To the Graduate Council:

I am submitting herewith a dissertation written by Giuseppe Settimo Iannelli entitled "A Globally Well-Posed Accurate and Efficient Finite Element CFD Algorithm for Compressible Aerodynamics". I have examined the final copy of this dissertation for form and content and recommend that it be accepted in partial fulfillment of the requirements for the degree of Doctor of Philosophy, with a major in Engineering Science and Mechanics.

Allen J. Baker, Major Professor

We have read this dissertation
and recommend its acceptance:

Wayman E. Scott

Eugene L Wachspress

Gerald C. Paynter

Accepted for the Council:

Vice Provost
and Dean of The Graduate School

A GLOBALLY WELL-POSED ACCURATE AND EFFICIENT FINITE ELEMENT CFD ALGORITHM FOR COMPRESSIBLE AERODYNAMICS

A Dissertation

Presented for the

Doctor of Philosophy

Degree

The University of Tennessee , Knoxville

Giuseppe Settimo Iannelli

May, 1991

Copyright © Giuseppe Settimo Iannelli, 1991
All rights reserved

ACKNOWLEDGEMENTS

The research program which has culminated in this dissertation could not have been absolutely performed without the continuous encouragement, guidance and assistance of my major professor Dr. A. J. Baker.

Our professional relationship has been truly outstanding with decisive scientific progress made. He has always arranged for adequate financial support to be available for me and repeatedly supported me especially in those moments when *slow convergence rates* seemed to daunt my efforts. I have always felt I was being treated by him more like a colleague than a doctoral candidate and I am grateful for the possibility he afforded me to participate in various specialist meetings and coauthor several technical papers. He has literally fostered the continuation of my intellectual growth, and with this dissertation I wish to express my heartfelt gratitude.

I am also immensely grateful to Dr. J. Stoneking, who provided my initial TA support, and presented me with an ineffably invaluable gift: the wondrously rewarding opportunity to teach.

My gratitude is then extended to the highly esteemed members of my dissertation commitee: Drs. Baker, Paynter, Scott, Stoneking, and Wachspress.

Finally, I wish to acknowledge the fundamental support of the Engineering College Computational Fluid Dynamics Laboratory, and the UT Computing Center that have provided the essential computational facilities for the development of this dissertation.

ABSTRACT

For the reliable determination of aerodynamic flows, a minimally dissipative generalized curvilinear-coordinate flux vector splitting implicit algorithm is developed within an optimal finite element integral statement for the two-dimensional (2-D) and axisymmetric compressible Navier-Stokes equations for ideal and reacting gases. Hypersonic-flow dissociated real air is modelled via a neutral mixture of five species, i.e. nitric oxide, molecular and atomic oxygen and nitrogen. The associated thermodynamic state is then determined via an original solution procedure for the classical chemical equilibrium equation system.

The analysis develops the curvilinear-coordinate flux vector jacobian matrices and associated characteristic equations. For any equation of state, the eigenvalues are the contravariant components of velocity in combination with the sound speed. Hence, the flow wave propagation in curvilinear space is rigorously represented using a tensor-field resolution of the flux vector into essentially kinematic and kinetic components. The streamwise semi-discretization is achieved using a Lyapunov-stable, Galerkin finite element integral statement for an eigenvalue-based "*companion conservation law system*", permitting classical test and trial space definitions. Thereafter, the accurate computation of the unsteady flow evolution is attained utilizing an implicit Runge-Kutta time-integration scheme, which is non-linearly stable and 2^{nd} order accurate.

Subsequently, a matrix tensor product factorization permits efficient numeri-

cal linear algebra handling for large Courant number. For 2-D and axisymmetric transonic, supersonic, and hypersonic inviscid and viscous flows, including real gas effect simulation, the algorithm is verified to yield reliable determination of velocity, pressure and temperature fields by generating accurate and monotone, essentially non-oscillatory numerical solutions in the presence of weak and strong shocks, attached and detached, and in boundary layer-inviscid flow interactions.

Contents

I The Continuum Statement 17

1 Governing Equations 18

1.1 Flux Vector Expressions 19

1.2 Equilibrium Real Gas Simulation 20

1.2.1 Chemical Equilibrium Equations 20

1.2.2 Pressure Partial Derivatives 25

1.3 Dimensional Analysis 26

1.4 Transport Coefficients 28

1.5 Curvilinear Coordinate Formulation 29

1.5.1 Coordinate Transformation 29

1.5.2 Curvilinear-Coordinate Equations 33

1.5.3 Contravariant Velocity Components 36

1.6 Mathematical Character 36

1.6.1 Canonical Form 36

1.6.2 Characteristic Eigenvalue Analysis 38

1.6.3 Homogeneous Gas Eigenvalues 40

1.6.4 Curvilinear Coordinate Mach Number 43

2 Integral Statements **44**

2.1 Strong Convection Form 44

2.2 Weak Statement 46

2.3 Jump Conditions 47

3 Boundary and Initial Conditions **54**

3.1 Boundary Conditions 54

3.1.1 Choice of Boundary Conditions 55

3.1.2 Implementation of Boundary Conditions 64

3.2 Initial Conditions 65

3.2.1 Transonic - Supersonic Flow Initialization 65

3.2.2 Hypersonic Flow Initialization 68

II Finite Element Semi-Discretization **73**

4 Hyberbolic System Semi-Discretization **74**

4.1 Analytical Solution Boundedness 74

4.2 Semi-Discrete Solution Boundedness 79

4.2.1 Uniform-Sign Eigenvalues 80

4.2.2 Mixed-Sign Eigenvalues 84

4.2.3 Fully Upwind and Companion System
Semi-Discretization 90
4.3 Companion Conservation Law System 93
4.4 Euler Equation Contravariant
Flux Vector Splittings 98
4.4.1 Contravariant Jacobian Matrix 98
4.4.2 Kinematic-Kinetic Flux Vector Splitting 100
4.4.3 Convection Acoustic Wave Flux Vector Splitting 104

5 Finite Element Integral Statements **107**

5.1 Domain Decomposition and Approximation Basis Functions 107
5.2 Exact and Approximate-Solution Spaces 109
5.3 Classical Galerkin Statement 110
5.4 Integral Statement Consistency 113
5.5 Directional Bias Character 114
5.6 Lyapunov Semi-Discretization Stability Analysis 117
5.6.1 One- Dimensional Stability Criteria 118
5.6.2 Multi-Dimensional Curvilinear Coordinate
Stability Criteria 122
5.7 Convection / Acoustic Flux Decomposition
Integral Statement 130
5.8 Optimal Metric Data Evaluations 133

6 Metric Data Handling for Accurate Semi-Discretizations on Arbitrary Curvilinear Meshes 136

6.1 Curvilinear-Coordinate Differential Operators 137

6.2 An Integration Identity 138

6.3 Spatial Approximation Functions 143

6.4 Determination of Optimal Metric-Data Evaluation Points for Convection Operator Semi-Discretizations 146

6.4.1 Integration in η Space 147

6.4.2 Metric-Data Evaluation Points 151

6.4.3 Accuracy Considerations 156

6.4.4 Second Order Accurate Semi-Discretizations on Arbitrary Meshes 157

6.4.5 Specific Applications 159

6.5 Determination of Optimal Metric Data Evaluation Points for Diffusion Operator Semi-Discretizations 160

6.5.1 Integrations in η Space 160

6.5.2 Metric-Data Evaluation Points 168

6.5.3 Accuracy Consideration 175

6.5.4 Second Order Accurate Semi-Discretizations on Arbitrary Meshes 176

6.5.5 Specific Applications 180

III Implicit Time Integration **182**

7 Solution Procedure **183**

7.1 Ordinary Differential Equation System and Implicit Integration 183

7.2 Newton Implementation and Tensor Matrix Product Factorization 185

8 A Non-Linearly Stable Implicit Runge-Kutta Algorithm for Conservation Law System Dissipative Semi-Discretizations **191**

8.1 Algorithm Derivation 191

8.1.1 Classical Accuracy and B-Consistency/Convergence Constraints 193

8.1.2 Stability Constraints 196

8.2 Solution of the IRK Coefficient Equations 201

8.3 Theoretical Comparisons 203

9 A Generalized Tensor Product Factorization for Implicit Finite Element Methods **207**

9.1 Jacobian Matrix Factorization 207

9.2 Computational Regions and Bilinear Tensor Product Basis Functions 209

9.3 Integration Identities 214

9.4 TPF Matrix Structure 217

9.5 Derivation of a Prototype TPF Scheme 220

9.6 Derivation of a Specific TPF Scheme 222

9.7 Mass Matrix Factorization 226

9.8 Inviscid Flux Vector Factorization 229

9.8.1 η_1 Direction Operators 230

9.8.2 η_2 Direction Operators 238

9.9 Viscous Flux Vector Factorization 245

9.9.1 η_1 Direction Operators 246

9.9.2 η_2 Direction Operators 254

9.10 TPF Error Structure 264

9.10.1 Generic Error Expression 264

9.10.2 Convection Term Errors 267

9.10.3 Diffusion Term Errors 270

9.10.4 $O(\Delta t^2)$ Errors 275

9.10.5 Error Order of Magnitude 275

9.11 An Alternative Iterative Solver 276

9.12 Examples of Application 278

IV Validations **282**

10 Discussion and Results: Quasi-1D

2-D and Axisymmetric Solutions **283**

10.1 Quasi-1-D Euler Benchmark 284

10.2 Linear Hyperbolic Conservation

Law System Case 289

10.3 Transonic Aerodynamics Benchmarks 291

10.3.1 Inviscid Airfoil Flows 291

10.3.2 Viscous Airfoil Flows at $Re = 2000$ and $Re = 4.6 \cdot 10^6$ 296

10.4 Supersonic Cases 301

10.4.1 Gasdynamic Inviscid Flows 301

10.4.2 Shock-Wave Flat-Plate Boundary Layer Interaction 306

10.5 Hypersonic Cases 309

10.5.1 Blunt Body Inviscid Flow 309

10.5.2 Missile Inviscid and Viscous Flows 310

11 Summary and Conclusions **357**

V Bibliography **360**

List of Figures

2.1 Shock Surface Control-Volume Detail 48

2.2 Local Normal Unit Vector Detail 49

2.3 Plane Oblique Shock Geometry 53

3.1 Internal Flow Domain Geometry 66

3.2 Missile and Bow Shock Configuration 69

3.3 Shock Segment and Representative Velocity Vector Resolution . . . 70

5.1 Representative Assembly of Four 2-D Lagrange Bilinear Elements with Optimal Evaluation Points 135

6.1 Example of domain transformation 144

6.2 Approximation Function Variation 145

6.3 Representative Computational Cell for Evaluation (6.44) 148

6.4 Representative Computational Cell for Evaluation (6.53) 150

6.5 Contiguous Elements and Evaluation Points for Integrals (6.97) . . . 161

6.6 Contiguous Elements and Evaluation Points for Integrals (6.104) . . 163

6.7 Contiguous Elements and Evaluation Points for Integrals (6.111) . . 166

6.8 Contiguous Elements and Evaluation Points for Integrals (6.117) . . 167

6.9 Contiguous Cells for Evaluation (6.148) 179

9.1 Assembly of Four Finite Elements Forming a Master Element 210

9.2 Assembly of Two Contiguous Elements 210

9.3 Variations of Bilinear Functions (9.4) over $\widehat{\Omega}$ 212

9.4 Variations of Functions (9.5) over ω 212

9.5 Union of Bilinear Elements. Nodes Numbered in the η_1 Topological Direction 218

9.6 Banded structure of A 218

9.7 Banded Structure of B and C 219

9.8 Representative TPF Computational Domain Correspondence 278

10.1 de Laval Nozzle and Initial Condition Mach Number Profile. 315

10.2 MDS Finite Element Quasi-1-D Euler Algorithm Steady-State Solution, $M_s \simeq 1.40$, Momentum Distribution 315

10.3 MDS Finite Element Quasi-1-D Euler Algorithm Steady-State Solution, $M_s \simeq 1.40$, Mach Number Distribution and Comparisons from [48]. 315

10.4 Unsteady Quasi-1-D Euler Solution. Implicit Runge-Kutta. Mach Number Profiles. $\Delta t = 0.005s$, a) $t = 0.4s$, b) $t = 1.0s$, c) $t = 1.2s$, e) $t = 1.8s$, f) $t = 2.8s$. 316

10.5 Unsteady Quasi-1-D Euler Solution. Implicit Runge-Kutta. $\Delta t =$ $0.005s$, $t = 1.8s$, a) Density, b) Momentum, c) Pressure. 317

10.6 Unsteady Quasi-1-D Euler Solution Comparisons, $t = 1.0s$, $\Delta t =$ $0.2s$, —from Fig. 10.4b, a) EU, b) CN, c) IRK. 317

10.7 Unsteady Quasi-1-D Euler Solution, $t = 1.8s$, $\Delta t = 0.2s$, —from Fig. 10.4e, a) EU, b) CN, c) IRK. 318

10.8 Unsteady Quasi-1-D Euler Solution, $t = 1.8s$, $\Delta t = 0.3s$, —from Fig. 10.4e, a) EU, b) CN, c) IRK. 318

10.9 Two-Dimensional Linear Problem Domain and Discretization Ω^h. . 319

10.10 Analytical Solution Interpolation on Nodes of Ω^h for q_1, $t = 2.0s$. . 319

10.11 Computed Solution Surface Perspectives for q_1, $t = 2.0s$, $\Delta t = 0.1s$, a) Backwards Euler, b) Trapezoidal, c) Implicit Runge-Kutta. 319

10.12 Computed Solution Surface Perspectives for q_1, $t = 2.0s$, $\Delta t = 0.2s$, a) Backwards Euler, b) Trapezoidal, c) Implicit Runge-Kutta. 319

10.13 Error Distribution Perspective for q_1, $t = 2.0s$, $\Delta t = 0.1s$, a) Backwards Euler, b) Trapezoidal Rule, c) Implicit Runge-Kutta. . . 320

10.14 Error Distribution Perspective for q_1, $t = 2.0s$, $\Delta t = 0.2s$, a) Backwards Euler, b) Trapezoidal Rule, c) Implicit Runge-Kutta. . . 320

10.15 M=65 $\times$ 35 Nonuniform Mesh for Transonic Parabolic Arc Problem. 321

10.16 MDS Algorithm Unsteady Solution, Euler Equations, $t - t_0 = 2.0s$, Transonic Mach Number Surface Perspective and Contours, a) Initial State, b) Backwards Euler Rule, c) Trapezoidal Rule, d) Implicit Runge-Kutta. 322

10.17 MDS Algorithm Unsteady Solution Perspective and Contours, Euler Equations, $t - t_0 = 14.65s$, $\Delta t = 0.15s$, Backwards Euler Rule, a) Pressure, b) Mach Number. 323

10.18 MDS Algorithm Unsteady Solution Perspective and Contours, Euler Equations, $t - t_0 = 14.65s$, $\Delta t = 0.15s$, Implicit Runge-Kutta, a) Pressure, b) Mach Number. 324

10.19 MDS Algorithm Steady-State Velocity Vector Field, Euler Equations, Parabolic Arc, $M_s \simeq 1.5$. 325

10.20 MDS Algorithm Steady-State Solution Contours, Euler Equations, Parabolic Arc, $M_s \simeq 1.5$, a) Entropy, b) Mach Number, c) Principal Momentum. 325

10.21 MDS Algorithm Steady-State Solution Perspectives and Contours, a) Principal Momentum, b) Transverse Momentum. 326

10.22 MDS Algorithm Steady-State Solution Perspectives and Contours, a) Mach Number, b) Pressure. 327

10.23 MDS Algorithm Steady-State Solution, Navier-Stokes Equations, Laminar $Re = 2000$, a) M=65 $\times$ 35 Element Discretization, b) Mach Number Distribution, c) Velocity Vector Field. 328

10.24 MDS Algorithm Steady-State Solution, Navier-Stokes Equations, Laminar $Re = 2000$, a) Trailing Edge Region Velocity Vector Field, b) Mach Number Isocline Distribution. 329

10.25 MDS Algorithm Steady-State Solution, Navier-Stokes Equations, Laminar $Re = 2000$, a) Transverse Momentum, b) Principal Momentum, c) Pressure, d) Temperature. 330

10.26 MDS Algorithm Steady-State Solution, Navier-Stokes Equations, Laminar $Re = 4 \times 10^6$, a) M=65 $\times$ 45 Element Discretization, b) Physical Space Principal Momentum Contour Distribution. 331

10.27 MDS Algorithm Steady-State Solution, Navier-Stokes Equations, Laminar $Re = 4 \times 10^6$, a) Transverse Nodal Space Contour Distribution, b) Perspective Surface Presentation. 332

10.28 MDS Algorithm Steady-State Pressure Solution, Navier-Stokes Equations, Laminar $Re = 4 \times 10^6$, a) Global Distribution, b) Trailing Edge Region Detail. 333

10.29 MDS Algorithm Steady-State Euler Solution, Supersonic Compression Ramp, $M_\infty = 3.0$, $\alpha = 20°$, a) Sheared Cartesian Mesh, M=65 $\times$ 35 b) Density Distribution on Mesh 1. 334

10.30 MDS Algorithm Steady-State Euler Solution, Supersonic Compression Ramp, $M_\infty = 3.0$, $\alpha = 20^o$, a) First Solution-Adapted Mesh b) Density Distribution on Mesh 2. 335

10.31 MDS Algorithm Steady-State Euler Solution, Supersonic Compression Ramp, $M_\infty = 3.0$, $\alpha = 20^o$, a) Second Solution-Adapted Mesh b) Density Distribution on Mesh 3. 336

10.32 MDS Algorithm Steady-State Euler Solution, Supersonic Compression Ramp, $M_\infty = 3.0$, $\alpha = 20^o$, Perspective Surface and Solution Contour Distributions, a) Mach Number, b) Pressure. 337

10.33 MDS Algorithm Steady-State Euler Solution, Supersonic Shock Reflection $M_\infty = 2.15$, $\alpha = -4^o$, a) Sheared Cartesian Mesh, M=65 $\times$ 35, b) Computed Density Distribution. 338

10.34 MDS Algorithm Steady-State Euler Solution, Supersonic Shock Reflection $M_\infty = 2.15$, $\alpha = -4^o$, a) First Solution-Adapted Mesh, b) Computed Density Distribution on Mesh 2. 338

10.35 MDS Algorithm Steady-State Euler Solution, Supersonic Shock Reflection $M_\infty = 2.15$, $\alpha = -4^o$, a) Second Solution-Adapted Mesh, b) Computed Density Distribution on Mesh 3. 339

10.36 MDS Algorithm Steady-State Euler Solution, Supersonic Shock Reflection $M_\infty = 2.15$, $\alpha = -4^o$, Mach Number Solution Contour and Perspective Surface Distributions on Mesh 3. 339

10.37 MDS Algorithm Steady-State Euler Solution, Supersonic Shock Reflection $M_\infty = 2.15$, $\alpha = -4^o$, Pressure Solution Contour and Perspective Surface Distributions on Mesh 3. 340

10.38 MDS Algorithm Steady-State Euler Solution, Supersonic Shock Reflection $M_\infty = 2.15$, $\alpha = -4^o$, Entropy Solution Contour and Perspective Surface Distributions on Mesh 3. 340

10.39 MDS Algorithm Steady-State Euler Solution, Double Supersonic Shock Reflection $M_\infty = 2.15$, $\alpha = -4^o$, a) Sheared Cartesian Mesh, M=65 $\times$ 35, b) Computed Density Distribution, c) Final Solution-Adapted Mesh, d) Final Density Distribution. 341

10.40 MDS Algorithm Steady-State Euler Solution, Double Supersonic Shock Reflection $M_\infty = 2.15$, $\alpha = -4^o$, Perspectives and Contour Distributions on Final Mesh, a) Static Pressure, b) Mach Number. . 342

10.41 MDS Algorithm Steady-State Navier-Stokes Solution, Shock-Wave Laminar Boundary Layer Interaction, $M_\infty = 2.15$, $Re = 1 \times 10^5$, a) Problem Schematic, b) Entropy Perspective Solution Surface and Contour Distribution. 343

10.42 MDS Algorithm Steady-State Navier-Stokes Solution, Shock-Wave Laminar Boundary Layer Interaction, $M_\infty = 2.15$, $Re = 1 \times 10^5$, Perspective Solution Surface and Contour Distributions, a) Temperature, b) Density. 344

10.43 MDS Algorithm Steady-State Navier-Stokes Solution, Shock-Wave Laminar Boundary Layer Interaction, $M_\infty = 2.15$, $Re = 1 \times 10^5$, Perspective Solution Surface and Contour Distributions, a) Axial Momentum b) Mach Number. 345

10.44 MDS Algorithm Steady-State Navier-Stokes Solution, Shock-Wave Laminar Boundary Layer Interaction, $M_\infty = 2.15$, $Re = 1 \times 10^5$, Pressure Perspective Solution Surface and Contour Distributions, a) Single Reflection, b) Double Reflection. 346

10.45 Surface Pressure Distributions and Comparisons from [46], Shock Boundary Layer Interaction, $M_\infty = 2.15$ 347

10.46 Surface Skin Friction Distributions and Comparisons from [46], Shock Boundary Layer Interaction, $M_\infty = 2.15$ 347

10.47 Steady-State Navier-Stokes Solution, Shock-Boundary Layer Interaction, $M_\infty = 2.15$, $Re = 1 \times 10^5$, a) Axial Velocity Surface Perspective and Contour Distribution, b) Recirculation Region Velocity Field Close-Up. 348

10.48 MDS Algorithm Steady-State Euler Solution, Hypersonic Blunt Body, $M_\infty = 6.5$, a) Third Solution-Adapted Mesh, M=65 $\times$ 35, b) Density Contour Distribution 349

10.49 Sphere-Biconic Axisymmetric Body, Computational Domain, A) Symmetry Streamline Inlet Point, B) Symmetry Streamline Shock Point, C) Stagnation Point, D) Sphere-Cone Juncture, E) Bicone Juncture. 350

10.50 $M_\infty = 8$ Hypersonic Viscous Flow Past Sphere-Biconic Axisymmetric Body, $Re_\infty = 500,000$, Steady State Perspective Surface and Contour Distributions, Mach Number. 351

10.51 $M_\infty = 8$ Hypersonic Viscous Flow Past Sphere-Biconic Axisymmetric Body, $Re_\infty = 500,000$, Steady State Perspective Surface and Contour Distributions, Temperature. 351

10.52 $M_\infty = 8$ Hypersonic Flow Past Sphere-Biconic Axisymmetric Body, Steady State Contour Distributions, Pressure, a) $Re_\infty = 500,000$ Viscous Flow, b) Inviscid Flow. Magnification-Induced Bow Shock Distortion. 352

10.53 $M_\infty = 8$ Hypersonic Inviscid Flow Past Sphere-Biconic Axisymmetric Body, Steady State Perspective Surface and Contour Distributions, Mach Number, C) Stagnation Point, D) Sphere-Cone Juncture, E) Bicone Juncture. 353

10.54 $M_\infty = 8$ Hypersonic Flow Past Sphere-Biconic Axisymmetric Body, Steady State Perspective Surface and Contour Distributions, Density. 353

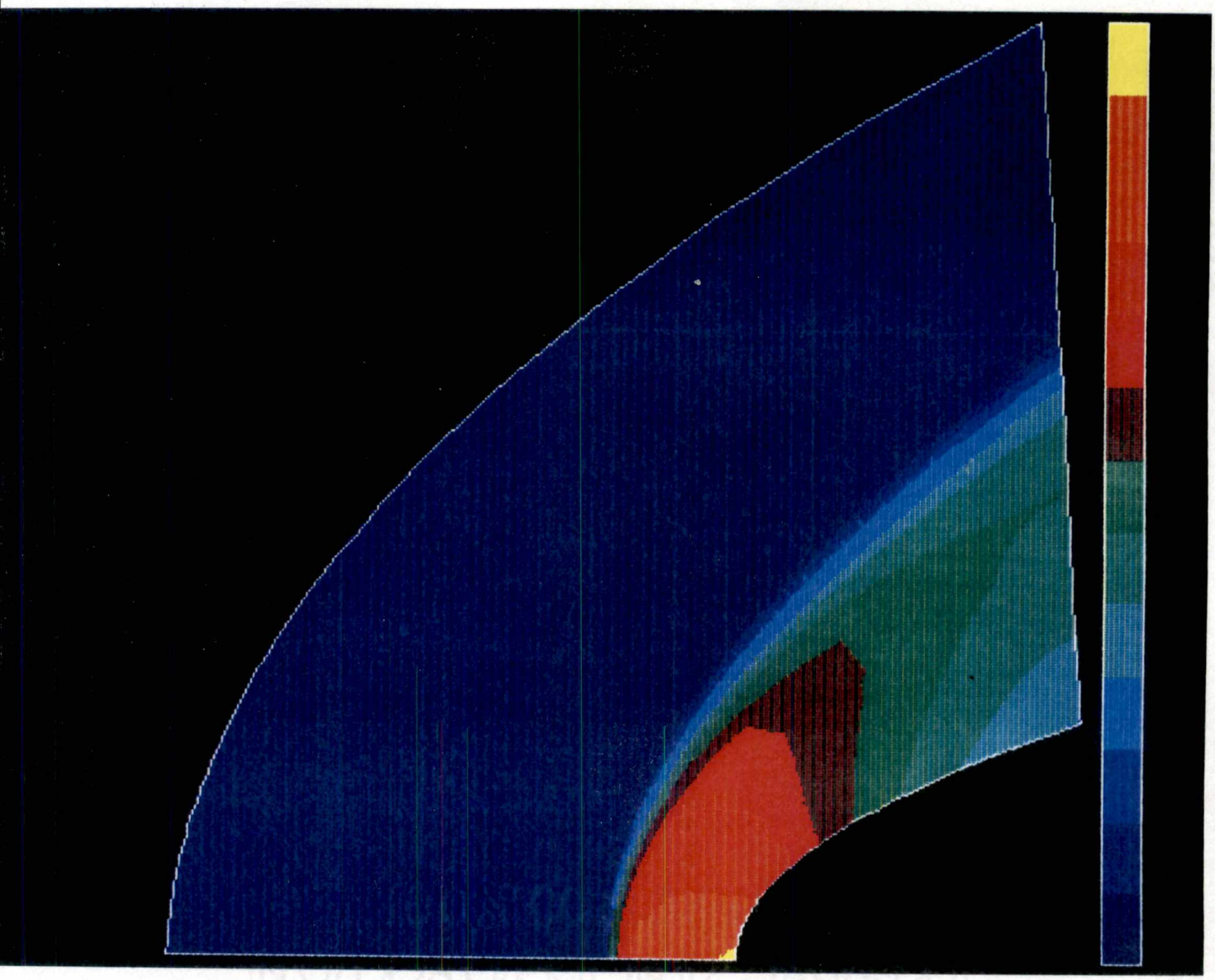
10.55 $M_\infty = 8$ Hypersonic Inviscid Flow Past Sphere-Biconic Axisymmetric Body, Steady State Contour Distributions, Pressure, a) Ideal Gas, b) Real Gas. Magnification-Induced Bow Shock Distortion. . . 354

10.56 $M_\infty = 8$ Hypersonic Inviscid Flow Past Sphere-Biconic Axisymmetric Body, Steady State Stagnation Streamline Distributions, B-Shock Point, C-Stagnation Point, D-Sphere Cone Juncture, – – – – Ideal Gas, —— Real Gas, a) Pressure, b) Temperature. 355

10.57 $M_\infty = 8$ Hypersonic Inviscid Flow Past Sphere-Biconic Axisymmetric Body, Detailed Steady-State Stagnation-Streamline Temperature Distributions. 355

10.58 $M_\infty = 8$ Hypersonic Inviscid Flow Past Sphere-Biconic Axisymmetric Body, Steady State Stagnation-Streamline Distributions, B-Shock Point, C-Stagnation Point, D-Sphere Cone Juncture, Mass Fractions, a) Molecular Nitrogen, b) Molecular Oxygen. 356

10.59 $M_\infty = 8$ Hypersonic Inviscid Flow Past Sphere-Biconic Axisymmetric Body, Detailed Steady-State Stagnation-Streamline Distributions for Nitric Oxide and Atomic Oxygen Mass Fractions. 356



Introduction

The reliable simulation of real gas supersonic and hypersonic aerodynamic flows presents subtle challenges, since strong-shock molecular dissociations /recombinations can occur, and bow shocks virtually coalesce with thick chemically reacting boundary layers. In these cases, the ensuing strong-interaction modification of the outer, essentially inviscid flow, and/or real-gas-effect pressure field variations, directly affect the aerodynamic surface pressure distribution and heat transfer.

For the accurate prediction of these flows, this dissertation documents derivation and performance verification of a minimally dissipative, generalized implicit flux vector split Galerkin finite element algorithm for the compressible Euler and Navier-Stokes equations in curvilinear coordinates for ideal and reacting gases, that is nonlinearly stable and uniformly 2^{nd} order accurate on absolutely arbitrary meshes of Lagrange bilinear elements. The transport coefficients are modelled via generalized temperature-dependent Sutherland laws, while real gas effects are simulated using an original solution procedure for the chemical equilibrium equations along with the internal energy and mass fraction conservation relations.

The algorithm allows improved understanding of reacting gas, high supersonic and hypersonic aerodynamic flows via theoretical and practical minimization of the sizable semi-discretization dissipation, that affect currently practiced upwind flux vector/difference splitting theories and /or central difference schemes with numerical damping within finite difference/ finite volume implementations. The theoretical developments are based on characteristic eigenvalue and finite element analyses. Significantly, two crucially distinct CFD algorithm stability aspects are elicited. The first concerns the stability of the multi-dimensional spatial semi-discretization, herein analyzed using a Lyapunov method. The second corresponds to the stability of the time integration, herein investigated using non-linear Runge-Kutta scheme theories. The minimization of the spatial semi-discretization dissipation is obtained for a Lyapunov-stable, consistent-order-of-accuracy conservative scheme, in totally arbitrary curvilinear coordinates, hence completely general body-fitted meshes, that efficiently accomodates any real gas state equation. Further, the procedure admits reliable simulation of transients, within reacting flows, as obtained using a time-accurate and non-linearly stable implicit Runge-Kutta integration scheme.

The resultant fully discrete algebraic system can be solved iteratively or non-iteratively for large Courant numbers. The terminal implementation has selected and evaluated a quasi-Newton sub-iteration option, via an efficient tensor matrix product factorization, specifically appropriate for parallel processing.

The national interest in reliable, aerodynamically-active hypersonic missiles,

both tactical and strategic, and hypersonic aircrafts, such as advanced interceptors, strike/reconnaissance vehicles, including the national aerospace plane, motivates the development of this CFD procedure. Thus, the reliable computation of transonic, supersonic, and hypersonic inviscid and viscous flows with significant real gas effects including molecular dissociations, directly addresses this interest.

A wide variety of CFD algorithms has been developed for transonic and supersonic aerodynamic flow predictions over the last two decades, in an attempt to meet the fundamental requirements of stability, accuracy and efficiency for arbitrary meshes in a single practical scheme. The spatial semi-discretizations in these algorithms can be broadly classified in two classes, namely central difference schemes with suitable numerical damping and upwind schemes.

A notable contribution to the central-difference dissipative class was published by Beam and Warming [25], who proposed an implicit factored scheme for the Euler equations, wherein the unknown state variable constitutes the solution of an efficient sequence of block-tridiagonal linear systems. This theory and procedure forms the basis of the NASA Ames-developed ARC-2D and ARC-3D code family [44], that has supported investigation of a wide range of transonic and supersonic aerodynamic flows. However, as confirmed by Pulliam [44], the basic scheme must be augmented by a blend of 2^{nd} and 4^{th} order dissipative difference operators to maintain stability in the presence of shocks, or for smooth solution stability in 3-dimensions. This leads to a block-pentadiagonal matrix system, if the full jacobian matrix of the necessary

artificial dissipation is included in the implicit-side formulation. The original block tri-diagonal matrix structure can be maintained by using only explicit 4^{th} order damping, which limits the magnitude of stable time steps. The associated Courant number may not be much larger than unity, for accurate unsteady simulations, since the time integrator is the intrinsically non-dissipative Crank-Nicolson rule.

An alternative formulation is proposed by Lerat [38], who develops a fully discrete space centered finite difference scheme for the Euler equations that, importantly, introduces an inherent coupling in the time derivatives of the unknown state variable at various adjacent nodes. This feature distinguishes this scheme from that of Beam and Warming, and intrinsically introduces an adequate amount of numerical dissipation without explicitly added 4^{th} order difference expressions. This mechanism produces an algorithm that remains stable in the presence of shocks. The original development is based on uniform mesh, and time step increments, and leads to a family of algorithms, upon selection of specific numerical values for embedded parameters.

The notion of time derivative coupling is natural in the finite element method, via the semi-discretization mass matrix, and leads to schemes that are not affected by odd-even node decoupling for dissipative spatial semi-discretizations devoid of 4^{th} order difference terms. In this framework, Fletcher [16] proposed a group-approximation least-squares algorithm for subsonic flows, while Tezduyar and Hughes [37] developed Petrov-Galerkin schemes to introduce adequate dissipation

in a weak statement formulation. In distinction to these developments, Donea [39] derived the "Taylor Galerkin" finite element algorithm for hyperbolic equations. This formulational procedure employs a truncated Taylor series to generate a time semi-discrete conservation law statement which is subsequenly discretized in space using bilinear basis functions. In this instance, several stability mechanisms are introduced in continuum form, upon restatement of the time derivatives with spatial derivatives via the original conservation law system.

This fundamental procedure has been thoroughly analyzed by Baker and Kim [47], who develop the "Taylor Weak Statement" generalization for hyperbolic conservation law systems. This construction develops a so-called *companion conservation law* system that contains continuum expressions representing intrinsic dissipative and anti-dissipative mechanisms. Whereupon, the classical Galerkin finite element fully discrete algorithm yields over a dozen independently derived schemes, upon identification of the embedded parameter set. The analysis indicates that the companion conservation law system approach can lead to stable, centered semi-discrete schemes upon selection of opportune length and velocity scales in the continuum dissipation operators.

In parallel with these developments, research efforts have increasingly focused on the class of upwind, intrinsically dissipative difference methods which do not require explicit addition of empirical numerical dissipation. Procedures advancing flux-vector and flux-difference splitting developments, and applications, include

those developed by Steger-Warming [33], van Leer [35], Roe [32], and Grossman [65], wherein the upwind differencing is performed in directions opposite to the characteristic directions, and thereby induces an amount of relevant artificial dissipation. These algorithms have been implemented using both explicit and implicit time integration schemes [35,48], and have generated crisp non-oscillatory shocks for significant aerodynamic simulations. Recently, Liou and van Leer [48] present a thorough comparisons of various splittings, and conclude that a robust algorithm is best achieved by using different splittings in the quasi-Newton jacobian and residual operators. They also extend various standard splitting procedures to real gas flows [50].

The geometric rigor and appeal of eigenvalue analyses for hyperbolic conservation law systems is considerable, since the derivations pivot on classical notions of characteristics, hence signal propagation directions. The common thread of recent vector splitting theories is geometric extension of 1-D derived schemes to multidimensional formulations. However, this extrapolation leads to formulational ambiguities, and results in algorithms that are tightly coupled to the underlying grid. Powell and van Leer [56], among others, have addressed this crucial issue, and developed a "cell-vertex scheme where the grid components of the convection speed are known". This entails local decomposition of the Euler equations into a set of convection equations leading to discrete conservation of mass, momentum and energy. Therefore, the resulting scheme is algebraically rather involved for non-cartesian

meshings.

Recently, Colella [62] presents an explicit Godunov-type multi-dimensional and upwind second-order algorithm for the Euler equations. His construction solves a characteristic form of the equations at a moderate CFL number. The procedure renders good discontinuity resolution for the standard shock reflection problem, with the exception of small isolated regions where dispersion error is noticeable. In the same year, Yee et al. [63] published a shock capturing finite volume TVD algorithm for hypersonic flows, that can be third-order accurate on uniform grids. However, they report that some of the procedure formulae may not preserve free-stream values on highly skewed grids, even though usage of the implicit backward Euler time integration and finite elements on such grids can lead to stability and convergence enhancements. Nevertheless, it is also indicated that accuracy and/or stability may be compromised by discontinuities in the thermodynamic derivatives supplied by the Srinivasan curve-fits [53,63].

Furthermore, as identified in recent US Air Force sponsored research [61], the basic upwind constructions can induce sizable numerical dissipation, which may require use of much too expensive, highly-refined computational meshes for acceptable solution accuracy. For example, it is shown in [61] that the Steger-Warming construction requires four times the number of grid points of Roe's scheme to adequately resolve a laminar boundary layer, even though the latter scheme is 25% more CPU expensive. Moreover, an exaustive study conducted at Wright-Patterson

AFB [59] shows that the solutions generated by both schemes do not "compare extremely well" with available experimental data for a hypersonic compression ramp flow benchmark.

Further, these procedures have been mainly tested for essentially inviscid flows, and only grudgingly admit real gas and curvilinear-coordinate generalizations, yielding non-unique formulae that need extra computations of several auxiliary quantities. For example, the 1-D generalization of Roe's scheme [66], introduces artificial thermodynamic states that aggravate solution accuracy especially along contact discontinuities. On the other hand, a real gas equation in the 1-D van Leer scheme causes the smallest eigenvalue, associated with the "positive" flux, to become negative (for some states) in the whole subsonic range [66,67], which in turn engenders semi-discretization instability. Moreover, in non-equilibrium simulations, where the vastly different chemical time scales considerably stiffen the semi-discrete Euler equations, these potential instabilities then reduce the practical stability margins to the extent that bounded solutions with these schemes are reported attained only for CFL $\leq 10^{-2}$, [68]. Moreover, in most conventional multi-dimensional constructions, the final upwind direction remains normal to the local computational cell face, regardless of the genuine kinematic convection direction. Consequently, numerically captured oblique shocks may be smeared over several cells. The need of high accuracy for practical meshes then becomes more acute in real gas and/or viscous hypersonic simulations, where strong shocks virtually coalesce with thick

boundary layers within a chemically reacting flow. In these cases, the ensuing strong-interaction modification of the surrounding, essentially-inviscid flow, and/or the real gas effect pressure field variations, directly affect the aerodynamic surface pressure distributions and skin friction, hence lift, drag and heat transfer.

Even though both classes of spatial semi-discretizations employ formulae of stated unambiguous order of accuracy, for a uniform cartesian mesh, and lead to bounded solutions for significant aerodynamics simulations, uncertainties regarding the level of induced artificial dissipation and the objective accuracy of the corresponing numerical solutions remain, since the current research lacks complete quantitative stability analyses for the multi-dimensional, real-gas Euler equations in curvilinear coordinates. Therefore, not even the crucial effect of the coordinate transformation metric data upon algorithm stability is sufficiently investigated.

In order to resolve these cited limitations, this dissertation documents a dimensionally complete Lyapunov semi-discretization stability analysis for the full real gas Euler equations in curvilinear coordinates, within a generalized finite element Navier-Stokes CFD algorithm. The developed minimal-dissipation scheme utilizes a fully generalized, curvilinear coordinate kinematic-kinetic flux vector splitting, where the split fluxes partition the pressure gradient using the local contravariant Mach number resolution. Importantly, the procedure efficiently accomodates an arbitrary real gas equation of state, while the eigenvalues of the positive contravariant flux remain unequivocally non-negative on absolutely arbitrary meshes,

in sharp contrast to the cited potential negative-eigenvalue instability of the van Leer scheme.

As detailed in the following sections, the coordinate transformation metric data intrinsically enter the jacobian eigenvalue expressions, and consequently, the stable directional semi-discretization can be rigorously obtained in totally arbitrary curvilinear coordinates. The developed finite element semi-discretization intrinsically corresponds to a linear combination of second order schemes, as formulated on all sides of any computational node. This leads to a linear combination of jacobian matrices over the multi-dimensional computational cell. A crucial Lyapunov stability analysis for the full semi-discrete Navier-Stokes equations, then yields a rigorous, eigenvalue matrix non-negativeness stability condition, which at each semi-discretization node "r" then allows local dissipation minimization using the embedded dissipation parameter β_r. Importantly, $\beta_r = 0.5$ corresponds to the classical fully upwind formula, and the maximum of semi-discretization dissipation. Whereupon, the intrinsic presence of the coordinate transformation metric data in this criterion allows the rigorous assessment of mesh non-uniformity and non-orthogonality issues on semi-discretization stability. Further, β_r is allowed to vary nodally, thus ensuring uniform minimal dissipation throughout the mesh. Conversely, for a fixed β_r the mesh can be locally adapted, hence the metric data varied, to satisfy this rigorous stability criterion and attain an optimal order-of-accuracy semi-discretization.

The Galerkin integral statement is directly formulated in curvilinear coordinates and associates the local value of the coordinate-transformation jacobian determinant with the dependent variable. For accuracy and efficiency, the crucial metric data are evaluated at optimal locations within each element. The curvilinear coordinates of these points are invariant under any coordinate transformation, and are theoretically determined so that the developed semi-discrete operators allow primitive-coordinate second order accuracy on arbitrary grids, along with unconditional preservation of a uniform free stream, a property that some schemes are cited to lack. Thus, the algorithm implementation dispenses with element-by-element Gaussian quadratures, and directly leads to terminal recursion relations in closed form. Hence, the computational procedure implementation becomes competitive with difference methodology.

A significant advancement in the determination of well-posedness for the full compressible Navier-Stokes equations was presented by Dutt [49], who derived statements for "maximally dissipative" boundary conditions. In his analysis, these were determined such that the time variation of a Navier-Stokes system energy functional is bounded. The development focused on essentially uni-directional flows, and heuristically assumed that a bounded energy time variation induced a bounded solution.

In this dissertation, Dutt's analysis is generalized and interpreted as an application of a generalized Lyapunov stability theory, [4,5,7,8]. Stable boundary condi-

tions for the Navier-Stokes equations are derived, and their dependence on inflow and outflow Mach number is clearly identified and assessed. Further, the connection between bounded energy variation and a stable solution is analytically established. The derived conditions constrain the outflow static pressure and the surface deviatoric tractions, as well as momentum and heat fluxes, and can be effectively enforced via the Galerkin weak statement-derived surface integrals. The evaluation of these algorithm integrals then completes the terminal stiff and non-linear ordinary differential equation (ODE) system.

Inclusion of real gas physics, in addition to local mesh refinements, considerably stiffens the semi-discrete Euler and Navier-Stokes equations. Stiffness and non-linearity make it particularly challenging to establish a stable time integration procedure which can also generate accurate solutions using relatively large time steps (CFL numbers) for efficiency. The backwards Euler and trapezoidal rule (Crank-Nicolson) time integration algorithms are commonly employed in implicit CFD applications, [25,48], in a one iteration per time step mode. Both algorithms enjoy theoretical linear absolute stability which portends use of an arbitrarily large time step Δt. The A-stable trapezoidal rule is second order accurate, yet when the linear-analysis ODE system has a large eigenvalue spread, and if Δt is not relatively small, the scheme amplification ratio decays very slowly or not at all. Conversely, the backwards Euler amplification factor always tends to zero with large time steps, however, the algorithm is highly dissipative and only first order accurate.

The notions of *absolute stability* and *strong* A-stability have both been developed and analyzed [10] for a model linear ordinary differential equation which indeed propounds use of arbitrarily large time steps Δt. However, when a highly non-linear ODE system results, e.g., in the spatial semi-discretization of the Euler/Navier-Stokes equations, stability can be preserved only at the cost of limiting the time step Δt to values well below those predicted as admissible by linear model stability analyses, if the temporal algorithm remains non-iterative throughout the solution process. Progressing towards the elimination of this stability limitation, this dissertation presents a two-stage implicit Runge-Kutta scheme that combines second order time accuracy with non-linear stability. Further, it can be implemented as iterative within any two consecutive time levels.

The theoretical analysis is based on the recently developed theories of B- consistency, B- convergence, and B- stability, [15,18]. It is shown that the implicit Runge-Kutta (IRK) theoretical framework affords *non-linear stability* for the full semi-discrete dissipative Euler and Navier-Stokes equations for *arbitrary* grids and time-steps. Further, it contains both the Euler and trapezoidal rule schemes as special cases. Subsequently, the *algebraic stability* analysis is applied to these CFD standard implicit algorithms to elicit their stability features.

The investment of two iterative implicit solutions per time step is ultimately expected to lead to an economic solver, when the overall cost of obtaining a reliable solution for several time steps is considered. This derives from the robust stability

characteristics of the present algorithm and relevant practical implementation. The latter is based on a quasi-Newton iteration per stage, which is realized via an efficient tensor matrix product approximate factorization of the Newton algorithm system jacobian.

Tensor product factorizations (TPF) are nowadays applied to the solution of non-linear conservation law systems of PDE's, by suitably extending the original algorithms for the solution of a scalar linear parabolic PDE. Various improvements in the pioneering procedure have been developed, over the years, seeking to increase the order of accuracy, incorporate finite element algorithms and handle arbitrary curvilinear geometries. Hayes [28,29] utilized an isoparametric transformation to generate an accurate "patch" approximation of the local element measures on an arbitrary grid of bilinear finite elements. More recently, Celia and Pinder [40] have critically analyzed various implementations and emphasized the structure of the $O(\Delta t^2)$ factorization error generated by the discretization of a parabolic PDE.

The common thread of all of these important developments is the replacement of a multi-dimensional jacobian sparse matrix, with an operationally efficient sequence employing block m-diagonal one-dimensional matrices. This approximation clearly calls for the synthesis of adequate methods to handle non-regular multi-dimensional geometries. In this connection the accurate representation of the 2-D metric data is crucial. In this dissertation, a new TPF algorithm is developed that associates the determinant of the coordinate-transformation Jacobian with the

dependent variable, within the time derivative, and directly utilizes 2-D metric data in the computation of the curvilinear 1-D differential operators. This procedure departs totally from traditional finite element practice, and results in a 2-D mass-matrix free from any mesh measure dependency. This eliminates the need to approximate this determinant [28,29], hence eliminates the associated error and permits the exact factorization of the 2-D mass matrix in terms of 1-D mass-matrix components which, in turn, allows an accurate factorization of the 2-D differential operators on arbitrary meshes.

The present scheme is developed upon capitalization on the topology of an arbitrary mesh of Lagrangian bilinear finite elements. The specific factorization formulae are presented for 2-D convection and diffusion operators and the relevant errors identified. These involve metric-data averages and jacobian term approximations. Whereupon, a novel iterative procedure is discussed to minimize such errors. This procedure utilizes the TPF matrix as the implicit part of an iterative solution algorithm.

The developed finite element CFD algorithm is verified for benchmark probelms in quasi-1-D, 2-D and axisymmetric geometries for transonic, supersonic and hypersonic ideal and real gas inviscid and viscous flows. These include a de Laval nozzle configuration for various flow criticalities, an $M_\infty = 0.65$ flow about a parabolic arc airfoil, an $M_\infty = 2.2$ inviscid and viscous schock reflection problem, an $M_\infty = 3.0$ wedge flow, and an $M_\infty = 8.0$ flow about a sphere-bicone missile configuration. All

CFD solutions are verified monotone and essentially non-oscillatory throughout the computational domain, including the boundaries, and each accurately resolves all flow features including weak and strong shocks, attached and detached, expansion waves, and boundary layer-inviscid flow interactions.

This dissertation is organized as follows. The governing conservation law system and associated curvilinear-coordinate characteristic analysis are presented in Chapter 1. Chapter 2 then details formulation of the fundamental strong and weak integral statements, with well-posed boundary and initial conditions discussed in Chapter 3. The crucial issue of dissipative spatial semi-discretizations for hyperbolic systems is then considered in Chapter 4, where the essentially kinematic-kinetic curvilinear-coordinate flux vector splittings are developed. Whereupon, the finite element directionally biased semi-discrete integral statements and associated Lyapunov stability analysis are developed in Chapter 5, while the optimal metric data evaluations are formulated in Chapter 6. The terminal solution procedure is presented in Chapter 7 and the implicit non-linearly stable Runge-Kutta scheme is derived in Chapter 8. Chapter 9 then details the tensor matrix product factorization. To conclude, Chapter 10 presents thorough validations for a comprehensive set of benchmark problems in quasi 1-D, 2-D and axisymmetric geometries for transonic, supersonic and hypersonic flows.

Part I

The Continuum Statement

Chapter 1

Governing Equations

The non-linear Eulerian partial differential equation conservation law system governing unsteady and compressible aerodynamic viscous flows is,

$$L(q) = \frac{\partial q}{\partial t} + \nabla \cdot (\boldsymbol{f} - \boldsymbol{f}^{\nu}) = 0, \quad \text{on } \Re^{+} \times \Omega, \ \ \Omega \subset \Re^{n}, \ \ t \geq t_0 \qquad (1.1)$$

where $\Re^{+}$ denotes the positive real number field and n indicates the spatial dimensionality. Further, $q = q(\boldsymbol{x}, t)$ is the dependent state variable, $\boldsymbol{f} = \boldsymbol{f}(q)$ is the kinematic-kinetic flux vector and $\boldsymbol{f}^{\nu} = \boldsymbol{f}^{\nu}(q)$ contains the constitutive dissipation fluxes. In the sequel, a lower case letter denotes an array, capital letter denotes a square matrix and boldface signifies a vector.

1.1 Flux Vector Expressions

The cartesian-component Navier-Stokes equations are obtained for (1.1), using subscript i, j tensor indices, through the following specifications

$$q \equiv \left\{ \begin{array}{c} \rho \\ m_i \\ E \end{array} \right\} \; , \; \boldsymbol{f} \Rightarrow f_j = \left\{ \begin{array}{c} m_j \\ m_i m_j/\rho + p\delta_{ij} \\ (E+p)m_j/\rho \end{array} \right\} \; , \; \boldsymbol{f}^{\nu} \Rightarrow f_j^{\nu} = \left\{ \begin{array}{c} 0 \\ \sigma_{ij} \\ \sigma_{ij} m_i/\rho - q_j \end{array} \right\} \tag{1.2}$$

In expressions (1.2), ρ is the fluid density, $m_i = \rho u_i$ is the linear momentum vector resolution, E is the volume specific total energy, and p is the static pressure. Further, for a laminar flow the deviatoric stress tensor σ_{ij} and heat flux q_j definitions are

$$\sigma_{ij} = \mu(T) \left\{ \frac{\partial(m_i/\rho)}{\partial x_j} + \frac{\partial(m_j/\rho)}{\partial x_i} - \frac{2}{3} \frac{\partial(m_k/\rho)}{\partial x_k} \delta_{ij} \right\} \tag{1.3}$$

$$q_j = -k(T) \left\{ \frac{\partial T}{\partial x_j} \right\} \tag{1.4}$$

In (1.3), (1.4), T is the static temperature, while $\mu(T)$ and $k(T)$ are respectively the temperature-dependent dynamic viscosity and heat conductivity coefficients.

Definitions (1.1)-(1.4) model the unsteady laminar flow of any newtonian fluid satisfying the Stokes' hypothesis. A specific fluid is then mathematically identified using specific expressions for $\mu(T)$ and $k(T)$, along with an equation of state definition for the static pressure p and temperature T. For homogeneous air, the latter equations can be expressed as

$$p = p(\rho, \varepsilon) \quad , \quad T = T(\rho, \varepsilon) \tag{1.5}$$

where ε is the specific internal energy per unit mass with state variable q resolution

$$\varepsilon = \frac{E}{\rho} - \frac{m_i m_i}{2\rho^2} \tag{1.6}$$

Therefore, E corresponds to the sum of internal and kinetic energy, while p and T are function of q in the form

$$p = p(\rho, \varepsilon(\rho, m_i, E)) \tag{1.7}$$

$$T = T(\rho, \varepsilon(\rho, m_i, E)) \tag{1.8}$$

The theoretical developments in the following Sections are valid for any form of (1.7)-(1.8), hence universally apply for both reacting and ideal gas situations.

1.2 Equilibrium Real Gas Simulation

1.2.1 Chemical Equilibrium Equations

Real gas simulation is efficiently and accurately performed, in the equilibrium high-temperature regime, using a five species air model coupled with an equilibrium-constant equation solution as follows. The Dalton's law equation of state for a reacting gas is

$$p = R\rho T \sum_{i=1}^{5} \frac{Y_i}{M_i} \tag{1.9}$$

where R is the universal gas constant, M_i is the molecular mass of the i^{th} species, and Y_i is the associated mass fraction. In the sequel, $1 \leq i \leq 5$ corresponds to the species O, N, NO, O_2 and N_2 respectively.

The reacting gas energy expression in terms of the specific internal energy ε is

$$\varepsilon + RT\sum_{i=1}^{5}\frac{Y_i}{M_i} - \sum_{i=1}^{5}Y_i c_{pi}T - \sum_{i=3}^{5}Y_i\frac{R\theta_i^v/M_i}{\exp(\theta_i^v/T)-1} - \sum_{i=1}^{3}Y_i h_i^0 = 0 \qquad (1.10)$$

where $c_{pi} = 5/2(R/M_i)$, $i = 1,2$, and $c_{pi} = 7/2(R/M_i)$, $i = 3,4,5$. Further, h_i^0 is the formation enthalpy and θ_i^v is the characteristic vibrational temperature. In these conditions, the internal energy ε comprises the species formation chemical energy, the molecular translational and rotational kinetic energies, and the molecular vibrational potential energy with equilibrium magnitude characterized by the static temperature T. Expressions (1.9) and (1.10) clearly constitute special cases of (1.7) and (1.8).

If no chemical reactions occur, then the mass fractions Y_i are constant, and the last term in (1.10) vanishes. Further, if no vibrational modes are excited, the exponential term in (1.10) also vanishes. These constraints yield the ideal gas model which consists of a volumetric mixture of 21% of oxygen and 79% of nitrogen for atmospheric air. The state equations for this gas are obtained from (1.10) and (1.9) as

$$\varepsilon = c_v T \qquad (1.11)$$

$$p = \mathcal{R}\rho T = \frac{\mathcal{R}}{c_v}\rho\varepsilon = (\gamma - 1)\rho\varepsilon \qquad (1.12)$$

where $\mathcal{R}$ is the inert air constant

$$\mathcal{R} = R\sum_{i=4}^{5}\frac{Y_i}{M_i} \qquad (1.13)$$

Relations (1.12)-(1.13) imply Mayer's relation $c_p - c_v = \mathcal{R}$ and the (constant) specific-heat ratio $\gamma = c_p/c_v$. Whereupon, insertion of (1.6) into (1.11)-(1.12) yields

the state variable q resolution for p and T as

$$p = (\gamma - 1)\left(E - \frac{m_i m_i}{2\rho}\right) \tag{1.14}$$

$$T = \frac{(\gamma - 1)}{\mathcal{R}\rho}\left(E - \frac{m_i m_i}{2\rho}\right) \tag{1.15}$$

In the general case of a neutral reacting gas, the full expressions (1.9), (1.10) are used along with the fundamental independent dissociation and exchange reaction equations

$$\begin{aligned} O_2 + \mathcal{M} &\rightleftarrows 2O + \mathcal{M} \\ N_2 + \mathcal{M} &\rightleftarrows 2N + \mathcal{M} \\ N_2 + O_2 + \mathcal{M} &\rightleftarrows 2NO + \mathcal{M} \end{aligned} \tag{1.16}$$

where $\mathcal{M}$ denotes a species collision factor. The law of mass action for (1.16) yields

$$\frac{Y_2^2}{Y_5} = \frac{M_2^2 K_1(T)}{M_5 \rho} \quad , \quad \frac{Y_1^2}{Y_4} = \frac{M_1^2 K_2(T)}{M_4 \rho} \quad , \quad \frac{Y_3^2}{Y_4 Y_5} = \frac{M_3^2 K_3(T)}{M_4 M_5} \tag{1.17}$$

where $K_1(T)$, $K_2(T)$, and $K_3(T)$ are equilibrium relations available from latest spectroscopic data as well as atomic and molecular constant calculations [42,57]. Equations (1.17) supply three constraints on the five mass fractions Y_i. Consequently, two more equations must be formulated for closure. The first is global mass conservation,

$$\sum_{i=1}^{5} Y_i = 1 \quad , \quad \text{since} \quad Y_i \equiv \frac{\rho_i}{\rho} \quad , \quad \sum_{i=1}^{5} \rho_i = \rho \tag{1.18}$$

while the second expresses the uniformity of local proportion of oxygen nuclei rela-

tive to nitrogen nuclei for air, as

$$\left(\frac{Y_1}{M_1}+\frac{Y_3}{M_3}+2\frac{Y_4}{M_4}\right)/21=\left(\frac{Y_2}{M_2}+\frac{Y_3}{M_3}+2\frac{Y_5}{M_5}\right)/79 \tag{1.19}$$

In current analyses, for a given thermodynamic state (ρ,ε), the temperature T and composition mass fractions Y_i, $1\leq i\leq 5$ are determined through a simultaneous solution of the six equations (1.10), (1.17)-(1.19), with eventual multi-dimensional interpolation. As an innovation, and of efficiency impact, the same analytical solution of these equations is herein developed in terms of T and the nitric oxide mass fraction Y_3, using a far more convenient two-equation system, also amenable to analytical pressure derivative determination as follows. Equations (1.18) and (1.19) are linear and yield, for α_{ij} dependent only on the molecular masses

$$Y_1-(\alpha_{10}-Y_4+\alpha_{13}Y_3)=0\quad,\quad Y_2-(\alpha_{20}-Y_5+\alpha_{23}Y_3)=0 \tag{1.20}$$

Further, insertion of the second of (1.20) into the first of (1.17) yields a quadratic equation in Y_5 alone, with physical solution

$$Y_5=\left(\alpha_{20}+\alpha_{23}Y_3+\frac{M_2^2K_1(T)}{2\rho M_5}\right)-\left(\frac{M_2^2K_1(T)}{\rho M_5}\left(\alpha_{20}+\alpha_{23}Y_3+\frac{M_2^2K_1(T)}{4\rho M_5}\right)\right)^{1/2} \tag{1.21}$$

The analogous solution for Y_4 is

$$Y_4=\left(\alpha_{10}+\alpha_{13}Y_3+\frac{M_1^2K_2(T)}{2\rho M_4}\right)-\left(\frac{M_1^2K_2(T)}{\rho M_4}\left(\alpha_{10}+\alpha_{13}Y_3+\frac{M_1^2K_2(T)}{4\rho M_4}\right)\right)^{1/2} \tag{1.22}$$

whereupon, for any Y_3, Y_1 and Y_2 are determined via (1.20). Hence, for given Y_3 and T the mass fractions Y_i, i =1,2,4 and 5 are directly determined, yielding pressure

via (1.9).

Temperature T and nitric oxide mass fraction Y_3 are then determined as the solution of the two-equation system

$$\left\{ \begin{array}{rcl} f_1 & \equiv & Y_3 - M_3 \left(Y_4 Y_5 \dfrac{K_3(T)}{M_4 M_5} \right)^{1/2} = 0 \\ f_2 & \equiv & \varepsilon + RT \displaystyle\sum_{i=1}^{5} \frac{Y_i}{M_i} - \sum_{i=1}^{5} Y_i c_{pi} T - \sum_{i=1}^{3} Y_i h_i^0 - \sum_{i=3}^{5} Y_i \frac{R\theta_i^v / M_i}{\exp(\theta_i^v / T) - 1} = 0 \end{array} \right. \tag{1.23}$$

with Y_i, i =1,2,4 and 5 expressed via (1.20)-(1.22). For a given input state $q \equiv (\rho, m_i, E)$, hence given ρ and ε, and $Q \equiv \{Y_3, T\}^T$ this system is cast as

$$F(Q) \equiv F(Y_3, T) \equiv \left\{ \begin{array}{c} f_1(Y_3, T) \\ \\ f_2(Y_3, T) \end{array} \right\} = 0 \tag{1.24}$$

The Newton algorithm for (1.24) is

$$\delta Q^{s+1} = - \left[\left(\frac{\partial F}{\partial Q} \right)_{\rho, \varepsilon} \right]_s^{-1} \{F^s\} \tag{1.25}$$

with initial conditions $Q^j = Q^{j^-}$, where j^- denotes a location adjacent to a neighboring one where system (1.24) has already been solved.

The other key innovation is that iteration (1.25) is in closed-form, since the 2×2 jacobian inverse can be analytically established. Thus, evaluating (1.25) is relatively inexpensive, leads to a quadratically convergent process (two or three iterations, owing to the good initial estimates), and directly yields Y_3 and T, hence p via (1.20)-(1.22) and (1.9).

1.2.2 Pressure Partial Derivatives

An implicit CFD algorithm requires the accurate computation of the jacobians of pressure with respect to the state variable q. These are analytically established via the partial derivatives of Y_i, $1 \leq i \leq 5$, and T with respect to ρ and ε as follows. Considering that $Q = Q(\rho, \varepsilon)$, the differential of both sides of expression (1.24) yields

$$\left(\left(\frac{\partial F}{\partial Q}\right)_{\rho,\varepsilon}\left(\frac{\partial Q}{\partial \rho}\right)_{\varepsilon} + \left(\frac{\partial F}{\partial \rho}\right)_{Q,\varepsilon}\right) d\rho + \left(\left(\frac{\partial F}{\partial Q}\right)_{\rho,\varepsilon}\left(\frac{\partial Q}{\partial \varepsilon}\right)_{\rho} + \left(\frac{\partial F}{\partial \varepsilon}\right)_{Q,\rho}\right) d\varepsilon = 0 \tag{1.26}$$

This constitutes a linear combination on the linearly independent differentials $d\rho$ and $d\varepsilon$, which holds true if and only if their coefficients independently vanish, producing the two linear systems

$$\left(\frac{\partial Q}{\partial \rho}\right)_{\varepsilon} = -\left[\left(\frac{\partial F}{\partial Q}\right)_{\rho,\varepsilon}\right]^{-1}\left(\frac{\partial F}{\partial \rho}\right)_{Q,\varepsilon} \quad , \quad \left(\frac{\partial Q}{\partial \varepsilon}\right)_{\rho} = -\left[\left(\frac{\partial F}{\partial Q}\right)_{\rho,\varepsilon}\right]^{-1}\left(\frac{\partial F}{\partial \varepsilon}\right)_{Q,\rho} \tag{1.27}$$

The jacobian in (1.27) is invariant and coincides with that in (1.25). Therefore, (1.27) directly supply the required derivatives of Y_3 and T. The derivatives of Y_i, i =1,2,4 and 5, are then determined via these expressions and (1.20)-(1.22). Consequently, the thermodynamic pressure derivatives are analytically expressed as

$$\left(\frac{\partial p}{\partial \rho}\right)_{\varepsilon} = RT\sum_{i=1}^{5}\frac{Y_i}{M_i} + R\rho\left(\frac{\partial T}{\partial \rho}\right)_{\varepsilon}\sum_{i=1}^{5}\frac{Y_i}{M_i} + R\rho T\sum_{i=1}^{5}\frac{1}{M_i}\left(\frac{\partial Y_i}{\partial \rho}\right)_{\varepsilon} \tag{1.28}$$

$$\left(\frac{\partial p}{\partial \varepsilon}\right)_{\rho} = R\rho\left(\frac{\partial T}{\partial \varepsilon}\right)_{\rho}\sum_{i=1}^{5}\frac{Y_i}{M_i} + R\rho T\sum_{i=1}^{5}\frac{1}{M_i}\left(\frac{\partial Y_i}{\partial \varepsilon}\right)_{\rho} \tag{1.29}$$

Finally, the pressure derivatives with respect to the flow state variable q are computed as

$$p_\rho \equiv \left(\frac{\partial p}{\partial \rho}\right)_{m_i,E} = \left(\frac{\partial p}{\partial \rho}\right)_{\varepsilon} + \left(\frac{\partial p}{\partial \varepsilon}\right)_{\rho} \left(\frac{\partial \varepsilon}{\partial \rho}\right)_{m_i,E} \tag{1.30}$$

$$p_E \equiv \left(\frac{\partial p}{\partial E}\right)_{\rho,m_i} = \left(\frac{\partial p}{\partial \varepsilon}\right)_{\rho} \left(\frac{\partial \varepsilon}{\partial E}\right)_{\rho,m_i} \; ; \; p_{m_i} \equiv \left(\frac{\partial p}{\partial m_i}\right)_{\rho,m_j,E} = \left(\frac{\partial p}{\partial \varepsilon}\right)_{\rho} \left(\frac{\partial \varepsilon}{\partial m_i}\right)_{\rho,m_j,E} \tag{1.31}$$

Therefore, (1.20)-(1.22), (1.25) and (1.27)-(1.31) can be implemented for accurate computation of equilibrium real gas pressure and pressure derivatives.

1.3 Dimensional Analysis

For aerodynamic simulations, the typical reference state for the non- dimensionalization of $q(\boldsymbol{x},t)$ and the flux vectors $\boldsymbol{f}(q)$ and $\boldsymbol{f}^{\nu}(q)$ is the inlet state, with density ρ_∞ and principal velocity component U_∞, as well as a convenient length measure L. Time is scaled by L/U_∞ whereas static pressure and total specific energy E are scaled by the reference dynamic pressure $\rho_\infty U_\infty^2$. The reference temperatute T_{ref} is then obtained using the ideal gas state equation as

$$T_{ref} = \frac{p_{ref}}{\mathcal{R}\rho_{ref}} = \frac{U_\infty^2}{\mathcal{R}} = \gamma\left(\frac{U_\infty^2}{\gamma\mathcal{R}T_\infty}\right)T_\infty = \gamma M_\infty^2 T_\infty \tag{1.32}$$

Here M_∞ denotes the (freestream) reference Mach number associated with U_∞ and T_∞. Using these reference values, the non-dimensional inlet variables are expressed as

$$\frac{\rho_\infty}{\rho_{ref}} = 1 \quad , \quad \frac{U_\infty}{U_{ref}} = 1 \tag{1.33}$$

$$\frac{p_\infty}{p_{ref}} = \frac{1}{\gamma M_\infty^2} \quad , \quad \frac{T_\infty}{T_{ref}} = \frac{1}{\gamma M_\infty^2} \tag{1.34}$$

$$\frac{E_\infty}{p_{ref}} = \frac{p_\infty}{(\gamma-1)\rho_\infty U_\infty^2} + \frac{1}{2} = \frac{1}{\gamma(\gamma-1)M_\infty^2} + \frac{1}{2} \tag{1.35}$$

With this non-dimensionalization, the state variable q and flux vector $f_j(q)$ remain invariant, hence the reference Mach number M_∞ does not explicitly appear as a multiplier in the convection terms in (1.1). However, its influence on the flow field is reflected in the magnitude of the inlet static pressure, temperature and total volume specific energy via (1.34),(1.35). These relations indicate that for growing M_∞, the non-dimensional values of the inlet pressure, temperature, and volume specific energy approach the limits 0.0 and 0.5 respectively, which express the Mach number invariance principle for hypersonic flows [22].

Finally, the non-dimensional deviatoric stress tensor and heat flux vector are expressed as

$$\sigma_{ij} = \frac{\mu^*(T)}{Re}\left\{\frac{\partial(m_i/\rho)}{\partial x_j} + \frac{\partial(m_j/\rho)}{\partial x_i} - \frac{2}{3}\frac{\partial(m_k/\rho)}{\partial x_k}\delta_{ij}\right\} \tag{1.36}$$

$$q_j = -\frac{\gamma k^*(T)}{(\gamma-1)Re\ Pr}\left\{\frac{\partial T}{\partial x_j}\right\} \tag{1.37}$$

In these relations, Re and Pr denote the Reynolds and Prandtl numbers respectively defined as

$$Re \equiv \frac{\rho_\infty U_\infty L}{\mu_\infty} \quad , \quad Pr \equiv \frac{c_p \mu_\infty}{k_\infty} \tag{1.38}$$

where c_p is the specific heat at constant pressure while μ_∞ and k_∞ denote the freestream dynamic viscosity and heat conductivity, respectively, evaluated at T_∞.

1.4 Transport Coefficients

The non-dimensional transport coefficients k^* and μ^* in (1.36) and (1.37) are defined as

$$\mu^*(T) \equiv \frac{\mu(T)}{\mu_\infty} \quad , \quad k^*(T) \equiv \frac{k(T)}{k_\infty} \tag{1.39}$$

These ratios are derived from the Sutherland formulae [11]

$$\left(\frac{\mu}{\mu_0}\right) = \left(\frac{T}{T_0}\right)^{3/2} \left(\frac{1+\omega_0}{T/T_0+\omega_0}\right) \tag{1.40}$$

$$\left(\frac{k}{k_0}\right) = \left(\frac{T}{T_0}\right)^{3/2} \left(\frac{1+\phi_0}{T/T_0+\phi_0}\right) \tag{1.41}$$

Here, $T_0 = 273.1K^o$ is the Sutherland reference temperature and the constants are

$$\omega_0 = 0.404800651\ldots \tag{1.42}$$

$$\phi_0 = 0.711960944\ldots \tag{1.43}$$

Thus, k^* and μ^* are computed using

$$\left(\frac{k}{k_\infty}\right) = \left(\frac{k}{k_0}\right)\left(\frac{k_\infty}{k_0}\right)^{-1} \quad , \quad \left(\frac{\mu}{\mu_\infty}\right) = \left(\frac{\mu}{\mu_0}\right)\left(\frac{\mu_\infty}{\mu_0}\right)^{-1} \tag{1.44}$$

which yields

$$\left(\frac{\mu}{\mu_\infty}\right) = \left(\frac{T}{T_\infty}\right)^{3/2} \left(\frac{1+\frac{\omega_0}{T_\infty/T_0}}{T/T_\infty+\frac{\omega_0}{T_\infty/T_0}}\right) \tag{1.45}$$

$$\left(\frac{k}{k_\infty}\right) = \left(\frac{T}{T_\infty}\right)^{3/2} \left(\frac{1+\frac{\phi_0}{T_\infty/T_0}}{T/T_\infty+\frac{\phi_0}{T_\infty/T_0}}\right) \tag{1.46}$$

However, the non-dimensional temperature variable is T/T_{ref}, hence

$$\left(\frac{T}{T_\infty}\right) = \left(\frac{T}{T_{ref}}\right)\left(\frac{T_{ref}}{T_\infty}\right) = \gamma M_\infty^2 \left(\frac{T}{T_{ref}}\right) \tag{1.47}$$

Insertion of (1.47) into (1.45)-(1.46) yields the terminal generalized Sutherland formulae

$$\left(\frac{\mu}{\mu_\infty}\right) = \left(\gamma M_\infty^2\right)^{3/2}\left(\frac{T}{T_{ref}}\right)^{3/2}\left(\frac{1/(\gamma M_\infty^2)+\omega}{T/T_{ref}+\omega}\right) \tag{1.48}$$

$$\left(\frac{k}{k_\infty}\right) = \left(\gamma M_\infty^2\right)^{3/2}\left(\frac{T}{T_{ref}}\right)^{3/2}\left(\frac{1/(\gamma M_\infty^2)+\phi}{T/T_{ref}+\phi}\right) \tag{1.49}$$

where ω and ϕ are now defined as

$$\omega = \frac{\omega_0}{\gamma M_\infty^2 T_\infty/T_0} \quad , \quad \phi = \frac{\phi_0}{\gamma M_\infty^2 T_\infty/T_0} \tag{1.50}$$

In the sequel, (1.48) and (1.49) are denoted as g_μ and g_θ. Further, the term $\frac{\gamma}{Re\,Pr\,(\gamma-1)}$ in (1.37) is replaced by $(Pe)^{-1}$, the inverse generalized Peclet number.

1.5 Curvilinear Coordinate Formulation

1.5.1 Coordinate Transformation

Among several advantages, useful simplifications in surface definition, and boundary condition enforcement accrue from a curvilinear coordinate formulation of the governing equations. For example, an aerodynamic surface, say a fuselage, can be uniquely defined by the expression $\eta_3 = \text{const}$, with η_3 denoting the curvilinear coordinate issuing from the surface. Likewise, the no-penetration flow boundary

condition can be stated as $v_3 = 0$, where v_3 denotes the contravariant component of velocity along the normal direction to the $\eta_3 = \text{const}$ surface, see Section 1.5.3.

The cartesian coordinates $\boldsymbol{x}$ are transformed into curvilinear coordinates $\boldsymbol{\eta}$ via the relation

$$\boldsymbol{x} = \boldsymbol{x}(\boldsymbol{\eta}) \tag{1.51}$$

Function (1.51) is assumed to be single valued and have continuous first partial derivatives. The jacobian J of the coordinate transformation (1.51) is expressed as

$$J \equiv \left[\frac{\partial \boldsymbol{x}}{\partial \boldsymbol{\eta}}\right] = \left[\frac{\partial x_j}{\partial \eta_i}\right] \tag{1.52}$$

The relation between the x_i and η_j partial derivatives is then

$$\left\{\frac{\partial}{\partial \eta_i}\right\} = \left[\frac{\partial x_j}{\partial \eta_i}\right]\left\{\frac{\partial}{\partial x_j}\right\} = J\left\{\frac{\partial}{\partial x_j}\right\} \tag{1.53}$$

Therefore, the partial derivatives with respect to the cartesian coordinates x_j are expressed using the inverse of (1.53) as

$$\left\{\frac{\partial}{\partial x_j}\right\} = J^{-1}\left\{\frac{\partial}{\partial \eta_k}\right\} = \frac{1}{\det J}\left[\det J \cdot J^{-1}\right]\left\{\frac{\partial}{\partial \eta_k}\right\} \tag{1.54}$$

where $\det J$ does not vanish and keeps a uniform sign in Ω. With these specifications, the entries of the matrix $\det J \cdot J^{-1}$ are denoted as $[e_{jk}]$. In the general 3-D case, the expressions for $\det J$ and $[e_{jk}]$ are

$$\begin{aligned} \det J \;=\; & \frac{\partial x_1}{\partial \eta_1}\frac{\partial x_2}{\partial \eta_2}\frac{\partial x_3}{\partial \eta_3} + \frac{\partial x_2}{\partial \eta_1}\frac{\partial x_3}{\partial \eta_2}\frac{\partial x_1}{\partial \eta_3} + \\ & \frac{\partial x_3}{\partial \eta_1}\frac{\partial x_1}{\partial \eta_2}\frac{\partial x_2}{\partial \eta_3} - \frac{\partial x_1}{\partial \eta_3}\frac{\partial x_2}{\partial \eta_2}\frac{\partial x_3}{\partial \eta_1} - \\ & \frac{\partial x_2}{\partial \eta_3}\frac{\partial x_3}{\partial \eta_2}\frac{\partial x_1}{\partial \eta_1} - \frac{\partial x_3}{\partial \eta_3}\frac{\partial x_1}{\partial \eta_2}\frac{\partial x_2}{\partial \eta_1} \end{aligned} \tag{1.55}$$

$$
\begin{aligned}
e_{11} &= \frac{\partial x_2}{\partial \eta_2}\frac{\partial x_3}{\partial \eta_3} - \frac{\partial x_2}{\partial \eta_3}\frac{\partial x_3}{\partial \eta_2} \\
e_{12} &= \frac{\partial x_2}{\partial \eta_3}\frac{\partial x_3}{\partial \eta_1} - \frac{\partial x_2}{\partial \eta_1}\frac{\partial x_3}{\partial \eta_3} \\
e_{13} &= \frac{\partial x_2}{\partial \eta_1}\frac{\partial x_3}{\partial \eta_2} - \frac{\partial x_2}{\partial \eta_2}\frac{\partial x_3}{\partial \eta_1}
\end{aligned} \tag{1.56}
$$

$$
\begin{aligned}
e_{21} &= \frac{\partial x_1}{\partial \eta_3}\frac{\partial x_3}{\partial \eta_2} - \frac{\partial x_1}{\partial \eta_2}\frac{\partial x_3}{\partial \eta_3} \\
e_{22} &= \frac{\partial x_1}{\partial \eta_1}\frac{\partial x_3}{\partial \eta_3} - \frac{\partial x_1}{\partial \eta_3}\frac{\partial x_3}{\partial \eta_1} \\
e_{23} &= \frac{\partial x_1}{\partial \eta_2}\frac{\partial x_3}{\partial \eta_1} - \frac{\partial x_1}{\partial \eta_1}\frac{\partial x_3}{\partial \eta_2}
\end{aligned} \tag{1.57}
$$

$$
\begin{aligned}
e_{31} &= \frac{\partial x_1}{\partial \eta_2}\frac{\partial x_2}{\partial \eta_3} - \frac{\partial x_1}{\partial \eta_3}\frac{\partial x_2}{\partial \eta_2} \\
e_{32} &= \frac{\partial x_1}{\partial \eta_3}\frac{\partial x_2}{\partial \eta_1} - \frac{\partial x_1}{\partial \eta_1}\frac{\partial x_2}{\partial \eta_3} \\
e_{33} &= \frac{\partial x_1}{\partial \eta_1}\frac{\partial x_2}{\partial \eta_2} - \frac{\partial x_1}{\partial \eta_2}\frac{\partial x_2}{\partial \eta_1}
\end{aligned} \tag{1.58}
$$

In 2-D, these expressions simplify to

$$
\det J = \frac{\partial x_1}{\partial \eta_1}\frac{\partial x_2}{\partial \eta_2} - \frac{\partial x_2}{\partial \eta_1}\frac{\partial x_1}{\partial \eta_2} \tag{1.59}
$$

$$
e_{11} = +\frac{\partial x_2}{\partial \eta_2} \quad ; \quad e_{12} = -\frac{\partial x_2}{\partial \eta_1} \tag{1.60}
$$

$$
e_{21} = -\frac{\partial x_1}{\partial \eta_2} \quad ; \quad e_{22} = +\frac{\partial x_1}{\partial \eta_1} \tag{1.61}
$$

These functional forms for the metric data e_{jk}, with continuous partial derivatives in their definition domain, lead to the fundamental invariance relation

$$
\sum_{k=1}^{n} \frac{\partial e_{jk}}{\partial \eta_k} = 0 \quad , \quad \forall \; j \tag{1.62}
$$

in both 2-D and 3-D. Furthermore, for each k, the metric data e_{jk} constitute the components of a vector $\boldsymbol{n}_k$ orthogonal to the surface $\eta_k = \text{const.}$ as follows

$$\begin{aligned} \boldsymbol{n}_1 &= \frac{\partial x_j}{\partial \eta_2}\boldsymbol{e}_j \times \frac{\partial x_j}{\partial \eta_3}\boldsymbol{e}_j \\ \boldsymbol{n}_2 &= \frac{\partial x_j}{\partial \eta_3}\boldsymbol{e}_j \times \frac{\partial x_j}{\partial \eta_1}\boldsymbol{e}_j \\ \boldsymbol{n}_3 &= \frac{\partial x_j}{\partial \eta_1}\boldsymbol{e}_j \times \frac{\partial x_j}{\partial \eta_2}\boldsymbol{e}_j \end{aligned} \tag{1.63}$$

where $\times$ denotes the vector cross product, and $\boldsymbol{e}_j$ corresponds to the cartesian unit vector set. In the expression defining $\boldsymbol{n}_1$, for example, the two vectors $\frac{\partial x_j}{\partial \eta_2}\boldsymbol{e}_j$ and $\frac{\partial x_j}{\partial \eta_3}\boldsymbol{e}_j$ are tangent to the η_2 and η_3 axes respectively, at (η_1, η_2, η_3). Thus, $\boldsymbol{n}_1$ is locally orthogonal to the $\eta_2 - \eta_3$ facet. The components of $\boldsymbol{n}_1$ are determined from its definition with the classical determinant rule as

$$\begin{aligned} (n_1)_1 &= \frac{\partial x_2}{\partial \eta_2}\frac{\partial x_3}{\partial \eta_3} - \frac{\partial x_2}{\partial \eta_3}\frac{\partial x_3}{\partial \eta_2} \\ (n_1)_2 &= \frac{\partial x_1}{\partial \eta_3}\frac{\partial x_3}{\partial \eta_2} - \frac{\partial x_1}{\partial \eta_2}\frac{\partial x_3}{\partial \eta_3} \\ (n_1)_3 &= \frac{\partial x_1}{\partial \eta_2}\frac{\partial x_2}{\partial \eta_3} - \frac{\partial x_1}{\partial \eta_3}\frac{\partial x_2}{\partial \eta_2} \end{aligned} \tag{1.64}$$

which coincide with e_{j1}, $1 \leq j \leq 3$. Analogous derivations then verify that the components of $\boldsymbol{n}_k$ are indeed e_{jk}, $1 \leq j \leq 3$, $2 \leq k \leq 3$. In 2-D, similar conclusions regarding the geometric meaning of e_{jk}, $1 \leq j, k \leq 2$, are obtained setting $x_3 = \eta_3$, and $x_k = x_k(\eta_1, \eta_2)$, $1 \leq k \leq 2$.

Whereupon, this fundamental metric data e_{jk} meaning leads to a significant interpretation for the contravariant components of velocity resolution, as detailed in Section 1.5.3.

1.5.2 Curvilinear-Coordinate Equations

The non-dimensional Navier-Stokes equations (1.1) under the generalized curvilinear coordinate transformation (1.51)-(1.54) and in tensor notation are

$$\frac{\partial q}{\partial t} + \frac{e_{jk}}{\det J}\frac{\partial}{\partial \eta_k}\left(f_j - f_j^{\nu}\right) = 0 \tag{1.65}$$

The non-dimensional deviatoric stress tensor σ_{ij} and heat flux vector q_j are analogously transformed to

$$\sigma_{ij} = \frac{g_\mu}{Re}\left[\frac{e_{jr}}{\det J}\frac{\partial(m_i/\rho)}{\partial \eta_r} + \frac{e_{i\ell}}{\det J}\frac{\partial(m_j/\rho)}{\partial \eta_\ell} - \frac{2}{3}\frac{e_{kp}}{\det J}\frac{\partial(m_k/\rho)}{\partial \eta_p}\delta_{ij}\right] \tag{1.66}$$

$$q_j = \frac{g_\theta}{Pe}\left[\frac{e_{j\ell}}{\det J}\frac{\partial T}{\partial \eta_\ell}\right] \tag{1.67}$$

For a time-independent coordinate transformation, $\det J$ does not depend upon time hence can be brought inside the time derivative, yielding

$$\frac{\partial}{\partial t}(q \cdot \det J) + e_{jk}\frac{\partial}{\partial \eta_k}\left(f_j - f_j^{\nu}\right) = 0 \tag{1.68}$$

Equation (1.68) constitutes the so-called "*weak conservation law form*"[44], since the metric data stand outside the differential operators. Conversely, the "*strong form*" [44] is obtained by bringing these data inside the spatial partial derivative operator. Invoking the fundamental metric invariance identity (1.62), the equivalent final form is

$$\frac{\partial}{\partial t}(q \cdot \det J) + \frac{\partial}{\partial \eta_k}\left(e_{jk}\left(f_j - f_j^{\nu}\right)\right) = 0 \tag{1.69}$$

For definitiveness, system (1.69), by components of q defines

$$\frac{\partial}{\partial t}(\rho \cdot \det J) + \frac{\partial}{\partial \eta_k}(e_{jk} m_j) = 0 \tag{1.70}$$

as the continuity equation,

$$\frac{\partial}{\partial t}(m_i \cdot \det J) + \frac{\partial}{\partial \eta_k}\left(e_{jk}\frac{m_j}{\rho}m_i + e_{jk}p\delta_{ij}\right)$$
$$-\frac{1}{Re}\frac{\partial}{\partial \eta_k}\left(e_{jk}g_\mu\left(\frac{e_{jr}}{\det J}\frac{\partial(m_i/\rho)}{\partial \eta_r} + \frac{e_{i\ell}}{\det J}\frac{\partial(m_j/\rho)}{\partial \eta_\ell} - \frac{2}{3}\frac{e_{ks}}{\det J}\frac{\partial(m_k/\rho)}{\partial \eta_s}\delta_{ij}\right)\right) = 0 \tag{1.71}$$

as the momentum equation set, $1 \leq i \leq n$, and

$$\frac{\partial}{\partial t}(E \cdot \det J) + \frac{\partial}{\partial \eta_k}\left(e_{jk}\frac{m_j}{\rho}(E+p)\right) - \frac{1}{Pe}\frac{\partial}{\partial \eta_k}\left(e_{jk}g_\theta\frac{e_{j\ell}}{\det J}\frac{\partial T}{\partial \eta_\ell}\right)$$
$$-\frac{1}{Re}\frac{\partial}{\partial \eta_k}\left(e_{jk}g_\mu\frac{m_i}{\rho}\left(\frac{e_{jr}}{\det J}\frac{\partial(m_i/\rho)}{\partial \eta_r} + \frac{e_{i\ell}}{\det J}\frac{\partial(m_j/\rho)}{\partial \eta_\ell} - \frac{2}{3}\frac{e_{ks}}{\det J}\frac{\partial(m_k/\rho)}{\partial \eta_s}\delta_{ij}\right)\right) = 0 \tag{1.72}$$

as the energy equation.

In (1.70)-(1.72), the partial derivative expression

$$\frac{\partial K_k}{\partial \eta_k} = \frac{\partial}{\partial \eta_k}\left(e_{jk}\frac{m_j}{\rho}\cdot\tilde{q}\right) \tag{1.73}$$

for the intrinsically kinematic flux K_k

$$K_k \equiv e_{jk}\frac{m_j}{\rho}\cdot\tilde{q} = e_{jk}\frac{m_j}{\rho}\left\{\begin{array}{c}\rho\\ m_i\\ E+p\end{array}\right\} \tag{1.74}$$

corresponds to a fundamental streamline-differentiation expression for the flux $\|\boldsymbol{V}\|\cdot\tilde{q}$ as follows. The η_k partial derivatives in (1.74) can be restated as

$$\left\{\frac{\partial}{\partial \eta_k}\right\} = \frac{\overline{e}_{kj}}{\det \overline{J}}\left\{\frac{\partial}{\partial \xi_j}\right\} \tag{1.75}$$

$$\overline{e}_{kj} = \det \overline{J}\cdot\left\{\frac{\partial \eta_k}{\partial \xi_j}\right\}^{-1} \tag{1.76}$$

using the analysis of Section 1.5.1. The coordinates ξ_j, $1 \leq j \leq n$, define the streamline coordinate system, with ξ_1 axis parallel to the positive velocity direction and ξ_k, $2 \leq k \leq n$, mutually orthogonal to ξ_1. Therefore, relations (1.75)-(1.76) correspond to the unique coordinate transformation that maps the $\boldsymbol{\eta}$ system into the $\boldsymbol{\xi}$ system, and allows restatement of the k^{th} contravariant velocity component as

$$e_{jk}\frac{m_j}{\rho} = \|\boldsymbol{V}\| \cdot \frac{\partial \eta_k}{\partial \xi_j}\delta_j^1 \tag{1.77}$$

for $\boldsymbol{V}$ lying along ξ_1. Such a transformation exists and is unique since the n velocity components and n coordinate directions yield exactly $n + (n-1)n = n^2$ linearly independent constraints for the determination of the n^2 elements in $\overline{J}$.

Inserting (1.75)-(1.77) into (1.73) yields

$$\begin{aligned}
\frac{\partial}{\partial \eta_k}\left(e_{jk}\frac{m_j}{\rho}\cdot\tilde{q}\right) &= \frac{1}{\det \overline{J}}\frac{\partial}{\partial \xi_\ell}\left(\delta_j^1\frac{\partial \eta_k}{\partial \xi_j}\overline{e}_{\ell k}\|\boldsymbol{V}\|\cdot\tilde{q}\right) \\
&= \frac{1}{\det \overline{J}}\frac{\partial}{\partial \xi_\ell}\left(\det \overline{J}\delta_j^1\delta_j^\ell\|\boldsymbol{V}\|\cdot\tilde{q}\right) \\
&= \frac{\partial}{\partial \xi_1}\left(\|\boldsymbol{V}\|\cdot\tilde{q}\right) + \|\boldsymbol{V}\|\cdot\tilde{q}\left(\frac{1}{\det \overline{J}}\frac{\partial(\det \overline{J})}{\partial \xi_1}\right)
\end{aligned} \tag{1.78}$$

Consequently, (1.73) in the governing equations (1.70)-(1.72) expresses the streamline differentiation of $\|\boldsymbol{V}\| \cdot \tilde{q}$, augmented with a measure of the deviation between the $\boldsymbol{\eta}$ and $\boldsymbol{\xi}$ systems. Evidently, those coordinate systems with vanishing streamline-system deviation measure are particularly interesting.

1.5.3 Contravariant Velocity Components

In (1.70)-(1.72), the momentum vector resolution and deviatoric stress tensor remain cartesian, even though the governing equations are cast in generalized curvilinear coordinates. Consequently, the relation

$$v_k = e_{jk}\left(\frac{m_j}{\rho}\right) \tag{1.79}$$

pervades these equations, and constitutes the contravariant velocity component resolution. For each value of k, expression (1.79) coincides with the vector dot product of $\boldsymbol{n}_k$ and velocity $\boldsymbol{V}$

$$\boldsymbol{n}_k \cdot \boldsymbol{V} = e_{jk}\left(\frac{m_j}{\rho}\right) \tag{1.80}$$

owing to the expressions (1.63) for $\boldsymbol{n}_k$. Consequently, the k^{th} contravariant component (1.79) is proportional to the component of velocity $\boldsymbol{V}$ in the direction orthogonal to the surface $\eta_k = \text{const}$. With this fundamental interpretation, the efficient enforcement of the no-through flow boundary condition along the $\eta_k = \text{const}$. surface is then obtained setting $v_k = 0$.

1.6 Mathematical Character

1.6.1 Canonical Form

The governing equations (1.70)-(1.72) constitute a second order partial differential equation system, owing to the presence of the second order physical-diffusion spatial

partial derivatives with coefficients Re^{-1} and Pe^{-1}. Consequently, as the Reynolds number increases, the governing system (1.69) tends to the limit first order Euler conservation law system

$$\frac{\partial q}{\partial t} + \frac{1}{\det J}\frac{\partial}{\partial \eta_k}(e_{jk} f_j) = 0 \tag{1.81}$$

which is cast in the canonical form

$$\frac{\partial q}{\partial t} + \frac{1}{\det J}\left(\frac{\partial (e_{jk} f_j)}{\partial q}\right)\frac{\partial q}{\partial \eta_k} = 0 \tag{1.82}$$

since the flux vector $f_j = f_j(q)$ is a function of q. The corresponding flux vector jacobian matrix $A_k \equiv \dfrac{\partial (e_{jk} f_j)}{\partial q}$ is $A_k =$

$$\begin{pmatrix} 0 & , & e_{\ell k} & , & 0 \\ -e_{jk}\dfrac{m_j}{\rho^2} m_i + e_{ik} p_\rho & , & e_{\ell k}\dfrac{m_i}{\rho} + e_{ik} p_{m_\ell} + e_{jk}\dfrac{m_j}{\rho}\delta_{i\ell} & , & e_{ik} p_E \\ -e_{jk}\dfrac{m_j}{\rho^2}(E+p) + e_{jk}\dfrac{m_j}{\rho} p_\rho & , & \dfrac{e_{\ell k}}{\rho}(E+p) + e_{jk}\dfrac{m_j}{\rho} p_{m_\ell} & , & e_{jk}\dfrac{m_j}{\rho}(1+p_E) \end{pmatrix} \tag{1.83}$$

Here, $1 \le (i, \ell) \le n$ are the row and column indices, for the n-dimensional resolution of momentum, whereas the subscript notations p_ρ, p_{m_j}, and p_E are defined via (1.30)-(1.31).

Thus the mathematical character of (1.82) depends upon the real or complex nature of the eigenvalues of the matrix [21]

$$A_\omega \equiv \sum_{k=1}^{n} \omega_k \frac{\partial (e_{jk} f_j)}{\partial q} \quad ; \quad \sum_{k=1}^{n} \omega_k = 1 \quad ; \quad \forall \ \omega_k \in \Re^1 \tag{1.84}$$

Due to the linear structure of A_k with respect to the metric data $e_{\ell k}$, $\forall \quad \ell, k$, the terminal form of A_ω coincides with that of A_k upon substitution of $e_{\ell k}$ with

$e_{\ell\omega} \equiv \omega_k e_{\ell k}$, $\forall\ \ell$. Therefore, the eigenvalues of A_ω are real (or complex) if and only if the eigenvalues of A_k are real (or complex).

1.6.2 Characteristic Eigenvalue Analysis

The eigenvalues of A_k are the solutions of the characteristic equation

$$\det\left(\frac{\partial(e_{jk}f_j(q))}{\partial q} - \lambda_k I\right) = 0 \tag{1.85}$$

which corresponds to a real-coefficient algebraic equation of degree $m = n+2$, with exactly m roots. This characteristic equation can be expressed as

$$\lambda_k^m - \kappa_{1_{\underline{k}}}\lambda_k^{m-1} + \kappa_{2_{\underline{k}}}\lambda_k^{m-2} + \ldots + (-1)^m \kappa_{m_{\underline{k}}} = 0 \tag{1.86}$$

with coefficients κ_i expressed in terms of the trace s_i of the i^{th} power $(A_k)^i$ of A_k through the Newton formulae [21]

$$\begin{aligned}
\kappa_1 &= +s_1 \\
\kappa_2 &= -\frac{1}{2}(s_2 - \kappa_1 s_1) \\
\kappa_3 &= +\frac{1}{3}(s_3 - \kappa_1 s_2 + \kappa_2 s_1) \\
&\cdot \\
&\cdot \\
\kappa_m &= +\frac{(-1)^{m-1}}{m}\left(s_m - \kappa_1 s_{m-1} + \kappa_2 s_{m-2} \ldots + (-1)^{m-1}\kappa_{m-1} s_1\right)
\end{aligned} \tag{1.87}$$

Significantly, these formulae eliminate the formidable algebraic task of developing the determinant in (1.85). In 2-D, the coefficients κ_{i_k} are developed as

$$\begin{aligned}
\kappa_{1_k} &= 4e_{jk}\frac{m_j}{\rho} + e_{jk}p_{m_j} + e_{jk}\frac{m_j}{\rho}p_E \\
\kappa_{2_k} &= 3\left(e_{jk}\frac{m_j}{\rho}\right)^2 + 3e_{jk}\frac{m_j}{\rho}\left(e_{jk}\frac{m_j}{\rho}(1+p_E) + e_{jk}p_{m_j}\right) \\
&\quad -e_{j\underline{k}}e_{j\underline{k}}\left(\frac{m_j}{\rho}p_{m_j} + p_\rho + \frac{p_E}{\rho}(E+p)\right) \\
\kappa_{3_k} &= 2\kappa_{2_k}\left(e_{jk}\frac{m_j}{\rho}\right) - 3\kappa_{1_k}\left(e_{jk}\frac{m_j}{\rho}\right)^2 + 4\left(e_{jk}\frac{m_j}{\rho}\right)^3 \\
\kappa_{4_k} &= \kappa_{3_k}\left(e_{jk}\frac{m_j}{\rho}\right) - \kappa_{2_k}\left(e_{jk}\frac{m_j}{\rho}\right)^2 + \kappa_{1_k}\left(e_{jk}\frac{m_j}{\rho}\right)^3 - \left(e_{jk}\frac{m_j}{\rho}\right)^4
\end{aligned} \tag{1.88}$$

Correspondingly, the roots of (1.86), hence the eigenvalues of A_k are determined as

$$\left\{\begin{aligned}
\lambda_{k_{1,2}} &= e_{jk}\frac{m_j}{\rho} \\
\lambda_{k_{3,4}} &= e_{jk}\frac{m_j}{\rho} + \frac{1}{2}\left(e_{jk}p_{m_j} + e_{jk}\frac{m_j}{\rho}p_E\right) \\
&= \pm\left(\frac{1}{4}\left(e_{jk}p_{m_j} + e_{jk}\frac{m_j}{\rho}p_E\right)^2 + e_{j\underline{k}}e_{j\underline{k}}\left(\frac{m_j}{\rho}p_{m_j}p_\rho + \frac{p_E}{\rho}(E+p)\right)\right)^{1/2}
\end{aligned}\right. \tag{1.89}$$

For a homogeneous gas, the argument of the square root is always positive, as proven in the following section. Therefore, for any integer value of k, hence any value of the coordinate transformation metric data $e_{\ell k}$, the eigenvalues $\lambda_{k_{1,4}}$ are always real. Further, A_k has a complete set of eigenvectors, since this property is classically verified for $e_{jk} = \delta_{jk}$ [21]. Consequently, the real gas Euler conservation law system (1.82) is a hyperbolic system which, as such, models wave propagation phenomena. According to the eigenvalues (1.89), the flow field waves are convection waves, with characteristic speed $v_{k_{1,2}} = \dfrac{\lambda_{k_{1,2}}}{\sqrt{e_{j\underline{k}}e_{j\underline{k}}}}$, and a combination of convection and pressure

waves with characteristic speed $v_{k_{3,4}} = \dfrac{\lambda_{k_{3,4}}}{\sqrt{e_{jk}e_{j\underline{k}}}}$. For an aerodynamic large but finite Reynolds number, the governing Navier-Stokes equation system (1.1), (1.69), thus constitutes a parabolic perturbation to the Euler hyperbolic system.

1.6.3 Homogeneous Gas Eigenvalues

The eigenvalues (1.89) are determined for totally arbitrary state equations, even more general than (1.6)-(1.7), since the fundamental pressure partial derivatives $\dfrac{\partial p}{\partial q}$ are not replaced by any specialized relation. For a homogeneous gas, relations (1.6)-(1.7) lead to a considerable simplification of $\lambda_{k_{3,4}}$, by allowing the restatement of the partial derivatives of pressure with respect to the components of q in terms of q, $\left(\dfrac{\partial p}{\partial \rho}\right)_{\varepsilon}$, and $\left(\dfrac{\partial p}{\partial \varepsilon}\right)_{\rho}$ alone, as follows

$$e_{jk}p_{m_j} = e_{jk}\left(\frac{\partial p}{\partial \varepsilon}\right)_{\rho}\left(\frac{\partial \varepsilon}{\partial m_j}\right)_{\rho,E} = -\left(\frac{\partial p}{\partial \varepsilon}\right)_{\rho} e_{jk}\frac{m_j}{\rho^2} \tag{1.90}$$

$$e_{jk}\frac{m_j}{\rho}p_E = e_{jk}\frac{m_j}{\rho}\left(\frac{\partial p}{\partial \varepsilon}\right)_{\rho}\left(\frac{\partial \varepsilon}{\partial \rho}\right)_{m_i,E} = +\left(\frac{\partial p}{\partial \varepsilon}\right)_{\rho} e_{jk}\frac{m_j}{\rho^2} \tag{1.91}$$

Therefore, $\lambda_{k_{3,4}}$ simplify to

$$\lambda_{k_{3,4}} = e_{jk}\frac{m_j}{\rho} \pm \left(e_{j\underline{k}}e_{j\underline{k}}\left(\frac{m_j}{\rho}p_{m_j} + p_\rho + \frac{p_E}{\rho}(E+p)\right)\right)^{1/2} \tag{1.92}$$

For a uniform cartesian coordinate system, this expression reduces to

$$\lambda_{k_{3,4}} = \frac{m_k}{\rho} \pm \left(\frac{m_j}{\rho}p_{m_j} + p_\rho + \frac{p_E}{\rho}(E+p)\right)^{1/2} \tag{1.93}$$

In such a coordinate system, the eigenvalues $\lambda_{k_{3,4}}$ are classically known as

$$\lambda_{k_{3,4}} = \frac{m_k}{\rho} \pm c \tag{1.94}$$

where c denotes the speed of sound [21,44]. Consequently, the pressure-derivative square root expression in (1.92)-(1.93) must correspond to an alternative relation for the sound speed c. Thus

$$c \equiv \left(a^2\right)^{1/2} = \left(\frac{m_j}{\rho} p_{m_j} + p_\rho + \frac{p_E}{\rho}\left(E + p\right)\right)^{1/2} \tag{1.95}$$

This assertion holds true for any form of (1.7) as follows. The definition of the square of the sound speed for a homogeneous gas is

$$c^2 \equiv \left(\frac{\partial p}{\partial \rho}\right)_{\text{isen}} \tag{1.96}$$

Considering that $\varepsilon = \varepsilon(\rho, s)$, with s denoting entropy, (1.96) is expressed using (1.7) as

$$\left(\frac{\partial p}{\partial \rho}\right)_{\text{isen}} = \left(\frac{\partial p}{\partial \rho}\right)_{\varepsilon} + \left(\frac{\partial p}{\partial \varepsilon}\right)_{\rho} \cdot \left(\frac{\partial \varepsilon}{\partial \rho}\right)_{\text{isen}} \tag{1.97}$$

Whereupon, invoking the first principle of thermodynamics

$$d\varepsilon = \delta \mathcal{Q} - \delta \mathcal{L} = \delta \mathcal{Q} - p\, \delta\left(\frac{1}{\rho}\right) = \delta \mathcal{Q} + \frac{p}{\rho^2}\delta\rho \tag{1.98}$$

leads to the following expression for the isentropic partial derivative of ε with respect to ρ

$$\left(\frac{\partial \varepsilon}{\partial \rho}\right)_{\text{isen}} = \frac{p}{\rho^2} \tag{1.99}$$

Therefore, the square of the sound speed is expressed as

$$c^2 \equiv \left(\frac{\partial p}{\partial \rho}\right)_{\text{isen}} = \left(\frac{\partial p}{\partial \rho}\right)_{\varepsilon} + \frac{p}{\rho^2}\left(\frac{\partial p}{\partial \varepsilon}\right)_{\rho} \tag{1.100}$$

The pressure partial derivatives in the argument a^2 of the square root (1.95) can also be expressed using (1.7), leading to relations (1.30)-(1.31), cast as

$$\begin{aligned} p_{m_j} &= \left(\frac{\partial p}{\partial \varepsilon}\right)_\rho \cdot \left(-\frac{m_j}{\rho^2}\right) \\ p_\rho &= \left(\frac{\partial p}{\partial \rho}\right)_\varepsilon + \left(\frac{\partial p}{\partial \varepsilon}\right)_\rho \cdot \left(-\frac{E}{\rho^2} + \frac{m_j m_j}{\rho^3}\right) \\ p_E &= \left(\frac{\partial p}{\partial \varepsilon}\right)_\rho \cdot \left(\frac{1}{\rho}\right) \end{aligned} \tag{1.101}$$

Therefore, the terminal expression for a^2 is

$$\begin{aligned} a^2 &= \frac{m_j}{\rho} p_{m_j} + p_\rho + \left(\frac{E+p}{\rho}\right) p_E \\ &= \left(\frac{\partial p}{\partial \varepsilon}\right)_\rho \cdot \left(-\frac{m_j m_j}{\rho^3}\right) + \left(\frac{\partial p}{\partial \rho}\right)_\varepsilon + \\ &\quad \left(\frac{\partial p}{\partial \varepsilon}\right)_\rho \cdot \left(-\frac{E}{\rho^2} + \frac{m_j m_j}{\rho^3}\right) + \left(\frac{\partial p}{\partial \varepsilon}\right)_\rho \cdot \left(\frac{E}{\rho^2} + \frac{p}{\rho^2}\right) \\ &= \left(\frac{\partial p}{\partial \rho}\right)_\varepsilon + \frac{p}{\rho^2}\left(\frac{\partial p}{\partial \varepsilon}\right)_\rho \end{aligned} \tag{1.102}$$

which coincides with (1.100). Consequently, (1.95) is indeed an alternative relation for c, hence the argument of the square root in $\lambda_{k_{3,4}}$ is positive, which proves that these eigenvalues are real.

Finally, for an ideal gas, the pressure state equation (1.12) yields the following expression for the square of the sound speed

$$c^2 = (\gamma - 1)\varepsilon + \frac{p}{\rho^2}(\gamma - 1)\rho = \frac{p}{\rho} + (\gamma - 1)\frac{p}{\rho} = \gamma \frac{p}{\rho} \tag{1.103}$$

which coincides with the classical form.

1.6.4 Curvilinear Coordinate Mach Number

The developed interpretation for the argument of the square root in (1.92) shows that the combination of convection and pressure waves corresponds to acoustic waves emanating from a representative fluid particle flowing with local contravariant velocity $v_{k_{1,2}}$. These acoustic waves can propagate upstream in the k^{th} curvilinear direction if the following inequality is satisfied

$$\frac{\left(\frac{e_{jk}m_j}{\rho}\right)^2}{e_{j\underline{k}}e_{j\underline{k}}} < c^2 \tag{1.104}$$

This inequality directly leads to the curvilinear-coordinate definition of the square of the Mach number

$$(M_k)^2 \equiv \frac{\left(\frac{e_{jk}m_j}{\rho}\right)^2}{e_{j\underline{k}}e_{j\underline{k}} \cdot c^2} \tag{1.105}$$

Therefore, if $(M_k)^2 > 1$, the flow, as referred to the $\boldsymbol{\eta}$ curvilinear coordinate system, is supersonic. Finally, for a uniform cartesian coordinate system, (1.105) reverts to the classical expression

$$(M_k)^2 \equiv \frac{\left(\frac{m_k}{\rho}\right)^2}{c^2} \tag{1.106}$$

Thus, (1.105) constitutes the appropriate curvilinear-coordinate generalization of the Mach number.

Chapter 2

Integral Statements

2.1 Strong Convection Form

An integral statement for the cartesian form of (1.1) is

$$\int_{\Omega} w \left[\frac{\partial q}{\partial t} + \frac{\partial}{\partial x_j} \left(f_j - f_j^{\nu} \right) \right] d\boldsymbol{x} = 0, \quad \forall \ w \in S^m \tag{2.1}$$

whereupon, the associated $\boldsymbol{\eta}$-space integral statement for (1.69) is

$$\int_{\widehat{\Omega}} w \left[\frac{\partial}{\partial t} (q \cdot \det J) + \frac{\partial}{\partial \eta_\ell} (e_{k\ell} (f_k - f_k^{\nu})) \right] d\boldsymbol{\eta} = 0, \quad \forall \ w \in S^m \tag{2.2}$$

In (2.2), $\widehat{\Omega}$ is the image of Ω in $\boldsymbol{\eta}$ space and w is an arbitrary element of the Hilbert space S^m for $m \geq 0$. This form is termed "*strong convection form*", or "*non-divergence form*" [14] since the divergence of the inviscid kinematic-kinetic flux vector are not integrated by parts. For $w \in S^m$, $m \geq 1$, the symmetrized weak statement form [14] associated with (2.2) is obtained via a Green-Gauss theorem

applied to the divergence of the diffusion flux vector as

$$\int_{\hat{\Omega}} w \frac{\partial}{\partial t}(q \cdot \det J)\ d\boldsymbol{\eta} + \int_{\hat{\Omega}} w \frac{\partial}{\partial \eta_\ell}(e_{k\ell} f_k)\ d\boldsymbol{\eta} + \int_{\hat{\Omega}} \frac{\partial w}{\partial \eta_\ell}(e_{k\ell} f_k^\nu)\ d\boldsymbol{\eta}$$

$$- \oint_{\partial\hat{\Omega}} w e_{k\ell} f_k^\nu n_\ell\ d\Gamma = 0, \quad \forall w \in S^1 \tag{2.3}$$

where n_ℓ denotes the ℓ^{th} component of the normal outward pointing unit vector $\boldsymbol{n}$ on the boundary $\partial\hat{\Omega}$ of $\hat{\Omega}$.

The system (2.3) is, by components of q

$$\int_{\hat{\Omega}} w \frac{\partial}{\partial t}(\rho \cdot \det J)\ d\boldsymbol{\eta} + \int_{\hat{\Omega}} w \frac{\partial e_{k\ell} m_k}{\partial \eta_\ell}\ d\boldsymbol{\eta} = 0 \tag{2.4}$$

for the continuity equation,

$$\int_{\hat{\Omega}} w \frac{\partial}{\partial t}(m_i \cdot \det J)\ d\boldsymbol{\eta} + \int_{\hat{\Omega}} w \frac{\partial}{\partial \eta_\ell}\left(e_{k\ell}\frac{m_k}{\rho} m_i + p e_{k\ell}\delta_{ki}\right)\ d\boldsymbol{\eta}$$

$$+ \int_{\hat{\Omega}} \frac{\partial w}{\partial \eta_\ell} e_{k\ell}\sigma_{ik}\ d\boldsymbol{\eta} - \oint_{\partial\hat{\Omega}} w e_{kj}\sigma_{ij} n_k\ d\Gamma = 0 \tag{2.5}$$

for the momentum equations, $1 \le i \le n = 2$, and

$$\int_{\hat{\Omega}} w \frac{\partial}{\partial t}(E \cdot \det J)\ d\boldsymbol{\eta} + \int_{\hat{\Omega}} w \frac{\partial}{\partial \eta_\ell}\left(e_{k\ell}\frac{m_k}{\rho}(E+p)\right)\ d\boldsymbol{\eta} + \int_{\hat{\Omega}} \frac{\partial w}{\partial \eta_\ell} e_{k\ell}\left(\frac{m_i}{\rho}\sigma_{ik}\right)\ d\boldsymbol{\eta}$$

$$+ \frac{1}{Pe}\int_{\hat{\Omega}} \frac{\partial w}{\partial \eta_\ell}\frac{e_{k\ell}e_{kj}}{\det J}\frac{\partial T}{\partial \eta_j}\ d\boldsymbol{\eta} - \oint_{\partial\hat{\Omega}} w e_{k\ell}\frac{m_i}{\rho}\sigma_{ik} n_\ell\ d\Gamma - \frac{1}{Pe}\oint_{\partial\hat{\Omega}} w \frac{e_{k\ell}e_{kj}}{\det J}\frac{\partial T}{\partial \eta_j} n_\ell\ d\Gamma = 0 \tag{2.6}$$

for the energy equation.

Any continuous solution of (1.1), hence (1.69), also satisfies the integral statement (2.3). However, the classical weak solutions with embedded discontinuities, shock waves for example, can only satisfy the weak statement, as developed next.

2.2 Weak Statement

For $w \in S^m$, $m \geq 1$, a weak statement form associated with (2.2) is obtained via a Green-Gauss theorem applied to the divergence of the inviscid kinematic-kinetic flux vector as

$$\int_{\widehat{\Omega}} w \frac{\partial}{\partial t}(q \cdot \det J)\, d\boldsymbol{\eta} - \int_{\widehat{\Omega}} \frac{\partial w}{\partial \eta_\ell}\left(e_{k\ell}\left(f_k - f_k^\nu\right)\right)\, d\boldsymbol{\eta}$$

$$+ \oint_{\partial\widehat{\Omega}} w e_{k\ell} f_k n_\ell \, d\Gamma - \oint_{\partial\widehat{\Omega}} w e_{k\ell} f_k^\nu n_\ell \, d\Gamma = 0, \quad \forall w \in S^1 \tag{2.7}$$

For an inviscid-flow specification, (2.7) can be satisfied by any suitable, possibly-discontinuous Lebesgue integrable distribution [12], since the kinematic-kinetic flux vector is not differentiated.

The system (2.7) is, by components of q

$$\int_{\widehat{\Omega}} w \frac{\partial}{\partial t}(\rho \cdot \det J)\, d\boldsymbol{\eta} - \int_{\widehat{\Omega}} \frac{\partial w}{\partial \eta_\ell} e_{k\ell} m_k \, d\boldsymbol{\eta} + \oint_{\partial\widehat{\Omega}} w \rho e_{j\ell} \frac{m_j}{\rho} n_\ell \, d\Gamma = 0 \tag{2.8}$$

for the continuity equation,

$$\int_{\widehat{\Omega}} w \frac{\partial}{\partial t}(m_i \cdot \det J)\, d\boldsymbol{\eta} - \int_{\widehat{\Omega}} \frac{\partial w}{\partial \eta_\ell} e_{k\ell}\left(\frac{m_k}{\rho} m_i + p\delta_{ki}\right)\, d\boldsymbol{\eta} + \int_{\widehat{\Omega}} \frac{\partial w}{\partial \eta_\ell} e_{k\ell}\sigma_{ik}\, d\boldsymbol{\eta}$$

$$+ \oint_{\partial\widehat{\Omega}} w m_i e_{j\ell} \frac{m_j}{\rho} n_\ell \, d\Gamma + \oint_{\partial\widehat{\Omega}} w e_{k\ell}\left(p\delta_{ik} - \sigma_{ik}\right) n_\ell \, d\Gamma = 0 \tag{2.9}$$

for the momentum equations, $1 \leq i \leq n = 2$, and

$$\int_{\widehat{\Omega}} w \frac{\partial}{\partial t}(E \cdot \det J)\, d\boldsymbol{\eta} - \int_{\widehat{\Omega}} \frac{\partial w}{\partial \eta_\ell} e_{k\ell}\left(\frac{m_k}{\rho}(E+p)\right)\, d\boldsymbol{\eta}$$

$$+ \int_{\widehat{\Omega}} \frac{\partial w}{\partial \eta_\ell} e_{k\ell}\left(\frac{m_i}{\rho}\sigma_{ik}\right)\, d\boldsymbol{\eta} + Pe^{-1} \int_{\widehat{\Omega}} \frac{\partial w}{\partial \eta_\ell} e_{k\ell} \frac{e_{kj}}{\det J} \frac{\partial T}{\partial \eta_j}\, d\boldsymbol{\eta}$$

$$+\oint_{\partial\widehat{\Omega}} wEe_{j\ell}\frac{m_j}{\rho}n_\ell\,d\Gamma+\oint_{\partial\widehat{\Omega}} we_{k\ell}\frac{m_i}{\rho}\left(p\delta_{ik}-\sigma_{ik}\right)n_\ell\,d\Gamma-Pe^{-1}\oint_{\partial\widehat{\Omega}} we_{k\ell}q_k n_\ell\,d\Gamma=0 \tag{2.10}$$

for the energy equation.

Of theoretical significance, since the weak statement surface integrals depend upon the contravariant momentum flux, total surface tractions and contravariant heat flux, well-posed boundary conditions can be obtained in terms of these physically meaningful integrands, as proved in Chapter 3. Hence, such identified boundary conditions can be efficiently imposed via the developed surface integrals in (2.8)-(2.10). As another theoretical advantage, the continuum weak statement directly leads to generalized, inviscid-flow jump conditions as developed next.

2.3 Jump Conditions

For a cartesian reference, hence $x_j \equiv \eta_j$, and a steady state inviscid flow, the weak statement (2.7) specializes to

$$-\int_\Omega \frac{\partial w}{\partial \eta_\ell}\left(f_k(q)\right)\,d\boldsymbol{x}+\oint_{\partial\Omega} wf_k(q)n_k\,d\Gamma=0,\quad \forall w\in S^1 \tag{2.11}$$

In (2.11), Ω can be interpreted as an arbitrary control volume with surface $\partial\Omega$, and differential elements $d\Omega$ and $d\Gamma$, while n_k denotes the appropriate resolution of the outward pointing unit vector $\boldsymbol{n}$ orthogonal to $\partial\Omega$, see Figure 2.1.

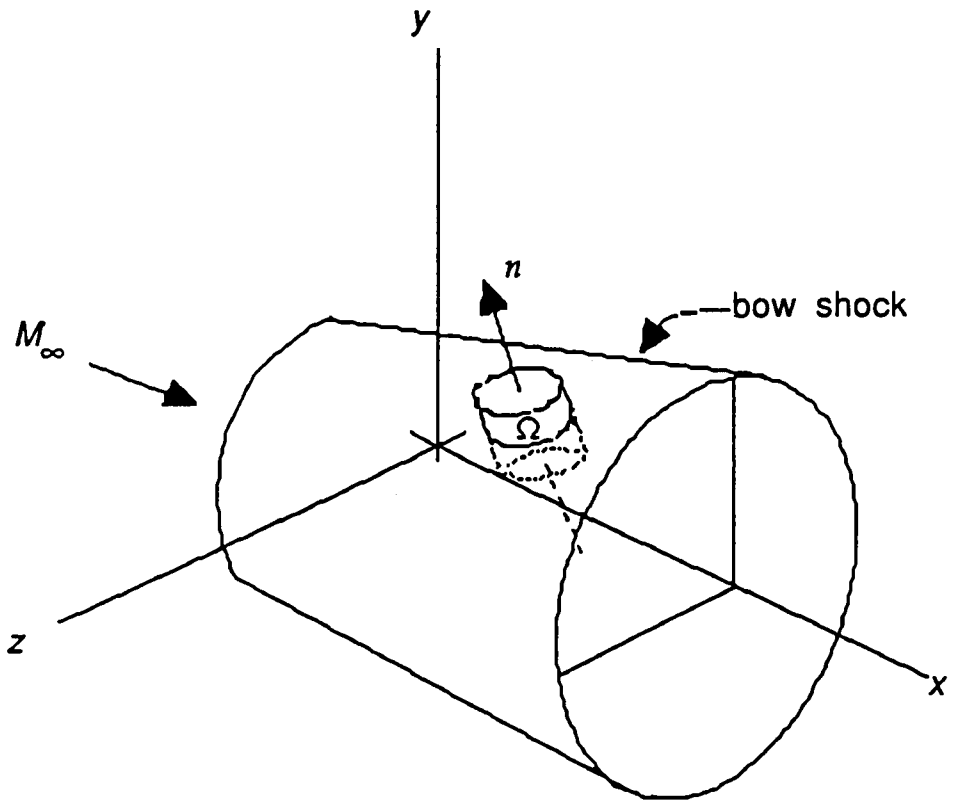


Figure 2.1: Shock Surface Control-Volume Detail

For an arbitrary cylindrical control volume that 1) intersects an arbitrary shock, 2) keeps its bases constantly parallel to the shock surface, and 3) shrinks to zero measure in the $\boldsymbol{n}$ direction, then (2.11) yields

$$\sum_{j=1}^{3} w\Delta\left(f_j(q)\right) n_j = 0 \tag{2.12}$$

Hence, since w is arbitrary, the jump conditions as expressed in (2.11) become

$$\sum_{j=1}^{3} \left\{\Delta\left(f_j(q)\right) n_j\right\} = 0 \tag{2.13}$$

In (2.12), $\Delta f_j(q)$ is the jump in $f_j(q)$ across the shock. Thus, (2.13) stipulates that the vector of variations is orthogonal to $\boldsymbol{n}$.

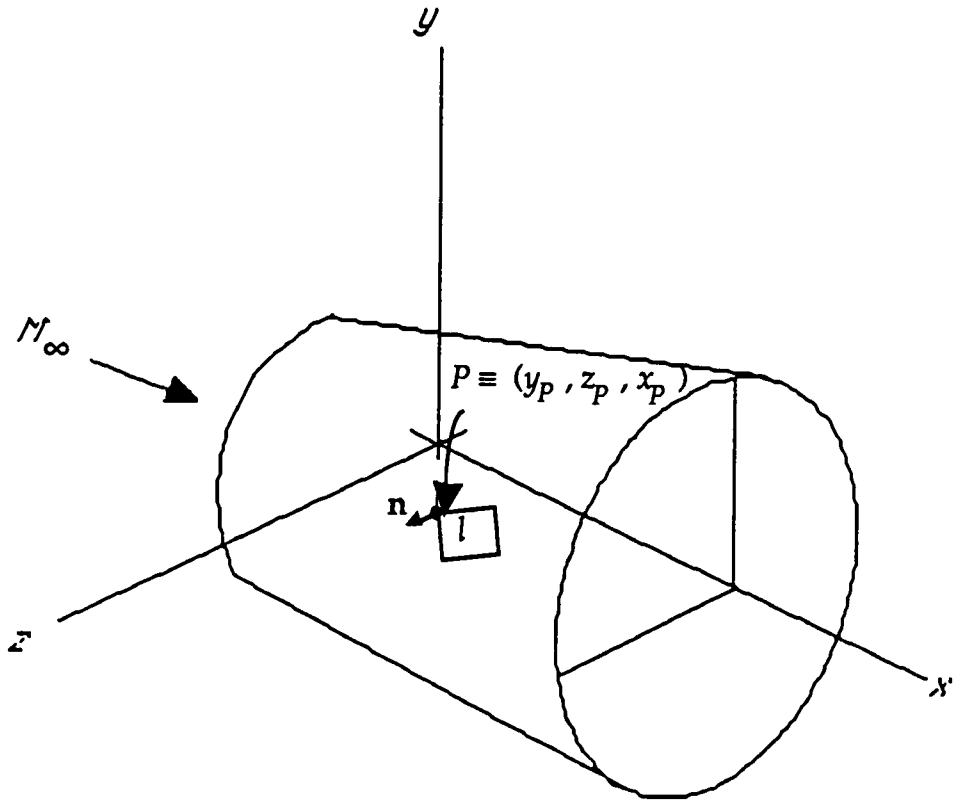


Figure 2.2: Local Normal Unit Vector Detail

The jump conditions (2.13) are conveniently cast in terms of the local shock surface directional derivatives. With reference to Figure 2.2, let the differentiable function

$$F(x_1, x_2, x_3) = 0 \tag{2.14}$$

describe the shock surface.

At any point P in the definition domain of $F(\cdot) = 0$, the local orthogonal unit vector $\boldsymbol{n}$ and tangent plane facet ℓ exist. Consequently, the expression for $\boldsymbol{n}$ is

$$\boldsymbol{n} = \frac{\nabla F}{|\nabla F|} = \frac{\dfrac{\partial F}{\partial x_j}\boldsymbol{e}_j}{|\nabla F|} \tag{2.15}$$

with local directional derivatives

$$\tan\theta_{x_1x_2} = \frac{\partial x_1}{\partial x_2} \quad , \quad \tan\theta_{x_1x_3} = \frac{\partial x_1}{\partial x_3} \tag{2.16}$$

Since the differentiable function (2.13) implicitly defines $x_1 = x_1(x_2, x_3)$, expressions (2.16) are given as

$$\frac{\partial x_1}{\partial x_2} = -\frac{\dfrac{\partial F}{\partial x_2}}{\dfrac{\partial F}{\partial x_1}} \quad , \quad \frac{\partial x_1}{\partial x_3} = -\frac{\dfrac{\partial F}{\partial x_3}}{\dfrac{\partial F}{\partial x_1}} \tag{2.17}$$

Therefore, the terminal relation for $\boldsymbol{n}$ is

$$\boldsymbol{n} = \frac{1 - \sum_{j=2}^{3} \dfrac{\partial F}{\partial x_j} e_j}{\dfrac{\partial F}{\partial x_1} |\nabla F|} \tag{2.18}$$

Hence, the multidimensional jump condition relation (2.13) is

$$\Delta\left(f_1(q)\right) = \Delta\left(f_2(q)\right)\frac{\partial x_1}{\partial x_2} + \Delta\left(f_3(q)\right)\frac{\partial x_1}{\partial x_3} \tag{2.19}$$

For an arbitrary equation of state, the unabridged form of this expression then yields jump conditions in terms of density, velocity resolution, pressure, and total volume specific energy in the form

$$\rho_1 u_1 - \rho_2 u_2 = \left(\rho_1 v_1 - \rho_2 v_2\right)\frac{\partial x_1}{\partial x_2} + \left(\rho_1 w_1 - \rho_2 w_2\right)\frac{\partial x_1}{\partial x_3} \tag{2.20}$$

$$\left(\rho_1 u_1^2 + p_1\right) - \left(\rho_2 u_2^2 + p_2\right) = \left(\rho_1 v_1 u_1 - \rho_2 v_2 u_2\right)\frac{\partial x_1}{\partial x_2} + \left(\rho_1 w_1 u_1 - \rho_2 w_2 u_2\right)\frac{\partial x_1}{\partial x_3} \tag{2.21}$$

$$\left(\rho_1 u_1 v_1 - \rho_2 u_2 v_2\right) = \left(\rho_1 v_1^2 + p_1 - \rho_2 v_2^2 - p_2\right)\frac{\partial x_1}{\partial x_2} + \left(\rho_1 w_1 v_1 - \rho_2 w_2 v_2\right)\frac{\partial x_1}{\partial x_3} \tag{2.22}$$

$$(\rho_1 u_1 w_1 - \rho_2 u_2 w_2) = (\rho_1 v_1 w_1 - \rho_2 v_2 w_2)\frac{\partial x_1}{\partial x_2} + \left(\rho_1 w_1^2 + p_1 - \rho_2 w_2^2 - p_2\right)\frac{\partial x_1}{\partial x_3} \tag{2.23}$$

$$u_1(E_1 + p_1) - u_2(E_2 + p_2) = (v_1(E_1 + p_1) - v_2(E_2 + p_2))\frac{\partial x_1}{\partial x_2} + (w_1(E_1 + p_1) - w_2(E_2 + p_2))\frac{\partial x_1}{\partial x_3} \tag{2.24}$$

In (2.20)-(2.24), the scalar components of freestream velocity $\boldsymbol{V}$ are denoted as (u_1, v_1, w_1); the analogous components across the shock are (u_2, v_2, w_2). A convenient algebraic rearrangement of (2.20)-(2.24) then yields the terminal generalized jump conditions as

$$\left(\frac{\rho_2}{\rho_1}\right) = \frac{1 - \left(\frac{v_1}{u_1}\right)\frac{\partial x_1}{\partial x_2} - \left(\frac{w_1}{u_1}\right)\frac{\partial x_1}{\partial x_3}}{\left(\frac{u_2}{u_1}\right) - \left(\frac{v_2}{u_1}\right)\frac{\partial x_1}{\partial x_2} - \left(\frac{w_2}{u_1}\right)\frac{\partial x_1}{\partial x_3}} \tag{2.25}$$

$$\left(\frac{u_2}{u_1}\right) = 1 - \frac{\left(\frac{p_2}{p_1} - 1\right)}{\gamma M_1^2\left(1 - \left(\frac{v_1}{u_1}\right)\frac{\partial x_1}{\partial x_2} - \left(\frac{w_1}{u_1}\right)\frac{\partial x_1}{\partial x_3}\right)} \tag{2.26}$$

$$\left(\frac{v_2}{u_1}\right) = \left(\frac{v_1}{u_1}\right) + \frac{\left(\frac{p_2}{p_1} - 1\right)}{\gamma M_1^2\left(1 - \left(\frac{v_1}{u_1}\right)\frac{\partial x_1}{\partial x_2} - \left(\frac{w_1}{u_1}\right)\frac{\partial x_1}{\partial x_3}\right)}\left(\frac{\partial x_1}{\partial x_2}\right) \tag{2.27}$$

$$\left(\frac{w_2}{u_1}\right) = \left(\frac{w_1}{u_1}\right) + \frac{\left(\frac{p_2}{p_1} - 1\right)}{\gamma M_1^2\left(1 - \left(\frac{v_1}{u_1}\right)\frac{\partial x_1}{\partial x_2} - \left(\frac{w_1}{u_1}\right)\frac{\partial x_1}{\partial x_3}\right)}\left(\frac{\partial x_1}{\partial x_3}\right) \tag{2.28}$$

$$\left(\frac{\partial x_1}{\partial x_2}\right)^2 + \left(\frac{\partial x_1}{\partial x_3}\right)^2 = \frac{\gamma M_1^2\left(\frac{H_2}{H_1} - 1\right)}{\frac{H_2}{H_1}\left(\frac{H_2}{H_1} - 1\right)}\left(1 - \left(\frac{v_1}{u_1}\right)\frac{\partial x_1}{\partial x_2} - \left(\frac{w_1}{u_1}\right)\frac{\partial x_1}{\partial x_3}\right)^2 - 1 \tag{2.29}$$

In (2.25)-(2.29), $(M_1)^2$ denotes the freestream axial mach number defined as

$$(M_1)^2 \equiv \frac{u_1^2}{\gamma\left(\frac{p_1}{\rho_1}\right)} \tag{2.30}$$

while H defines the total volume specific enthalpy as

$$H = E + p \tag{2.31}$$

Of theoretical significance, equation (2.29) constitutes the "*shock surface partial differential equation*", with solution the bow shock-surface function $x_1 = x_1(x_2, x_3)$, and hence the directional derivatives (2.17), for specified freestream axial Mach number M_1, velocity $\boldsymbol{V}_1$, and thermodynamic state p_2/p_1, H_2/H_1. Once the directional partial derivatives are computed, the shock flow velocity and density ratios are determined from (2.26)-(2.28), and then (2.25).

Expressions (2.25)-(2.29) revert to the classical formulae for a plane shock in a perfect gas flow, via the specialization

$$\left(\frac{\partial x_1}{\partial x_3}\right) = 0 \quad , \quad \left(\frac{\partial x_1}{\partial x_2}\right) = (\tan\beta)^{-1} \tag{2.32}$$

$$v_1 = 0 \quad , \quad w_1 = 0 \tag{2.33}$$

Referring to Figure 2.3, (2.29) simplifies to

$$1 + \left(\frac{\partial x_1}{\partial x_2}\right)^2 + \left(\frac{\partial x_1}{\partial x_3}\right)^2 = 1 + \frac{1}{\tan^2\beta} = \frac{\tan^2\beta + 1}{\tan^2\beta} = \frac{1}{\sin^2\beta} \tag{2.34}$$

Hence, (2.25)-(2.29) yield

$$\left(\frac{p_2}{p_1}\right) \;=\; 1 + \frac{2\gamma}{\gamma+1}\left(M_1^2\sin^2\beta - 1\right) \tag{2.35}$$

$$\left(\frac{u_2}{u_1}\right) = 1 - \frac{2\left(M_1^2 \sin^2\beta - 1\right)}{(\gamma+1)\,M_1^2} \tag{2.36}$$

$$\left(\frac{v_2}{u_1}\right) = \frac{2\left(M_1^2 \sin^2\beta - 1\right)}{\tan\beta\,(\gamma+1)\,M_1^2} \tag{2.37}$$

$$\left(\frac{w_2}{u_1}\right) = 0 \tag{2.38}$$

$$\left(\frac{\rho_2}{\rho_1}\right) = \frac{(\gamma+1)M_1^2 \sin^2\beta}{(\gamma-1)M_1^2 \sin^2\beta + 2} \tag{2.39}$$

which coincide with the classical expressions [22].

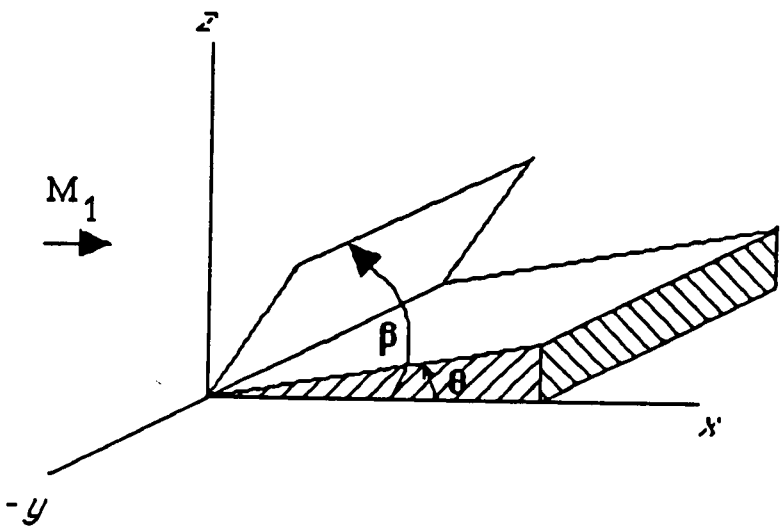


Figure 2.3: Plane Oblique Shock Geometry

Chapter 3

Boundary and Initial Conditions

3.1 Boundary Conditions

The number of Dirichlet boundary conditions for (1.1) is

Euler Equations:

$n+2$ conditions for supersonic inflow

$n+1$ conditions for subsonic inflow

1 condition for subsonic outflow

0 condition for supersonic outflow

Navier-Stokes Equations:

$n+2$ conditions on an inflow boundary

$n+1$ conditions on an outflow boundary

as derived from Strikwerda's work [26]. An admissible specific boundary condition

set is then derived following Dutt's analysis [49], whereupon it is shown that the weak statement (2.8)-(2.10) provides by default the venue to enforce the determined well-posed conditions, both rigorously and efficiently.

3.1.1 Choice of Boundary Conditions

This analysis details derivation of a specific set of boundary conditions that promote solution boundedness for (1.1), hence (2.4)-(2.10). For an arbitrary partial differential equation system, this analysis is established invoking Lyapunov stability theory, [4,5,7,8]. This theory employs a non-decreasing functional, or generalized "system energy", and its total time derivative as associated with the given equation set. As shown in the sequel, the stability expression can be cast in terms of functions on the boundary Γ of the domain Ω, which can be constrained to satisfy the following generalized stability theorem.

Theorem 1 (Iannelli) *Let $V = V(t,q)$ be a Lyapunov function defined on $\Re^+ \times \Re^n$, with $t \in \Re^+$, and $q \in \Re^n$, which satisfies the conditions:*

1. *$c(\|q\|) \leq V(t,q)$, where $c(\|q\|)$ is a continuously increasing function and $c(\|q\|) \to \infty$ as $\|q\| \to \infty$;*

2. *$\left(\frac{dV}{dt}\right)_{PDE} = f(t,q) - g(t,q)$, where subscript "PDE" denotes the time derivative along a solution q of the given partial differential equation, f is a con-*

tinuous function bounded above and g is a positive continuously increasing function.

Then the solutions q are bounded.

Proof. If $f(t,q) \leq 0$, then this theorem reverts to the classical Lyapunov-theory stability condition proved in [7]. Conversely, if $f(t,q) > 0$, then the theorem is proved by contradiction as:

1. Suppose $\exists\ t^*\ \setminus\ \left(\frac{dV}{dt}\right)_{PDE} = f(t,q) - g(t,q) > 0,\ \forall\ t > t^*$

2. $\Rightarrow g(t,q) < f(t,q),\ \forall\ q(\boldsymbol{x},t)\ \setminus\ t > t^*$

3. $\Rightarrow V(t,q)$ grows $\forall\ t > t^*$

4. $\Rightarrow \|q(\boldsymbol{x},t)\|$ grows $\forall\ t > t^*$, since $V(t,q)$ is continuously increasing

5. $\Rightarrow \exists\ \boldsymbol{x}_b,\ \tilde{t}\ \setminus\ g(t,q(\boldsymbol{x},t)) > \max\{f(t,q(\boldsymbol{x},t))\}\ \forall\ t > \tilde{t}$,

   $\forall\ \boldsymbol{x} \in S \equiv \{\boldsymbol{x} : \|\boldsymbol{x} - \boldsymbol{x}_b\| \leq \delta\} \subset \Omega,\ \delta > 0$, since $g(t,q(\boldsymbol{x},t))$ is continuously increasing and $\max\{f(t,q(\boldsymbol{x},t))\} \leq K = \text{const.}$, since f is bounded.

However, 5) contradicts 2) hence 1) does not hold $\forall\ t > t^*$, and consequently $q(\boldsymbol{x},t)$ does not grow $\forall\ t > \tilde{t}$. An analogous contradiction is reached by assuming in 1) an opposite inequality for the time derivative of V. Therefore, $q(\boldsymbol{x},t)$ can be at most a bounded oscillatory function since $V(t,q)$ is not less than a norm of $q(\boldsymbol{x},t)$ and $V_{\min}(t,q) \leq V(t,q) \leq V_{\max}(t,q)$, with $V_{\max}(t,q) \leq K = \text{const.}$, since 1) does not hold $\forall\ t > t^*$. □

The application of this theorem can be exemplified via determination of the well-known admissible boundary condition for a linear hyperbolic partial differential equation. Thereafter, the corresponding boundary conditions for the full Navier-Stokes system are established. The linear model equation is

$$\frac{\partial q}{\partial t} + u\frac{\partial q}{\partial x} = 0 \tag{3.1}$$

defined in the domain $[a, b] \times [t_0, \infty)$, where u is a positive constant. The known well-posed boundary condition for (3.1) is,

$$q(a, t) = q_a(t) \tag{3.2}$$

without any constraint at $x = b$, which is readily derived as follows. An admissible Lyapunov functional associated to (3.1) is,

$$V(t) = \frac{1}{2}\int_a^b q^2\, dx \tag{3.3}$$

with time derivative

$$\frac{dV}{dt} = \int_a^b q\frac{\partial q}{\partial t}\, dx \tag{3.4}$$

Equation (3.4), upon substitution of $\dfrac{\partial q}{\partial t}$ via (3.1), becomes

$$\frac{dV}{dt} = -u\int_a^b q\frac{\partial q}{\partial x}\, dx = -u\int_a^b \frac{\partial}{\partial x}\left[\frac{q^2}{2}\right]\, dx \tag{3.5}$$

which can be integrated exactly exposing the boundary function

$$\frac{dV}{dt} = u\left[\frac{q^2}{2}\right]_{x=a} - u\left[\frac{q^2}{2}\right]_{x=b} \tag{3.6}$$

Note that (3.6) satisfies the hypotheses of Theorem 1 upon setting $q(a,t) = q_a(t)$, for $q_a(t)$ a continuous function bounded above. Consequently, the boundary condition (3.2) is well-posed.

Dutt's analysis [49] indicates that a system energy functional, appropriate for the full Navier-Stokes equations, can be derived utilizing an Euler-equation "entropy" functional herein cast as

$$V(q) = \rho\left[\gamma \log\left(\frac{\rho}{\overline{\rho}}\right) - \log\left(\frac{p}{\overline{p}}\right) + \frac{(\gamma-1)\overline{\rho}\,(m_i m_i)}{2\overline{p}\rho^2} - \gamma + \frac{p\overline{\rho}}{\overline{p}\rho}\right] + (\gamma-1)\overline{\rho} \qquad (3.7)$$

where $\overline{p}$ and $\overline{\rho}$, to be determined, represent a reference thermodynamic state such that

$$V(q) - (\gamma-1)\overline{\rho} \geq 0 \qquad (3.8)$$

and

$$\left(\frac{\overline{\rho}}{\overline{p}} - \frac{\rho}{p}\right) \leq 0 \qquad (3.9)$$

As shown in [49], V is a strictly positive and convex function that satisfies the relation

$$\frac{\partial V}{\partial q}\frac{\partial f_j}{\partial q} = \frac{\partial F_j}{\partial q} \qquad (3.10)$$

where the expressions for F_j and $\dfrac{\partial V}{\partial q}$ are herein reexpressed as

$$F_j = \frac{m_j}{\rho}\left[V(q) - (\gamma-1)\overline{\rho}\right] \qquad (3.11)$$

$$\frac{\partial V}{\partial q} = \begin{Bmatrix} \gamma \log\left(\frac{\rho}{\overline{\rho}}\right) - \log\left(\frac{p}{\overline{p}}\right) - \frac{(\gamma-1)m_i m_i}{2\rho p} \\ \frac{m_i(\gamma-1)}{p} \\ (\gamma-1)\left(\frac{\overline{\rho}}{\overline{p}} - \frac{\rho}{p}\right) \end{Bmatrix}^T \qquad (3.12)$$

Herein, the Lyapunov functional is defined as

$$S(t) \equiv \int_{\Omega} V\left(q(\boldsymbol{x},t)\right)\, d\Omega \tag{3.13}$$

and $\dfrac{\partial V}{\partial t}$ is derived utilizing the Navier-Stokes equations (1.1) as follows. First

$$\frac{\partial V}{\partial q}\frac{\partial q}{\partial t} + \frac{\partial V}{\partial q}\frac{\partial f_j}{\partial x_j} - \frac{\partial V}{\partial q}\frac{\partial f_j^{\nu}}{\partial x_j} = 0 \tag{3.14}$$

hence,

$$\frac{\partial V}{\partial t} + \frac{\partial V}{\partial q}\frac{\partial f_j}{\partial q}\frac{\partial q}{\partial x_j} - \frac{\partial V}{\partial q}\frac{\partial f_j^{\nu}}{\partial x_j} = 0 \tag{3.15}$$

whereupon, using (3.10)

$$\frac{\partial V}{\partial t} + \frac{\partial F_j}{\partial x_j} - \frac{\partial V}{\partial q}\frac{\partial f_j^{\nu}}{\partial x_j} = 0 \tag{3.16}$$

Consequently, the Lyapunov functional time derivative is

$$\frac{dS}{dt} = -\int_{\Omega}\left(\frac{\partial F_j}{\partial x_j} - \frac{\partial V}{\partial q}\frac{\partial f_j^{\nu}}{\partial x_j}\right)\, d\Omega \tag{3.17}$$

Integrating (3.17) via the Green-Gauss theorem yields

$$\frac{dS}{dt} = -\oint_{\partial\Omega}\left(F_j n_j - \frac{\partial V}{\partial q} f_j^{\nu} n_j\right)\, d\Gamma - \int_{\Omega}\frac{\partial}{\partial x_j}\left(\frac{\partial V}{\partial q}\right) f_j^{\nu}\, d\Omega \tag{3.18}$$

Since the domain integral in (3.18) is proved positive in [49], its elimination form (3.18) yields the following inequality for the time derivative of S

$$\begin{aligned}\frac{dS}{dt} \leq & -\oint_{\partial\Omega}\frac{m_j}{\rho} n_j \left(V(q) - (\gamma-1)\overline{\rho}\right) d\Gamma \\ & + \oint_{\partial\Omega}(\gamma-1)\frac{\overline{\rho}}{\overline{p}}\frac{m_i}{\rho}\sigma_{ij} n_j\, d\Gamma + \oint_{\partial\Omega}(\gamma-1)\left(\frac{\overline{\rho}}{\overline{p}} - \frac{\rho}{p}\right) Pe^{-1}\frac{\partial T}{\partial x_j} n_j\, d\Gamma\end{aligned} \tag{3.19}$$

For $\partial\Omega = \partial\Omega_{in} \bigcup \partial\Omega_{wall} \bigcup \partial\Omega_{out}$, where $\partial\Omega_{in}$, $\partial\Omega_{wall}$ and $\partial\Omega_{out}$ are the boundary segments along which $m_j n_j < 0$, $m_j n_j = 0$ and $m_j n_j > 0$, respectively, expression (3.19) becomes, in expanded form

$$\begin{aligned}
\frac{dS}{dt} \leq & -\int_{\partial\Omega_{in}} \frac{m_j}{\rho} n_j \left(V(q) - (\gamma-1)\overline{\rho}\right) d\Gamma \\
& + \int_{\partial\Omega_{in}} (\gamma-1)\frac{\overline{\rho}}{\overline{p}}\frac{m_i}{\rho}\sigma_{ij} n_j \, d\Gamma + \int_{\partial\Omega_{in}} (\gamma-1)\left(\frac{\overline{\rho}}{\overline{p}} - \frac{\rho}{p}\right) Pe^{-1}\frac{\partial T}{\partial x_j} n_j \, d\Gamma \\
& - \int_{\partial\Omega_{wall}} \frac{m_j}{\rho} n_j \left(V(q) - (\gamma-1)\overline{\rho}\right) d\Gamma + \int_{\partial\Omega_{wall}} (\gamma-1)\frac{\overline{\rho}}{\overline{p}}\frac{m_i}{\rho}\sigma_{ij} n_j \, d\Gamma \\
& + \int_{\partial\Omega_{wall}} (\gamma-1)\left(\frac{\overline{\rho}}{\overline{p}} - \frac{\rho}{p}\right) Pe^{-1}\frac{\partial T}{\partial x_j} n_j \, d\Gamma - \int_{\partial\Omega_{out}} \frac{m_j}{\rho} n_j \left(V(q) - (\gamma-1)\overline{\rho}\right) d\Gamma \\
& + \int_{\partial\Omega_{out}} (\gamma-1)\frac{\overline{\rho}}{\overline{p}}\frac{m_i}{\rho}\sigma_{ij} n_j \, d\Gamma + \int_{\partial\Omega_{out}} (\gamma-1)\left(\frac{\overline{\rho}}{\overline{p}} - \frac{\rho}{p}\right) Pe^{-1}\frac{\partial T}{\partial x_j} n_j \, d\Gamma \quad (3.20)
\end{aligned}$$

Inequality (3.20) is instrumental for deriving Navier-Stokes system boundary conditions that satisfy the hypotheses of Theorem 1, and thereby guarantee solution stability in the sense of bounded energy. Note that (3.20) depends upon the momentum flux, deviatoric tractions and heat flux, in direct correspondence with the analogous terms in the weak statement (2.8)-(2.10). Consequently, the extracted boundary conditions constrain the values of these terms and are directly enforceable in (2.8)-(2.10). Note also that expressing p, via the state equation (1.14), leads to the equality

$$\int_{\Omega_{in}} \frac{m_j}{\rho} n_j (V(q) - (\gamma-1)\overline{\rho}) \, d\Gamma =$$

$$\int_{\Omega_{in}} \frac{m_j}{\rho} n_j \left(\rho\left(\gamma \log\left(\frac{\rho}{\overline{\rho}}\right) - \log\left(\frac{(\gamma-1)(E - m_i m_i/2\rho)}{\overline{p}}\right) + (\gamma-1)\frac{\overline{\rho}}{\rho}\frac{E}{p} - \gamma\right)\right) d\Gamma \quad (3.21)$$

which is instrumental in the derivation of admissible inlet conditions.

The function $g(t,q)$ of Theorem 1 can be identified as

$$g(t, q(\boldsymbol{x},t)) = \int_{\Omega_{out}} \frac{m_j}{\rho} n_j (V(q) - (\gamma-1)\overline{\rho}) \, d\Gamma \quad (3.22)$$

while the function $f(t, q(\boldsymbol{x}, t))$ corresponds to the sum of the remaining integrals. The following Navier-Stokes boundary conditions prevent the positive growth of these integrals. Importantly, they revert to admissible boundary conditions as $Re \rightarrow \infty$ for Euler equation system.

Subsonic inflow:

$$\begin{aligned} \rho &= \rho_{in} \\ E &= E_{in} \\ \sigma_{ij} n_j &= \left[a_{ij} \frac{m_j}{\rho} s_j^k + g_i \right] \end{aligned} \tag{3.23}$$

where s_j^k, $1 \leq k \leq n-1$, is the tangent unit vector resolution in the k^{th} coordinate direction on $d\Gamma$ with unit normal n_j. Note that the third expression in (3.23) constitutes a Robin mixed boundary condition statement for the momentum equations for any finite Re. The rank of the matrix $[a_{i1}, a_{i2}, g_i]$ must be $n-1$, so that (3.23) reduces to $n-1$ boundary conditions as $Re \rightarrow \infty$. Further, the matrices a_{ij} must be bounded negative definite and g_i must be a bounded function. This choice is valid since for subsonic flows

$$\frac{m_i m_i}{\rho} < \gamma p, \text{ hence } m_i m_i < \frac{\gamma(\gamma-1)}{\gamma+1} E\rho \tag{3.24}$$

Consequently both $m_j n_j$ and T are bounded since both ρ and E are constrained.

Supersonic inflow:

$$\begin{aligned} \rho &= \rho_{in} \\ E &= E_{in} \end{aligned}$$

$$(m_j) \;=\; (m_j)_{in} \tag{3.25}$$

This choice is valid since it leads to bounded inflow integrals in (3.20).

Wall boundaries:

$$\begin{aligned} m_j n_j &= 0 \quad , \text{ inviscid flow} \\ m_j = 0 \;\forall\; j \;,\; \left(aT + \frac{1}{Pe}\frac{\partial T}{\partial n}\right) &= g_T \quad , \text{ viscous flow} \end{aligned} \tag{3.26}$$

where $a < 0$ and g_T is a bounded function. Note that in either instance, (3.26) leads to bounded surface integrals on $\partial\Omega_{\text{wall}}$ in (3.20).

Concerning outflow boundary conditions, these must lead to a positive function (3.22) as required by Theorem 1. The function is herein cast as

$$g(t, q(\boldsymbol{x}, t)) = \int_{\partial\Omega_{out}} m_j n_j \left(\gamma \log\left(\frac{\rho}{\overline{\rho}}\right) - \log\left(\frac{p}{\overline{p}}\right) + (\gamma - 1)\frac{\overline{\rho}}{\rho}\frac{E}{\overline{p}} - \gamma\right) d\Gamma \tag{3.27}$$

and is positive if the expression in parentheses remains positive, since $(m_j n_j)_{out} > 0$. This requirement is met if the following sufficient conditions are satisfied.

$$\log\left(\frac{\rho}{\overline{\rho}}\right) > 1, \quad \forall \quad \rho_{out} \tag{3.28}$$

$$\log\left(\frac{\overline{p}}{p}\right) > 0, \quad \forall \quad p_{out} \tag{3.29}$$

Hence

$$\overline{\rho} \;<\; \frac{(\rho_{\min})_{out}}{e^1} \tag{3.30}$$

$$\overline{p} \;>\; (p_{\max})_{out} \tag{3.31}$$

where e=2.718.... . The constraint on $\overline{\rho}$ is evidently satisfied without any additional Mach number-dependent specification on outflow density. Conversely, the constraint

on $\overline{p}$ is met for subsonic outflows when a surface traction / pressure boundary condition is imposed. This is detailed in the sequel, where suitable specifications are introduced that contribute to the positivity of (3.27), and to the boundedness and/or negativity of the remaining outflow integrals in (3.20).

Subsonic outflow:

$$\begin{aligned} (p\delta_{ij} - \sigma_{ij})\, n_j &= p_{out} > 0 \\ \left(aT + \frac{1}{Pe}\frac{\partial T}{\partial n}\right) &= 0 \end{aligned} \tag{3.32}$$

where $a \leq 0$. These constraints reduce to a single boundary condition on p as $Re \rightarrow \infty$. Note that the constant $\overline{p}$ in (3.29), and (3.31) exists since p_{out}, hence $(p_{\max})_{out}$, is constrained.

Supersonic outflow:

$$\begin{aligned} \sigma_{ij} n_j &= 0 \\ \left(aT + \frac{1}{Pe}\frac{\partial T}{\partial n}\right) &= 0 \end{aligned} \tag{3.33}$$

where $a \leq 0$. These constraints also vanish identically as $Re \rightarrow \infty$, and the constant $\overline{p}$ exists since p_{out} decreases with increasing supersonic Mach number.

In summary, (3.23), (3.25), (3.26), (3.32), (3.33) specify admissible constraints on the surface momentum flux, deviatoric/total tractions and heat flux vector. Note thereby, that no steady state solution q can exist if the heat flux surface integral in (3.19) does not asymptotically vanish in time.

The boundary conditions (3.23), (3.25), (3.26), (3.32), (3.33) collectively prevent the positive growth of all integrals in (3.20) except the term

$$\int_{\partial\Omega_{out}} \frac{1}{\rho}(m_j n_j)\,[V(q) - (\gamma - 1)\overline{\rho}]\; d\Gamma > 0 \tag{3.34}$$

which is allowed to vary. Consequently, the hypotheses of Theorem 1 are satisfied, and therefore the solution q of system (1.1), as complemented by the derived boundary conditions, is bounded.

3.1.2 Implementation of Boundary Conditions

The enforcement of Dirichlet boundary conditions on any entry q_j in the state variable q is effected by replacing the associated conservation equation with the statement $\dfrac{\partial q_j}{\partial t} = 0$, and utilizing the given data as local initial conditions. The other derived constraints are then keyed to the weak statement surface integrals in (2.8)-(2.10). Therefore, the wall tangency boundary condition (3.26) is efficiently imposed via deletion of the momentum flux surface integrals in (2.8)-(2.10) that would otherwise be computed along any wall segment. The total surface traction and heat flux boundary conditions are analogously enforced for all values of Re by replacing the arguments of the relevant integrals in (2.9)-(2.10) with (3.23), (3.26), (3.32), (3.33). Very likely, the efficacy of this enforcement procedure translate into the overall monotonicity displayed by the benchmark test case solutions discussed in Chapter 10.

3.2 Initial Conditions

To attain a steady-state expeditiously, the state variable initialization $q(\boldsymbol{x}, t_0)$ should model in some sense the asymptotic solution. For transonic and supersonic ($M_\infty \leq 3$) external and/or internal flows, an isentropic initialization has yielded a stable and efficient relaxation to a steady state for the various cases investigated. Conversely, the efficient numerical evolution to a steady-state hypersonic flowfield about blunt bodies requires that the initial conditions simulate, to a non-trivial extent, the sharp entropy gradient existing across the strong bow shock. The determined appropriate transonic, supersonic and hypersonic initialization procedures are now detailed.

3.2.1 Transonic - Supersonic Flow Initialization

For two-dimensional confined flow problems, the computation is easily initialized using the isentropic, quasi-1-D steady solution for ρ and E, with the initial distribution for axial momentum, $(m_x)_{2D}$, determined after establishing the initial values for transverse momentum, $(m_y)_{2D}$. Expressing the quasi-1-D continuity equation source term with the initial $(m_x)_{2D}$, and equating it with the partial derivative of $(m_y)_{2D}$ with respect to y yields

$$(m_x)_{2D} = (m_x)_{Q1d} \cos[\theta(y)] \tag{3.35}$$

$$\frac{(m_x)_{2D}}{A(x)} \frac{dA(x)}{dx} = \frac{\partial m_y}{\partial y} \tag{3.36}$$

where $\theta(y)$ is local the geometric angularity. Since $(m_x)_{Q1D}$ is a function of x only, and the variation of $\theta(y)$ is assumed to satisfy $\cos\theta \approx 1$, then the approximate direct integration of (3.36) yields

$$(m_y)_{2D} \approx \frac{(m_x)_{2D}}{A(x)} \frac{dA(x)}{dx} (y - y_T) \tag{3.37}$$

where y_T is the center plane ordinate along which $m_y = 0$, see Figure 3.1.

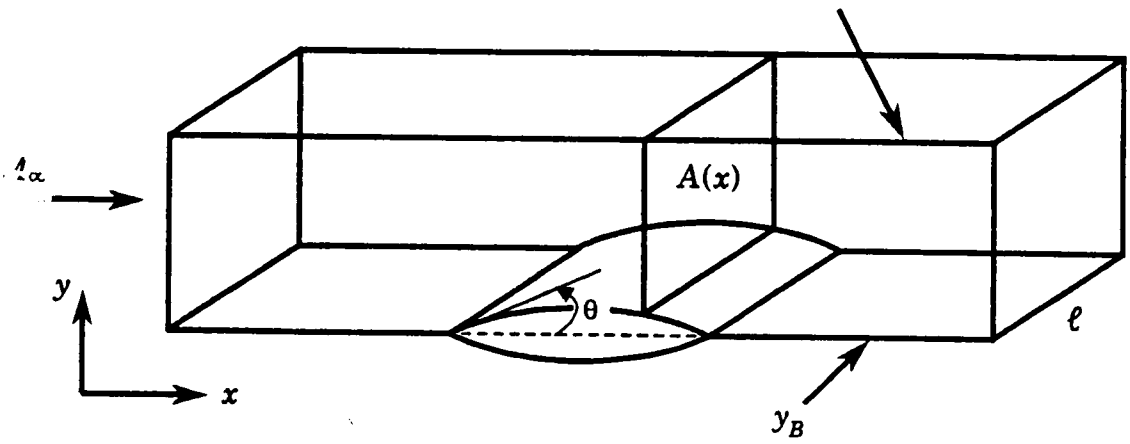


Figure 3.1: Internal Flow Domain Geometry

Importantly, the distribution of $(m_y)_{2D}$ computed via (3.37) satisfies the wall tangency constraint as is easily shown. Assume the geometric form is mathematically expressed as

$$A(x) = \ell\,(y_T - y_B) \tag{3.38}$$

where $\ell = 1$ is the channel unit transverse width. Consequently,

$$\frac{1}{A(x)}\frac{dA(x)}{dx}\,(y - y_T) = \left[-\frac{dy_B}{dx}\frac{(y - y_T)}{(y_T - y_B)}\right] \equiv \tan\left[\theta\,(y)\right] \tag{3.39}$$

therefore

$$(m_y)_{2D} = \left[-\frac{dy_B}{dx}\frac{(y - y_T)}{(y_T - y_B)}\right](m_x)_{2D} = \tan\left[\theta\,(y)\right] \cdot (m_x)_{2D} \tag{3.40}$$

which upon setting $y = y_B$ specializes to

$$m_y = m_x \cdot \tan\left[\theta\,(y)\right] \tag{3.41}$$

i.e., the wall tangency constraint. Finally, the corresponding $(m_x)_{2D}$ is obtained via (3.35) so that

$$(m_x)^2_{2D} + (m_y)^2_{2D} = (m_x)^2_{Q1D} \tag{3.42}$$

For an external flowfield problem, the procedure is analogous. Specifically, one replaces y_T with an appropriate reference level y_R in (3.37) so that the values of $(m_y)_{2D}$, as obtained with $y = y_T$, correspond to an admissible outer boundary distribution for this momentum component.

3.2.2 Hypersonic Flow Initialization

A satisfactory solution initialization for hypersonic flows about blunt bodies with bow-shock entropy rise approximation can be established via an accurate estimate of the bow shock location in concert with the Rankine-Hugoniot shock conditions, for pressure rise determination, and a Newtonian impact model for surface pressure distribution [22]. The surface velocity is in turn computed using linear interpolation from nought, at the blunt body stagnation point, to the conical flow value, at the last body surface point. The field velocity is then determined via interpolation from shock to surface values. Thereafter, density and total volume-specific energy are computed via the steady-state adiabatic flow equation. The detailed initial field determination is as follows.

With reference to Figure 3.2, an empirical equation [22] approximating the bow shock is

$$x = -|R| - |\delta| + \Delta + \frac{R_c}{\tan^2 \beta_a} \left[\left(1 + \frac{y^2 \tan^2 \beta_a}{R_a^2} \right)^{1/2} - 1 \right] \tag{3.43}$$

where R is the spherical nose radius, δ is the shock standoff distance, Δ is the x coordinate of the nose center, R_c is the bow shock vertex radius of curvature, and β_a is the bow shock asymptotic angle to freestream, as determined for conical flow at given M_∞ and θ_c.

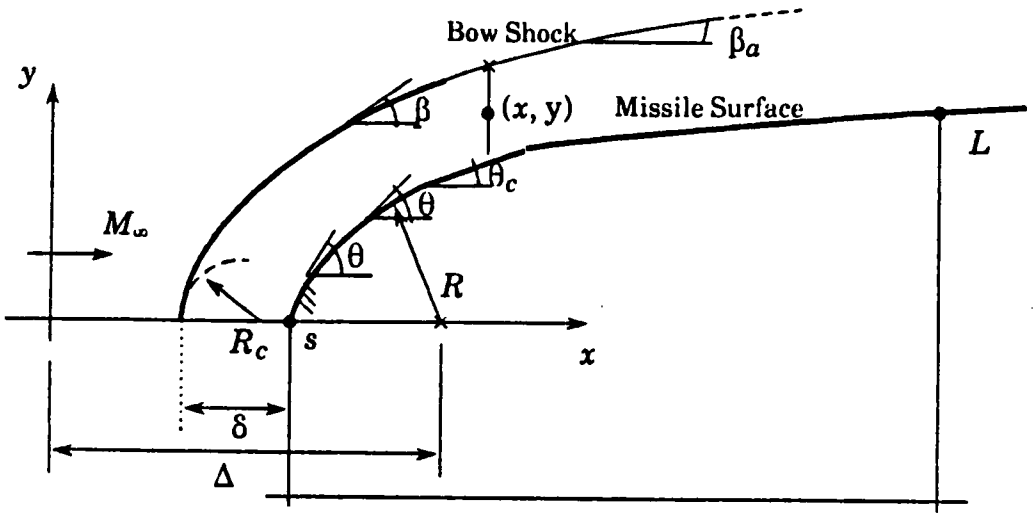


Figure 3.2: Missile and Bow Shock Configuration

The geometric parameters δ and R_c for sphere-cone bodies [22] are correlated as

$$\begin{aligned} \frac{\delta}{R} &= 0.143 \exp\left(\frac{3.24}{M_\infty^2}\right) \\ \frac{R_c}{R} &= 1.143 \exp\left(\frac{0.54}{(M_\infty - 1)^{1.2}}\right) \end{aligned} \tag{3.44}$$

Therefore, for a given missile geometry, hence R, Δ, θ_c and onset flow Mach number M_∞, the initial bow shock location is completely estimated via (3.43)-(3.44). The local bow shock angle β is then determined via differentiation of (3.43) yielding

$$\frac{dx}{dy} \equiv \frac{1}{\tan\beta} = \frac{y}{(R_c^2 + y^2 \tan^2\beta)^{1/2}} \tag{3.45}$$

Note that as $y \to \infty$, $\dfrac{1}{\tan\beta} \to \dfrac{1}{\tan\beta_a}$.

The angle β is instrumental for determination of bow shock pressure rise and post-shock velocity components as follows. With reference to Figure 3.3

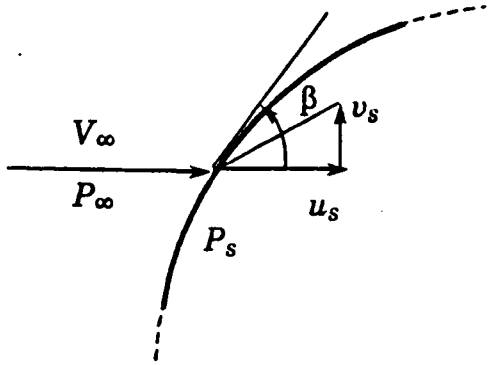


Figure 3.3: Shock Segment and Representative Velocity Vector Resolution

the Rankine-Hugoniot jump conditions are

$$\frac{p_s}{\rho_\infty V_\infty^2} = \frac{p_\infty}{\rho_\infty V_\infty^2}\left(1+\frac{2\gamma}{1+\gamma}\left(M_\infty^2\sin^2\beta-1\right)\right) \tag{3.46}$$

$$\frac{u_s}{V_\infty} = 1-\frac{2\left(M_\infty^2\sin^2\beta-1\right)}{(1+\gamma)M_\infty^2} \tag{3.47}$$

$$\frac{v_s}{V_\infty} = \frac{1}{\tan\beta}\cdot\frac{2\left(M_\infty^2\sin^2\beta-1\right)}{(1+\gamma)M_\infty^2} \tag{3.48}$$

and $\sin^2\beta$ is available from (3.45) as

$$\sin^2\beta = \frac{1}{\left(\frac{1}{\tan^2\beta}\right)+1} \tag{3.49}$$

Therefore, for each abscissa x of a grid point $P \equiv (x,y)$, see Figure 3.2, the appropriate values of y_S (the shock ordinate) and y_B (the body surface ordinate) are determined. The value y_S is computed via (3.43)-(3.44). Thereafter, $\tan\beta$ is determined via (3.45) and, consequently, the shock jump data $\frac{p_s}{\rho_\infty V_\infty^2}$, $\frac{u_s}{V_\infty}$, $\frac{v_s}{V_\infty}$, across the shock are established via (3.46)-(3.48). Subsequently, the values for $\frac{p}{\rho_\infty V_\infty^2}$, $\frac{u}{V_\infty}$,

$\frac{v}{V_\infty}$, are calculated via interpolation from the shock values to the surface pressure and velocity.

The surface pressure is initialized using the Newtonian impact model for the surface coefficient of pressure

$$C_p = 2\sin^2\theta \tag{3.50}$$

Consequently, using (3.50) the surface pressure distribution is

$$\left(\frac{p}{\rho_\infty V_\infty^2}\right) = \frac{p_\infty}{\rho_\infty V_\infty^2} + \sin^2\theta \tag{3.51}$$

for given θ and onset flow conditions, p_∞, ρ_∞, and V_∞.

The non-dimensional body tangent velocity component V_b is determined via linear interpolation from the stagnation point value, at s, to the conical value V_L, at L, thus V_b at (x_b, y_b) is

$$V_b = \left(\frac{x_b - x_s}{x_L - x_s}\right) \cdot V_L \tag{3.52}$$

Hence, the cartesian components $\frac{u_b}{V_\infty}$ and $\frac{v_b}{V_\infty}$ are determined as

$$\frac{u_b}{V_\infty} = V_b(x_b) \cdot \cos\theta(x_b, y_b) \tag{3.53}$$

$$\frac{v_b}{V_\infty} = V_b(x_b) \cdot \sin\theta(x_b, y_b) \tag{3.54}$$

Therefore, for a given onset flow condition M_∞ and V_∞, and missile geometry, hence V_L and θ, the body tangent velocity component resolution is determined.

As soon as the intial values of $\frac{p}{\rho_\infty V_\infty^2}$, $\frac{u}{V_\infty}$, $\frac{v}{V_\infty}$, are computed, density $\frac{\rho}{\rho_\infty}$ and volume specific total energy $\frac{E}{\rho_\infty V_\infty^2}$ are determined for a steady state adiabatic flow.

In these conditions, the constant total enthalpy

$$2c_pT_\infty + V_\infty^2 = 2c_pT + V^2 \tag{3.55}$$

and the ideal gas law $p = \rho\mathcal{R}T$ yield

$$\frac{\rho}{\rho_\infty} = \frac{\dfrac{2\gamma}{\gamma-1}\cdot\dfrac{p}{\rho_\infty V_\infty^2}}{\dfrac{2\gamma}{\gamma-1}\left(\dfrac{p_\infty}{\rho_\infty V_\infty^2}\right) + 1 - \left(\dfrac{V}{V_\infty}\right)^2} \tag{3.56}$$

which allows straightforward computation of density. Then, $\dfrac{E}{\rho_\infty V_\infty^2}$ is established via (1.14) as

$$\frac{E}{\rho_\infty V_\infty^2} = \frac{1}{\gamma-1}\frac{p}{\rho_\infty V_\infty^2} + \frac{1}{2}\frac{\rho}{\rho_\infty}\left[\left(\frac{u}{V_\infty}\right)^2\left(\frac{v}{V_\infty}\right)^2\right] \tag{3.57}$$

Finally, a convenient real-gas hypersonic flow initialization is assumed to coincide with an ideal gas hypersonic steady-state for the same configuration.

Part II

Finite Element

Semi-Discretization

Chapter 4

Hyberbolic System Semi-Discretization

The theory formulated in this chapter yields a minimally dissipative, spatial semi-discretization procedure for general non-linear dominantly hyperbolic conservation law systems in arbitrary curvilinear coordinates. The analytical developments proceed from the pivotal notions of approximate solution accuracy and boundedness, hence elucidate the unambiguous relation of these solution attributes with flux vector splitting constructions. The classical characteristic analysis developments, thus far the sole province of upwind schemes, are then generalized for dissipative curvilinear-coordinate integral statement synthesis.

4.1 Analytical Solution Boundedness

The fundamental relation between solution boundedness and the eigenvalues of an hyperbolic system flux vector jacobian is exemplified in this section through deter-

mination of the analytical solution for the representative conservation law system

$$\frac{\partial \overline{q}}{\partial t} + \frac{\partial \overline{f}}{\partial x} = 0 \tag{4.1}$$

$$\frac{\partial \overline{q}}{\partial t} + A\frac{\partial \overline{q}}{\partial x} = 0 \tag{4.2}$$

The analysis focuses on a jacobian matrix $A = \dfrac{\partial \overline{f}}{\partial \overline{q}}$ that exhibits the properties

1. A is constant

2. A possesses real eigenvalues and a complete set of eigenvectors X

The first property allows determination of a closed form solution, while the second is inherent in the definition of a hyperbolic system [20]. Both properties then permits identification of (4.2) with the linearized Euler equations that satisfy such an eigenvector property. The matrix A in (4.2) is then restated using the similarity transformation

$$A = X\Lambda X^{-1} \tag{4.3}$$

where the diagonal matrix Λ contains the real eigenvalues of A. Inserting (4.3) into (4.2) yields

$$\frac{\partial \overline{q}}{\partial t} + X\Lambda X^{-1}\frac{\partial \overline{q}}{\partial x} = 0 \tag{4.4}$$

Hence

$$\frac{\partial}{\partial t}\left(X^{-1}\overline{q}\right) + \Lambda\frac{\partial}{\partial x}\left(X^{-1}\overline{q}\right) = 0$$

$$\frac{\partial q}{\partial t} + \Lambda\frac{\partial q}{\partial x} = 0 \quad ; \quad q \equiv X^{-1}\overline{q} \tag{4.5}$$

since X is a constant matrix.

A solution for (4.5), hence (4.1), can be expressed in the form

$$q(x,t) = v(t)\exp(\boldsymbol{j}\omega x) \tag{4.6}$$

In (4.6), $\boldsymbol{j} \equiv \sqrt{-1}$ denotes the imaginary unit, $\frac{\omega}{2\pi}$ corresponds to the representative Fourier frequency, and $v(t)$ is an array function of time only, to be determined. Insertion of (4.6) into (4.5) yields

$$\exp(\boldsymbol{j}\omega x)\frac{dv(t)}{dt} + \boldsymbol{j}\omega\Lambda v(t)\exp(\boldsymbol{j}\omega x) = 0 \tag{4.7}$$

Consequently

$$\frac{dv(t)}{dt} + \boldsymbol{j}\omega\Lambda v(t) = 0 \tag{4.8}$$

The solution of this first order ordinary differential equation system defining $v(t)$ can be cast as

$$v(t) = \sum_{\ell=1}^{m} c_\ell \exp(-\boldsymbol{j}\omega\lambda_\ell t) \tag{4.9}$$

where m is the number of entries in $v(t)$, λ_ℓ is the representative eigenvalue in Λ, and c_ℓ are the eigenvectors of the diagonal matrix Λ expressed as

$$c_1 = b\begin{Bmatrix} 1 \\ 0 \\ \vdots \\ \vdots \\ 0 \end{Bmatrix} \; ; \; c_2 = b\begin{Bmatrix} 0 \\ 1 \\ \vdots \\ \vdots \\ 0 \end{Bmatrix} \; ; \; \cdots \; ; \; c_m = b\begin{Bmatrix} 0 \\ 0 \\ \vdots \\ \vdots \\ 1 \end{Bmatrix} \tag{4.10}$$

with b indicating an arbitrary scalar constants. Insertion of (4.9) into (4.6) yields the solution $q(x,t)$ as

$$\begin{aligned} q(x,t) &= \sum_{\ell=1}^{m} c_\ell \exp(-j\omega\lambda_\ell t)\exp(j\omega x) \\ &= \sum_{\ell=1}^{m} c_\ell \exp(j\omega(x-\lambda_\ell t)) \end{aligned} \tag{4.11}$$

which leads to classical characteristic speed interpretation for the eigenvalues λ_ℓ, owing to the explicit presence of the argument $(x - \lambda_\ell \cdot t)$. The terminal solution $\overline{q}(x,t)$ is then

$$\overline{q} = X \sum_{\ell=1}^{m} c_\ell \exp(j\omega(x-\lambda_\ell t)) \tag{4.12}$$

As a key analytical feature, the argument of the exponential remains imaginary for any value of the real eigenvalue λ_ℓ, either non-negative or non-positive. Thus, the solution $q(x,t)$ remains bounded at all times, and expresses the constant amplitude propagation of the initial $\exp(j\omega x) = \cos(\omega x) + j\sin(\omega x)$ waves in the positive and negative x-axis direction, for positive and negative eigenvalues respectively. Of theoretical significance, the solution of the parabolic perturbation to (4.1)

$$\frac{\partial \overline{q}}{\partial t} + A\frac{\partial \overline{q}}{\partial x} - \frac{1}{Pe}\frac{\partial^2 \overline{q}}{\partial x^2} = 0 \tag{4.13}$$

also remains bounded at all times, and exhibits an analogous wave propagation character, but with an exponential amplitude damping dependent upon the inverse of the Peclet number Pe as follows. System (4.13) is recast using (4.3) as

$$\frac{\partial q}{\partial t} + \Lambda\frac{\partial q}{\partial x} - \frac{1}{Pe}\frac{\partial^2 q}{\partial x^2} = 0 \tag{4.14}$$

whereupon inserting (4.6) into (4.14) yields

$$\exp(\boldsymbol{j}\omega x)\frac{dv(t)}{dt} + \left(\boldsymbol{j}\omega\Lambda + \frac{\omega^2}{Pe}I\right) v(t)\exp(\boldsymbol{j}\omega x) = 0 \tag{4.15}$$

and I is the identity matrix. Consequently,

$$\frac{dv(t)}{dt} + \boldsymbol{j}\omega\overline{\Lambda}v(t) = 0 \tag{4.16}$$

where the diagonal matrix $\overline{\Lambda}$ is

$$\overline{\Lambda} \equiv \Lambda + \frac{\omega}{\boldsymbol{j}Pe}I \tag{4.17}$$

In analogy with (4.8)-(4.9), the solution of (4.16) is then

$$\begin{aligned} v(t) &= \sum_{\ell=1}^{m} c_\ell \exp(-\boldsymbol{j}\omega\overline{\lambda_\ell}t) \\ &= \sum_{\ell=1}^{m} c_\ell \exp\left(-\boldsymbol{j}\omega\left(\lambda_\ell + \frac{\omega}{\boldsymbol{j}Pe}\right)t\right) \\ &= \exp\left(-\frac{\omega^2}{Pe}\cdot t\right)\cdot\sum_{\ell=1}^{m} c_\ell \exp\left(-\boldsymbol{j}\omega\lambda_\ell t\right) \end{aligned} \tag{4.18}$$

Therefore, the solution $q(x,t)$ of (4.14) is

$$q(x,t) = \exp\left(-\frac{\omega^2}{Pe}\cdot t\right)\cdot\sum_{\ell=1}^{m} c_\ell \exp(\boldsymbol{j}\omega(x-\lambda_\ell t)) \tag{4.19}$$

which displays the indentical wave propagation structure of (4.11), even though the wave amplitude undergoes a time damping through the exponential function $\exp\left(-\frac{\omega^2}{Pe}\cdot t\right)$ with argument proportional to the inverse Peclet number.

Therefore, any approximate solution to (4.1) or (4.13) is accurate when it exhibits an analogous wave-propagation structure, with either minimal amplitude decay, in the case of a purely hyperbolic system, or a high fidelity amplitude decrease

for a parabolic perturbation. Finally, considering that for a two-point boundary value problem a real solution of (4.13) contains components of the form

$$\begin{aligned} q_\ell(x,t) &= q_\ell(0) + \left(q_\ell\left(\frac{2\pi}{\omega}\right) - q_\ell(0) \right) \cdot \frac{\exp(\lambda_\ell Pe x) - 1}{\exp\left(\dfrac{2\pi\lambda_\ell Pe}{\omega}\right) - 1} \\ &+ \alpha \exp\left(-\frac{\omega^2}{Pe} \cdot t \right) \cdot \sin(\omega(x - \lambda_\ell t)) \ , \\ & 0 \le x \le \frac{2\pi}{\omega} \quad ; \quad \forall \ \alpha = \text{const} \end{aligned} \tag{4.20}$$

an accurate approximate solution is indispensable for the quality resolution of boudary layer structures inherent in the steady part of (4.20).

4.2 Semi-Discrete Solution Boundedness

The semi-discrete solution boundedness critically depends on the sign of the characteristic eigenvalues λ_ℓ, as developed in this section for representative second order semi-discrete schemes. Therefore, the two cases of uniform sign and mixed sign eigenvalue sets are appropriately detailed.

For a unified tratment of upwind and centered spatial semi-discretization schemes, and accurate semi-discrete equation consistent with (4.5) and (4.13) is obtained by a centered semi-discretization of a "*companion conservation law system*" associated with either (4.5) or (4.13). As developed in Section 4.3, the companion system augments (4.5) or (4.13) with a variable coefficient, characteristic-based dissipation mechanism, such that the centered semi-discretization of the terminal system yields the classical upwind or centered scheme for (4.5) or (4.13), depending on a dissipa-

tion coefficient specification. As exemplified in the following sections, the specific requirement of a characteristic based dissipation totally eliminates the need for any "foggy" empirical and trial-and-error numerical damping.

4.2.1 Uniform-Sign Eigenvalues

System (4.5) is expressed as

$$\frac{\partial q}{\partial t} + \frac{\partial f}{\partial x} = 0 \tag{4.21}$$

where $f \equiv \Lambda q$. The second time derivative of q is then

$$\frac{\partial^2 q}{\partial \tau^2}\Delta\tau = \frac{\partial}{\partial \tau}\left(\frac{\partial q}{\partial \tau}\Delta\tau\right) = -\frac{\partial}{\partial \tau}\left(\frac{\partial f}{\partial x}\Delta\tau\right)$$

$$= -\frac{\partial}{\partial \tau}\left(\frac{\partial f}{\partial q}\frac{\partial q}{\partial \tau}\Delta\tau\right) = \frac{\partial}{\partial \tau}\left(\left(\frac{\partial f}{\partial q}\right)^2 \Delta\tau \frac{\partial q}{\partial x}\right) \tag{4.22}$$

Therefore, the presence of the positive-eigenvalue matrix $\left(\frac{\partial f}{\partial q}\right)^2$ leads to a dissipative operator, expressed in the form $\beta\mathcal{L}\mathrm{sgn}(\Lambda)\frac{\partial^2 f}{\partial x^2}$, as developed in Section 4.3.

Hence, the companion conservation law system associated with (4.21) is

$$\frac{\partial q}{\partial t} + \frac{\partial f}{\partial x} - \beta\mathcal{L}\mathrm{sgn}(\Lambda)\frac{\partial^2 f}{\partial x^2} = 0 \tag{4.23}$$

The spatial semi-discretization of this system then yields an equation system consistent with (4.21) with accurate and bounded solution. The dissipation mechanism in (4.23) is characteristic based because it utilizes the second derivative of the flux vector f, as multiplied by the unique sign $\mathrm{sgn}(\Lambda)$ of the eigenvalues λ_ℓ, for the uniform sign hypothesis. Further, since $\mathrm{sgn}(\Lambda)\frac{\partial^2 f}{\partial x^2} = \frac{\partial}{\partial x}\left(\left(\mathrm{sgn}(\Lambda)\frac{\partial f}{\partial q}\right)\frac{\partial q}{\partial x}\right)$, non-negative

dissipation is induced in the companion system through the non-negative-eigenvalue matrix $\left(\text{sgn}(\Lambda)\frac{\partial f}{\partial q}\right)$. Finally, β is a positive parameter, and $\mathcal{L}$ is a reference length.

For the model system (4.5), the companion system (4.23) simplifies to

$$\frac{\partial q}{\partial t} + \Lambda\frac{\partial q}{\partial x} - \beta\mathcal{L}\text{sgn}(\Lambda)\Lambda\frac{\partial^2 q}{\partial x^2} = 0 \tag{4.24}$$

With reference to a uniform semi-discretization of the x-axis with mesh spacing Δx, $\mathcal{L}$ logically coincides with Δx, and the classical second order centered scheme for (4.24) is

$$\frac{dq_i(t)}{dt} + \Lambda\frac{q_{i+1} - q_{i-1}}{2\Delta x} - \beta\text{sgn}(\Lambda)\Lambda\left(\frac{q_{i+1} - q_i}{\Delta x} - \frac{q_i - q_{i-1}}{\Delta x}\right) = 0 \tag{4.25}$$

Thereafter, a convenient algebraic rearrangement of terms in (4.25) yields the final expression for analysis as

$$\frac{dq_i(t)}{dt} + \frac{\Lambda}{2}\left[(1 - 2\text{sgn}(\Lambda)\beta)\frac{q_{i+1} - q_i}{\Delta x} + (1 + 2\text{sgn}(\Lambda)\beta)\frac{q_i - q_{i-1}}{\Delta x}\right] = 0 \tag{4.26}$$

Significantly, (4.26) expresses a linear combination of a downwind and an upwind scheme. Thus, $\beta = 0.5$ yields the classical fully upwind scheme for (4.5), depending on sgn(Λ), while $\beta = 0$ corresponds to the centered scheme.

In direct analogy with the continuum expression (4.6), the solution of (4.24)-(4.26) is expressable as

$$q_i(t) = v(t)\exp(\boldsymbol{j}k \cdot i) \quad ; \quad 0 \leq k = \omega\Delta x \leq \pi \quad ; \quad 1 \leq i \leq M \tag{4.27}$$

for M discrete node points. Insertion of (4.27) into (4.26) yields

$$\frac{dv(t)}{dt} = -\frac{\Lambda}{2\Delta x}v(t)\left[(1 - 2\text{sgn}(\Lambda)\beta)(\exp(\boldsymbol{j}k) - 1)\right.$$

$$
\begin{aligned}
&+(1+2\mathrm{sgn}(\Lambda)\beta)(1-\exp(-\boldsymbol{j}k))] \\
= \; & -\frac{\Lambda}{2\Delta x}v(t)\left[(\exp(\boldsymbol{j}k)-\exp(-\boldsymbol{j}k))+4\mathrm{sgn}(\Lambda)\beta\right. \\
& \left.-2\mathrm{sgn}(\Lambda)\beta(\exp(\boldsymbol{j}k)+\exp(-\boldsymbol{j}k))\right] \qquad (4.28)
\end{aligned}
$$

Consequently

$$
\frac{dv(t)}{dt}+\left[\frac{2\mathrm{sgn}(\Lambda)\beta(1-\cos k)}{\Delta x}+\frac{\boldsymbol{j}\sin k}{\Delta x}\right]\Lambda v(t)=0 \qquad (4.29)
$$

The direct comparison of this fundamental ordinary differential equation system with its fully continuous counterpart (4.8) i.e.,

$$
\frac{dv(t)}{dt}+\boldsymbol{j}\omega\Lambda v(t)=0 \qquad (4.8)
$$

reveals that the spatial semi-discretization modifies the imaginary unit coefficient and induces the real term $2\mathrm{sgn}(\Lambda)\beta(1-\cos(k))/\Delta x$ in the multiplier of Λ, which engenders wave amplitude modifications. The solution of (4.29) is

$$
v(t)=\sum_{\ell=1}^{m}c_\ell\exp\left(-\lambda_\ell\left(\frac{2\mathrm{sgn}(\Lambda)\beta(1-\cos k)}{\Delta x}+\frac{\boldsymbol{j}\sin k}{\Delta x}\right)t\right) \qquad (4.30)
$$

Inserting (4.30) into (4.27) yields the solution $q_i(t)$ as

$$
\begin{aligned}
q_i(t) &= \sum_{\ell=1}^{m}c_\ell\exp\left(-\lambda_\ell\left(\frac{2\mathrm{sgn}(\Lambda)\beta(1-\cos k)}{\Delta x}+\frac{\boldsymbol{j}\sin k}{\Delta x}\right)t\right)\cdot\exp(\boldsymbol{j}ki) \\
&= \sum_{\ell=1}^{m}\exp\left(-\frac{2\lambda_\ell\mathrm{sgn}(\Lambda)\beta(1-\cos(\omega\Delta x))}{\Delta x}t\right)c_\ell\exp\left(\boldsymbol{j}\omega\left(x_i-\lambda_\ell\frac{\sin(\omega\Delta x)}{\omega\Delta x}t\right)\right)
\end{aligned} \qquad (4.31)
$$

A further direct comparison of this semi-discrete relation with its fully continuous counterpart (4.11)

$$
q(x_i,t) = \sum_{\ell=1}^{m}c_\ell\exp(\boldsymbol{j}\omega(x_i-\lambda_\ell t)) \qquad (4.11)
$$

shows that the spatial discretization triggers emergence of the dissipative term

$$d_\ell \equiv \exp\left(-\frac{2\lambda_\ell \mathrm{sgn}(\Lambda)\beta(1-\cos(\omega\Delta x))}{\Delta x}t\right) \tag{4.32}$$

in the approximate solution, and forces the semi-discrete characteristic speed

$$\widehat{\lambda}_\ell = \lambda_\ell \frac{\sin(\omega\Delta x)}{\omega\Delta x} \tag{4.33}$$

to differ from λ_ℓ in the form of a dispersive error. Expression (4.32) is certainly dissipative since the real exponential argument is constantly non-positive, while the dispersive error induces a wave phase modification. These conclusions derive from the inequalities

$$\lambda_\ell \cdot \mathrm{sgn}(\Lambda) \geq 0 \quad ; \quad 1-\cos(\omega\Delta x) \geq 0 \tag{4.34}$$

$$|\lambda_\ell| \frac{\sin(\omega\Delta x)}{\omega\Delta x} \leq |\lambda_\ell| \tag{4.35}$$

It follows that (4.31) remains bounded at all times for any non-negative value of β. Further, the exponential in (4.32) is constantly less than one, while the semi-discrete characteristic speed does not coincide with λ_ℓ. Hence, the semi-discretization error manifests itself as a wave-amplitude reduction and characteristic speed modification. Therefore, an accurate semi-discrete solution is achievable only when the wave-amplitude attenuation and the characteristic speed alteration are both minimized. This minimization is partly achieved using a refined mesh with $\Delta x \to 0$, since by the De L' Hospital rule

$$\lim_{\Delta x \to 0} \frac{1-\cos(\omega\Delta x)}{\Delta x} = \omega \lim_{\Delta x \to 0} \sin(\omega\Delta x) = 0 \tag{4.36}$$

$$\lim_{\omega\Delta x\to 0} \lambda_\ell \frac{\sin(\omega\Delta x)}{\omega\Delta x} = \lambda_\ell \tag{4.37}$$

hence both the dissipation and dispersion errors converge to zero. Therefore, for vanishing Δx and arbitrary non-negative finite value of β the semi-discrete solution (4.31) reverts to (4.11) by virtue of (4.36)-(4.37), thereby verifying for the representative case the validity of the companion conservation law system procedure. Note that a $\beta \geq 0$ is indispensable to annihilate the finite arithmetic round off errors. Whereupon, only $\beta > 0$ can generally promote stability as shown in Sections 5.61, 5.52.

4.2.2 Mixed-Sign Eigenvalues

When the eigenvalues in Λ have mixed signs, then $\text{sgn}(\Lambda)$ is no longer uniquely defined, since no uniform eigenvalue sign can exist in this case. If $\text{sgn}(\Lambda)$ is set to $+1$, then (4.32) is dissipative for the positive eigenvalues, but certainly anti-dissipative for the negative eigenvalues, and vice-versa if $\text{sgn}(\Lambda)$ is set to -1. This situation is resolved by the flux-vector splitting procedure that provides separate flux vector components with uniform eigenvalue-sign jacobians. The representative developments of the preceding section then directly apply to the semi-discretization of each flux-vector component in the governing equations.

Thus, the flux vector splitting, companion conservation law system is

$$\frac{\partial q}{\partial t} + \frac{\partial f}{\partial x} - \beta\mathcal{L}\left(\text{sgn}(\Lambda^q)\frac{\partial^2 f^q}{\partial x^2} + \text{sgn}(\Lambda^p)\frac{\partial^2 f^p}{\partial x^2}\right) = 0 \tag{4.38}$$

In (4.38), the flux vector decmposition into components f^q and f^p is arbitrary,

subject to the consistency requirement

$$f = f^q + f^p \tag{4.39}$$

Further, the diagonal matrix $\Lambda^{q,p}$, which denotes the eigenvalues of $\frac{\partial f^q}{\partial q}$ and $\frac{\partial f^p}{\partial q}$ respectively, have entries of uniform sign.

For the model system (4.5), the companion system (4.38) simplifies to

$$\frac{\partial q}{\partial t} + \Lambda \frac{\partial q}{\partial x} - \beta \mathcal{L} \left(\mathrm{sgn}(\Lambda^q) \Lambda^q \frac{\partial^2 q}{\partial x^2} + \mathrm{sgn}(\Lambda^p) \Lambda^p \frac{\partial^2 q}{\partial x^2} \right) = 0 \tag{4.40}$$

where

$$\Lambda = \Lambda^q + \Lambda^p \tag{4.41}$$

The representative uniform-spacing second order centered scheme for (4.40) is

$$\begin{aligned} \frac{dq_i(t)}{dt} &+ \Lambda^q \frac{q_{i+1} - q_{i-1}}{2\Delta x} - \mathrm{sgn}(\Lambda^q) \Lambda^q \beta \left(\frac{q_{i+1} - q_i}{\Delta x} - \frac{q_i - q_{i-1}}{\Delta x} \right) \\ &+ \Lambda^p \frac{q_{i+1} - q_{i-1}}{2\Delta x} - \mathrm{sgn}(\Lambda^p) \Lambda^p \beta \left(\frac{q_{i+1} - q_i}{\Delta x} - \frac{q_i - q_{i-1}}{\Delta x} \right) = 0 \end{aligned} \tag{4.42}$$

which, after a convenient algebraic rearrangement of terms, becomes

$$\begin{aligned} \frac{dq_i(t)}{dt} &+ \frac{\Lambda^q}{2} \left[(1 - 2\mathrm{sgn}(\Lambda^q)\beta) \frac{q_{i+1} - q_i}{\Delta x} + (1 + 2\mathrm{sgn}(\Lambda^q)\beta) \frac{q_i - q_{i-1}}{\Delta x} \right] \\ &+ \frac{\Lambda^p}{2} \left[(1 - 2\mathrm{sgn}(\Lambda^p)\beta) \frac{q_{i+1} - q_i}{\Delta x} + (1 + 2\mathrm{sgn}(\Lambda^p)\beta) \frac{q_i - q_{i-1}}{\Delta x} \right] = 0 \end{aligned} \tag{4.43}$$

This expression again corresponds to a linear combination of downwind and upwind semi-discretizations. Thus, for $\beta = 0.5$, (4.43) supplies the classical flux-vector split fully upwind scheme, depending upon both $\mathrm{sgn}(\Lambda^q)$ and $\mathrm{sgn}(\Lambda^p)$.

In direct analogy with both (4.6) and (4.27), the solution of (4.43) is expressed as

$$q_i(t) = v(t)\exp(\boldsymbol{j}k \cdot i) \quad ; \quad 0 \leq k = \omega\Delta x \leq \pi \quad ; \quad 1 \leq i \leq M \tag{4.44}$$

Inserting (4.44) into (4.43), and invoking the developments of the previous section yields

$$\begin{aligned} \frac{dv(t)}{dt} &+ \Lambda^q v(t)\left[\frac{2\mathrm{sgn}(\Lambda^q)\beta(1-\cos k)}{\Delta x} + \frac{\boldsymbol{j}\sin k}{\Delta x}\right] \\ &+ \Lambda^p v(t)\left[\frac{2\mathrm{sgn}(\Lambda^p)\beta(1-\cos k)}{\Delta x} + \frac{\boldsymbol{j}\sin k}{\Delta x}\right] = 0 \end{aligned} \tag{4.45}$$

The solution is

$$\begin{aligned} v(t) &= \sum_{\ell=m_1}^{m_2} c_\ell \exp\left(-\lambda_\ell^q\left(\frac{2\mathrm{sgn}(\Lambda^q)\beta(1-\cos k)}{\Delta x} + \frac{\boldsymbol{j}\sin k}{\Delta x}\right)t\right) \\ &+ \sum_{\ell=m_3}^{m_4} c_\ell \exp\left(-\lambda_\ell^p\left(\frac{2\mathrm{sgn}(\Lambda^p)\beta(1-\cos k)}{\Delta x} + \frac{\boldsymbol{j}\sin k}{\Delta x}\right)t\right) \end{aligned} \tag{4.46}$$

with $m_2 - m_1 + 1$ and $m_4 - m_3 + 1$ uniform-sign eigenvalues, such that $2 + m_4 + m_2 - m_1 - m_3 = m$. Insertion of (4.46) into (4.44) yields the terminal solution $q_i(t)$ as

$$\begin{aligned} q_i(t) &= \sum_{\ell=m_1}^{m_2} \exp\left(-\frac{2\lambda_\ell^q \mathrm{sgn}(\Lambda^q)\beta(1-\cos(\omega\Delta x))}{\Delta x}t\right) c_\ell \exp\left(\boldsymbol{j}\omega\left(x_i - \lambda_\ell^q\frac{\sin(\omega\Delta x)}{\omega\Delta x}t\right)\right) \\ &+ \sum_{\ell=m_3}^{m_4} \exp\left(-\frac{2\lambda_\ell^p \mathrm{sgn}(\Lambda^p)\beta(1-\cos(\omega\Delta x))}{\Delta x}t\right) c_\ell \exp\left(\boldsymbol{j}\omega\left(x_i - \lambda_\ell^p\frac{\sin(\omega\Delta x)}{\omega\Delta x}t\right)\right) \end{aligned} \tag{4.47}$$

The expression $d_\ell^{q,p}$ in (4.47), i.e.,

$$d_\ell^{q,p} \equiv \exp\left(-\frac{2\lambda_\ell^{q,p}\mathrm{sgn}(\Lambda^{q,p})\beta(1-\cos(\omega\Delta x))}{\Delta x}t\right) \tag{4.48}$$

is certainly dissipative, since the exponential real argument is constantly non-positive by virtue of

$$\lambda_\ell^{q,p} \cdot \mathrm{sgn}(\Lambda^{q,p}) \geq 0 \quad ; \quad 1 - \cos(\omega \Delta x) \geq 0 \tag{4.49}$$

Therefore, also in this case (4.47) remains bounded for any non-negative value of β.

The companion system procedure also leads to an accurate approximate solution for the parabolic perturbation (4.14). In this case, the companion system is

$$\frac{\partial q}{\partial t} + \Lambda \frac{\partial q}{\partial x} - \beta \mathcal{L}\left(\mathrm{sgn}(\Lambda^q)\Lambda^q \frac{\partial^2 q}{\partial x^2} + \mathrm{sgn}(\Lambda^p)\Lambda^p \frac{\partial^2 q}{\partial x^2}\right) - \frac{1}{Pe}\frac{\partial^2 q}{\partial x^2} = 0 \tag{4.50}$$

As detailed in Chapter 5, an accurate spatial semi-discretization consistent with (4.14) is achieved using the classical Galerkin finite element integral statement

$$\int_\Omega w \left(\frac{\partial q}{\partial t} + \Lambda \frac{\partial q}{\partial x} - \beta \mathcal{L}\left(\mathrm{sgn}(\Lambda^q)\Lambda^q \frac{\partial^2 q}{\partial x^2} + \mathrm{sgn}(\Lambda^p)\Lambda^p \frac{\partial^2 q}{\partial x^2}\right) - \frac{1}{Pe}\frac{\partial^2 q}{\partial x^2}\right) d\Omega = 0 \tag{4.51}$$

Hence, the corresponding semi-discrete statement is

$$\begin{aligned} &\int_{\Omega^h} w_i^h \left(\frac{\partial q^h}{\partial t} + \Lambda \frac{\partial q^h}{\partial x}\right) d\Omega + \\ &\quad \int_{\Omega^h} \frac{\partial w_i^h}{\partial x} \left(\beta \mathcal{L}\left(\mathrm{sgn}(\Lambda^q)\Lambda^q \frac{\partial q^h}{\partial x} + \mathrm{sgn}(\Lambda^p)\Lambda^p \frac{\partial q^h}{\partial x}\right) + \frac{1}{Pe}\frac{\partial q^h}{\partial x}\right) d\Omega = 0 \end{aligned} \tag{4.52}$$

where $\Omega^h \in \Re^1$ is the cartesian solution domain. For the representative linear trial and test space w_i^h, statement (4.52) yields

$$\begin{aligned} &\frac{1}{6}\frac{dq_{i-1}(t)}{dt} + \frac{4}{6}\frac{dq_i(t)}{dt} + \frac{1}{6}\frac{dq_{i+}(t)}{dt} = \\ &+ \Lambda^q \frac{q_{i+1} - q_{i-1}}{2\Delta x} - \left(\mathrm{sgn}(\Lambda^q)\Lambda^q \beta + \frac{1}{2\Delta x Pe}\right)\left(\frac{q_{i+1} - q_i}{\Delta x} - \frac{q_i - q_{i-1}}{\Delta x}\right) \\ &+ \Lambda^p \frac{q_{i+1} - q_{i-1}}{2\Delta x} - \left(\mathrm{sgn}(\Lambda^p)\Lambda^p \beta + \frac{1}{2\Delta x Pe}\right)\left(\frac{q_{i+1} - q_i}{\Delta x} - \frac{q_i - q_{i-1}}{\Delta x}\right) = 0 \end{aligned} \tag{4.53}$$

which, after a convenient algebraic rearrangement of terms, becomes

$$\begin{aligned}
&\frac{1}{6}\frac{dq_{i-1}(t)}{dt} + \frac{4}{6}\frac{dq_i(t)}{dt} + \frac{1}{6}\frac{dq_{i+}(t)}{dt} = \\
&+ \frac{\Lambda^q}{2}\left[(1 - 2\mathrm{sgn}(\Lambda^q)\tilde{\beta}^q)\frac{q_{i+1} - q_i}{\Delta x} + (1 + 2\mathrm{sgn}(\Lambda^q)\tilde{\beta}^q)\frac{q_i - q_{i-1}}{\Delta x}\right] \\
&+ \frac{\Lambda^p}{2}\left[(1 - 2\mathrm{sgn}(\Lambda^p)\tilde{\beta}^p)\frac{q_{i+1} - q_i}{\Delta x} + (1 + 2\mathrm{sgn}(\Lambda^p)\tilde{\beta}^p)\frac{q_i - q_{i-1}}{\Delta x}\right] = 0 \quad (4.54)
\end{aligned}$$

where

$$\tilde{\beta}^{q,p} \equiv \beta + (2\mathrm{sgn}(\lambda^{q,p})\lambda^{q,p})^{-1} \cdot \frac{1}{\Delta x Pe} \quad (4.55)$$

Inserting (4.44) into (4.54), and invoking the developments of the previous section yields

$$\begin{aligned}
a\frac{dv(t)}{dt} &+ \Lambda^q v(t)\left[\frac{2\mathrm{sgn}(\Lambda^q)\tilde{\beta}^q(1 - \cos k)}{\Delta x} + \frac{j \sin k}{\Delta x}\right] \\
&+ \Lambda^p v(t)\left[\frac{2\mathrm{sgn}(\Lambda^p)\tilde{\beta}^p(1 - \cos k)}{\Delta x} + \frac{j \sin k}{\Delta x}\right] = 0 \quad (4.56) \\
a &= \frac{2 + \cos(\omega\Delta x)}{3} \quad (4.57)
\end{aligned}$$

with solution

$$\begin{aligned}
v(t) &= \sum_{\ell=m_1}^{m_2} c_\ell \exp\left(-\lambda_\ell^q\left(\frac{2\mathrm{sgn}(\Lambda^q)\tilde{\beta}^q(1 - \cos k)}{a\Delta x} + \frac{j \sin k}{a\Delta x}\right)t\right) \\
&+ \sum_{\ell=m_3}^{m_4} c_\ell \exp\left(-\lambda_\ell^p\left(\frac{2\mathrm{sgn}(\Lambda^p)\tilde{\beta}^p(1 - \cos k)}{a\Delta x} + \frac{j \sin k}{a\Delta x}\right)t\right) \quad (4.58)
\end{aligned}$$

Therefore, the solution $q_i(t)$ is

$$\begin{aligned}
q_i(t) &= \sum_{\ell=m_1}^{m_2} \exp\left(-\frac{2\lambda_\ell^q \mathrm{sgn}(\Lambda^q)\tilde{\beta}^q(1 - \cos(\omega\Delta x))}{a\Delta x}t\right) c_\ell \exp\left(j\omega\left(x_i - \lambda_\ell^q\frac{\sin(\omega\Delta x)}{a\omega\Delta x}t\right)\right) \\
&+ \sum_{\ell=m_3}^{m_4} \exp\left(-\frac{2\lambda_\ell^p \mathrm{sgn}(\Lambda^p)\tilde{\beta}^p(1 - \cos(\omega\Delta x))}{a\Delta x}t\right) c_\ell \exp\left(j\omega\left(x_i - \lambda_\ell^p\frac{\sin(\omega\Delta x)}{a\omega\Delta x}t\right)\right) \quad (4.59)
\end{aligned}$$

Inserting (4.55) into this expression yields the terminal solution

$$\begin{aligned} q_i(t) &= \exp\left(-\frac{\omega^2}{Pe}\frac{2(1-\cos(\omega\Delta x))}{a(\omega\Delta x)^2}t\right)\times \\ &\quad \sum_{\ell=m_1}^{m_2}\exp\left(-\frac{2\lambda_\ell^q \mathrm{sgn}(\Lambda^q)\beta(1-\cos(\omega\Delta x))}{a\Delta x}t\right)c_\ell \exp\left(j\omega\left(x_i-\lambda_\ell^q\frac{\sin(\omega\Delta x)}{a\omega\Delta x}t\right)\right) \\ &+ \exp\left(-\frac{\omega^2}{Pe}\frac{2(1-\cos(\omega\Delta x))}{a(\omega\Delta x)^2}t\right)\times \\ &\quad \sum_{\ell=m_3}^{m_4}\exp\left(-\frac{2\lambda_\ell^p \mathrm{sgn}(\Lambda^p)\beta(1-\cos(\omega\Delta x))}{a\Delta x}t\right)c_\ell \exp\left(j\omega\left(x_i-\lambda_\ell^p\frac{\sin(\omega\Delta x)}{a\omega\Delta x}t\right)\right) \end{aligned} \tag{4.60}$$

which also remains bounded at all times for any non-negative value of β.

Of theoretical significance, the time derivative integral (mass matrix) in the Galerkin statement (4.52), induces the exponential argument divisor a which drastically reduces the (finite element) dispersion and natural diffusion errors in comparison to those associated with the classical finite difference analogue since

$$1 \geq \frac{3}{2+\cos(\omega\Delta x)}\cdot\frac{\sin(\omega\Delta x)}{\omega\Delta x} \geq \frac{\sin(\omega\Delta x)}{\omega\Delta x} \tag{4.61}$$

$$\left|1-\frac{3}{2+\cos(\omega\Delta x)}\cdot\frac{2(1-\cos(\omega\Delta x)}{(\omega\Delta)^2}\right| \leq \left|1-\frac{2(1-\cos(\omega\Delta x)}{(\omega\Delta)^2}\right| \tag{4.62}$$

Hence, the total dissipation in (4.60) is comprised of the natural diffusion with argument $\frac{1}{Pe}$, and the semi-discretization damping with argument β. Therefore, an accurate solution is achieved when the semi-discretization damping does not overwhelm the natural diffusion. This condition is certainly achieved for any value $\beta = \mathcal{O}(1)$, using an appropriately refined mesh, since

$$\lim_{\omega\Delta x\to 0}\frac{\omega^2}{Pe}\frac{2(1-\cos(\omega\Delta x))}{a(\omega\Delta x)^2} = \lim_{\omega\Delta x\to 0}\frac{\omega^2}{aPe}\cdot\lim_{\omega\Delta x\to 0}\frac{\sin(\omega\Delta x)}{(\omega\Delta x)} = \frac{\omega^2}{Pe} \tag{4.63}$$

is finite and converges to the continuous dissipation argument in (4.19), whereas the semi-discretization damping vanishes under the same conditions, since

$$\lim_{\omega\Delta x\to 0}\frac{1-\cos(\omega\Delta x)}{a\Delta x}=\omega\lim_{\omega\Delta x\to 0}\frac{3}{2+\cos(\omega\Delta x)}\cdot\lim_{\omega\Delta x\to 0}\sin(\omega\Delta x)=0 \qquad (4.64)$$

Further, for a fixed β and owing to the mass-matrix divisor a, the finite element damping in (4.60) is larger than the corresponding finite difference form in (4.48). Consequently, the finite element statement (4.52) yields a given dissipation magnitude with a smaller value of β which in turn leads to a more accurate semi-discretization.

In conlusion, for any non-negative value of β derivations (4.40)-(4.60) show that for the representative hyperbolic system (4.5) and parabolic perturbation (4.14), a bounded semi-discrete solution is achieved in the general mixed-sign eigenvalue case using a dissipative semi-discretization of the flux vector splitting systems (4.40) or (4.50). Also in this case, the semi-discretization induced dissipation and dispersion are reduced using a refined mesh, by virtue of relations (4.64), (4.37). Hence, the semi-discrete solutions (4.47), (4.60) also revert to their respective analytical counterparts (4.11), (4.19), which corroborates the utility of the companion system approach.

4.2.3 Fully Upwind and Companion System Semi-Discretization

The bounded approximate solution (4.60) is achievable with a general upwind semi-discretization of (4.50). For a finite ("*small*") Δx, the classical finite difference,

fully upwind scheme dissipation $(d_\ell^{q,p})_u$ is obtained from (4.60) setting $\beta = 0.5$ and $a = 1$ as

$$(d_\ell^{q,p})_u \equiv \exp\left(-\frac{\lambda_\ell^{q,p}\mathrm{sgn}(\Lambda^{q,p})(1-\cos(\omega\Delta x))}{\Delta x}t\right) \tag{4.65}$$

which corresponds to the maximum of (4.48) with respect to β. Note that an identical expression is obtained for this semi-discretization of the Euler equations subset of (1.1) with frozen jacobian. Therefore, the entire fully-upwind scheme philosophy, with or without flux vector splitting, is mathematically predicated upon the important notion of dissipative semi-discretizations leading to bounded solutions, independently of the common "more-physically-accurate-procedure" statements.

In this connection, attributing a specific physical meaning to $(d_\ell^{q,p})_u$ is a difficult issue, since this term is totally absent in the continuum solutions (4.11) and (4.19). Therefore, fully upwind schemes, with or without flux vector splitting, are important, not because they "more appropriately" represent wave propagation phenomena, but because a spatial semi-discretization in the direction opposite to the characteristic direction yields a bounded-solution dissipative scheme, even though the intrinsic dissipation, which depends upon the flux vector jacobian eigenvalues, is absent in the analytical solution.

Of theoretical significance, flux vector splittting procedures are totally independent of any upwind semi-discretization, their sole purpose being the identification of component fluxes with uniform-sign eigenvalue jacobians. Whereupon, the semi-discretization of the derivatives of these component fluxes leads to a dissipative

expression in the terminal equations, with magnitude depending on the specific semi-discretization scheme. For a fixed Δx, fully upwind scheme theories then promote induced-dissipation reduction using either a sophisticated extrapolation procedure, a limited ("clipped") anti-diffusive flux, or a higher order semi-discretization which expands the computational stencil one-sidedness.

Conversely, the companion conservation law system semi-discretization procedure can attain a minimally dissipative semi-discrete scheme within the second order centered stencil without any extrapolation technique. Considering that the induced dissipation $d^{q,p}$ (4.48) is directly proportional to β, dissipation reduction is attainable for suitable values of $\beta < 0.5$, with a rigorous selection procedure detailed in Section 5.6. The terminal scheme then retains a directional bias character.

The theoretical derivations in Section 4.2 focused on a 1-D uniform semi- discretization for a linear hyperbolic/parabolic perturbation systems, and led to conveniently interpretable results. However, for multi-dimensional curvilinear coordinate semi-discretizations of non-linear systems, the clear identification of an effective flux vector splitting, fully upwind truly multi-dimensional formula becomes algebraically rather involved. The derived companion conservation law system procedure considerably simplifies this task, as detailed in the next section, and leads to an elegant generalization of flux vector decompositions to obtain the directionally-biased Galerkin integral statements discussed in the next Chapter.

4.3 Companion Conservation Law System

The approximate solution of non-linear and multi-dimensional hyperbolic conservation law systems, like the Euler equations, requires a robust dissipative semi-discretization compatible with attainment of accurate solutions. This requirement exists since a non-dissipative convection term spatial semi-discretization may yield an unbounded dispersive error mode that propagates as mesh scale oscillations throughout the computational domain. This mode may totally corrupt the approximate solution process as well, leading to iterative divergence, especially in the presence of shock waves, rarefactions and contact discontinuities.

To prevent this degradation of the approximate solution, the companion conservation law system for general mixed hyperbolic/parabolic partial differential equation systems embeds an intrinsically non-linear multi-dimensional, hyperbolic flux characteristic-based, positive-eigenvalue dissipation term which can lead to an optimal, minimally dissipative semi-discrete statement. The induced dissipation is then minimized, to preserve physical diffusion integrity, and kept positive, to prevent an unbounded dispersive mode. The companion system dissipation is extracted from the second time derivative of the term $q \cdot \det J$, as follows.

According to the Cauchy-Kowalewski theorem [21], the solution of

$$\frac{\partial(q \cdot \det J)}{\partial t} + \frac{\partial(e_{jk} f_j)}{\partial \eta_k} = 0 \tag{4.66}$$

exists and is unique as well as analytical, in the neighborhood G of any $\boldsymbol{\eta}$-space point, where $\det J$ and A_k are analytic. Hence, a Taylor series for $q \cdot \det J$ exists in

G, and is expressed as

$$\frac{1}{\Delta\tau}(q\cdot\det J)^{n+1}=\frac{1}{\Delta\tau}(q\cdot\det J)^{n}+\left(\frac{\partial(q\cdot\det J)}{\partial\tau}\right)^{n}+\left(\frac{\partial^2(q\cdot\det J)}{\partial\tau^2}\right)^{n}\frac{\Delta\tau}{2}+\cdots \tag{4.67}$$

Therefore, the second order time derivative of $q\cdot\det J$ exists, and can be cast in terms of η_k spatial derivatives using (4.66) as

$$\begin{aligned}
\widehat{d}^{n} &\equiv \left(\frac{\partial^2(q\cdot\det J)}{\partial\tau^2}\right)^{n}\frac{\Delta\tau}{2}=\frac{\partial}{\partial\tau}\left(\frac{\partial(q\cdot\det J)}{\partial\tau}\frac{\Delta\tau}{2}\right)^{n}\\
&= \frac{\partial}{\partial\tau}\left(-\frac{\partial}{\partial\eta_k}(e_{jk}f_j)\frac{\Delta\tau}{2}\right)^{n}=\frac{\partial}{\partial\eta_k}\left(-\frac{\partial}{\partial\tau}(e_{jk}f_j)\frac{\Delta\tau}{2}\right)^{n}\\
&= \frac{\partial}{\partial\eta_k}\left(-\frac{1}{\det J}\frac{\partial(e_{jk}f_j)}{\partial q}\frac{\partial(q\cdot\det J)}{\partial\tau}\frac{\Delta\tau}{2}\right)^{n}\\
&= \frac{\partial}{\partial\eta_k}\left(\frac{1}{\det J}A_k\frac{\partial(e_{j\ell}f_j)}{\partial\eta_\ell}\frac{\Delta\tau}{2}\right)^{n}\\
&= \frac{\partial}{\partial\eta_k}\left(\frac{1}{\det J}A_kA_\ell\frac{\partial q}{\partial\eta_\ell}\frac{\Delta\tau}{2}\right)^{n}
\end{aligned} \tag{4.68}$$

The matrix product A_kA_ℓ contains the positive-eigenvalue matrices $(A_{\underline{k}})^2$, $1\le k\le n$. Hence, a dissipation operator $\widehat{d}$ at each time level is obtainable from (4.68) by contracting the indices k and ℓ.

The parameter $\Delta\tau$ in (4.68), crucial for dimensional consistency of $\widehat{d}$ with (4.66), can be recast using the generalized Courant number definition

$$C_k=\frac{a_k\Delta\tau}{\mathcal{L}_{\underline{k}}}\;\Rightarrow\;\Delta\tau=\frac{\mathcal{L}_{\underline{k}}C_{\underline{k}}}{a_{\underline{k}}} \tag{4.69}$$

where underbar denotes an indicator index not eligible for implied summation. Thus, for $\Delta\tau$, $C_{\underline{k}}$ is the k^{th} curvilinear direction Courant number, while $\mathcal{L}_{\underline{k}}$ and $a_{\underline{k}}$ are a parallel reference length and speed, respectively. The expression of the

jacobian matrix A_k with a complete set of eigenvectors X_k is

$$A_k = X_{\underline{k}} \Lambda_k X_{\underline{k}}^{-1} \tag{4.70}$$

Thus, (4.68) is expressed as

$$\begin{aligned} \widehat{d} &= \frac{\partial}{\partial \eta_k} \left(\frac{\Delta\tau}{2} \frac{1}{\det J} X_{\underline{k}} \Lambda_{\underline{k}} X_{\underline{k}}^{-1} \frac{\partial (e_{jk} f_j)}{\partial \eta_{\underline{k}}} \right) \\ &= \frac{\partial}{\partial \eta_k} \left(\frac{\Delta\tau}{2} \frac{\sqrt{e_{j\underline{k}} e_{j\underline{k}}}}{\det J} X_{\underline{k}} \left(\frac{1}{\sqrt{e_{j\underline{k}} e_{j\underline{k}}}} \Lambda_{\underline{k}} \right) X_{\underline{k}}^{-1} \frac{\partial (e_{jk} f_j)}{\partial \eta_{\underline{k}}} \right) \end{aligned} \tag{4.71}$$

The factor $\sqrt{e_{j\underline{k}} e_{j\underline{k}}}$ is associated with (4.71) for eigenvalue dimensional consistency as follows. If the curvilinear coordinates η_k are dimensionless, then the term $\frac{\sqrt{e_{j\underline{k}} e_{j\underline{k}}}}{\det J}$ is always homogeneous to the inverse of a length, whereas $\frac{\Lambda_k}{\sqrt{e_{j\underline{k}} e_{j\underline{k}}}}$ is always homogeneous to a speed. Conversely, if the curvilinear coordinates η_k are dimensional, then $\frac{\sqrt{e_{j\underline{k}} e_{j\underline{k}}}}{\det J}$ becomes a dimensionless term, whereas $\frac{\Lambda_k}{\sqrt{e_{j\underline{k}} e_{j\underline{k}}}}$ remains homogeneous to a speed. Consequently, the eigenvalues of $\frac{\Lambda_k}{\sqrt{e_{j\underline{k}} e_{j\underline{k}}}}$ are dimensionally appropriate as reference speeds for the Courant number in (4.69). Likewise, the reference length can be chosen as

$$\mathcal{L}_{\underline{k}} = \frac{\det J}{\sqrt{e_{j\underline{k}} e_{j\underline{k}}}} \mathcal{L} \tag{4.72}$$

where $\mathcal{L}$ is a single scalar parameter, homogeneous to a length when η_k is dimensionless. For the case of uniform sign eigenvalues, the reference speed is selected as the absolute value of the trace of $\frac{\Lambda_k}{\sqrt{e_{j\underline{k}} e_{j\underline{k}}}}$. Thus

$$a_{\underline{k}} \equiv |\mathrm{tr}| \equiv \left| \mathrm{tr} \left(A_{\underline{k}} / \sqrt{e_{j\underline{k}} e_{j\underline{k}}} \right) \right| \tag{4.73}$$

leading to the $\Delta\tau$ replacement

$$\Delta\tau = \frac{\dfrac{\det J}{\sqrt{e_{jk}e_{jk}}}\mathcal{L}C_{\underline{k}}}{\left|\mathrm{tr}\left(A_{\underline{k}}/\sqrt{e_{jk}e_{jk}}\right)\right|} \tag{4.74}$$

Insertion of (4.74) into (4.71) yields

$$\begin{aligned}\widehat{d} &= \frac{\partial}{\partial\eta_k}\left(\mathcal{L}\frac{C_{\underline{k}}}{2}X_{\underline{k}}\left(\frac{\Lambda_{\underline{k}}}{|\mathrm{tr}|\sqrt{e_{jk}e_{jk}}}\right)X_{\underline{k}}^{-1}\frac{\partial(e_{jk}f_j)}{\partial\eta_{\underline{k}}}\right)\\ &= \frac{\partial}{\partial\eta_k}\left(\mathcal{L}\frac{C_{\underline{k}}}{2}\mathrm{sgn}(\Lambda_{\underline{k}})X_{\underline{k}}\left(\frac{|\Lambda_{\underline{k}}|}{|\mathrm{tr}|\sqrt{e_{jk}e_{jk}}}\right)X_{\underline{k}}^{-1}\frac{\partial(e_{jk}f_j)}{\partial\eta_{\underline{k}}}\right)\end{aligned} \tag{4.75}$$

where the terminal diagonal matrix in

$$\widehat{A}_k = X_{\underline{k}}\left(\frac{|\Lambda_k|}{|\mathrm{tr}|\sqrt{e_{j\underline{k}}e_{j\underline{k}}}}\right)X_{\underline{k}}^{-1} \tag{4.76}$$

has positive eigenvalues. Furthermore, this diagonal matrix clearly satisfies the norm inequality

$$\left\|\left(\frac{|\Lambda_k|}{|\mathrm{tr}|\sqrt{e_{j\underline{k}}e_{j\underline{k}}}}\right)\right\| \leq \|I_k\| \tag{4.77}$$

where I_k is the identity matrix. Therefore, $\widehat{d}$ is simplified by replacing the diagonal matrix in (4.76) with the identity matrix , owing to (4.77). This yields

$$\begin{aligned}\widehat{d} &= \frac{\partial}{\partial\eta_k}\left(\mathcal{L}\frac{C_{\underline{k}}}{2}\mathrm{sgn}(\Lambda_{\underline{k}})X_{\underline{k}}I_{\underline{k}}X_{\underline{k}}^{-1}\frac{\partial(e_{jk}f_j)}{\partial\eta_{\underline{k}}}\right)\\ &= \frac{\partial}{\partial\eta_k}\left(\mathcal{L}\frac{C_{\underline{k}}}{2}\mathrm{sgn}(\Lambda_{\underline{k}})\frac{\partial(e_{jk}f_j)}{\partial\eta_{\underline{k}}}\right)\\ &= \frac{\partial}{\partial\eta_k}\left(\mathcal{L}\beta\mathrm{sgn}(\Lambda_{\underline{k}})\frac{\partial(e_{jk}f_j)}{\partial\eta_{\underline{k}}}\right)\end{aligned} \tag{4.78}$$

which corresponds to the multi-dimensional, curvilinear coordinate generalization of the cartesian term in (4.23). Of theoretical significance, the reference speed

specification (4.73) induces in (4.78) the non-negative eigenvalue dissipation matrix $\left(\mathrm{sgn}(\Lambda_{\underline{k}})\frac{\partial(e_{jk}f_j)}{\partial q}\right)$, with uniform-sign eigenvalues.

If the eigenvalues of $A_k = \frac{\partial(e_{jk}f_j)}{\partial q}$ have mixed sign, then flux vector splitting is utilized and the contravariant flux $(e_{jk}f_j)$ is decomposed in analogy to (4.39) as

$$e_{jk}f_j = e_{jk}f_j^q + e_{jk}f_j^p \tag{4.79}$$

such that the jacobians of the component fluxes have uniform-sign eigenvalues. Consequently, the flux vector-splitting generalization of (4.78) is

$$\begin{aligned}\hat{d} &= \frac{\partial}{\partial\eta_k}\left(\mathcal{L}\beta\mathrm{sgn}(\Lambda^q_{\underline{k}})\frac{\partial(e_{jk}f_j)^q}{\partial\eta_{\underline{k}}}\right)\\ &+ \frac{\partial}{\partial\eta_k}\left(\mathcal{L}\beta\mathrm{sgn}(\Lambda^p_{\underline{k}})\frac{\partial(e_{jk}f_j)^p}{\partial\eta_{\underline{k}}}\right)\end{aligned} \tag{4.80}$$

where the diagonal matrices $\Lambda^{q,p}$ contain the eigenvalues of $(e_{jk}f_j)^{q,p}$ respectively. Expression (4.80) is further recast to

$$\begin{aligned}\hat{d} &= \frac{\partial}{\partial\eta_k}\left(\mathcal{L}\beta\mathrm{sgn}(\Lambda^q_{\underline{k}})\frac{\partial(e_{jk}f_j)^q}{\partial q}\frac{\partial q}{\partial\eta_{\underline{k}}}\right)\\ &+ \frac{\partial}{\partial\eta_k}\left(\mathcal{L}\beta\mathrm{sgn}(\Lambda^p_{\underline{k}})\frac{\partial(e_{jk}f_j)^p}{\partial q}\frac{\partial q}{\partial\eta_{\underline{k}}}\right)\end{aligned} \tag{4.81}$$

and considering that the matrices

$$\hat{A}^{q,p}_k \equiv \mathrm{sgn}(\Lambda^{q,p}_{\underline{k}})\frac{\partial(e_{jk}f_j)^{q,p}}{\partial q} \tag{4.82}$$

both have non-negative eigenvalues, it follows that also in this case (4.80) corresponds to a dissipative operator.

The multi-dimensional curvilinear coordinate companion conservation law sys-

tem associated with the hyperbolic system (4.66) is then

$$\frac{\partial(q \cdot \det J)}{\partial t} + \frac{\partial (e_{jk} f_j)}{\partial \eta_k} -$$
$$\mathcal{L}\beta \left(\frac{\partial}{\partial \eta_k} \left(\text{sgn}(\Lambda^q_{\underline{k}}) \frac{\partial (e_{jk} f_j)^q}{\partial \eta_{\underline{k}}} \right) + \frac{\partial}{\partial \eta_k} \left(\text{sgn}(\Lambda^p_{\underline{k}}) \frac{\partial (e_{jk} f_j)^p}{\partial \eta_{\underline{k}}} \right) \right) = 0 \tag{4.83}$$

Finally, the companion system for the parabolic perturbation of (4.66) is

$$\frac{\partial(q \cdot \det J)}{\partial t} + \frac{\partial}{\partial \eta_k} \left(e_{jk} \left(f_j - f^\nu_j \right) \right) -$$
$$\mathcal{L}\beta \left(\frac{\partial}{\partial \eta_k} \left(\text{sgn}(\Lambda^q_{\underline{k}}) \frac{\partial (e_{jk} f_j)^q}{\partial \eta_{\underline{k}}} \right) + \frac{\partial}{\partial \eta_k} \left(\text{sgn}(\Lambda^p_{\underline{k}}) \frac{\partial (e_{jk} f_j)^p}{\partial \eta_{\underline{k}}} \right) \right) = 0 \tag{4.84}$$

These systems then lead to a directionally biased semi-discretization within arbitrary integral statements as shown in Chapter 5.

4.4 Euler Equation Contravariant Flux Vector Splittings

4.4.1 Contravariant Jacobian Matrix

The companion system derivations (4.67)-(4.82) apply to arbitrary hyperbolic systems with or without parabolic perturbation, since no specific form for the contravariant flux vector $e_{jk} f_j$ has been invoked. Specific relations are now developed for the Euler/Navier-Stokes equations, using the results of the generalized characteristic analysis in Section 1.6.

Recalling that the homogeneous-gas eigenvalues of $A_k \equiv \dfrac{\partial (e_{jk} f_j)}{\partial q}$ are

$$\begin{aligned} \lambda_{k_{1,n}} &= e_{jk} \frac{m_j}{\rho} \\ \lambda_{k_{n+1,n+2}} &= e_{jk} \frac{m_j}{\rho} \pm \sqrt{e_{j\underline{k}} e_{j\underline{k}}} \cdot c \end{aligned} \tag{4.85}$$

the diagonal matrix $\dfrac{\Lambda_k}{\sqrt{e_{j\underline{k}}e_{j\underline{k}}}}$ is expressable as

$$\frac{\Lambda_k}{\sqrt{e_{j\underline{k}}e_{j\underline{k}}}} = \begin{pmatrix} \dfrac{e_{jk}m_j/\rho}{\sqrt{e_{j\underline{k}}e_{j\underline{k}}}} & & & & & \\ & \dfrac{e_{jk}m_j/\rho}{\sqrt{e_{j\underline{k}}e_{j\underline{k}}}} & & & & \\ & & \dfrac{e_{jk}m_j/\rho}{\sqrt{e_{j\underline{k}}e_{j\underline{k}}}} & & & \\ & & & \dfrac{e_{jk}m_j/\rho}{\sqrt{e_{j\underline{k}}e_{j\underline{k}}}} + c & & \\ & & & & \dfrac{e_{jk}m_j/\rho}{\sqrt{e_{j\underline{k}}e_{j\underline{k}}}} - c & \end{pmatrix} \tag{4.86}$$

with absolute-value trace

$$|\mathrm{tr}| \equiv |\mathrm{tr}\left(\Lambda_k/\sqrt{e_{j\underline{k}}e_{j\underline{k}}}\right)| = (n+2)\frac{e_{jk}m_j/\rho}{\sqrt{e_{j\underline{k}}e_{j\underline{k}}}} \tag{4.87}$$

Consequently, the diagonal matrix $\dfrac{\Lambda_k}{|\mathrm{tr}|\sqrt{e_{j\underline{k}}e_{j\underline{k}}}}$ in (4.76) becomes $\dfrac{\Lambda_k}{|\mathrm{tr}|\sqrt{e_{j\underline{k}}e_{j\underline{k}}}} =$

$$\frac{\mathrm{sgn}(e_{j\underline{k}}m_j/\rho)}{n+2}\begin{pmatrix} 1 & & & & & \\ & 1 & & & & \\ & & 1 & & & \\ & & & 1+\dfrac{1}{|M_k|\mathrm{sgn}(e_{j\underline{k}}m_j/\rho)} & & \\ & & & & 1-\dfrac{1}{|M_k|\mathrm{sgn}(e_{j\underline{k}}m_j/\rho)} & \end{pmatrix} \tag{4.88}$$

This form clearly satisfies inequality (4.77). Further, for high supersonic / hypersonic flows, where $|M_k| >> 1$, (4.88) specializes to

$$\frac{\Lambda_k}{|\mathrm{tr}|\sqrt{e_{j\underline{k}}e_{j\underline{k}}}} \simeq \frac{\mathrm{sgn}(e_{j\underline{k}}m_j/\rho)}{n+2}I_k \tag{4.89}$$

which legitimizes the simplification in (4.78). Of theoretical significance, for totally arbitrary curvilinear coordinates, the eigenvalues (4.85) have uniform sign if the

magnitude of the generalized Mach number in (1.105) is not less than one. Thus, even in a curvilinear coordinate formulation, the eigenvalues (4.85) have uniform sign if the flow is locally supersonic for the generalized Mach number determination. For these conditions, no flux-vector splitting is needed to achieve a dissipative scheme. Conversely, for a locally subsonic flow, hence mixed sign eigenvalues, flux vector splitting is required to yield separate flux components with uniform-sign eigenvalue jacobians.

Any flux vector splitting theory consistent with (4.79) is admissible in the companion system procedure. As recently established [66,68], the classical flux vector splitting schemes developed for essentially uni-directional cartesian frames, and ideal gas hypotheses, undergo a reduction in stability margin for equilibrium and non-equilibrium real gas simulations, which may also become aggravated in straightforward curvilinear coordinate extensions. Therefore, the following section presents a kinematic-kinetic flux-vector splitting specifically designed for accurate real gas and multi-dimensional curvilinear coordinate bounded-solution dissipative scheme determination.

4.4.2 Kinematic-Kinetic Flux Vector Splitting

An effective flux vector splitting for accurate curvilinear coordinate real gas simulations is obtained by splitting the contravariant inviscid flux vector $e_{jk}f_j$ into

kinematic and kinetic components as follows

$$e_{jk}f_j = e_{jk}f_j^q + e_{jk}f_j^p \quad , \quad e_{jk}f_j^q \equiv \left\{ \begin{array}{c} e_{jk}m_j \\ e_{jk}\frac{m_j}{\rho}m_i + \delta_{\underline{k}}e_{ik}p \\ e_{jk}\frac{m_j}{\rho}(E+p) \end{array} \right\} \; , \; e_{jk}f_j^p \equiv \left\{ \begin{array}{c} 0 \\ (1-\delta_{\underline{k}})e_{ik}p \\ 0 \end{array} \right\} \tag{4.90}$$

where $\delta_{\underline{k}}$ is a positive partition parameter. Importantly, the explicit presence of the metric data e_{jk} in (4.90) allows direct accounting for the crucial effect of arbitrary computational cell aspect ratio upon semi-discrete algorithm stability through the contravariant flux vector component eigenvalues. This flux vector splitting, among those published, is "closest" to the unsplit inviscid flux vector, and thus preserves kinematic flux integrity.

Significantly, for arbitrary reacting gases and curvilinear coordinates, the eigenvalues of the associated jacobian matrices

$$A_k^q \equiv \frac{\partial(e_{jk}f_j^q)}{\partial q} \quad , \quad A_k^p \equiv \frac{\partial(e_{jk}f_j^p)}{\partial q} \tag{4.91}$$

are uniquely determined in closed form using the characteristic analysis procedure of Section 1.6 as: $(\lambda_k^q)_{1,3} = e_{jk}\frac{m_j}{\rho}$, $(\lambda_k^q)_{4,5} =$

$$e_{jk}\frac{m_j}{\rho} + \frac{1-\delta_{\underline{k}}}{2}e_{jk}\frac{m_j}{\rho}\left(\frac{\partial p}{\partial E}\right)_{\rho,m_j} \pm \left(\left(\frac{1-\delta_{\underline{k}}}{2}e_{jk}\frac{m_j}{\rho}\left(\frac{\partial p}{\partial E}\right)_{\rho,m_j} \right)^2 + \delta_{\underline{k}}e_{j\underline{k}}e_{jk}c^2 \right)^{1/2} \tag{4.92}$$

and

$$(\lambda_k^p)_{1,4} = 0 \; , \; (\lambda_k^p)_5 = (1-\delta_{\underline{k}})e_{jk}\left(\frac{\partial p}{\partial m_j}\right)_{\rho,E} = -\frac{(1-\delta_{\underline{k}})}{\rho}\left(\frac{\partial p}{\partial \varepsilon}\right)_\rho \left(e_{jk}\frac{m_j}{\rho}\right) \tag{4.93}$$

These eigenvalue determinations are valid for any state equation, since the pressure partial derivatives have not been replaced by any specialized relation. Therefore, the square of the speed of sound c^2 remains expressed using (1.95), repeated here for convenience as

$$c^2 = \left(\frac{\partial p}{\partial \rho}\right)_{\varepsilon} + \frac{p}{\rho^2}\left(\frac{\partial p}{\partial \varepsilon}\right)_{\rho} = \frac{m_j}{\rho}\left(\frac{\partial p}{\partial m_j}\right)_{\rho,E} + \left(\frac{\partial p}{\partial E}\right)_{\rho,m_j}\frac{(E+p)}{\rho} + \left(\frac{\partial p}{\partial \rho}\right)_{m_j,E} \tag{4.94}$$

For $\delta_{\underline{k}} = 1$, the full contravariant flux eigenvalues have uniform sign, either positive or negative, provided that

$$\left(e_{jk}\frac{m_j}{\rho}\right)^2 \geq e_{j\underline{k}}e_{jk}c^2 \quad , \quad \text{hence} \quad (M_k)^2 = \frac{(e_{jk}m_j/\rho)^2}{(e_{j\underline{k}}e_{j\underline{k}})\cdot c^2} \geq 1 \tag{4.95}$$

Consequently, if the curvilinear coordinate flow is locally supersonic, then $\delta_{\underline{k}}$ is set to one and no flux vector splitting is necessary. Conversely, if $0 \leq M_k^2 < 1$, then the flux vector splitting (4.90) yields eigenvalue sign uniformity for each split flux using an appropriate positive value of the partition parameter $0 \leq \delta_{\underline{k}} \leq 1$.

Therefore, if $\delta_{\underline{k}} < 1$ the sign of the kinematic eigenvalue coincides with the sign of $-(e_{jk}m_j/\rho)$. Concerning the kinetic flux eigenvalues, if the contravariant component of velocity $e_{jk}m_j/\rho$ is positive, then $(\lambda_k^q)_4$ is always positive, while $(\lambda_k^q)_5$ is non-negative if

$$\left(e_{jk}\frac{m_j}{\rho}\right) + \frac{(1-\delta_{\underline{k}})}{2}\left(e_{jk}\frac{m_j}{\rho}\right)\left(\frac{\partial p}{\partial E}\right)_{\rho,m_j} \geq \left(\left(\frac{(1-\delta_{\underline{k}})}{2}\left(e_{jk}\frac{m_j}{\rho}\right)\left(\frac{\partial p}{\partial E}\right)_{\rho,m_j}\right)^2 + \delta_{\underline{k}}e_{j\underline{k}}e_{jk}c^2\right)^{1/2} \tag{4.96}$$

yielding

$$\left(e_{jk}\frac{m_j}{\rho}\right)^2 + (1-\delta_{\underline{k}})\left(e_{jk}\frac{m_j}{\rho}\right)^2\left(\frac{\partial p}{\partial E}\right)_{\rho,m_j} \geq \delta_{\underline{k}} e_{j\underline{k}} e_{jk} c^2 = \frac{\delta_{\underline{k}}}{M_{\underline{k}}^2}\left(e_{jk}\frac{m_j}{\rho}\right)^2 \quad (4.97)$$

At this point, it is possible to force $(\lambda_k^q)_5$ to vanish for $0 \leq M_k \leq 1$, as in the ideal gas van Leer scheme, or to have the same sign of $(\lambda_k^q)_4$ and vanish at $M_k^2 = 1$. These two cases are respectively achieved for

$$\text{I)}\ \delta_{\underline{k}} = \frac{1+\left(\frac{\partial p}{\partial E}\right)_{\rho,m_j}}{M_{\underline{k}}^{-2}+\left(\frac{\partial p}{\partial E}\right)_{\rho,m_j}} \quad , \quad \text{II)}\ \delta_{\underline{k}} = M_{\underline{k}}^2 \quad (4.98)$$

thus, $0 < \delta_k \leq 1$ for $0 < M_k^2 \leq 1$. Note that if the k^{th} contravariant velocity component is non-positive, then identical expressions are obtained for $\delta_{\underline{k}}$ by enforcing non positivity of $(\lambda_k^q)_4$.

The analysis supplies two unique forms for $\delta_{\underline{k}}$. Therefore, a convenient terminal expression is

$$\delta_{\underline{k}} = \frac{1+\left(\frac{\partial p}{\partial E}\right)_{\rho,m_j}}{M_{\underline{k}}^{-2}+\left(\frac{\partial p}{\partial E}\right)_{\rho,m_j}}(1-\theta) + M_{\underline{k}}^2\,\theta \quad ; \quad 0 \leq \theta \leq 1 \quad (4.99)$$

Finally, the partition parameter $\delta_{\underline{k}}$ must be a piece-wise constant function, since the useful and convenient closed form for the eigenvalues (4.92)-(4.93) is only valid for a vanishing jacobian $\frac{\partial \delta_{\underline{k}}}{\partial q}$. Therefore, it is crucial for algorithm consistency and stability that expressions (4.98)-(4.99) remain constant in each and every semi-discretization computational cell.

4.4.3 Convection Acoustic Wave Flux Vector Splitting

A dissipative semi-discrete scheme can also be achieved for an appropriate value of β by employing a directional semi-discretization of only one uniform-sign flux vector component, provided that the jacobian eigenvalues of the other flux component are equal in magnitude and opposite in sign.

This situation corresponds to developing the companion system with only one uniform-sign eigenvalue split flux component, as obtained, for the Euler equations, with the following convection/acoustic wave flux vector decomposition

$$e_{jk} f_j = e_{jk} f_j^q + e_{jk} f_j^p \tag{4.100}$$

$$e_{jk} f_j^q \equiv \left\{ \begin{array}{c} e_{jk} m_j \\ e_{jk} \frac{m_j}{\rho} m_i \\ e_{jk} \frac{m_j}{\rho} E \end{array} \right\} \; , \; e_{jk} f_j^p \equiv \left\{ \begin{array}{c} 0 \\ e_{jk} p \delta_i^j \\ e_{jk} \frac{m_j}{\rho} p \end{array} \right\} \tag{4.101}$$

The eigenvalues of the associated jacobian matrices

$$A_k^q \equiv \frac{\partial (e_{jk} f_j^q)}{\partial q} \quad , \quad A_k^p \equiv \frac{\partial (e_{jk} f_j^p)}{\partial q} \tag{4.102}$$

are

$$\left\{ \begin{array}{l} \lambda_{k_{1,n+2}}^q = e_{jk} \frac{m_j}{\rho} \\ \lambda_{k_{1,n}}^p = 0 \qquad\qquad , \; \lambda_{k_{n+1,n+2}}^p = \pm \sqrt{e_{jk} e_{j\underline{k}}} \left(\frac{p}{\rho^2} \left(\frac{\partial p}{\partial \varepsilon} \right)_\rho \right)^{1/2} \end{array} \right. \tag{4.103}$$

The acoustic flux eigenvalues are equal in magnitude and opposite in sign, while the convection flux eigenvalues always have uniform sign.

Hence, $e_{jk}f_j^q$ in (4.101) is an adequate component for companion system formulation. Further, the convection flux vector $e_{jk}f_j^q$ can be expressed as

$$e_{jk}f_j^q = \left\{ \begin{array}{c} \rho \\ m_i \\ E \end{array} \right\} e_{jk}\frac{m_j}{\rho} = q \cdot e_{jk}\frac{m_j}{\rho} \tag{4.104}$$

consequently, its partial derivative with respect to η_k is

$$\frac{\partial(e_{jk}f_j^q)}{\partial \eta_k} = \frac{\partial}{\partial \eta_k}\left\{ \begin{array}{c} \rho \\ m_i \\ E \end{array} \right\} e_{jk}\frac{m_j}{\rho} + \left\{ \begin{array}{c} \rho \\ m_i \\ E \end{array} \right\} \frac{\partial}{\partial \eta_k}\left(e_{jk}\frac{m_j}{\rho}\right) \tag{4.105}$$

The eigenvalues of the jacobian matrix

$$\left(\frac{\partial q}{\partial q}\right) \cdot \left(e_{jk}\frac{m_j}{\rho}\right) = \left(\frac{\partial}{\partial q}\left\{ \begin{array}{c} \rho \\ m_i \\ E \end{array} \right\} \right) \left(e_{jk}\frac{m_j}{\rho}\right) \tag{4.106}$$

coincide with λ_k^q, whereas the eigenvalues of the matrix

$$q\frac{\partial}{\partial q}\left(e_{jk}\frac{m_j}{\rho}\right) = \left\{ \begin{array}{c} \rho \\ m_i \\ E \end{array} \right\} \frac{\partial}{\partial q}\left(e_{jk}\frac{m_j}{\rho}\right) \tag{4.107}$$

are evidently zero. Thus, the associated companion system is simply based on the lead convection term in (4.105), with $e_{jk}\dfrac{m_j}{\rho}$ conservatively replaced by the reference contravariant velocity magnitude $|\boldsymbol{u}|$

$$|\boldsymbol{u}| = \left(|e_{j1}\frac{m_j}{\rho}|^2 + |e_{j2}\frac{m_j}{\rho}|^2 + |e_{j3}\frac{m_j}{\rho}|^2 \right)^{1/2} \tag{4.108}$$

to ensure an adequate level of dissipation in regions of vanishing $e_{jk}\frac{m_j}{\rho}$, for the single convection flux component directional semi-discretization.

The terminal form of the companion conservation law system in this case is

$$\frac{\partial(q \cdot \det J)}{\partial t} + \frac{\partial}{\partial \eta_k}\left(e_{jk}\left(f_j - f_j^{\nu}\right)\right) - \beta \mathcal{L}\frac{\partial}{\partial \eta_k}\left(|\boldsymbol{u}|\frac{\partial q}{\partial \eta_k}\right) = 0 \tag{4.109}$$

The benchmark validations discussed in Chapter 10 confirm the efficiency of the Galerkin algorithm for (4.109), since it leads to stable and accurate monotone solutions for transonic, supersonic, and hypersonic flows. Therefore, (4.109) constitutes a convenient and efficient companion system for solution determinations in challenging flow regimes, and is the one considered in detail for practical implementation in this dissertation. Future investigations will undoubtedly establish the specific utility of the companion conservation law system (4.84) for the kinematic-kinetic flux vector splitting (4.90).

Chapter 5

Finite Element Integral Statements

The theoretical developments in this chapter establish that the classical Galerkin finite element integral statement coincides with a Hilbert space L_2 least-square error extremization for arbitrary non-linear conservation law systems in generalized curvilinear coordinates. Several consistent companion-system Navier Stokes statements are then formulated, which expose an appropriate directional bias character in generalized curvilinear coordinates for arbitrary sets of trial functions. The stability of the terminal semi-discrete system is then assessed using a generalized Lyapunov stability analysis within an optimal metric data procedure for an accurate and efficient algorithm.

5.1 Domain Decomposition and Approximation Basis Functions

The discretization $\hat{\Omega}^h$ to the η-space solution domain $\hat{\Omega}$

$$\hat{\Omega}^h \equiv \bigcup_e^{M_e} \left(\hat{\Omega}_e \cup \partial\hat{\Omega}_e\right) \subseteq \hat{\Omega} \cup \partial\hat{\Omega} \tag{5.1}$$

is obtained by subdividing $\hat{\Omega}$ into M_e non-overlapping finite elements, each denoted $\hat{\Omega}_e$, with exterior boundaries $\bigcup_e^{M_e} \partial\hat{\Omega}_e^h$ possibly not coincident with the outer frontier $\partial\hat{\Omega}$ of $\hat{\Omega}$. Each $\boldsymbol{\eta}$-space element $\hat{\Omega}_e$ has a constant measure (equal to 4 in 2-D). Further, the closed set $\overline{\hat{\Omega}}_e \equiv \hat{\Omega}_e \bigcup \partial\hat{\Omega}_e \subset \hat{\Omega}$ contains at least one node $\boldsymbol{x}^r$ of the discretization. Therefore, a master region $\hat{\Omega}_{e,r}$ is defined as the union of all closed sets $\overline{\hat{\Omega}}_e$ sharing node $\boldsymbol{x}^r$. This region $\hat{\Omega}_{e,r}$ constitutes the compact support of the continuous nodal trial functions $w_r^h(\boldsymbol{\eta})$, $1 \leq r \leq M$ which attain the value one at node $\boldsymbol{x}^r$, zero at all other nodes, belong to a complete set of continuous functions, differentiable within each $\hat{\Omega}_e$, and which identically vanish on all elements $\hat{\Omega}_e \notin \hat{\Omega}_{e,r}$ elsewhere in $\hat{\Omega}^h$.

Therefore, the (isoparametric) coordinate transformation [14] from the $\boldsymbol{x}$-space domain Ω onto the $\boldsymbol{\eta}$-space computational domain $\hat{\Omega}^h$ is

$$\boldsymbol{x}(\boldsymbol{\eta}) = \sum_{r=1}^{M} w_r^h(\boldsymbol{\eta}) \boldsymbol{x}^r \tag{5.2}$$

where $\boldsymbol{\eta}$ spans the finite coordinate range in each $\hat{\Omega}_e$ where $w_r^h(\boldsymbol{\eta})$ is supported. The specific relation between the partial derivatives with respect to η_i and x_j follows by direct application of (1.53)-(1.54) to (5.2). Considering that in each element $\hat{\Omega}_e$ the functions $w_r^h(\boldsymbol{\eta})$ are differentiable, the transformation partial derivatives exist, hence the fundamental invariance relation (1.62) is satisfied for transformation (5.2). Furthermore, the metric data $\left[\dfrac{\partial x_\ell}{\partial \eta_k}\right]$ computed with (5.2) become infinitesimal in any element $\hat{\Omega}_e$ coinciding with the image of a vanishing measure $\boldsymbol{x}$-space subdomain

Ω_e. This conclusion follows from, 1) the relation

$$1 = \sum_{r=1}^{M} w_r^h(\boldsymbol{\eta}) \quad , \quad \forall \quad \boldsymbol{\eta} \in \widehat{\Omega}_e \quad , \quad \forall \quad e \tag{5.3}$$

since $w_r^h(\boldsymbol{\eta})$ belongs to a complete set of functions, and 2) the convergence of all $\boldsymbol{x}^\ell$ to the single constant $\boldsymbol{x}^r$ within the vanishing Ω_e, since the coordinate transformation (5.2) is continuous.

Finally, the semi-discrete approximation $(q(\boldsymbol{x},t) \cdot \det J)^h$ to $(q(\boldsymbol{x},t) \cdot \det J)$ is then expressed in terms of the trial function set members $w_r^h(\boldsymbol{\eta})$ using a relation similar to (5.2).

5.2 Exact and Approximate-Solution Spaces

Let $\mathcal{H}$ denote the infinite dimensional Hilbert space containing the exact analytical and weak solutions $q(\boldsymbol{x},t)$ of (1.1). Since these solutions generally depend upon time, the scalar field $\mathcal{F}$ associated with $\mathcal{H}$ contains the space of Lebesgue integrable [12] functions of time $a(t)$. Therefore, the square of the L_2 norm, or "*magnitude*", of any element $h(\boldsymbol{x},t) \in \mathcal{H}$ is the function of time

$$\mathcal{V}(t) = \|h\|_{L_2}^2 \equiv \int_{\widehat{\Omega}} h(\boldsymbol{x}(\boldsymbol{\eta}),t) \cdot h(\boldsymbol{x}(\boldsymbol{\eta}),t) d\Omega \tag{5.4}$$

where $h(\boldsymbol{x},t)$ can be cast as an infinite series of elements of $\mathcal{H}$. Therefore, the semi-discrete approximate solution $(q(\boldsymbol{x},t) \cdot \det J)^h$ constitutes the projection of $(q(\boldsymbol{x},t) \cdot \det J)$ onto the finite, M dimensional and complete subspace $\mathcal{S}_M^h \subset \mathcal{H}$ of continuous functions $w_r^h(\boldsymbol{\eta})$ differentiable within each $\widehat{\Omega}_e$. Thus, $q(\boldsymbol{x},t)^h$ is expressable as the

finite summation

$$(q(\boldsymbol{x}(\boldsymbol{\eta}),t) \cdot \det J(\boldsymbol{x}(\boldsymbol{\eta})))^h = \sum_{r=1}^{M} w_r^h(\boldsymbol{\eta}) q^r(t) \det J^r \tag{5.5}$$

In (5.5), the approximate values $q^r(t)$ of $q(\boldsymbol{x},t)$ at node "r" are time dependent coefficients to be determined using an appropriate error extremization constraint.

5.3 Classical Galerkin Statement

In general, the projection $(q(\boldsymbol{x},t) \cdot \det J)^h$ does not coincide with the exact solution $q(\boldsymbol{x},t) \cdot \det J$. Hence, insertion of expansion (5.5) into the governing conservation law system

$$\frac{\partial(q \cdot \det J)}{\partial t} + \frac{\partial}{\partial \eta_k}\left(e_{jk}\left(f_j - f_j^\nu\right)\right) = 0 \tag{5.6}$$

with inclusion of the companion-system dissipation term (4.81), yields the fundamental expression

$$\begin{aligned} &\frac{\partial(q \cdot \det J)^h}{\partial t} + \frac{\partial}{\partial \eta_k}\left(e_{jk} f_j^h\right) \\ &= \varepsilon(\boldsymbol{\eta},t) + \delta(\boldsymbol{\eta},t) + \frac{\partial}{\partial \eta_k}\left(e_{jk} f_j^{\nu h}\right) \\ &+ \mathcal{L}\beta\left(\frac{\partial}{\partial \eta_k}\left(\operatorname{sgn}(\Lambda_{\underline{k}}^q)\frac{\partial(e_{jk} f_j^q)^h}{\partial \eta_{\underline{k}}}\right) + \frac{\partial}{\partial \eta_k}\left(\operatorname{sgn}(\Lambda_{\underline{k}}^p)\frac{\partial(e_{jk} f_j^p)^h}{\partial \eta_{\underline{k}}}\right)\right) \end{aligned} \tag{5.7}$$

In (5.7), $\dfrac{\partial\left(e_{jk} f_j^{\nu h}\right)}{\partial \eta_k}$ approximates $\dfrac{\partial\left(e_{jk} f_j^{\nu}\right)}{\partial \eta_k}$ and accrues to an expression analogous to, but not necessarily coincident with (5.5). Further, $\delta(\boldsymbol{\eta},t)$ denotes the component of the spatial approximation error *not* belonging to $\mathcal{S}_M^h$, which collectively corresponds to both the approximation of the fluxes in (5.6) and the inclusion of

the companion system terms. Consequently, $\varepsilon(\boldsymbol{\eta}, t)$ denotes the component of the spatial approximation error that *does* belong to $\mathcal{S}_M^h$, which may or may not coincide with the total hyperbolic-system spatial approximation error, depending on the specific approximation for the contravariant fluxes $e_{jk} f_j$. Therefore, $\varepsilon(\boldsymbol{\eta}, t) \in \mathcal{S}_M^h$ is expressable as

$$\varepsilon(\boldsymbol{\eta}, t) = \sum_{r=1}^{M} w_r^h(\boldsymbol{\eta}) a^r(t) \tag{5.8}$$

where $a^r(t)$ are time dependent (error) coefficients.

Consequently, using (5.4), the square of the L_2-norm of the total error

$$\varepsilon^T(\boldsymbol{\eta}, t) = \varepsilon(\boldsymbol{\eta}, t) + \delta(\boldsymbol{\eta}, t) \tag{5.9}$$

over $\widehat{\Omega}^h$ is

$$\begin{aligned} \mathcal{E}(t) &= \int_{\widehat{\Omega}^h} \left(\varepsilon(\boldsymbol{\eta}, t) + \delta(\boldsymbol{\eta}, t)\right)^2 d\Omega \\ &= \int_{\widehat{\Omega}^h} \left(\sum_{r=1}^{M} w_r^h(\boldsymbol{\eta}) a^r(t) + \delta(\boldsymbol{\eta}, t) \right)^2 d\Omega \end{aligned} \tag{5.10}$$

This global error $\mathcal{E}(t)$ is spatially extremizable with respect to the coefficients $a^r(t)$, yielding

$$\frac{\partial \mathcal{E}(t)}{\partial a^r(t)} = 2 \int_{\widehat{\Omega}^h} w_r^h \left(\sum_{\ell=1}^{M} w_\ell^h(\boldsymbol{\eta}) a^\ell(t) + \delta(\boldsymbol{\eta}, t) \right) d\Omega \equiv 0 \tag{5.11}$$

which prescribes the orthogonality of the total error $\varepsilon^T(\boldsymbol{\eta}, t)$ with respect to every member $w_r^h(\boldsymbol{\eta}) \in \mathcal{S}_M^h$.

Thereafter, replacing the argument of (5.11) with (5.7) leads to the classical Galerkin integral statement for (4.84) as

$$\int_{\widehat{\Omega}^h} w_r^h \frac{\partial (q \cdot \det J)^h}{\partial t} d\Omega + \int_{\widehat{\Omega}^h} w_r^h \frac{\partial}{\partial \eta_k} \left(e_{jk} \left(f_j^h - f^{\nu h} \right) \right) d\Omega -$$

$$\mathcal{L}\beta \int_{\widehat{\Omega}^h} w_r^h \left(\frac{\partial}{\partial \eta_k} \left(\mathrm{sgn}(\Lambda_{\underline{k}}^q) \frac{\partial (e_{jk} f_j^q)^h}{\partial \eta_{\underline{k}}} \right) + \frac{\partial}{\partial \eta_k} \left(\mathrm{sgn}(\Lambda_{\underline{k}}^p) \frac{\partial (e_{jk} f_j^p)^h}{\partial \eta_{\underline{k}}} \right) \right) d\Omega \equiv 0 \quad (5.12)$$

which yields exactly M ordinary differential equations for the M unknown coefficients $q^r(t)$ of the approximation (5.5). Therefore, for arbitrary conservation law systems (5.6), the classical statement (5.12) coincides with a least-square error extremization. Further, (5.5) yields an approximate solution continuous everywhere in the computational domain, with physical discontinuities to be represented by steep narrow fronts. The terminal strong convection form (5.12) thus constitutes an appropriate statement for approximate solution determination, since the integrand spatial derivatives of the convection fluxes exist almost everywhere in $\widehat{\Omega}^h$, with the possible exception of a finite number of sets with Lebesgue null-measure [12].

Of significance, the association of $\det J$ with the state variable expression (5.5), and hence within the time derivative integral in (5.12), departs from traditional finite element developments and leads to a robust and efficient numerical linear algebra solver as detailed in Chapter 9. The integral statement (5.12) is implemented with appropriate semi-discrete specifications for $\boldsymbol{f}^h$ and $\boldsymbol{f}^{\nu h}$ as

$$\boldsymbol{f}(q) \simeq \boldsymbol{f}^h(q) = \sum_{r=1}^{M} w_r^h(\boldsymbol{\eta}) \boldsymbol{f}(q^r(t)) \quad (5.13)$$

$$\boldsymbol{f}^\nu(q) \simeq \boldsymbol{f}^{\nu h}(q) = \sum_{r=1}^{M} w_r^h(\boldsymbol{\eta}) \boldsymbol{f}^\nu(q^r(t)) \quad (5.14)$$

Even though the global error $\mathcal{E}(t)$ is spatially extremized, it remains a function of time with bounded evolution not *a-priori* guaranteed. Consequently, the final con-

straint of time boundedness must be enforced on (5.12) to complete the algorithm specification. As shown in Sections 5.5 and 5.6, the presence of the companion system terms renders (5.12) an optimal dissipative, directionally biased semi-discrete system with stable solution. The induced dissipation can be efficiently minimized, to preserve physical diffusion integrity, and is kept positive to prevent an unbounded dispersive mode.

5.4 Integral Statement Consistency

Equation (5.12) is consistent with (2.1) in the sense that, for vanishing mesh measures $\left[\frac{\partial x_\ell}{\partial \eta_k}\right]$, it reverts to (2.1) without appended dissipation terms. The reference cartesian equivalent of (5.12), for an $\boldsymbol{\eta}$-space Gauss-Green transformation of the dissipation term, yields

$$
\begin{aligned}
&\int_{\Omega^h} w_r^h \frac{\partial q^h}{\partial t} d\boldsymbol{x} + \int_{\Omega^h} w_r^h \frac{\partial}{\partial x_j}\left(f_j^h - f_j^{\nu h}\right) d\boldsymbol{x} = \\
&\quad - \beta\mathcal{L} \int_{\widehat{\Omega}^h} \operatorname{sgn}(\Lambda_{\underline{k}}^q) \frac{\partial w_r^h}{\partial \eta_k} \frac{\partial}{\partial \eta_{\underline{k}}} \left(e_{jk} f_j^h\right)^q d\Omega \\
&\quad - \beta\mathcal{L} \int_{\widehat{\Omega}^h} \operatorname{sgn}(\Lambda_{\underline{k}}^p) \frac{\partial w_r^h}{\partial \eta_k} \frac{\partial}{\partial \eta_{\underline{k}}} \left(e_{jk} f_j^h\right)^p d\Omega \\
&\quad - \beta\mathcal{L} \oint_{\partial\widehat{\Omega}^h} \operatorname{sgn}(\Lambda_{\underline{k}}^q) w_r^h \frac{\partial}{\partial \eta_{\underline{k}}} \left(e_{jk} f_j^h\right)^q \widehat{n}_k d\Gamma_\eta \\
&\quad - \beta\mathcal{L} \oint_{\partial\widehat{\Omega}^h} \operatorname{sgn}(\Lambda_{\underline{k}}^p) w_r^h \frac{\partial}{\partial \eta_{\underline{k}}} \left(e_{jk} f_j^h\right)^p \widehat{n}_k d\Gamma_\eta = \\
&\quad - \beta\mathcal{L} \int_{\Omega^h} \operatorname{sgn}(\Lambda_{\underline{k}}^q) \frac{\partial w_r^h}{\partial x_\ell} \left(\frac{\partial x_\ell}{\partial \eta_k} \frac{e_{jk}}{\det J} \frac{\partial x_n}{\partial \eta_{\underline{k}}}\right) \frac{\partial}{\partial x_n} \left(f_j^h\right)^q d\boldsymbol{x} \\
&\quad - \beta\mathcal{L} \int_{\Omega^h} \operatorname{sgn}(\Lambda_{\underline{k}}^p) \frac{\partial w_r^h}{\partial x_\ell} \left(\frac{\partial x_\ell}{\partial \eta_k} \frac{e_{jk}}{\det J} \frac{\partial x_n}{\partial \eta_{\underline{k}}}\right) \frac{\partial}{\partial x_n} \left(f_j^h\right)^p d\boldsymbol{x}
\end{aligned}
$$

$$
\begin{aligned}
&- \beta\mathcal{L}\oint_{\partial\Omega^h} \mathrm{sgn}(\Lambda^q_{\underline{k}}) w_r^h \frac{\partial (f_j^q)^h}{\partial x_\ell}\left(\frac{\partial x_\ell}{\partial \eta_{\underline{k}}} e_{jk} e^{-1}_{ik}\right) n_i d\Gamma \\
&- \beta\mathcal{L}\oint_{\partial\Omega^h} \mathrm{sgn}(\Lambda^p_{\underline{k}}) w_r^h \frac{\partial (f_j^p)^h}{\partial x_\ell}\left(\frac{\partial x_\ell}{\partial \eta_{\underline{k}}} e_{jk} e^{-1}_{ik}\right) n_i d\Gamma
\end{aligned} \tag{5.15}
$$

Whereupon, all the right hand integrals tend to zero for any value of β, since all terms in parentheses are directly proportional to the vanishing mesh measures $\left[\frac{\partial x_\ell}{\partial \eta_k}\right]$. Under these conditions, the following relations also hold

$$
\begin{aligned}
\int_{\Omega^h} w_r^h \frac{\partial q^h}{\partial t} d\boldsymbol{x} &\rightarrow \int_\Omega w_r \frac{\partial q}{\partial t} d\boldsymbol{x} \\
\int_{\Omega^h} w_r^h \frac{\partial}{\partial x_j}\left(f_j^h - f_j^{\nu h}\right) d\boldsymbol{x} &\rightarrow \int_\Omega w \frac{\partial}{\partial x_j}\left(f_j - f_j^\nu\right) d\boldsymbol{x}
\end{aligned} \tag{5.16}
$$

Consequently, (5.12) converges to, hence is consistent with (2.1). QED

5.5 Directional Bias Character

According to (4.79), the semi-discrete contravariant flux $\left(e_{jk} f_j^h\right)$ is expressed as

$$
e_{jk} f_j^h = \left(e_{jk} f_j^q\right)^h + \left(e_{jk} f_j^p\right)^h \tag{5.17}
$$

Hence, the integral statement (5.12) becomes

$$
\begin{aligned}
&\int_{\widehat{\Omega}^h_{e,\underline{r}}} w_r^h \frac{\partial (q \cdot \det J)^h}{\partial t} d\Omega - \int_{\widehat{\Omega}^h_{e,\underline{r}}} w_r^h \frac{\partial \left(e_{jk} f^{\nu h}\right)}{\partial \eta_k} d\Omega \\
&\quad + \int_{\widehat{\Omega}^h_{e,\underline{r}}} w_r^h \left(\frac{\partial}{\partial \eta_k}\left(e_{jk} f_j^q\right)^h - \mathcal{L}\beta \mathrm{sgn}(\Lambda^q_{\underline{k}})\left(\frac{\partial}{\partial \eta_k}\left(\frac{\partial (e_{j\underline{k}} f_j)^q}{\partial \eta_k}\right)\right)\right) d\Omega \\
&\quad + \int_{\widehat{\Omega}^h_{e,\underline{r}}} w_r^h \left(\frac{\partial}{\partial \eta_k}\left(e_{jk} f_j^p\right)^h - \mathcal{L}\beta \mathrm{sgn}(\Lambda^p_{\underline{k}})\left(\frac{\partial}{\partial \eta_k}\left(\frac{\partial (e_{j\underline{k}} f_j)^p}{\partial \eta_k}\right)\right)\right) d\Omega = 0
\end{aligned} \tag{5.18}
$$

where $\widehat{\Omega}^h_{e,\underline{r}} \subset \widehat{\Omega}^h$ is the representative master region where $w_r^h(\boldsymbol{\eta})$ is supported.

In analogy with (5.15), and using the relation $w_r^h(\partial\widehat{\Omega}_{e,\underline{r}}^h) = 0$, the dissipation integrals are restated, using an $\boldsymbol{\eta}$-space Gauss-Green transformation, as

$$\int_{\widehat{\Omega}_{e,\underline{r}}^h} w_r^h \frac{\partial(q \cdot \det J)^h}{\partial t} d\Omega - \int_{\widehat{\Omega}_{e,\underline{r}}^h} w^h \frac{\partial\left(e_{jk} f^{\nu h}\right)}{\partial \eta_k} d\Omega$$

$$+ \int_{\widehat{\Omega}_{e,\underline{r}}^h} \left(w_r^h + \mathcal{L}\beta \mathrm{sgn}(\Lambda_{\underline{k}}^q) \frac{\partial w_r^h}{\partial \eta_{\underline{k}}}\right) \frac{\partial}{\partial \eta_k} \left(e_{jk} f_j^q\right)^h d\Omega$$

$$+ \int_{\widehat{\Omega}_{e,\underline{r}}^h} \left(w_r^h + \mathcal{L}\beta \mathrm{sgn}(\Lambda_{\underline{k}}^p) \frac{\partial w_r^h}{\partial \eta_{\underline{k}}}\right) \frac{\partial}{\partial \eta_k} \left(e_{jk} f_j^p\right)^h d\Omega = 0 \tag{5.19}$$

Further, the region $\widehat{\Omega}_{e,\underline{r}}^h \subset \widehat{\Omega}^h$ is decomposed as

$$\widehat{\Omega}_{e,\underline{r}}^h = \widehat{\Omega}_{e,\underline{r}}^{h_{k^+}} \bigcup \widehat{\Omega}_{e,\underline{r}}^{h_{k^-}} \tag{5.20}$$

such that

$$\frac{\partial w_r^h}{\partial \eta_k} \left(\widehat{\Omega}_{e,\underline{r}}^{h_{k^+}}\right) \geq 0 \quad , \quad \frac{\partial w_r^h}{\partial \eta_k} \left(\widehat{\Omega}_{e,\underline{r}}^{h_{k^-}}\right) \leq 0 \tag{5.21}$$

This decomposition exists since $w_r^h(\boldsymbol{\eta})$ is continuous and belongs to a complete set of functions satisfying (5.3).

Inserting (5.20)-(5.21) into (5.19) then yields

$$\int_{\widehat{\Omega}_{e,\underline{r}}^h} w_r^h \frac{\partial(q \cdot \det J)^h}{\partial t} d\Omega - \int_{\widehat{\Omega}_{e,\underline{r}}^h} w_r^h \frac{\partial}{\partial \eta_k} \left(e_{jk} f^{\nu h}\right) d\Omega$$

$$+ \int_{\widehat{\Omega}_{e,\underline{r}}^{h_{k^+}}} \left(w_r^h + \mathcal{L}\beta \mathrm{sgn}(\Lambda_{\underline{k}}^q) \left|\frac{\partial w_r^h}{\partial \eta_{\underline{k}}}\right|\right) \frac{\partial}{\partial \eta_k} \left(e_{jk} f_j^q\right)^h d\Omega$$

$$+ \int_{\widehat{\Omega}_{e,\underline{r}}^{h_{k^-}}} \left(w_r^h - \mathcal{L}\beta \mathrm{sgn}(\Lambda_{\underline{k}}^q) \left|\frac{\partial w^h}{\partial \eta_{\underline{k}}}\right|\right) \frac{\partial}{\partial \eta_k} \left(e_{jk} f_j^q\right)^h d\Omega$$

$$+ \int_{\widehat{\Omega}_{e,\underline{r}}^{h_{k^+}}} \left(w_r^h + \mathcal{L}\beta \mathrm{sgn}(\Lambda_{\underline{k}}^p) \left|\frac{\partial w_r^h}{\partial \eta_{\underline{k}}}\right|\right) \frac{\partial}{\partial \eta_k} \left(e_{jk} f_j^p\right)^h d\Omega$$

$$+ \int_{\widehat{\Omega}_{e,\underline{r}}^{h_{k^-}}} \left(w_r^h - \mathcal{L}\beta \mathrm{sgn}(\Lambda_{\underline{k}}^p) \left|\frac{\partial w_r^h}{\partial \eta_k}\right|\right) \frac{\partial}{\partial \eta_k} \left(e_{jk} f_j^p\right)^h d\Omega = 0 \tag{5.22}$$

Expression (5.22) constitutes the fundamental semi-discrete integral statement with embedded directional biased integration of the inviscid-flux partial derivatives, depending on $\mathrm{sgn}(\Lambda_k^{q,p})$, for each contravariant flux component. This conclusion follows from the presence of the terminal weight functions $w_r^{\widehat{d}\pm}$

$$w_r^{\widehat{d}\pm} \equiv w_r^h \pm \mathcal{L}\beta \mathrm{sgn}(\Lambda_{\underline{k}}^{q,p}) \left| \frac{\partial w_r^h}{\partial \eta_k} \right| \tag{5.23}$$

Hence, (5.22) represents a linear combination of $\boldsymbol{\eta}$-space "upwind" and "downwind schemes". Of theoretical significance, (5.22) constitutes the rigorous curvilinear coordinate generalization of the directionally biased cartesian scheme (4.54).

This generalization applies to arbitrary curvilinear coordinates, owing to the contravariant flux vector splitting. Furthermore, this pivotal result is achieved without any restriction on the shape of the region $\widehat{\Omega}_{e,\underline{r}}^h$, or type of the continuous piece-wise differentiable trial/weight functions $w_r^h(\boldsymbol{\eta})$.

Therefore, (5.22) is crucial for arbitrary unstructured grid semi-discretizations, providing an unambiguous statement for direct and non-empirical, directionally-biased scheme determinations. Further, (5.22) also shows that the companion conservation law procedure yields a terminal statement that preserves integrity of the inviscid contravariant fluxes in (5.6), since the terminal semi-discretization corresponds to a linear combination of flux derivative integrations with weights (5.23). The magnitute of the combination weights then varies in direct proportion to β. The variable or constant value for this fundamental parameter is rigorously determined, using the generalized Lyapunov semi-discretization stability analysis, in the

following section.

5.6 Lyapunov Semi-Discretization Stability Analysis

The fundamental semi-discretization stability analysis is formulated for the real-gas Navier-Stokes CFD integral statement (5.22) for the unequivocal assessment in curvilinear coordinates of the effect of actual solution distribution as well as mesh non-uniformity and non-orthogonality on semi-discrete algorithm stability. The analysis completes the synthesis of the minimally dissipative scheme on totally arbitrary meshes. This analysis is performed using a generalization of the classical Lyapunov method, presented in Section 3.11. Therefore, after identifying a suitable, positive definite Lyapunov functional $\mathcal{V}$, its time derivative is formulated in terms of any subset of (5.6) to yields unambiguous and general sufficient stability conditions. These constraints then show that β can be optimally selected as a nodal parameter $\beta_{\underline{r}}$ to minimize a local oscillatory Gibbs phenomenon.

For an accurate Navier-Stokes CFD algorithm with uncompromised physical diffusion effects, the contravariant convection flux semi-discretization must be minimally dissipative, as outlined at the end of Section 4.22. Therefore, the minimal dissipation stability analysis naturally focuses on the Euler equation subset of (5.6). The convenient Lyapunov functional for weak statement replacement has been determined as

$$\mathcal{V} = \sum_{r=1}^{M} \left(\int_{\widehat{\Omega}^h} w_r^h \overline{\left(X_{\underline{r}}^{-1} q \det J \right)}^T d\boldsymbol{\eta} \cdot \int_{\widehat{\Omega}^h} w_r^h \left(X_{\underline{r}}^{-1} q \det J \right) d\boldsymbol{\eta} \right) \geq 0 \qquad (5.24)$$

where overbar signifies complex conjugation, and $X_{\underline{r}}$ is an element-wise constant matrix of eigenvectors. The time derivative of $\mathcal{V}$, and associated sufficient non-linear stability condition, is then

$$\begin{aligned}
\frac{d\mathcal{V}}{dt} &= \sum_{r=1}^{M}\left(\int_{\widehat{\Omega}^h} w_r^h\left(X_{\underline{r}}^{-1}\frac{\partial(\overline{q\det J})}{\partial t}\right)^T d\boldsymbol{\eta}\cdot\int_{\widehat{\Omega}^h} w_r^h\left(X_{\underline{r}}^{-1}q\det J\right)d\boldsymbol{\eta}\right) \\
&+ \sum_{r=1}^{M}\left(\int_{\widehat{\Omega}^h} w_r^h\overline{\left(X_{\underline{r}}^{-1}q\det J\right)}^T d\boldsymbol{\eta}\cdot\int_{\widehat{\Omega}^h} w_r^h\left(X_{\underline{r}}^{-1}\frac{\partial(q\det J)}{\partial t}\right)d\boldsymbol{\eta}\right) \\
&= \sum_{r=1}^{M}\left(\int_{\widehat{\Omega}^h} w_r^h\left(X_{\underline{r}}^{-1}q\det J\right)^T d\boldsymbol{\eta}\cdot\int_{\widehat{\Omega}^h} w_r^h\left(X_{\underline{r}}^{-1}\frac{\partial(\overline{q\det J})}{\partial t}\right)d\boldsymbol{\eta}\right) \\
&+ \sum_{r=1}^{M}\left(\int_{\widehat{\Omega}^h} w_r^h\overline{\left(X_{\underline{r}}^{-1}q\det J\right)}^T d\boldsymbol{\eta}\cdot\int_{\widehat{\Omega}^h} w_r^h\left(X_{\underline{r}}^{-1}\frac{\partial(q\det J)}{\partial t}\right)d\boldsymbol{\eta}\right)\leq 0 \qquad (5.25)
\end{aligned}$$

Note that the sum of the real parts of all terms in (5.25) leads to an equivalent and convenient stability condition.

5.6.1 One- Dimensional Stability Criteria

For the representative 1-D linear companion system

$$\frac{\partial q}{\partial t}+\frac{\partial f}{\partial \eta}-\mathcal{L}\beta\left(\frac{\partial}{\partial\eta}\left(\mathrm{sgn}(\Lambda^q)\frac{\partial f^q}{\partial\eta}+\frac{\partial}{\partial\eta}\left(\mathrm{sgn}(\Lambda^p)\frac{\partial f^p}{\partial\eta}\right)\right)\right)=0 \qquad (5.26)$$

with

$$x\equiv\eta \quad ; \quad \frac{\partial f}{\partial\eta}=A\frac{\partial q}{\partial\eta}=X\Lambda X^{-1}\frac{\partial q}{\partial\eta} \qquad (5.27)$$

and

$$f=f^q+f^p \quad ; \quad f^q=X\Lambda^q X^{-1}q \quad ; \quad f^p=X\Lambda^p X^{-1}q \qquad (5.28)$$

the Galerkin statement (5.19) is

$$\int_{\widehat{\Omega}^h} w_r^h\frac{\partial q^h}{\partial t}d\Omega = \; - \; \int_{\widehat{\Omega}^h}\left(w_r^h+\mathcal{L}\beta\mathrm{sgn}(\Lambda_{\underline{k}}^q)\frac{\partial w_r^h}{\partial\eta}\right)\frac{\partial f^{qh}}{\partial\eta}d\Omega$$

$$- \int_{\widehat{\Omega}^h} \left(w_r^h + \mathcal{L}\beta \mathrm{sgn}(\Lambda_{\underline{k}}^q) \frac{\partial w_r^h}{\partial \eta} \right) \frac{\partial f^{qh}}{\partial \eta} d\Omega \tag{5.29}$$

Introducing the compact notation

$$w_r^h (1 + \beta^{q,p}) \equiv \left(w_r^h + \mathcal{L}\beta \mathrm{sgn}(\Lambda_{\underline{k}}^{q,p}) \frac{\partial w_r^h}{\partial \eta} \right) \tag{5.30}$$

and replacing the time derivative integrals in (5.25) with (5.29) yields

$$\begin{aligned}
&\sum_{r=1}^{M} \left(\int_{\widehat{\Omega}^h} w_r^h \left(X_{\underline{r}}^{-1} q^h \right)^T \, d\eta \cdot \right. \\
&\quad \left. \left(\int_{\widehat{\Omega}^h} w_r^h \left(X_{\underline{r}}^{-1} \frac{\partial \overline{f}^{qh}}{\partial \eta} (1 + \beta^q) + \frac{\partial \overline{f}^{ph}}{\partial \eta} (1 + \beta^p) \right) \, d\eta \right) \right) + \\
&\sum_{r=1}^{M} \left(\int_{\widehat{\Omega}^h} w_r^h \left(X_{\underline{r}}^{-1} \overline{q}^h \right)^T \, d\eta \cdot \right. \\
&\quad \left. \left(\int_{\widehat{\Omega}^h} w_r^h \left(X_{\underline{r}}^{-1} \frac{\partial f^{qh}}{\partial \eta} (1 + \beta^q) + \frac{\partial f^{ph}}{\partial \eta} (1 + \beta^p) \right) \, d\eta \right) \right) \geq 0
\end{aligned} \tag{5.31}$$

Inserting (5.28) into (5.31), and identifying $X_{\underline{r}}$ with X then yields

$$\begin{aligned}
&\sum_{r=1}^{M} \left(\int_{\widehat{\Omega}^h} w_r^h \left(X^{-1} q^h \right)^T \, d\eta \cdot \right. \\
&\quad \left. \left(\int_{\widehat{\Omega}^h} w_r^h \left(\Lambda^q \frac{\partial (X^{-1} \overline{q}^h)}{\partial \eta} (1 + \beta^q) + \Lambda^p \frac{\partial (X^{-1} \overline{q}^h)}{\partial \eta} (1 + \beta^p) \right) \, d\eta \right) \right) + \\
&\sum_{r=1}^{M} \left(\int_{\widehat{\Omega}^h} w_r^h \left(X^{-1} \overline{q}^h \right)^T \, d\eta \cdot \right. \\
&\quad \left. \left(\int_{\widehat{\Omega}^h} w_r^h \left(\Lambda^q \frac{\partial (X^{-1} q^h)}{\partial \eta} (1 + \beta^q) + \Lambda^p \frac{\partial (X^{-1} q^h)}{\partial \eta} (1 + \beta^p) \right) \, d\eta \right) \right) \geq 0
\end{aligned} \tag{5.32}$$

which constitutes a rigorous stability condition.

In analogy with (4.27), $q(\eta,t)^h$ can be expressed as

$$q(\eta,t)^h = \sum_{r=1}^{M} \tilde{v}(t) w_r^h(\eta) \exp(j\overline{\omega}\cdot r) \quad ; \quad 0 \le \overline{\omega} \le \pi \tag{5.33}$$

since (5.26) is linear. Inserting this resolution into (5.32) yields

$$\sum_{r=1}^{M} v(t)^T \left(\int_{\widehat{\Omega}^h} w_r^h \cdot s(\overline{\omega},\eta) d\eta \cdot \left(\int_{\widehat{\Omega}^h} w_r^h \cdot g(\overline{\omega},\eta) \left(\Lambda^q (1+\beta^q) + \Lambda^p (1+\beta^p) \right) \, d\eta \right) \right) v(t) \ge 0 \tag{5.34}$$

where $s(\overline{\omega},\eta)$ and $g(\overline{\omega},\eta)$ are positive real functions and $v(t) \equiv X^{-1}\tilde{v}(t)$. Recalling now the directional biased expression (5.22), the analytical integration of (5.34) for the representative 1-D linear basis with $\mathcal{L} = 2$, and with (5.30), yields

$$\sum_{r=1}^{M} h(\overline{\omega}) v(t)^T \left(\Lambda^q (1 + 2\mathrm{sgn}(\Lambda^q)\beta) - \Lambda^q (1 - 2\mathrm{sgn}(\Lambda^q)\beta) \right) v(t) + \sum_{r=1}^{M} h(\overline{\omega}) v(t)^T \left(\Lambda^p (1 + 2\mathrm{sgn}(\Lambda^p)\beta) - \Lambda^p (1 - 2\mathrm{sgn}(\Lambda^p)\beta) \right) v(t) \ge 0 \tag{5.35}$$

where $h(\overline{\omega})$ is a positive real function.

At this point, the single β in (5.76) is replaced with a local $\beta_{\underline{r}}$ for a minimally dissipative algorithm. Thus, (5.35) becomes

$$\sum_{r=1}^{M} h(\overline{\omega}) v(t)^T \left(\mathrm{sgn}(\Lambda^q) \Lambda^q \beta_{\underline{r}} \right) v(t) + \sum_{r=1}^{M} h(\overline{\omega}) v(t)^T \left(\mathrm{sgn}(\Lambda^p) \Lambda^p \beta_{\underline{r}} \right) v(t) \ge 0 \tag{5.36}$$

which stipulates non-negative definiteness of the argument matrices. Evidently, (5.20) is satisfied if each term is non-negative. Thus, to minimize emergence of a local Gibbs oscillatory phenomenon, this stability condition is enforced at each and every node "r" with local value of $\beta_{\underline{r}}$ determined by the constraint

$$v(t)^T \left(\mathrm{sgn}(\Lambda^q) \Lambda^q \beta_{\underline{r}} \right) v(t) + v(t)^T \left(\mathrm{sgn}(\Lambda^p) \Lambda^p \beta_{\underline{r}} \right) v(t) \ge 0 \tag{5.37}$$

However, the diagonal matrices in (5.37) are already non-negative definite due to the flux vector splitting (5.28). Therefore stability under these conditions is achieved for any

$$\beta_{\underline{r}} \geq 0 \tag{5.38}$$

This condition conforms with the independently obtained results in Section 4.2. Therefore, derivations (5.31)-(5.37) corroborate the validity of the Lyapunov analysis. Further, for the non-linear case they lead to a sharper stability constraint than that supplied by classical linearized stability analysis, as follows. For a quasi non-linear stability analysis, expressions (5.28) are obtained after freezing the jacobian matrix A in each element $\widehat{\Omega}_e^h \in \widehat{\Omega}_{e,r}^h$. Thereafter, identifying $X_{\underline{r}}$ with the frozen value of X at node "$r-1/2$" and repeating derivations (5.31)-(5.35) yields the global stability condition

$$\begin{aligned}
&\sum_{r=1}^{M} h(k) v(t)^T \left(\Lambda^q_{r-1/2}(1 + 2\mathrm{sgn}(\Lambda^q)\beta_{\underline{r}}) - \tilde{\Lambda}^q_{r+1/2}(1 - 2\mathrm{sgn}(\Lambda^q)\beta_{\underline{r}}) \right) v(t) + \\
&\sum_{r=1}^{M} h(k) v(t)^T \left(\Lambda^p_{r-1/2}(1 + 2\mathrm{sgn}(\Lambda^p)\beta_{\underline{r}}) - \tilde{\Lambda}^p_{r+1/2}(1 - 2\mathrm{sgn}(\Lambda^q)\beta_{\underline{r}}) \right) v(t) \geq 0
\end{aligned} \tag{5.39}$$

where

$$\begin{aligned}
\tilde{\Lambda}^q_{r+1/2} &= X^{-1}_{r-1/2} X_{r+1/2} \Lambda^q_{r+1/2} X^{-1}_{r+1/2} X_{r-1/2} \\
\tilde{\Lambda}^q_{r+1/2} &= X^{-1}_{r-1/2} X_{r+1/2} \Lambda^p_{r+1/2} X^{-1}_{r+1/2} X_{r-1/2}
\end{aligned} \tag{5.40}$$

The associated nodal constraint is then

$$v(t)^T \left(\Lambda^q_{r-1/2}(1 + 2\mathrm{sgn}(\Lambda^q)\beta_{\underline{r}}) - \tilde{\Lambda}^q_{r+1/2}(1 - 2\mathrm{sgn}(\Lambda^q)\beta_{\underline{r}}) \right) v(t) +$$

$$v(t)^T \left(\Lambda^p_{r-1/2}(1 + 2\text{sgn}(\Lambda^p)\beta_{\underline{r}}) - \tilde{\Lambda}^p_{r+1/2}(1 - 2\text{sgn}(\Lambda^q)\beta_{\underline{r}}) \right) v(t) \geq 0 \quad (5.41)$$

For the approximations $X^{-1}_{r-1/2}X_{r+1/2} \simeq I$ and $X^{-1}_{r-1/2}X_{r+1/2} \simeq I$, with I denoting the identity matrix, (5.41) simplifies to

$$v(t)^T \left(\Lambda^q_{r-1/2}(1 + 2\text{sgn}(\Lambda^q)\beta_{\underline{r}}) - \Lambda^q_{r+1/2}(1 - 2\text{sgn}(\Lambda^q)\beta_{\underline{r}}) \right) v(t) +$$

$$v(t)^T \left(\Lambda^p_{r-1/2}(1 + 2\text{sgn}(\Lambda^p)\beta_{\underline{r}}) - \Lambda^p_{r+1/2}(1 - 2\text{sgn}(\Lambda^q)\beta_{\underline{r}}) \right) v(t) \geq 0 \quad (5.42)$$

If $\beta_r = 0.5$, then (5.42) is certainly verified, since non-negative definite diagonal matrices remain in (5.42). Conversely, if $\beta_r = 0.0$, then (5.42) may fail, since differences of non-negative definite matrices remain. Therefore, a value of β_r exists in the range

$$0.0 < \beta_r < 0.5 \quad (5.43)$$

satisfying (5.42).

The classical linearized stability analysis [9] assumes a frozen jacobian matrix A throughout the master region $\widehat{\Omega}_{e,r}$. Hence, the terminal stability constraint for β_r is (5.38) itself. However, such an inequality yields an unacceptably vague value for β_r in the non-linear case. Conversely, the Lyapunov constraint (5.42) sharpens the classical result, and provides an unambiguous relation to determine β_r.

5.6.2 Multi-Dimensional Curvilinear Coordinate Stability Criteria

For a general multi-dimensional, curvilinear coordinate and non-linear hyperbolic conservation law system, the time derivative integrals in the sufficient stability

condition (5.25) with local $\beta_{\underline{r}}$ are

$$\int_{\widehat{\Omega}^h} w_r^h \frac{\partial (q \cdot \det J)^h}{\partial t} d\Omega = - \int_{\widehat{\Omega}^h} \left(w_r^h + \mathcal{L}\beta_{\underline{r}} \mathrm{sgn}(\Lambda_{\underline{k}}^q) \frac{\partial w_r^h}{\partial \eta_{\underline{k}}} \right) \frac{\partial}{\partial \eta_k} \left(e_{jk} f_j^q \right)^h d\Omega$$
$$- \int_{\widehat{\Omega}^h} \left(w_r^h + \mathcal{L}\beta_{\underline{r}} \mathrm{sgn}(\Lambda_{\underline{k}}^p) \frac{\partial w_r^h}{\partial \eta_{\underline{k}}} \right) \frac{\partial}{\partial \eta_k} \left(e_{jk} f_j^p \right)^h d\Omega \tag{5.44}$$

Introducing the compact notation

$$w_r^h \left(1 + \beta_{\underline{r},\underline{k}}^{q,p} \right) \equiv \left(w_r^h + \mathcal{L}\beta_{\underline{r}} \mathrm{sgn} \left(\Lambda_{\underline{k}}^{q,p} \right) \frac{\partial w_r^h}{\partial \eta_{\underline{k}}} \right) \tag{5.45}$$

and replacing the time derivative integrals in (5.25) with (5.44) yields

$$\sum_{r=1}^{M} \left(\int_{\widehat{\Omega}^h} w_r^h \left(X_{\underline{r}}^{-1} (q \det J)^h \right)^T d\boldsymbol{\eta} \cdot \right.$$
$$\left. \left(\int_{\widehat{\Omega}^h} w_r^h X_{\underline{r}}^{-1} e_{jk} \left(\frac{\partial \overline{f}_j^{qh}}{\partial \eta_k} (1 + \beta_{\underline{r},\underline{k}}^q) + \frac{\partial \overline{f}_j^{ph}}{\partial \eta_k} (1 + \beta_{\underline{r},\underline{k}}^p) \right) d\boldsymbol{\eta} \right) \right) +$$

$$\sum_{r=1}^{M} \left(\int_{\widehat{\Omega}^h} w_r^h \left(X_{\underline{r}}^{-1} (\overline{q \det J})^h \right)^T d\boldsymbol{\eta} \cdot \right.$$
$$\left. \left(\int_{\widehat{\Omega}^h} w_r^h X_{\underline{r}}^{-1} e_{jk} \left(\frac{\partial f_j^{qh}}{\partial \eta_k} (1 + \beta_{\underline{r},\underline{k}}^q) + \frac{\partial f_j^{ph}}{\partial \eta_k} (1 + \beta_{\underline{r},\underline{k}}^{ph}) \right) d\boldsymbol{\eta} \right) \right) \geq 0 \tag{5.46}$$

This inequality can be expressed in terms of jacobian matrices as

$$\sum_{r=1}^{M} \left(\int_{\widehat{\Omega}^h} w_r^h \left(X_{\underline{r}}^{-1} (q \det J)^h \right)^T d\boldsymbol{\eta} \cdot \right.$$
$$\left. \left(\int_{\widehat{\Omega}^h} w_r^h X_{\underline{r}}^{-1} \frac{e_{jk}}{\det J} \left(\overline{A}_j^{qh} (1 + \beta_{\underline{r},\underline{k}}^q) + \overline{A}_j^{ph} (1 + \beta_{\underline{r},\underline{k}}^p) \right) X_{\underline{r}} X_{\underline{r}}^{-1} \frac{\partial \overline{q \det J}}{\partial \eta_k} d\boldsymbol{\eta} \right) \right) +$$

$$\sum_{r=1}^{M} \left(\int_{\widehat{\Omega}^h} w_r^h \left(X_{\underline{r}}^{-1} (\overline{q \det J})^h \right)^T d\boldsymbol{\eta} \cdot \right.$$
$$\left. \left(\int_{\widehat{\Omega}^h} w_r^h X_{\underline{r}}^{-1} \frac{e_{jk}}{\det J} \left(A_j^{qh} (1 + \beta_{\underline{r},\underline{k}}^q) + A_j^{ph} (1 + \beta_{\underline{r},\underline{k}}^p) \right) X_{\underline{r}} X_{\underline{r}}^{-1} \frac{\partial q \det J}{\partial \eta_k} d\boldsymbol{\eta} \right) \right) \geq 0 \tag{5.47}$$

which constitutes a rigorous, fully non-linear sufficient stability condition.

Equation (5.47) then leads to a stability condition for a CFD algorithm that allows wave propagation at all grid-supported frequencies, but prevents unbounded amplitude growth. This refinement corresponds to a generalized quasi-non-linear stability analysis, which employs frozen jacobians in each element $\widehat{\Omega}_e \in \widehat{\Omega}_{e,r}$, as introduced in the previous section. With this specification, and in analogy with (4.27) and (5.33), the dependent variable $(q(\boldsymbol{\eta},t)\cdot \det J)^h$ can be expressed as

$$(q(\boldsymbol{\eta},t)\cdot \det J)^h = \sum_{r=1}^{M} v(t) w_r^h(\boldsymbol{\eta}) \exp(\boldsymbol{j}\overline{\boldsymbol{\omega}}_k \cdot r_k) \quad ; \quad 0 \le \overline{\omega}_k \le \pi \quad ; \quad \forall \ k \qquad (5.48)$$

where r_k denotes the k^{th}-direction node number associated with the global node r. For notational compactness, the grid frequencies $\overline{\omega}_r$ are denoted as $\overline{\boldsymbol{\omega}} \equiv \{\overline{\omega}_k\}$. Inserting resolution (5.48) into (5.47) yields

$$\begin{aligned}
&\sum_{r=1}^{M} v(t)^T \int_{\widehat{\Omega}^h} w_r^h s(\overline{\boldsymbol{\omega}},\boldsymbol{\eta})\, d\boldsymbol{\eta} \cdot \\
&\quad \left(\int_{\widehat{\Omega}^h} w_r^h \overline{g}_k(\overline{\boldsymbol{\omega}},\boldsymbol{\eta}) X_{\underline{r}}^{-1} \frac{e_{jk}}{\det J} \left(A_j^{qh}(1+\beta_{\underline{r},\underline{k}}^{q}) + A_j^{ph}(1+\beta_{\underline{r},\underline{k}}^{ph}) \right) X_{\underline{r}}\, d\boldsymbol{\eta} \right) v(t) + \\
&\sum_{r=1}^{M} v(t)^T \int_{\widehat{\Omega}^h} w_r^h s(\overline{\boldsymbol{\omega}},\boldsymbol{\eta})\, d\boldsymbol{\eta} \cdot \\
&\quad \left(\int_{\widehat{\Omega}^h} w_r^h g_k(\overline{\boldsymbol{\omega}},\boldsymbol{\eta}) X_{\underline{r}}^{-1} \frac{e_{jk}}{\det J} \left(A_j^{qh}(1+\beta_{\underline{r},\underline{k}}^{q}) + A_j^{ph}(1+\beta_{\underline{r},\underline{k}}^{p}) \right) X_{\underline{r}}\, d\boldsymbol{\eta} \right) v(t) = \\
&\sum_{r=1}^{M} v(t)^T \int_{\widehat{\Omega}^h} w_r^h s(\overline{\boldsymbol{\omega}},\boldsymbol{\eta}) d\boldsymbol{\eta} \cdot \\
&\quad \left(\int_{\widehat{\Omega}^h} w_r^h g_{kR}(\overline{\boldsymbol{\omega}},\boldsymbol{\eta}) X_{\underline{r}}^{-1} \frac{e_{jk}}{\det J} \left(A_j^{qh}(1+\beta_{\underline{r},\underline{k}}^{q}) + A_j^{ph}(1+\beta_{\underline{r},\underline{k}}^{p}) \right) X_{\underline{r}}\, d\boldsymbol{\eta} \right) v(t) \ge 0
\end{aligned} \qquad (5.49)$$

where $s(\overline{\boldsymbol{\omega}},\boldsymbol{\eta})$ and $g_{kR}(\overline{\boldsymbol{\omega}},\boldsymbol{\eta})$ are strictly positive real functions, and $v(t) = X_{\underline{r}}^{-1}\tilde{v}(t)$.

Of theoretical significance, (5.49) can be integrated analytically, upon identification of a specific trial/test space function. Recalling the directional biased expression (5.22), and using (5.45), the closed form integration of (5.49) for the representative case of a positive eigenvalue matrix $e_{jk}A_j^{qh}$ and a 2-D Lagrange bilinear basis, with $\mathcal{L} = \Delta\eta_{\underline{k}} = 2$, yields

$$\begin{aligned}
\sum_{r=1}^{M} v^T(t) X_{\underline{r}}^{-1} \Bigg(\Bigg(& h_{11}(\overline{\omega}) \cdot \frac{(e_{j1})_{P_{r1}}}{(\det J)_{P_{r1}}} \left(A_j^{qh}\right)_{P_{r1}} + h_{12}(\overline{\omega}) \cdot \frac{(e_{j2})_{P_{r1}}}{(\det J)_{P_{r1}}} \left(A_j^{qh}\right)_{P_{r1}} \Bigg) (1+2\beta_{\underline{r}}) \\
& + \left(h_{11}(\overline{\omega}) \cdot \frac{(e_{j1})_{P_{r1}}}{(\det J)_{P_{r1}}} \left(A_j^{ph}\right)_{P_{r1}} + h_{12}(\overline{\omega}) \cdot \frac{(e_{j2})_{P_{r1}}}{(\det J)_{P_{r1}}} \left(A_j^{ph}\right)_{P_{r1}} \right) (1-2\beta_{\underline{r}}) \\
& + \left(h_{21}(\overline{\omega}) \cdot \frac{(e_{j1})_{P_{r4}}}{(\det J)_{P_{r4}}} \left(A_j^{qh}\right)_{P_{r4}} + h_{22}(\overline{\omega}) \cdot \frac{(e_{j2})_{P_{r2}}}{(\det J)_{P_{r2}}} \left(A_j^{qh}\right)_{P_{r2}} \right) (1+2\beta_{\underline{r}}) \\
& + \left(h_{21}(\overline{\omega}) \cdot \frac{(e_{j1})_{P_{r4}}}{(\det J)_{P_{r4}}} \left(A_j^{ph}\right)_{P_{r4}} + h_{22}(\overline{\omega}) \cdot \frac{(e_{j2})_{P_{r2}}}{(\det J)_{P_{r2}}} \left(A_j^{ph}\right)_{P_{r2}} \right) (1-2\beta_{\underline{r}}) \\
& - \left(h_{11}(\overline{\omega}) \cdot \frac{(e_{j1})_{P_{r3}}}{(\det J)_{P_{r3}}} \left(A_j^{qh}\right)_{P_{r3}} + h_{12}(\overline{\omega}) \cdot \frac{(e_{j2})_{P_{r3}}}{(\det J)_{P_{r3}}} \left(A_j^{qh}\right)_{P_{r3}} \right) (1-2\beta_{\underline{r}}) \\
& - \left(h_{11}(\overline{\omega}) \cdot \frac{(e_{j1})_{P_{r3}}}{(\det J)_{P_{r3}}} \left(A_j^{ph}\right)_{P_{r3}} + h_{12}(\overline{\omega}) \cdot \frac{(e_{j2})_{P_{r3}}}{(\det J)_{P_{r3}}} \left(A_j^{ph}\right)_{P_{r3}} \right) (1+2\beta_{\underline{r}}) \\
& - \left(h_{21}(\overline{\omega}) \cdot \frac{(e_{j1})_{P_{r2}}}{(\det J)_{P_{r2}}} \left(A_j^{qh}\right)_{P_{r2}} + h_{22}(\overline{\omega}) \cdot \frac{(e_{j2})_{P_{r4}}}{(\det J)_{P_{r4}}} \left(A_j^{qh}\right)_{P_{r4}} \right) (1-2\beta_{\underline{r}}) \\
& - \left(h_{21}(\overline{\omega}) \cdot \frac{(e_{j1})_{P_{r2}}}{(\det J)_{P_{r2}}} \left(A_j^{ph}\right)_{P_{r2}} + h_{22}(\overline{\omega}) \cdot \frac{(e_{j2})_{P_{r4}}}{(\det J)_{P_{r4}}} \left(A_j^{ph}\right)_{P_{r4}} \right) (1+2\beta_{\underline{r}}) \Bigg) X_{\underline{r}} v(t) \geq 0
\end{aligned} \tag{5.50}$$

which can expressed in compact form as

$$\begin{aligned}
& \sum_{r=1}^{M} v^T(t) X_{\underline{r}}^{-1} \left(A_r^{h1}(1+2\beta_{\underline{r}}) - A_r^{h3}(1-2\beta_{\underline{r}}) \right) X_{\underline{r}} v(t) + \\
& \sum_{r=1}^{M} v^T(t) X_{\underline{r}}^{-1} \left(A_r^{h4}(1+2\beta_{\underline{r}}) - A_r^{h2}(1-2\beta_{\underline{r}}) \right) X_{\underline{r}} v(t) \geq 0
\end{aligned} \tag{5.51}$$

In (5.51), the matrices $A_r^{h\ell}$, $1 \leq \ell \leq 4$ are defined as

$$A_r^{h\ell} \equiv h_{i(\ell)k}(\overline{\omega}) \cdot \frac{(e_{jk})_{P_{r\ell}}}{(\det J)_{P_{r\ell}}} \left[\left(A_j^{qh}\right)_{P_{r\ell_{\underline{k}}}} + \left(A_j^{ph}\right)_{P_{r\ell_{\underline{k}}}} \frac{1-2\beta_{\underline{r}}}{1+2\beta_{\underline{r}}} \right], \ell = 1,4 \tag{5.52}$$

$$A_r^{h\ell} \equiv h_{i(\ell)k}(\overline{\omega}) \cdot \frac{(e_{jk})_{P_{r\ell}}}{(\det J)_{P_{r\ell}}} \left[\left(A_j^{qh}\right)_{P_{r\ell_{\underline{k}}}} + \left(A_j^{ph}\right)_{P_{r\ell_{\underline{k}}}} \frac{1+2\beta_{\underline{r}}}{1-2\beta_{\underline{r}}} \right], \ell = 2,3 \quad (5.53)$$

with $i(1) = i(3) = 1$, $i(2) = i(4) = 2$, as well as $P_{r\ell_{\underline{1}}} = P_{r\ell_{\underline{2}}} = P_{r\ell}$ for $\ell = 1,3$, $P_{r\ell_{\underline{2}}} = P_{r4}$ for $\ell = 2$, and $P_{r\ell_{\underline{2}}} = P_{r2}$ for $\ell = 4$. The terms $h_{ij}(\overline{\omega})$ in (5.50) then denote the real functions

$$\begin{aligned}
h_{11}(\overline{\omega}) &= 2\left(2\left(1-\cos\left(\overline{\omega}_1\right)\right)+\cos\left(\overline{\omega}_2\right)-\cos\left(\overline{\omega}_1+\overline{\omega}_2\right)\right) \\
h_{12}(\overline{\omega}) &= 2\left(2\left(1-\cos\left(\overline{\omega}_2\right)\right)+\cos\left(\overline{\omega}_1\right)-\cos\left(\overline{\omega}_1+\overline{\omega}_2\right)\right) \\
h_{21}(\overline{\omega}) &= 2\left(2\left(1-\cos\left(\overline{\omega}_1\right)\right)+\cos\left(\overline{\omega}_2\right)-\cos\left(\overline{\omega}_1-\overline{\omega}_2\right)\right) \\
h_{22}(\overline{\omega}) &= 2\left(2\left(1-\cos\left(\overline{\omega}_2\right)\right)+\cos\left(\overline{\omega}_1\right)-\cos\left(\overline{\omega}_1-\overline{\omega}_2\right)\right) \qquad (5.54)
\end{aligned}$$

which are strictly non-negative when $0 \leq \overline{\omega}_k \leq \pi$. The locations $P_{r\ell}$ the become identified with the optimal evaluation points developed in Section 5.8 and Chapter 6.

Of fundamental importance, (5.50)-(5.51) stipulate non-negative definiteness of the argument matrices. Evidently, (5.51) is satisfied if each term is non-negative. Thus, in order to minimize emergence of a local Gibbs oscillatory phenomenon, this bounded wave amplitude stability condition is enforced at each and every mesh node "r" with value of β_r determined by imposing the pivotal stability-matrix non-negative definiteness local condition

$$\begin{aligned}
v^T(t)X_{\underline{r}}^{-1} \quad & \left(A_r^{h1}(1+2\beta_{\underline{r}}) - A_r^{h3}(1-2\beta_{\underline{r}}) + \right. \\
& \left. A_r^{h4}(1+2\beta_{\underline{r}}) - A_r^{h2}(1-2\beta_{\underline{r}})\right) X_{\underline{r}} v(t) \geq 0 \qquad (5.55)
\end{aligned}$$

This expression can be considerably simplified from a theoretical point of view

by equating $X_{\underline{r}}$ to the matrix of eigenvectors associated with the whole linear combination of matrices in (5.55). Inserting this specification for $X_{\underline{r}}$ into (5.55) yields the efficient stability condition

$$v^T(t)\ \Lambda_r\ v(t) \geq 0 \tag{5.56}$$

which is directly satisfied by determining β_r such that the eigenvalues in the diagonal matrix Λ_r become all non-negative. However, it may be arduous, if not impractical to determine these eigenvalues in closed form for this X_r.

As an alternative, X_r may be equated to the eigenvectors X_r^ℓ of the simpler matrix $A_r^{h\ell}$ (5.52)-(5.53). Inserting this specification for $X_{\underline{r}}$ into (5.55) yields

$$\begin{aligned} v(t)^T \quad & \left(\tilde{\Lambda}_r^{h1}(1+2\beta_{\underline{r}}) - \tilde{\Lambda}_r^{h3}(1-2\beta_{\underline{r}}) + \right. \\ & \left. \tilde{\Lambda}_r^{h4}(1+2\beta_{\underline{r}}) - \tilde{\Lambda}_r^{h2}(1-2\beta_{\underline{r}})\right) v(t) \geq 0 \end{aligned} \tag{5.57}$$

where

$$\left(\tilde{\Lambda}_r^{hs}\right) \ = \ \left((X_r^\ell)^{-1}\right) X_r^s \Lambda_r^{hs} \left((X_r^s)^{-1}\right) X_r^\ell \tag{5.58}$$

for the diagonal eigenvalue matrix Λ_r^{hs}. The fundamental condition (5.57) can then be directly enforced, hence the local value of $\beta_{\underline{r}}$ is determined using the simple and convenient non-negativity constraint for the Gauss LU decomposition pivots of the given matrix symmetric part. Importantly, these purely analytical selections of X_r, and associated value of β_r, correspond to the geometric requirement of an intrinsically multi-dimensional directionally biased semi-discretization.

For the approximations

$$\left((X_r^\ell)^{-1}\right) X_r^s \simeq I \quad ; \quad \left((X_r^s)^{-1}\right) X_r^\ell \simeq I \quad ; \quad \ell \neq s \tag{5.59}$$

the constraint (5.57) is even simpler, since the matrices $\left(\tilde{\Lambda}_r^{h\ell}\right)$ reduce to diagonal eigenvalue matrices. Furthermore, the simplest form of (5.57) is obtained at a node "r" where flux vector splitting is either not required, or required only along a few directions, since in this case some, if not all, matrices $\left(A_j^{ph}\right)_{P_{r\ell}}$ are no longer present in $A_r^{h\ell}$.

If the eigenvalues of the jacobian matrix $e_{jk}A_j^q$ are positive, then for $\beta_r = 0$, the matrices in (5.50) may be negative definite, since they result from a difference of positive eigenvalue matrices. Conversely, if $\beta_r = 0.5$, only positive eigenvalues matrices are left in (5.50). Consequently, the developed stability condition can be satisfied for $0 \leq \beta_r \leq 0.5$. Identical conclusions are then reached for a negative-eigenvalue matrix $e_{jk}A_j$, by replacing β_r with $-\beta_r$. Furthermore, it is readily verified that β_r reduces to zero under mesh refinement for any choice of X_r. To reach this conclusion, express (5.55), for example, in the form

$$2\beta_{\underline{r}} v(t)^T X_{\underline{r}}^{-1} \left(\left(A_r^{h1} + A_r^{h3}\right) + \left(A_r^{h4} + A_r^{h2}\right)\right) X_{\underline{r}} v(t) \geq$$

$$v(t)^T X_{\underline{r}}^{-1} \left(\left(A_r^{h3} - A_r^{h1}\right) + \left(A_r^{h2} - A_r^{h4}\right)\right) X_{\underline{r}} v(t) \tag{5.60}$$

Thus, as the mesh is refined, the rhs of (5.60) tends to zero, hence $\beta_{\underline{r}}$ also tends to zero, since the lhs matrix does not reduce to the zero matrix. Therefore, the product of $\beta_{\underline{r}}$ and the dissipation terms in (5.44) converges to zero at a high rate

with mesh refinement since both the companion system dissipation (see Section 5.4) and β_τ simultaneously tend to zero.

The developed stability condition intrinsically depends upon the local mesh aspect ratios via the presence of the metric data in (5.50)-(5.51). Therefore, the value of β_τ will depend upon the solution level and local mesh distribution. Consequently, for any given mesh, the developed procedure can always generate an optimal minimal dissipation semi-discretization in a direct manner. Conversely, any fully upwind scheme corresponds to $\beta_\tau = 0.5$, hence introduces maximum local dissipation. Of fundamental significance, for a fixed β_τ the mesh can be locally adapted, hence the metric data $\frac{e_{jk}}{\det J}$ varied, to satisfy the developed stability criteria and therefore attain an optimal order-of-accuracy semi-discretization. The feasibility of this approach awaits to be fully ascertained in future investigations.

Evidently, the magnitude of the induced dissipation, hence the value of β_τ, directly affects the convergence rate. This recognition yields an optimal convergence rate control in conjunction with an accurate solution determination using the variation of β_τ. Specifically, if only a steady-state is desired then $\beta_\tau = 0.5$ during the transient is suitable. Therafter, at convergence, β_τ is progressively reduced locally to satisfy (5.50)-(5.51), hence achieve the optimally stable and accurate solution for the given grid. If instead, accurate transients are also needed, then β_τ must satisfy (5.50)-(5.51) at each time level and sub-iteration stage. Therefore, implementation of the developed jacobian matrix non-negative definitness condition for the dynamic

determination of β_r, hence achievement of the strategic convergence rate control, yields a distinctively efficient overall CFD algorithm.

5.7 Convection / Acoustic Flux Decomposition Integral Statement

The Galerkin integral statement for the companion system (4.109) is

$$\int_{\widehat{\Omega}^h} w_r^h \left[\frac{\partial}{\partial t} (q \cdot \det J)^h + \frac{\partial}{\partial \eta_\ell} \left(e_{k\ell} \left(f_k^h - f_k^{\nu h} \right) \right) - \mathcal{L} \beta_r \frac{\partial}{\partial \eta_\ell} \left(|\boldsymbol{u}| \frac{\partial q^h}{\partial \eta_\ell} \right) \right] d\boldsymbol{\eta} = 0 \quad (5.61)$$

For the finite element Lagrange bilinear basis specification $w_\ell^h(\boldsymbol{\eta}) = N_\ell(\boldsymbol{\eta})$, the expansions for $\boldsymbol{f}^h$ and $\boldsymbol{f}^{\nu h}$ in terms of cartesian components are selected as

$$\boldsymbol{f}^h \Rightarrow f_j^h \equiv \left\{ \begin{array}{c} N_\ell m_j^\ell(t) \\ u_j^k(t) N_k N_\ell m_i^\ell(t) + N_\ell p^\ell(t) \delta_{ij} \\ u_j^k(t) N_k N_\ell (E^\ell(t) + p^\ell(t)) \end{array} \right\} \quad (5.62)$$

$$\boldsymbol{f}^{\nu h} \Rightarrow f_j^{\nu h} \equiv \left\{ \begin{array}{c} 0 \\ \frac{g_\mu^v(t) N_v}{Re} \left[\frac{e_{js}}{\det J} \frac{\partial N_\ell}{\partial \eta_s} u_i^\ell(t) + \frac{e_{is}}{\det J} \frac{\partial N_\ell}{\partial \eta_s} u_j^\ell(t) - \frac{2}{3} \frac{e_{rs}}{\det J} \frac{\partial N_\ell}{\partial \eta_s} u_r^\ell(t) \delta_{ij} \right] \\ \frac{u_i^v(t) g_\mu^v(t) N_v}{Re} \left[\frac{e_{js}}{\det J} \frac{\partial N_\ell}{\partial \eta_s} u_i^\ell(t) + \frac{e_{is}}{\det J} \frac{\partial N_\ell}{\partial \eta_s} u_j^\ell(t) \right. \\ \left. - \frac{2}{3} \frac{e_{rs}}{\det J} \frac{\partial N_\ell}{\partial \eta_s} u_r^\ell(t) \delta_{ij} \right] + \frac{g_\theta^v(t) N_v}{Pe} \frac{e_{js}}{\det J} \frac{\partial N_\ell}{\partial \eta_s} T^\ell(t) \end{array} \right\} \quad (5.63)$$

where

$$u_j^\ell(t) \equiv \frac{m_j^\ell(t)}{\rho^\ell(t)} \quad (5.64)$$

Inserting specifications (5.5) and (5.62)-(5.64) into (5.61) yields the terminal ordinary differential equation system containing

$$\int_{\widehat{\Omega}^h} N_r N_\ell \frac{d}{dt}(\rho^\ell(t) \det J^\ell)\, d\boldsymbol{\eta} + \int_{\widehat{\Omega}^h} e_{jk} N_r \frac{\partial N_\ell}{\partial \eta_k} m_j^\ell(t)\, d\boldsymbol{\eta}$$
$$+ \mathcal{L}\beta_{\underline{r}} \int_{\widehat{\Omega}^h} |\boldsymbol{u}^s(t)| N_s \frac{\partial N_r}{\partial \eta_\ell} \frac{\partial N_k}{\partial \eta_\ell} \rho^k(t)\, d\boldsymbol{\eta} = 0 \tag{5.65}$$

for the continuity equation,

$$\int_{\widehat{\Omega}^h} N_r N_\ell \frac{d}{dt}(m_i^\ell(t) \det J^\ell)\, d\boldsymbol{\eta}$$
$$+ \int_{\widehat{\Omega}^h} e_{jk} N_r u_j^s(t) \frac{\partial (N_s N_\ell)}{\partial \eta_k} m_i^\ell(t)\, d\boldsymbol{\eta} + \int_{\widehat{\Omega}^h} e_{jk} N_r \frac{\partial N_\ell}{\partial \eta_k} p^\ell(t) \delta_{ij}\, d\boldsymbol{\eta}$$
$$+ \frac{1}{Re} \int_{\widehat{\Omega}^h} g_\mu^v(t) N_v \frac{e_{jk}}{\det J} \frac{\partial N_r}{\partial \eta_k} \left[e_{js} \frac{\partial N_\ell}{\partial \eta_s} u_i^\ell(t) + e_{is} \frac{\partial N_\ell}{\partial \eta_s} u_j^\ell(t) - \frac{2}{3} e_{ks} \frac{\partial N_\ell}{\partial \eta_s} u_k^\ell(t) \delta_{ij} \right] d\boldsymbol{\eta}$$
$$+ \mathcal{L}\beta_{\underline{r}} \int_{\widehat{\Omega}^h} |\boldsymbol{u}^s(t)| N_s \frac{\partial N_r}{\partial \eta_\ell} \frac{\partial N_k}{\partial \eta_\ell} m_i^k(t)\, d\boldsymbol{\eta} = 0 \tag{5.66}$$

for the momentum equations, $1 \leq i \leq n$, and

$$\int_{\widehat{\Omega}^h} N_r N_\ell \frac{d}{dt}(E^\ell(t) \det J^\ell)\, d\boldsymbol{\eta} + \int_{\widehat{\Omega}^h} e_{jk} N_r u_j^s(t) \frac{\partial (N_s N_\ell)}{\partial \eta_k} (\, E^\ell(t) + p^\ell(t)\,)\, d\boldsymbol{\eta}$$
$$+ \frac{1}{Re} \int_{\widehat{\Omega}^h} u_i^v(t) g_\mu^v(t) N_v \frac{e_{jk}}{\det J} \frac{\partial N_r}{\partial \eta_k} \left[e_{js} \frac{\partial N_\ell}{\partial \eta_s} u_i^\ell(t) + e_{is} \frac{\partial N_\ell}{\partial \eta_s} u_j^\ell(t) - \frac{2}{3} e_{ks} \frac{\partial N_\ell}{\partial \eta_s} u_k^\ell(t) \delta_{ij} \right] d\boldsymbol{\eta}$$
$$+ \frac{1}{Pe} \int_{\widehat{\Omega}^h} g_\theta^v(t) N_v \frac{e_{jk}}{\det J} \frac{\partial N_r}{\partial \eta_k} e_{js} \frac{\partial N_\ell}{\partial \eta_s} T^\ell(t)\, d\boldsymbol{\eta} + \mathcal{L}\beta_{\underline{r}} \int_{\widehat{\Omega}^h} |\boldsymbol{u}^s(t)| N_s \frac{\partial N_r}{\partial \eta_\ell} \frac{\partial N_k}{\partial \eta_\ell} E^k(t)\, d\boldsymbol{\eta} = 0 \tag{5.67}$$

for the energy equation. These statements apply by components at all internal grid nodes, and unconstrained boundary nodes. An associated weak statement, employed at all non-Dirichlet constrained boundary nodes for efficient surface-integral boundary condition enforcement, is by components

$$\int_{\widehat{\Omega}^h} N_r N_\ell \frac{d}{dt}(\rho^\ell(t) \det J^\ell)\, d\boldsymbol{\eta} - \int_{\widehat{\Omega}^h} e_{jk} \frac{\partial N_r}{\partial \eta_k} N_\ell m_j^\ell(t)\, d\boldsymbol{\eta}$$

$$+\mathcal{L}\beta_{\underline{r}}\int_{\widehat{\Omega}^h}|\boldsymbol{u}^s(t)|N_s\frac{\partial N_r}{\partial\eta_\ell}\frac{\partial N_k}{\partial\eta_\ell}\rho^k(t)\,d\boldsymbol{\eta}+\oint_{\partial\widehat{\Omega}^h}N_r m_j^h e_{jk}n_k d\Gamma=0 \tag{5.68}$$

for the continuity equation,

$$\int_{\widehat{\Omega}^h}N_rN_\ell\frac{d}{dt}(m_i^\ell(t)\det J^\ell)\,d\boldsymbol{\eta}$$

$$-\int_{\widehat{\Omega}^h}u_j^s(t)N_se_{jk}\frac{\partial N_r}{\partial\eta_k}N_\ell m_i^\ell(t)\,d\boldsymbol{\eta}-\int_{\widehat{\Omega}^h}e_{jk}\frac{\partial N_r}{\partial\eta_k}N_\ell p^\ell(t)\delta_{ij}\,d\boldsymbol{\eta}$$

$$+\frac{1}{Re}\int_{\widehat{\Omega}^h}g_\mu^v(t)N_v\frac{e_{jk}}{detJ}\frac{\partial N_r}{\partial\eta_k}\left[e_{js}\frac{\partial N_\ell}{\partial\eta_s}u_i^\ell(t)+e_{is}\frac{\partial N_\ell}{\partial\eta_s}u_j^\ell(t)-\frac{2}{3}e_{ks}\frac{\partial N_\ell}{\partial\eta_s}u_k^\ell(t)\delta_{ij}\right]d\boldsymbol{\eta}$$

$$+\mathcal{L}\beta_{\underline{r}}\int_{\widehat{\Omega}^h}|\boldsymbol{u}^s(t)|N_s\frac{\partial N_r}{\partial\eta_\ell}\frac{\partial N_k}{\partial\eta_\ell}m_i^k(t)\,d\boldsymbol{\eta}$$

$$+\oint_{\partial\widehat{\Omega}^h}N_rN_\ell m_i^\ell(t)u_j^he_{jk}n_kd\Gamma+\oint_{\partial\widehat{\Omega}^h}N_r\left(p^h\delta_{ij}-\sigma_{ij}^h\right)e_{jk}n_kd\Gamma=0 \tag{5.69}$$

for the momentum equations, $1\leq i\leq n$, and

$$\int_{\widehat{\Omega}^h}N_rN_\ell\frac{d}{dt}(E^\ell(t)\det J^\ell)\,d\boldsymbol{\eta}-\int_{\widehat{\Omega}^h}u_j^s(t)N_se_{jk}\frac{\partial N_r}{\partial\eta_k}N_\ell(E^\ell(t)+p^\ell(t))\,d\boldsymbol{\eta}$$

$$+\frac{1}{Re}\int_{\widehat{\Omega}^h}u_i^v(t)g_\mu^v(t)N_v\frac{e_{jk}}{\det J}\frac{\partial N_r}{\partial\eta_k}\left[e_{js}\frac{\partial N_\ell}{\partial\eta_s}u_i^\ell(t)+e_{is}\frac{\partial N_\ell}{\partial\eta_s}u_j^\ell(t)-\frac{2}{3}e_{ks}\frac{\partial N_\ell}{\partial\eta_s}u_k^\ell(t)\delta_{ij}\right]d\boldsymbol{\eta}$$

$$+\frac{1}{Pe}\int_{\widehat{\Omega}^h}g_\theta^v(t)N_v\frac{e_{jk}}{\det J}\frac{\partial N_r}{\partial\eta_k}e_{js}\frac{\partial N_\ell}{\partial\eta_s}T^\ell(t)\,d\boldsymbol{\eta}+\mathcal{L}\beta_{\underline{\ell}}^E\int_{\widehat{\Omega}^h}|\boldsymbol{u}^s(t)|N_s\frac{\partial N_r}{\partial\eta_\ell}\frac{\partial N_k}{\partial\eta_\ell}E^k(t)\,d\boldsymbol{\eta}$$

$$+\oint_{\partial\widehat{\Omega}^h}N_ru_j^h\left(p^h\delta_{ij}-\sigma_{ij}^h\right)e_{jk}n_kd\Gamma-\oint_{\partial\widehat{\Omega}^h}N_rq_j^he_{jk}n_kd\Gamma=0 \tag{5.70}$$

for the energy equation. The boundary conditions developed in Chapter 3 are then directly inserted in the arguments of the surface integrals in this statement.

In (5.65)-(5.70), the time derivative integrals contain nodal values of $\det J$, whereas the viscous flux vector integrals depend upon the element variation of this determinant. Both $\det J$ and the metric data e_{jk} that pervade all integrals in (5.65)-(5.67) and (5.68)-(5.70), are consistently evaluated following the optimal metric data strategy outlined in the next Section, and detailed in Chapter 6.

5.8 Optimal Metric Data Evaluations

For the general Galerkin integral statement (5.12), the optimal metric data integration procedure is

$$\sum_{\ell=1}^{M_r}\left(\int_{\widehat{\Omega}^h_{\ell,\underline{r}}} N_r \frac{\partial(q\cdot\det J)^h}{\partial t}d\Omega + (e_{jk})_{P_{r\ell}}\int_{\widehat{\Omega}^h_{\ell,\underline{r}}} N_r\frac{\partial}{\partial\eta_k}\left(\left(f_j^h - f_j^{\nu h}\right)\right)d\Omega + \right.$$
$$\left.(e_{jk})_{P_{r\ell}}\mathcal{L}\beta_{\underline{r}}\int_{\widehat{\Omega}^h_{\ell,\underline{r}}}\frac{\partial N_r}{\partial\eta_k}\left(\operatorname{sgn}\left(\Lambda^q_{\underline{k}}\right)\frac{\partial}{\partial\eta_k}\left(f_j^{qh}\right) + \operatorname{sgn}\left(\Lambda^p_{\underline{k}}\right)\frac{\partial}{\partial\eta_k}\left(f_j^{ph}\right)\right)d\Omega\right) = 0 \quad (5.71)$$

where now the metric data e_{jk} are extracted from the associated integrals. In (5.71), M_r is the number of elements $\widehat{\Omega}_\ell \in \widehat{\Omega}_{\ell,r}$, and $P_{r\ell}$ corresponds to the optimal evaluation point within each $\widehat{\Omega}^h_\ell$. As exhaustively detailed in Chapter 6, the optimal metric data evaluation coordinates are determined such that the fundamental linear-solution compatibility condition

$$\left[(\det J)\,\delta^i_j\right]_{P_{r\ell}} \equiv \frac{\int_{\widehat{\Omega}^h_e} N_r \det J\frac{\partial x_i}{\partial x_j}\,d\boldsymbol{\eta}}{\int_{\widehat{\Omega}^h_e} N_r\,d\boldsymbol{\eta}} = \frac{\int_{\widehat{\Omega}^h_e} N_r e_{jk}\frac{\partial x_i}{\partial\eta_k}\,d\boldsymbol{\eta}}{\int_{\widehat{\Omega}^h_e} N_r\,d\boldsymbol{\eta}} = \frac{(e_{jk})_{P_{r\ell}}\cdot\int_{\widehat{\Omega}^h_e} N_r\frac{\partial x_i}{\partial\eta_k}\,d\boldsymbol{\eta}}{\int_{\widehat{\Omega}^h_e} N_r\,d\boldsymbol{\eta}} \quad (5.72)$$

is identically satisfied on arbitrary grids for any e_{jk}. In (5.72), δ^i_j is the Kronecker delta, and the integral on N_r is a normalization factor. Cartesian and curvilinear coordinate 2-*nd* order accuracy is achieved if the quadratic-solution compatibility condition

$$\left[x_i\,(\det J)\,\delta^i_j\right]_{P_{r\ell}} \equiv \frac{\int_{\widehat{\Omega}^h_e} N_r\frac{\det J}{2}\frac{\partial(x_i)^2}{\partial x_j}\,d\boldsymbol{\eta}}{\int_{\widehat{\Omega}^h_e} N_r\,d\boldsymbol{\eta}}$$
$$= \frac{\int_{\widehat{\Omega}^h_e}\frac{N_r}{2}e_{jk}\frac{\partial(x_i)^2}{\partial\eta_k}\,d\boldsymbol{\eta}}{\int_{\widehat{\Omega}^h_e} N_r\,d\boldsymbol{\eta}} = \frac{(e_{jk})_{P_{r\ell}}\cdot\int_{\widehat{\Omega}^h_e}\frac{N_r}{2}\frac{\partial(x_i)^2}{\partial\eta_k}\,d\boldsymbol{\eta}}{\int_{\widehat{\Omega}^h_e} N_r\,d\boldsymbol{\eta}} \quad (5.73)$$

is also identically satisfied for any value of e_{jk}. Therefore, usage of these optimal metric data will afford consistent order of accuracy on totally arbitrary grids.

For the bilinear lagrangian basis functions, and conventional counter clock-wise numbering of the elements sharing node r, see Figure 5.1, the appropriate evaluation points for the metric data e_{jk} that identically satisfy (5.72) and (5.73) are developed in the next Chapter as

$$P_{r1} \equiv \left(+\frac{1}{3};+\frac{1}{3}\right) \quad P_{r2} \equiv \left(-\frac{1}{3};+\frac{1}{3}\right) \quad P_{r3} \equiv \left(-\frac{1}{3};-\frac{1}{3}\right) \quad P_{r1} \equiv \left(+\frac{1}{3};-\frac{1}{3}\right) \tag{5.74}$$

Note that these optimal-point curvilinear coordinates are invariant in each element, regardless of its physical shape. The analysis for evaluation points for the dissipation and physical diffusion integrals in (5.65)-(5.67) and (5.68)-(5.70) is analogous. and fully documented in the next Chapter.

The efficiency of these metric data evaluations, is exemplified for the following representative expression

$$\int_{\widehat{\Omega}_e^h} e_{jk}(\boldsymbol{\eta}) N_r \frac{\partial N_\ell}{\partial \eta_k} m_j^\ell(t)\, d\boldsymbol{\eta} = (e_{jk})_{P_{re}} \int_{\widehat{\Omega}_e^h} N_r \frac{\partial N_\ell}{\partial \eta_k}\ d\boldsymbol{\eta}\ \ m_j^\ell(t) = (e_{jk})_{P_{re}} \{\text{array}\} \{m_j^\ell(t)\} \tag{5.75}$$

Here, $(e_{jk})_{P_{re}}$ is the metric data evaluation and {array} denotes the (metric-data independent) exact integrations for the remaining integral, [14]. The illustrated procedure (5.75), which also involves an optimal det J evaluation within the viscous flux vector integrals, is extended to all metric-data handling in (5.65)-(5.67) and/or (5.68)-(5.70), thereby permitting extraction of all metric data from the associated integrals. This consequently, allows dispensing with the traditional finite

element Gaussian quadrature loop, yielding an algorithm statement operationally competitive with difference scheme methodology. Furthermore, this evaluation procedure renders use of the bilinear quadrilaterals as efficient as the linear triangles with element-constant metric data.

Finally, the analysis leading to (5.74) shows that the bilinear element mass matrix integrals in (5.65)-(5.70) satisfy the fundamental relation

$$\int_{\widehat{\Omega}^h_{r\ell}} N_r(\boldsymbol{\eta}) N_j(\boldsymbol{\eta}) d\Omega = N_j(\boldsymbol{\eta}_{P_{r\ell}}) \quad \forall r \quad , j \tag{5.76}$$

Therefore, in each element $\widehat{\Omega}_\ell$, the mass matrix integral (5.76) yields the value of the basis function $N_j(\boldsymbol{\eta})$ at the optimal point P_{r_ℓ}.

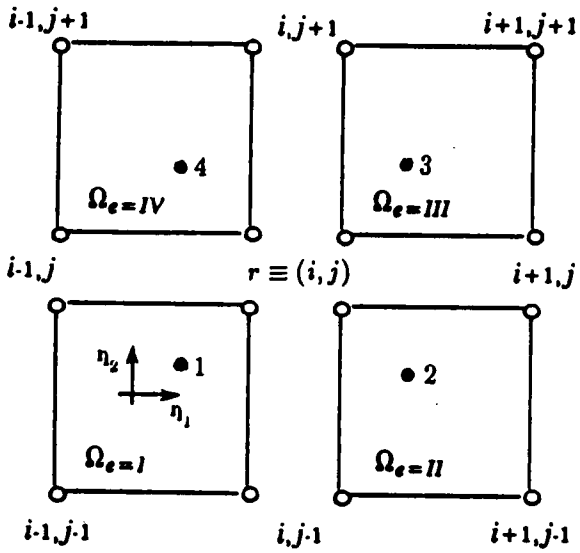


Figure 5.1: Representative Assembly of Four 2-D Lagrange Bilinear Elements with Optimal Evaluation Points

Chapter 6

Metric Data Handling for Accurate Semi-Discretizations on Arbitrary Curvilinear Meshes

In this Chapter, an efficient metric data procedure is detailed such that the semi-discrete weak statements (5.65)-(5.67) and/or (5.68)-(5.70) remain uniformly second order accurate on arbitrary grids of bilinear lagrangian elements. This accrues to metric data evaluations at optimal points, such that (5.65)-(5.67) and/or (5.68)-(5.70) satisfy linear and quadratic solution compatibility conditions for first and second order differential operators. This condition is required on both cartesian and curvilinear coordinates, as developed in the following sections, wherein $\widehat{\Omega}^h$ is denoted as simply $\widehat{\Omega}$ for notational clarity.

6.1 Curvilinear-Coordinate Differential Operators

A second-order curvilinear-coordinate PDE system is obtained from its cartesian counterpart through the following differential operator transformations

$$\det J \left(\frac{\partial(\cdot)}{\partial x_i} \right) = e_{ik} \left(\frac{\partial(\cdot)}{\partial \eta_k} \right) \tag{6.1}$$

$$\det J \left[\frac{\partial}{\partial x_i} \left((\cdot) \frac{\partial(\cdot)}{\partial x_j} \right) \right] = e_{ik} \frac{\partial}{\partial \eta_k} \left[\frac{e_{j\ell}}{\det J} (\cdot) \left(\frac{\partial(\cdot)}{\partial \eta_\ell} \right) \right] \tag{6.2}$$

complemented by the fundamental identity

$$\sum_{k=1}^{n} \frac{\partial e_{ik}}{\partial \eta_k} = 0 \ , \ 1 \leq i \leq n \tag{6.3}$$

Equalities (6.1)-(6.2) express the first and second order primitive coordinate differential operators in terms of associated curvilinear-coordinate operators via the transformation metric data e_{ik}, with the symbol "$(\cdot)$" representing a differentiable function upon which (6.1) and (6.2) operate.

An "optimal" metric data evaluation method is developed, such that a second order accurate semi-discretization of all the rhs curvilinear-coordinate operators in (6.1)-(6.2) on arbitrary grids also yields a second-order accurate representation of the associated lhs primitive-coordinate differential operators. This method derives from a consistent and accurate evaluation of following mean value theorem integral expressions for operators (6.1)-(6.2) as

$$\left[(\det J) \frac{\partial(\cdot)}{\partial x_i} \right]_{\boldsymbol{\eta}^P} \equiv \frac{\int_{\widehat{\Omega}} N_r \det J \left[\frac{\partial(\cdot)}{\partial x_i} \right] d\boldsymbol{\eta}}{\int_{\widehat{\Omega}} N_r \, d\boldsymbol{\eta}} = \frac{\int_{\widehat{\Omega}} N_r e_{ik} \left[\frac{\partial(\cdot)}{\partial \eta_k} \right] d\boldsymbol{\eta}}{\int_{\widehat{\Omega}} N_r \, d\boldsymbol{\eta}} \tag{6.4}$$

$$\left[(\det J)\frac{\partial}{\partial x_i}\left((\cdot)\frac{\partial}{\partial x_j}(\cdot)\right)\right]_{\boldsymbol{\eta}^P} \equiv \frac{\int_{\widehat{\Omega}} N_r \det J\left[\frac{\partial}{\partial x_i}\left((\cdot)\frac{\partial(\cdot)}{\partial x_j}\right)\right] d\boldsymbol{\eta}}{\int_{\widehat{\Omega}} N_r \, d\boldsymbol{\eta}}$$

$$= \frac{\int_{\widehat{\Omega}} N_r e_{ik}\frac{\partial}{\partial \eta_k}\left[\frac{e_{j\ell}}{\det J}(\cdot)\left(\frac{\partial(\cdot)}{\partial \eta_\ell}\right)\right] d\boldsymbol{\eta}}{\int_{\widehat{\Omega}} N_r \, d\boldsymbol{\eta}} \tag{6.5}$$

Herein, $\boldsymbol{\eta}^P$ indicates a suitable coordinate point in the region $\widehat{\Omega}$, to be determined. In (6.4)-(6.5) the coordinate transformation Jacobian determinant in 2-dimensions is defined as

$$\det J(\boldsymbol{\eta}) = e_{11}(\boldsymbol{\eta})e_{22}(\boldsymbol{\eta}) - e_{21}(\boldsymbol{\eta})e_{12}(\boldsymbol{\eta}) \tag{6.6}$$

Further, the function N_r is a weight function that satisfies the condition

$$\int_{\widehat{\Omega}} N_r \, d\boldsymbol{\eta} = \alpha \tag{6.7}$$

where $\alpha = 1$ or $\alpha = 4$ depending on the region.

6.2 An Integration Identity

In view of the fundamental importance of (6.4)-(6.5), for the practical metric data evaluation method, a generalized mean value theorem is now proved in the following section. The integrals (6.4)-(6.5) express the first and second order differential operators which can be evaluated when suitable functions are inserted into the integrands in an appropriate order.

Let the product of functions

$$F(\boldsymbol{x}) = \varphi(\boldsymbol{x}) \cdot \psi(\boldsymbol{x}) = \varphi(\boldsymbol{x}(\boldsymbol{\eta})) \cdot \psi(\boldsymbol{x}(\boldsymbol{\eta})) \tag{6.8}$$

represent a differentiable function in both cartesian and curvilinear coordinates. Application of (6.4)-(6.5) to (6.8) yields

$$\left[(\det J)\,\frac{\partial}{\partial x_i}\varphi\psi\right]_{\boldsymbol{\eta}^P}\int_{\widehat{\Omega}} N_r\,d\boldsymbol{\eta} = \int_{\widehat{\Omega}} e_{jk}N_r\left[\frac{\partial}{\partial \eta_k}\varphi\psi\right]\,d\boldsymbol{\eta} \tag{6.9}$$

$$\left[(\det J)\,\frac{\partial}{\partial x_i}\left(\varphi\frac{\partial}{\partial x_i}\psi\right)\right]_{\boldsymbol{\eta}^P}\int_{\widehat{\Omega}} N_r\,d\boldsymbol{\eta} = \int_{\widehat{\Omega}} e_{ik}N_r\frac{\partial}{\partial \eta_k}\left[\frac{e_{j\ell}}{\det J}\varphi\left(\frac{\partial}{\partial \eta_\ell}\psi\right)\right]\,d\boldsymbol{\eta} \tag{6.10}$$

where $\boldsymbol{\eta}^P$ denotes a suitable evaluation point in the domain $\widehat{\Omega}$. Integrals (6.9)-(6.10) can be recast as

$$\int_{\widehat{\Omega}} e_{jk}N_r\left[\frac{\partial}{\partial \eta_k}\varphi\psi\right]\,d\boldsymbol{\eta} = -\int_{\widehat{\Omega}} e_{jk}\frac{\partial N_r}{\partial \eta_k}\varphi\psi\,d\boldsymbol{\eta} \tag{6.11}$$

$$\int_{\widehat{\Omega}} N_r e_{ik}\frac{\partial}{\partial \eta_k}\left[\frac{e_{j\ell}}{\det J}\varphi\left(\frac{\partial}{\partial \eta_\ell}\psi\right)\right]\,d\boldsymbol{\eta} = -\int_{\widehat{\Omega}} e_{ik}\frac{\partial N_r}{\partial \eta_k}\left[\frac{e_{j\ell}}{\det J}\varphi\left(\frac{\partial}{\partial \eta_\ell}\psi\right)\right]\,d\boldsymbol{\eta} \tag{6.12}$$

In the sequel, (6.9) is called strong form integral, to distinguish it from the companion weak form (6.11). The surface integral associated with the Gauss-Green transformation in (6.11)-(6.12) is deleted using the assumption

$$N_r(\partial\widehat{\Omega}) = 0 \quad , \quad \partial\widehat{\Omega} \quad \Rightarrow \quad \text{boundary of} \quad \widehat{\Omega} \tag{6.13}$$

Whenever (6.13) is not met, then deletion of the surface integrals amounts to enforcing a Neumann constraint for the associated differential term.

Integrals (6.9)-(6.12) are synthetically written as

$$\mathcal{F} = \int_{\widehat{\Omega}} p(\boldsymbol{\eta})q(\boldsymbol{\eta})r(\boldsymbol{\eta})s(\boldsymbol{\eta})\,d\boldsymbol{\eta} \tag{6.14}$$

where the functions p, q, r and s are identified by inspection. An integration identity is now proved for the simplified and rigorous evaluation of integrals (6.9)-(6.12) that allows second order accurate spatial semi-discretization of operators (6.1)-(6.2) on arbitrary meshes.

Lemma 1 *Consider the integral (6.14)*

$$\mathcal{F} = \int_{\widehat{\Omega}} p(\boldsymbol{\eta}) q(\boldsymbol{\eta}) r(\boldsymbol{\eta}) s(\boldsymbol{\eta})\, d\boldsymbol{\eta}$$

If in the integration domain $\widehat{\Omega}$ the functions $q(\boldsymbol{\eta})$ and $r(\boldsymbol{\eta})$ are continuous, $p(\boldsymbol{\eta})$ and $s(\boldsymbol{\eta})$ are integrable, and both $p(\boldsymbol{\eta}) \cdot s(\boldsymbol{\eta})$ and $p(\boldsymbol{\eta}) \cdot r(\boldsymbol{\eta}) \cdot s(\boldsymbol{\eta})$ do not change sign then the following relation holds

$$\mathcal{F} = \int_{\widehat{\Omega}} p(\boldsymbol{\eta}) q(\boldsymbol{\eta}) r(\boldsymbol{\eta}) s(\boldsymbol{\eta})\, d\boldsymbol{\eta} = q(\boldsymbol{\eta}^{P1}) r(\boldsymbol{\eta}^{P2}) \int_{\widehat{\Omega}} p(\boldsymbol{\eta}) s(\boldsymbol{\eta})\, d\boldsymbol{\eta} \tag{6.15}$$

where $\boldsymbol{\eta}^{P1}$ and $\boldsymbol{\eta}^{P1}$ are suitable coordinate pairs lying in the domain $\widehat{\Omega}$.

Proof:

Integration theory leads to the fundamental inequality

$$q_{\min} \int_{\widehat{\Omega}} p(\boldsymbol{\eta}) r(\boldsymbol{\eta}) s(\boldsymbol{\eta})\, d\boldsymbol{\eta} \leq \int_{\widehat{\Omega}} p(\boldsymbol{\eta}) q(\boldsymbol{\eta}) r(\boldsymbol{\eta}) s(\boldsymbol{\eta})\, d\boldsymbol{\eta} \leq q_{\max} \int_{\widehat{\Omega}} p(\boldsymbol{\eta}) r(\boldsymbol{\eta}) s(\boldsymbol{\eta})\, d\boldsymbol{\eta} \tag{6.16}$$

The limits in this relation constitute the extrema of the auxiliary function

$$f(\boldsymbol{\eta}) = q(\boldsymbol{\eta}) \int_{\widehat{\Omega}} p(\boldsymbol{\eta}) r(\boldsymbol{\eta}) s(\boldsymbol{\eta})\, d\boldsymbol{\eta} \tag{6.17}$$

This is a continuous function of $\boldsymbol{\eta}$ since $q(\boldsymbol{\eta})$ is continuous and the rhs integral is

finite. Therefore, the following relations hold

$$q_{\min} \int_{\widehat{\Omega}} p(\boldsymbol{\eta}) r(\boldsymbol{\eta}) s(\boldsymbol{\eta})\, d\boldsymbol{\eta} \leq q(\boldsymbol{\eta}) \int_{\widehat{\Omega}} p(\boldsymbol{\eta}) r(\boldsymbol{\eta}) s(\boldsymbol{\eta})\, d\boldsymbol{\eta} \leq q_{\max} \int_{\widehat{\Omega}} p(\boldsymbol{\eta}) r(\boldsymbol{\eta}) s(\boldsymbol{\eta})\, d\boldsymbol{\eta} \tag{6.18}$$

Moreover, (6.17) attains all values between its extrema by virtue of the function theory Heine-Cantor theorem [12]. The middle term in (6.16) is certainly one such value. Consequently, in particular, the auxiliary function also satisfies the following equality

$$\int_{\widehat{\Omega}} p(\boldsymbol{\eta}) q(\boldsymbol{\eta}) r(\boldsymbol{\eta}) s(\boldsymbol{\eta})\, d\boldsymbol{\eta} = q(\boldsymbol{\eta}^{P_1}) \int_{\widehat{\Omega}} p(\boldsymbol{\eta}) r(\boldsymbol{\eta}) s(\boldsymbol{\eta})\, d\boldsymbol{\eta} \tag{6.19}$$

where $\boldsymbol{\eta}^{P1}$ is a suitable coordinate point. The preceding discussion can be applied almost verbatim to the integral

$$\mathcal{I} = \int_{\widehat{\Omega}} p(\boldsymbol{\eta}) r(\boldsymbol{\eta}) s(\boldsymbol{\eta})\, d\boldsymbol{\eta} \tag{6.20}$$

and directly leads to the companion equality

$$\int_{\widehat{\Omega}} p(\boldsymbol{\eta}) r(\boldsymbol{\eta}) s(\boldsymbol{\eta})\, d\boldsymbol{\eta} = r(\boldsymbol{\eta}^{P2}) \int_{\widehat{\Omega}} p(\boldsymbol{\eta}) s(\boldsymbol{\eta})\, d\boldsymbol{\eta} \tag{6.21}$$

where $\boldsymbol{\eta}^{P2}$ is another appropriate coordinate point. Whereupon, combining (6.19) and (6.21) leads to identity (6.16), □.

By virtue of this identity, and for N_r, φ and ψ satisfying the hypotheses of Lemma 1, then the rhs of integrals (6.9)-(6.12) can be equivalently expressed as

$$\int_{\widehat{\Omega}} e_{ik}(\boldsymbol{\eta}) N_r \psi(\boldsymbol{\eta}) \frac{\partial}{\partial \eta_k} \varphi(\boldsymbol{\eta})\, d\boldsymbol{\eta} = e_{ik}(\boldsymbol{\eta}^{P1}) \psi(\boldsymbol{\eta}^{P2}) \int_{\widehat{\Omega}} N_r \frac{\partial}{\partial \eta_k} \varphi(\boldsymbol{\eta})\, d\boldsymbol{\eta} \tag{6.22}$$

$$\int_{\widehat{\Omega}} e_{ik}(\boldsymbol{\eta}) \frac{\partial N_r}{\partial \eta_k} \psi(\boldsymbol{\eta}) \varphi(\boldsymbol{\eta})\, d\boldsymbol{\eta} = e_{ik}(\boldsymbol{\eta}^{P1}) \psi(\boldsymbol{\eta}^{P2}) \int_{\widehat{\Omega}} \frac{\partial N_r}{\partial \eta_k} \varphi(\boldsymbol{\eta})\, d\boldsymbol{\eta} \tag{6.23}$$

$$\int_{\widehat{\Omega}} e_{ik}(\boldsymbol{\eta})\frac{\partial N_r}{\partial \eta_k}\frac{e_{j\ell}}{\det J}\psi(\boldsymbol{\eta})\frac{\partial}{\partial \eta_\ell}\varphi(\boldsymbol{\eta})\, d\boldsymbol{\eta}$$
$$= e_{ik}(\boldsymbol{\eta}^{P1})\psi(\boldsymbol{\eta}^{P2})\left(\frac{e_{j\ell}}{\det J}\right)_{\boldsymbol{\eta}^{P3}}\int_{\widehat{\Omega}}\frac{\partial N_r}{\partial \eta_k}\frac{\partial}{\partial \eta_\ell}\varphi(\boldsymbol{\eta})\, d\boldsymbol{\eta} \qquad (6.24)$$

The evaluation point choice in (6.24) is readily justified by a straightforward extension of Lemma 1.

It is observed that (6.22)-(6.24) permit a simple and direct evaluation of integrals (6.9)-(6.12) whenever the functions N_r, ψ and φ are easily integrable on the region $\widehat{\Omega}$ and whenever the evaluation points $\boldsymbol{\eta}^j$ are determined. This determination generally depends upon the coordinate-transformation and upon the primitive coordinate distribution over each transformed region. However, if on such regions the exact value of integrals (6.9)-(6.12) are known for specific compatibility conditions that all solutions of (5.65)-(5.67) and (5.68)-(5.70) should satisfy, then equalities (6.22)-(6.24) allow the determination of unique local evaluation points which are totally independent of primitive coordinate values and allow consistent second-order accurate semi-discretizations on truly arbitrary meshes. This determination is accomplished for (6.22)-(6.24) by enforcing the following fundamental linear and quadratic compatibility conditions for first and second order differential operators,

$$\left[(\det J)\frac{\partial x_j}{\partial x_i}\right]_{\boldsymbol{\eta}^P}\int_{\widehat{\Omega}} N_r\, d\boldsymbol{\eta} = \int_{\widehat{\Omega}} N_r e_{ik}\left[\frac{\partial x_j}{\partial \eta_k}\right]\, d\boldsymbol{\eta} = \left[\det J\cdot\delta_i^j\right]_{\boldsymbol{\eta}^P}\int_{\widehat{\Omega}} N_r\, d\boldsymbol{\eta} \qquad (6.25)$$

$$\left[(\det J)\frac{\partial x_j}{\partial x_i}\right]_{\boldsymbol{\eta}^P}\int_{\widehat{\Omega}} N_r\, d\boldsymbol{\eta} = -\int_{\widehat{\Omega}} e_{ik}\left[\frac{\partial N_r}{\partial \eta_k}\right] x_j\, d\boldsymbol{\eta} = \left[\det J\cdot \delta_i^j\right]_{\boldsymbol{\eta}^P}\int_{\widehat{\Omega}} N_r\, d\boldsymbol{\eta} \quad (6.26)$$

$$\left[\left(\frac{\det J}{2}\right)\frac{\partial x_j x_j}{\partial x_i}\right]_{\boldsymbol{\eta}^P}\int_{\widehat{\Omega}} N_r\, d\boldsymbol{\eta} = \int_{\widehat{\Omega}} \frac{e_{ik}}{2} N_r\left[\frac{\partial x_j x_j}{\partial \eta_k}\right]\, d\boldsymbol{\eta} = \left[\det J\cdot x_j\delta_i^j\right]_{\boldsymbol{\eta}^P}\int_{\widehat{\Omega}} N_r\, d\boldsymbol{\eta} \quad (6.27)$$

$$\left[\left(\frac{\det J}{2}\right)\frac{\partial x_j x_j}{\partial x_i}\right]_{\boldsymbol{\eta}^P}\int_{\widehat{\Omega}} N_r\, d\boldsymbol{\eta} = -\int_{\widehat{\Omega}} \frac{e_{ik}}{2}\frac{\partial N_r}{\partial \eta_k} x_j x_j\, d\boldsymbol{\eta} = \left[\det J\cdot x_j\delta_i^j\right]_{\boldsymbol{\eta}^P}\int_{\widehat{\Omega}} N_r\, d\boldsymbol{\eta} \quad (6.28)$$

$$\left[(\det J)\frac{\partial}{\partial x_i}\left(\frac{\partial x_m}{\partial x_j}\right)\right]_{\boldsymbol{\eta}^P}\int_{\widehat{\Omega}} N_r\, d\boldsymbol{\eta} = -\int_{\widehat{\Omega}} e_{ik}\frac{\partial N_r}{\partial \eta_k}\left[\frac{e_{j\ell}}{\det J}\left(\frac{\partial x_m}{\partial \eta_\ell}\right)\right]\, d\boldsymbol{\eta} = 0 \quad (6.29)$$

$$\left[\left(\frac{\det J}{2}\right)\frac{\partial}{\partial x_i}\left(\frac{\partial (x_m x_n)}{\partial x_j}\right)\right]_{\boldsymbol{\eta}^P}\int_{\widehat{\Omega}} N_r\, d\boldsymbol{\eta} =$$
$$-\int_{\widehat{\Omega}} e_{ik}\frac{\partial N_r}{\partial \eta_k}\left[\frac{e_{j\ell}}{2\det J}\left(\frac{\partial (x_m x_n)}{\partial \eta_\ell}\right)\right]\, d\boldsymbol{\eta} = \left[\frac{\det J}{2}\left(\delta_j^m\delta_i^n + \delta_i^m\delta_j^n\right)\right]_{\boldsymbol{\eta}^P}\int_{\widehat{\Omega}} N_r\, d\boldsymbol{\eta} \quad (6.30)$$

6.3 Spatial Approximation Functions

This section details the properties of a class of bilinear functions that permit second order accurate semi-discretizations on both primitive and curvilinear coordinate

computational cells. Each curvilinear-coordinate cell is obtained upon transformation of an arbitrary quadrilateral cartesian region Ω, as illustrated by the 2-D example in Figure 6.1.

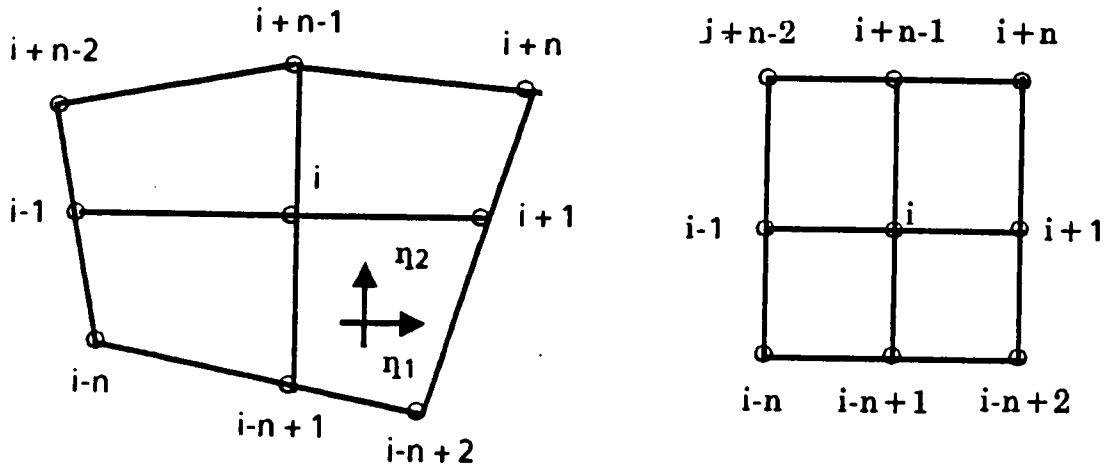


Figure 6.1: Example of domain transformation

It is convenient to define the local reference frame $\{\eta_1, \eta_2\}$, with each coordinate spanning the range $[-1; +1]$, in which the approximation functions are specified. The bilinear Lagrange polynomials of interest herein are

$$N_1 = \frac{1}{4}(1-\eta_1)(1-\eta_2) \quad , \quad N_2 = \frac{1}{4}(1+\eta_1)(1-\eta_2)$$
$$N_3 = \frac{1}{4}(1+\eta_1)(1+\eta_2) \quad , \quad N_4 = \frac{1}{4}(1-\eta_1)(1+\eta_2) \tag{6.31}$$

The subscript ℓ on N_ℓ refers to the computational-cell nodes and uniquely identify these functions for the conventional counter-clockwise ordering in Figure 6.2. Note that a one-to-one correspondence is established between the global numbering index pair (i, j) and the element nodal index $\ell = 1, 2, 3, 4$.

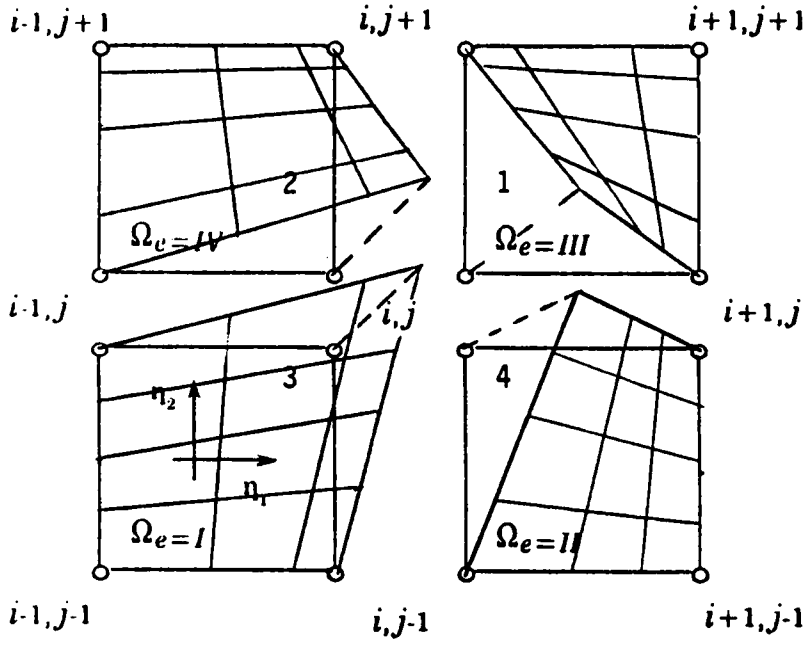


Figure 6.2: Approximation Function Variation

The metric data e_{ik} are then expressed in terms of the partial derivatives of the primitive coordinates with respect to the curvilinear coordinates $\boldsymbol{\eta}$. Consequently, the distribution of these metrics over each cell can be obtained via differentiation of (6.31) yielding

$$e_{11}(\eta) = +\frac{\partial x_2}{\partial \eta_2} = \frac{\partial N_\ell(\boldsymbol{\eta})}{\partial \eta_2} x_2^\ell \quad , \quad e_{12}(\eta) = -\frac{\partial x_2}{\partial \eta_1} = \frac{\partial N_\ell(\boldsymbol{\eta})}{\partial \eta_1} x_2^\ell \tag{6.32}$$

$$e_{21}(\eta) = -\frac{\partial x_1}{\partial \eta_2} = \frac{\partial N_\ell(\boldsymbol{\eta})}{\partial \eta_2} x_1^\ell \quad , \quad e_{22}(\eta) = +\frac{\partial x_1}{\partial \eta_1} = \frac{\partial N_\ell(\boldsymbol{\eta})}{\partial \eta_1} x_1^\ell \tag{6.33}$$

These expressions are crucial in the determination of the optimal metric-data evaluation points.

The following highlights a fundamental feature of the partial derivatives of N_ℓ.

Specifically,

$$\frac{\partial N_1}{\partial \eta_1} = -(1-\eta_2)/4 \quad , \quad \frac{\partial N_1}{\partial \eta_2} = -(1-\eta_1)/4 \tag{6.34}$$

$$\frac{\partial N_2}{\partial \eta_1} = +(1-\eta_2)/4 \quad , \quad \frac{\partial N_2}{\partial \eta_2} = -(1+\eta_1)/4 \tag{6.35}$$

$$\frac{\partial N_3}{\partial \eta_1} = +(1+\eta_2)/4 \quad , \quad \frac{\partial N_3}{\partial \eta_2} = +(1+\eta_1)/4 \tag{6.36}$$

$$\frac{\partial N_4}{\partial \eta_1} = -(1+\eta_2)/4 \quad , \quad \frac{\partial N_4}{\partial \eta_2} = +(1-\eta_1)/4 \tag{6.37}$$

hence the partial derivatives $\partial N_j/\partial \eta_i$ do not depend upon η_i itself. As will be shown, this characteristic plays a key role for the identification of the metric-data optimal evaluation points.

6.4 Determination of Optimal Metric-Data Evaluation Points for Convection Operator Semi-Discretizations

This section is divided into two parts. First, ψ is set to one, the integrations are performed over the region cell $\hat{\Omega}$ and the resultant expressions analyzed. In the second part, the derived expressions are combined with the metric data e_{ik} to form relations (6.25)-(6.28) after setting $\varphi = x_j$. Thereupon, the optimal evaluations points are determined.

6.4.1 Integration in η Space

The evaluation of the strong statement integral

$$\mathcal{I}_1^r = \int_{\widehat{\Omega}} N_r \frac{\partial N_\ell}{\partial \eta_1}\, d\boldsymbol{\eta}\, \varphi^\ell = \sum_{e=1}^{4} \int_{\widehat{\Omega}_e} N_r \frac{\partial N_\ell}{\partial \eta_1}\, d\boldsymbol{\eta}\, \varphi^\ell \tag{6.38}$$

over the computational domain $\widehat{\Omega}$ of Figure 6.1 yields, for node $r \equiv$ node (i,j)

$$\begin{aligned} \int_{\widehat{\Omega}_1} N_r \frac{\partial N_\ell}{\partial \eta_1}\, d\boldsymbol{\eta}\, \varphi^\ell &= \left(\frac{\partial N_\ell}{\partial \eta_1}\right)_{P_1^1} \varphi^\ell \quad , \quad \int_{\widehat{\Omega}_2} N_r \frac{\partial N_\ell}{\partial \eta_1}\, d\boldsymbol{\eta}\, \varphi^\ell = \left(\frac{\partial N_\ell}{\partial \eta_1}\right)_{P_2^1} \varphi^\ell \\ \int_{\widehat{\Omega}_3} N_r \frac{\partial N_\ell}{\partial \eta_1}\, d\boldsymbol{\eta}\, \varphi^\ell &= \left(\frac{\partial N_\ell}{\partial \eta_1}\right)_{P_3^1} \varphi^\ell \quad , \quad \int_{\widehat{\Omega}_4} N_r \frac{\partial N_\ell}{\partial \eta_1}\, d\boldsymbol{\eta}\, \varphi^\ell = \left(\frac{\partial N_\ell}{\partial \eta_1}\right)_{P_4^1} \varphi^\ell \end{aligned} \tag{6.39}$$

where the coordinates of points P_e^1 are

$$P_1^1 \equiv \left(0; +\tfrac{1}{3}\right) \quad P_2^1 \equiv \left(0; +\tfrac{1}{3}\right) \quad P_3^1 \equiv \left(0; -\tfrac{1}{3}\right) \quad P_4^1 \equiv \left(0; -\tfrac{1}{3}\right) \tag{6.40}$$

Consequently, the evaluation of integral $\mathcal{I}_1^r$ is expressed as

$$\mathcal{I}_1^r = \left\{ \left(\frac{\partial N_\ell}{\partial \eta_1}\right)_{P_1^1} \varphi^\ell + \left(\frac{\partial N_\ell}{\partial \eta_1}\right)_{P_2^1} \varphi^\ell + \left(\frac{\partial N_\ell}{\partial \eta_1}\right)_{P_3^1} \varphi^\ell + \left(\frac{\partial N_\ell}{\partial \eta_1}\right)_{P_4^1} \varphi^\ell \right\} \tag{6.41}$$

and for $\varphi^r \equiv \phi_{i,j}$ it coincides with the recursion formula

$$\mathcal{I}_1^r = \left(-\frac{1}{6}\phi_{i-1,j-1} - \frac{4}{6}\phi_{i-1,j} - \frac{1}{6}\phi_{i-1,j+1} + \frac{1}{6}\phi_{i+1,j-1} + \frac{4}{6}\phi_{i+1,j} + \frac{1}{6}\phi_{i+1,j+1} \right) \tag{6.42}$$

Note that a one-to-one correspondence is established between of r and the index pair (i,j).

Expression (6.41) supplies the sum of four second-order centered difference formulae for $\dfrac{\partial \varphi}{\partial \eta_1}$, each evaluated at P_e^1. For example, the following expression is obtained on $\widehat{\Omega}_1$ at point $(0; 1/3)$

$$\left(\frac{\partial N_\ell}{\partial \eta_1}\right)_{(0;1/3)} \varphi^\ell = \left(\frac{2}{6}\varphi^3 + \frac{1}{6}\varphi^2\right) - \left(\frac{2}{6}\varphi^4 + \frac{1}{6}\varphi^1\right) \tag{6.43}$$

which, with reference to Figure 6.3, coincides with the approximation

$$\frac{\partial \varphi}{\partial \eta_1} \simeq \frac{1}{\Delta \eta_1}\left(\varphi^{\alpha} - \varphi^{\beta}\right) \tag{6.44}$$

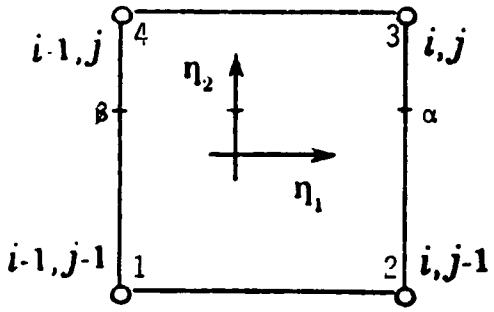


Figure 6.3: Representative Computational Cell for Evaluation (6.44)

Whereupon, the expressions for φ^{α} and φ^{β} at points $(-1;1/3)$ and $(+1;1/3)$, respectively, are

$$\varphi^{\alpha} = \frac{4}{6}\phi_{i,j} + \frac{2}{6}\phi_{i,j-1} \quad , \quad \varphi^{\beta} = \frac{4}{6}\phi_{i-1,j} + \frac{2}{6}\phi_{i-1,j-1} \tag{6.45}$$

Insertion of (6.45) into (6.44) yields

$$\frac{\partial \varphi}{\partial \eta_1} \simeq \left(\frac{2}{6}\phi_{i,j} + \frac{1}{6}\phi_{i,j-1}\right) - \left(\frac{2}{6}\phi_{i-1,j} + \frac{1}{6}\phi_{i-1,j-1}\right) \tag{6.46}$$

which reverts to (6.43). Likewise the evaluation of the integral

$$\mathcal{I}_2^r = \int_{\widehat{\Omega}} N_r \frac{\partial N_\ell}{\partial \eta_2}\, d\boldsymbol{\eta}\, \varphi^\ell = \sum_{e=1}^{4} \int_{\widehat{\Omega}_e} N_r \frac{\partial N_\ell}{\partial \eta_2}\, d\boldsymbol{\eta}\, \varphi^\ell \tag{6.47}$$

over the computational domain of Figure 6.1 yields

$$\begin{aligned} \int_{\widehat{\Omega}_1} N_r \frac{\partial N_\ell}{\partial \eta_2}\, d\boldsymbol{\eta}\, \varphi^\ell &= \left(\frac{\partial N_\ell}{\partial \eta_2}\right)_{P_1^2} \varphi^\ell \quad , \quad \int_{\widehat{\Omega}_2} N_r \frac{\partial N_\ell}{\partial \eta_2}\, d\boldsymbol{\eta}\, \varphi^\ell = \left(\frac{\partial N_\ell}{\partial \eta_2}\right)_{P_2^2} \varphi^\ell \\ \int_{\widehat{\Omega}_3} N_r \frac{\partial N_\ell}{\partial \eta_2}\, d\boldsymbol{\eta}\, \varphi^\ell &= \left(\frac{\partial N_\ell}{\partial \eta_2}\right)_{P_3^2} \varphi^\ell \quad , \quad \int_{\widehat{\Omega}_4} N_r \frac{\partial N_\ell}{\partial \eta_2}\, d\boldsymbol{\eta}\, \varphi^\ell = \left(\frac{\partial N_\ell}{\partial \eta_2}\right)_{P_4^2} \varphi^\ell \end{aligned} \tag{6.48}$$

where the coordinates of points P_e^2 are

$$P_1^2 \equiv \left(+\tfrac{1}{3};0\right) \quad P_2^2 \equiv \left(-\tfrac{1}{3};0\right) \quad P_3^2 \equiv \left(-\tfrac{1}{3};0\right) \quad P_4^2 \equiv \left(+\tfrac{1}{3};0\right) \tag{6.49}$$

Consequently, the evaluation of integral $\mathcal{I}_2^r$ is expressed as

$$\mathcal{I}_2^r = \left\{ \left(\frac{\partial N_\ell}{\partial \eta_2}\right)_{P_1^2} \varphi^\ell + \left(\frac{\partial N_\ell}{\partial \eta_2}\right)_{P_2^2} \varphi^\ell + \left(\frac{\partial N_\ell}{\partial \eta_2}\right)_{P_3^2} \varphi^\ell + \left(\frac{\partial N_\ell}{\partial \eta_2}\right)_{P_4^2} \varphi^\ell \right\} \tag{6.50}$$

and coincides with the recursion formula

$$\mathcal{I}_2^r = \left(-\frac{1}{6}\phi_{i-1,j-1} - \frac{4}{6}\phi_{i,j-1} - \frac{1}{6}\phi_{i+1,j-1} + \frac{1}{6}\phi_{i-1,j+1} + \frac{4}{6}\phi_{i,j+1} + \frac{1}{6}\phi_{i+1,j+1} \right) \tag{6.51}$$

Expression (6.50) supplies the sum of four second-order centered difference formulae for $\dfrac{\partial \varphi}{\partial \eta_2}$, each evaluated at P_e^2. For example, the following expression is obtained on $\widehat{\Omega}_1$ at point $(1/3;0)$

$$\left(\frac{\partial N_\ell}{\partial \eta_2}\right)_{(1/3;0)} \varphi^\ell = \left(\frac{2}{6}\varphi^3 + \frac{1}{6}\varphi^4\right) - \left(\frac{2}{6}\varphi^2 + \frac{1}{6}\varphi^1\right) \tag{6.52}$$

which, by referring to Figure 6.4, coincides with the approximation

$$\frac{\partial \varphi}{\partial \eta_2} \simeq \frac{1}{\Delta \eta_2}\left(\varphi^\alpha - \varphi^\beta\right) \tag{6.53}$$

Hence, the expressions for φ^α and φ^β at points $(1/3;+1)$ and $(1/3;-1)$, respectively, are

$$\varphi^\alpha = \frac{4}{6}\phi_{i,j} + \frac{2}{6}\phi_{i-1,j} \quad , \quad \varphi^\beta = \frac{4}{6}\phi_{i,j-1} + \frac{2}{6}\phi_{i-1,j-1} \tag{6.54}$$

Insertion of (6.54) into (6.53) yields

$$\frac{\partial \varphi}{\partial \eta_2} \simeq \left(\frac{2}{6}\phi_{i,j} + \frac{1}{6}\phi_{i-1,j}\right) - \left(\frac{2}{6}\phi_{i,j-1} + \frac{1}{6}\phi_{i-1,j-1}\right) \tag{6.55}$$

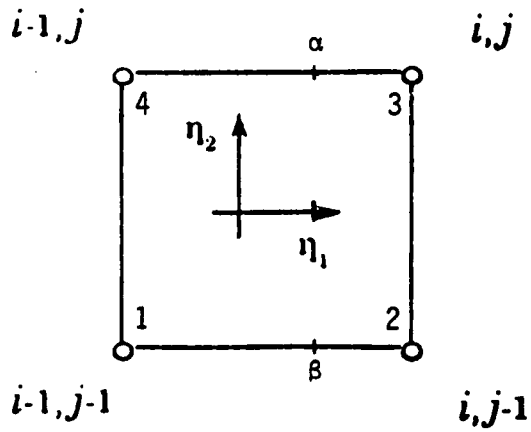


Figure 6.4: Representative Computational Cell for Evaluation (6.53)

which reverts to (6.52).

The evaluation of the weak statement integral

$$\mathcal{J}_1^r = -\int_{\widehat{\Omega}} \frac{\partial N_r}{\partial \eta_1} N_\ell \, d\boldsymbol{\eta} \, \varphi^\ell = -\sum_{e=1}^{4} \int_{\widehat{\Omega}_e} \frac{\partial N_r}{\partial \eta_1} N_\ell \, d\boldsymbol{\eta} \, \varphi^\ell \tag{6.56}$$

over $\widehat{\Omega}$, see Figure 6.3, yields

$$\begin{aligned} -\int_{\widehat{\Omega}_1} \frac{\partial N_r}{\partial \eta_1} N_\ell \, d\boldsymbol{\eta} \, \varphi^\ell &= -(N_\ell)_{P_1^1} \varphi^\ell \quad , \quad -\int_{\widehat{\Omega}_2} \frac{\partial N_r}{\partial \eta_1} N_\ell \, d\boldsymbol{\eta} \, \varphi^\ell = +(N_\ell)_{P_2^1} \varphi^\ell \\ -\int_{\widehat{\Omega}_3} \frac{\partial N_r}{\partial \eta_1} N_\ell \, d\boldsymbol{\eta} \, \varphi^\ell &= +(N_\ell)_{P_3^1} \varphi^\ell \quad , \quad -\int_{\widehat{\Omega}_4} \frac{\partial N_r}{\partial \eta_1} N_\ell \, d\boldsymbol{\eta} \, \varphi^\ell = -(N_\ell)_{P_4^1} \varphi^\ell \end{aligned} \tag{6.57}$$

where the evaluation points P_e^1 coincide with (6.40). Consequently, $\mathcal{J}_1^r$ is expressed as

$$\mathcal{J}_1^r = \left\{ \left[(N_\ell)_{P_2^1} \varphi^\ell - (N_\ell)_{P_1^1} \varphi^\ell \right] + \left[(N_\ell)_{P_3^1} \varphi^\ell - (N_\ell)_{P_4^1} \varphi^\ell \right] \right\} \tag{6.58}$$

and coincides with expression (6.42) via evaluation of each basis function in the element indicated by the subscript in P_e^1.

Analogously, the evaluation of the weak statement integral

$$\mathcal{J}_2^r = -\int_{\widehat{\Omega}} \frac{\partial N_r}{\partial \eta_2} N_\ell \, d\boldsymbol{\eta} \, \varphi^\ell = -\sum_{e=1}^{4} \int_{\widehat{\Omega}_e} \frac{\partial N_r}{\partial \eta_2} N_\ell \, d\boldsymbol{\eta} \, \varphi^\ell \tag{6.59}$$

over $\widehat{\Omega}$, see Figure 6.4, yields

$$-\int_{\widehat{\Omega}_1} \frac{\partial N_r}{\partial \eta_2} N_\ell \, d\boldsymbol{\eta} \, \varphi^\ell = -(N_\ell)_{P_1^2} \varphi^\ell \quad , \quad -\int_{\widehat{\Omega}_2} \frac{\partial N_r}{\partial \eta_2} N_\ell \, d\boldsymbol{\eta} \, \varphi^\ell = -(N_\ell)_{P_2^2} \varphi^\ell$$
$$-\int_{\widehat{\Omega}_3} \frac{\partial N_r}{\partial \eta_2} N_\ell \, d\boldsymbol{\eta} \, \varphi^\ell = +(N_\ell)_{P_3^2} \varphi^\ell \quad , \quad -\int_{\widehat{\Omega}_4} \frac{\partial N_r}{\partial \eta_2} N_\ell \, d\boldsymbol{\eta} \, \varphi^\ell = +(N_\ell)_{P_4^2} \varphi^\ell \tag{6.60}$$

where the evaluation points P_e^2 coincide with (6.49). Consequently, $\mathcal{J}_2^r$ is expressed as

$$\mathcal{J}_2^r = \left\{ \left[(N_\ell)_{P_4^2} \varphi^\ell - (N_\ell)_{P_1^2} \varphi^\ell \right] + \left[(N_\ell)_{P_3^2} \varphi^\ell - (N_\ell)_{P_2^2} \varphi^\ell \right] \right\} \tag{6.61}$$

and coincides with expression (6.51) via evaluation of each basis function in the element indicated by the subscript in P_e^2. Therefore, the assembly of the weak statement integrals (6.56) and (6.59) coincide with the assembly of their respective strong statement counterparts on uniform rectangular grids. However, this identity no longer holds on each individual element, compare (6.39), (6.48) with (6.57), (6.60). Consequently, significant differences originate in the terminal formulae resulting from the evaluations of these two sets of integrals on arbitrary meshes, hence variable metric data e_{jk}, as shown in the next section.

6.4.2 Metric-Data Evaluation Points

The fundamental identity (6.25) is expressed in each region $\widehat{\Omega}_e$, see Figure 6.1, as

$$\left[\det J \cdot \frac{\partial x_j}{\partial x_i} \right]_{\boldsymbol{\eta}_e^P} \cdot \int_{\widehat{\Omega}_e} N_r \, d\boldsymbol{\eta} \;=\; \int_{\widehat{\Omega}} e_{ik} N_r \frac{\partial x_j}{\partial \eta_k} \, d\boldsymbol{\eta} = \left[\det J \cdot \frac{\partial x_j}{\partial x_i} \delta_i^j \right]_{\boldsymbol{\eta}_e^P} \tag{6.62}$$

since $\int_{\Omega_e} N_r \, d\boldsymbol{\eta} = 1$. The unabridged form of this integral is

$$\int_{\widehat{\Omega}_e} e_{ik} N_r \frac{\partial x_j}{\partial \eta_k} \, d\boldsymbol{\eta} = \int_{\widehat{\Omega}_e} e_{i1} N_r \frac{\partial x_j}{\partial \eta_1} \, d\boldsymbol{\eta} + \int_{\widehat{\Omega}_e} e_{i2} N_r \frac{\partial x_j}{\partial \eta_2} \, d\boldsymbol{\eta} \tag{6.63}$$

Whereupon, expressing x_j via basis functions (6.31) in this integral, and invoking Lemma 1 yields

$$\mathcal{E}_e = \int_{\widehat{\Omega}_e} e_{ik} N_r \frac{\partial N_\ell}{\partial \eta_k}\, d\boldsymbol{\eta}\, x_j^\ell = \left\{ e_{i1}\left(\boldsymbol{\eta}_e^1\right)\left(\int_{\widehat{\Omega}_e} N_r \frac{\partial N_\ell}{\partial \eta_1}\, d\boldsymbol{\eta}\right) x_j^\ell + e_{i2}\left(\boldsymbol{\eta}_e^2\right)\left(\int_{\widehat{\Omega}_e} N_r \frac{\partial N_\ell}{\partial \eta_2}\, d\boldsymbol{\eta}\right) x_j^\ell \right\} \tag{6.64}$$

This expression is then transformed via relations (6.39), (6.48) to yield

$$\mathcal{E}_e = e_{i1}(\boldsymbol{\eta}_e^1)\left(\frac{\partial N_\ell}{\partial \eta_1}\right)_{P_e^1} x_j^\ell + e_{i2}(\boldsymbol{\eta}_e^2)\left(\frac{\partial N_\ell}{\partial \eta_2}\right)_{P_e^2} x_j^\ell \tag{6.65}$$

which for $i \neq j$ and for the metric data definitions (6.32), (6.33) should identically vanish. It appears that this expression can indeed vanish only if $\boldsymbol{\eta}_e^1 \neq \boldsymbol{\eta}_e^2$ since $P_e^1 \neq P_e^2$. But, if this were the case, then for $i = j = 1$ the unique evaluation point $\boldsymbol{\eta}_P$ at the lhs (6.62) would not exist, since the value of $\det J$ must result from products of metric data evaluated at one point only, see (6.6). However, a unique point can be determined for the bilinear lagrangian basis. In this connection, note that the partial derivative $\partial N_\ell/\partial \eta_1$ is a function of η_2 alone, and $\partial N_\ell/\partial \eta_2$ is a function of η_1 alone. Consequently, the following equalities hold

$$\left(\frac{\partial N_\ell}{\partial \eta_1}\right)_{(0;\pm 1/3)} = \left(\frac{\partial N_\ell}{\partial \eta_1}\right)_{(\pm 1/3;\pm 1/3)}, \quad \left(\frac{\partial N_\ell}{\partial \eta_2}\right)_{(\pm 1/3;0)} = \left(\frac{\partial N_\ell}{\partial \eta_2}\right)_{(\pm 1/3;\pm 1/3)} \tag{6.66}$$

Therefore, for $i = 1$ and $j = 2$ expression (6.65) is cast as

$$\mathcal{E}_e = x_2^\ell \left(\frac{\partial N_\ell}{\partial \eta_2}\right)_{\boldsymbol{\eta}_e^1} \left(\frac{\partial N_\ell}{\partial \eta_1}\right)_{(\pm 1/3;\pm 1/3)} x_2^\ell - x_2^\ell \left(\frac{\partial N_\ell}{\partial \eta_1}\right)_{\boldsymbol{\eta}_e^2} \left(\frac{\partial N_\ell}{\partial \eta_2}\right)_{(\pm 1/3;\pm 1/3)} x_2^\ell \tag{6.67}$$

and consequently, the appropriate evaluation points for both e_{11} and e_{12} that make (6.67) identically vanish are

$$\boldsymbol{\eta}_1^1 \equiv \boldsymbol{\eta}_1^2 \equiv \boldsymbol{\eta}_1 \equiv \left(+\frac{1}{3}; +\frac{1}{3}\right)$$

$$\boldsymbol{\eta}_2^1 \equiv \boldsymbol{\eta}_2^2 \equiv \boldsymbol{\eta}_2 \equiv \left(-\frac{1}{3}; +\frac{1}{3}\right)$$

$$\boldsymbol{\eta}_3^1 \equiv \boldsymbol{\eta}_3^2 \equiv \boldsymbol{\eta}_3 \equiv \left(-\frac{1}{3}; -\frac{1}{3}\right)$$

$$\boldsymbol{\eta}_4^1 \equiv \boldsymbol{\eta}_4^2 \equiv \boldsymbol{\eta}_4 \equiv \left(+\frac{1}{3}; -\frac{1}{3}\right) \tag{6.68}$$

where $\equiv$ denotes equivalence but not coincidence. These points are also adequate when $i = 2$ and $j = 1$ in (6.65), since

$$\mathcal{E}_e = e_{21}(\boldsymbol{\eta}_e)\left(\frac{\partial N_\ell}{\partial \eta_1}\right)_{P_e} x_1^\ell + e_{22}(\boldsymbol{\eta}_e)\left(\frac{\partial N_\ell}{\partial \eta_2}\right)_{P_e} x_1^\ell$$

$$= -x_1^\ell \left(\frac{\partial N_\ell}{\partial \eta_2}\right)_{P_e}\left(\frac{\partial N_\ell}{\partial \eta_1}\right)_{P_e} x_1^\ell + x_1^\ell \left(\frac{\partial N_\ell}{\partial \eta_1}\right)_{P_e}\left(\frac{\partial N_\ell}{\partial \eta_2}\right)_{P_e} x_1^\ell = 0 \tag{6.69}$$

Of significance, the derived coordinates remain valid when $\delta_i^j = 1$ in (6.62), since this expression then becomes

$$\mathcal{E}_e = x_2^\ell \left(\frac{\partial N_\ell}{\partial \eta_2}\right)_{P_e}\left(\frac{\partial N_\ell}{\partial \eta_1}\right)_{P_e} x_1^\ell - x_2^\ell \left(\frac{\partial N_\ell}{\partial \eta_1}\right)_{P_e}\left(\frac{\partial N_\ell}{\partial \eta_2}\right)_{P_e} x_1^\ell \tag{6.70}$$

for $i = j = 1$ and

$$\mathcal{E}_e = -x_1^\ell \left(\frac{\partial N_\ell}{\partial \eta_2}\right)_{P_e}\left(\frac{\partial N_\ell}{\partial \eta_1}\right)_{P_e} x_2^\ell + x_1^\ell \left(\frac{\partial N_\ell}{\partial \eta_1}\right)_{P_e}\left(\frac{\partial N_\ell}{\partial \eta_2}\right)_{P_e} x_2^\ell \tag{6.71}$$

for $i = j = 2$, which both correctly constitute the value of $\det J$ at point P_e.

To conclude these derivations, note that the fundamental relation (6.62) is exactly satisfied by the strong statement integrals on each individual element. Conversely, as shown next, the weak statement integrals can only satisfy such cardinal relation on average and on an assembly of four contiguous elements.

Considering that $\int_{\widehat{\Omega}} N_r \, d\boldsymbol{\eta} = 4$, the fundamental identity (6.25) is expressed in the region $\widehat{\Omega}$, see Figure 6.1, as

$$\left[\det J \cdot \frac{\partial x_j}{\partial x_i}\right]_{\boldsymbol{\eta}^P} \cdot \int_{\widehat{\Omega}} N_r \, d\boldsymbol{\eta} \;=\; -\int_{\widehat{\Omega}} e_{ik} \frac{\partial N_r}{\partial \eta_k} x_j \, d\boldsymbol{\eta} = 4 \cdot [\det J]_{\boldsymbol{\eta}^P} \cdot \delta_i^j \quad (6.72)$$

Here $\boldsymbol{\eta}^P$ now denotes a point on the assembly of four contiguous elements. The unabridged form of this integral is

$$-\int_{\widehat{\Omega}} e_{ik} \frac{\partial N_r}{\partial \eta_k} x_j \, d\boldsymbol{\eta} = -\int_{\widehat{\Omega}} e_{i1} \frac{\partial N_r}{\partial \eta_1} x_j \, d\boldsymbol{\eta} - \int_{\widehat{\Omega}} e_{i2} \frac{\partial N_r}{\partial \eta_2} x_j \, d\boldsymbol{\eta} \quad (6.73)$$

Whereupon, expressing x_j via basis functions (6.31) in this integral and invoking Lemma 1 yields

$$\mathcal{E} = -\int_{\widehat{\Omega}} e_{ik} \frac{\partial N_r}{\partial \eta_k} N_\ell \, d\boldsymbol{\eta} \; x_j^\ell =$$
$$\sum_{e=1}^{4} \quad \left\{ e_{i1}\left(\boldsymbol{\eta}_e^1\right) \left(-\int_{\widehat{\Omega}_e} \frac{\partial N_r}{\partial \eta_1} N_\ell \, d\boldsymbol{\eta} \right) x_j^\ell + e_{i2}\left(\boldsymbol{\eta}_e^2\right) \left(-\int_{\widehat{\Omega}_e} \frac{\partial N_r}{\partial \eta_2} N_\ell \, d\boldsymbol{\eta} \right) x_j^\ell \right\} \quad (6.74)$$

This expression is further transformed via relations (6.57), (6.60) and is cast as

$$\begin{aligned}
\mathcal{E} \;=\; & -e_{i1}(\boldsymbol{\eta}_1^1)\,(N_\ell)_{P_1^1}\, x_j^\ell + e_{i1}(\boldsymbol{\eta}_2^1)\,(N_\ell)_{P_2^1}\, x_j^\ell \\
& + e_{i1}(\boldsymbol{\eta}_3^1)\,(N_\ell)_{P_3^1}\, x_j^\ell - e_{i1}(\boldsymbol{\eta}_4^1)\,(N_\ell)_{P_4^1}\, x_j^\ell \\
& - e_{i2}(\boldsymbol{\eta}_1^2)\,(N_\ell)_{P_1^2}\, x_j^\ell - e_{i2}(\boldsymbol{\eta}_2^2)\,(N_\ell)_{P_2^2}\, x_j^\ell \\
& + e_{i2}(\boldsymbol{\eta}_3^2)\,(N_\ell)_{P_3^1}\, x_j^\ell + e_{i2}(\boldsymbol{\eta}_4^2)\,(N_\ell)_{P_4^1}\, x_j^\ell \qquad (6.75)
\end{aligned}$$

This relation must vanish for both x_j^ℓ replaced by a constant, for example 1, and i set different from j. In the former case, this requirement can be satisfied since such an expression then reduces to

$$\mathcal{E} \;=\; -e_{i1}(\boldsymbol{\eta}_1^1) - e_{i2}(\boldsymbol{\eta}_1^2) + e_{i1}(\boldsymbol{\eta}_2^1) - e_{i2}(\boldsymbol{\eta}_2^2)$$

$$+e_{i1}(\boldsymbol{\eta}_3^1) + e_{i2}(\boldsymbol{\eta}_3^2) - e_{i1}(\boldsymbol{\eta}_4^1) + e_{i2}(\boldsymbol{\eta}_4^2) \tag{6.76}$$

and if

$$\begin{aligned} e_{i1}(\boldsymbol{\eta}_1^1) = e_{i1}(\boldsymbol{\eta}_2^1) \quad &, \quad e_{i1}(\boldsymbol{\eta}_3^1) = e_{i1}(\boldsymbol{\eta}_4^1) \\ e_{i2}(\boldsymbol{\eta}_1^2) = e_{i2}(\boldsymbol{\eta}_4^2) \quad &, \quad e_{i2}(\boldsymbol{\eta}_2^2) = e_{i2}(\boldsymbol{\eta}_3^2) \end{aligned} \tag{6.77}$$

then this expression vanishes as needed. Considering that the basis functions N_ℓ are bilinear and e_{jk} are expressed via (6.32)-(6.33), then relations (6.77) are satisfied if

$$\begin{aligned} \boldsymbol{\eta}_1^1 \equiv \boldsymbol{\eta}_2^1 \quad &, \quad \boldsymbol{\eta}_3^1 \equiv \boldsymbol{\eta}_4^1 \\ \boldsymbol{\eta}_1^2 \equiv \boldsymbol{\eta}_4^2 \quad &, \quad \boldsymbol{\eta}_2^2 \equiv \boldsymbol{\eta}_3^2 \end{aligned} \tag{6.78}$$

Conversely, for $i \neq j$, expression (6.75) does not identically vanish. For example, setting $i = 1$ and $j = 2$, and using (6.77), hence (6.78) yields

$$\begin{aligned} \mathcal{E} \;=\; & +e_{11}(\boldsymbol{\eta}_1^1)\left[(N_\ell)_{P_2^1}\, x_2^\ell - (N_\ell)_{P_1^1}\, x_2^\ell\right] + e_{11}(\boldsymbol{\eta}_4^1)\left[(N_\ell)_{P_3^1}\, x_2^\ell - (N_\ell)_{P_4^1}\, x_2^\ell\right] \\ & +e_{12}(\boldsymbol{\eta}_1^2)\left[(N_\ell)_{P_4^2}\, x_2^\ell - (N_\ell)_{P_1^2}\, x_2^\ell\right] + e_{12}(\boldsymbol{\eta}_2^2)\left[(N_\ell)_{P_3^2}\, x_2^\ell - (N_\ell)_{P_2^2}\, x_2^\ell\right] \end{aligned} \tag{6.79}$$

which cannot be forced to vanish for arbitrary values of x_2^j, since on each element the metric data e_{jk} with (6.77), (6.78) couple only two nodes whereas the relations between brackets couple four nodes. However, the magnitude of this expression is modest since it satisfies the following order-of-magnitude constraint

$$O(\mathcal{E}) = O\left(\max_{e=1,4}\left(\left(\frac{\partial x_2}{\partial \eta_2}\right)_{\boldsymbol{\eta}_e^1}\left(\frac{\Delta x_2}{\Delta \eta_1}\right)_e \Delta\eta_1 - \left(\frac{\partial x_2}{\partial \eta_1}\right)_{\boldsymbol{\eta}_e^2}\left(\frac{\Delta x_2}{\Delta \eta_2}\right)_e \Delta\eta_2\right)\right) \tag{6.80}$$

Consequently, evaluation (6.74) may be accurate for suitable element aspect ratios.

The coordinate of the evaluation points $\boldsymbol{\eta}_e^1$ and $\boldsymbol{\eta}_e^2$ are determined by setting $i = j = 1$ in (6.75). For this index specification, this expresion is cast as

$$\mathcal{E} = \left[\left(\frac{\partial x_2}{\partial \eta_2}\right)_{\boldsymbol{\eta}_1^1}\left(\frac{\Delta x_1}{\Delta \eta_1}\right)_{(1;+1/3),e=1}\Delta\eta_1 + \left(\frac{\partial x_2}{\partial \eta_2}\right)_{\boldsymbol{\eta}_4^1}\left(\frac{\Delta x_1}{\Delta \eta_1}\right)_{(1;-1/3),e=4}\Delta\eta_1\right] - \left[\left(\frac{\partial x_2}{\partial \eta_1}\right)_{\boldsymbol{\eta}_1^2}\left(\frac{\Delta x_1}{\Delta \eta_2}\right)_{(+1/3;1),e=1}\Delta\eta_2 + \left(\frac{\partial x_2}{\partial \eta_1}\right)_{\boldsymbol{\eta}_2^2}\left(\frac{\Delta x_1}{\Delta \eta_2}\right)_{(-1/3;1),e=2}\Delta\eta_2\right] \quad (6.81)$$

which, for the following choices of $\boldsymbol{\eta}_e^1 \equiv \boldsymbol{\eta}_e^2 \equiv \tilde{\boldsymbol{\eta}}_e$

$$\begin{aligned}
&\boldsymbol{\eta}_1^1 = (+1;+\tfrac{1}{3}) \equiv \boldsymbol{\eta}_2^1 = (-1;+\tfrac{1}{3}) \quad , \quad \boldsymbol{\eta}_3^1 = (-1;-\tfrac{1}{3}) \equiv \boldsymbol{\eta}_4^1 = (+1;-\tfrac{1}{3}) \\
&\boldsymbol{\eta}_1^2 = (+\tfrac{1}{3};+1) \equiv \boldsymbol{\eta}_4^2 = (+\tfrac{1}{3};-1) \quad , \quad \boldsymbol{\eta}_2^2 = (-\tfrac{1}{3};+1) \equiv \boldsymbol{\eta}_3^2 = (-\tfrac{1}{3};-1) \\
&\tilde{\boldsymbol{\eta}}_1 = (+1;+1) \equiv \tilde{\boldsymbol{\eta}}_4 = (+1;-1) \quad , \quad \tilde{\boldsymbol{\eta}}_2 = (-1;+1) \equiv \tilde{\boldsymbol{\eta}}_3 = (-1;-1)
\end{aligned} \quad (6.82)$$

reduces to

$$\mathcal{E} \approx 4 \cdot \det J(\boldsymbol{\eta}^r), \quad \boldsymbol{\eta}^r \equiv \text{ node } (i,j) \quad (6.83)$$

since e_{jk} is independent of the η_{3-k} coordinate in 2-D. Therefore, (6.75) approximates expression (6.72). Note that for $i = 2$ and $j = 1,2$ identical conclusions are reached for (6.80), (6.81). In particular, the accuracy level of the latter expressions critically depends on element aspect ratios. Conversely, the accuracy of the corresponding strong statement expressions is not affected by truly arbitrary meshes.

6.4.3 Accuracy Considerations

Expression (6.62) constitutes the fundamental consistency and/or first order accuracy constraint that all consistent semi-discretization theories verify on a uniform

mesh. For arbitrary meshes such a verification is in general more involved. However, the semi-discretization procedure herein detailed has yielded this crucial verification in a rather straightforward manner, via determination and use of metric-data optimal evaluation points. This procedure is now expanded to achieve a semi-discretization for nonlinear terms that is second order accurate on both primitive and computational coordinate spaces. This is accomplished by devising a semi-discrete formula that identically satisfies constraint (6.27) on arbitrary meshes.

6.4.4 Second Order Accurate Semi-Discretizations on Arbitrary Meshes

Setting $\psi = x_i^\ell N_\ell$ allows expressing the fundamental identity (6.27) as

$$\mathcal{G}_e = \int_{\widehat{\Omega}_e} w \frac{e_{jk}}{2} \frac{\partial (x_i)^2}{\partial \eta_k} \, d\boldsymbol{\eta} = \int_{\widehat{\Omega}_e} e_{jk} N_r x_i^\ell N_\ell \frac{\partial N_s}{\partial \eta_k} x_i^s \, d\boldsymbol{\eta} = \left[\det J x_i \delta_j^i \right]_{\boldsymbol{\eta}^P} \tag{6.84}$$

and using Lemma (6.1) yields

$$\mathcal{G}_e = \int_{\widehat{\Omega}_e} e_{jk} N_r x_i^\ell N_\ell \frac{\partial N_s}{\partial \eta_k} x_i^s \, d\boldsymbol{\eta} = x_i^\ell N_\ell(\boldsymbol{\eta}_e^*) e_{jk}(\boldsymbol{\eta}_e) \int_{\widehat{\Omega}_e} N_r \frac{\partial N_s}{\partial \eta_k} x_i^s \, d\boldsymbol{\eta} \tag{6.85}$$

where $\boldsymbol{\eta}_e^*$ is a suitable evaluation point that permits satisfying (6.84), hence yields 2^{nd} order accuracy. Capitalizing on the results (6.39), (6.48), (6.70) and (6.71) allows expressing (6.85) as

$$\mathcal{G}_e = x_i^\ell N_\ell(\boldsymbol{\eta}_e^*) \left((e_{j1})_{P_e} \left(\frac{\partial N_\ell}{\partial \eta_1} \right)_{P_e} x_i^\ell + (e_{j2})_{P_e} \left(\frac{\partial N_\ell}{\partial \eta_2} \right)_{P_e} x_i^\ell \right) = x_i^\ell N_\ell(\boldsymbol{\eta}_e^*) (\det J)_{P_e} \delta_j^i \tag{6.86}$$

And upon identification of $\boldsymbol{\eta}_e^*$ with P_e, recall (6.68), expression (6.86) becomes

$$\mathcal{G}_e = x_i^\ell (N_\ell)_{P_e} (\det J)_{P_e} \delta_j^i \tag{6.87}$$

which by corresponding to the lhs of (6.84) for arbitrary e_{jk}, hence $\det J$, proves the accuracy assertion.

For the weak statement integrals (6.56), (6.59) the counterpart of relation (6.84) is

$$\tilde{\mathcal{G}} = \int_{\widehat{\Omega}} N_r \frac{e_{jk}}{2} \frac{\partial (x_i)^2}{\partial \eta_k} \, d\boldsymbol{\eta} = -\frac{1}{2} \int_{\widehat{\Omega}} e_{jk} \frac{\partial N_r}{\partial \eta_k} N_m x_i^m N_\ell x_i^\ell \, d\boldsymbol{\eta} =$$

$$\frac{1}{2} \sum_{e=1}^{4} \left(- \int_{\widehat{\Omega}_e} \frac{\partial N_r}{\partial \eta_k} e_{jk} N_\ell x_i^\ell N_m x_i^m \, d\boldsymbol{\eta} \right) = \frac{1}{2} \sum_{e=1}^{4} e_{jk}(\tilde{\boldsymbol{\eta}}_e) N_m(\boldsymbol{\eta}_e^k) x_i^m \left(- \int_{\widehat{\Omega}_e} \frac{\partial N_r}{\partial \eta_k} N_\ell \, d\boldsymbol{\eta} \right) =$$

$$\begin{aligned}
&\frac{1}{2} e_{j1}(\tilde{\boldsymbol{\eta}}_1) \cdot \left[-N_m(\boldsymbol{\eta}_1^1) (N_\ell)_{P_1^1} x_i^\ell + N_m(\boldsymbol{\eta}_2^1) (N_\ell)_{P_2^1} x_i^\ell \right] + \\
&\frac{1}{2} e_{j1}(\tilde{\boldsymbol{\eta}}_4) \cdot \left[+N_m(\boldsymbol{\eta}_3^1) (N_\ell)_{P_3^1} x_i^\ell - N_m(\boldsymbol{\eta}_4^1) (N_\ell)_{P_4^1} x_i^\ell \right] + \\
&\frac{1}{2} e_{j2}(\tilde{\boldsymbol{\eta}}_1) \cdot \left[-N_m(\boldsymbol{\eta}_1^2) (N_\ell)_{P_1^2} x_i^\ell + N_m(\boldsymbol{\eta}_4^2) (N_\ell)_{P_4^2} x_i^\ell \right] + \\
&\frac{1}{2} e_{j2}(\tilde{\boldsymbol{\eta}}_2) \cdot \left[+N_m(\boldsymbol{\eta}_3^2) (N_\ell)_{P_3^2} x_i^\ell - N_m(\boldsymbol{\eta}_2^2) (N_\ell)_{P_2^2} x_i^\ell \right]
\end{aligned} \tag{6.88}$$

Whereupon, setting

$$\boldsymbol{\eta}_e^k \equiv P_e^k \quad 1 \le e \le 4 \tag{6.89}$$

see (6.42) and (6.49), leads to the result

$$\begin{aligned}
\tilde{\mathcal{G}} \;=\; & \frac{1}{2} e_{j1}(\tilde{\boldsymbol{\eta}}_1) \left[\left((N_\ell)_{P_2^1} x_i^\ell \right)^2 - \left((N_\ell)_{P_1^1} x_i^\ell \right)^2 \right] \\
+ \; & \frac{1}{2} e_{j1}(\tilde{\boldsymbol{\eta}}_3) \left[\left((N_\ell)_{P_3^1} x_i^\ell \right)^2 - \left((N_\ell)_{P_4^1} x_i^\ell \right)^2 \right] \\
+ \; & \frac{1}{2} e_{j2}(\tilde{\boldsymbol{\eta}}_2) \left[\left((N_\ell)_{P_3^2} x_i^\ell \right)^2 - \left((N_\ell)_{P_2^1} x_i^\ell \right)^2 \right] \\
+ \; & \frac{1}{2} e_{j2}(\tilde{\boldsymbol{\eta}}_1) \left[\left((N_\ell)_{P_4^2} x_i^\ell \right)^2 - \left((N_\ell)_{P_1^2} x_i^\ell \right)^2 \right] = \\
& \frac{1}{2} e_{j1}(\tilde{\boldsymbol{\eta}}_1) \left(\frac{\Delta x_i^2}{\Delta \eta_1} \right)_{\boldsymbol{\eta}_1^1} \Delta \eta_1 + \frac{1}{2} e_{j1}(\tilde{\boldsymbol{\eta}}_3) \left(\frac{\Delta x_i^2}{\Delta \eta_1} \right)_{\boldsymbol{\eta}_3^1} \Delta \eta_1 + \\
& \frac{1}{2} e_{j2}(\tilde{\boldsymbol{\eta}}_2) \left(\frac{\Delta x_i^2}{\Delta \eta_2} \right)_{\boldsymbol{\eta}_2^2} \Delta \eta_2 + \frac{1}{2} e_{j2}(\tilde{\boldsymbol{\eta}}_4) \left(\frac{\Delta x_i^2}{\Delta \eta_2} \right)_{\boldsymbol{\eta}_4^2} \Delta \eta_2 =
\end{aligned}$$

$$
\begin{aligned}
& e_{j1}(\tilde{\boldsymbol{\eta}}_1)\left(x_i\frac{\Delta x_i}{\Delta\eta_1}\right)_{\boldsymbol{\eta}_1^1}\Delta\eta_1 + e_{j1}(\tilde{\boldsymbol{\eta}}_3)\left(x_i\frac{\Delta x_i}{\Delta\eta_1}\right)_{\boldsymbol{\eta}_3^1}\Delta\eta_1 + \\
& e_{j2}(\tilde{\boldsymbol{\eta}}_2)\left(x_i\frac{\Delta x_i}{\Delta\eta_2}\right)_{\boldsymbol{\eta}_2^2}\Delta\eta_2 + e_{j2}(\tilde{\boldsymbol{\eta}}_4)\left(x_i\frac{\Delta x_i}{\Delta\eta_2}\right)_{\boldsymbol{\eta}_4^2}\Delta\eta_2 + O_{\max,i}\left((\Delta x_i)^2\right) \\
& \approx 4\cdot[\det J]_{\boldsymbol{\eta}^r}x_j^r\delta_i^j
\end{aligned}
\tag{6.90}
$$

Note again that the strong statement integral yields an exact representation of (6.84) for arbitrary meshes, whereas the weak form can only approximate it.

6.4.5 Specific Applications

Utilization of formula (6.85) and/or (6.90) for the semi-discretization of non-linear second or higher-degree terms within the convection operator, yields a recursion formula that can be second order accurate in both primitive and computational coordinate spaces for arbitrary meshes. The following semi-discretization for a representative Euler equation convection term exemplifies the use of such formulae. This term is written as

$$
\det J\cdot\mathcal{C}\equiv\det J\frac{\partial}{\partial x}\left[\frac{m_x}{\rho}m_x\right]=e_{1k}\frac{\partial}{\partial\eta_k}\left[\frac{m_x}{\rho}m_x\right] \tag{6.91}
$$

An integral representation for this expression is

$$
\int_{\widehat{\Omega}_e}N_r\det J\cdot C\;d\boldsymbol{\eta}=\int_{\widehat{\Omega}_e}N_re_{1k}(\boldsymbol{\eta})\frac{\partial}{\partial\eta_k}\left[\frac{m_x}{\rho}\cdot m_x\right]\;d\boldsymbol{\eta} \tag{6.92}
$$

hence

$$
\int_{\widehat{\Omega}_e}N_r\det J\cdot C\;d\boldsymbol{\eta}\simeq\int_{\widehat{\Omega}_e}N_re_{1k}(\boldsymbol{\eta})\frac{\partial}{\partial\eta_k}[N_jN_\ell]\;d\boldsymbol{\eta}\;\frac{m_x^j}{\rho^j}\cdot m_x^\ell \tag{6.93}
$$

Thereafter, (6.85) leads to the terminal relation

$$\int_{\widehat{\Omega}_e} N_r \det J \cdot C \; d\boldsymbol{\eta} \simeq$$
$$\left\{ e_{1k}(\boldsymbol{\eta}_e) N_j(\boldsymbol{\eta}_e) \frac{m_x^j}{\rho^j} \int_{\widehat{\Omega}_e} N_r \frac{\partial}{\partial \eta_k} [N_\ell] \; d\boldsymbol{\eta} \; m_x^\ell \right.$$
$$\left. e_{1k}(\boldsymbol{\eta}_e) N_\ell(\boldsymbol{\eta}_e) m_x^\ell \int_{\widehat{\Omega}_e} N_r \frac{\partial}{\partial \eta_k} [N_j] \; d\boldsymbol{\eta} \; \frac{m_x^j}{\rho^j} \right\} \tag{6.94}$$

The corresponding expression for the weak form (6.89) is

$$\int_{\widehat{\Omega}} N_r \det J \cdot C \; d\boldsymbol{\eta} \approx -\sum_{e=1}^{M} \left\{ e_{1k}(\tilde{\boldsymbol{\eta}}_e) N_j(\boldsymbol{\eta}_e^k) \frac{m_x^j}{\rho^j} \int_{\widehat{\Omega}_e} \frac{\partial N_r}{\partial \eta_k} [N_\ell] \; d\boldsymbol{\eta} \; m_x^\ell \right\} \tag{6.95}$$

6.5 Determination of Optimal Metric Data Evaluation Points for Diffusion Operator Semi-Discretizations

This section is also divided into two parts. In the first part ψ is set to one, the required integrations are performed over each computational cell illustrated in Figure 6.5, and the attendant results are appropriately summed. In the second part the derived expressions are multiplied by the metric data to form relations (6.29) and (6.30), after setting $\varphi = x_j$. Finally, the optimal evaluation points are determined.

6.5.1 Integrations in η Space

The evaluation of the parallel-derivative integral

$$\mathcal{I}_{11}^r = -\int_{\widehat{\Omega}} \frac{\partial N_r}{\partial \eta_1} \frac{\partial N_j}{\partial \eta_1} \, d\boldsymbol{\eta} \, \varphi^j = -\sum_{e=1}^{4} \int_{\widehat{\Omega}_e} \frac{\partial N_r}{\partial \eta_1} \frac{\partial N_j}{\partial \eta_1} \, d\boldsymbol{\eta} \, \varphi^j \tag{6.96}$$

over $\widehat{\Omega}$, see Figure 6.5, yields

$$
\begin{aligned}
-\int_{\widehat{\Omega}_1} \frac{\partial N_r}{\partial \eta_1}\frac{\partial N_j}{\partial \eta_1}\, d\boldsymbol{\eta}\, \varphi^j &= -\left(\frac{\partial N_j}{\partial \eta_1}\right)_{P_1^1} \varphi^j \quad , \quad -\int_{\widehat{\Omega}_2} \frac{\partial N_r}{\partial \eta_1}\frac{\partial N_j}{\partial \eta_1}\, d\boldsymbol{\eta}\, \varphi^j = +\left(\frac{\partial N_j}{\partial \eta_1}\right)_{P_2^1} \varphi^j \\
-\int_{\widehat{\Omega}_3} \frac{\partial N_r}{\partial \eta_1}\frac{\partial N_j}{\partial \eta_1}\, d\boldsymbol{\eta}\, \varphi^j &= +\left(\frac{\partial N_j}{\partial \eta_1}\right)_{P_3^1} \varphi^j \quad , \quad -\int_{\widehat{\Omega}_4} \frac{\partial N_r}{\partial \eta_1}\frac{\partial N_j}{\partial \eta_1}\, d\boldsymbol{\eta}\, \varphi^j = -\left(\frac{\partial N_j}{\partial \eta_1}\right)_{P_4^1} \varphi^j
\end{aligned}
\tag{6.97}
$$

Note that the evaluation points in these expressions coincide with (6.40).

Consequently $\mathcal{I}_{11}^r$ is expressed as

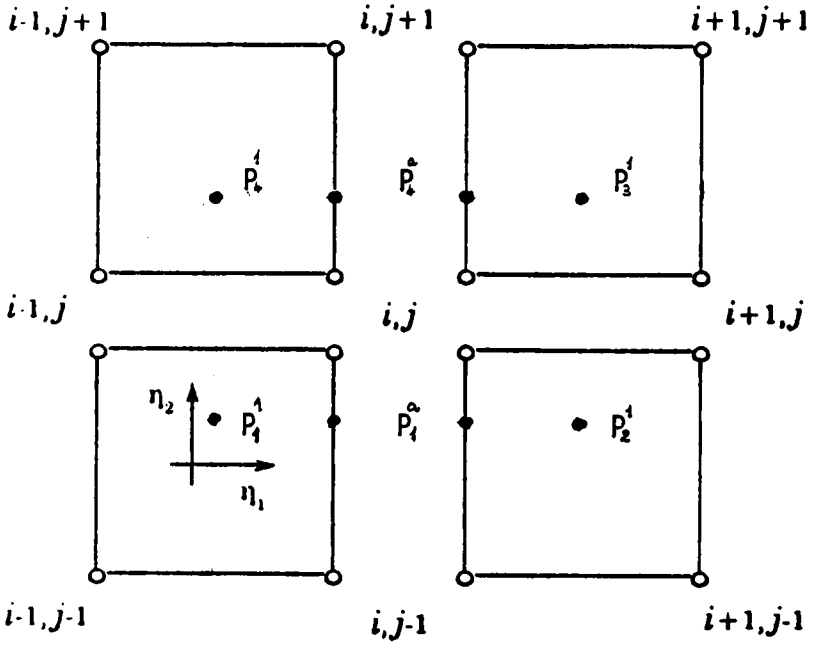


Figure 6.5: Contiguous Elements and Evaluation Points for Integrals (6.97)

$$
\mathcal{I}_{11}^r = \left\{ \left[\left(\frac{\partial N_j}{\partial \eta_1}\right)_{P_2^1} \varphi^j - \left(\frac{\partial N_j}{\partial \eta_1}\right)_{P_1^1} \varphi^j \right] + \left[\left(\frac{\partial N_j}{\partial \eta_1}\right)_{P_3^1} \varphi^j - \left(\frac{\partial N_j}{\partial \eta_1}\right)_{P_4^1} \varphi^j \right] \right\} \tag{6.98}
$$

with each partial derivative computed in the element identified by the subscript in P_e^1, and coincides with the recursion formula

$$
\mathcal{I}_{11}^r = \frac{1}{2}\left(\frac{2}{6}\phi_{i-1,j-1} - \frac{4}{6}\phi_{i,j-1} + \frac{2}{6}\phi_{i+1,j-1}\frac{4}{6}\phi_{i-1,j} - \frac{8}{6}\phi_{i,j} + \frac{4}{6}\phi_{i+1,j}\right.
$$

$$+\frac{4}{6}\phi_{i-1,j} - \frac{8}{6}\phi_{i,j} + \frac{4}{6}\phi_{i+1,j} + \frac{2}{6}\phi_{i-1,j+1} + \frac{4}{6}\phi_{i,j+1} + \frac{2}{6}\phi_{i+1,j+1}\Big) \quad (6.99)$$

Expression (6.98), hence (6.99), supplies the average of two second-order centered difference formulae evaluated at points $P_1^a \equiv (1, 1/3)$ and $P_4^a \equiv (1, -1/3)$ respectively, as is easily shown by referring to Figure 6.6. The second-order accurate centered formula approximating the partial derivative $\frac{\partial}{\partial \eta_1}\left(\frac{\partial \varphi}{\partial \eta_1}\right)\Delta\eta_1^2$ at point P_1^a is

$$\left[\Delta\eta_1^2 \frac{\partial}{\partial \eta_1}\left(\frac{\partial \varphi}{\partial \eta_1}\right)\right]_{P_1^a} \simeq \left(\left(\frac{\partial \varphi}{\partial \eta_1}\right)_{P_2^1} - \left(\frac{\partial \varphi}{\partial \eta_1}\right)_{P_1^1}\right)\Delta\eta_1 \quad (6.100)$$

Whereupon utilization of expression (6.43) for the semi-discretization of these rhs partial derivatives leads to the recursion formula

$$\begin{aligned}\left[\frac{\partial}{\partial \eta_1}\left(\frac{\partial \varphi}{\partial \eta_1}\right)\right]_{P_1^a}\Delta\eta_1^2 \simeq &\left[\left(\left(\frac{4}{6}\phi_{i+1,j} + \frac{2}{6}\phi_{i+1,j-1}\right) - \left(\frac{4}{6}\phi_{i,j} + \frac{2}{6}\phi_{i,j-1}\right)\right) - \right. \\ &\left.\left(\left(\frac{4}{6}\phi_{i,j} + \frac{2}{6}\phi_{i,j-1}\right) - \left(\frac{4}{6}\phi_{i-1,j} + \frac{2}{6}\phi_{i-1,j-1}\right)\right)\right] = \\ &\left[\frac{2}{6}\phi_{i-1,j-1} - \frac{4}{6}\phi_{i,j-1} + \frac{2}{6}\phi_{i+1,j-1} + \frac{4}{6}\phi_{i-1,j} - \frac{8}{6}\phi_{i,j} + \frac{4}{6}\phi_{i+1,j}\right]\Delta\eta_1 \quad (6.101)\end{aligned}$$

The companion expression formed at point P_4^a is

$$\begin{aligned}&\left[\frac{\partial}{\partial \eta_1}\left(\frac{\partial \varphi}{\partial \eta_1}\right)\right]_{P_4^a}\Delta\eta_1^2 \simeq \\ &\left[\frac{4}{6}\phi_{i-1,j} - \frac{8}{6}\phi_{i,j} + \frac{4}{6}\phi_{i+1,j} + \frac{2}{6}\phi_{i-1,j+1} - \frac{4}{6}\phi_{i,j+1} + \frac{2}{6}\phi_{i+1,j+1}\right]\Delta\eta_1 \quad (6.102)\end{aligned}$$

Whereupon the average of expressions (6.101) and (6.102) reverts to (6.99). Note that the latter is also interpreted as a semi-discretization of the lhs of (6.100) at node r.

Following an analogous procedure, the evaluation of the integral

$$\mathcal{I}_{22}^{r} = -\int_{\widehat{\Omega}} \frac{\partial N_r}{\partial \eta_2}\frac{\partial N_j}{\partial \eta_2}\, d\boldsymbol{\eta}\, \varphi^j = -\sum_{e=1}^{4}\int_{\widehat{\Omega}_e} \frac{\partial N_r}{\partial \eta_2}\frac{\partial N_j}{\partial \eta_2}\, d\boldsymbol{\eta}\, \varphi^j \tag{6.103}$$

over $\widehat{\Omega}$, see Figure 6.6, yields

$$\begin{aligned}
-\int_{\widehat{\Omega}_1} \frac{\partial N_r}{\partial \eta_2}\frac{\partial N_j}{\partial \eta_2}\, d\boldsymbol{\eta}\, \varphi^j &= -\left(\frac{\partial N_j}{\partial \eta_2}\right)_{P_1^2} \varphi^j \quad , \quad -\int_{\widehat{\Omega}_2} \frac{\partial N_r}{\partial \eta_2}\frac{\partial N_j}{\partial \eta_2}\, d\boldsymbol{\eta}\, \varphi^j = -\varphi^j \left(\frac{\partial N_j}{\partial \eta_2}\right)_{P_2^2} \\
-\int_{\widehat{\Omega}_3} \frac{\partial N_r}{\partial \eta_2}\frac{\partial N_j}{\partial \eta_2}\, d\boldsymbol{\eta}\, \varphi^j &= +\left(\frac{\partial N_j}{\partial \eta_2}\right)_{P_3^2} \varphi^j \quad , \quad -\int_{\widehat{\Omega}_4} \frac{\partial N_r}{\partial \eta_2}\frac{\partial N_j}{\partial \eta_2}\, d\boldsymbol{\eta}\, \varphi^j = +\varphi^j \left(\frac{\partial N_j}{\partial \eta_2}\right)_{P_4^2}
\end{aligned} \tag{6.104}$$

where the evaluation points P_e^2 are the same as (6.49).

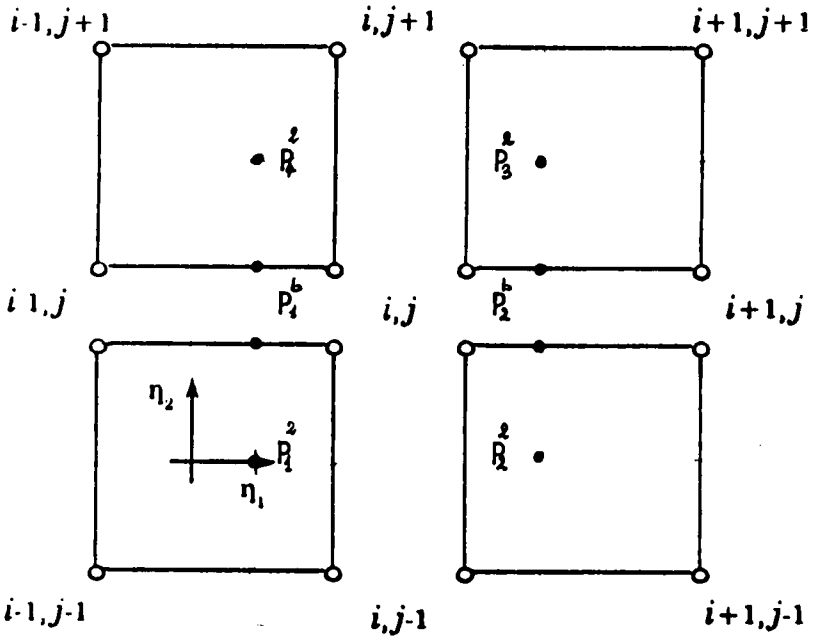


Figure 6.6: Contiguous Elements and Evaluation Points for Integrals (6.104)

Consequently, $\mathcal{I}_{22}^{r}$ is expressed as

$$\mathcal{I}_{22}^{r} = \left\{ \left[\left(\frac{\partial N_j}{\partial \eta_2}\right)_{P_4^2} \varphi^j - \left(\frac{\partial N_j}{\partial \eta_2}\right)_{P_1^2} \varphi^j \right] + \left[\left(\frac{\partial N_j}{\partial \eta_2}\right)_{P_3^2} \varphi^j - \left(\frac{\partial N_j}{\partial \eta_2}\right)_{P_2^2} \varphi^j \right] \right\} \tag{6.105}$$

with each partial derivative computed in the cell corresponding to the subscript in P_e^2, and coincides with the recursion formula

$$\mathcal{I}_{22}^r = \tfrac{1}{2}\left(\frac{2}{6}\phi_{i-1,j-1} - \frac{4}{6}\phi_{i-1,j} + \frac{2}{6}\phi_{i-1,j+1} + \frac{4}{6}\phi_{i,j-1} - \frac{8}{6}\phi_{i,j} + \frac{4}{6}\phi_{i,j+1} \right.$$
$$\left. \frac{4}{6}\phi_{i,j-1} - \frac{8}{6}\phi_{i,j} + \frac{4}{6}\phi_{i,j+1} + \frac{2}{6}\phi_{i+1,j-1} - \frac{4}{6}\phi_{i+1,j} + \frac{2}{6}\phi_{i+1,j+1}\right) \quad (6.106)$$

Relation (6.105), hence (6.106), expresses the average of the two second-order centered difference formulae evaluated at points $P_1^b \equiv (1/3;1)$ and $P_2^b \equiv (-1/3;1)$ respectively, as is easily shown by referring to Figure 6.8. The second-order accurate formula approximating the partial derivative $\frac{\partial}{\partial\eta_2}\left(\frac{\partial\varphi}{\partial\eta_2}\right)\Delta\eta_2^2$ at point P_1^b is

$$\left[\Delta\eta_2^2 \frac{\partial}{\partial\eta_2}\left(\frac{\partial\varphi}{\partial\eta_2}\right)\right]_{P_1^b} \simeq \left(\left(\frac{\partial\varphi}{\partial\eta_2}\right)_{P_4^2} - \left(\frac{\partial\varphi}{\partial\eta_2}\right)_{P_1^2}\right)\Delta\eta_2 \quad (6.107)$$

Whereupon utilization of expression (6.52) for the semi-discretization of the rhs partial derivatives leads to the recursion formula

$$\left[\frac{\partial}{\partial\eta_2}\left(\frac{\partial\varphi}{\partial\eta_2}\right)\right]_{P_1^b}\Delta\eta_2^2 \simeq$$
$$\left[\frac{2}{6}\phi_{i-1,j-1} - \frac{4}{6}\phi_{i-1,j} + \frac{2}{6}\phi_{i-1,j+1} + \frac{4}{6}\phi_{i,j-1} - \frac{8}{6}\phi_{i,j} + \frac{4}{6}\phi_{i,j+1}\right]\Delta\eta_2 \quad (6.108)$$

The companion expression at point P_2^b is

$$\left[\frac{\partial}{\partial\eta_2}\left(\frac{\partial\varphi}{\partial\eta_2}\right)\right]_{P_2^a}\Delta\eta_2^2 \simeq$$
$$\left[\frac{4}{6}\phi_{i,j-1} - \frac{8}{6}\phi_{i,j} + \frac{4}{6}\phi_{i,j+1} + \frac{2}{6}\phi_{i+1,j-1} - \frac{4}{6}\phi_{i+1,j} + \frac{2}{6}\phi_{i+1,j+1}\right]\Delta\eta_2 \quad (6.109)$$

Whereupon the average of expressions (6.108) and (6.109) reverts to evaluation (106), which is also interpreted as the semi-discretization of the lhs of (6.107) at node r.

Finally, the evaluation of the cross-derivative integral

$$\mathcal{I}_{12}^{r} = -\int_{\widehat{\Omega}} \frac{\partial N_r}{\partial \eta_1}\frac{\partial N_j}{\partial \eta_2}\, d\boldsymbol{\eta}\, \varphi_j = -\sum_{e=1}^{4} \int_{\widehat{\Omega}_e} \frac{\partial N_r}{\partial \eta_1}\frac{\partial N_j}{\partial \eta_2}\, d\boldsymbol{\eta}\, \varphi^j \tag{6.110}$$

on $\widehat{\Omega}$, see Figure 6.7, yields

$$\begin{aligned}
&-\int_{\widehat{\Omega}_1} \frac{\partial N_r}{\partial \eta_1}\frac{\partial N_j}{\partial \eta_2}\, d\boldsymbol{\eta}\, \varphi^j = -\left(\frac{\partial N_j}{\partial \eta_2}\right)_{P_1^o} \varphi^j \quad , \quad -\int_{\widehat{\Omega}_2} \frac{\partial N_r}{\partial \eta_1}\frac{\partial N_j}{\partial \eta_2}\, d\boldsymbol{\eta}\, \varphi^j = +\varphi^j \left(\frac{\partial N_j}{\partial \eta_2}\right)_{P_2^o} \\
&-\int_{\widehat{\Omega}_3} \frac{\partial N_r}{\partial \eta_1}\frac{\partial N_j}{\partial \eta_2}\, d\boldsymbol{\eta}\, \varphi^j = +\left(\frac{\partial N_j}{\partial \eta_2}\right)_{P_3^o} \varphi^j \quad , \quad -\int_{\widehat{\Omega}_4} \frac{\partial N_r}{\partial \eta_1}\frac{\partial N_j}{\partial \eta_2}\, d\boldsymbol{\eta}\, \varphi^j = -\varphi^j \left(\frac{\partial N_j}{\partial \eta_2}\right)_{P_4^o}
\end{aligned} \tag{6.111}$$

The coordinates of the evaluation points in these expressions are

$$P_1^o \equiv (0; +\frac{1}{3}), \quad P_2^o \equiv (0; +\frac{1}{3}), \quad P_3^o \equiv (0; -\frac{1}{3}), \quad P_4^o \equiv (0; -\frac{1}{3}) \tag{6.112}$$

Consequently, $\mathcal{I}_{12}^{r}$ is written as

$$\mathcal{I}_{12}^{r} = \left\{ \left[\left(\frac{\partial N_j}{\partial \eta_2}\right)_{P_2^o} \varphi^j - \left(\frac{\partial N_j}{\partial \eta_2}\right)_{P_1^o} \varphi^j \right] + \left[\left(\frac{\partial N_j}{\partial \eta_2}\right)_{P_3^o} \varphi^j - \left(\frac{\partial N_j}{\partial \eta_2}\right)_{P_4^o} \varphi_j \right] \right\} \tag{6.113}$$

with each partial derivative computed in the cell corresponding to the subscript in P_e^o, and corresponds to the recursion formula

$$\mathcal{I}_{12}^{r} \;\; = \tfrac{1}{4} \;\; (\phi_{i-1,j-1} - \phi_{i+1,j-1} - \phi_{i+1,j+1} + \phi_{i+1,j+1}) \tag{6.114}$$

This expression coincides with the standard second-order accurate centered finite difference formula approximating the expression

$$c_1 = \frac{\partial}{\partial \eta_1}\left(\frac{\partial \varphi}{\partial \eta_2}\Delta\eta_1\Delta\eta_2\right) \tag{6.115}$$

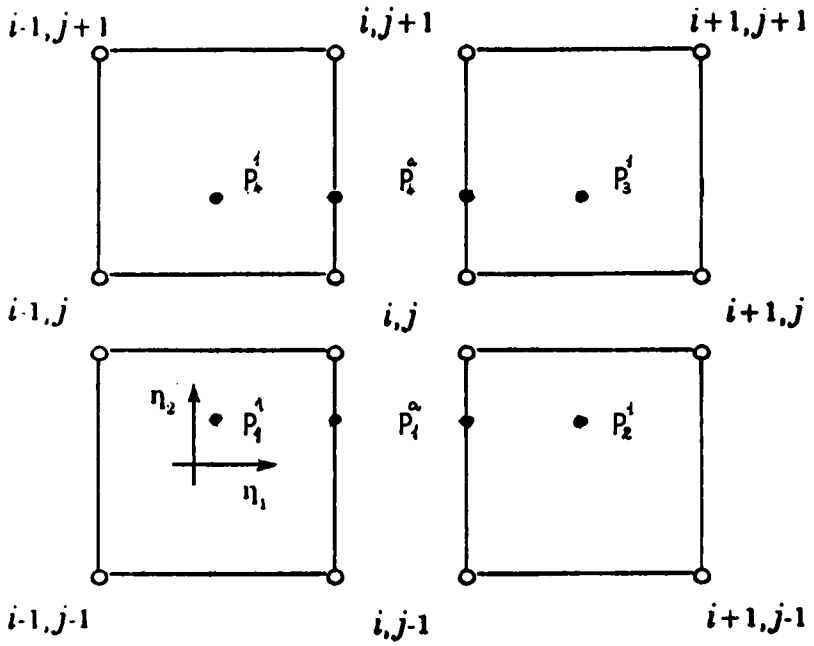


Figure 6.7: Contiguous Elements and Evaluation Points for Integrals (6.111)

at node r and can also be interpreted as the average of the second-order approximations for itself as determined at nodes $P_1^{oa} \equiv (1; +\frac{1}{3})$ and $P_4^{oa} \equiv (1; -\frac{1}{3})$.

Note that the evaluation of the integral

$$\mathcal{I}_{21}^{r} = -\int_{\widehat{\Omega}} \frac{\partial N_r}{\partial \eta_2} \frac{\partial N_j}{\partial \eta_1} \, d\boldsymbol{\eta} \, \varphi^j \tag{6.116}$$

over $\widehat{\Omega}$, see Figure 6.8, identically yields formula (6.114). Such an expression results from the sum of the integrals

$$\begin{aligned}
&-\int_{\widehat{\Omega}_1} \frac{\partial N_r}{\partial \eta_2} \frac{\partial N_j}{\partial \eta_1} \, d\boldsymbol{\eta} \, \varphi^j = -\left(\frac{\partial N_j}{\partial \eta_1}\right)_{P_1^2} \varphi^j \quad , \quad -\int_{\widehat{\Omega}_2} \frac{\partial N_r}{\partial \eta_2} \frac{\partial N_j}{\partial \eta_1} \, d\boldsymbol{\eta} \, \varphi^j = -\varphi^j \left(\frac{\partial N_j}{\partial \eta_1}\right)_{P_2^2} \\
&-\int_{\widehat{\Omega}_3} \frac{\partial N_r}{\partial \eta_2} \frac{\partial N_j}{\partial \eta_1} \, d\boldsymbol{\eta} \, \varphi^j = +\left(\frac{\partial N_j}{\partial \eta_1}\right)_{P_3^2} \varphi^j \quad , \quad -\int_{\widehat{\Omega}_4} \frac{\partial N_r}{\partial \eta_2} \frac{\partial N_j}{\partial \eta_1} \, d\boldsymbol{\eta} \, \varphi^j = -\varphi^j \left(\frac{\partial N_j}{\partial \eta_1}\right)_{P_4^2}
\end{aligned} \tag{6.117}$$

where the evaluation points are the same as (6.49).

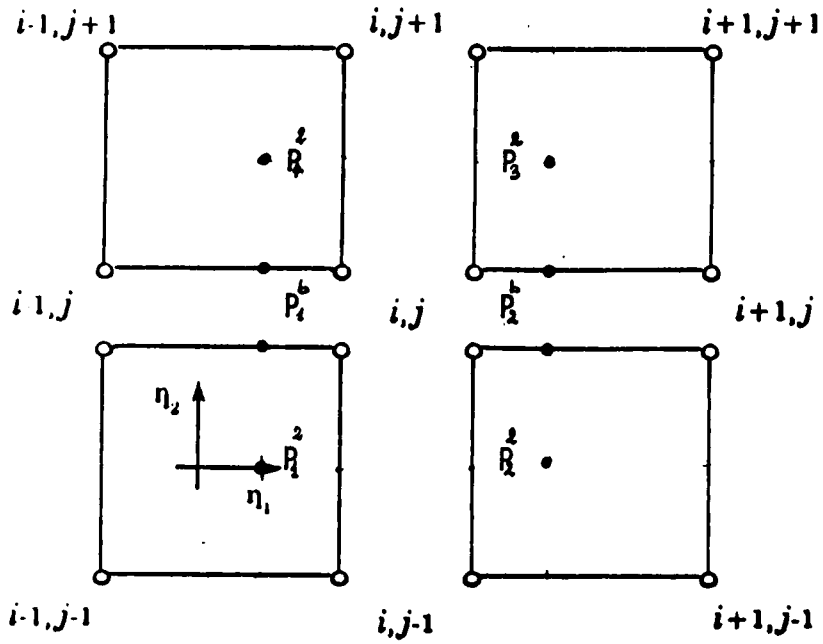


Figure 6.8: Contiguous Elements and Evaluation Points for Integrals (6.117)

Therefore, $\mathcal{I}_{21}^{r}$ is expressed as

$$\mathcal{I}_{21}^{r} = \left\{ \left[\left(\frac{\partial N_j}{\partial \eta_1} \right)_{P_4^2} \varphi^j - \left(\frac{\partial N_j}{\partial \eta_1} \right)_{P_1^2} \varphi^j \right] + \left[\left(\frac{\partial N_j}{\partial \eta_1} \right)_{P_3^2} \varphi^j - \left(\frac{\partial N_j}{\partial \eta_1} \right)_{P_2^2} \varphi^j \right] \right\} \quad (6.118)$$

and it is found to coincide with (6.113). This relation alternatively constitutes the standard second-order accurate finite-difference formula approximating the expression

$$c_2 = \frac{\partial}{\partial \eta_2} \left(\frac{\partial \varphi}{\partial \eta_1} \Delta\eta_2 \Delta\eta_1 \right) \quad (6.119)$$

at node r and can also be interpreted as the average of the second-order approximations for itself as evaluated at nodes $P_1^{ob} \equiv (+\frac{1}{3}; 1)$ and $P_2^{ob} \equiv (-\frac{1}{3}; 1)$.

6.5.2 Metric-Data Evaluation Points

The fundamental identity (6.29) is expressed in the region $\widehat{\Omega}$, see Figure 6.1, as

$$\left[\det J \cdot \frac{\partial^2 x_m}{\partial x_i \partial x_j}\right]_{\boldsymbol{\eta}^P} \cdot \int_{\widehat{\Omega}} N_r \, d\boldsymbol{\eta} \;=\; -\int_{\widehat{\Omega}} e_{ik} \frac{\partial N_r}{\partial \eta_k} \frac{e_{j\ell}}{\det J} \frac{\partial x_m}{\partial \eta_\ell} \, d\boldsymbol{\eta} = 0 \quad (6.120)$$

The unabridged form of this integral is

$$\begin{aligned} -\int_{\widehat{\Omega}} e_{ik} \frac{\partial N_r}{\partial \eta_k} \frac{e_{j\ell}}{\det J} \frac{\partial x_m}{\partial \eta_\ell} \, d\boldsymbol{\eta} = \\ -\int_{\widehat{\Omega}} e_{i1} \frac{\partial N_r}{\partial \eta_1} \frac{e_{j1}}{\det J} \frac{\partial x_m}{\partial \eta_1} \, d\boldsymbol{\eta} - \int_{\widehat{\Omega}} e_{i1} \frac{\partial N_r}{\partial \eta_1} \frac{e_{j2}}{\det J} \frac{\partial x_m}{\partial \eta_2} \, d\boldsymbol{\eta} \\ -\int_{\widehat{\Omega}} e_{i2} \frac{\partial N_r}{\partial \eta_2} \frac{e_{j1}}{\det J} \frac{\partial x_m}{\partial \eta_1} \, d\boldsymbol{\eta} - \int_{\widehat{\Omega}} e_{i2} \frac{\partial N_r}{\partial \eta_2} \frac{e_{j2}}{\det J} \frac{\partial x_m}{\partial \eta_2} \, d\boldsymbol{\eta} \end{aligned} \quad (6.121)$$

Whereupon expressing x_m via basis functions (6.31) in this integral and invoking Lemma 1 yields

$$\begin{aligned} \mathcal{E} = -\int_{\widehat{\Omega}} e_{ik} \frac{\partial N_r}{\partial \eta_k} \left(\frac{e_{jn}}{\det J}\right) \frac{\partial N_\ell}{\partial \eta_n} \, d\boldsymbol{\eta} \;\; x_m^\ell = \\ \sum_{e=1}^{4} \quad \left\{ e_{i1}\left(\boldsymbol{\eta}_e^1\right) \left(\frac{e_{j1}}{\det J}\right)_{\tilde{\boldsymbol{\eta}}_e^1} \left(-\int_{\widehat{\Omega}_e} \frac{\partial N_r}{\partial \eta_1} \frac{\partial N_\ell}{\partial \eta_1} \, d\boldsymbol{\eta}\right) x_m^\ell \right. \\ + e_{i1}\left(\boldsymbol{\eta}_e^\circ\right) \left(\frac{e_{j2}}{\det J}\right)_{\tilde{\boldsymbol{\eta}}_e^\circ} \left(-\int_{\widehat{\Omega}_e} \frac{\partial N_r}{\partial \eta_1} \frac{\partial N_\ell}{\partial \eta_2} \, d\boldsymbol{\eta}\right) x_m^\ell \\ + e_{i2}\left(\overline{\boldsymbol{\eta}}_e^\circ\right) \left(\frac{e_{j1}}{\det J}\right)_{\bar{\tilde{\boldsymbol{\eta}}}_e^\circ} \left(-\int_{\widehat{\Omega}_e} \frac{\partial N_r}{\partial \eta_2} \frac{\partial N_\ell}{\partial \eta_1} \, d\boldsymbol{\eta}\right) x_m^\ell \\ \left. + e_{i2}\left(\boldsymbol{\eta}_e^2\right) \left(\frac{e_{j2}}{\det J}\right)_{\tilde{\boldsymbol{\eta}}_e^2} \left(-\int_{\widehat{\Omega}_e} \frac{\partial N_r}{\partial \eta_2} \frac{\partial N_\ell}{\partial \eta_2} \, d\boldsymbol{\eta}\right) x_m^\ell \right\} \end{aligned} \quad (6.122)$$

This expression is further transformed via relations (6.97), (6.104), (6.111) and (6.117) yielding

$$\begin{aligned} \mathcal{E} = \; -\left(e_{i1}(\boldsymbol{\eta}_1^1) \left(\frac{e_{j1}}{\det J}\right)_{\tilde{\boldsymbol{\eta}}_1^1} \left(\frac{\partial N_\ell}{\partial \eta_1}\right)_{P_1^1} x_m^\ell + e_{i1}(\boldsymbol{\eta}_1^\circ) \left(\frac{e_{j2}}{\det J}\right)_{\tilde{\boldsymbol{\eta}}_1^\circ} \left(\frac{\partial N_\ell}{\partial \eta_2}\right)_{P_1^\circ} x_m^\ell \right) \\ -\left(e_{i2}(\overline{\boldsymbol{\eta}}_1^\circ) \left(\frac{e_{j1}}{\det J}\right)_{\bar{\tilde{\boldsymbol{\eta}}}_1^\circ} \left(\frac{\partial N_\ell}{\partial \eta_1}\right)_{P_1^\circ} x_m^\ell + e_{i2}(\boldsymbol{\eta}_1^2) \left(\frac{e_{j2}}{\det J}\right)_{\tilde{\boldsymbol{\eta}}_1^2} \left(\frac{\partial N_\ell}{\partial \eta_2}\right)_{P_1^2} x_m^\ell \right) \end{aligned}$$

$$
\begin{aligned}
&+\left(e_{i1}(\boldsymbol{\eta}_2^1)\left(\frac{e_{j1}}{\det J}\right)_{\tilde{\boldsymbol{\eta}}_2^1}\left(\frac{\partial N_\ell}{\partial \eta_1}\right)_{P_2^1} x_m^\ell + e_{i1}(\boldsymbol{\eta}_2^o)\left(\frac{e_{j2}}{\det J}\right)_{\tilde{\boldsymbol{\eta}}_2^o}\left(\frac{\partial N_\ell}{\partial \eta_2}\right)_{P_2^o} x_m^\ell\right)\\
&-\left(e_{i2}(\overline{\boldsymbol{\eta}}_2^o)\left(\frac{e_{j1}}{\det J}\right)_{\bar{\tilde{\boldsymbol{\eta}}}_2^o}\left(\frac{\partial N_\ell}{\partial \eta_1}\right)_{P_2^o} x_m^\ell + e_{i2}(\boldsymbol{\eta}_2^2)\left(\frac{e_{j2}}{\det J}\right)_{\tilde{\boldsymbol{\eta}}_2^2}\left(\frac{\partial N_\ell}{\partial \eta_2}\right)_{P_2^2} x_m^\ell\right)\\
&+\left(e_{i1}(\boldsymbol{\eta}_3^1)\left(\frac{e_{j1}}{\det J}\right)_{\tilde{\boldsymbol{\eta}}_3^1}\left(\frac{\partial N_\ell}{\partial \eta_1}\right)_{P_3^1} x_m^\ell + e_{i1}(\boldsymbol{\eta}_3^o)\left(\frac{e_{j2}}{\det J}\right)_{\tilde{\boldsymbol{\eta}}_3^o}\left(\frac{\partial N_\ell}{\partial \eta_2}\right)_{P_3^o} x_m^\ell\right)\\
&+\left(e_{i2}(\overline{\boldsymbol{\eta}}_3^o)\left(\frac{e_{j1}}{\det J}\right)_{\bar{\tilde{\boldsymbol{\eta}}}_3^o}\left(\frac{\partial N_\ell}{\partial \eta_1}\right)_{P_3^o} x_m^\ell + e_{i2}(\boldsymbol{\eta}_3^2)\left(\frac{e_{j2}}{\det J}\right)_{\tilde{\boldsymbol{\eta}}_3^2}\left(\frac{\partial N_\ell}{\partial \eta_2}\right)_{P_3^2} x_m^\ell\right)\\
&-\left(e_{i1}(\boldsymbol{\eta}_4^1)\left(\frac{e_{j1}}{\det J}\right)_{\tilde{\boldsymbol{\eta}}_4^1}\left(\frac{\partial N_\ell}{\partial \eta_1}\right)_{P_4^1} x_m^\ell + e_{i1}(\boldsymbol{\eta}_4^o)\left(\frac{e_{j2}}{\det J}\right)_{\tilde{\boldsymbol{\eta}}_4^o}\left(\frac{\partial N_\ell}{\partial \eta_2}\right)_{P_4^o} x_m^\ell\right)\\
&+\left(e_{i2}(\overline{\boldsymbol{\eta}}_4^o)\left(\frac{e_{j1}}{\det J}\right)_{\bar{\tilde{\boldsymbol{\eta}}}_4^o}\left(\frac{\partial N_\ell}{\partial \eta_1}\right)_{P_4^o} x_m^\ell + e_{i2}(\boldsymbol{\eta}_4^2)\left(\frac{e_{j2}}{\det J}\right)_{\tilde{\boldsymbol{\eta}}_4^2}\left(\frac{\partial N_\ell}{\partial \eta_2}\right)_{P_4^2} x_m^\ell\right)
\end{aligned}
\tag{6.123}
$$

This relation must vanish for arbitrary values of the metric data. Considering that the outer metrics e_{i1} and e_{i2} are linearly independent of each other in any one element, it follows that each expression in parentheses must be separately equal to nought. This is achieved if, preliminarily,

$$\boldsymbol{\eta}_e^1 = \boldsymbol{\eta}_e^o \quad , \quad \tilde{\boldsymbol{\eta}}_e^1 = \tilde{\boldsymbol{\eta}}_e^o \tag{6.124}$$

$$\overline{\boldsymbol{\eta}}_e^o = \boldsymbol{\eta}_e^2 \quad , \quad \bar{\tilde{\boldsymbol{\eta}}}_e^o = \tilde{\boldsymbol{\eta}}_e^2 \tag{6.125}$$

The coordinates of these points are conveniently derived by setting $i = 1$, $j = 1$ and $x_m^\ell = x_2^\ell$. Whereupon, they are found valid for any other value $1 \leq i, j, n \leq 2$.

For the specified settings of the indices i, j, and m, the first relation for $\widehat{\Omega}_1$ in

(6.123) is

$$\mathcal{E}_1 = -\frac{e_{11}(\boldsymbol{\eta}_1^1)}{\det J(\tilde{\boldsymbol{\eta}}_1^1)} \left[\left[\frac{\partial N_\ell}{\partial \eta_2}\right]_{\tilde{\boldsymbol{\eta}}_1^1} x_2^\ell \left(\frac{\partial N_\ell}{\partial \eta_1}\right)_{(0;1/3)} x_2^\ell - \left[\frac{\partial N_\ell}{\partial \eta_1}\right]_{\tilde{\boldsymbol{\eta}}_1^1} x_2^\ell \left(\frac{\partial N_\ell}{\partial \eta_2}\right)_{(0;0)} x_2^\ell \right] \tag{6.126}$$

A unique evaluation point $\tilde{\boldsymbol{\eta}}_1^1$ is now determined by capitalizing on the single-variable dependency feature of the approximation function partial derivatives. This characteristic stipulates the validity of

$$\left(\frac{\partial N_\ell}{\partial \eta_2}\right)_{(0;0)} = \left(\frac{\partial N_\ell}{\partial \eta_2}\right)_{(0;\pm 1/3)} \quad , \quad \forall \ \ell \tag{6.127}$$

Consequently relation (6.126) becomes

$$\mathcal{E}_1 = -\frac{e_{11}(\boldsymbol{\eta}_1^1)}{\det J(\tilde{\boldsymbol{\eta}}_1^1)} \left[\left[\frac{\partial N_\ell}{\partial \eta_2}\right]_{\tilde{\boldsymbol{\eta}}_1^1} x_2^\ell \left(\frac{\partial N_\ell}{\partial \eta_1}\right)_{(0;1/3)} x_2^\ell - \left[\frac{\partial N_\ell}{\partial \eta_1}\right]_{\tilde{\boldsymbol{\eta}}_1^1} x_2^\ell \left(\frac{\partial N_\ell}{\partial \eta_2}\right)_{(0;1/3)} x_2^\ell \right] \tag{6.128}$$

which shows that it can be made to vanish identically upon setting $\tilde{\boldsymbol{\eta}}_1^1 \equiv (0;1/3)$. The second relation for $\widehat{\Omega}_1$ in (6.123) is

$$\mathcal{E}_2 = -\frac{e_{12}(\boldsymbol{\eta}_1^2)}{\det J(\tilde{\boldsymbol{\eta}}_1^2)} \left[\left[\frac{\partial N_\ell}{\partial \eta_2}\right]_{\tilde{\boldsymbol{\eta}}_1^2} x_2^\ell \left(\frac{\partial N_\ell}{\partial \eta_1}\right)_{(0;0)} x_2^\ell - \left[\frac{\partial N_\ell}{\partial \eta_1}\right]_{\tilde{\boldsymbol{\eta}}_1^2} x_2^\ell \left(\frac{\partial N_\ell}{\partial \eta_2}\right)_{(1/3;0)} x_2^\ell \right] \tag{6.129}$$

and the evaluation point $\tilde{\boldsymbol{\eta}}_1^2$ is determined via the identity

$$\left(\frac{\partial N_\ell}{\partial \eta_1}\right)_{(0;0)} = \left(\frac{\partial N_\ell}{\partial \eta_1}\right)_{(\pm 1/3;0)} \quad , \quad \forall \ \ell \tag{6.130}$$

Therefore, expression (6.129) becomes

$$\mathcal{E}_2 = -\frac{e_{12}(\boldsymbol{\eta}_1^2)}{\det J(\tilde{\boldsymbol{\eta}}_1^2)} \left[\left[\frac{\partial N_\ell}{\partial \eta_2}\right]_{\tilde{\boldsymbol{\eta}}_1^2} x_2^\ell \left(\frac{\partial N_\ell}{\partial \eta_1}\right)_{(1/3;0)} x_2^\ell - \left[\frac{\partial N_\ell}{\partial \eta_1}\right]_{\tilde{\boldsymbol{\eta}}_1^2} x_2^\ell \left(\frac{\partial N_\ell}{\partial \eta_2}\right)_{(1/3;0)} x_2^\ell \right] \tag{6.131}$$

which shows that it can be made to vanish identically upon setting $\tilde{\boldsymbol{\eta}}_1^2 \equiv (1/3;0)$.

A sequence of derivations analogous to (6.126)-(6.131) leads to the determination of points $\tilde{\boldsymbol{\eta}}_e^1$ and $\tilde{\boldsymbol{\eta}}_e^2$ for $2 \leq e \leq 4$. Their coordinates with those of $\tilde{\boldsymbol{\eta}}_1^1$ and $\tilde{\boldsymbol{\eta}}_1^2$ are

$$\tilde{\boldsymbol{\eta}}_1^1 = \left(0;+\tfrac{1}{3}\right) \quad , \quad \tilde{\boldsymbol{\eta}}_2^1 = \left(0;+\tfrac{1}{3}\right) \quad , \quad \tilde{\boldsymbol{\eta}}_3^1 = \left(0;-\tfrac{1}{3}\right) \quad , \quad \tilde{\boldsymbol{\eta}}_4^1 = \left(0;-\tfrac{1}{3}\right) \tag{6.132}$$

$$\tilde{\boldsymbol{\eta}}_1^2 = \left(+\tfrac{1}{3};0\right) \quad , \quad \tilde{\boldsymbol{\eta}}_2^2 = \left(-\tfrac{1}{3};0\right) \quad , \quad \tilde{\boldsymbol{\eta}}_3^2 = \left(-\tfrac{1}{3};0\right) \quad , \quad \tilde{\boldsymbol{\eta}}_4^2 = \left(+\tfrac{1}{3};0\right) \tag{6.133}$$

which coincide with (6.40) and (6.49) respectively.

It is important to note that the evaluation points $\tilde{\boldsymbol{\eta}}_e^1$ and $\tilde{\boldsymbol{\eta}}_e^2$ are valid for an arbitrary distribution of the primitive coordinate x_2^ℓ over $\widehat{\Omega}$. Moreover, as is now shown, they are correct for the accurate representation of expression (6.123) when $x_m^\ell = x_1^\ell$. With this substitution relation (6.123), which must vanish again, is cast as

$$\begin{aligned}
\mathcal{E} \;=\; & -\frac{e_{11}(\boldsymbol{\eta}_1^1)}{\det J(\tilde{\boldsymbol{\eta}}_1^1)}\left[e_{11}(\tilde{\boldsymbol{\eta}}_1^1)\left(\frac{\partial N_\ell}{\partial \eta_1}\right)_{P_1^1} x_1^\ell + e_{12}(\tilde{\boldsymbol{\eta}}_1^1)\left(\frac{\partial N_\ell}{\partial \eta_2}\right)_{P_1^1} x_1^\ell\right] \\
& -\frac{e_{12}(\boldsymbol{\eta}_1^2)}{\det J(\tilde{\boldsymbol{\eta}}_1^2)}\left[e_{11}(\tilde{\boldsymbol{\eta}}_1^2)\left(\frac{\partial N_\ell}{\partial \eta_1}\right)_{P_1^2} x_1^\ell + e_{12}(\tilde{\boldsymbol{\eta}}_1^2)\left(\frac{\partial N_\ell}{\partial \eta_2}\right)_{P_1^2} x_1^\ell\right] \\
& +\frac{e_{11}(\boldsymbol{\eta}_2^1)}{\det J(\tilde{\boldsymbol{\eta}}_2^1)}\left[e_{11}(\tilde{\boldsymbol{\eta}}_2^1)\left(\frac{\partial N_\ell}{\partial \eta_1}\right)_{P_2^1} x_1^\ell + e_{12}(\tilde{\boldsymbol{\eta}}_2^1)\left(\frac{\partial N_\ell}{\partial \eta_2}\right)_{P_2^1} x_1^\ell\right] \\
& -\frac{e_{12}(\boldsymbol{\eta}_2^2)}{\det J(\tilde{\boldsymbol{\eta}}_2^2)}\left[e_{11}(\tilde{\boldsymbol{\eta}}_2^2)\left(\frac{\partial N_\ell}{\partial \eta_1}\right)_{P_2^2} x_1^\ell + e_{12}(\tilde{\boldsymbol{\eta}}_2^2)\left(\frac{\partial N_\ell}{\partial \eta_2}\right)_{P_2^2} x_1^\ell\right] \\
& +\frac{e_{11}(\boldsymbol{\eta}_3^1)}{\det J(\tilde{\boldsymbol{\eta}}_3^1)}\left[e_{11}(\tilde{\boldsymbol{\eta}}_3^1)\left(\frac{\partial N_\ell}{\partial \eta_1}\right)_{P_3^1} x_1^\ell + e_{12}(\tilde{\boldsymbol{\eta}}_3^1)\left(\frac{\partial N_\ell}{\partial \eta_2}\right)_{P_3^1} x_1^\ell\right] \\
& +\frac{e_{12}(\boldsymbol{\eta}_3^2)}{\det J(\tilde{\boldsymbol{\eta}}_3^2)}\left[e_{11}(\tilde{\boldsymbol{\eta}}_3^2)\left(\frac{\partial N_\ell}{\partial \eta_1}\right)_{P_3^2} x_1^\ell + e_{12}(\tilde{\boldsymbol{\eta}}_3^2)\left(\frac{\partial N_\ell}{\partial \eta_2}\right)_{P_3^2} x_1^\ell\right] \\
& -\frac{e_{11}(\boldsymbol{\eta}_4^1)}{\det J(\tilde{\boldsymbol{\eta}}_4^1)}\left[e_{11}(\tilde{\boldsymbol{\eta}}_4^1)\left(\frac{\partial N_\ell}{\partial \eta_1}\right)_{P_4^1} x_1^\ell + e_{12}(\tilde{\boldsymbol{\eta}}_4^1)\left(\frac{\partial N_\ell}{\partial \eta_2}\right)_{P_4^1} x_1^\ell\right]
\end{aligned}$$

$$+\frac{e_{12}(\boldsymbol{\eta}_4^2)}{\det J(\tilde{\boldsymbol{\eta}}_4^2)}\left[e_{11}(\tilde{\boldsymbol{\eta}}_4^2)\left(\frac{\partial N_\ell}{\partial \eta_1}\right)_{P_4^2} x_1^\ell + e_{12}(\tilde{\boldsymbol{\eta}}_4^2)\left(\frac{\partial N_\ell}{\partial \eta_2}\right)_{P_4^2} x_1^\ell\right] \qquad (6.134)$$

This relation considerably simplifies, since the sum of the terms between brackets defines $\det J$. Consequently, the terminal expression is

$$\begin{aligned}\mathcal{E} \;=\; & -e_{11}(\boldsymbol{\eta}_1^1) - e_{12}(\boldsymbol{\eta}_1^2) + e_{11}(\boldsymbol{\eta}_2^1) - e_{12}(\boldsymbol{\eta}_2^2) \\ & +e_{11}(\boldsymbol{\eta}_3^1) + e_{12}(\boldsymbol{\eta}_3^2) - e_{11}(\boldsymbol{\eta}_4^1) + e_{12}(\boldsymbol{\eta}_4^2)\end{aligned} \qquad (6.135)$$

and if

$$\begin{aligned} & e_{11}(\boldsymbol{\eta}_1^1) = e_{11}(\boldsymbol{\eta}_2^1) \quad , \quad e_{11}(\boldsymbol{\eta}_3^1) = e_{11}(\boldsymbol{\eta}_4^1) \\ & e_{12}(\boldsymbol{\eta}_1^2) = e_{12}(\boldsymbol{\eta}_4^2) \quad , \quad e_{12}(\boldsymbol{\eta}_2^2) = e_{12}(\boldsymbol{\eta}_3^2)\end{aligned} \qquad (6.136)$$

then this expression vanishes as needed. Considering that the basis functions N_ℓ are bilinear, and e_{11} and e_{12} are expressed via (6.32), then relations (6.135) are satisfied if

$$\begin{aligned} & \boldsymbol{\eta}_1^1 \equiv \boldsymbol{\eta}_2^1 \quad , \quad \boldsymbol{\eta}_3^1 \equiv \boldsymbol{\eta}_4^1 \\ & \boldsymbol{\eta}_1^2 \equiv \boldsymbol{\eta}_4^2 \quad , \quad \boldsymbol{\eta}_2^2 \equiv \boldsymbol{\eta}_3^2\end{aligned} \qquad (6.137)$$

The coordinates of these points are determined in the following section.

The derived points (6.132) and (6.133) are also adequate for the evaluation of expression (6.123) when $i = 2$ and $j = 1$. With this selection the outer metric data e_{21} and e_{22} replace e_{11} and e_{12}, respectively, in (6.126)-(6.131). However, these outer metrics have not entered the determination procedure for points (6.132) and (6.133).

Consequently, expression (6.123) will also vanish identically for both $x_m^\ell = x_1^\ell$ and $x_m^\ell = x_2^\ell$, upon evaluating the inner metrics at $\tilde{\boldsymbol{\eta}}_e^1$ and $\tilde{\boldsymbol{\eta}}_e^2$.

The following section presents the proof that (6.132) and (6.133) are correct metric-data evaluation points for the accurate representation of expression (6.120) for the two cases $(i = 2, j = 2)$ and $(i = 1, j = 2)$. The case $(i = 2, j = 2)$ is considered first. Hence, upon setting $x_m^\ell = x_1^\ell$, expression (6.123) is

$$
\begin{aligned}
\mathcal{E} \;=\; & -e_{21}(\boldsymbol{\eta}_1^1)\left(\left(\frac{e_{21}}{\det J}\right)_{\tilde{\boldsymbol{\eta}}_1^1}\left(\frac{\partial N_\ell}{\partial \eta_1}\right)_{P_1^1} x_1^\ell + \left(\frac{e_{22}}{\det J}\right)_{\tilde{\boldsymbol{\eta}}_1^1}\left(\frac{\partial N_j}{\partial \eta_2}\right)_{P_1^1} x_1^\ell\right) \\
& -e_{22}(\boldsymbol{\eta}_1^2)\left(\left(\frac{e_{21}}{\det J}\right)_{\tilde{\boldsymbol{\eta}}_1^2}\left(\frac{\partial N_\ell}{\partial \eta_1}\right)_{P_1^2} x_1^\ell + \left(\frac{e_{22}}{\det J}\right)_{\tilde{\boldsymbol{\eta}}_1^2}\left(\frac{\partial N_j}{\partial \eta_2}\right)_{P_1^2} x_1^\ell\right) \\
& +e_{21}(\boldsymbol{\eta}_2^1)\left(\left(\frac{e_{21}}{\det J}\right)_{\tilde{\boldsymbol{\eta}}_2^1}\left(\frac{\partial N_\ell}{\partial \eta_1}\right)_{P_2^1} x_1^\ell + \left(\frac{e_{22}}{\det J}\right)_{\tilde{\boldsymbol{\eta}}_2^1}\left(\frac{\partial N_j}{\partial \eta_2}\right)_{P_2^1} x_1^\ell\right) \\
& -e_{22}(\boldsymbol{\eta}_2^2)\left(\left(\frac{e_{21}}{\det J}\right)_{\tilde{\boldsymbol{\eta}}_2^2}\left(\frac{\partial N_\ell}{\partial \eta_1}\right)_{P_2^2} x_1^\ell + \left(\frac{e_{22}}{\det J}\right)_{\tilde{\boldsymbol{\eta}}_2^2}\left(\frac{\partial N_j}{\partial \eta_2}\right)_{P_2^2} x_1^\ell\right) \\
& +e_{21}(\boldsymbol{\eta}_3^1)\left(\left(\frac{e_{21}}{\det J}\right)_{\tilde{\boldsymbol{\eta}}_3^1}\left(\frac{\partial N_\ell}{\partial \eta_1}\right)_{P_3^1} x_1^\ell + \left(\frac{e_{22}}{\det J}\right)_{\tilde{\boldsymbol{\eta}}_3^1}\left(\frac{\partial N_j}{\partial \eta_2}\right)_{P_3^1} x_1^\ell\right) \\
& +e_{22}(\boldsymbol{\eta}_3^2)\left(\left(\frac{e_{21}}{\det J}\right)_{\tilde{\boldsymbol{\eta}}_3^2}\left(\frac{\partial N_\ell}{\partial \eta_1}\right)_{P_3^2} x_1^\ell + \left(\frac{e_{22}}{\det J}\right)_{\tilde{\boldsymbol{\eta}}_3^2}\left(\frac{\partial N_j}{\partial \eta_2}\right)_{P_3^2} x_1^\ell\right) \\
& -e_{21}(\boldsymbol{\eta}_4^1)\left(\left(\frac{e_{21}}{\det J}\right)_{\tilde{\boldsymbol{\eta}}_4^1}\left(\frac{\partial N_\ell}{\partial \eta_1}\right)_{P_4^1} x_1^\ell + \left(\frac{e_{22}}{\det J}\right)_{\tilde{\boldsymbol{\eta}}_4^1}\left(\frac{\partial N_j}{\partial \eta_2}\right)_{P_4^1} x_1^\ell\right) \\
& +e_{22}(\boldsymbol{\eta}_4^2)\left(\left(\frac{e_{21}}{\det J}\right)_{\tilde{\boldsymbol{\eta}}_4^2}\left(\frac{\partial N_\ell}{\partial \eta_1}\right)_{P_4^2} x_1^\ell + \left(\frac{e_{22}}{\det J}\right)_{\tilde{\boldsymbol{\eta}}_4^2}\left(\frac{\partial N_j}{\partial \eta_2}\right)_{P_4^2} x_1^\ell\right) \qquad (6.138)
\end{aligned}
$$

This relation must vanish for arbitrary values of the metric data. Considering that the outer metrics e_{21} and e_{22} are linearly independent in any one element, then the expressions in parentheses must be separately equal to nought. The first set of

relations is written as

$$\mathcal{E}_1 = \frac{e_{21}(\boldsymbol{\eta}_e^1)}{\det J(\tilde{\boldsymbol{\eta}}_e^1)} \left[-\left[\frac{\partial N_k}{\partial \eta_2}\right]_{\tilde{\boldsymbol{\eta}}_e^1} x_1^k \left(\frac{\partial N_\ell}{\partial \eta_1}\right)_{(0;\pm 1/3)} x_1^\ell + \left[\frac{\partial N_k}{\partial \eta_1}\right]_{\tilde{\boldsymbol{\eta}}_e^1} x_1^k \left(\frac{\partial N_\ell}{\partial \eta_2}\right)_{(0;\pm 1/3)} x_1^\ell \right] \tag{6.139}$$

which identically vanishes for the previous selection of $\tilde{\boldsymbol{\eta}}_e^1$.

The second set of relations is

$$\mathcal{E}_2 = \frac{e_{22}(\boldsymbol{\eta}_e^2)}{\det J(\tilde{\boldsymbol{\eta}}_e^2)} \left[-\left[\frac{\partial N_k}{\partial \eta_2}\right]_{\tilde{\boldsymbol{\eta}}_e^2} x_1^k \left(\frac{\partial N_\ell}{\partial \eta_1}\right)_{(\pm 1/3;0)} x_1^\ell + \left[\frac{\partial N_k}{\partial \eta_1}\right]_{\tilde{\boldsymbol{\eta}}_e^2} x_1^k \left(\frac{\partial N_\ell}{\partial \eta_2}\right)_{(\pm 1/3;0)} x_1^\ell \right] \tag{6.140}$$

which also vanishes identically for the previous selction of $\tilde{\boldsymbol{\eta}}_1^2$.

When $x_m^\ell = x_2^\ell$, expression (6.123) is written as

$$\begin{aligned}
\mathcal{E} \;=\; & -\frac{e_{21}(\boldsymbol{\eta}_1^1)}{\det J(\tilde{\boldsymbol{\eta}}_1^1)} \left[e_{21}(\tilde{\boldsymbol{\eta}}_1^1) \left(\frac{\partial N_\ell}{\partial \eta_1}\right)_{P_1^1} x_2^\ell + e_{22}(\tilde{\boldsymbol{\eta}}_1^1) \left(\frac{\partial N_\ell}{\partial \eta_2}\right)_{P_1^1} x_2^\ell \right] \\
& -\frac{e_{22}(\boldsymbol{\eta}_1^2)}{\det J(\tilde{\boldsymbol{\eta}}_1^2)} \left[e_{21}(\tilde{\boldsymbol{\eta}}_1^2) \left(\frac{\partial N_\ell}{\partial \eta_1}\right)_{P_1^2} x_2^\ell + e_{22}(\tilde{\boldsymbol{\eta}}_1^2) \left(\frac{\partial N_\ell}{\partial \eta_2}\right)_{P_1^2} x_2^\ell \right] \\
& +\frac{e_{21}(\boldsymbol{\eta}_2^1)}{\det J(\tilde{\boldsymbol{\eta}}_2^1)} \left[e_{21}(\tilde{\boldsymbol{\eta}}_2^1) \left(\frac{\partial N_\ell}{\partial \eta_1}\right)_{P_2^1} x_2^\ell + e_{22}(\tilde{\boldsymbol{\eta}}_2^1) \left(\frac{\partial N_\ell}{\partial \eta_2}\right)_{P_2^1} x_2^\ell \right] \\
& -\frac{e_{22}(\boldsymbol{\eta}_2^2)}{\det J(\tilde{\boldsymbol{\eta}}_2^2)} \left[e_{21}(\tilde{\boldsymbol{\eta}}_2^2) \left(\frac{\partial N_\ell}{\partial \eta_1}\right)_{P_2^2} x_2^\ell + e_{22}(\tilde{\boldsymbol{\eta}}_2^2) \left(\frac{\partial N_\ell}{\partial \eta_2}\right)_{P_2^2} x_2^\ell \right] \\
& +\frac{e_{21}(\boldsymbol{\eta}_3^1)}{\det J(\tilde{\boldsymbol{\eta}}_3^1)} \left[e_{21}(\tilde{\boldsymbol{\eta}}_3^1) \left(\frac{\partial N_\ell}{\partial \eta_1}\right)_{P_3^1} x_2^\ell + e_{22}(\tilde{\boldsymbol{\eta}}_3^1) \left(\frac{\partial N_\ell}{\partial \eta_2}\right)_{P_3^1} x_2^\ell \right] \\
& +\frac{e_{22}(\boldsymbol{\eta}_3^2)}{\det J(\tilde{\boldsymbol{\eta}}_3^2)} \left[e_{21}(\tilde{\boldsymbol{\eta}}_3^2) \left(\frac{\partial N_\ell}{\partial \eta_1}\right)_{P_3^2} x_2^\ell + e_{22}(\tilde{\boldsymbol{\eta}}_3^2) \left(\frac{\partial N_\ell}{\partial \eta_2}\right)_{P_3^2} x_2^\ell \right] \\
& -\frac{e_{21}(\boldsymbol{\eta}_4^1)}{\det J(\tilde{\boldsymbol{\eta}}_4^1)} \left[e_{21}(\tilde{\boldsymbol{\eta}}_4^1) \left(\frac{\partial N_\ell}{\partial \eta_1}\right)_{P_4^1} x_2^\ell + e_{22}(\tilde{\boldsymbol{\eta}}_4^1) \left(\frac{\partial N_\ell}{\partial \eta_2}\right)_{P_4^1} x_2^\ell \right] \\
& +\frac{e_{22}(\boldsymbol{\eta}_4^2)}{\det J(\tilde{\boldsymbol{\eta}}_4^2)} \left[e_{21}(\tilde{\boldsymbol{\eta}}_4^2) \left(\frac{\partial N_\ell}{\partial \eta_1}\right)_{P_4^2} x_2^\ell + e_{22}(\tilde{\boldsymbol{\eta}}_4^2) \left(\frac{\partial N_\ell}{\partial \eta_2}\right)_{P_4^2} x_2^\ell \right]
\end{aligned} \tag{6.141}$$

Since the expressions between brackets correspond to det J, the terminal expression

is

$$\begin{aligned}\mathcal{E} &= -e_{21}(\boldsymbol{\eta}_1^1) - e_{22}(\boldsymbol{\eta}_1^2) + e_{21}(\boldsymbol{\eta}_2^1) - e_{22}(\boldsymbol{\eta}_2^2) \\ &\quad + e_{21}(\boldsymbol{\eta}_3^1) + e_{22}(\boldsymbol{\eta}_3^2) - e_{21}(\boldsymbol{\eta}_4^1) + e_{22}(\boldsymbol{\eta}_4^2) \end{aligned} \tag{6.142}$$

and, in analogy with (6.136), if

$$\begin{aligned} e_{21}(\boldsymbol{\eta}_1^1) = e_{21}(\boldsymbol{\eta}_2^1) \quad , \quad e_{21}(\boldsymbol{\eta}_3^1) = e_{21}(\boldsymbol{\eta}_4^1) \\ e_{22}(\boldsymbol{\eta}_1^2) = e_{22}(\boldsymbol{\eta}_4^2) \quad , \quad e_{22}(\boldsymbol{\eta}_2^2) = e_{22}(\boldsymbol{\eta}_3^2) \end{aligned} \tag{6.143}$$

then this expression vanishes as needed. Considering that the basis functions N_ℓ are bilinear and e_{21} and e_{22} are expressed via (6.33), then relations (6.143) are satisfied if equivalences (6.137) hold.

Finally, for the case $(i = 1, j = 2)$ the outer metric-data e_{11} and e_{12} replace e_{21} and e_{22} respectively, in (6.138)-(6.141) However, these outer metric data have not entered the determination procedure for points (6.132) and (6.133). Consequently, also in this case expression (6.123) identically vanishes for both $x_m^\ell = x_1^\ell$ and $x_m^\ell = x_2^\ell$ upon evaluating the inner metrics at $\tilde{\boldsymbol{\eta}}_e^1$ and $\tilde{\boldsymbol{\eta}}_e^2$.

6.5.3 Accuracy Consideration

Expression (6.120) constitutes a fundamental consistency and/or first order accuracy constraint for the approximation of diffusion operators that any semi- discretization theory should verify on arbitrary meshes. The semi-discretization procedure detailed in this section has yielded this crucial verification in a straightforward

manner via determination/utilization of optimal metric data evaluation points. It is noted that the proofs of this section do not place specific constraints on the coordinates of the outer-metric evaluation points, other than requirement (6.137). Hence, it should be possible to capitalize on these remaining degrees of freedom to identify additional evaluation points that lead to second-order accurate spatial semi-discretizations in both primitive and computational coordinates on arbitrary meshes.

6.5.4 Second Order Accurate Semi-Discretizations on Arbitrary Meshes

The fundamental identity (6.30) is cast as

$$\left[\frac{\det J}{2}\left(\delta_j^m\cdot\delta_i^n+\delta_i^m\cdot\delta_j^n\right)\right]_{\boldsymbol{\eta}_P}\cdot\int_{\widehat{\Omega}}N_r\,d\boldsymbol{\eta}=-\int_{\widehat{\Omega}}e_{ik}\frac{\partial N_r}{\partial\eta_k}\frac{e_{j\ell}}{\det J}\frac{\partial\left(x_m x_n\right)}{\partial\eta_\ell}\,d\boldsymbol{\eta}=$$
$$-\int_{\widehat{\Omega}}e_{i1}\frac{\partial N_r}{\partial\eta_1}\frac{e_{j1}}{\det J}\frac{\partial\left(x_m x_n\right)}{\partial\eta_1}\,d\boldsymbol{\eta}-\int_{\widehat{\Omega}}e_{i1}\frac{\partial N_r}{\partial\eta_1}\frac{e_{j2}}{\det J}\frac{\partial\left(x_m x_n\right)}{\partial\eta_2}\,d\boldsymbol{\eta}$$
$$-\int_{\widehat{\Omega}}e_{i2}\frac{\partial N_r}{\partial\eta_2}\frac{e_{j1}}{\det J}\frac{\partial\left(x_m x_n\right)}{\partial\eta_1}\,d\boldsymbol{\eta}-\int_{\widehat{\Omega}}e_{i2}\frac{\partial N_r}{\partial\eta_2}\frac{e_{j2}}{\det J}\frac{\partial\left(x_m x_n\right)}{\partial\eta_2}\,d\boldsymbol{\eta}\quad(6.144)$$

Thereafter, setting $\psi\equiv x_s^\ell N_\ell$ and using Lemma 1 allows casting (6.144) as

$$\left[\frac{\det J}{2}\left(\delta_j^m\cdot\delta_i^n+\delta_i^m\cdot\delta_j^n\right)\right]_{\boldsymbol{\eta}_P}=\mathcal{I}=$$
$$\frac{1}{2\alpha}\sum_{e=1}^{4}\Bigg\{e_{i1}\left(\boldsymbol{\eta}_e^1\right)\left(\frac{e_{j1}}{\det J}\right)_{\tilde{\boldsymbol{\eta}}_e^1}N_\ell\left(\widehat{\boldsymbol{\eta}}_e^1\right)\left(-\int_{\widehat{\Omega}_e}\frac{\partial N_r}{\partial\eta_1}\frac{\partial N_k}{\partial\eta_1}\,d\boldsymbol{\eta}\right)\left(x_m^\ell x_n^k+x_n^\ell x_m^k\right)$$
$$+e_{i1}\left(\boldsymbol{\eta}_e^1\right)\left(\frac{e_{j2}}{\det J}\right)_{\tilde{\boldsymbol{\eta}}_e^2}N_\ell\left(\widehat{\boldsymbol{\eta}}_e^1\right)\left(-\int_{\widehat{\Omega}_e}\frac{\partial N_r}{\partial\eta_1}\frac{\partial N_k}{\partial\eta_2}\,d\boldsymbol{\eta}\right)\left(x_m^\ell x_n^k+x_n^\ell x_m^k\right)$$
$$+e_{i2}\left(\boldsymbol{\eta}_e^2\right)\left(\frac{e_{j1}}{\det J}\right)_{\tilde{\boldsymbol{\eta}}_e^1}N_\ell\left(\widehat{\boldsymbol{\eta}}_e^2\right)\left(-\int_{\widehat{\Omega}_e}\frac{\partial N_r}{\partial\eta_2}\frac{\partial N_k}{\partial\eta_1}\,d\boldsymbol{\eta}\right)\left(x_m^\ell x_n^k+x_n^\ell x_m^k\right)$$
$$+e_{i2}\left(\boldsymbol{\eta}_e^2\right)\left(\frac{e_{j2}}{\det J}\right)_{\tilde{\boldsymbol{\eta}}_e^2}N_\ell\left(\widehat{\boldsymbol{\eta}}_e^2\right)\left(-\int_{\widehat{\Omega}_e}\frac{\partial N_r}{\partial\eta_2}\frac{\partial N_k}{\partial\eta_2}\,d\boldsymbol{\eta}\right)\left(x_m^\ell x_n^k+x_n^\ell x_m^k\right)\Bigg\}$$
$$(6.145)$$

where $\alpha = \int_{\widehat{\Omega}} N_r \, d\boldsymbol{\eta} = 4$, and $\hat{\boldsymbol{\eta}}_e^1$, $\hat{\boldsymbol{\eta}}_e^2$ are suitable points, to be determined.

The coordinates of points $\boldsymbol{\eta}_e^1$ and $\boldsymbol{\eta}_e^2$ are conveniently determined upon setting $i = 1$, $j = 1$ as well as $x_m^k = x_1^k$ and $x_n^\ell = x_1^\ell$. Whereupon, they are found to be valid for any value $1 \leq i, j, m, n, \leq 2$. For the specified index setting, relation (6.145) becomes

$$\begin{aligned}
\mathcal{I} = \frac{1}{\alpha} \sum_{e=1}^{4} \quad & \left\{ e_{11}\left(\boldsymbol{\eta}_e^1\right) \left(\frac{e_{11}}{\det J}\right)_{\tilde{\boldsymbol{\eta}}_e^1} \left(- \int_{\widehat{\Omega}_e} \frac{\partial N_r}{\partial \eta_1} \frac{\partial N_k}{\partial \eta_1} \, d\boldsymbol{\eta} \right) N_\ell\left(\hat{\boldsymbol{\eta}}_e^1\right) x_1^\ell x_1^k \right. \\
& + e_{11}\left(\boldsymbol{\eta}_e^1\right) \left(\frac{e_{12}}{\det J}\right)_{\tilde{\boldsymbol{\eta}}_e^2} \left(- \int_{\widehat{\Omega}_e} \frac{\partial N_r}{\partial \eta_1} \frac{\partial N_k}{\partial \eta_2} \, d\boldsymbol{\eta} \right) N_\ell\left(\hat{\boldsymbol{\eta}}_e^1\right) x_1^\ell x_1^k \\
& + e_{12}\left(\boldsymbol{\eta}_e^2\right) \left(\frac{e_{11}}{\det J}\right)_{\tilde{\boldsymbol{\eta}}_e^1} \left(- \int_{\widehat{\Omega}_e} \frac{\partial N_r}{\partial \eta_2} \frac{\partial N_k}{\partial \eta_1} \, d\boldsymbol{\eta} \right) N_\ell\left(\hat{\boldsymbol{\eta}}_e^2\right) x_1^\ell x_1^k \\
& \left. + e_{12}\left(\boldsymbol{\eta}_e^2\right) \left(\frac{e_{12}}{\det J}\right)_{\tilde{\boldsymbol{\eta}}_e^2} \left(- \int_{\widehat{\Omega}_e} \frac{\partial N_r}{\partial \eta_2} \frac{\partial N_k}{\partial \eta_2} \, d\boldsymbol{\eta} \right) N_\ell\left(\hat{\boldsymbol{\eta}}_e^2\right) x_1^\ell x_1^k \right\} \quad (6.146)
\end{aligned}$$

which is expanded via relations (6.97), (6.104), (6.111) and (6.117) as

$$\begin{aligned}
\mathcal{I} \;=\; & -\frac{e_{11}(\boldsymbol{\eta}_1^1)}{\alpha \det J(\tilde{\boldsymbol{\eta}}_1^1)} \left[\left[\frac{\partial N_m}{\partial \eta_2}\right]_{\tilde{\boldsymbol{\eta}}_1^1} x_2^m \left(\frac{\partial N_n}{\partial \eta_1}\right)_{P_1^1} x_1^n + \left[-\frac{\partial N_m}{\partial \eta_1}\right]_{\tilde{\boldsymbol{\eta}}_1^1} x_2^m \left(\frac{\partial N_n}{\partial \eta_2}\right)_{P_1^1} x_1^n \right] N_\ell(\hat{\boldsymbol{\eta}}_1^1) x_1^\ell \\
& - \frac{e_{12}(\boldsymbol{\eta}_1^2)}{\alpha \det J(\tilde{\boldsymbol{\eta}}_1^2)} \left[\left[\frac{\partial N_m}{\partial \eta_2}\right]_{\tilde{\boldsymbol{\eta}}_1^2} x_2^m \left(\frac{\partial N_n}{\partial \eta_1}\right)_{P_1^2} x_1^n + \left[-\frac{\partial N_m}{\partial \eta_1}\right]_{\tilde{\boldsymbol{\eta}}_1^2} x_2^m \left(\frac{\partial N_n}{\partial \eta_2}\right)_{P_1^2} x_1^n \right] N_\ell(\hat{\boldsymbol{\eta}}_1^2) x_1^\ell \\
& + \frac{e_{11}(\boldsymbol{\eta}_2^1)}{\alpha \det J(\tilde{\boldsymbol{\eta}}_2^1)} \left[\left[\frac{\partial N_m}{\partial \eta_2}\right]_{\tilde{\boldsymbol{\eta}}_2^1} x_2^m \left(\frac{\partial N_n}{\partial \eta_1}\right)_{P_2^1} x_1^n + \left[-\frac{\partial N_m}{\partial \eta_1}\right]_{\tilde{\boldsymbol{\eta}}_2^1} x_2^m \left(\frac{\partial N_n}{\partial \eta_2}\right)_{P_2^1} x_1^n \right] N_\ell(\hat{\boldsymbol{\eta}}_2^1) x_1^\ell \\
& - \frac{e_{12}(\boldsymbol{\eta}_2^2)}{\alpha \det J(\tilde{\boldsymbol{\eta}}_2^2)} \left[\left[\frac{\partial N_m}{\partial \eta_2}\right]_{\tilde{\boldsymbol{\eta}}_2^2} x_2^m \left(\frac{\partial N_n}{\partial \eta_1}\right)_{P_2^2} x_1^n + \left[-\frac{\partial N_m}{\partial \eta_1}\right]_{\tilde{\boldsymbol{\eta}}_2^2} x_2^m \left(\frac{\partial N_n}{\partial \eta_2}\right)_{P_2^2} x_1^n \right] N_\ell(\hat{\boldsymbol{\eta}}_2^2) x_1^\ell \\
& + \frac{e_{11}(\boldsymbol{\eta}_3^1)}{\alpha \det J(\tilde{\boldsymbol{\eta}}_3^1)} \left[\left[\frac{\partial N_m}{\partial \eta_2}\right]_{\tilde{\boldsymbol{\eta}}_3^1} x_2^m \left(\frac{\partial N_n}{\partial \eta_1}\right)_{P_3^1} x_1^n + \left[-\frac{\partial N_m}{\partial \eta_1}\right]_{\tilde{\boldsymbol{\eta}}_3^1} x_2^m \left(\frac{\partial N_n}{\partial \eta_2}\right)_{P_3^1} x_1^n \right] N_\ell(\hat{\boldsymbol{\eta}}_3^1) x_1^\ell \\
& + \frac{e_{12}(\boldsymbol{\eta}_3^2)}{\alpha \det J(\tilde{\boldsymbol{\eta}}_3^2)} \left[\left[\frac{\partial N_m}{\partial \eta_2}\right]_{\tilde{\boldsymbol{\eta}}_3^2} x_2^m \left(\frac{\partial N_n}{\partial \eta_1}\right)_{P_3^2} x_1^n + \left[-\frac{\partial N_m}{\partial \eta_1}\right]_{\tilde{\boldsymbol{\eta}}_3^2} x_2^m \left(\frac{\partial N_n}{\partial \eta_2}\right)_{P_3^2} x_1^n \right] N_\ell(\hat{\boldsymbol{\eta}}_3^2) x_1^\ell \\
& - \frac{e_{11}(\boldsymbol{\eta}_4^1)}{\alpha \det J(\tilde{\boldsymbol{\eta}}_4^1)} \left[\left[\frac{\partial N_m}{\partial \eta_2}\right]_{\tilde{\boldsymbol{\eta}}_4^1} x_2^m \left(\frac{\partial N_n}{\partial \eta_1}\right)_{P_4^1} x_1^n + \left[-\frac{\partial N_m}{\partial \eta_1}\right]_{\tilde{\boldsymbol{\eta}}_4^1} x_2^m \left(\frac{\partial N_n}{\partial \eta_2}\right)_{P_4^1} x_1^n \right] N_\ell(\hat{\boldsymbol{\eta}}_4^1) x_1^\ell \\
& + \frac{e_{12}(\boldsymbol{\eta}_4^2)}{\alpha \det J(\tilde{\boldsymbol{\eta}}_4^2)} \left[\left[\frac{\partial N_m}{\partial \eta_2}\right]_{\tilde{\boldsymbol{\eta}}_4^2} x_2^m \left(\frac{\partial N_n}{\partial \eta_1}\right)_{P_4^2} x_1^n + \left[-\frac{\partial N_m}{\partial \eta_1}\right]_{\tilde{\boldsymbol{\eta}}_4^2} x_2^m \left(\frac{\partial N_n}{\partial \eta_2}\right)_{P_4^2} x_1^n \right] N_\ell(\hat{\boldsymbol{\eta}}_4^2) x_1^\ell
\end{aligned} \quad (6.147)$$

Recognizing again the det J definition in the expressions between brackets, allows simplifying expression (6.147) as

$$\begin{aligned}\mathcal{I} = \frac{1}{2} \quad & \left\{\frac{1}{2}\left[\left(e_{11}(\boldsymbol{\eta}_2^1)N_\ell(\widehat{\boldsymbol{\eta}}_2^1)x_1^\ell\right) - \left(e_{11}(\boldsymbol{\eta}_1^1)N_\ell(\widehat{\boldsymbol{\eta}}_1^1)x_1^\ell\right)\right]\right. \\ & \left. +\frac{1}{2}\left[\left(e_{11}(\boldsymbol{\eta}_3^1)N_\ell(\widehat{\boldsymbol{\eta}}_3^1)x_1^\ell\right) - \left(e_{11}(\boldsymbol{\eta}_4^1)N_\ell(\widehat{\boldsymbol{\eta}}_4^1)x_1^\ell\right)\right]\right\} \\ +\frac{1}{2} \quad & \left\{\frac{1}{2}\left[\left(e_{12}(\boldsymbol{\eta}_4^2)N_\ell(\widehat{\boldsymbol{\eta}}_4^2)x_1^\ell\right) - \left(e_{12}(\boldsymbol{\eta}_1^2)N_\ell(\widehat{\boldsymbol{\eta}}_1^2)x_1^\ell\right)\right]\right. \\ & \left. +\frac{1}{2}\left[\left(e_{12}(\boldsymbol{\eta}_3^2)N_\ell(\widehat{\boldsymbol{\eta}}_3^2)x_1^\ell\right) - \left(e_{12}(\boldsymbol{\eta}_2^2)N_\ell(\widehat{\boldsymbol{\eta}}_2^2)x_1^\ell\right)\right]\right\} \end{aligned} \tag{6.148}$$

At this stage the evaluation points $\boldsymbol{\eta}_e^1$, $\boldsymbol{\eta}_e^2$ and $\widehat{\boldsymbol{\eta}}_e^1$, $\widehat{\boldsymbol{\eta}}_e^2$, $1 \leq e \leq 4$, are determined such that expression (6.148) accurately represents the relation

$$\mathcal{I} = \det J\left(\boldsymbol{\eta}^P\right) \tag{6.149}$$

where $\boldsymbol{\eta}^P$ is a suitable evaluation point in the region formed by the union of four computational cells as illustrated in Figure 6.9. With reference to this figure, and in harmony with requirements (6.137), the evaluation of the outer metric data e_{11} at points $\boldsymbol{\eta}_1^1 = (+1; +\frac{1}{3}) \equiv \boldsymbol{\eta}_2^1 = (-1; +\frac{1}{3})$ as well as $\boldsymbol{\eta}_3^1 = (-1; -\frac{1}{3}) \equiv \boldsymbol{\eta}_4^1 = (+1; -\frac{1}{3})$ and the outer metric e_{12} at points $\boldsymbol{\eta}_1^2 = (+\frac{1}{3}; +1) \equiv \boldsymbol{\eta}_4^2 = (+\frac{1}{3}; -1)$ as well as $\boldsymbol{\eta}_2^2 = (-\frac{1}{3}; +1) \equiv \boldsymbol{\eta}_3^2 = (-\frac{1}{3}; -1)$ permits recasting expression (6.148) as

$$\begin{aligned}\mathcal{I} \;=\; & \frac{1}{2}\left\{\frac{1}{2}e_{11}(\boldsymbol{\eta}_2^1)\left[N_\ell(\widehat{\boldsymbol{\eta}}_2^1)x_1^\ell - N_\ell(\widehat{\boldsymbol{\eta}}_1^1)x_1^\ell\right] + \frac{1}{2}e_{11}(\boldsymbol{\eta}_3^1)\left[N_\ell(\widehat{\boldsymbol{\eta}}_3^1)x_1^\ell - N_\ell(\widehat{\boldsymbol{\eta}}_4^1)x_1^\ell\right]\right\} + \\ & \frac{1}{2}\left\{\frac{1}{2}e_{12}(\boldsymbol{\eta}_1^2)\left[N_\ell(\widehat{\boldsymbol{\eta}}_4^2)x_1^\ell - N_\ell(\widehat{\boldsymbol{\eta}}_1^2)x_1^\ell\right] + \frac{1}{2}e_{12}(\boldsymbol{\eta}_2^2)\left[N_\ell(\widehat{\boldsymbol{\eta}}_3^2)x_1^\ell - N_\ell(\widehat{\boldsymbol{\eta}}_2^2)x_1^\ell\right]\right\}\end{aligned} \tag{6.150}$$

It is noted that the single evaluation point

$$\{\boldsymbol{\eta}_1^* = (1;1)\} \equiv \{\boldsymbol{\eta}_2^* = (-1;1)\} \equiv \{\boldsymbol{\eta}_3^* = (-1;-1)\} \equiv \{\boldsymbol{\eta}_4^* = (1;-1)\} \tag{6.151}$$

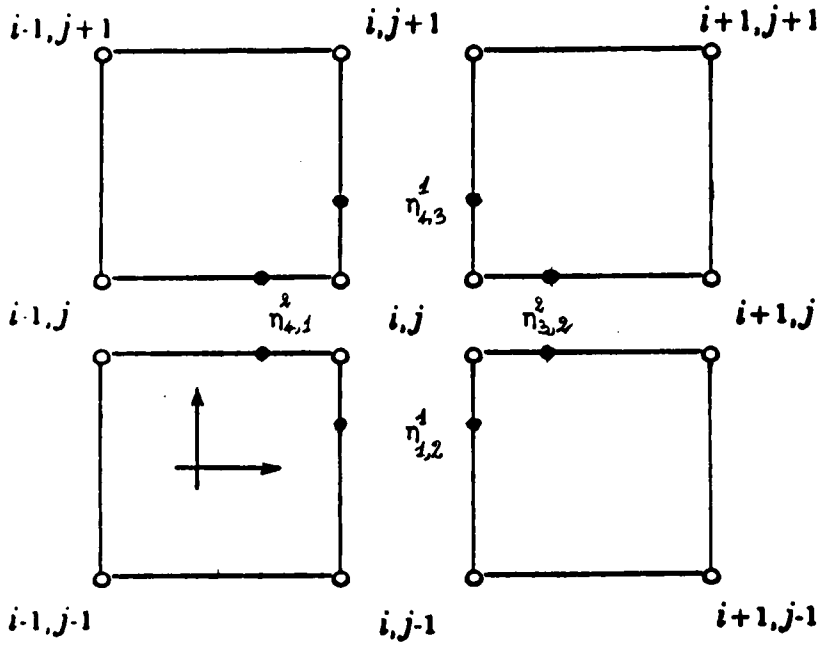


Figure 6.9: Contiguous Cells for Evaluation (6.148)

can be utilized to compute the outer metric data in (6.150) since the following relations hold true

$$\begin{aligned} (e_{11})_{(\pm 1;\pm 1/3)} &= (e_{11})_{(\pm 1;\pm 1)} \\ (e_{12})_{(\pm 1/3;\pm 1)} &= (e_{12})_{(\pm 1;\pm 1)} \end{aligned} \tag{6.152}$$

Whereupon, identification of points $\hat{\eta}_e^1$ and $\hat{\eta}_e^2$ with $\tilde{\eta}_e^1$ $\tilde{\eta}_e^2$ respectively, see (6.132), (6.133) and Figure 6.8, leads to the following form of relation (6.150)

$$\begin{aligned} \mathcal{I} = & \frac{1}{2}\left\{ e_{11}(\eta_2)\left(\frac{\Delta x_1}{\Delta \eta_1}\right)_{\eta_2^1} + e_{11}(\eta_3)\left(\frac{\Delta x_1}{\Delta \eta_1}\right)_{\eta_3^1} \right\} \\ & \frac{1}{2}\left\{ e_{12}(\eta_1)\left(\frac{\Delta x_1}{\Delta \eta_2}\right)_{\eta_1^2} + e_{12}(\eta_2)\left(\frac{\Delta x_1}{\Delta \eta_2}\right)_{\eta_2^2} \right\} \end{aligned} \tag{6.153}$$

which coincides with expression (6.149) upon identification of point η^P with node r in Figure 6.8. Therefore, the fundamental relation (6.144) is verified for an arbitrary

distribution of primitive coordinates over each computational cell. Importantly, (6.152) reduces to the well known uniform grid 2^{nd} order centered schemes for the diffusion operator when selected metric data e_{ij} vanish. Consequently,employing formula (6.146) for the semi-discretization of non-linear second or higher degree terms within the diffusion operator yields a second-order accurate recursion formula on both primitive and computational spaces on arbitrary meshes. Finally a straightforward repetion of derivations (6.145) and (6.153) leads to the result that expression (6.145) in concert with the determined diffusion-operator optimal evaluation points also constitutes an arbitrary mesh second-order accurate evaluation of relation (6.144) for the important cases $(i = 1, j = 2)$, $(i = 2, j = 1)$ and $(i = 2, j = 2)$. This conclusion is readily attained upon setting $x_m = x_i$ and $x_n = x_j$ in each derivation.

6.5.5 Specific Applications

To exemplify the use of formula (6.146), the spatial semi-discretization of the following Navier-Stokes equation diffusion term is developed

$$\det J \cdot D = \det J \frac{\partial}{\partial x}\left[\left(\frac{m_x}{\rho}\right)\frac{\partial}{\partial x}\left(\frac{m_x}{\rho}\right)\right] = e_{1k}\frac{\partial}{\partial \eta_1}\left[\left(\frac{m_x}{\rho}\right)\frac{e_{1\ell}}{\det J}\frac{\partial}{\partial \eta_\ell}\left(\frac{m_x}{\rho}\right)\right] \quad (6.154)$$

An integral representation of this term is

$$\int_{\widehat{\Omega}} N_r \det J \cdot D \, d\boldsymbol{\eta} = \int_{\widehat{\Omega}} N_r e_{1k}\frac{\partial}{\partial \eta_1}\left[\left(\frac{m_x}{\rho}\right)\frac{e_{1\ell}}{\det J}\frac{\partial}{\partial \eta_\ell}\left(\frac{m_x}{\rho}\right)\right] d\boldsymbol{\eta} =$$
$$-\sum_{e=1}^{4}\left\{\int_{\widehat{\Omega}_e} e_{1k}\frac{\partial N_r}{\partial \eta_k}\left(\frac{m_x}{\rho}\right)\frac{e_{1\ell}}{\det J}\frac{\partial}{\partial \eta_\ell}\left(\frac{m_x}{\rho}\right) d\boldsymbol{\eta}\right\} \quad (6.155)$$

hence

$$\int_{\widehat{\Omega}} N_r \det J \cdot D \, d\boldsymbol{\eta} \simeq -\sum_{e=1}^{4} \left\{ e_{1k}(\boldsymbol{\eta}_e^k) \int_{\widehat{\Omega}_e} \frac{\partial N_r}{\partial \eta_k} \frac{e_{1\ell}}{\det J} N_j \frac{\partial N_i}{\partial \eta_\ell} \, d\boldsymbol{\eta} \, \frac{m_x^j}{\rho^j} \frac{m_x^i}{\rho^i} \right\} \tag{6.156}$$

and capitalization on formula (6.146) leads to the terminal relation

$$\int_{\widehat{\Omega}} N_r \det J \cdot D \, d\boldsymbol{\eta} \simeq -\sum_{e=1}^{4} \left\{ e_{1k}(\boldsymbol{\eta}_e^k) \left(\frac{e_{1\ell}}{\det J} \right)_{\tilde{\boldsymbol{\eta}}_e^k} N_j \left(\tilde{\boldsymbol{\eta}}_e^k \right) \int_{\widehat{\Omega}_e} \frac{\partial N_r}{\partial \eta_k} \frac{\partial N_i}{\partial \eta_\ell} \, d\boldsymbol{\eta} \, \frac{m_x^j}{\rho^j} \frac{m_x^i}{\rho^i} \right\} \tag{6.157}$$

Part III

Implicit Time Integration

Chapter 7

Solution Procedure

7.1 Ordinary Differential Equation System and Implicit Integration

Equations (5.65)-(5.67) and/or (5.68)-(5.70) constitute the finite element semi-discretization which yields the global ODE system. This statement for the 2-D domain $\widehat{\Omega}^h$ is

$$\mathcal{M}\frac{d\tilde{q}}{dt} + \tilde{f}_1(t,\tilde{q}) + \tilde{f}_2(t,\tilde{q}) = 0 \tag{7.1}$$

where $\mathcal{M}$ is the semi-discretization mass matrix

$$\mathcal{M} \equiv \int_{\widehat{\Omega}^h} N_r N_\ell \, d\boldsymbol{\eta} \tag{7.2}$$

and $\tilde{q}$ is the array of nodal values of $(q \cdot \det J)^h$ constituted of four components at each node. The arrays $\tilde{f}_\ell$ define the algebraic sum of the semi-discrete, η_ℓ partial derivatives of the inviscid, viscous and dissipation fluxes, containing the appropriate metric data, see (5.65)-(5.67) and/or (5.68)-(5.70). Note that each array entry is

obtained by multiplication of $q(t)^\ell$, in the original entry, by $1 = \det J^\ell / \det J^\ell$, and subsequent association of the numerator $\det J^\ell$ with $q(t)^\ell$ itself. For example, the continuity equation entry in $\tilde{f}_1$ corresponding to node r, see (5.68), is

$$\begin{aligned} \left(\tilde{f}_1\right)_\rho^r &= -\int_{\widehat{\Omega}^h} e_{j1} \frac{\partial N_r}{\partial \eta_1} \frac{N_\ell}{\det J^\ell} (m_j^\ell(t) \det J^\ell)\, d\boldsymbol{\eta} \\ &+ \mathcal{L}\beta_{\underline{r}} \int_{\widehat{\Omega}^h} |\boldsymbol{u}^s(t)| \frac{N_s}{\det J^k} \frac{\partial N_r}{\partial \eta_1} \frac{\partial N_k}{\partial \eta_1} (\rho^k(t) \det J^k)\, d\boldsymbol{\eta} \end{aligned} \tag{7.3}$$

This algebraic rearrangement allows for straightforward determination of the Newton algorithm Jacobian expressions $\partial \tilde{f}_\ell / \partial \tilde{q}$.

The analytical solution of the semi-discretization ODE system (7.1) closely models the solution of (1.1), augmented with well-posed boundary conditions, since the finite element semi-discretization is stable for adequate choice of $\beta_{\underline{r}}$. Hence, the resultant ODE system is dissipative, and consequently the convergence of the terminal approximate solution depends on the evolution stability of the ODE solver.

For the numerical integration of (7.1), a two-stage, diagonally implicit Runge-Kutta (IRK) scheme is established, which remains non-linearly and absolutely stable for the stiff dissipative semi-discrete Navier-Stokes equations on arbitrary meshes. As detailed in Chapter 8, this algorithm family is constituted of the sequence

$$\tilde{q}_{n+1} - \tilde{q}_n = \Delta t (b_1 k_1 + b_2 k_2) \tag{7.4}$$

$$k_1 = g(t_n + c_1 \Delta t, \tilde{q}_n + \alpha_1 \Delta t k_1) \tag{7.5}$$

$$k_2 = g(t_n + c_2 \Delta t, \tilde{q}_n + \beta_{21} \Delta t k_1 + \alpha_2 \Delta t k_2) \tag{7.6}$$

In (7.4)-(7.6), n denotes the time step index, while the operator $g(\cdot,\cdot)$ is defined as

$$g(t,\tilde{q}_n) \equiv -\mathcal{M}^{-1}\left(\tilde{f}_1(t,\tilde{q}_n) + \tilde{f}_2(t,\tilde{q}_n)\right) \tag{7.7}$$

Further, the seven coefficients b_1, b_2, c_1, c_2, α_1, β_{21}, and α_2, defining the IRK scheme (7.4)-(7.6), allow simultaneous 2^{nd} order accuracy and non-linear absolute stability, as proved in the following Chapter.

For this diagonally implicit algorithm, the solutions k_1 and k_2 for (7.5) and (7.6) exist and are unique. For comparison, the following determination

$$\begin{aligned} \alpha_1 = \theta \quad &, \quad \alpha_2 = 0 \\ \beta_{21} = 0 \quad &, \quad c_1 = 1 \quad , \quad c_2 = 0 \end{aligned} \tag{7.8}$$

for (7.4)-(7.6) produces the single-stage, "θ" implicit algorithm family. Numerical validations, presented in Chapter 10, verify that the range of stable integration steps permitted by the IRK procedure significantly exceeds those for the A-stable backwards Euler rule ($\theta = 1$) while maintaining second order accuracy in time. Likewise, these results confirm that IRK allows expeditious attainment of a steady state, when one exists.

7.2 Newton Implementation and Tensor Matrix Product Factorization

The practical solution of the IRK expressions (7.5)-(7.6) may be pursued iteratively. Letting p denote the iteration index, the Newton algorithm for solving (7.5)-(7.6) is

$$\left(\mathcal{M}+\alpha_1\Delta t\left[\frac{\partial\tilde{f}_1}{\partial\tilde{q}}\right]_{\tilde{q}_n+\alpha_1\Delta t k_1^p}+\alpha_1\Delta t\left[\frac{\partial\tilde{f}_2}{\partial\tilde{q}}\right]_{\tilde{q}_n+\alpha_1\Delta t k_1^p}\right)\left(k_1^{p+1}-k_1^p\right)$$

$$=-\sum_{\ell=1}^{2}\tilde{f}_\ell(t_n+c_1\Delta t,\tilde{q}_n+\alpha_1\Delta t k_1^p)-\mathcal{M}k_1^p \tag{7.9}$$

iterated to accepted convergence for k_1, followed by the similar operation

$$\left(\mathcal{M}+\alpha_2\Delta t\left[\frac{\partial\tilde{f}_1}{\partial\tilde{q}}\right]_{\tilde{q}_n+\beta_{21}\Delta t k_1+\alpha_2\Delta t k_2^p}+\alpha_2\Delta t\left[\frac{\partial\tilde{f}_2}{\partial\tilde{q}}\right]_{\tilde{q}_n+\beta_{21}\Delta t k_1+\alpha_2\Delta t k_2^p}\right)\left(k_2^{p+1}-k_2^p\right)$$

$$=-\sum_{\ell=1}^{2}\tilde{f}_\ell(t_n+c_2\Delta t,\tilde{q}_n+\beta_{21}\Delta t k_1+\alpha_2\Delta t k_2^p)-\mathcal{M}k_2^p \tag{7.10}$$

The diagonal implicitness in these expressions allows the independent computation of the arrays k_1 and k_2, which are set to zero to begin the iteration. However, the direct LU factorization of the lhs matrices in (7.9)-(7.10) is prohibitively expensive on adequate semi-discretizations. Therefore, as detailed in Chapter 9, the Newton algorithm jacobian is approximated by a tensor matrix product as

$$\left[\mathcal{M}+\alpha_{\underline{i}}\Delta t\left[\frac{\partial\tilde{f}_1}{\partial\tilde{q}}\right]_{(\tilde{q}_n)_{\underline{i}}^*}+\alpha_{\underline{i}}\Delta t\left[\frac{\partial\tilde{f}_2}{\partial\tilde{q}}\right]_{(\tilde{q}_n)_{\underline{i}}^*}\right]$$

$$\simeq\left[\mathcal{M}_1+\alpha_{\underline{i}}\Delta t\left[\frac{\partial\tilde{\mathrm{f}}_1}{\partial\tilde{q}}\right]_{(\tilde{q}_n)_{\underline{i}}^*}\right]\otimes\left[\mathcal{M}_2+\alpha_{\underline{i}}\Delta t\left[\frac{\partial\tilde{\mathrm{f}}_2}{\partial\tilde{q}}\right]_{(\tilde{q}_n)_{\underline{i}}^*}\right] \tag{7.11}$$

where $\mathcal{M}_1$, $\mathcal{M}_2$, $\tilde{\mathrm{f}}_1$, and $\tilde{\mathrm{f}}_2$ are the 1-D factors intrinsic in (7.1)-(7.2), as indicated by (7.14)-(7.15) and detailed in Chapter 8. Further, $(\tilde{q}_n)_{\underline{i}}^*$ indicates the Jacobian matrix evaluation state in (7.9)-(7.10) and $\otimes$ denotes the matrix tensor product [14].

Significantly, the 2-D-formulation large, albeit sparse, matrix in the lhs of (7.11) is replaced with the product of two 1-D problem matrices, which remain block

tri-diagonal independent of the order and bandwidth of the associated multi- dimensional matrix [14,40]. The approximate solution of systems (7.9) and (7.10) is obtained via the sequence

$$\left[\mathcal{M}_1 + \alpha_{\underline{i}}\Delta t\left[\frac{\partial \tilde{\mathrm{f}}_1}{\partial \tilde{q}}\right]_{(\tilde{q}_n)^*_{\underline{i}}}\right]\ell_i = -\Delta t\sum_{\ell=1}^{2}\tilde{f}_\ell\left(t + c_{\underline{i}}\Delta t, \tilde{q}_n + \beta_{21}k_1\delta_i^2\right) - \mathcal{M}k_i^p$$

$$\left[\mathcal{M}_2 + \alpha_{\underline{i}}\Delta t\left[\frac{\partial \tilde{\mathrm{f}}_2}{\partial \tilde{q}}\right]_{(\tilde{q}_n)^*_{\underline{i}}}\right]\delta k_i^{p+1} = \ell_i\,,\ for\ 1 \le i \le 2 \qquad (7.12)$$

where $\delta k_i^{p+1} \equiv k_i^{p+1} - k_i^p$. Noting in (7.12) the subscript range for i, the IRK solution arrays are specifically computed by the following steps:

1. Number all nodes sequentially along η_1 coordinate curves, form $\left[\mathcal{M}_1 + \alpha_i\Delta t[\partial\tilde{\mathrm{f}}_1/\partial\tilde{q}]_{(\tilde{q}_n)^*_{\underline{i}}}\right]$ and $-\Delta t\sum_{\ell=1}^{2}\tilde{f}_\ell(t + c_i\Delta t, \tilde{q}_n + \beta_{21}k_1\delta_i^2)$ as well as $\mathcal{M}k_i^p$ along these curves. Enforce appropriate boundary conditions and solve for the intermediate array ℓ_1.

2. For all nodes renumbered sequentially along η_2 coordinate curves, form $\left[\mathcal{M}_2 + \alpha_i\Delta t[\partial\tilde{\mathrm{f}}_2/\partial\tilde{q}]_{(\tilde{q}_n)^*_{\underline{i}}}\right]$. Enforce appropriate boundary conditions and solve for the intermediate array δk_1^{p+1}.

3. Iterate steps 1-2 to convergence (or for a fixed number of steps) for k_1

4. Repeat steps 1-3 for $i = 2$ hence determine k_2

The desirable stability properties of the IRK algorithm could certainly become compromized by this approximation, since the convergence of the resultant quasi-Newton algorithm depends on problem stiffness, which may affect the conditions of

the Newton-Kantorovich theorem, [12,15]. To limit such a contamination, the tensor factored jacobians are re-evaluated (inexpensively) at each iteration. A solution is accepted after a specified number of iterations, or when it meets the constraint

$$\|k_j^{p+1} - k_j^p\| \leq TOL \quad , \quad j = 1,2 \tag{7.13}$$

for $\|\cdot\|$ a convenient norm and TOL a user-defined tolerance. This procedure is found to be robust via determination that the cost of factored jacobian evaluation, and subsequent linear equation solutions, is negligible in comparison to the rhs evaluation expenditure.

Each block tri-diagonal matrix component in the rhs of (7.11) contains decoupled inner matrices that correspond to the jacobians of the semi-discrete equations formulated at the nodes on independent grid lines that begin and end on boundary segments. Hence, as indicated by the subscripts 1 and 2 in (7.11), the two component matrices are formed using strictly one-dimensional bases n_ℓ associated with the individual curvilinear coordinates η_1 and η_2. For instance, the tensor factor $\mathcal{M}_1$ for $\mathcal{M}$ in (7.2) is

$$\mathcal{M}_1 \equiv \int_{\widehat{\Omega}_{\eta_1}} n_r n_\ell \, d\eta_1 \tag{7.14}$$

and the corresponding counterpart of $\left(\tilde{f}_1\right)_\rho^r$ in (7.3) is

$$\begin{aligned} \left(\tilde{f}_1\right)_\rho^r &= -\int_{\widehat{\Omega}_{\eta_1}} e_{j1} \frac{dn_r}{d\eta_1} \frac{n_\ell}{\det J^\ell} (m_j^\ell(t) \det J^\ell) \, d\eta_1 \\ &+ \mathcal{L}\beta_r \int_{\widehat{\Omega}_{\eta_1}} |\boldsymbol{u}^s(t)| \frac{n_s}{\det J^k} \frac{dn_r}{d\eta_1} \frac{dn_k}{d\eta_1} (\rho^k(t) \det J^k) \, d\eta_1 \end{aligned} \tag{7.15}$$

In (7.14)-(7.15), the values of the indices ℓ, s and k are limited to the range

$[\, r-1,\, r,\, r+1\,]$. Further, $\widehat{\Omega}_{\eta_1}$ is the η_1 coordinate curve spanning $\widehat{\Omega}^h$, in the η_2 direction, and n_r constitutes the η_1 direction tensor factor in N_r.

The association of $\det J$ with q within the time partial derivative, see (5.65)-(5.67) and/or (5.68)-(5.70), leads to a $\det J$-independent mass matrix (7.2), hence (7.14). As a result, the factorization of this matrix is exact, i.e.,

$$\mathcal{M} = \mathcal{M}_1 \otimes \mathcal{M}_2 \tag{7.16}$$

Furthermore, owing to the $\det J$ independent mass matrix, the $\boldsymbol{\eta}$-space first and second order partial derivative weak statement terms also factor exactly as

$$\int_{\widehat{\Omega}^h} N_r \frac{\partial N_\ell}{\partial \eta_j}\, d\boldsymbol{\eta} \equiv \mathcal{M}_{3-\underline{j}} \otimes \int_{\widehat{\Omega}_{\eta_{\underline{j}}}} n_r \frac{dn_\ell}{d\eta_j}\, d\eta_{\underline{j}} \tag{7.17}$$

$$\int_{\widehat{\Omega}^h} \frac{\partial N_r}{\partial \eta_{\underline{j}}} \frac{\partial N_\ell}{\partial \eta_j}\, d\boldsymbol{\eta} \equiv \mathcal{M}_{3-\underline{j}} \otimes \int_{\widehat{\Omega}_{\eta_{\underline{j}}}} \frac{dn_r}{d\eta_{\underline{j}}} \frac{dn_\ell}{d\eta_j}\, d\eta_{\underline{j}} \tag{7.18}$$

which allow usage of 2-D metric data in the 1-D operators, see (7.15) and Chapter 9, since no element measure is present in $\mathcal{M}_j$.

Therefore, these matrix tensor products do not require any approximate factorization of the metric data $\det J$ and e_{kj}. Consequently, the error associated with such approximate metric data is totally absent in this formulation. This new and robust finite element tensor product factorization, detailed in Chapter 9, thus significantly departs from "patch" factorization algorithms reported in [28,29] that require approximate factors of $\det J$ and e_{kj} Further, the present formulation is naturally cast in curvilinear coordinates and employs full 2-D metric data in the curvilinear 1-D factors in (5.65)-(5.67) and/or (5.68)-(5.70), see (7.15). Consequently,

the factorization can be used on arbitrary 2-D grids, and quasi-Newton algorithm convergence and stability, as well as unsteady solution accuracy, are not adversely affected on non-rectangular non-uniform meshes. The overall solution procedure is thoroughly detailed in Chapters 8 and 9, with validations documented in Chapter 10.

Chapter 8

A Non-Linearly Stable Implicit Runge-Kutta Algorithm for Conservation Law System Dissipative Semi-Discretizations

In this Chapter, a non-linearly and absolutely stable implicit Runge-Kutta algorithm is developed for the accurate temporal integration of the semi-discrete 2-D compressible Navier-Stokes Equations.

8.1 Algorithm Derivation

Following the classical method of lines, the semi-discrete integral statement (5.61), repeated here for convenience,

$$\int_{\widehat{\Omega}^h} w_r^h \left[\frac{\partial}{\partial t} \left(q \cdot \det J \right)^h + \frac{\partial}{\partial \eta_\ell} \left(e_{k\ell} \left(f_k^h - f_k^{h\nu} \right) \right) - \mathcal{L} \beta_{\underline{r}} \frac{\partial}{\partial \eta_\ell} \left(|\boldsymbol{u}^h| \frac{\partial q^h}{\partial \eta_\ell} \right) \right] d\boldsymbol{\eta} = 0, \quad \forall \ w \tag{8.1}$$

yields an ODE system of the form (5.65)-(5.67) and/or (5.68)-(5.70), hence (7.1), which is recast as

$$\frac{d\tilde{q}(t)}{dt} - g(t, \tilde{q}(t)) = 0 \tag{8.2}$$

where the operator $g(\cdot,\cdot)$ is defined by (7.7). In the sequel, the tilde superscript is deleted without loss of clarity.

As given by (7.4)-(7.6), and repeated here for convenience, the two-stage diagonally implicit Runge-Kutta (IRK) algorithm family is

$$q_{n+1} - q_n = \Delta t(b_1 k_1 + b_2 k_2) \tag{8.3}$$

$$k_1 = g(t_n + c_1\Delta t, q_n + \alpha_1 \Delta t k_1) \tag{8.4}$$

$$k_2 = g(t_n + c_2\Delta t, q_n + \beta_{21}\Delta t k_1 + \alpha_2 \Delta t k_2) \tag{8.5}$$

where subscript n denotes the time step index. The coefficients c_1 and c_2 satisfy the conditions

$$\begin{cases} c_1 = \alpha_1 \\ c_2 = \beta_{21} + \alpha_2 \end{cases} \tag{8.6}$$

The explicit dependence on time of the operator $g(\cdot,\cdot)$ allows straightforward implementation of time-dependent Dirichlet boundary conditions. In the sequel, a capital letter denotes a square matrix and lower case signifies a column matrix.

It is common practice, [15,18], to gather the ODE algorithm coefficients in the

form of a synoptic table, i.e.,

$$\begin{array}{c|c} c & A \\ \hline & b^T \end{array} = \begin{array}{c|cc} c_1 & \alpha_1 & 0 \\ c_2 & \beta_{21} & \alpha_2 \\ \hline & b_1 & b_2 \end{array} \tag{8.7}$$

The diagonal implicitness of algorithm (8.3)-(8.5) permits the independent determination of the arrays k_1 and k_2. This is pursued via the tensor product factorization of the Newton algorithm matrices, for the iterative solution of (8.4)-(8.5), as introduced in Chapter 7, and to be detailed in Chapter 9. The affordability of this procedure permits the 2^{nd}-stage recomputation of the jacobian matrix, hence the coefficient α_2 in (8.5) is in principle allowed to differ from α_1.

A two stage algorithm is selected so that enough coefficients are present to allow the combination, within a single implicit procedure, of the strong A-stability properties of the backwards Euler rule with the classical second order accuracy of the Crank-Nicolson rule. These constants are then determined such that the algorithm is second order accurate, in the classical sense, and also meets the requirements of the recent B-*consistency/convergence* and B-*stability* theories, [15,18].

8.1.1 Classical Accuracy and B-Consistency/Convergence Constraints

The constraints on the IRK constants, [10], guaranteeing second order accuracy in the classical sense are

$$b_1 + b_2 = 1 \tag{8.8}$$

$$b_1\alpha_1 + b_2(\beta_{21} + \alpha_2) \;=\; \frac{1}{2} \tag{8.9}$$

When equations (8.8)-(8.9) are satisfied, the following local time discretization error

$$\hat{l}_{n+1} = q(t_{n+1}) - \hat{q}_{n+1} \tag{8.10}$$

with

$$\hat{q}_{n+1} = q(t_n) + \Delta t(\;\; b_1 k_1(t_n, q(t_n)\;) + b_2 k_2(t_n, q(t_n)\;)\;\;) \tag{8.11}$$

is bounded by the inequality

$$\|\hat{l}_{n+1}\| \leq S\Delta t^3\;,\; \forall \Delta t \in (0, \Delta t_s] \tag{8.12}$$

where S and Δt_s in general depend upon the stiffness of the ODE system. For the stiff equations resulting from the spatial semi-discretization of the compressible viscous Navier-Stokes equations, inequality (8.12) is insufficient to ensure the expected accuracy for practical time steps Δt, since the constant S grows with increasing stiffness, while Δt_s may concurrently decrease.

The algorithm suitable for the numerical integration of the subject class of nonlinear stiff ODE system should instead maintain a uniform order of accuracy irrespective of the stiffness magnitude. This is the essence of the fundamental notion of B-*consistency*, which is mathematically characterized by the inequality

$$\|\hat{l}_{n+1}\| \leq D\Delta t^{p+1}\;,\; \forall \Delta t \in (0, \Delta t_1] \tag{8.13}$$

where the constants D and Δt_1 are totally independent of stiffness and exponent p is the order of consistency. For the IRK algorithm (8.3)-(8.5) this order is bounded

by the inequality $1 \leq p \leq 2$ and the sufficient conditions for B-consistency of order one, at least, are

$$\alpha_1 > 0 \quad , \quad \alpha_2 > 0 \tag{8.14}$$

Additional B-consistency expressions are [15]

$$b^T A^{-1} V e_j = 1 \quad , \quad j = 1, 2 \tag{8.15}$$

where V is the Van der Monde matrix

$$V = \begin{pmatrix} 1 & , & c_1 \\ 1 & , & c_2 \end{pmatrix} \tag{8.16}$$

and e_j defines the j^{th} unit vector, hence

$$e_1 = \begin{pmatrix} 1 \\ 0 \end{pmatrix} \quad , \quad e_2 = \begin{pmatrix} 0 \\ 1 \end{pmatrix} \tag{8.17}$$

Expression (8.15) yields the equations

$$b_1 \alpha_2 + b_2(\alpha_1 - \beta_{21}) = \alpha_1 \alpha_2 \tag{8.18}$$

$$b_1 + b_2 = 1 \tag{8.19}$$

Equation (8.18) provides an important auxiliary condition on the algorithm free parameters that leads to strong A-stability, as indicated in Section 8.1.2.

The efficient numerical integration of system (8.2) demands that convergence rate not degrade with increasing stiffness. This is the allied concept of B-convergence which is formulated in terms of the global time discretization error

$$\hat{e}_{n+1} = q(t_{n+1}) - q_{n+1} \tag{8.20}$$

via the inequality

$$\|\hat{e}_{n+1}\| \leq C\Delta t^r \ , \ \forall \Delta t \in (0, \Delta t_2] \tag{8.21}$$

In estimate (8.21), the exponent r is the convergence order and satisfies the inequality $r \ \leq \ p+1$. Further, the constants C and Δt_2 do not depend on stiffness. For the present diagonal algorithm, inequality (8.21) is satisfied if, in addition to constraints (8.14), the following inequalities are also satisfied [15]

$$b_1 > 0 \tag{8.22}$$

$$b_2 > 0 \tag{8.23}$$

8.1.2 Stability Constraints

The numerical stability of algorithm (8.3)-(8.5) is investigated in connection with the class of dissipative ODE systems, that is those that satisfy the inequality

$$\langle \ q(t) - \hat{q}(t), g(t, q(t)) - g(t, \hat{q}(t)) \ \rangle \ \ \leq 0 \tag{8.24}$$

In (8.24) $\langle \cdot, \cdot \rangle$ is a suitable real inner product and $q(t)$ and $\hat{q}(t)$ are any two arrays in the definition domain of $g(t, \cdot)$. Note that this expression resembles a Lyapunov stability constraint, [4,5,7,8].

Provided that appropriate well posed boundary conditions for (1.1), and a suitable dissipative spatial semi-discretization, e.g. that developed in Chapter 5, leads to an operator $g(\cdot, \cdot)$ that satisfies condition (8.24), then it is possible to capitalize on the results of the B-stability theory in the derivation of the IRK algorithm. This

theory dictates that the norm of the error $\varepsilon_n = q_n - \hat{q}_n$ meausring the distance between any two discrete solutions q_n and $\hat{q}_n$ corresponding to an identical Cauchy problem must not increase during the numerical integration for *any positive time step* Δt and *any arbitrary non-linear and stiff operator* $g(\cdot,\cdot)$ that meets constraint (8.24).

The notion of B-stability is thus characterized by the inequality

$$\|q_{n+1} - \hat{q}_{n+1}\| \leq \|q_n - \hat{q}_n\| \quad , \quad \Delta t > 0 \tag{8.25}$$

which, under the present hypotheses, implies classical linear absolute stability (A-stability). In (8.25), $\|\cdot\|$ indicates a Hilbert-space norm induced by the inner product in (8.24). The sufficient conditions for B-stability require the positive semi-definiteness of the two matrices

$$B = diag(b_1, \ldots, b_s) \tag{8.26}$$

$$M = BA + A^T B - bb^T \tag{8.27}$$

where s is the number of algorithm stages. This matrix property is used in the following proof, based on Butcher's and Verwer's developments [15,18], to yield inequality (8.25) after expressing q_{n+1} in terms of q_n via (8.3)-(8.5). To accomplish this, it is convenient to define the auxiliary variable p_i in terms of k_j as

$$p_i = q_n + \Delta t \sum_{j=1}^{2} a_{ij} k_j \quad , \quad i = 1, 2 \tag{8.28}$$

The following definitions are also needed

$$\delta q_n = q_n - \hat{q}_n \ , \ \delta q_{n+1} = q_{n+1} - \hat{q}_{n+1} \ , \ \delta p_i = p_i - \hat{p}_i \tag{8.29}$$

$$\delta g_i = g(t_n + c_i\Delta t, p_i) - g(t_n + c_i\Delta t, \hat{p}_i) \tag{8.30}$$

whereupon algorithm (8.3)-(8.5) leads to the relations

$$\delta q_{n+1} = \delta q_n + \Delta t \sum_{i=1}^{2} b_i \delta g_i \tag{8.31}$$

$$\begin{aligned} \delta q_n - \delta p_i &= (q_n - p_i) - (\hat{q}_n - \hat{p}_i) = -\Delta t \sum_{j=1}^{2} a_{ij}(k_j - \hat{k}_j) \\ &= -\Delta t a_{ij}\left(g(t_n + c_j\Delta t, p_j) - g(t_n + c_j\Delta t, \hat{p}_j)\right) = -\Delta t \sum_{j=1}^{2} a_{ij}\delta g_j \end{aligned} \tag{8.32}$$

Consequently, the square of the norm $\|q_{n+1} - \hat{q}_{n+1}\|$ is

$$\begin{aligned} \|q_{n+1} - \hat{q}_{n+1}\|^2 &= \|q_n - \hat{q}_n + \Delta t \sum_{i=1}^{2} b_i \delta g_i\|^2 = \langle \delta q_n + \Delta t \sum_{i=1}^{2} b_i \delta g_i, \delta q_n + \Delta t \sum_{i=1}^{2} b_j \delta g_j \rangle \\ &= \|q_n - \hat{q}_n\|^2 + 2\Delta t \sum_{i=1}^{2} b_i \langle \delta q_n, \delta g_i \rangle + \Delta t^2 \sum_{i,j=1}^{2} b_i b_j \langle \delta g_i, \delta g_j \rangle \\ &= \|q_n - \hat{q}_n\|^2 + 2\Delta t \sum_{i=1}^{2} b_i \langle \delta p_{\underline{i}}, \delta g_i \rangle + 2\Delta t \sum_{i=1}^{2} b_i \langle \delta q_n - \delta p_{\underline{i}}, \delta g_i \rangle \\ &+ \Delta t^2 \sum_{i,j=1}^{2} b_i b_j \langle \delta g_i, \delta g_j \rangle \\ &= \|q_n - \hat{q}_n\|^2 + 2\Delta t \sum_{i=1}^{2} b_i \langle \delta p_{\underline{i}}, \delta g_i \rangle - 2\Delta t^2 \sum_{i,j=1}^{2} b_i a_{ij} \langle \delta g_j, \delta g_i \rangle \\ &+ \Delta t^2 \sum_{i,j=1}^{2} b_i b_j \langle \delta g_i, \delta g_j \rangle \\ &= \|q_n - \hat{q}_n\|^2 + 2\Delta t \sum_{i=1}^{2} b_i \langle \delta p_{\underline{i}}, \delta g_i \rangle - \Delta t^2 \sum_{i,j=1}^{2} (b_i a_{ij} + b_j a_{ji} - b_i b_j) \langle \delta g_i, \delta g_j \rangle \\ &= \|q_n - \hat{q}_n\|^2 + 2\Delta t \sum_{i=1}^{2} b_i \langle \delta p_{\underline{i}}, \delta g_i \rangle - \Delta t^2 \sum_{i,j=1}^{2} m_{ij} \langle \delta g_i, \delta g_j \rangle \end{aligned} \tag{8.33}$$

where m_{ij} denotes the the set of entries in the matrix M. The last two inner-products in the final expression are non-positive since the differential equation system (8.2) is dissipative, that is $\langle \delta p_{\underline{i}}, \delta g_i \rangle \leq 0$, and the matrices B and M are assumed

positive semi-definite. Therefore, the fundamental inequality

$$\|q_{n+1} - \hat{q}_{n+1}\|^2 \leq \|q_n - \hat{q}_n\|^2 \tag{8.34}$$

results. Consequently B-stability is obtained for an implicit s-stage Runge-Kutta algorithm if its coefficients satisfy the cited matrix non-negativity property.

Any IRK algorithm that satisfies this property is called *algebraically stable*. Its significance for the CFD implicit algorithms, and the subject IRK procedure, is investigated in Section 8.3. In the derivation of inequality (8.34), no hypothesis has been made on the structure of the residual $g(\cdot,\cdot)$ and/or the semi-discretization employed. Consequently, procedure (8.3)-(8.5) is absolutely stable for the full Navier-Stokes dissipative semi-discrete equations on arbitrary meshes.

For algorithm (8.3)-(8.5), matrices B and M are

$$B = \begin{pmatrix} b_1 & , & 0 \\ 0 & , & b_2 \end{pmatrix} \tag{8.35}$$

$$M = \begin{pmatrix} b_1(2\alpha_1 - b_1) & , & b_2(\beta_{21} - b_1) \\ b_2(\beta_{21} - b_1) & , & b_2(2\alpha_2 - b_2) \end{pmatrix} \tag{8.36}$$

These symmetric matrices are positive semi- definite when their Gauss LU- decomposition pivots are non-negative. This requirement translates into the inequalities

$$b_1 \geq 0 \quad , \quad b_2 \geq 0 \tag{8.37}$$

for matrix B, and

$$\begin{aligned} & b_1(2\alpha_1 - b_1) \geq 0 \\ & b_1 b_2(4\alpha_2\alpha_1 - 2\alpha_2 b_1 - 2\alpha_1 b_2 + b_1 b_2) - b_2^2(\beta_{21} - b_1)^2 \geq 0 \end{aligned} \tag{8.38}$$

for matrix M.

As anticipated in Section 8.1.1, the present IRK algorithm is, in particular, linearly strongly A-stable, or L-stable, according to the definition of Ehle [10,15], by virtue of the B-consistency constraint (8.18). Therefore, the linear amplification ratio for (8.2) vanishes with increasing stiffness and/or solution component frequency, hence $\Delta\bar{t} \rightarrow \infty$. Consequently, the integration scheme linear dissipation increases with increasing stiffness. To verify this assertion, form the amplification ratio for the classical linear model problem

$$\frac{dq}{dt} = \lambda q \tag{8.39}$$

The result is

$$\frac{q_{n+1}}{q_n} = \frac{\gamma\overline{\Delta t}^2 + (b_1 + b_2 - \alpha_1 - \alpha_2)\overline{\Delta t} + 1}{(1 - \alpha_1\overline{\Delta t})(1 - \alpha_2\overline{\Delta t})} \tag{8.40}$$

wherein $\overline{\Delta t} \equiv \lambda\Delta t$ and the coefficient γ is defined as

$$\gamma = \alpha_1\alpha_2 - \alpha_2 b_1 - \alpha_1 b_2 + b_2\beta_{21} \tag{8.41}$$

It is then noted that $\gamma = 0$ coincides with constraint (8.18). When γ vanishes, the amplification ratio (8.40) tends to zero as the denominator becomes large. Further, due to the B-consistency constraint (8.14), the roots

$$\overline{\Delta t}_1 = (\alpha_1)^{-1} \quad , \quad \overline{\Delta t}_2 = (\alpha_2)^{-1} \tag{8.42}$$

of the denominator in (8.40) are positive. Therefore the amplification ratio remains always bounded for any $\Delta t > 0$, since $\Re(\overline{\Delta t})$ is constantly negative for dissipative

systems. Further, $\|q_{n+1}/q_n\| \leq 1$, following from (8.34) since $\hat{q}_n \equiv 0$ for the linear problem, and $\|q_{n+1}/q_n\| \to 0$, following from (8.40) and (8.18). Consequently the subject Runge-Kutta scheme is L-stable.

8.2 Solution of the IRK Coefficient Equations

The derived expressions for the algorithm coefficients that guarantee 2^{nd} order accuracy, B-consistency/convergence, and algebraic stability are

$$\begin{cases} b_1 + b_2 = 1 \\ b_1\alpha_1 + b_2(\beta_{21} + \alpha_2) = \frac{1}{2} \\ \alpha_1 > 0\ ,\ \alpha_2 > 0 \\ b_1\alpha_2 + b_2(\alpha_1 - \beta_{21}) = \alpha_1\alpha_2 \\ \beta_{21} > 0 \\ b_1 > 0\ ,\ b_2 > 0 \\ b_1(2\alpha_1 - b_1) \geq 0 \\ b_1 b_2(4\alpha_2\alpha_1 - 2\alpha_2 b_1 - 2\alpha_1 b_2 + b_1 b_2) - b_2^2(\beta_{21} - b_1)^2 \geq 0 \end{cases} \tag{8.43}$$

A real solution is then easily determined using the following normalization condition

$$b^T A^{-1} b = (\alpha_1\alpha_2)^{-1}(b_1^2\alpha_2 + b_2(b_2\alpha_1 - b_1\beta_{21})) = 1 \tag{8.44}$$

Correspondingly, the analytical solution of the following subset

$$\begin{cases} b_1 + b_2 = 1 \\ b_1\alpha_1 + b_2(\beta_{21} + \alpha_2) = \frac{1}{2} \\ b_1\alpha_1 + b_2(\alpha_1 - \beta_{21}) = \alpha_1\alpha_2 \\ b_1^2\alpha_2 + b_2(b_2\alpha_1 - b_1\beta_{21}) = \alpha_1\alpha_2 \end{cases} \tag{8.45}$$

is

$$\begin{cases} b_1 = \dfrac{1-\alpha_2}{2} \quad , \quad b_2 = \dfrac{1+\alpha_2}{2} \\ \alpha_1 = \dfrac{1-2\alpha_2}{2(1-\alpha_2)} \quad , \quad \beta_{21} = \dfrac{1-2\alpha_2^2}{2(1+\alpha_2)} \end{cases} \tag{8.46}$$

Substitution of both these relations, and the inequalities

$$\begin{cases} \alpha_1 > 0 \, , \; \alpha_2 > 0 \\ \beta_{21} > 0 \, , \; b_1 > 0 \, , \; b_2 > 0 \\ b_1(2\alpha_1 - b_1) \geq 0 \end{cases} \tag{8.47}$$

into the inequality

$$b_1 b_2(4\alpha_2\alpha_1 - 2\alpha_2 b_1 - 2\alpha_1 b_2 + b_1 b_2) - b_2^2(\beta_{21} - b_1)^2 \geq 0 \tag{8.48}$$

leads to the terminal constraint

$$-4\alpha_2^4 - 8\alpha_2^3 + 4\alpha_2 - 1 \geq 0 \tag{8.49}$$

The unique solution that satisfies system (8.47) and inequality (8.49) is

$$\alpha_2 = \frac{\sqrt{3}-1}{2} \tag{8.50}$$

The corresponding solution for (8.46) is

$$\begin{cases} \alpha_1 &= \frac{3-\sqrt{3}}{6} \\ \beta_{21} &= 2-\sqrt{3} \\ b_1 &= \frac{3-\sqrt{3}}{4} \\ b_2 &= \frac{1+\sqrt{3}}{4} \end{cases} \tag{8.51}$$

Note that, for the present diagonally implicit IRK algorithm, the solutions k_1 and k_2 for equations (8.4) and (8.5) do exist and are unique, since matrix B is positive definite and both coefficients α_1 and α_2 are positive, [15].

8.3 Theoretical Comparisons

Within the implicit Runge-Kutta framework, algebraic stability can be comparatively assessed for the CFD backwards Euler and trapezoidal (Crank-Nicolson) implicit algorithms. To derive these schemes from (8.3)-(8.5), consider the "theta" ODE algorithm family applied to (8.2) yielding

$$q_{n+1} - q_n = \Delta t(\ (1-\theta)g(t_n, q_n) + \theta g(t_{n+1}, q_{n+1})\ ) \tag{8.52}$$

Equation (8.52) can be recast as

$$q_{n+1} - q_n = \Delta t(\ (1-\theta)k_1 + \theta k_2\ ) \tag{8.53}$$

$$k_1 = g(t_n, q_n) \tag{8.54}$$

$$k_2 = g(t_n + \Delta t, q_n + (1-\theta)\Delta t k_1 + \theta \Delta t k_2) \tag{8.55}$$

and this form coincides with the structure of (8.3)-(8.5).

The synoptic table for algorithm (8.53)-(8.55) is

$$\begin{array}{c|c} c & A \\ \hline & b^T \end{array} = \begin{array}{c|cc} 0 & 0 & 0 \\ 1 & (1-\theta) & \theta \\ \hline & (1-\theta) & \theta \end{array} \tag{8.56}$$

and the matrices B and M are

$$B = \begin{pmatrix} 1-\theta & , & 0 \\ 0 & , & \theta \end{pmatrix} \tag{8.57}$$

$$M = \begin{pmatrix} -(1-\theta)^2 & , & 0 \\ 0 & , & \theta \end{pmatrix} \tag{8.58}$$

The algebraic-stability constraints are

$$\begin{cases} (1-\theta) \geq 0 \\ \theta \geq 0 \\ -(1-\theta)^2 \geq 0 \\ \theta^2 \geq 0 \end{cases} \tag{8.59}$$

from which it is deduced that the backwards Euler ($\theta = 1$) algorithm is algebraically stable, whereas the Crank-Nicolson rule ($\theta = \frac{1}{2}$) is not, even though the B-consistency constraint (8.18) is identically satisfied by both algorithms. The dependence of numerical growth or decay upon algebraic stability can be inferred from the fundamental relation

$$\|q_{n+1} - \hat{q}_{n+1}\|^2 = \|q_n - \hat{q}_n\|^2 + 2\Delta t b_i \langle \delta p_{\underline{i}}, \delta g_i \rangle - \Delta t^2 m_{ij} \langle \delta g_i, \delta g_j \rangle \tag{8.60}$$

According to (8.60), a Runge-Kutta temporal algorithm is B-stable, hence is characterized by (8.25), if it satisfies the constraint

$$2\Delta t b_i \langle \delta p_{\underline{i}}, \delta g_i \rangle - \Delta t^2 m_{ij} \langle \delta g_i, \delta g_j \rangle \leq 0 \tag{8.61}$$

The backwards Euler and present IRK schemes unconditionally satisfy this constraint, since the operator $g(\cdot, \cdot)$ is dissipative by hypothesis and matrices B and M are positive definite for both algorithms. Therefore both terms in (8.61) are always negative. Conversely, the Crank-Nicolson rule does not unconditionally satisfy this constraint, since its matrix M is negative definite. Hence, the second term in (8.61) is negative and consequently the whole expression can be positive. Hence, B-stability can only be achieved in this case if the dissipation inner product $\langle \delta p_{\underline{i}}, \delta g_i \rangle < 0$ reaches a sufficient magnitude such that (8.61) is satisfied. Therefore, the stability of this scheme critically depends on the dissipation property of the operator $g(\cdot, \cdot)$, via the magnitude of $\langle \delta p_{\underline{i}}, \delta g_i \rangle < 0$.

Conversely, the backwards Euler and IRK algorithms may be stable, even for non dissipative operators, provided that the magnitude of the associated inner product $\langle \delta p_{\underline{i}}, \delta g_i \rangle \geq 0$ is suitably moderate so that constraint (8.61) is still satisfied. However this phenomenon is substantially less pronounced for the IRK scheme by virtue of the relation

$$(m_{ij})_{EUL} \langle \delta g_i, \delta g_j \rangle > (m_{ij})_{IRK} \langle \delta g_i, \delta g_j \rangle \tag{8.62}$$

that derives from the ratio

$$\frac{(\lambda_M)_{IRK}}{(\lambda_M)_{EUL}} = \frac{2 - \sqrt{3}}{8} \tag{8.63}$$

where (λ_M) is the largest eigenvalue of matrix M for each of the two algorithms.

Consequently, if some form of severe numerical instability develops in the implicit temporal integration with the subject IRK scheme, applied to the semi-discrete CFD evolution equations, it is likely that the spatial semi-discretization employed has not yielded a sufficiently dissipative operator $g(\cdot, \cdot)$.

Chapter 9

A Generalized Tensor Product Factorization for Implicit Finite Element Methods

9.1 Jacobian Matrix Factorization

The efficient solution of the algorithm terminal matrix algebra problem,

$$\left[\mathcal{M} + \theta\,\Delta t \left[\frac{\partial \tilde{f}_1}{\partial \tilde{q}}\right]_p + \theta\,\Delta t \left[\frac{\partial \tilde{f}_2}{\partial \tilde{q}}\right]_p\right] \left[\delta k^{p+1}\right] = b \tag{9.1}$$

for an implicit numerical integration of semi-discretized evolution equations, is obtained through an accurate and cost-effective factorization of the lhs matrix in (9.1). This replacement is necessary, since a direct LU decomposition procedure for (9.1) is prohibitively expensive on adequate semi-discretizations.

In this dissertation, the Newton algorithm jacobian is replaced by a tensor matrix product factorization,

$$\left[\mathcal{M} + \theta\,\Delta t\left[\frac{\partial \tilde{f}_1}{\partial \tilde{q}}\right]_p + \theta\,\Delta t\left[\frac{\partial \tilde{f}_2}{\partial \tilde{q}}\right]_p\right]$$

$$= \left[\mathcal{M}_1 + \theta\,\Delta t\left[\frac{\partial \tilde{f}_1}{\partial \tilde{q}}\right]\right]_p \otimes \left[\mathcal{M}_2 + \theta\Delta t\left[\frac{\partial \tilde{f}_2}{\partial \tilde{q}}\right]\right]_p + O(\theta\Delta t)^2$$

$$\simeq \left[\mathcal{M}_1 + \theta\,\Delta t\left[\frac{\partial \tilde{f}_1}{\partial \tilde{q}}\right]\right]_p \left[\mathcal{M}_2 + \theta\Delta t\left[\frac{\partial \tilde{f}_2}{\partial \tilde{q}}\right]\right]_p \tag{9.2}$$

Each factor matrix in (9.2) remains strictly block tri-diagonal independent of the dimension and bandwidth of the original multi-dimensional matrix. Further, each matrix component contains decoupled inner blocks. These correspond to the jacobians of the semi-discrete equations formulated on independent mesh nodal lines that begin and end on a boundary segment. As indicated by the subscripts 1 and 2 in (9.2), the two component matrices are formed using strictly one-dimensional operators, associated with the corresponding curvilinear coordinate lines η_1 and η_2.

In this chapter, a systematic method to synthesize such one-dimensional operators is developed so that factorization (9.2) is accurate on arbitrary meshes. This method yields products of one-dimensional jacobians and mass matrices that identically coincide with selected multi-dimensional terms. This is obtained via utilization of unfactored 2-D metric data for the one-dimensional operators, after associating the coordinate transformation $\det J$ with the solution δk itself. The mass matrix is thus $\det J$- independent, and consequently no factorization of metric data is required. This new algorithm significantly differs from reported patch techniques that approximate element measures [28,29]. The rigor of the factorization herein developed rests on both the accurate $\boldsymbol{\eta}$-space integration of the multi-dimensional

weak-statement terms, via element-wise constant metric data extractable from the relevant integrals as described in Chapter 6, and on the usage of tensor product bilinear basis functions, whose structure is presented in the following section.

9.2 Computational Regions and Bilinear Tensor Product Basis Functions

For notational convenience, the master computational region $\hat{\Omega}^h_{e,r}$ for the evaluation of the integral statement integrals of Chapter 5 is reexpressed throughout this Chapter as

$$\begin{aligned} \hat{\Omega} &\equiv \bigcup_{e=1}^{4} \hat{\Omega}_e \quad , \quad \hat{\Omega}_e \equiv [-1;+1] \times [-1;+1] \\ \omega &\equiv \bigcup_{e=1}^{2} \omega_e \quad , \quad \omega_e \equiv [-1;+1] \end{aligned} \tag{9.3}$$

for 2-D and 1-D evaluations, respectively. The domain unions $\hat{\Omega}$ and ω are graphed in Figures 9.1 and 9.2 respectively. In these two figures "n" denotes the block semi-bandwidth of the matrix in (9.1).

With reference to Figure 9.1, and for the conventional counter clock-wise ordering, the bilinear Lagrange polynomials are

$$\begin{aligned} N_1(\eta_1,\eta_2) &= \frac{1}{2}(1-\eta_1)\cdot\frac{1}{2}(1-\eta_2) \quad , \quad N_2(\eta_1,\eta_2) = \frac{1}{2}(1+\eta_1)\cdot\frac{1}{2}(1-\eta_2) \\ N_3(\eta_1,\eta_2) &= \frac{1}{2}(1+\eta_1)\cdot\frac{1}{2}(1+\eta_2) \quad , \quad N_4(\eta_1,\eta_2) = \frac{1}{2}(1-\eta_1)\cdot\frac{1}{2}(1+\eta_2) \end{aligned} \tag{9.4}$$

which are graphed in Figure 9.3.

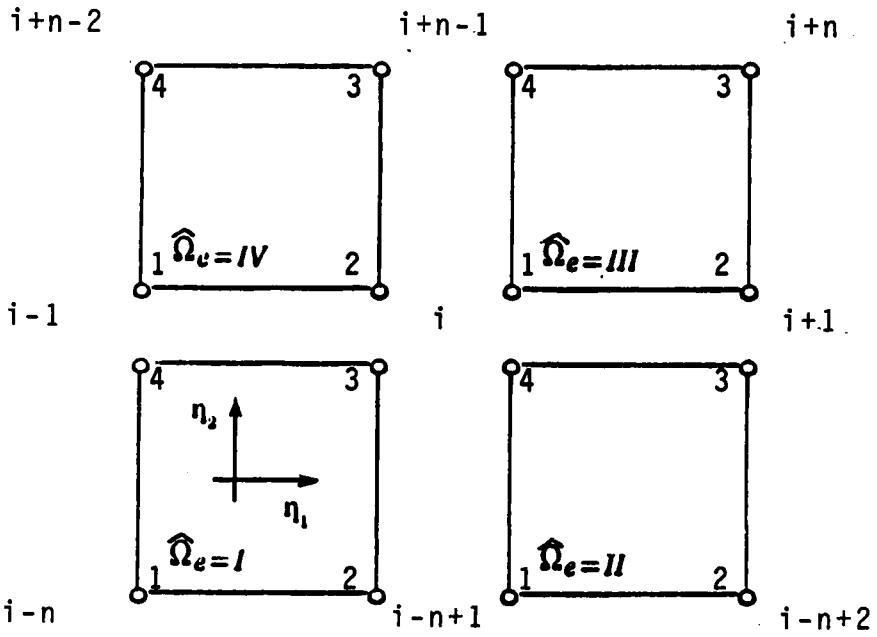


Figure 9.1: Assembly of Four Finite Elements Forming a Master Element

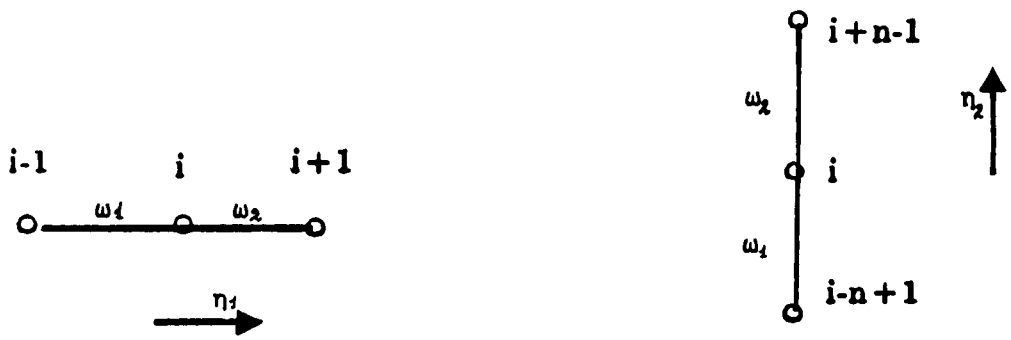


Figure 9.2: Assembly of Two Contiguous Elements

These 2-D functions are tensor products of the 1-D polynomials $n_1(\eta_\alpha)$ and $n_2(\eta_\alpha)$ which constitute the linear factors. These are defined as

$$\begin{aligned} n_1(\eta_1) &= \frac{1}{2}(1-\eta_1) \quad , \quad n_2(\eta_1) = \frac{1}{2}(1+\eta_1) \\ n_1(\eta_2) &= \frac{1}{2}(1-\eta_2) \quad , \quad n_2(\eta_2) = \frac{1}{2}(1+\eta_2) \end{aligned} \tag{9.5}$$

and are graphed in Figure 9.4. Therefore, the basis functions (9.4) are alternatively expressed as

$$\begin{aligned} N_1(\eta_1,\eta_2) &\equiv n_1(\eta_1)\cdot n_1(\eta_2) \quad , \quad N_2(\eta_1,\eta_2) \equiv n_2(\eta_1)\cdot n_1(\eta_2) \\ N_3(\eta_1,\eta_2) &\equiv n_2(\eta_1)\cdot n_2(\eta_2) \quad , \quad N_4(\eta_1,\eta_2) \equiv n_1(\eta_1)\cdot n_1(\eta_2) \end{aligned} \tag{9.6}$$

The functions in (9.4) and (9.5) constitute the building blocks of the generalized hat functions N_ℓ and n_ℓ, see Section 5.1. These attain the value one at node "ℓ" and zero at all other nodes, are supported on all elements that share node "ℓ" and vanish on all other elements and element boundaries that do not contain such a node. Therefore, an injective correspondence exists between the local 2-D element index "k"

$$k \in \{1,2,3,4\} \tag{9.7}$$

and the global numbering index "ℓ"

$$\ell \in \{i-n, i-n+1, i-n+2, i-1, i, i+1, i+n-2, i+n-1, i+n\} \tag{9.8}$$

as illustrated in Figures 9.1-9.2.

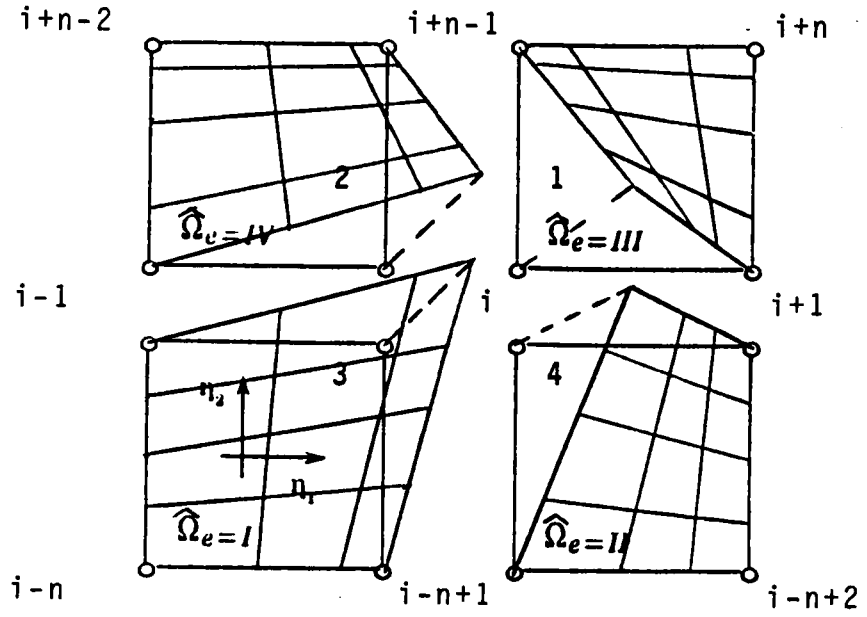


Figure 9.3: Variations of Bilinear Functions (9.4) over $\hat{\Omega}$

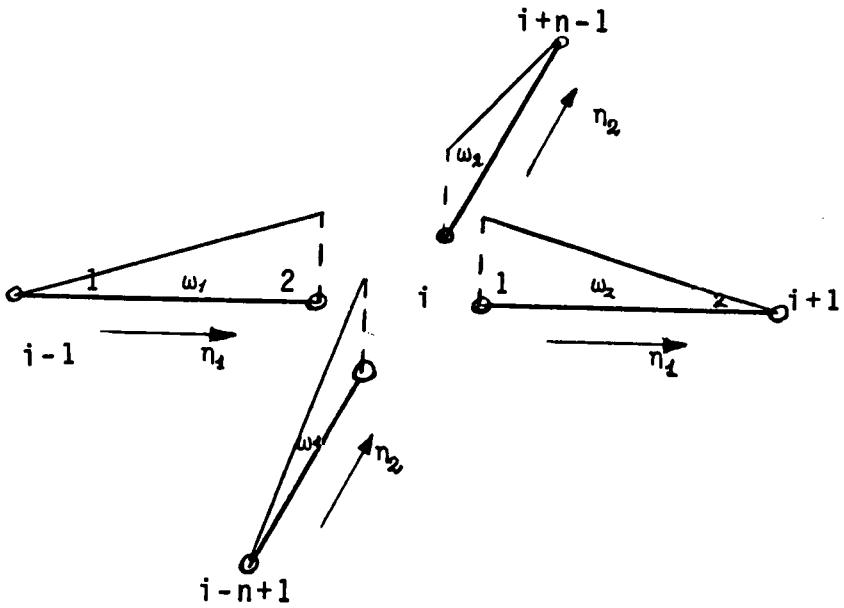


Figure 9.4: Variations of Functions (9.5) over ω

For example, $N_i(\eta_1, \eta_2)$ and $N_{i-1}(\eta_1, \eta_2)$ are defined as

$$N_i(\eta_1, \eta_2) = \begin{cases} N_3(\eta_1, \eta_2) & \text{on} \quad \hat{\Omega}_1 \\ N_4(\eta_1, \eta_2) & \text{on} \quad \hat{\Omega}_2 \\ N_1(\eta_1, \eta_2) & \text{on} \quad \hat{\Omega}_3 \\ N_2(\eta_1, \eta_2) & \text{on} \quad \hat{\Omega}_4 \end{cases} \tag{9.9}$$

and

$$N_{i-1}(\eta_1, \eta_2) = \begin{cases} N_4(\eta_1, \eta_2) & \text{on} \quad \hat{\Omega}_1 \\ 0 & \text{on} \quad \hat{\Omega}_2 \, , \, \hat{\Omega}_3, \\ N_1(\eta_1, \eta_2) & \text{on} \quad \hat{\Omega}_4 \end{cases} \tag{9.10}$$

Analogously, $n_i(\eta_\alpha)$ is defined as

$$n_i(\eta_\alpha) = \begin{cases} n_2(\eta_\alpha) & \text{on} \quad \omega_1 \\ n_1(\eta_\alpha) & \text{on} \quad \omega_2 \end{cases} \quad , \quad \alpha = 1, 2 \tag{9.11}$$

With all such definitions, the 2-D hat functions are also constituted by products of 1-D hat functions. Therefore, for "ℓ" defined by (9.8), the hat function $N_\ell(\eta_1, \eta_2)$ is expressed as

$$N_\ell(\eta_1, \eta_2) = n_\ell(\eta_1) \cdot n_\ell(\eta_2) \tag{9.12}$$

This pivotal global-index representation allows expressing a single $N_\ell(\eta_1, \eta_2)$ through several equivalent products of 1-D factors $n_\ell(\eta_\alpha)$. This is possible by virtue of the identities

$$\begin{aligned} n_{i-n}(\eta_1) &= n_{i-1}(\eta_1) = n_{i+n-2}(\eta_1) \\ n_{i-n+1}(\eta_1) &= n_i(\eta_1) = n_{i+n+1}(\eta_1) \\ n_{i-n+2}(\eta_1) &= n_{i+1}(\eta_1) = n_{i+n}(\eta_1) \end{aligned} \tag{9.13}$$

and

$$\begin{aligned} n_{i-n}(\eta_2) &= n_{i-n+1}(\eta_2) = n_{i-n+2}(\eta_2) \\ n_{i-1}(\eta_2) &= n_i(\eta_2) = n_{i+1}(\eta_2) \\ n_{i+n-2}(\eta_2) &= n_{i+n-1}(\eta_2) = n_{i+n}(\eta_2) \end{aligned} \tag{9.14}$$

as illustrated by graphing each such function on the 2-D master element in Figure 9.1. For example, $N_{i-1}(\eta_1, \eta_2)$ can be expressed as

$$\begin{aligned} N_{i-1}(\eta_1, \eta_2) &= n_{i-1}(\eta_1) \cdot n_{i-1}(\eta_2) \\ &= n_{i-n}(\eta_1) \cdot n_{i-1}(\eta_2) \\ &= n_{i+n-2}(\eta_1) \cdot n_i(\eta_2) \\ &= n_{i-n}(\eta_1) \cdot n_{i+1}(\eta_2) \\ &= \cdots \end{aligned} \tag{9.15}$$

All of these multiple equivalent representations are instrumental in the derivation of the tensor product factorization (TPF) algorithm, as detailed herein.

9.3 Integration Identities

The insertion of the generalized hat functions in each 2-D integral statement term affords the extension of the associated integration domain to the whole $\widehat{\Omega}$, see Figure 9.1, for the representative node "i". Concurrently, the 1-D integrations can be extended to the union of two adjacent elements as illustrated in Figure 9.2. Therefore all of these integrals are the sum of integrals over the component subregions

constituting $\widehat{\Omega}$ and ω. For instance, the integral

$$\int_{\widehat{\Omega}} N_i N_{i-1}\, d\boldsymbol{\eta} = \int_{\widehat{\Omega}_1} N_3 N_4\, d\boldsymbol{\eta} + \int_{\widehat{\Omega}_4} N_2 N_1\, d\boldsymbol{\eta} \tag{9.16}$$

is also written as

$$\begin{aligned}\int_{\widehat{\Omega}} N_i N_{i-1}\, d\boldsymbol{\eta} \;\; = \;\; & \int_{\widehat{\Omega}_1} N_3 N_4\, d\boldsymbol{\eta} + \int_{\widehat{\Omega}_2} N_4 \cdot 0\, d\boldsymbol{\eta} + \\ & \int_{\widehat{\Omega}_3} N_1 \cdot 0\, d\boldsymbol{\eta} + \int_{\widehat{\Omega}_4} N_2 N_1\, d\boldsymbol{\eta}\end{aligned} \tag{9.17}$$

since N_{i-1} vanishes all over elements $\widehat{\Omega}_2$ and $\widehat{\Omega}_3$. Likewise, the following integral expansion holds

$$\int_{\omega} n_i n_{i-1}\, d\eta = \int_{\omega_1} n_i n_{i-1}\, d\eta + \int_{\omega_2} n_i \cdot 0\, d\eta \tag{9.18}$$

since n_{i-1} vanishes on element ω_2. Analogous relations can be derived for the finite element statement integrals

$$M_{i,j} \equiv \int_{\widehat{\Omega}} N_i N_j\, d\boldsymbol{\eta} \quad , \quad \mathrm{m}_{i,j} \equiv \int_{\omega} n_i n_j\, d\eta \tag{9.19}$$

$$C^{\alpha}_{i,j} \equiv \int_{\widehat{\Omega}} N_i \frac{\partial N_j}{\partial \eta_\alpha}\, d\boldsymbol{\eta} \quad , \quad \mathrm{c}^{\alpha}_{i,j} \equiv \int_{\omega} n_i \frac{dn_j}{d\eta_\alpha}\, d\eta \tag{9.20}$$

$$F^{\alpha\beta}_{i,j} \equiv -\int_{\widehat{\Omega}} \frac{\partial N_i}{\partial \eta_\alpha}\frac{\partial N_j}{\partial \eta_\beta}\, d\boldsymbol{\eta} \quad , \quad \mathrm{f}^{\alpha\alpha}_{i,j} \equiv \int_{\omega} \frac{dn_i}{d\eta_\alpha}\frac{dn_j}{d\eta_\alpha}\, d\eta \tag{9.21}$$

for all admissible values of the indices "α", "i" and "j".

These integrals are denoted via the inner-product shorthand notation $< \cdot, \cdot >$, i.e.,

$$\begin{aligned}\langle N_i, N_j\rangle_{\widehat{\Omega}} \;\; &\equiv \;\; \int_{\widehat{\Omega}} N_i N_j\, d\boldsymbol{\eta} = \sum_{e=1}^{4}\int_{\widehat{\Omega}_e} N_i N_j\, d\boldsymbol{\eta} = \sum_{e=1}^{4}\langle N_i, N_j\rangle_{\widehat{\Omega}_e} \\ \langle N_i, \frac{\partial N_j}{\partial \eta_\alpha}\rangle_{\widehat{\Omega}} \;\; &\equiv \;\; \int_{\widehat{\Omega}} N_i \frac{\partial N_j}{\partial \eta_\alpha}\, d\boldsymbol{\eta} = \sum_{e=1}^{4}\int_{\widehat{\Omega}_e} N_i \frac{\partial N_j}{\partial \eta_\alpha}\, d\boldsymbol{\eta} = \sum_{e=1}^{4}\langle N_i, \frac{\partial N_j}{\partial \eta_\alpha}\rangle_{\widehat{\Omega}_e} \\ \langle \frac{\partial N_i}{\partial \eta_\beta}, \frac{\partial N_j}{\partial \eta_\alpha}\rangle_{\widehat{\Omega}} \;\; &\equiv \;\; \int_{\widehat{\Omega}} \frac{\partial N_i}{\partial \eta_\beta}\frac{\partial N_j}{\partial \eta_\alpha}\, d\boldsymbol{\eta} = \sum_{e=1}^{4}\int_{\widehat{\Omega}_e} \frac{\partial N_i}{\partial \eta_\beta}\frac{\partial N_j}{\partial \eta_\alpha}\, d\boldsymbol{\eta} = \sum_{e=1}^{4}\langle \frac{\partial N_i}{\partial \eta_\beta}, \frac{\partial N_j}{\partial \eta_\alpha}\rangle_{\widehat{\Omega}_e}\end{aligned} \tag{9.22}$$

and

$$\begin{aligned}
\langle n_i, n_j\rangle_\omega &\equiv \int_\omega n_i n_j \, d\eta = \sum_{e=1}^{2} \int_{\omega_e} n_i n_j \, d\eta = \sum_{e=1}^{2} \langle n_i, n_j\rangle_{\omega_e} \\
\langle n_i, \frac{dn_j}{d\eta_\alpha}\rangle_\omega &\equiv \int_\omega n_i \frac{dn_j}{d\eta_\alpha} \, d\eta = \sum_{e=1}^{2} \int_{\omega_e} n_i \frac{dn_j}{d\eta_\alpha} \, d\eta = \sum_{e=1}^{2} \langle n_i, \frac{dn_j}{d\eta_\alpha}\rangle_{\omega_e} \\
\langle \frac{dn_i}{d\eta_\alpha}, \frac{dn_j}{d\eta_\alpha}\rangle_\omega &\equiv \int_\omega \frac{dn_i}{d\eta_\alpha}\frac{dn_j}{d\eta_\alpha} \, d\eta = \sum_{e=1}^{2} \int_{\omega_e} \frac{dn_i}{d\eta_\alpha}\frac{dn_j}{d\eta_\alpha} \, d\eta = \sum_{e=1}^{2} \langle \frac{dn_i}{d\eta_\alpha}, \frac{dn_j}{d\eta_\alpha}\rangle_{\omega_e} \quad (9.23)
\end{aligned}$$

A useful relation can be established between (9.22) and (9.23) by virtue of the tensor product structure of their integrands. For $F_i(\eta_1, \eta_2)$ and $G_j(\eta_1, \eta_2)$ denoting any such integrand component, and with reference to Figure 9.1, the integrals in (9.22) are expressable as

$$\begin{aligned}
&\langle F_i(\eta_1, \eta_2), G_j(\eta_1, \eta_2)\rangle_{\widehat{\Omega}} = \sum_{e=1}^{4} \langle F_i(\eta_1, \eta_2), G_j(\eta_1, \eta_2)\rangle_{\widehat{\Omega}_e} = \\
&\quad \langle f_i(\eta_1), g_j(\eta_1)\rangle_{\omega_1} \cdot \langle f_i(\eta_2), g_j(\eta_2)\rangle_{\omega_1} + \langle f_i(\eta_1), g_j(\eta_1)\rangle_{\omega_2} \cdot \langle f_i(\eta_2), g_j(\eta_2)\rangle_{\omega_1} + \\
&\quad \langle f_i(\eta_1), g_j(\eta_1)\rangle_{\omega_1} \cdot \langle f_i(\eta_2), g_j(\eta_2)\rangle_{\omega_2} + \langle f_i(\eta_1), g_j(\eta_1)\rangle_{\omega_2} \cdot \langle f_i(\eta_2), g_j(\eta_2)\rangle_{\omega_2} = \\
&\quad \sum_{k=1}^{2} \langle f_i(\eta_1), g_j(\eta_1)\rangle_{\omega_k} \cdot \sum_{k=1}^{2} \langle f_i(\eta_2), g_j(\eta_2)\rangle_{\omega_k} = \\
&\quad \langle f_i(\eta_1), g_j(\eta_1)\rangle_{\omega} \cdot \langle f_i(\eta_2), g_j(\eta_2)\rangle_{\omega} \qquad (9.24)
\end{aligned}$$

where $f_i(\eta_\alpha)$ and $g_j(\eta_\alpha)$ correspond to the tensor factors in (9.23). Consequently, each 2-D integral (9.22) is cast as a direct product of two 1-D integrals (9.23).

These considerations facilitate the direct derivation of the TPF algorithm, as follows.

9.4 TPF Matrix Structure

Denote system (9.1) and the factored matrix in (9.2) as

$$A\delta k^{p+1} = b \tag{9.25}$$

$$A \simeq BC \tag{9.26}$$

for notational convenience. Further, the tilde superscript is deleted without loss of clarity.

Matrix A is block banded and each row contains 9 blocks at most, when the computational region $\hat{\Omega}$ results from the union of four neighboring bilinear elements, see Figure 9.5, where the nodes are numbered in the η_1 topological direction. The index "n" denotes the block semi-bandwidth, which consequently depends on the total number of nodes along lines parallel to the η_1 axis. Figure 9.6 illustrates the structure of A where, clearly, each element "a_{ij}" constitutes a $p \times p$ matrix, since both q and $f_\ell(q)$ in system (9.1) are arrays of order p. In order to solve (9.1) efficiently via a sequence of 1-D problems along the η_1 and η_2 axes, matrices B and C in (9.2) are block tri-diagonal such that the i^{th} row of B contains the three $p \times p$ blocks associated with the computational nodes $i-1, i, i+1$, and the i^{th} row of C contains the three $p \times p$ blocks associated with the computational nodes $i-n+1, i, i+n-1$. The structure of matrices B and C is illustrated in Figure 9.7.

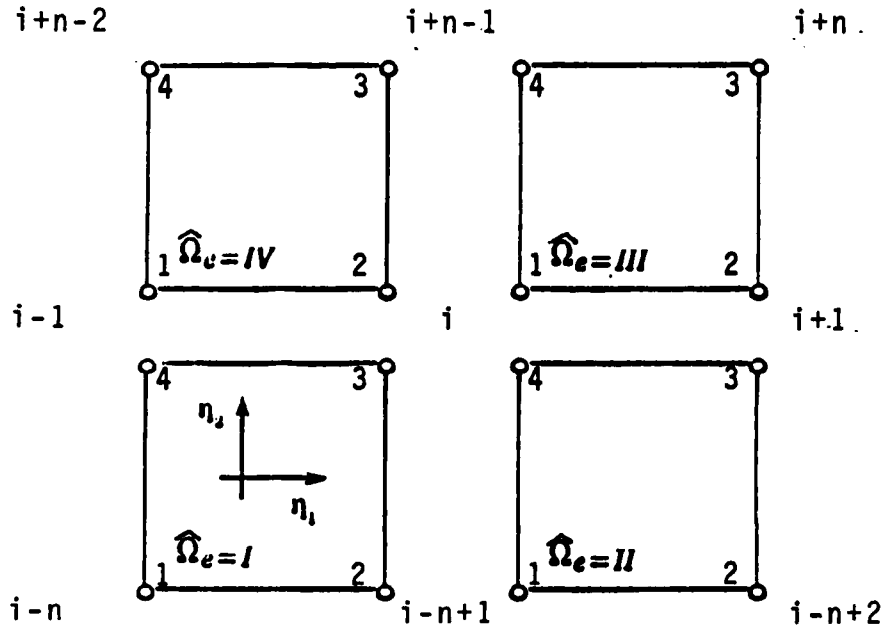


Figure 9.5: Union of Bilinear Elements. Nodes Numbered in the η_1 Topological Direction

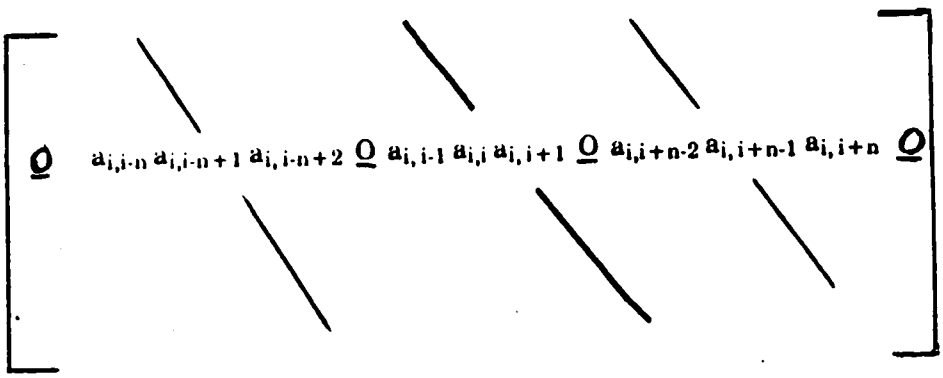


Figure 9.6: Banded structure of A

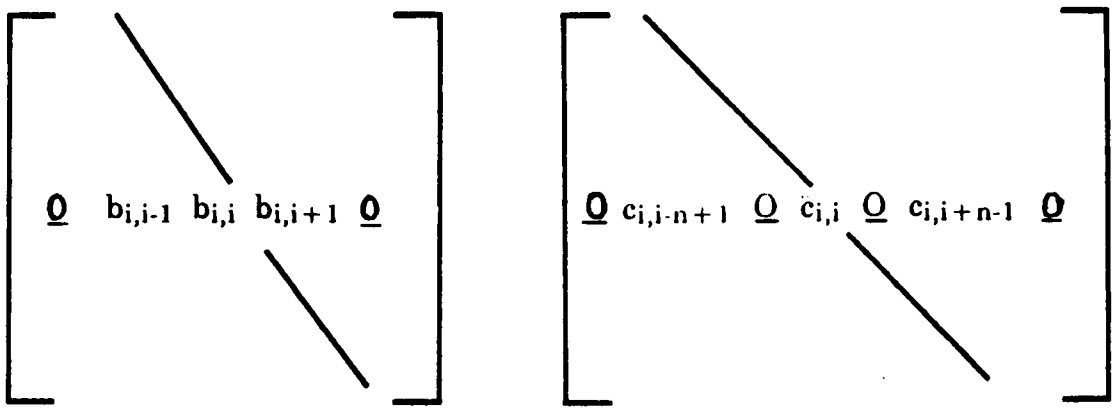


Figure 9.7: Banded Structure of B and C

Note that the semibandwidth "n" of matrix A does not influence the bandwidth of matrix B which, therefore, will always be block tri-diagonal for any number of mesh nodes. The bandwidth of matrix C can also be made independent of n upon renumbering for nodes along lines parallel to the η_2 axis. Hence, a typical procedure to solve system (9.1), via factorization (9.2), consists of the following steps:

1. Number mesh nodes sequentially along lines parallel to the η_1 axis

2. Solve $Bz = b$ for the intermediate array z

3. Number mesh nodes sequentially along lines parallel to the η_2 axis and reorder the entries in the arrays z and b accordingly

4. Solve $C\delta k^{p+1} = z$ for the terminal array δk^{p+1}

9.5 Derivation of a Prototype TPF Scheme

In the sequel, the symbol A is used to represent the factored matrix (9.2). This matrix product approximates matrix A of system (9.1) and the matrix-entry structure of this approximation is derived in this section. Consider factorization (9.2) and note the equality

$$A = BC \tag{9.27}$$

that is

$$a_{i,j} = \sum_{k=i-n}^{i+n} b_{i,k}c_{k,j} \tag{9.28}$$

By definition, the index "j" in "$a_{i,j}$" varies in the range

$$j \in \{i-n, i-n+1, i-n+2, i-1, i, i+1, i+n-2, i+n-1, i+n\} \tag{9.29}$$

Further, the non-zero blocks of B are

$$b_{i,i-1} \quad , \quad b_{i,i} \quad , \quad b_{i,i+1} \tag{9.30}$$

and the non-zero blocks of C are

$$c_{k,k-n+1} \quad , c_{k,k} \quad , c_{k,k+n-1} \tag{9.31}$$

Therefore, expression (9.28) in unabridged notation is

$$\begin{aligned}
a_{i,i-n} &= b_{i,i-1}c_{i-1,i-n} + b_{i,i}c_{i,i-n} + b_{i,i+1}c_{i+1,i-n} \\
a_{i,i-n+1} &= b_{i,i-1}c_{i-1,i-n+1} + b_{i,i}c_{i,i-n+1} + b_{i,i+1}c_{i+1,i-n+1} \\
a_{i,i-n+2} &= b_{i,i-1}c_{i-1,i-n+2} + b_{i,i}c_{i,i-n+2} + b_{i,i+1}c_{i+1,i-n+2}
\end{aligned} \tag{9.32}$$

$$
\begin{aligned}
a_{i,i-1} &= b_{i,i-1}c_{i-1,i-1} + b_{i,i}c_{i,i-1} + b_{i,i+1}c_{i+1,i-1} \\
a_{i,i} &= b_{i,i-1}c_{i-1,i} + b_{i,i}c_{i,i} + b_{i,i+1}c_{i+1,i} \\
a_{i,i+1} &= b_{i,i-1}c_{i-1,i+1} + b_{i,i}c_{i,i+1} + b_{i,i+1}c_{i+1,i+1} \qquad (9.33)
\end{aligned}
$$

$$
a_{i,i+n-2} = b_{i,i-1}c_{i-1,i+n-2} + b_{i,i}c_{i,i+n-2} + b_{i,i+1}c_{i+1,i+n-2}
$$

$$
\begin{aligned}
a_{i,i+n-1} &= b_{i,i-1}c_{i-1,i+n-1} + b_{i,i}c_{i,i+n-1} + b_{i,i+1}c_{i+1,i+n-1} \\
a_{i,i+n} &= b_{i,i-1}c_{i-1,i+n} + b_{i,i}c_{i,i+n} + b_{i,i+1}c_{i+1,i+n} \qquad (9.34)
\end{aligned}
$$

Whereupon, cancellation of the zero-blocks in (9.32)-(9.34) leads to the terminal equalities

$$
\begin{aligned}
a_{i,i-n} &= b_{i,i-1}c_{i-1,i-n} \\
a_{i,i-n+1} &= b_{i,i}c_{i,i-n+1} \\
a_{i,i-n+2} &= b_{i,i+1}c_{i+1,i-n+2} \qquad (9.35)
\end{aligned}
$$

$$
\begin{aligned}
a_{i,i-1} &= b_{i,i-1}c_{i-1,i-1} \\
a_{i,i} &= b_{i,i}c_{i,i} \\
a_{i,i+1} &= b_{i,i+1}c_{i+1,i+1} \qquad (9.36)
\end{aligned}
$$

$$
\begin{aligned}
a_{i,i+n-2} &= b_{i,i-1}c_{i-1,i+n-2} \\
a_{i,i+n-1} &= b_{i,i}c_{i,i+n-1} \\
a_{i,i+n} &= b_{i,i+1}c_{i+1,i+n} \qquad (9.37)
\end{aligned}
$$

Equations (9.35)-(9.37) constitute the prototype expressions of the TPF proce-

dure. They have been derived via use of algebraic and mesh topology considerations only, and verify that each block a_{ij} can be recast as a single product of two blocks, one from C and one from B. Moreover, they clearly indicate the presence of a spatial approximation to the block entries in matrix A of (9.1). This can be seen by noting in (9.35)-(9.37) that once the forms of blocks $c_{i,i-n+1}$, $c_{i,i}$, $c_{i,i+n-1}$ are prescribed, then so are the forms of the remaining blocks $c_{i,j}$ by induction on the subscripts. The three blocks from B are then the only ones to be assigned. Therefore, the described procedure allows the arbitrary selection of only *six* blocks to approximate the *nine* blocks of A.

9.6 Derivation of a Specific TPF Scheme

In harmony with (9.2), the definition of blocks $b_{i,j}$ and $c_{i,j}$ is

$$\begin{aligned} b_{i,j} &= m_{i,j} + \theta \Delta t d^1_{i,j} \\ c_{i,j} &= m_{i,j} + \theta \Delta t d^2_{i,j} \end{aligned} \tag{9.38}$$

where the $m_{i,j}$ is the one dimensional mass matrix

$$m_{i,j} = \int_\omega n_i \cdot n_j \, d\eta \tag{9.39}$$

and $d^2_{i,j}$ and $d^1_{i,j}$ are the one dimensional Jacobian terms

$$d^1_{i,j} \equiv \left[\frac{\partial \mathrm{f}_1}{\partial q}\right]_{i,j} \quad , \quad d^2_{i,j} \equiv \left[\frac{\partial \mathrm{f}_2}{\partial q}\right]_{i,j} \tag{9.40}$$

to be determined. Insertion of expressions (9.38) into formulae (9.35)-(9.37) yields the equalities

$$
\begin{aligned}
a_{i,i-n} &= b_{i,i-1}c_{i-1,i-n} = \left(m_{i,i-1} + \theta\Delta t d^1_{i,i-1}\right)\left(m_{i-1,i-n} + \theta\Delta t d^2_{i-1,i-n}\right) = \\
& m_{i,i-1}m_{i-1,i-n} + \theta\Delta t m_{i,i-1}d^2_{i-1,i-n} + \theta\Delta t d^1_{i,i-1}m_{i-1,i-n} + \theta^2\Delta t^2 d^1_{i,i-1}d^2_{i-1,i-n} \\
a_{i,i-n+1} &= b_{i,i}c_{i,i-n+1} = \left(m_{i,i} + \theta\Delta t d^1_{i,i}\right)\left(m_{i,i-n+1} + \theta\Delta t d^2_{i,i-n+1}\right) = \\
& m_{i,i}m_{i,i-n+1} + \theta\Delta t m_{i,i}d^2_{i,i-n+1} + \theta\Delta t d^1_{i,i}m_{i,i-n+1} + \theta^2\Delta t^2 d^1_{i,i}d^2_{i,i-n+1} \\
a_{i,i-n+2} &= b_{i,i+1}c_{i+1,i-n+2} = \left(m_{i,i+1} + \theta\Delta t d^1_{i,i+1}\right)\left(m_{i+1,i-n+2} + \theta\Delta t d^2_{i+1,i-n+2}\right) = \\
& m_{i,i+1}m_{i+1,i-n+2} + \theta\Delta t m_{i,i+1}d^2_{i+1,i-n+2} + \theta\Delta t d^1_{i,i+1}m_{i+1,i-n+2} + \\
& \theta^2\Delta t^2 d^1_{i,i+1}d^2_{i+1,i-n+2} \qquad (9.41) \\
a_{i,i-1} &= b_{i,i-1}c_{i-1,i-1} = \left(m_{i,i-1} + \theta\Delta t d^1_{i,i-1}\right)\left(m_{i-1,i-1} + \theta\Delta t d^2_{i-1,i-1}\right) = \\
& m_{i,i-1}m_{i-1,i-1} + \theta\Delta t m_{i,i-1}d^2_{i-1,i-1} + \theta\Delta t d^1_{i,i-1}m_{i-1,i-1} + \theta^2\Delta t^2 d^1_{i,i-1}d^2_{i-1,i-1} \\
a_{i,i} &= b_{i,i}c_{i,i} = \left(m_{i,i} + \theta\Delta t d^1_{i,i}\right)\left(m_{i,i} + \theta\Delta t d^2_{i,i}\right) = \\
& m_{i,i}m_{i,i} + \theta\Delta t m_{i,i}d^2_{i,i} + \theta\Delta t d^1_{i,i}m_{i,i} + \theta^2\Delta t^2 d^1_{i,i}d^2_{i,i} \\
a_{i,i+1} &= b_{i,i+1}c_{i+1,i+1} = \left(m_{i,i+1} + \theta\Delta t d^1_{i,i+1}\right)\left(m_{i+1,i+1} + \theta\Delta t d^2_{i+1,i-1}\right) = \\
& m_{i,i+1}m_{i+1,i+1} + \theta\Delta t m_{i,i+1}d^2_{i+1,i+1} + \theta\Delta t d^1_{i,i+1}m_{i+1,i+1} + \\
& \theta^2\Delta t^2 d^1_{i,i+1}d^2_{i+1,i+1} \qquad (9.42) \\
a_{i,i+n-2} &= b_{i,i-1}c_{i-1,i+n-2} = \left(m_{i,i-1} + \theta\Delta t d^1_{i,i-1}\right)\left(m_{i-1,i+n-2} + \theta\Delta t d^2_{i-1,i+n-2}\right) = \\
& m_{i,i-1}m_{i-1,i+n-2} + \theta\Delta t m_{i,i-1}d^2_{i-1,i+n-2} + \theta\Delta t d^1_{i,i-1}m_{i-1,i+n-2} + \\
& \theta^2\Delta t^2 d^1_{i,i-1}d^2_{i-1,i+n-2} \\
a_{i,i+n-1} &= b_{i,i}c_{i,i+n-1} = \left(m_{i,i} + \theta\Delta t d^1_{i,i}\right)\left(m_{i,i+n-1} + \theta\Delta t d^2_{i,i+n-1}\right) =
\end{aligned}
$$

$$
\begin{aligned}
& m_{i,i}m_{i,i+n-1} + \theta\Delta t m_{i,i} d^2_{i,i+n-1} + \theta\Delta t d^1_{i,i} m_{i,i+n-1} + \theta^2\Delta t^2 d^1_{i,i} d^2_{i,i+n-1} \\
a_{i,i+n} \;=\; & b_{i,i+1}c_{i+1,i+n} = \left(m_{i,i+1} + \theta\Delta t d^1_{i,i+1}\right)\left(m_{i+1,i+n} + \theta\Delta t d^2_{i+1,i+n}\right) = \\
& m_{i,i+1}m_{i+1,i+n} + \theta\Delta t m_{i,i+1} d^2_{i+1,i+n} + \theta\Delta t d^1_{i,i+1} m_{i+1,i+n} + \\
& \theta^2\Delta t^2 d^1_{i,i+1} d^2_{i+1,i+n}
\end{aligned} \tag{9.43}
$$

Formulae (9.41)-(9.43) maintain their validity when both the convection and diffusion operators are simultaneously present, for the $\theta\Delta t$ terms therein are linear. For example, a representative term is

$$
\mathcal{T}_{i,k} = m_{i,j}d_{j,k} = m_{i,j}\left((d_{j,k})^c + (d_{j,k})^d\right) = m_{i,j}(d_{j,k})^c + m_{i,j}(d_{j,k})^d \tag{9.44}
$$

where supescripts "c" and "d" denote convection and diffusion operators. Equations (9.41)-(9.43) define the computational grid form of blocks a_{ij}. A large albeit sparse 2-D matrix problem is replaced by a sequence of two banded 1-D problems. This sequence, as shown in the sequel, constitutes an optimal approximation to the full 2-D problem, under the constraints that matrices B and C are block tri-diagonal.

If no TPF procedure is employed, then the exact forms of blocks a_{ij} in (9.1) are

$$
\begin{aligned}
a_{i,i-n} &= M_{i,i-n} + \theta\Delta t D^1_{i,i-n} + \theta\Delta t D^2_{i,i-n} \\
a_{i,i-n+1} &= M_{i,i-n+1} + \theta\Delta t D^1_{i,i-n+1} + \theta\Delta t D^2_{i,i-n+1} \\
a_{i,i-n+2} &= M_{i,i-n+2} + \theta\Delta t D^1_{i,i-n+2} + \theta\Delta t D^2_{i,i-n+2}
\end{aligned} \tag{9.45}
$$

$$
\begin{aligned}
a_{i,i-1} &= M_{i,i-1} + \theta\Delta t D^1_{i,i-1} + \theta\Delta t D^2_{i,i-1} \\
a_{i,i} &= M_{i,i} + \theta\Delta t D^1_{i,i} + \theta\Delta t D^2_{i,i}
\end{aligned}
$$

$$a_{i,i+1} = M_{i,i+1} + \theta\Delta t D^1_{i,i+1} + \theta\Delta t D^2_{i,i+1} \tag{9.46}$$

$$\begin{aligned} a_{i,i+n-2} &= M_{i,i+n-2} + \theta\Delta t D^1_{i,i+n-2} + \theta\Delta t D^2_{i,i+n-2} \\ a_{i,i+n-1} &= M_{i,i+n-1} + \theta\Delta t D^1_{i,i+n-1} + \theta\Delta t D^2_{i,i+n-1} \\ a_{i,i+n} &= M_{i,i+n} + \theta\Delta t D^1_{i,i+n} + \theta\Delta t D^2_{i,i+n} \end{aligned} \tag{9.47}$$

where the symbols M_{ij} , D^α_{ij}, $\alpha = 1, 2$, are defined as

$$M_{i,j} = \int_{\widehat{\Omega}} N_i N_j \, d\boldsymbol{\eta} \tag{9.48}$$

$$\left(D^\alpha_{i,j}\right)^c \equiv \left(\frac{\partial f^i_\alpha}{\partial q^j}\right)^c = \left(\int_{\widehat{\Omega}} e_{\ell\alpha} N_i \frac{\partial N_k}{\partial \eta_\alpha} \, d\boldsymbol{\eta}\right) \frac{\partial f^k_\ell}{\partial q^j} \quad , \quad \alpha = 1, 2 \tag{9.49}$$

$$\left(D^\alpha_{i,j}\right)^d \equiv \left(\frac{\partial f^i_\alpha}{\partial q^j}\right)^d = -\left(\int_{\widehat{\Omega}} e_{\ell\alpha} \frac{e_{m\alpha}}{\det J} \frac{\partial N_i}{\partial \eta_\alpha} \frac{\partial N_k}{\partial \eta_\alpha} \, d\boldsymbol{\eta}\right) \frac{\partial f^k_{\ell m}}{\partial q^j} \, , \; \alpha = 1, 2 \tag{9.50}$$

and f_ℓ and $f_{\ell m}$ now denote the cartesian components of the convection and diffusion flux semi-discretization integrals respectively.

Comparing (9.41)-(9.43) with (9.45)-(9.47) highlights introduction of an error term of order $(\theta\Delta t)^2$ resulting from expansions (9.38), in the approximation of matrix A, in addition to the spatial approximation error identified at the end of Section 9.5. The latter is minimized through the selected 2-D basis functions N_i. Hence, the product of two appropriate 1-D mass-matrix elements (9.39) reproduces a specified 2-D mass-matrix element (9.48). Moreover the product of an adequate 1-D mass-matrix element with an opportune curvilinear Jacobian element (9.40) accurately represents a predetermined 2-D jacobian term (9.49)-(9.50). This notion is exemplified via examination of the representative block $a_{i,i-1}$ in formulae (9.42), resulting from the sum of three leading terms which the TPF procedure will approximate

with the following expressions

$$\begin{aligned} M_{i,i-1} &= m_{i,i-1} m_{i-1,i-1} \\ D^1_{i,i-1} &= d^1_{i,i-1} m_{i-1,i-1} \\ D^2_{i,i-1} &\simeq m_{i,i-1} d^2_{i-1,i-1} \end{aligned} \tag{9.51}$$

Finally, note that for the general case of an array f_ℓ (or $f_{\ell m}$) of order p the jacobians

$$(J)^c = \frac{\partial f_\ell}{\partial q} \quad , \quad (J)^d = \frac{\partial f_{\ell m}}{\partial q} \tag{9.52}$$

are $p \times p$ matrices. Therefore, the jacobian expressions (9.40) are matrices of order p. Concomitantly, the mass-matrix expressions $m_{i,j}$ and $M_{i,j}$ are leading-diagonal matrices of order p, since they have to be summed to $p \times p$ Jacobians in the factorization (9.2).

9.7 Mass Matrix Factorization

The 2-D mass matrix exactly factors without any error via the TPF expressions (9.41)-(9.43). With reference to Figure 9.1, the representative 2-D mass matrix term $M_{i,i}$ is

$$\begin{aligned} M_{i,i} = \int_{\widehat{\Omega}} N_i(\eta_1,\eta_2) \cdot N_i(\eta_1,\eta_2)\ d\boldsymbol{\eta} = \int_{\widehat{\Omega}} \mathrm{n}_i(\eta_1)\,\mathrm{n}_i(\eta_2) \cdot \mathrm{n}_i(\eta_1)\,\mathrm{n}_i(\eta_2)\ d\boldsymbol{\eta} = \\ \int_{\widehat{\Omega}_1} \mathrm{n}_i(\eta_1)\,\mathrm{n}_i(\eta_2) \cdot \mathrm{n}_i(\eta_1)\,\mathrm{n}_i(\eta_2)\ d\boldsymbol{\eta} + \int_{\widehat{\Omega}_2} \mathrm{n}_i(\eta_1)\,\mathrm{n}_i(\eta_2) \cdot \mathrm{n}_i(\eta_1)\,\mathrm{n}_i(\eta_2)\ d\boldsymbol{\eta} + \\ \int_{\widehat{\Omega}_4} \mathrm{n}_i(\eta_1)\,\mathrm{n}_i(\eta_2) \cdot \mathrm{n}_i(\eta_1)\,\mathrm{n}_i(\eta_2)\ d\boldsymbol{\eta} + \int_{\widehat{\Omega}_3} \mathrm{n}_i(\eta_1)\,\mathrm{n}_i(\eta_2) \cdot \mathrm{n}_i(\eta_1)\,\mathrm{n}_i(\eta_2)\ d\boldsymbol{\eta} = \\ \left(\int_{\omega_1} \mathrm{n}_i(\eta_1)\,\mathrm{n}_i(\eta_1)\ d\eta\right) \cdot \left(\int_{\omega_1} \mathrm{n}_i(\eta_2)\,\mathrm{n}_i(\eta_2)\ d\eta\right) + \end{aligned}$$

$$\left(\int_{\omega_2} n_i(\eta_1)\, n_i(\eta_1)\ d\eta\right) \cdot \left(\int_{\omega_1} n_i(\eta_2)\, n_i(\eta_2)\ d\eta\right) +$$
$$\left(\int_{\omega_1} n_i(\eta_1)\, n_i(\eta_1)\ d\eta\right) \cdot \left(\int_{\omega_2} n_i(\eta_2)\, n_i(\eta_2)\ d\eta\right) +$$
$$\left(\int_{\omega_2} n_i(\eta_1)\, n_i(\eta_1)\ d\eta\right) \cdot \left(\int_{\omega_2} n_i(\eta_2)\, n_i(\eta_2)\ d\eta\right) =$$
$$\left(\int_{\omega_1} n_i(\eta_1)\, n_i(\eta_1)\ d\eta + \int_{\omega_2} n_i(\eta_2)\, n_i(\eta_2)\ d\eta\right) \cdot \left(\int_{\omega_1} n_i(\eta_2)\, n_i(\eta_2)\ d\eta\right) +$$
$$\left(\int_{\omega_1} n_i(\eta_1)\, n_i(\eta_1)\ d\eta + \int_{\omega_2} n_i(\eta_2)\, n_i(\eta_2)\ d\eta\right) \cdot \left(\int_{\omega_2} n_i(\eta_2)\, n_i(\eta_2)\ d\eta\right) =$$
$$\left(\int_{\omega_1} n_i(\eta_1)\, n_i(\eta_1)\ d\eta + \int_{\omega_2} n_i(\eta_2)\, n_i(\eta_2)\ d\eta\right) \cdot$$
$$\left(\int_{\omega_1} n_i(\eta_1)\, n_i(\eta_1)\ d\eta + \int_{\omega_2} n_i(\eta_2)\, n_i(\eta_2)\ d\eta\right) =$$
$$\left(\int_{\omega} n_i(\eta_1)\, n_i(\eta_1)\ d\eta\right) \cdot \left(\int_{\omega} n_i(\eta_2)\, n_i(\eta_2)\ d\eta\right) = \langle n_i, n_i\rangle_\omega \cdot \langle n_i, n_i\rangle_\omega = m_{i,i} m_{i,i} \tag{9.53}$$

This verifies that the 2-D term $M_{i,i}$ is directly expressed as a product of 1-D terms, each computed on the full computational domain ω. Hence, this expression is directly cast via notations (9.22)-(9.23), whereupon the TPF representations of the nine 2-D mass matrix terms over the region $\widehat{\Omega}$ are

$$\begin{aligned}
M_{i,i-n} &= \langle N_i(\eta_1,\eta_2), N_{i-n}(\eta_1,\eta_2)\rangle_{\widehat{\Omega}} = \langle n_i(\eta_1)\, n_i(\eta_2), n_{i-n}(\eta_1)\, n_{i-n}(\eta_2)\rangle_{\widehat{\Omega}} = \\
&\quad \langle n_i(\eta_1)\, n_{i-1}(\eta_2), n_{i-1}(\eta_1)\, n_{i-n}(\eta_2)\rangle_{\widehat{\Omega}} = \\
&\quad \langle n_i(\eta_1)\, n_{i-1}(\eta_1), n_{i-1}(\eta_2)\, n_{i-n}(\eta_2)\rangle_{\widehat{\Omega}} = \\
&\quad \langle n_i(\eta_1), n_{i-1}(\eta_1)\rangle_\omega \cdot \langle n_{i-1}(\eta_2), n_{i-n}(\eta_2)\rangle_\omega = m_{i,i-1} m_{i-1,i-n} \\
M_{i,i-n+1} &= \langle N_i(\eta_1,\eta_2), N_{i-n+1}(\eta_1,\eta_2)\rangle_{\widehat{\Omega}} = \langle n_i(\eta_1)\, n_i(\eta_2), n_{i-n+1}(\eta_1)\, n_{i-n+1}(\eta_2)\rangle_{\widehat{\Omega}} = \\
&\quad \langle n_i(\eta_1)\, n_i(\eta_2), n_i(\eta_1)\, n_{i-n+1}(\eta_2)\rangle_{\widehat{\Omega}} = \langle n_i(\eta_1)\, n_i(\eta_1), n_i(\eta_2)\, n_{i-n+1}(\eta_2)\rangle_{\widehat{\Omega}} = \\
&\quad \langle n_i(\eta_1), n_i(\eta_1)\rangle_\omega \cdot \langle n_i(\eta_2), n_{i-n+1}(\eta_2)\rangle_\omega = m_{i,i} m_{i,i-n+1}
\end{aligned}$$

$$M_{i,i-n+2} = \langle N_i(\eta_1,\eta_2), N_{i-n+2}(\eta_1,\eta_2)\rangle_{\widehat{\Omega}} = \langle n_i(\eta_1)\, n_i(\eta_2), n_{i-n+2}(\eta_1)\, n_{i-n+2}(\eta_2)\rangle_{\widehat{\Omega}} =$$

$$\langle n_i(\eta_1)\, n_{i+1}(\eta_2), n_{i+1}(\eta_1)\, n_{i-n+2}(\eta_2)\rangle_{\widehat{\Omega}} =$$

$$\langle n_i(\eta_1)\, n_{i+1}(\eta_1), n_{i+1}(\eta_2)\, n_{i-n+2}(\eta_2)\rangle_{\widehat{\Omega}} =$$

$$\langle n_i(\eta_1), n_{i+1}(\eta_1)\rangle_\omega \cdot \langle n_{i+1}(\eta_2), n_{i-n+2}(\eta_2)\rangle_\omega = m_{i,i+1} m_{i+1,i-n+2} \tag{9.54}$$

$$M_{i,i-1} = \langle N_i(\eta_1,\eta_2), N_{i-1}(\eta_1,\eta_2)\rangle_{\widehat{\Omega}} = \langle n_i(\eta_1)\, n_i(\eta_2), n_{i-1}(\eta_1)\, n_{i-1}(\eta_2)\rangle_{\widehat{\Omega}} =$$

$$\langle n_i(\eta_1)\, n_{i-1}(\eta_2), n_{i-1}(\eta_1)\, n_{i-1}(\eta_2)\rangle_{\widehat{\Omega}} =$$

$$\langle n_i(\eta_1)\, n_{i-1}(\eta_1), n_{i-1}(\eta_2)\, n_{i-1}(\eta_2)\rangle_{\widehat{\Omega}} =$$

$$\langle n_i(\eta_1), n_{i-1}(\eta_1)\rangle_\omega \cdot \langle n_{i-1}(\eta_2), n_{i-1}(\eta_2)\rangle_\omega = m_{i,i-1} m_{i-1,i-1}$$

$$M_{i,i} = \langle N_i(\eta_1,\eta_2), N_i(\eta_1,\eta_2)\rangle_{\widehat{\Omega}} = \langle n_i(\eta_1)\, n_i(\eta_2), n_i(\eta_1)\, n_i(\eta_2)\rangle_{\widehat{\Omega}} =$$

$$\langle n_i(\eta_1)\, n_i(\eta_2), n_i(\eta_1)\, n_i(\eta_2)\rangle_{\widehat{\Omega}} = \langle n_i(\eta_1)\, n_i(\eta_1), n_i(\eta_2)\, n_i(\eta_2)\rangle_{\widehat{\Omega}} =$$

$$\langle n_i(\eta_1), n_i(\eta_1)\rangle_\omega \cdot \langle n_i(\eta_2), n_i(\eta_2)\rangle_\omega = m_{i,i} m_{i,i}$$

$$M_{i,i+1} = \langle N_i(\eta_1,\eta_2), N_{i+1}(\eta_1,\eta_2)\rangle_{\widehat{\Omega}} = \langle n_i(\eta_1)\, n_i(\eta_2), n_{i+1}(\eta_1)\, n_{i+1}(\eta_2)\rangle_{\widehat{\Omega}} =$$

$$\langle n_i(\eta_1)\, n_{i+1}(\eta_2), n_{i+1}(\eta_1)\, n_{i+1}(\eta_2)\rangle_{\widehat{\Omega}} =$$

$$\langle n_i(\eta_1)\, n_{i+1}(\eta_1), n_{i+1}(\eta_2)\, n_{i+1}(\eta_2)\rangle_{\widehat{\Omega}} =$$

$$\langle n_i(\eta_1), n_{i+1}(\eta_1)\rangle_\omega \cdot \langle n_{i+1}(\eta_2), n_{i+1}(\eta_2)\rangle_\omega = m_{i,i+1} m_{i+1,i+1} \tag{9.55}$$

$$M_{i,i+n-2} = \langle N_i(\eta_1,\eta_2), N_{i+n-2}(\eta_1,\eta_2)\rangle_{\widehat{\Omega}} = \langle n_i(\eta_1)\, n_i(\eta_2), n_{i+n-2}(\eta_1)\, n_{i+n-2}(\eta_2)\rangle_{\widehat{\Omega}} =$$

$$\langle n_i(\eta_1)\, n_{i-1}(\eta_2), n_{i-1}(\eta_1)\, n_{i+n-2}(\eta_2)\rangle_{\widehat{\Omega}} =$$

$$\langle n_i(\eta_1)\, n_{i-1}(\eta_1), n_{i-1}(\eta_2)\, n_{i+n-2}(\eta_2)\rangle_{\widehat{\Omega}} =$$

$$\langle n_i(\eta_1), n_{i-1}(\eta_1)\rangle_\omega \cdot \langle n_{i-1}(\eta_2), n_{i+n-2}(\eta_2)\rangle_\omega = m_{i,i-1} m_{i-1,i+n-2}$$

$$M_{i,i+n-1} = \langle N_i(\eta_1,\eta_2), N_{i+n-1}(\eta_1,\eta_2)\rangle_{\widehat{\Omega}} = \langle n_i(\eta_1)\, n_i(\eta_2), n_{i+n-1}(\eta_1)\, n_{i+n-1}(\eta_2)\rangle_{\widehat{\Omega}} =$$

$$\langle n_i(\eta_1)\, n_i(\eta_2), n_i(\eta_1)\, n_{i+n-1}(\eta_2)\rangle_{\widehat{\Omega}} = \langle n_i(\eta_1)\, n_i(\eta_1), n_i(\eta_2)\, n_{i+n-1}(\eta_2)\rangle_{\widehat{\Omega}} =$$

$$\langle n_i(\eta_1), n_i(\eta_1)\rangle_\omega \cdot \langle n_i(\eta_2), n_{i+n-1}(\eta_2)\rangle_\omega = m_{i,i} m_{i-1,i+n-1}$$

$$M_{i,i+n} = \langle N_i(\eta_1,\eta_2), N_{i+n}(\eta_1,\eta_2)\rangle_{\widehat{\Omega}} = \langle n_i(\eta_1)\, n_i(\eta_2), n_{i+n}(\eta_1)\, n_{i+n}(\eta_2)\rangle_{\widehat{\Omega}} =$$

$$\langle n_i(\eta_1)\, n_{i+1}(\eta_2), n_{i+1}(\eta_1)\, n_{i+n}(\eta_2)\rangle_{\widehat{\Omega}} =$$

$$\langle n_i(\eta_1)\, n_{i+1}(\eta_1), n_{i+1}(\eta_2)\, n_{i+n}(\eta_2)\rangle_{\widehat{\Omega}} =$$

$$\langle n_i(\eta_1), n_{i+1}(\eta_1)\rangle_\omega \cdot \langle n_{i+1}(\eta_2), n_{i+n}(\eta_2)\rangle_\omega = m_{i,i+1} m_{i+1,i+n} \tag{9.56}$$

These expressions clearly verify that no approximation is introduced in the representation of the full 2-D mass matrix terms through appropriate products of 1-D mass matrix components, as also demonstrated in the last section of this chapter. This feature holds true for arbitrary grids since no metric data enter the mass matrix, owing to the association of $\det J$ with the dependent variable q, hence δk, and its consequent elimination from the mass matrix iteself. Further, as a result of the absence of a $\det J$ factor in the 1-D mass matrix components, selected 2-D curvilinear convection and diffusion operators are exactly factored, as determined in the following sections.

9.8 Inviscid Flux Vector Factorization

In this section the one dimensional convection operators

$$\left(d^{\alpha}_{i,j}\right)^{c} \quad , \quad \alpha = 1,2 \tag{9.57}$$

are defined such that their product with 1-D mass matrix terms and 2-D metric data $e_{\ell\alpha}$ exactly represent selected 2-D convection jacobian terms $D^{\alpha}_{i,j}$ on arbitrary grids. These base 2-D jacobian expressions are

$$D^{\alpha}_{i,j} \equiv \int_{\widehat{\Omega}} e_{\ell\alpha} N_i \frac{\partial N_k}{\partial \eta_\alpha} \, d\boldsymbol{\eta} \frac{\partial f^k_\ell}{\partial q^j} \tag{9.58}$$

whereupon, the identity

$$\frac{\partial f^k_\ell}{\partial q^j} = \frac{\partial f^j_\ell}{\partial q^j} \delta^k_{\underline{j}} = \frac{\partial f^j_\ell}{\partial q^{\underline{j}}} \tag{9.59}$$

allows expressing (9.58) as

$$D^{\alpha}_{i,j} \equiv \int_{\widehat{\Omega}} e_{\ell\alpha} N_i \frac{\partial N_j}{\partial \eta_\alpha} \, d\boldsymbol{\eta} \left[\frac{\partial f^j_\ell}{\partial q^{\underline{j}}} \right] \tag{9.60}$$

and the associated 2-D differential operator is

$$\mathcal{D}^{\alpha\ell}_{i,j} \equiv \int_{\widehat{\Omega}} e_{\ell\alpha} N_i \frac{\partial N_j}{\partial \eta_\alpha} \, d\boldsymbol{\eta} \tag{9.61}$$

Therefore, $d^{\alpha}_{i,j}$ is defined as

$$d^{\alpha}_{i,j} \equiv \mathbf{d}^{\alpha\ell}_{i,j} \cdot \left[\frac{\partial f^j_\ell}{\partial q^{\underline{j}}} \right] \tag{9.62}$$

whereupon $d^{\alpha\ell}_{i,j}$, hence $d^{\alpha}_{i,j}$, is derived by setting it equal to the exact one dimensional operator intrinsic in the multi-dimensional operators $\mathcal{D}^{\alpha\ell}_{i,j}$ as now developed.

9.8.1 η_1 Direction Operators

The determination of $d^{1\ell}_{i,j}$ is attained via derivation of the exact decomposition of integrals $\mathcal{D}^{1\ell}_{i,i-1}$, $\mathcal{D}^{1\ell}_{i,i}$ and $\mathcal{D}^{1\ell}_{i,i+1}$ along the principal η_1 sweep line $\{i-1, i, i+1\}$ (see

Figure 9.1). The decomposition of integral $\mathcal{D}^{1\ell}_{i,i-1}$ is

$$\begin{aligned}
\mathcal{D}^{1\ell}_{i,i-1} &= \int_{\widehat{\Omega}} e_{\ell 1} N_i(\eta_1,\eta_2)\frac{\partial N_{i-1}}{\partial \eta_1}\,d\boldsymbol{\eta} = \int_{\widehat{\Omega}} e_{\ell 1} n_i(\eta_1)\, n_{i-1}(\eta_2)\frac{dn_{i-1}}{d\eta_1} n_{i-1}(\eta_2)\,d\boldsymbol{\eta} = \\
& e_{\ell 1}(\boldsymbol{\eta}_1)\int_{\widehat{\Omega}_1} n_i(\eta_1)\, n_{i-1}(\eta_2)\frac{dn_{i-1}}{d\eta_1} n_{i-1}(\eta_2)\,d\boldsymbol{\eta} + \\
& e_{\ell 1}(\boldsymbol{\eta}_4)\int_{\widehat{\Omega}_4} n_i(\eta_1)\, n_{i-1}(\eta_2)\frac{dn_{i-1}}{d\eta_1} n_{i-1}(\eta_2)\,d\boldsymbol{\eta} = \\
& \left(e_{\ell 1}(\boldsymbol{\eta}_1)\int_{\omega_1} n_i(\eta_1)\frac{dn_{i-1}}{d\eta_1}\,d\eta\right)\cdot\left(\int_{\omega_1} n_{i-1}(\eta_2)\, n_{i-1}(\eta_2)\,d\eta\right) + \\
& \left(e_{\ell 1}(\boldsymbol{\eta}_4)\int_{\omega_1} n_i(\eta_1)\frac{dn_{i-1}}{d\eta_1}\,d\eta\right)\cdot\left(\int_{\omega_2} n_{i-1}(\eta_2)\, n_{i-1}(\eta_2)\,d\eta\right)
\end{aligned} \tag{9.63}$$

and use of the equality

$$\int_{\omega_1} n_{i-1}(\eta_2)\, n_{i-1}(\eta_2)\,d\eta = \int_{\omega_2} n_{i-1}(\eta_2)\, n_{i-1}(\eta_2)\,d\eta \tag{9.64}$$

allows writing (9.63) as

$$\begin{aligned}
\mathcal{D}^{1\ell}_{i,i-1} &= \left(\frac{1}{2}\left(e_{\ell 1}(\boldsymbol{\eta}_1)+e_{\ell 1}(\boldsymbol{\eta}_4)\right)\int_{\omega_1} n_i(\eta_1)\frac{dn_{i-1}}{d\eta_1}\,d\eta\right)\times \\
& \left(\int_{\omega_1} n_{i-1}(\eta_2)\, n_{i-1}(\eta_2)\,d\eta + \int_{\omega_2} n_{i-1}(\eta_2)\, n_{i-1}(\eta_2)\,d\eta\right) = \\
& \left(\frac{1}{2}\left(e_{\ell 1}(\boldsymbol{\eta}_1)+e_{\ell 1}(\boldsymbol{\eta}_4)\right)\int_{\omega_1} n_i(\eta_1)\frac{dn_{i-1}}{d\eta_1}\,d\eta\right)\cdot\left(\int_{\omega} n_{i-1}(\eta_2)\, n_{i-1}(\eta_2)\,d\eta\right)
\end{aligned} \tag{9.65}$$

The leading 1-D convection integral in this expression is post-multiplied by a mass-matrix term and pre- multiplied by the average of two metrics. Each metric is evaluated in the 2-D element that shares the 1-D element on which the relevant integral is computed. Consequently, this operator is obtained via the formula

$$\overline{\langle e_{\ell 1} n_i, \frac{dn_j}{d\eta_1}\rangle_\omega} \equiv \sum_{k=1}^{2}\left(\frac{1}{2}\left(e_{\ell 1}\left(\boldsymbol{\eta}_{\widehat{\Omega}_{k1}}\right)+e_{\ell 1}\left(\boldsymbol{\eta}_{\widehat{\Omega}_{k2}}\right)\right)\int_{\omega_k} n_i(\eta_1)\frac{dn_j}{d\eta_1}\,d\eta\right) \tag{9.66}$$

where the subscripts $\widehat{\Omega}_{k1}$ and $\widehat{\Omega}_{k2}$ respectively, denote the two 2-D elements that share the 1-D element ω_k. Insertion of this expression into (9.65) leads to the formula

$$\mathcal{D}^{1\ell}_{i,i-1} = \overline{\langle e_{\ell 1}\, \mathrm{n}_i, \frac{d\mathrm{n}_{i-1}}{d\eta_1}\rangle_\omega \cdot \langle \mathrm{n}_{i-1}(\eta_2), , \mathrm{n}_{i-1}(\eta_2)\rangle_\omega} = \overline{\langle e_{\ell 1}\, \mathrm{n}_i, \frac{d\mathrm{n}_{i-1}}{d\eta_1}\rangle_\omega} \cdot m_{i-1,i-1} \tag{9.67}$$

The decomposition of integral $\mathcal{D}^{1\ell}_{i,i}$ is

$$\begin{aligned}
\mathcal{D}^{1\ell}_{i,i} &= \int_{\widehat{\Omega}} e_{\ell 1} N_i(\eta_1,\eta_2) \frac{\partial N_i}{\partial \eta_1}\, d\boldsymbol{\eta} = \int_{\widehat{\Omega}} e_{\ell 1}\, \mathrm{n}_i(\eta_1)\, \mathrm{n}_i(\eta_2) \frac{d\mathrm{n}_i}{d\eta_1} \mathrm{n}_i(\eta_2)\; d\boldsymbol{\eta} = \\
& e_{\ell 1}(\boldsymbol{\eta}_1) \int_{\widehat{\Omega}_1} \mathrm{n}_i(\eta_1)\, \mathrm{n}_i(\eta_2) \frac{d\mathrm{n}_i}{d\eta_1} \mathrm{n}_i(\eta_2)\; d\boldsymbol{\eta} \\
+ \;& e_{\ell 1}(\boldsymbol{\eta}_2) \int_{\widehat{\Omega}_2} \mathrm{n}_i(\eta_1)\, \mathrm{n}_i(\eta_2) \frac{d\mathrm{n}_i}{d\eta_1} \mathrm{n}_i(\eta_2)\; d\boldsymbol{\eta} + \\
& e_{\ell 1}(\boldsymbol{\eta}_3) \int_{\widehat{\Omega}_3} \mathrm{n}_i(\eta_1)\, \mathrm{n}_i(\eta_2) \frac{d\mathrm{n}_i}{d\eta_1} \mathrm{n}_i(\eta_2)\; d\boldsymbol{\eta} \\
+ \;& e_{\ell 1}(\boldsymbol{\eta}_4) \int_{\widehat{\Omega}_4} \mathrm{n}_i(\eta_1)\, \mathrm{n}_i(\eta_2) \frac{d\mathrm{n}_i}{d\eta_1} \mathrm{n}_i(\eta_2)\; d\boldsymbol{\eta} = \\
& \left(e_{\ell 1}(\boldsymbol{\eta}_1) \int_{\omega_1} \mathrm{n}_i(\eta_1) \frac{d\mathrm{n}_i}{d\eta_1}\, d\eta\right) \cdot \left(\int_{\omega_1} \mathrm{n}_i(\eta_2)\, \mathrm{n}_i(\eta_2)\; d\eta\right) + \\
& \left(e_{\ell 1}(\boldsymbol{\eta}_2) \int_{\omega_2} \mathrm{n}_i(\eta_1) \frac{d\mathrm{n}_i}{d\eta_1}\, d\eta\right) \cdot \left(\int_{\omega_1} \mathrm{n}_i(\eta_2)\, \mathrm{n}_i(\eta_2)\; d\eta\right) + \\
& \left(e_{\ell 1}(\boldsymbol{\eta}_4) \int_{\omega_1} \mathrm{n}_i(\eta_1) \frac{d\mathrm{n}_i}{d\eta_1}\, d\eta\right) \cdot \left(\int_{\omega_2} \mathrm{n}_i(\eta_2)\, \mathrm{n}_i(\eta_2)\; d\eta\right) + \\
& \left(e_{\ell 1}(\boldsymbol{\eta}_3) \int_{\omega_2} \mathrm{n}_i(\eta_1) \frac{d\mathrm{n}_i}{d\eta_1}\, d\eta\right) \cdot \left(\int_{\omega_2} \mathrm{n}_i(\eta_2)\, \mathrm{n}_i(\eta_2)\; d\eta\right)
\end{aligned} \tag{9.68}$$

Use of the equality

$$\int_{\omega_1} \mathrm{n}_i(\eta_2)\, \mathrm{n}_i(\eta_2)\; d\eta = \int_{\omega_2} \mathrm{n}_i(\eta_2)\, \mathrm{n}_i(\eta_2)\; d\eta \tag{9.69}$$

allows writing (9.68) as

$$\mathcal{D}^{1\ell}_{i,i} = \left(\frac{1}{2}\left(e_{\ell 1}(\boldsymbol{\eta}_1) + e_{\ell 1}(\boldsymbol{\eta}_4)\right) \int_{\omega_1} \mathrm{n}_i(\eta_1) \frac{d\mathrm{n}_i}{d\eta_1}\, d\eta\right.$$

$$
\begin{aligned}
&+\frac{1}{2}\left(e_{\ell 1}\left(\boldsymbol{\eta}_2\right)+e_{\ell 1}\left(\boldsymbol{\eta}_3\right)\right)\int_{\omega_2} n_i\left(\eta_1\right)\frac{dn_i}{d\eta_1}\,d\eta\Big)\times\\
&\Big(\int_{\omega_1} n_i\left(\eta_2\right)n_i\left(\eta_2\right)\,d\eta+\int_{\omega_2} n_i\left(\eta_2\right)n_i\left(\eta_2\right)\,d\eta\Big)=\\
&\Big(\frac{1}{2}\left(e_{\ell 1}\left(\boldsymbol{\eta}_1\right)+e_{\ell 1}\left(\boldsymbol{\eta}_4\right)\right)\int_{\omega_1} n_i\left(\eta_1\right)\frac{dn_i}{d\eta_1}\,d\eta\\
&+\frac{1}{2}\left(e_{\ell 1}\left(\boldsymbol{\eta}_2\right)+e_{\ell 1}\left(\boldsymbol{\eta}_3\right)\right)\int_{\omega_2} n_i\left(\eta_1\right)\frac{dn_i}{d\eta_1}\,d\eta\Big)\times\\
&\Big(\int_{\omega} n_i\left(\eta_2\right)n_i\left(\eta_2\right)\,d\eta\Big)
\end{aligned}
\tag{9.70}
$$

The leading 1-D convection operator is again expressable via (9.66). Hence, $\mathcal{D}_{i,j}^{1\ell}$ is synthesized as

$$
\mathcal{D}_{i,i}^{1\ell}=\overline{\langle e_{\ell 1}n_i,\frac{dn_i}{d\eta_1}\rangle_\omega}\cdot\langle n_i(\eta_2),n_i(\eta_2)\rangle_\omega=\overline{\langle e_{\ell 1}n_i,\frac{dn_i}{d\eta_1}\rangle_\omega}\cdot m_{i,i} \tag{9.71}
$$

Finally, the decomposition of integral $\mathcal{D}_{i,i+1}^{1\ell}$ is

$$
\begin{aligned}
\mathcal{D}_{i,i+1}^{1\ell} &= \int_{\widehat{\Omega}} e_{\ell 1}N_i\left(\eta_1,\eta_2\right)\frac{\partial N_{i+1}}{\partial\eta_1}\,d\boldsymbol{\eta}=\int_{\widehat{\Omega}} e_{\ell 1}n_i\left(\eta_1\right)n_{i+1}\left(\eta_2\right)\frac{dn_{i+1}}{d\eta_1}n_{i+1}\left(\eta_2\right)\,d\boldsymbol{\eta}=\\
&e_{\ell 1}\left(\boldsymbol{\eta}_2\right)\int_{\widehat{\Omega}_2} n_i\left(\eta_1\right)n_{i+1}\left(\eta_2\right)\frac{dn_{i+1}}{d\eta_1}n_{i+1}\left(\eta_2\right)\,d\boldsymbol{\eta}+\\
&e_{\ell 1}\left(\boldsymbol{\eta}_3\right)\int_{\widehat{\Omega}_3} n_i\left(\eta_1\right)n_{i+1}\left(\eta_2\right)\frac{dn_{i+1}}{d\eta_1}n_{i+1}\left(\eta_2\right)\,d\boldsymbol{\eta}=\\
&\Big(e_{\ell 1}\left(\boldsymbol{\eta}_2\right)\int_{\omega_2} n_i\left(\eta_1\right)\frac{dn_{i+1}}{d\eta_1}\,d\eta\Big)\cdot\Big(\int_{\omega_1} n_{i+1}\left(\eta_2\right)n_{i+1}\left(\eta_2\right)\,d\eta\Big)+\\
&\Big(e_{\ell 1}\left(\boldsymbol{\eta}_3\right)\int_{\omega_2} n_i\left(\eta_1\right)\frac{dn_{i+1}}{d\eta_1}\,d\eta\Big)\cdot\Big(\int_{\omega_2} n_{i+1}\left(\eta_2\right)n_{i+1}\left(\eta_2\right)\,d\eta\Big)
\end{aligned}
\tag{9.72}
$$

Use of the equality

$$
\int_{\omega_1} n_{i+1}\left(\eta_2\right)n_{i+1}\left(\eta_2\right)\,d\eta=\int_{\omega_2} n_{i+1}\left(\eta_2\right)n_{i+1}\left(\eta_2\right)\,d\eta \tag{9.73}
$$

allows writing (9.72) as

$$
\mathcal{D}_{i,i+1}^{1\ell} = \Big(\frac{1}{2}\left(e_{\ell 1}\left(\boldsymbol{\eta}_2\right)+e_{\ell 1}\left(\boldsymbol{\eta}_3\right)\right)\int_{\omega_2} n_i\left(\eta_1\right)\frac{dn_{i+1}}{d\eta_1}\,d\eta\Big)\times
$$

$$\left(\int_{\omega_1} n_{i+1}(\eta_2)\, n_{i+1}(\eta_2)\; d\eta + \int_{\omega_2} n_{i+1}(\eta_2)\, n_{i+1}(\eta_2)\; d\eta\right) =$$
$$\left(\frac{1}{2}\left(e_{\ell 1}(\boldsymbol{\eta}_2) + e_{\ell 1}(\boldsymbol{\eta}_3)\right)\int_{\omega_2} n_i(\eta_1)\,\frac{dn_{i+1}}{d\eta_1}\; d\eta\right)\cdot\left(\int_{\omega} n_{i+1}(\eta_2)\, n_{i+1}(\eta_2)\; d\eta\right) \tag{9.74}$$

whereupon, this expression is recast as

$$\mathcal{D}^{1\ell}_{i,i+1} = \overline{\langle e_{\ell 1} n_i, \frac{dn_{i+1}}{d\eta_1}\rangle_\omega} \cdot \langle n_{i+1}(\eta_2), n_{i+1}(\eta_2)\rangle_\omega = \overline{\langle e_{\ell 1} n_i, \frac{dn_{i+1}}{d\eta_1}\rangle_\omega} \cdot m_{i+1,i+1} \tag{9.75}$$

Therefore, formulae (9.65), (9.70) and (9.74) can be made to coincide with the $\theta\Delta t d^1_{i,j}$ terms in (9.42) via the following definitions for $d^{1\ell}_{i,j}$

$$d^{1\ell}_{i,i-1} = \frac{1}{2}\left(e_{\ell 1}(\boldsymbol{\eta}_1) + e_{\ell 1}(\boldsymbol{\eta}_4)\right)\int_{\omega_1} n_i(\eta_1)\,\frac{dn_{i-1}}{d\eta_1}\; d\eta \tag{9.76}$$

$$\begin{aligned} d^{1\ell}_{i,i} = {} & \frac{1}{2}\left(e_{\ell 1}(\boldsymbol{\eta}_1) + e_{\ell 1}(\boldsymbol{\eta}_4)\right)\int_{\omega_1} n_i(\eta_1)\,\frac{dn_i}{d\eta_1}\; d\eta + \\ & \frac{1}{2}\left(e_{\ell 1}(\boldsymbol{\eta}_2) + e_{\ell 1}(\boldsymbol{\eta}_3)\right)\int_{\omega_2} n_i(\eta_1)\,\frac{dn_i}{d\eta_1}\; d\eta \end{aligned} \tag{9.77}$$

$$d^{1\ell}_{i,i+1} = \frac{1}{2}\left(e_{\ell 1}(\boldsymbol{\eta}_2) + e_{\ell 1}(\boldsymbol{\eta}_3)\right)\int_{\omega_2} n_i(\eta_1)\,\frac{dn_{i+1}}{d\eta_1}\; d\eta \tag{9.78}$$

These one dimensional operators contain 2-D metric data and constitute a distinguishing feature of this TPF algorithm. The structure of these operators induces a metric-data approximation in the evaluation of the *off principal sweep line* TPF terms. Consider for example the evaluation of the representative term $\mathcal{D}^{1\ell}_{i,i-n+1}$. According to the TPF formula (9.41), its value is represented via the principal sweep line operator $d^{1\ell}_{i,i}$. Consequently, following (9.76)-(9.78), the associated TPF representation will embed the average of the four pieces of metric data corresponding to the elements sharing node "i". However, the selected 2-D integral results from the

contributions of elements $\widehat{\Omega}_1$ and $\widehat{\Omega}_2$ only, hence its exact expression contains two metrics, as evidenced by the following development

$$\begin{aligned}
\mathcal{D}^{1\ell}_{i,i-n+1} &= \int_{\widehat{\Omega}} e_{\ell 1} N_i(\eta_1,\eta_2)\,\frac{\partial N_{i-n+1}}{\partial \eta_1}\,d\boldsymbol{\eta} \\
&= \int_{\widehat{\Omega}} e_{\ell 1}\, n_i(\eta_1)\, n_i(\eta_2)\,\frac{dn_{i-n+1}}{d\eta_1} n_{i-n+1}(\eta_2)\; d\boldsymbol{\eta} \\
&= e_{\ell 1}(\boldsymbol{\eta}_1)\int_{\widehat{\Omega}_1} n_i(\eta_1)\, n_i(\eta_2)\,\frac{dn_i}{d\eta_1} n_{i-n+1}(\eta_2)\; d\boldsymbol{\eta} \\
&+ e_{\ell 1}(\boldsymbol{\eta}_2)\int_{\widehat{\Omega}_2} n_i(\eta_1)\, n_i(\eta_2)\,\frac{dn_i}{d\eta_1} n_{i-n+1}(\eta_2)\; d\boldsymbol{\eta} = \\
&\left(e_{\ell 1}(\boldsymbol{\eta}_1)\int_{\omega_1} n_i(\eta_1)\,\frac{dn_i}{d\eta_1}\,d\eta\right)\cdot\left(\int_{\omega_1} n_i(\eta_2)\, n_{i-n+1}(\eta_2)\; d\eta\right) + \\
&\left(e_{\ell 1}(\boldsymbol{\eta}_2)\int_{\omega_2} n_i(\eta_1)\,\frac{dn_i}{d\eta_1}\,d\eta\right)\cdot\left(\int_{\omega_1} n_i(\eta_2)\, n_{i-n+1}(\eta_2)\; d\eta\right) \\
&= \left(e_{\ell 1}(\boldsymbol{\eta}_1)\int_{\omega_1} n_i(\eta_1)\,\frac{dn_i}{d\eta_1}\,d\eta\right. \\
&\left.+ e_{\ell 1}(\boldsymbol{\eta}_2)\int_{\omega_2} n_i(\eta_1)\,\frac{dn_i}{d\eta_1}\,d\eta\right)\cdot\left(\int_{\omega} n_i(\eta_2)\, n_{i-n+1}(\eta_2)\; d\eta\right)
\end{aligned} \tag{9.79}$$

The leading 1-D convection operator is obtained from the formula

$$\langle e_{\ell\alpha} n_i \frac{dn_j}{d\eta_\alpha}\rangle_\omega = \sum_{k=1}^{2} e_{\ell\alpha}\left(\boldsymbol{\eta}_{\widehat{\Omega}_k}\right)\int_{\omega_k} n_i(\eta_1)\,\frac{dn_j}{d\eta_\alpha}\,d\eta \;\;,\;\; \alpha = 1 \tag{9.80}$$

where $\widehat{\Omega}_k$ denotes each element where $\mathcal{D}^{1\ell}_{i,j}$, $j \neq i-1, i, i+1$, is evaluated. The TPF representation associated with (9.79) is

$$\begin{aligned}
\mathcal{D}^{1\ell}_{i,i-n+1} \;\simeq\; &\left(\frac{1}{2}\left(e_{\ell 1}(\boldsymbol{\eta}_1) + e_{\ell 1}(\boldsymbol{\eta}_4)\right)\int_{\omega_1} n_i(\eta_1)\,\frac{dn_i}{d\eta_1}\,d\eta\right. \\
&\left.+\frac{1}{2}\left(e_{\ell 1}(\boldsymbol{\eta}_2) + e_{\ell 1}(\boldsymbol{\eta}_3)\right)\int_{\omega_2} n_i(\eta_1)\,\frac{dn_i}{d\eta_1}\,d\eta\right)\times\left(\int_{\omega} n_i(\eta_2)\, n_{i-n+1}(\eta_2)\; d\eta\right)
\end{aligned} \tag{9.81}$$

Therefore, comparing formulae (9.79) and (9.81) reveals that the TPF represen-

tation uses the following replacements

$$e_{\ell 1}(\boldsymbol{\eta}_1) \Rightarrow \frac{1}{2}\left(e_{\ell 1}(\boldsymbol{\eta}_1) + e_{\ell 1}(\boldsymbol{\eta}_4)\right) \quad , \quad e_{\ell 1}(\boldsymbol{\eta}_2) \Rightarrow \frac{1}{2}\left(e_{\ell 1}(\boldsymbol{\eta}_2) + e_{\ell 1}(\boldsymbol{\eta}_3)\right) \tag{9.82}$$

A similar comparison with the espression for the remaining *off principal sweep line* terms shows that the TPF formulae (9.41)-(9.43) employ the replacements

$$e_{\ell 1}(\boldsymbol{\eta}_4) \Rightarrow \frac{1}{2}\left(e_{\ell 1}(\boldsymbol{\eta}_1) + e_{\ell 1}(\boldsymbol{\eta}_4)\right) \quad , \quad e_{\ell 1}(\boldsymbol{\eta}_3) \Rightarrow \frac{1}{2}\left(e_{\ell 1}(\boldsymbol{\eta}_2) + e_{\ell 1}(\boldsymbol{\eta}_3)\right) \tag{9.83}$$

Consequently, in order to make the TPF algorithm an accurate representation of the 2-D convection operators, a mesh for TPF computations should be so developed as to minimize the differences between the lhs and rhs of (9.82)-(9.83).

Finally, the following expressions show that the exact $\mathcal{D}^{1\ell}_{i,j}$ are all consistently represented by the TPF formulae (9.41)-(9.43)

$$\begin{aligned}
\mathcal{D}^{1\ell}_{i,i-n} &= \langle e_{\ell 1} N_i(\eta_1,\eta_2), \frac{\partial}{\partial \eta_1} N_{i-n}(\eta_1,\eta_2)\rangle_{\widehat{\Omega}} = \langle e_{\ell 1} n_i(\eta_1) n_i(\eta_2), \frac{dn_{i-n}}{d\eta_1} n_{i-n}(\eta_2)\rangle_{\widehat{\Omega}} = \\
&\quad \langle e_{\ell 1} n_i(\eta_1) n_{i-1}(\eta_2), \frac{dn_{i-1}}{d\eta_1} n_{i-n}(\eta_2)\rangle_{\widehat{\Omega}} = \langle e_{\ell 1} n_i(\eta_1) \frac{dn_{i-1}}{d\eta}, n_{i-1}(\eta_2) n_{i-n}(\eta_2)\rangle_{\widehat{\Omega}} = \\
&\quad \langle e_{\ell 1} n_i(\eta_1), \frac{dn_{i-1}}{d\eta_1}\rangle_{\omega} \cdot \langle n_{i-1}(\eta_2), n_{i-n}(\eta_2)\rangle_{\omega} \simeq d^{1\ell}_{i,i-1}\, m_{i-1,i-n} \\
\mathcal{D}^{1\ell}_{i,i-n+1} &= \langle e_{\ell 1} N_i(\eta_1,\eta_2), \frac{\partial}{\partial \eta_1} N_{i-n+1}(\eta_1,\eta_2)\rangle_{\widehat{\Omega}} = \langle e_{\ell 1} n_i(\eta_1) n_i(\eta_2), \frac{dn_{i-n+1}}{d\eta_1} n_{i-n+1}(\eta_2)\rangle_{\widehat{\Omega}} \\
&\quad = \langle e_{\ell 1} n_i(\eta_1) n_i(\eta_2), \frac{dn_{i-n+1}}{d\eta_1} n_{i-n+1}(\eta_2)\rangle_{\widehat{\Omega}} = \langle e_{\ell 1} n_i(\eta_1) \frac{dn_i}{d\eta}, n_i(\eta_2) n_{i-n+1}(\eta_2)\rangle_{\widehat{\Omega}} \\
&\quad = \langle e_{\ell 1} n_i(\eta_1), \frac{dn_i}{d\eta_1}\rangle_{\omega} \cdot \langle n_i(\eta_2), n_{i-n+1}(\eta_2)\rangle_{\omega} \simeq d^{1\ell}_{i,i}\, m_{i,i-n+1} \\
\mathcal{D}^{1\ell}_{i,i-n+2} &= \langle e_{\ell 1} N_i(\eta_1,\eta_2), \frac{\partial}{\partial \eta_1} N_{i-n+2}(\eta_1,\eta_2)\rangle_{\widehat{\Omega}} = \langle e_{\ell 1} n_i(\eta_1) n_i(\eta_2), \frac{dn_{i-n+2}}{d\eta_1} n_{i-n+2}(\eta_2)\rangle_{\widehat{\Omega}} \\
&\quad = \langle e_{\ell 1} n_i(\eta_1) n_{i+1}(\eta_2), \frac{dn_{i+1}}{d\eta_1} n_{i-n+2}(\eta_2)\rangle_{\widehat{\Omega}} = \\
&\quad \langle e_{\ell 1} n_i(\eta_1) \frac{dn_{i+1}}{d\eta_1}, n_{i+1}(\eta_2) n_{i-n+2}(\eta_2)\rangle_{\widehat{\Omega}} = \\
&\quad \langle e_{\ell 1} n_i(\eta_1), \frac{dn_{i+1}}{d\eta_1}\rangle_{\omega} \cdot \langle n_{i+1}(\eta_2), n_{i-n+2}(\eta_2)\rangle_{\omega} \simeq d^{1\ell}_{i,i+1}\, m_{i+1,i-n+2}
\end{aligned} \tag{9.84}$$

$$\mathcal{D}^{1\ell}_{i,i-1} = \langle e_{\ell 1} N_i(\eta_1,\eta_2), \frac{\partial}{\partial\eta_1} N_{i-1}(\eta_1,\eta_2)\rangle_{\widehat{\Omega}} = \langle e_{\ell 1} n_i(\eta_1) n_i(\eta_2), \frac{dn_{i-1}}{d\eta_1} n_{i-1}(\eta_2)\rangle_{\widehat{\Omega}} =$$

$$\langle e_{\ell 1} n_i(\eta_1) n_{i-1}(\eta_2), \frac{dn_{i-1}}{d\eta_1} n_{i-1}(\eta_2)\rangle_{\widehat{\Omega}} = \langle e_{\ell 1} n_i(\eta_1) \frac{dn_{i-1}}{d\eta_1}, n_{i-1}(\eta_2) n_{i-1}(\eta_2)\rangle_{\widehat{\Omega}} =$$

$$\overline{\langle e_{\ell 1} n_i(\eta_1), \frac{dn_{i-1}}{d\eta_1}\rangle_{\omega}} \cdot \langle n_{i-1}(\eta_2), n_{i-1}(\eta_2)\rangle_{\omega} = d^{1\ell}_{i,i-1}\, m_{i-1,i-1}$$

$$\mathcal{D}^{1\ell}_{i,i} = \langle e_{\ell 1} N_i(\eta_1,\eta_2), \frac{\partial}{\partial\eta_1} N_i(\eta_1,\eta_2)\rangle_{\widehat{\Omega}} = \langle e_{\ell 1} n_i(\eta_1) n_i(\eta_2), \frac{dn_i}{d\eta_1} n_i(\eta_2)\rangle_{\widehat{\Omega}} =$$

$$\langle e_{\ell 1} n_i(\eta_1) n_i(\eta_2), \frac{dn_i}{d\eta_1} n_i(\eta_2)\rangle_{\widehat{\Omega}} = \langle e_{\ell 1} n_i(\eta_1) \frac{dn_i}{d\eta_1}, n_i(\eta_2) n_i(\eta_2)\rangle_{\widehat{\Omega}} =$$

$$\overline{\langle e_{\ell 1} n_i(\eta_1), \frac{dn_i}{d\eta_1}\rangle}_{\omega} \cdot \langle n_i(\eta_2), n_i(\eta_2)\rangle_{\omega} = d^{1\ell}_{i,i}\, m_{i,i}$$

$$\mathcal{D}^{1\ell}_{i,i+1} = \langle e_{\ell 1} N_i(\eta_1,\eta_2), \frac{\partial}{\partial\eta_1} N_{i+1}(\eta_1,\eta_2)\rangle_{\widehat{\Omega}} = \langle e_{\ell 1} n_i(\eta_1) n_i(\eta_2), \frac{dn_{i+1}}{d\eta_1} n_{i+1}(\eta_2)\rangle_{\widehat{\Omega}} =$$

$$\langle e_{\ell 1} n_i(\eta_1) n_{i+1}(\eta_2), \frac{dn_{i+1}}{d\eta_1} n_{i+1}(\eta_2)\rangle_{\widehat{\Omega}} = \langle e_{\ell 1} n_i(\eta_1) \frac{dn_{i+1}}{d\eta_1}, n_{i+1}(\eta_2) n_{i+1}(\eta_2)\rangle_{\widehat{\Omega}} =$$

$$\overline{\langle e_{\ell 1} n_i(\eta_1), \frac{dn_{i+1}}{d\eta_1}\rangle_{\omega}} \cdot \langle n_{i+1}(\eta_2), n_{i+1}(\eta_2)\rangle_{\omega} = d^{1\ell}_{i,i+1}\, m_{i+1,i+1} \tag{9.85}$$

$$\mathcal{D}^{1\ell}_{i,i+n-2} = \langle e_{\ell 1} N_i(\eta_1,\eta_2), \frac{\partial}{\partial\eta_1} N_{i+n-2}(\eta_1,\eta_2)\rangle_{\widehat{\Omega}} = \langle e_{\ell 1} n_i(\eta_1) n_i(\eta_2), \frac{dn_{i+n-2}}{d\eta_1} n_{i+n-2}(\eta_2)\rangle_{\widehat{\Omega}}$$

$$= \langle e_{\ell 1} n_i(\eta_1) n_{i-1}(\eta_2), \frac{dn_{i-1}}{d\eta_1} n_{i+n-2}(\eta_2)\rangle_{\widehat{\Omega}} =$$

$$\langle e_{\ell 1} n_i(\eta_1) \frac{dn_{i-1}}{d\eta_1}, n_{i-1}(\eta_2) n_{i+n-2}(\eta_2)\rangle_{\widehat{\Omega}} =$$

$$\langle e_{\ell 1} n_i(\eta_1), \frac{dn_{i-1}}{d\eta_1}\rangle_{\omega} \cdot \langle n_{i-1}(\eta_2), n_{i+n-2}(\eta_2)\rangle_{\omega} \simeq d^{1\ell}_{i,i-1}\, m_{i-1,i+n-2}$$

$$\mathcal{D}^{1\ell}_{i,i+n-1} = \langle e_{\ell 1} N_i(\eta_1,\eta_2), \frac{\partial}{\partial\eta_1} N_{i+n-1}(\eta_1,\eta_2)\rangle_{\widehat{\Omega}} = \langle e_{\ell 1} n_i(\eta_1) n_i(\eta_2), \frac{dn_{i+n-1}}{d\eta_1} n_{i+n-1}(\eta_2)\rangle_{\widehat{\Omega}}$$

$$= \langle e_{\ell 1} n_i(\eta_1) n_i(\eta_2), \frac{dn_i}{d\eta_1} n_{i+n-1}(\eta_2)\rangle_{\widehat{\Omega}} = \langle e_{\ell 1} n_i(\eta_1) \frac{dn_i}{d\eta_1}, n_i(\eta_2) n_{i+n-1}(\eta_2)\rangle_{\widehat{\Omega}} =$$

$$\langle e_{\ell 1} n_i(\eta_1), \frac{dn_i}{d\eta_1}\rangle_{\omega} \cdot \langle n_i(\eta_2), n_{i+n-1}(\eta_2)\rangle_{\omega} \simeq d^{1\ell}_{i,i}\, m_{i,i+n-1}$$

$$\mathcal{D}^{1\ell}_{i,i+n} = \langle e_{\ell 1} N_i(\eta_1,\eta_2), \frac{\partial}{\partial\eta_1} N_{i+n}(\eta_1,\eta_2)\rangle_{\widehat{\Omega}} = \langle e_{\ell 1} n_i(\eta_1) n_i(\eta_2), \frac{dn_{i+n}}{d\eta_1} n_{i+n}(\eta_2)\rangle_{\widehat{\Omega}} =$$

$$\langle e_{\ell 1} n_i(\eta_1) n_{i+1}(\eta_2), \frac{dn_{i+1}}{d\eta_1} n_{i+n}(\eta_2)\rangle_{\widehat{\Omega}} = \langle e_{\ell 1} n_i(\eta_1) \frac{dn_{i+1}}{d\eta_1}, n_{i+1}(\eta_2) n_{i+n}(\eta_2)\rangle_{\widehat{\Omega}} =$$

$$\langle e_{\ell 1} n_i(\eta_1), \frac{dn_{i+1}}{d\eta_1}\rangle_{\omega} \cdot \langle n_{i+1}(\eta_2), n_{i+n}(\eta_2)\rangle_{\omega} \simeq d^{1\ell}_{i,i+1}\, m_{i+1,i+n} \tag{9.86}$$

9.8.2 η_2 Direction Operators

For the determination of $d_{i,j}^{2\ell}$, the decompositions of $\mathcal{D}_{i,i-n+1}^{2\ell}$, $\mathcal{D}_{i,i}^{2\ell}$ and $\mathcal{D}_{i,i+n-1}^{2\ell}$, along the principal η_2 sweep line $\{i-n+1, i, i+n-1\}$ (see Figure 9.1), are now developed. The decomposition of integral $\mathcal{D}_{i,i-n+1}^{2\ell}$ is

$$\begin{aligned}
\mathcal{D}_{i,i-n+1}^{2\ell} &= \int_{\widehat{\Omega}} e_{\ell 2} N_i(\eta_1,\eta_2) \frac{\partial N_{i-n+1}}{\partial \eta_2}\, d\boldsymbol{\eta} \\
&= \int_{\widehat{\Omega}} e_{\ell 2} n_i(\eta_1)\, n_i(\eta_2) \frac{dn_{i-n+1}}{d\eta_2} n_{i-n+1}(\eta_1)\, d\boldsymbol{\eta} \\
&= e_{\ell 2}(\boldsymbol{\eta}_1) \int_{\widehat{\Omega}_1} n_i(\eta_1)\, n_i(\eta_2) \frac{dn_{i-n+1}}{d\eta_2} n_i(\eta_1)\, d\boldsymbol{\eta} + \\
&\quad e_{\ell 2}(\boldsymbol{\eta}_2) \int_{\widehat{\Omega}_2} n_i(\eta_1)\, n_i(\eta_2) \frac{dn_{i-n+1}}{d\eta_2} n_i(\eta_1)\, d\boldsymbol{\eta} = \\
&\quad \left(\int_{\omega_1} n_i(\eta_1)\, n_i(\eta_1)\, d\eta\right) \cdot \left(e_{\ell 2}(\boldsymbol{\eta}_1) \int_{\omega_1} n_i(\eta_2) \frac{dn_{i-n+1}}{d\eta_2}\, d\eta\right) + \\
&\quad \left(\int_{\omega_2} n_i(\eta_1)\, n_i(\eta_1)\, d\eta\right) \cdot \left(e_{\ell 2}(\boldsymbol{\eta}_2) \int_{\omega_1} n_i(\eta_2) \frac{dn_{i-n+1}}{d\eta_2}\, d\eta\right)
\end{aligned} \tag{9.87}$$

Use of the equality

$$\int_{\omega_1} n_i(\eta_1)\, n_i(\eta_1)\, d\eta = \int_{\omega_2} n_i(\eta_1)\, n_i(\eta_1)\, d\eta \tag{9.88}$$

allows writing (9.87) as

$$\begin{aligned}
\mathcal{D}_{i,i-n+1}^{2\ell} &= \left(\int_{\omega_1} n_i(\eta_1)\, n_i(\eta_1)\, d\eta + \int_{\omega_2} n_i(\eta_1)\, n_i(\eta_1)\, d\eta\right) \times \\
&\quad \left(\frac{1}{2}\left(e_{\ell 2}(\boldsymbol{\eta}_1) + e_{\ell 2}(\boldsymbol{\eta}_2)\right) \int_{\omega_1} n_i(\eta_2) \frac{dn_{i-n+1}}{d\eta_2}\, d\eta\right) \\
&= \left(\int_{\omega} n_i(\eta_1)\, n_i(\eta_1)\, d\eta\right) \times \\
&\quad \left(\frac{1}{2}\left(e_{\ell 2}(\boldsymbol{\eta}_1) + e_{\ell 2}(\boldsymbol{\eta}_2)\right) \int_{\omega_1} n_i(\eta_2) \frac{dn_{i-n+1}}{d\eta_2}\, d\eta\right)
\end{aligned} \tag{9.89}$$

In analogy with (9.65), the 1-D convection integral in this expression is pre- multiplied by a mass-matrix term and by the average of two metrics. Each metric is

evaluated in the 2-D element that shares the 1-D element on which the relevant integral is computed. Consequently, this operator is obtained via the formula

$$\overline{\langle e_{\ell 2} n_i, \frac{dn_j}{d\eta_2} \rangle_\omega} \equiv \sum_{k=1}^{2} \left(\frac{1}{2} \left(e_{\ell 2} \left(\boldsymbol{\eta}_{\widehat{\Omega}_{k1}} \right) + e_{\ell 2} \left(\boldsymbol{\eta}_{\widehat{\Omega}_{k2}} \right) \right) \int_{\omega_k} n_i \left(\eta_2 \right) \frac{dn_j}{d\eta_2} \, d\eta \right) \tag{9.90}$$

where the subscripts $\widehat{\Omega}_{k1}$ and $\widehat{\Omega}_{k2}$ respectively, denote the two 2-D elements that share the 1-D element ω_k. Insertion of this expression into (9.89) leads to the formula

$$\mathcal{D}^{2\ell}_{i,i-n+1} = \langle n_i(\eta_1), n_i(\eta_1) \rangle_\omega \cdot \overline{\langle e_{\ell 2} n_i, \frac{dn_{i-n+1}}{d\eta_2} \rangle_\omega} = m_{i,i} \cdot \overline{\langle e_{\ell 2} n_i, \frac{dn_{i-n+1}}{d\eta_2} \rangle_\omega} \tag{9.91}$$

The decomposition of integral $\mathcal{D}^{2\ell}_{i,i}$ is

$$\begin{aligned}
\mathcal{D}^{2\ell}_{i,i} &= \int_{\widehat{\Omega}} e_{\ell 2} N_i \left(\eta_1, \eta_2 \right) \frac{\partial N_i}{\partial \eta_2} \, d\boldsymbol{\eta} = \int_{\widehat{\Omega}} e_{\ell 2} n_i \left(\eta_1 \right) n_i \left(\eta_2 \right) \frac{dn_i}{d\eta_2} n_i \left(\eta_1 \right) \, d\boldsymbol{\eta} \\
&= e_{\ell 2} \left(\boldsymbol{\eta}_1 \right) \int_{\widehat{\Omega}_1} n_i \left(\eta_1 \right) n_i \left(\eta_2 \right) \frac{dn_i}{d\eta_2} n_i \left(\eta_1 \right) \, d\boldsymbol{\eta} \\
&+ e_{\ell 2} \left(\boldsymbol{\eta}_2 \right) \int_{\widehat{\Omega}_2} n_i \left(\eta_1 \right) n_i \left(\eta_2 \right) \frac{dn_i}{d\eta_2} n_i \left(\eta_1 \right) \, d\boldsymbol{\eta} \\
&+ e_{\ell 2} \left(\boldsymbol{\eta}_3 \right) \int_{\widehat{\Omega}_3} n_i \left(\eta_1 \right) n_i \left(\eta_2 \right) \frac{dn_i}{d\eta_2} n_i \left(\eta_1 \right) \, d\boldsymbol{\eta} \\
&+ e_{\ell 2} \left(\boldsymbol{\eta}_4 \right) \int_{\widehat{\Omega}_4} n_i \left(\eta_1 \right) n_i \left(\eta_2 \right) \frac{dn_i}{d\eta_2} n_i \left(\eta_1 \right) \, d\boldsymbol{\eta} \\
&= \left(\int_{\omega_1} n_i \left(\eta_1 \right) n_i \left(\eta_1 \right) \, d\eta \right) \cdot \left(e_{\ell 2} \left(\boldsymbol{\eta}_1 \right) \int_{\omega_1} n_i \left(\eta_2 \right) \frac{dn_i}{d\eta_2} \, d\eta \right) \\
&+ \left(\int_{\omega_2} n_i \left(\eta_1 \right) n_i \left(\eta_1 \right) \, d\eta \right) \cdot \left(e_{\ell 2} \left(\boldsymbol{\eta}_2 \right) \int_{\omega_1} n_i \left(\eta_2 \right) \frac{dn_i}{d\eta_2} \, d\eta \right) \\
&+ \left(\int_{\omega_1} n_i \left(\eta_1 \right) n_i \left(\eta_1 \right) \, d\eta \right) \cdot \left(e_{\ell 2} \left(\boldsymbol{\eta}_4 \right) \int_{\omega_2} n_i \left(\eta_2 \right) \frac{dn_i}{d\eta_2} \, d\eta \right) \\
&+ \left(\int_{\omega_2} n_i \left(\eta_1 \right) n_i \left(\eta_1 \right) \, d\eta \right) \cdot \left(e_{\ell 2} \left(\boldsymbol{\eta}_3 \right) \int_{\omega_2} n_i \left(\eta_2 \right) \frac{dn_i}{d\eta_2} \, d\eta \right)
\end{aligned} \tag{9.92}$$

and use of equality (9.88) allows writing (9.92) as

$$\mathcal{D}^{1\ell}_{i,i} = \left(\int_{\omega_1} n_i \left(\eta_1 \right) n_i \left(\eta_1 \right) \, d\eta + \int_{\omega_2} n_i \left(\eta_1 \right) n_i \left(\eta_1 \right) \, d\eta \right) \times$$

$$
\begin{aligned}
&\left(\frac{1}{2}\left(e_{\ell 2}\left(\boldsymbol{\eta}_1\right)+e_{\ell 2}\left(\boldsymbol{\eta}_2\right)\right)\int_{\omega_1} n_i\left(\eta_2\right)\frac{dn_i}{d\eta_2}\,d\eta\right.\\
&\left.+\frac{1}{2}\left(e_{\ell 2}\left(\boldsymbol{\eta}_3\right)+e_{\ell 2}\left(\boldsymbol{\eta}_4\right)\right)\int_{\omega_2} n_i\left(\eta_2\right)\frac{dn_i}{d\eta_2}\,d\eta\right)\\
=\;&\left(\int_{\omega} n_i\left(\eta_1\right)n_i\left(\eta_1\right)\,d\eta\right)\times\\
&\left(\frac{1}{2}\left(e_{\ell 2}\left(\boldsymbol{\eta}_1\right)+e_{\ell 2}\left(\boldsymbol{\eta}_2\right)\right)\int_{\omega_1} n_i\left(\eta_2\right)\frac{dn_i}{d\eta_2}\,d\eta\right.\\
&\left.+\frac{1}{2}\left(e_{\ell 2}\left(\boldsymbol{\eta}_3\right)+e_{\ell 2}\left(\boldsymbol{\eta}_4\right)\right)\int_{\omega_2} n_i\left(\eta_2\right)\frac{dn_i}{d\eta_2}\,d\eta\right)
\end{aligned}
\tag{9.93}
$$

The 1-D convection operator in this expression is again expressable via (9.90), hence $\mathcal{D}_{i,i}^{2\ell}$ is cast as

$$
\mathcal{D}_{i,i}^{2\ell}=\langle n_i(\eta_1),n_i(\eta_1)\rangle_{\omega}\cdot\overline{\langle e_{\ell 2}n_i,\frac{dn_i}{d\eta_2}\rangle_{\omega}}=m_{i,i}\cdot\overline{\langle e_{\ell 2}n_i,\frac{dn_i}{d\eta_2}\rangle_{\omega}} \tag{9.94}
$$

Finally, the decomposition of integral $\mathcal{D}_{i,i+n-1}^{2\ell}$ is

$$
\begin{aligned}
\mathcal{D}_{i,i+n-1}^{2\ell}\;=\;&\int_{\widehat{\Omega}} e_{\ell 2}N_i\left(\eta_1,\eta_2\right)\frac{\partial N_{i+n-1}}{\partial\eta_2}\,d\boldsymbol{\eta}=\\
&\int_{\widehat{\Omega}} e_{\ell 2}n_i\left(\eta_1\right)n_i\left(\eta_2\right)\frac{dn_{i+n-1}}{d\eta_2}n_{i+n-1}\left(\eta_1\right)\,d\boldsymbol{\eta}=\\
&e_{\ell 2}\left(\boldsymbol{\eta}_3\right)\int_{\widehat{\Omega}_3} n_i\left(\eta_1\right)n_i\left(\eta_2\right)\frac{dn_{i+n-1}}{d\eta_2}n_i\left(\eta_1\right)\,d\boldsymbol{\eta}+\\
&e_{\ell 2}\left(\boldsymbol{\eta}_4\right)\int_{\widehat{\Omega}_4} n_i\left(\eta_1\right)n_i\left(\eta_2\right)\frac{dn_{i+n-1}}{d\eta_2}n_i\left(\eta_1\right)\,d\boldsymbol{\eta}=\\
&\left(\int_{\omega_1} n_i\left(\eta_1\right)n_i\left(\eta_1\right)\,d\eta\right)\cdot\left(e_{\ell 2}\left(\boldsymbol{\eta}_3\right)\int_{\omega_2} n_i\left(\eta_2\right)\frac{dn_{i+n-1}}{d\eta_2}\,d\eta\right)+\\
&\left(\int_{\omega_2} n_i\left(\eta_1\right)n_i\left(\eta_1\right)\,d\eta\right)\cdot\left(e_{\ell 2}\left(\boldsymbol{\eta}_4\right)\int_{\omega_2} n_i\left(\eta_2\right)\frac{dn_{i+n-1}}{d\eta_2}\,d\eta\right)
\end{aligned}
\tag{9.95}
$$

and continued use of equality (9.88) allows expressing (9.95) as

$$
\mathcal{D}_{i,i+n-1}^{2\ell}\;=\;\left(\int_{\omega_1} n_i\left(\eta_1\right)n_i\left(\eta_1\right)\,d\eta+\int_{\omega_2} n_i\left(\eta_1\right)n_i\left(\eta_1\right)\,d\eta\right)\times
$$

$$\left(\frac{1}{2}\left(e_{\ell 2}\left(\boldsymbol{\eta}_3\right)+e_{\ell 2}\left(\boldsymbol{\eta}_4\right)\right)\int_{\omega_2} n_i\left(\eta_2\right)\frac{dn_{i+n-1}}{d\eta_2}\,d\eta\right)=$$
$$\left(\int_{\omega} n_i\left(\eta_1\right)n_i\left(\eta_1\right)\,d\eta\right)\cdot\left(\frac{1}{2}\left(e_{\ell 2}\left(\boldsymbol{\eta}_3\right)+e_{\ell 2}\left(\boldsymbol{\eta}_4\right)\right)\int_{\omega_2} n_i\left(\eta_2\right)\frac{dn_{i+n-1}}{d\eta_2}\,d\eta\right) \tag{9.96}$$

which is recast via (9.90) as

$$\mathcal{D}^{2\ell}_{i,i+n-1}=\langle n_i(\eta_1),n_i(\eta_1)\rangle_\omega\cdot\overline{\langle e_{\ell 2}n_i,\frac{dn_{i+n-1}}{d\eta_2}\rangle_\omega}=m_{i,i}\cdot\overline{\langle e_{\ell 2}n_i,\frac{dn_{i+n-1}}{d\eta_2}\rangle_\omega} \tag{9.97}$$

Therefore, formulae (9.89), (9.93) and (9.96) can be made to coincide with the $\theta\Delta t d^2_{ij}$ terms in (9.41)-(9.43) via the following definitions for $d^{2\ell}_{i,j}$

$$d^{2\ell}_{i,i-n+1} = \frac{1}{2}\left(e_{\ell 2}\left(\boldsymbol{\eta}_1\right)+e_{\ell 2}\left(\boldsymbol{\eta}_2\right)\right)\int_{\omega_1} n_i\left(\eta_2\right)\frac{dn_{i-n+1}}{d\eta_2}\,d\eta \tag{9.98}$$

$$\begin{aligned} d^{2\ell}_{i,i} = {} & \frac{1}{2}\left(e_{\ell 2}\left(\boldsymbol{\eta}_1\right)+e_{\ell 2}\left(\boldsymbol{\eta}_2\right)\right)\int_{\omega_1} n_i\left(\eta_2\right)\frac{dn_i}{d\eta_2}\,d\eta + \\ & \frac{1}{2}\left(e_{\ell 2}\left(\boldsymbol{\eta}_3\right)+e_{\ell 2}\left(\boldsymbol{\eta}_4\right)\right)\int_{\omega_2} n_i\left(\eta_2\right)\frac{dn_i}{d\eta_2}\,d\eta \end{aligned} \tag{9.99}$$

$$d^{2\ell}_{i,i+n-1} = \frac{1}{2}\left(e_{\ell 2}\left(\boldsymbol{\eta}_3\right)+e_{\ell 2}\left(\boldsymbol{\eta}_4\right)\right)\int_{\omega_2} n_i\left(\eta_2\right)\frac{dn_{i+n-1}}{d\eta_2}\,d\eta \tag{9.100}$$

In strict analogy with (9.76)-(9.78), these operators also contain 2-D metric data. Their structure also induces a metric-data approximation for the *off principal sweep line* TPF terms. Consider for example the evaluation of the representative term $\mathcal{D}^{2\ell}_{i,i-1}$. According to the TPF formula (9.42), its value is represented via the principal sweep line operator $d^{2\ell}_{i-1,i-1}$. Consequently, following (9.98)-(9.100) the associated TPF representation will embed the average of the four pieces of metric data corresponding to the elements sharing node "i". However, the selected 2-D integral results from the contributions of elements $\widehat{\Omega}_1$ and $\widehat{\Omega}_4$ only, hence its exact expression

contains two metrics. Specifically

$$\begin{aligned}
\mathcal{D}_{i,i-1}^{2\ell} &= \int_{\widehat{\Omega}} e_{\ell 2} N_i(\eta_1,\eta_2)\frac{\partial N_{i-1}}{\partial \eta_2}\,d\boldsymbol{\eta} = \int_{\widehat{\Omega}} e_{\ell 1}\, n_i(\eta_1)\, n_i(\eta_2)\frac{dn_{i-1}}{d\eta_2} n_{i-1}(\eta_2)\,d\boldsymbol{\eta} = \\
& e_{\ell 2}(\boldsymbol{\eta}_1)\int_{\widehat{\Omega}_1} n_i(\eta_1)\, n_{i-1}(\eta_2)\frac{dn_{i-1}}{d\eta_2} n_{i-1}(\eta_1)\,d\boldsymbol{\eta} + \\
& e_{\ell 2}(\boldsymbol{\eta}_4)\int_{\widehat{\Omega}_4} n_i(\eta_1)\, n_{i-1}(\eta_2)\frac{dn_{i-1}}{d\eta_2} n_{i-1}(\eta_1)\,d\boldsymbol{\eta} = \\
& \left(\int_{\omega_1} n_i(\eta_1)\, n_{i-1}(\eta_1)\,d\eta\right)\cdot\left(e_{\ell 2}(\boldsymbol{\eta}_1)\int_{\omega_1} n_{i-1}(\eta_2)\frac{dn_{i-1}}{d\eta_2}\,d\eta\right) + \\
& \left(\int_{\omega_1} n_i(\eta_1)\, n_{i-1}(\eta_1)\,d\eta\right)\cdot\left(e_{\ell 2}(\boldsymbol{\eta}_4)\int_{\omega_2} n_{i-1}(\eta_2)\frac{dn_{i-1}}{d\eta_2}\,d\eta\right) = \\
& \left(\int_{\omega} n_i(\eta_1)\, n_{i-1}(\eta_1)\,d\eta\right)\times \\
& \left(e_{\ell 2}(\boldsymbol{\eta}_1)\int_{\omega_1} n_{i-1}(\eta_2)\frac{dn_{i-1}}{d\eta_2}\,d\eta + e_{\ell 2}(\boldsymbol{\eta}_4)\int_{\omega_2} n_{i-1}(\eta_2)\frac{dn_{i-1}}{d\eta_2}\,d\eta\right) \qquad (9.101)
\end{aligned}$$

and the 1-D convection operator is obtained via (9.80). The TPF representation associated with (9.101) is

$$\begin{aligned}
\mathcal{D}_{i,i-1}^{2\ell} &\simeq \left(\int_{\omega} n_i(\eta_1)\, n_{i-1}(\eta_1)\,d\eta\right)\times \\
& \left(\frac{1}{2}\left(e_{\ell 2}^{i-1}(\boldsymbol{\eta}_1)+e_{\ell 2}^{i-1}(\boldsymbol{\eta}_2)\right)\int_{\omega_1} n_{i-1}(\eta_2)\frac{dn_{i-1}}{d\eta_2}\,d\eta + \right. \\
& \left.\frac{1}{2}\left(e_{\ell 2}^{i-1}(\boldsymbol{\eta}_3)+e_{\ell 2}^{i-1}(\boldsymbol{\eta}_4)\right)\int_{\omega_2} n_{i-1}(\eta_1)\frac{dn_{i-1}}{d\eta_1}\,d\eta\right) \qquad (9.102)
\end{aligned}$$

Therefore, comparing (9.101) and (9.102) reveals that the TPF representation uses the following replacements

$$e_{\ell 2}^{i}(\boldsymbol{\eta}_1) \Rightarrow \frac{1}{2}\left(e_{\ell 2}^{i-1}(\boldsymbol{\eta}_1)+e_{\ell 2}^{i-1}(\boldsymbol{\eta}_2)\right) \quad , \quad e_{\ell 2}^{i}(\boldsymbol{\eta}_4) \Rightarrow \frac{1}{2}\left(e_{\ell 2}^{i-1}(\boldsymbol{\eta}_3)+e_{\ell 2}^{i-1}(\boldsymbol{\eta}_4)\right) \qquad (9.103)$$

where superscript $i-1$ indicates evaluation on the elements associated with node $i-1$.

A similar comparison with the expression for the remaining *off principal sweep line* terms shows that the TPF formulae (9.41)-(9.43) employ the replacements

$$e^i_{\ell 2}(\boldsymbol{\eta}_2) \Rightarrow \frac{1}{2}\left(e^{i+1}_{\ell 2}(\boldsymbol{\eta}_1) + e^{i+1}_{\ell 2}(\boldsymbol{\eta}_2)\right) \quad , \quad e^i_{\ell 2}(\boldsymbol{\eta}_2) \Rightarrow \frac{1}{2}\left(e^{i+1}_{\ell 2}(\boldsymbol{\eta}_3) + e^{i+1}_{\ell 2}(\boldsymbol{\eta}_4)\right) \tag{9.104}$$

where superscript "$i+1$" now indicates evaluation on the elements associated with node "$i+1$". Consequently, this approximation is inherently distinct from that of (9.82)-(9.83). Hence, the mesh variations should indeed be smooth to minimize the difference between the lhs and rhs in (9.103)-(9.104).

Finally, the following expressions show that the exact $\mathcal{D}^{2\ell}_{i,j}$ are all consistently represented by the TPF formulae (9.41)-(9.43)

$$\begin{aligned}
\mathcal{D}^{2\ell}_{i,i-n} &= \langle e_{\ell 2} N_i(\eta_1,\eta_2), \frac{\partial}{\partial \eta_2} N_{i-n}(\eta_1,\eta_2)\rangle_{\widehat{\Omega}} = \langle e_{\ell 2} n_i(\eta_1) n_i(\eta_2), \frac{dn_{i-n}}{d\eta_2} n_{i-n}(\eta_1)\rangle_{\widehat{\Omega}} = \\
&\quad \langle e_{\ell 2} n_i(\eta_1) n_{i-1}(\eta_2), \frac{dn_{i-n}}{d\eta_2} n_{i-1}(\eta_1)\rangle_{\widehat{\Omega}} = \langle n_i(\eta_1) n_{i-1}(\eta_1), e_{\ell 2} n_{i-1}(\eta_2) \frac{dn_{i-n}}{d\eta_2}\rangle_{\widehat{\Omega}} = \\
&\quad \langle n_i(\eta_1), n_{i-1}(\eta_1)\rangle_\omega \cdot \langle e_{\ell 2} n_{i-1}(\eta_2), \frac{dn_{i-n}}{d\eta_2}\rangle_\omega \simeq m_{i,i-1}\ d^{2\ell}_{i-1,i-n} \\
\mathcal{D}^{2\ell}_{i,i-n+1} &= \langle e_{\ell 2} N_i(\eta_1,\eta_2), \frac{\partial}{\partial \eta_2} N_{i-n+1}(\eta_1,\eta_2)\rangle_{\widehat{\Omega}} = \langle e_{\ell 2} n_i(\eta_1) n_i(\eta_2), \frac{dn_{i-n+1}}{d\eta_2} n_{i-n+1}(\eta_1)\rangle_{\widehat{\Omega}} \\
&\quad = \langle e_{\ell 2} n_i(\eta_1) n_i(\eta_2), \frac{dn_{i-n+1}}{d\eta_2} n_i(\eta_1)\rangle_{\widehat{\Omega}} = \langle n_i(\eta_1) n_i(\eta_1), e_{\ell 2} n_i(\eta_2) \frac{dn_{i-n+1}}{d\eta_2}\rangle_{\widehat{\Omega}} = \\
&\quad \langle n_i(\eta_1), n_i(\eta_1)\rangle_\omega \cdot \langle e_{\ell 2} n_i(\eta_2), \frac{dn_{i-n+1}}{d\eta_2}\rangle_\omega = m_{i,i}\ d^{2\ell}_{i,i-n+1} \\
\mathcal{D}^{2\ell}_{i,i-n+2} &= \langle e_{\ell 2} N_i(\eta_1,\eta_2), \frac{\partial}{\partial \eta_2} N_{i-n+2}(\eta_1,\eta_2)\rangle_{\widehat{\Omega}} = \langle e_{\ell 2} n_i(\eta_1) n_i(\eta_2), \frac{dn_{i-n+2}}{d\eta_2} n_{i-n+2}(\eta_1)\rangle_{\widehat{\Omega}} \\
&\quad = \langle e_{\ell 2} n_i(\eta_1) n_{i+1}(\eta_2), \frac{dn_{i-n+2}}{d\eta_2} n_{i+1}(\eta_1)\rangle_{\widehat{\Omega}} = \\
&\quad \langle n_i(\eta_1) n_{i+1}(\eta_1), e_{\ell 2} n_{i+1}(\eta_2) \frac{dn_{i-n+2}}{d\eta_2},\rangle_{\widehat{\Omega}} = \\
&\quad \langle n_i(\eta_1), n_{i+1}(\eta_1)\rangle_\omega \cdot \langle e_{\ell 2} n_{i+1}(\eta_2), \frac{dn_{i-n+2}}{d\eta_2}\rangle_\omega \simeq m_{i,i+1}\ d^{2\ell}_{i+1,i-n+2}
\end{aligned} \tag{9.105}$$

$$\mathcal{D}^{2\ell}_{i,i-1} = \langle e_{\ell 2} N_i(\eta_1,\eta_2), \frac{\partial}{\partial \eta_2} N_{i-1}(\eta_1,\eta_2)\rangle_{\widehat{\Omega}} = \langle e_{\ell 2} n_i(\eta_1) n_i(\eta_2), \frac{dn_{i-1}}{d\eta_2} n_{i-1}(\eta_1)\rangle_{\widehat{\Omega}} =$$

$$\langle e_{\ell 2} n_i(\eta_1) n_{i-1}(\eta_2), \frac{dn_{i-1}}{d\eta_2} n_{i-1}(\eta_1)\rangle_{\widehat{\Omega}} = \langle n_i(\eta_1) n_{i-1}(\eta_1), e_{\ell 2} n_{i-1}(\eta_2) \frac{dn_{i-1}}{d\eta_2}\rangle_{\widehat{\Omega}} =$$

$$\langle n_i(\eta_1), n_{i-1}(\eta_1)\rangle_\omega \cdot \langle e_{\ell 2} n_{i-1}(\eta_2), \frac{dn_{i-1}}{d\eta_2}\rangle_\omega \simeq m_{i,i-1}\ d^{2\ell}_{i-1,i-1}$$

$$\mathcal{D}^{2\ell}_{i,i} = \langle e_{\ell 2} N_i(\eta_1,\eta_2), \frac{\partial}{\partial \eta_2} N_i(\eta_1,\eta_2)\rangle_{\widehat{\Omega}} = \langle e_{\ell 2} n_i(\eta_1) n_i(\eta_2), \frac{dn_i}{d\eta_2} n_i(\eta_1)\rangle_{\widehat{\Omega}} =$$

$$\langle e_{\ell 2} n_i(\eta_1) n_i(\eta_2), \frac{dn_i}{d\eta_2} n_i(\eta_1)\rangle_{\widehat{\Omega}} = \langle n_i(\eta_1) n_i(\eta_1), e_{\ell 2} n_i(\eta_2) \frac{dn_i}{d\eta_2}\rangle_{\widehat{\Omega}} =$$

$$\langle n_i(\eta_1), n_i(\eta_1)\rangle_\omega \cdot \overline{\langle e_{\ell 2} n_i(\eta_2), \frac{dn_i}{d\eta_2}\rangle_\omega} = m_{i,i}\ d^{2\ell}_{i,i}$$

$$\mathcal{D}^{2\ell}_{i,i+1} = \langle e_{\ell 2} N_i(\eta_1,\eta_2), \frac{\partial}{\partial \eta_2} N_{i+1}(\eta_1,\eta_2)\rangle_{\widehat{\Omega}} = \langle e_{\ell 2} n_i(\eta_1) n_i(\eta_2), \frac{dn_{i+1}}{d\eta_2} n_{i+1}(\eta_1)\rangle_{\widehat{\Omega}} =$$

$$\langle e_{\ell 2} n_i(\eta_1) n_{i+1}(\eta_2), \frac{dn_{i+1}}{d\eta_2} n_{i+1}(\eta_1)\rangle_{\widehat{\Omega}} = \langle n_i(\eta_1) n_{i+1}(\eta_1), e_{\ell 2} n_{i+1}(\eta_2) \frac{dn_{i+1}}{d\eta_2}\rangle_{\widehat{\Omega}} =$$

$$\langle n_i(\eta_1), n_{i+1}(\eta_1)\rangle_\omega \cdot \langle e_{\ell 2} n_{i+1}(\eta_2), \frac{dn_{i+1}}{d\eta_2}\rangle_\omega \simeq m_{i,i+1}\ d^{2\ell}_{i+1,i+1} \qquad (9.106)$$

$$\mathcal{D}^{2\ell}_{i,i+n-2} = \langle e_{\ell 2} N_i(\eta_1,\eta_2), \frac{\partial}{\partial \eta_2} N_{i+n-2}(\eta_1,\eta_2)\rangle_{\widehat{\Omega}} = \langle e_{\ell 2} n_i(\eta_1) n_i(\eta_2), \frac{dn_{i+n-2}}{d\eta_2} n_{i+n-2}(\eta_1)\rangle_{\widehat{\Omega}}$$

$$= \langle e_{\ell 2} n_i(\eta_1) n_{i-1}(\eta_2), \frac{dn_{i+n-2}}{d\eta_2} n_{i-1}(\eta_1)\rangle_{\widehat{\Omega}} =$$

$$\langle n_i(\eta_1) n_{i-1}(\eta_1), e_{\ell 2} n_{i-1}(\eta_2) \frac{dn_{i+n-2}}{d\eta_2}\rangle_{\widehat{\Omega}} =$$

$$\langle n_i(\eta_1), n_{i-1}(\eta_1)\rangle_\omega \cdot \langle e_{\ell 2} n_{i-1}(\eta_2), \frac{dn_{i+n-2}}{d\eta_2}\rangle_\omega \simeq m_{i,i-1}\ d^{2\ell}_{i-1,i+n-2}$$

$$\mathcal{D}^{2\ell}_{i,i+n-1} = \langle e_{\ell 2} N_i(\eta_1,\eta_2), \frac{\partial}{\partial \eta_2} N_{i+n-1}(\eta_1,\eta_2)\rangle_{\widehat{\Omega}} = \langle e_{\ell 2} n_i(\eta_1) n_i(\eta_2), \frac{dn_{i+n-1}}{d\eta_2} n_{i+n-1}(\eta_1)\rangle_{\widehat{\Omega}}$$

$$= \langle e_{\ell 2} n_i(\eta_1) n_i(\eta_2), \frac{dn_{i+n-1}}{d\eta_2} n_i(\eta_1)\rangle_{\widehat{\Omega}} = \langle n_i(\eta_1) n_i(\eta_1), e_{\ell 2} n_i(\eta_2) \frac{dn_{i+n-1}}{d\eta_2}\rangle_{\widehat{\Omega}} =$$

$$\langle n_i(\eta_1), n_i(\eta_1)\rangle_\omega \cdot \overline{\langle e_{\ell 2} n_i(\eta_2), \frac{dn_{i-n}}{d\eta_2}\rangle_\omega} = m_{i,i}\ d^{2\ell}_{i,i+n-1}$$

$$\mathcal{D}^{2\ell}_{i,i+n} = \langle e_{\ell 2} N_i(\eta_1,\eta_2), \frac{\partial}{\partial \eta_2} N_{i+n}(\eta_1,\eta_2)\rangle_{\widehat{\Omega}} = \langle e_{\ell 2} n_i(\eta_1) n_i(\eta_2), \frac{dn_{i+n}}{d\eta_2} n_{i+n}(\eta_1)\rangle_{\widehat{\Omega}} =$$

$$\langle e_{\ell 2} n_i(\eta_1) n_{i+1}(\eta_2), \frac{dn_{i+n}}{d\eta_2} n_{i+1}(\eta_1)\rangle_{\widehat{\Omega}} = \langle n_i(\eta_1) n_{i+1}(\eta_1), e_{\ell 2} n_{i+1}(\eta_2) \frac{dn_{i+n}}{d\eta_2}\rangle_{\widehat{\Omega}} =$$

$$\langle n_i(\eta_1), n_{i+1}(\eta_1)\rangle_\omega \cdot \langle e_{\ell 2} n_{i+1}(\eta_2), \frac{dn_{i+n}}{d\eta}\rangle_\omega \simeq m_{i,i+1}\ d^{2\ell}_{i+1,i+n} \qquad (9.107)$$

9.9 Viscous Flux Vector Factorization

In this section the one dimensional diffusion operators

$$\left(d^{\alpha}_{i,j}\right)^{d} \quad , \quad \alpha = 1,2 \tag{9.108}$$

are defined such that their product with 1-D mass matrix terms and the 2-D metric data $e_{\ell\alpha}$ and $\det J$ exactly represent select 2-D diffusion jacobian terms $D^{\alpha}_{i,j}$ on arbitrary grids. The basic 2-D jacobian expressions are

$$D^{\alpha}_{i,j} \equiv -\int_{\widehat{\Omega}} e_{\ell\alpha} \frac{e_{m\alpha}}{\det J} \frac{\partial N_i}{\partial \eta_\alpha} \frac{\partial N_k}{\partial \eta_\alpha} \, d\boldsymbol{\eta} \;\; \frac{\partial f^{k}_{\ell m}}{\partial q^{j}} \tag{9.109}$$

The extension of identity (9.59) for the jacobian term in this integral is

$$\frac{\partial f^{k}_{\ell m}}{\partial q^{j}} = \frac{\partial f^{j}_{\ell m}}{\partial q^{j}} \delta^{k}_{\underline{j}} = \frac{\partial f^{j}_{\ell m}}{\partial q^{\underline{j}}} \tag{9.110}$$

This allows expressing (9.109) as

$$D^{\alpha}_{i,j} \equiv -\int_{\widehat{\Omega}} e_{\ell\alpha} \frac{e_{m\alpha}}{\det J} \frac{\partial N_i}{\partial \eta_\alpha} \frac{\partial N_j}{\partial \eta_\alpha} \, d\boldsymbol{\eta} \;\; \left[\frac{\partial f^{j}_{\ell m}}{\partial q^{\underline{j}}}\right] \tag{9.111}$$

and the associated 2-D differential operator is

$$\mathcal{D}^{\alpha\ell m}_{i,j} \equiv -\int_{\widehat{\Omega}} e_{\ell\alpha} \frac{e_{m\alpha}}{\det J} \frac{\partial N_i}{\partial \eta_\alpha} \frac{\partial N_j}{\partial \eta_\alpha} \, d\boldsymbol{\eta} \tag{9.112}$$

In analogy with (9.62), $d^{\alpha}_{i,j}$ is defined as

$$d^{\alpha}_{i,j} \equiv d^{\alpha\ell m}_{i,j} \left[\frac{\partial f_{\ell m}}{\partial q^{\underline{j}}}\right] \tag{9.113}$$

whereupon, $d^{\alpha\ell m}_{i,j}$, hence $d^{\alpha}_{i,j}$ is derived by setting it equal to the exact one dimensional operator intrinsic to $\mathcal{D}^{\alpha\ell m}_{i,j}$ as now developed.

9.9.1 η_1 Direction Operators

The determination of $d_{i,j}^{1\ell m}$ is attained via derivation of the exact decomposition for integrals $\mathcal{D}_{i,i-1}^{1\ell m}$, $\mathcal{D}_{i,i}^{1\ell m}$ and $\mathcal{D}_{i,i+1}^{1\ell m}$ along the principal η_1 sweep line $\{i-1, i, i+1\}$ (see Figure 9.1). The decomposition of integral $\mathcal{D}_{i,i-1}^{1\ell m}$ is

$$
\begin{aligned}
\mathcal{D}_{i,i-1}^{1\ell m} \;=\; & -\int_{\widehat{\Omega}} e_{\ell 1} \frac{e_{m1}}{\det J} \frac{\partial N_i}{\partial \eta_1} \frac{\partial N_{i-1}}{\partial \eta_1}\, d\boldsymbol{\eta} = \\
& -\int_{\widehat{\Omega}} e_{\ell 1} \frac{e_{m1}}{\det J} \frac{dn_i}{d\eta_1} n_{i-1}(\eta_2) \frac{dn_{i-1}}{d\eta_1} n_{i-1}(\eta_2)\, d\boldsymbol{\eta} = \\
& -e_{\ell 1}(\boldsymbol{\eta}_1) \left(\frac{e_{m1}}{\det J}\right)_{\tilde{\boldsymbol{\eta}}_1} \int_{\widehat{\Omega}_1} \frac{dn_i}{d\eta_1} n_{i-1}(\eta_2) \frac{dn_{i-1}}{d\eta_1} n_{i-1}(\eta_2)\, d\boldsymbol{\eta} \\
& -e_{\ell 1}(\boldsymbol{\eta}_4) \left(\frac{e_{m1}}{\det J}\right)_{\tilde{\boldsymbol{\eta}}_4} \int_{\widehat{\Omega}_4} \frac{dn_i}{d\eta} n_{i-1}(\eta_2) \frac{dn_{i-1}}{d\eta_1} n_{i-1}(\eta_2)\, d\boldsymbol{\eta} = \\
& -\left(e_{\ell 1}(\boldsymbol{\eta}_1) \left(\frac{e_{m1}}{\det J}\right)_{\tilde{\boldsymbol{\eta}}_1} \int_{\omega_1} \frac{dn_i}{d\eta_1} \frac{dn_{i-1}}{d\eta_1}\, d\eta\right) \cdot \left(\int_{\omega_1} n_{i-1}(\eta_2)\, n_{i-1}(\eta_2)\, d\eta\right) \\
& -\left(e_{\ell 1}(\boldsymbol{\eta}_4) \left(\frac{e_{m1}}{\det J}\right)_{\tilde{\boldsymbol{\eta}}_4} \int_{\omega_1} \frac{dn_i}{d\eta_1} \frac{dn_{i-1}}{d\eta_1}\, d\eta\right) \cdot \left(\int_{\omega_2} n_{i-1}(\eta_2)\, n_{i-1}(\eta_2)\, d\eta\right)
\end{aligned}
\tag{9.114}
$$

Use of equality (9.64) allows writing (9.114) as

$$
\begin{aligned}
\mathcal{D}_{i,i-1}^{1\ell m} = \; & -\left(\frac{1}{2}\left(e_{\ell 1}(\boldsymbol{\eta}_1) \left(\frac{e_{m1}}{\det J}\right)_{\tilde{\boldsymbol{\eta}}_1} + e_{\ell 1}(\boldsymbol{\eta}_4) \left(\frac{e_{m1}}{\det J}\right)_{\tilde{\boldsymbol{\eta}}_4}\right) \int_{\omega_1} \frac{dn_i}{d\eta_1} \frac{dn_{i-1}}{d\eta_1}\, d\eta\right) \times \\
& \left(\int_{\omega_1} n_{i-1}(\eta_2)\, n_{i-1}(\eta_2)\, d\eta + \int_{\omega_2} n_{i-1}(\eta_2)\, n_{i-1}(\eta_2)\, d\eta\right) = \\
& -\left(\frac{1}{2}\left(e_{\ell 1}(\boldsymbol{\eta}_1) \left(\frac{e_{m1}}{\det J}\right)_{\tilde{\boldsymbol{\eta}}_1} + e_{\ell 1}(\boldsymbol{\eta}_4) \left(\frac{e_{m1}}{\det J}\right)_{\tilde{\boldsymbol{\eta}}_4}\right) \int_{\omega_1} \frac{dn_i}{d\eta} \frac{dn_{i-1}}{d\eta_1}\, d\eta\right) \times \\
& \left(\int_{\omega} n_{i-1}(\eta_2)\, n_{i-1}(\eta_2)\, d\eta\right)
\end{aligned}
\tag{9.115}
$$

The leading 1-D diffusion operator in this expression is post-multiplied by a mass-matrix term and pre- multiplied by the average of two metric-data expressions. Each expression is evaluated in the 2-D element that shares the 1-D element on

which the relevant integral is computed. Consequently, this operator is obtained via the formula

$$\overline{\langle e_{\ell 1}\frac{e_{m1}}{\det J}\frac{dn_i}{d\eta_1},\frac{dn_j}{d\eta_1}\rangle_\omega} \equiv \sum_{k=1}^{2}\left(\frac{1}{2}\left(e_{\ell 1}\left(\boldsymbol{\eta}_{\widehat{\Omega}_{k1}}\right)\left(\frac{e_{m1}}{\det J}\right)_{\tilde{\boldsymbol{\eta}}_{\widehat{\Omega}_{k1}}} + e_{\ell 1}\left(\boldsymbol{\eta}_{\widehat{\Omega}_{k2}}\right)\left(\frac{e_{m1}}{\det J}\right)_{\tilde{\boldsymbol{\eta}}_{\widehat{\Omega}_{k2}}}\right)\int_{\omega_k}\frac{dn_i}{d\eta_1}\frac{dn_j}{d\eta_1}\,d\eta\right) \tag{9.116}$$

where the subscripts $\widehat{\Omega}_{k1}$ and $\widehat{\Omega}_{k2}$ respectively denote the two 2-D elements that share the 1-D element ω_k. Insertion of this expression into (9.115) leads to the formula

$$\mathcal{D}_{i,i-1}^{1\ell m} = -\overline{\langle e_{\ell 1}\frac{e_{m1}}{\det J}\frac{dn_i}{d\eta_1},\frac{dn_{i-1}}{d\eta_1}\rangle_\omega}\cdot\langle n_{i-1},n_{i-1}\rangle_\omega = -\overline{\langle e_{\ell 1}\frac{e_{m1}}{\det J}\frac{dn_i}{d\eta_1},\frac{dn_{i-1}}{d\eta_1}\rangle_\omega}\cdot m_{i-1,i-1} \tag{9.117}$$

The decomposition of integral $\mathcal{D}_{i,i}^{1\ell m}$ is

$$\begin{aligned}
\mathcal{D}_{i,i}^{1\ell m} &= -\int_{\widehat{\Omega}} e_{\ell 1}\frac{e_{m1}}{\det J}\frac{\partial N_i}{\partial\eta_1}\frac{\partial N_i}{\partial\eta_1}\,d\boldsymbol{\eta} = \\
&\quad -\int_{\widehat{\Omega}} e_{\ell 1}\frac{e_{m1}}{\det J}\frac{dn_i}{d\eta_1}n_i(\eta_2)\frac{dn_i}{d\eta_1}n_i(\eta_2)\,d\boldsymbol{\eta} = \\
&\quad -e_{\ell 1}(\boldsymbol{\eta}_1)\left(\frac{e_{m1}}{\det J}\right)_{\tilde{\boldsymbol{\eta}}_1}\int_{\widehat{\Omega}_1}\frac{dn_i}{d\eta_1}n_i(\eta_2)\frac{dn_i}{d\eta_1}n_i(\eta_2)\,d\boldsymbol{\eta} \\
&\quad -e_{\ell 1}(\boldsymbol{\eta}_2)\left(\frac{e_{m1}}{\det J}\right)_{\tilde{\boldsymbol{\eta}}_2}\int_{\widehat{\Omega}_2}\frac{dn_i}{d\eta_1}n_i(\eta_2)\frac{dn_i}{d\eta_1}n_i(\eta_2)\,d\boldsymbol{\eta} \\
&\quad -e_{\ell 1}(\boldsymbol{\eta}_3)\left(\frac{e_{m1}}{\det J}\right)_{\tilde{\boldsymbol{\eta}}_3}\int_{\widehat{\Omega}_3}\frac{dn_i}{d\eta_1}n_i(\eta_2)\frac{dn_i}{d\eta_1}n_i(\eta_2)\,d\boldsymbol{\eta} \\
&\quad -e_{\ell 1}(\boldsymbol{\eta}_4)\left(\frac{e_{m1}}{\det J}\right)_{\tilde{\boldsymbol{\eta}}_4}\int_{\widehat{\Omega}_4}\frac{dn_i}{d\eta_1}n_i(\eta_2)\frac{dn_i}{d\eta_1}n_i(\eta_2)\,d\boldsymbol{\eta} = \\
&\quad -\left(e_{\ell 1}(\boldsymbol{\eta}_1)\left(\frac{e_{m1}}{\det J}\right)_{\tilde{\boldsymbol{\eta}}_1}\int_{\omega_1}\frac{dn_i}{d\eta_1}\frac{dn_i}{d\eta_1}\,d\eta\right)\cdot\left(\int_{\omega_1}n_i(\eta_2)\,n_i(\eta_2)\,d\eta\right) \\
&\quad -\left(e_{\ell 1}(\boldsymbol{\eta}_2)\left(\frac{e_{m1}}{\det J}\right)_{\tilde{\boldsymbol{\eta}}_2}\int_{\omega_2}\frac{dn_i}{d\eta_1}\frac{dn_i}{d\eta_1}\,d\eta\right)\cdot\left(\int_{\omega_1}n_i(\eta_2)\,n_i(\eta_2)\,d\eta\right)
\end{aligned}$$

$$
\begin{aligned}
&- \left(e_{\ell 1}(\boldsymbol{\eta}_3) \left(\frac{e_{m1}}{\det J} \right)_{\tilde{\boldsymbol{\eta}}_3} \int_{\omega_2} \frac{dn_i}{d\eta_1} \frac{dn_i}{d\eta_1} \, d\eta \right) \cdot \left(\int_{\omega_2} n_i(\eta_2)\, n_i(\eta_2) \, d\eta \right) \\
&- \left(e_{\ell 1}(\boldsymbol{\eta}_4) \left(\frac{e_{m1}}{\det J} \right)_{\tilde{\boldsymbol{\eta}}_4} \int_{\omega_1} \frac{dn_i}{d\eta_1} \frac{dn_i}{d\eta_1} \, d\eta \right) \cdot \left(\int_{\omega_2} n_i(\eta_2)\, n_i(\eta_2) \, d\eta \right)
\end{aligned}
\tag{9.118}
$$

and equality (9.69) allows writing (9.118) as

$$
\begin{aligned}
\mathcal{D}_{i,i}^{1\ell m} \;=\; & - \left(\frac{1}{2} \left(e_{\ell 1}(\boldsymbol{\eta}_1) \left(\frac{e_{m1}}{\det J} \right)_{\tilde{\boldsymbol{\eta}}_1} + e_{\ell 1}(\boldsymbol{\eta}_4) \left(\frac{e_{m1}}{\det J} \right)_{\tilde{\boldsymbol{\eta}}_4} \right) \int_{\omega_1} \frac{dn_i}{d\eta_1} \frac{dn_i}{d\eta_1} \, d\eta \right. \\
& \left. - \frac{1}{2} \left(e_{\ell 1}(\boldsymbol{\eta}_2) \left(\frac{e_{m1}}{\det J} \right)_{\tilde{\boldsymbol{\eta}}_2} + e_{\ell 1}(\boldsymbol{\eta}_3) \left(\frac{e_{m1}}{\det J} \right)_{\tilde{\boldsymbol{\eta}}_3} \right) \int_{\omega_2} \frac{dn_i}{d\eta_1} \frac{dn_i}{d\eta_1} \, d\eta \right) \times \\
& \left(\int_{\omega_1} n_i(\eta_2)\, n_i(\eta_2) \, d\eta + \int_{\omega_2} n_i(\eta_2)\, n_i(\eta_2) \, d\eta \right) = \\
& - \left(\frac{1}{2} \left(e_{\ell 1}(\boldsymbol{\eta}_1) \left(\frac{e_{m1}}{\det J} \right)_{\tilde{\boldsymbol{\eta}}_1} + e_{\ell 1}(\boldsymbol{\eta}_4) \left(\frac{e_{m1}}{\det J} \right)_{\tilde{\boldsymbol{\eta}}_4} \right) \int_{\omega_1} \frac{dn_i}{d\eta_1} \frac{dn_i}{d\eta_1} \, d\eta \right. \\
& \left. - \frac{1}{2} \left(e_{\ell 1}(\boldsymbol{\eta}_2) \left(\frac{e_{m1}}{\det J} \right)_{\tilde{\boldsymbol{\eta}}_2} + e_{\ell 1}(\boldsymbol{\eta}_3) \left(\frac{e_{m1}}{\det J} \right)_{\tilde{\boldsymbol{\eta}}_3} \right) \int_{\omega_2} \frac{dn_i}{d\eta_1} \frac{dn_i}{d\eta_1} \, d\eta \right) \times \\
& \left(\int_{\omega} n_i(\eta_2)\, n_i(\eta_2) \, d\eta \right)
\end{aligned}
\tag{9.119}
$$

The leading 1-D diffusion operator is again expressable via (9.116), hence $\mathcal{D}_{i,i}^{1\ell m}$ is cast as

$$
\mathcal{D}_{i,i}^{1\ell m} = -\overline{\langle e_{\ell 1} \frac{e_{m1}}{\det J} \frac{dn_i}{d\eta_1}, \frac{dn_i}{d\eta_1} \rangle_\omega} \cdot \langle n_i, n_i \rangle_\omega = -\overline{\langle e_{\ell 1} \frac{e_{m1}}{\det J} \frac{dn_i}{d\eta_1}, \frac{dn_i}{d\eta_1} \rangle_\omega} \cdot m_{i,i} \tag{9.120}
$$

Finally, the decomposition of integral $\mathcal{D}_{i,i+1}^{1\ell m}$ is

$$
\begin{aligned}
\mathcal{D}_{i,i+1}^{1\ell m} \;=\; & - \int_{\widehat{\Omega}} e_{\ell 1} \frac{e_{m1}}{\det J} \frac{\partial N_i}{\partial \eta_1} \frac{\partial N_{i+1}}{\partial \eta_1} \, d\boldsymbol{\eta} = \\
& - \int_{\widehat{\Omega}} e_{\ell 1} \frac{e_{m1}}{\det J} \frac{dn_i}{d\eta_1} n_{i+1}(\eta_2) \frac{dn_{i+1}}{d\eta_1} n_{i+1}(\eta_2) \, d\boldsymbol{\eta} = \\
& - e_{\ell 1}(\boldsymbol{\eta}_2) \left(\frac{e_{m1}}{\det J} \right)_{\tilde{\boldsymbol{\eta}}_2} \int_{\widehat{\Omega}_1} \frac{dn_i}{d\eta_1} n_{i+1}(\eta_2) \frac{dn_{i+1}}{d\eta_1} n_{i+1}(\eta_2) \, d\boldsymbol{\eta} \\
& - e_{\ell 1}(\boldsymbol{\eta}_3) \left(\frac{e_{m1}}{\det J} \right)_{\tilde{\boldsymbol{\eta}}_3} \int_{\widehat{\Omega}_3} \frac{dn_i}{d\eta_1} n_{i+1}(\eta_2) \frac{dn_{i+1}}{d\eta_1} n_{i+1}(\eta_2) \, d\boldsymbol{\eta} =
\end{aligned}
$$

$$
\begin{aligned}
&- \left(e_{\ell 1}(\boldsymbol{\eta}_2) \left(\frac{e_{m1}}{\det J} \right)_{\tilde{\boldsymbol{\eta}}_2} \int_{\omega_2} \frac{dn_i}{d\eta_1} \frac{dn_{i+1}}{d\eta_1} \, d\eta \right) \cdot \left(\int_{\omega_1} n_{i+1}(\eta_2) \, n_{i+1}(\eta_2) \; d\eta \right) \\
&- \left(e_{\ell 1}(\boldsymbol{\eta}_3) \left(\frac{e_{m1}}{\det J} \right)_{\tilde{\boldsymbol{\eta}}_3} \int_{\omega_2} \frac{dn_i}{d\eta_1} \frac{dn_{i+1}}{d\eta_1} \, d\eta \right) \cdot \left(\int_{\omega_2} n_{i+1}(\eta_2) \, n_{i+1}(\eta_2) \; d\eta \right)
\end{aligned}
\tag{9.121}
$$

and equality (9.73) allows writing (9.121) as

$$
\begin{aligned}
\mathcal{D}^{1\ell m}_{i,i+1} = \; &- \left(\frac{1}{2} \left(e_{\ell 1}(\boldsymbol{\eta}_2) \left(\frac{e_{m1}}{\det J} \right)_{\tilde{\boldsymbol{\eta}}_2} + e_{\ell 1}(\boldsymbol{\eta}_3) \left(\frac{e_{m1}}{\det J} \right)_{\tilde{\boldsymbol{\eta}}_3} \right) \int_{\omega_2} \frac{dn_i}{d\eta_1} \frac{dn_{i+1}}{d\eta_1} \, d\eta \right) \times \\
&\left(\int_{\omega_1} n_{i+1}(\eta_2) \, n_{i+1}(\eta_2) \; d\eta + \int_{\omega_2} n_{i+1}(\eta_2) \, n_{i+1}(\eta_2) \; d\eta \right) = \\
&- \left(\frac{1}{2} \left(e_{\ell 1}(\boldsymbol{\eta}_2) \left(\frac{e_{m1}}{\det J} \right)_{\tilde{\boldsymbol{\eta}}_2} + e_{\ell 1}(\boldsymbol{\eta}_3) \left(\frac{e_{m1}}{\det J} \right)_{\tilde{\boldsymbol{\eta}}_3} \right) \int_{\omega_2} \frac{dn_i}{d\eta_1} \frac{dn_{i+1}}{d\eta_1} \, d\eta \right) \times \\
&\left(\int_{\omega} n_{i+1}(\eta_2) \, n_{i+1}(\eta_2) \; d\eta \right)
\end{aligned}
\tag{9.122}
$$

whereupon, this expression is recast as

$$
\mathcal{D}^{1\ell m}_{i,i+1} = -\overline{\langle e_{\ell 1} \frac{e_{m1}}{\det J} \frac{dn_i}{d\eta_1}, \frac{dn_{i+1}}{d\eta_1} \rangle_{\omega}} \cdot \langle n_{i+1}, n_{i+1} \rangle_{\omega} = -\overline{\langle e_{\ell 1} \frac{e_{m1}}{\det J} \frac{dn_i}{d\eta_1}, \frac{dn_{i+1}}{d\eta_1} \rangle_{\omega}} \cdot m_{i+1,i+1}
\tag{9.123}
$$

Therefore, formulae (9.115), (9.119) and (9.122) can be made to coincide with the $\theta \Delta t d^1_{i,j}$ terms in (9.42) via the following definitions for $d^{1\ell m}_{i,j}$

$$
d^{1\ell m}_{i,i-1} = -\frac{1}{2} \left(e_{\ell 1}(\boldsymbol{\eta}_1) \left(\frac{e_{m1}}{\det J} \right)_{\tilde{\boldsymbol{\eta}}_1} + e_{\ell 1}(\boldsymbol{\eta}_4) \left(\frac{e_{m1}}{\det J} \right)_{\tilde{\boldsymbol{\eta}}_4} \right) \int_{\omega_1} \frac{dn_i}{d\eta_1} \frac{dn_{i-1}}{d\eta_1} \, d\eta
\tag{9.124}
$$

$$
\begin{aligned}
d^{1\ell m}_{i,i} = \; &-\frac{1}{2} \left(e_{\ell 1}(\boldsymbol{\eta}_1) \left(\frac{e_{m1}}{\det J} \right)_{\tilde{\boldsymbol{\eta}}_1} + e_{\ell 1}(\boldsymbol{\eta}_4) \left(\frac{e_{m1}}{\det J} \right)_{\tilde{\boldsymbol{\eta}}_4} \right) \int_{\omega_1} \frac{dn_i}{d\eta_1} \frac{dn_i}{d\eta_1} \, d\eta \\
&-\frac{1}{2} \left(e_{\ell 1}(\boldsymbol{\eta}_2) \left(\frac{e_{m1}}{\det J} \right)_{\tilde{\boldsymbol{\eta}}_2} + e_{\ell 1}(\boldsymbol{\eta}_3) \left(\frac{e_{m1}}{\det J} \right)_{\tilde{\boldsymbol{\eta}}_3} \right) \int_{\omega_2} \frac{dn_i}{d\eta_1} \frac{dn_i}{d\eta_1} \, d\eta
\end{aligned}
\tag{9.125}
$$

$$
d^{1\ell m}_{i,i+1} = -\frac{1}{2} \left(e_{\ell 1}(\boldsymbol{\eta}_2) \left(\frac{e_{m1}}{\det J} \right)_{\tilde{\boldsymbol{\eta}}_2} + e_{\ell 1}(\boldsymbol{\eta}_3) \left(\frac{e_{m1}}{\det J} \right)_{\tilde{\boldsymbol{\eta}}_3} \right) \int_{\omega_2} \frac{dn_i}{d\eta_1} \frac{dn_{i+1}}{d\eta_1} \, d\eta
$$

These one dimensional operators contain 2-D metric data expressions and constitute a distinguishing feature of this TPF algorithm for diffusion jacobians. The structure of these operators induces a metric-data approximation in the evaluation of the *off principal sweep line* TPF terms. Consider for example the evaluation of the representative term $\mathcal{D}^{1\ell m}_{i,i-n+1}$. According to the TPF formula (9.41), its value is represented via the principal sweep line operator $d^{1\ell m}_{i,i}$. Consequently, following (9.124)-(9.126) the associated TPF representation will embed the average of the four pieces of metric data corresponding to the elements sharing node "i". However, the selected 2-D integral results from the contributions of elements $\widehat{\Omega}_1$ and $\widehat{\Omega}_2$ only, hence its exact expression contains two metric data expressions as evidenced by the following development

$$
\begin{aligned}
\mathcal{D}^{1\ell m}_{i,i-n+1} \;=\; & -\int_{\widehat{\Omega}} e_{\ell 1}\frac{e_{m1}}{\det J}\frac{\partial N_i}{\partial \eta_1}\frac{\partial N_{i-n+1}}{\partial \eta_1}\,d\boldsymbol{\eta} = \\
& -\int_{\widehat{\Omega}} e_{\ell 1}\frac{e_{m1}}{\det J}\frac{dn_i}{d\eta_1}n_i(\eta_2)\,\frac{dn_{i-n+1}}{d\eta_1}n_{i-n+1}(\eta_2)\;d\boldsymbol{\eta} = \\
& -e_{\ell 1}(\boldsymbol{\eta}_1)\left(\frac{e_{m1}}{\det J}\right)_{\tilde{\boldsymbol{\eta}}_1}\int_{\widehat{\Omega}_1}\frac{dn_i}{d\eta_1}n_i(\eta_2)\,\frac{dn_i}{d\eta_1}n_{i-n+1}(\eta_2)\;d\boldsymbol{\eta} \\
& -e_{\ell 1}(\boldsymbol{\eta}_2)\left(\frac{e_{m1}}{\det J}\right)_{\tilde{\boldsymbol{\eta}}_2}\int_{\widehat{\Omega}_2}\frac{dn_i}{d\eta_1}n_i(\eta_2)\,\frac{dn_i}{d\eta_1}n_{i-n+1}(\eta_2)\;d\boldsymbol{\eta} = \\
& -\left(e_{\ell 1}(\boldsymbol{\eta}_1)\left(\frac{e_{m1}}{\det J}\right)_{\tilde{\boldsymbol{\eta}}_1}\int_{\omega_1}\frac{dn_i}{d\eta_1}\frac{dn_i}{d\eta_1}\,d\eta\right)\cdot\left(\int_{\omega_1}n_i(\eta_2)\,n_{i-n+1}(\eta_2)\;d\eta\right) \\
& -\left(e_{\ell 1}(\boldsymbol{\eta}_2)\left(\frac{e_{m1}}{\det J}\right)_{\tilde{\boldsymbol{\eta}}_2}\int_{\omega_2}\frac{dn_i}{d\eta_1}\frac{dn_i}{d\eta_1}\,d\eta\right)\cdot\left(\int_{\omega_1}n_i(\eta_2)\,n_{i-n+1}(\eta_2)\;d\eta\right) = \\
& -\left(e_{\ell 1}(\boldsymbol{\eta}_1)\left(\frac{e_{m1}}{\det J}\right)_{\tilde{\boldsymbol{\eta}}_1}\int_{\omega_1}\frac{dn_i}{d\eta_1}\frac{dn_i}{d\eta_1}\,d\eta\right. \\
& \left.+\,e_{\ell 1}(\boldsymbol{\eta}_2)\left(\frac{e_{m1}}{\det J}\right)_{\tilde{\boldsymbol{\eta}}_1}\int_{\omega_2}\frac{dn_i}{d\eta_1}\frac{dn_i}{d\eta_1}\,d\eta\right)\times
\end{aligned}
$$

$$\left(\int_{\omega} n_i(\eta_2)\, n_{i-n+1}(\eta_2)\; d\eta\right) \tag{9.127}$$

Here, the leading one dimensional diffusion operator is obtained from the formula

$$\langle e_{\ell\alpha}\frac{e_{m\alpha}}{\det J}\frac{dn_i}{d\eta_\alpha}, \frac{dn_j}{d\eta_\alpha}\rangle_\omega = \sum_{k=1}^{2} e_{\ell\alpha}\left(\boldsymbol{\eta}_{\widehat{\Omega}_k}\right)\left(\frac{e_{m\alpha}}{\det J}\right)_{\boldsymbol{\eta}_{\widehat{\Omega}_k}} \int_{\omega_k} \frac{dn_i}{d\eta_\alpha}\frac{dn_j}{d\eta_\alpha}\, d\eta \;\;,\;\; \alpha = 1 \tag{9.128}$$

where $\widehat{\Omega}_k$ denotes each element where $\mathcal{D}_{i,j}^{1\ell m}$, $j \neq i-1, i, i+1$, is evaluated. The TPF representation associated with (9.127) is

$$\begin{aligned}
\mathcal{D}_{i,i-n+1}^{1\ell m} \;\simeq\; & \left(-\frac{1}{2}\left(e_{\ell 1}(\boldsymbol{\eta}_1)\left(\frac{e_{m1}}{\det J}\right)_{\tilde{\boldsymbol{\eta}}_1} + e_{\ell 1}(\boldsymbol{\eta}_4)\left(\frac{e_{m1}}{\det J}\right)_{\tilde{\boldsymbol{\eta}}_4}\right)\int_{\omega_1}\frac{dn_i}{d\eta_1}\frac{dn_i}{d\eta_1}\, d\eta\right. \\
& \left.-\frac{1}{2}\left(e_{\ell 1}(\boldsymbol{\eta}_2)\left(\frac{e_{m1}}{\det J}\right)_{\tilde{\boldsymbol{\eta}}_2} + e_{\ell 1}(\boldsymbol{\eta}_3)\left(\frac{e_{m1}}{\det J}\right)_{\tilde{\boldsymbol{\eta}}_3}\right)\int_{\omega_2}\frac{dn_i}{d\eta_1}\frac{dn_i}{d\eta_1}\, d\eta\right)\times \\
& \left(\int_{\omega} n_i(\eta_2)\, n_{i-n+1}(\eta_2)\; d\eta\right)
\end{aligned} \tag{9.129}$$

Therefore, comparing formulae (9.127) and (9.129) reveals that the TPF representation uses the following replacements

$$\begin{aligned}
e_{\ell 1}(\boldsymbol{\eta}_1)\left(\frac{e_{m1}}{\det J}\right)_{\tilde{\boldsymbol{\eta}}_1} &\Rightarrow \frac{1}{2}\left(e_{\ell 1}(\boldsymbol{\eta}_1)\left(\frac{e_{m1}}{\det J}\right)_{\tilde{\boldsymbol{\eta}}_1} + e_{\ell 1}(\boldsymbol{\eta}_4)\left(\frac{e_{m1}}{\det J}\right)_{\tilde{\boldsymbol{\eta}}_4}\right) \\
e_{\ell 1}(\boldsymbol{\eta}_2)\left(\frac{e_{m1}}{\det J}\right)_{\tilde{\boldsymbol{\eta}}_2} &\Rightarrow \frac{1}{2}\left(e_{\ell 1}(\boldsymbol{\eta}_2)\left(\frac{e_{m1}}{\det J}\right)_{\tilde{\boldsymbol{\eta}}_2} + e_{\ell 1}(\boldsymbol{\eta}_3)\left(\frac{e_{m1}}{\det J}\right)_{\tilde{\boldsymbol{\eta}}_3}\right)
\end{aligned} \tag{9.130}$$

A similar comparison with the espression for the remaining *off principal sweep line* terms shows that the TPF formulae (9.41)-(9.43) employ the replacements

$$\begin{aligned}
e_{\ell 1}(\boldsymbol{\eta}_4)\left(\frac{e_{m1}}{\det J}\right)_{\tilde{\boldsymbol{\eta}}_4} &\Rightarrow \frac{1}{2}\left(e_{\ell 1}(\boldsymbol{\eta}_1)\left(\frac{e_{m1}}{\det J}\right)_{\tilde{\boldsymbol{\eta}}_1} + e_{\ell 1}(\boldsymbol{\eta}_4)\left(\frac{e_{m1}}{\det J}\right)_{\tilde{\boldsymbol{\eta}}_4}\right) \\
e_{\ell 1}(\boldsymbol{\eta}_3)\left(\frac{e_{m1}}{\det J}\right)_{\tilde{\boldsymbol{\eta}}_3} &\Rightarrow \frac{1}{2}\left(e_{\ell 1}(\boldsymbol{\eta}_2)\left(\frac{e_{m1}}{\det J}\right)_{\tilde{\boldsymbol{\eta}}_2} + e_{\ell 1}(\boldsymbol{\eta}_3)\left(\frac{e_{m1}}{\det J}\right)_{\tilde{\boldsymbol{\eta}}_3}\right)
\end{aligned} \tag{9.131}$$

Consequently, in order to make the TPF algorithm an accurate representation of the 2-D diffusion operators, a mesh for TPF computations should be so developed as to minimize the differences between the lhs and rhs of expressions (9.130)-(9.131).

Finally, the following expressions show that all $\mathcal{D}_{i,j}^{1\ell m}$ are all consistently represented by the TPF formulae (9.41)-(9.43)

$$
\begin{aligned}
\mathcal{D}_{i,i-n}^{1\ell m} &= -\langle e_{\ell 1}\frac{e_{m1}}{\det J}\frac{\partial}{\partial\eta_1}N_i(\eta_1,\eta_2),\frac{\partial}{\partial\eta_1}N_{i-n}(\eta_1,\eta_2)\rangle_{\widehat{\Omega}} = \\
&\quad -\langle e_{\ell 1}\frac{e_{m1}}{\det J}\frac{dn_i}{d\eta_1}n_i(\eta_2),\frac{dn_{i-n}}{d\eta_1}n_{i-n}(\eta_2)\rangle_{\widehat{\Omega}} = \\
&\quad -\langle e_{\ell 1}\frac{e_{m1}}{\det J}\frac{dn_i}{d\eta_1}n_{i-1}(\eta_2),\frac{dn_{i-1}}{d\eta}n_{i-n}(\eta_2)\rangle_{\widehat{\Omega}} = \\
&\quad -\langle e_{\ell 1}\frac{e_{m1}}{\det J}\frac{dn_i}{d\eta_1}\frac{dn_{i-1}}{d\eta_1},n_{i-1}(\eta_2)n_{i-n}(\eta_2)\rangle_{\widehat{\Omega}} = \\
&\quad -\langle e_{\ell 1}\frac{e_{m1}}{\det J}\frac{dn_i}{d\eta_1},\frac{dn_{i-1}}{d\eta_1}\rangle_\omega\cdot\langle n_{i-1}(\eta_2),n_{i-n}(\eta_2)\rangle_\omega \simeq d_{i,i-1}^{1\ell m}\ m_{i-1,i-n} \\
\mathcal{D}_{i,i-n+1}^{1\ell m} &= -\langle e_{\ell 1}\frac{e_{m1}}{\det J}\frac{\partial}{\partial\eta_1}N_i(\eta_1,\eta_2),\frac{\partial}{\partial\eta_1}N_{i-n+1}(\eta_1,\eta_2)\rangle_{\widehat{\Omega}} = \\
&\quad -\langle e_{\ell 1}\frac{e_{m1}}{\det J}\frac{dn_i}{d\eta_1}n_i(\eta_2),\frac{dn_{i-n+1}}{d\eta_1}n_{i-n+1}(\eta_2)\rangle_{\widehat{\Omega}} = \\
&\quad -\langle e_{\ell 1}\frac{e_{m1}}{\det J}\frac{dn_i}{d\eta_1}n_i(\eta_2),\frac{dn_i}{d\eta_1}n_{i-n+1}(\eta_2)\rangle_{\widehat{\Omega}} = \\
&\quad -\langle e_{\ell 1}\frac{e_{m1}}{\det J}\frac{dn_i}{d\eta_1}\frac{dn_i}{d\eta_1},n_i(\eta_2)n_{i-n+1}(\eta_2)\rangle_{\widehat{\Omega}} = \\
&\quad -\langle e_{\ell 1}\frac{e_{m1}}{\det J}\frac{dn_i}{d\eta_1},\frac{dn_i}{d\eta_1}\rangle_\omega\cdot\langle n_i(\eta_2),n_{i-n+1}(\eta_2)\rangle_\omega \simeq d_{i,i}^{1\ell m}\ m_{i,i-n+1} \\
\mathcal{D}_{i,i-n+2}^{1\ell m} &= -\langle e_{\ell 1}\frac{e_{m1}}{\det J}\frac{\partial}{\partial\eta_1}N_i(\eta_1,\eta_2),\frac{\partial}{\partial\eta_1}N_{i-n+2}(\eta_1,\eta_2)\rangle_{\widehat{\Omega}} = \\
&\quad -\langle e_{\ell 1}\frac{e_{m1}}{\det J}\frac{dn_i}{d\eta_1}n_i(\eta_2),\frac{dn_{i-n+2}}{d\eta_1}n_{i-n+2}(\eta_2)\rangle_{\widehat{\Omega}} = \\
&\quad -\langle e_{\ell 1}\frac{e_{m1}}{\det J}\frac{dn_i}{d\eta_1}n_{i+1}(\eta_2),\frac{dn_{i+1}}{d\eta_1}n_{i-n+2}(\eta_2)\rangle_{\widehat{\Omega}} = \\
&\quad -\langle e_{\ell 1}\frac{e_{m1}}{\det J}\frac{dn_i}{d\eta_1}\frac{dn_{i+1}}{d\eta_1},n_{i+1}(\eta_2)n_{i-n+2}(\eta_2)\rangle_{\widehat{\Omega}} = \\
&\quad -\langle e_{\ell 1}\frac{e_{m1}}{\det J}\frac{dn_i}{d\eta_1},\frac{dn_{i+1}}{d\eta_1}\rangle_\omega\cdot\langle n_{i+1}(\eta_2),n_{i-n+2}(\eta_2)\rangle_\omega \\
&\quad \simeq d_{i,i+1}^{1\ell m}\ m_{i+1,i-n+2} \qquad (9.132) \\
\mathcal{D}_{i,i-1}^{1\ell m} &= -\langle e_{\ell 1}\frac{e_{m1}}{\det J}\frac{\partial}{\partial\eta_1}N_i(\eta_1,\eta_2),\frac{\partial}{\partial\eta_1}N_{i-1}(\eta_1,\eta_2)\rangle_{\widehat{\Omega}} = \\
&\quad -\langle e_{\ell 1}\frac{e_{m1}}{\det J}\frac{dn_i}{d\eta_1}n_i(\eta_2),\frac{dn_{i-1}}{d\eta_1}n_{i-1}(\eta_2)\rangle_{\widehat{\Omega}} =
\end{aligned}
$$

$$
\begin{aligned}
&-\langle e_{\ell 1}\frac{e_{m1}}{\det J}\frac{dn_i}{d\eta_1}n_{i-1}(\eta_2),\frac{dn_{i-1}}{d\eta_1}n_{i-1}(\eta_2)\rangle_{\widehat{\Omega}}=\\
&-\langle e_{\ell 1}\frac{e_{m1}}{\det J}\frac{dn_i}{d\eta_1}\frac{dn_{i-1}}{d\eta_1},n_{i-1}(\eta_2)n_{i-1}(\eta_2)\rangle_{\widehat{\Omega}}=\\
&\overline{-\langle e_{\ell 1}\frac{e_{m1}}{\det J}\frac{dn_i}{d\eta_1}\frac{dn_{i-1}}{d\eta_1}\rangle_{\omega}\cdot\langle n_{i-1}(\eta_2),n_{i-1}(\eta_2)\rangle_{\omega}}=d_{i,i-1}^{1\ell m}\ m_{i-1,i-1}\\
\mathcal{D}_{i,i}^{1\ell m}\ =\ &-\langle e_{\ell 1}\frac{e_{m1}}{\det J}\frac{\partial}{\partial\eta_1}N_i(\eta_1,\eta_2),\frac{\partial}{\partial\eta_1}N_i(\eta_1,\eta_2)\rangle_{\widehat{\Omega}}=\\
&-\langle e_{\ell 1}\frac{e_{m1}}{\det J}\frac{dn_i}{d\eta_1}n_i(\eta_2),\frac{dn_i}{d\eta_1}n_i(\eta_2)\rangle_{\widehat{\Omega}}=\\
&-\langle e_{\ell 1}\frac{e_{m1}}{\det J}\frac{dn_i}{d\eta_1}n_i(\eta_2),\frac{dn_i}{d\eta_1}n_i(\eta_2)\rangle_{\widehat{\Omega}}=\\
&-\langle e_{\ell 1}\frac{e_{m1}}{\det J}\frac{dn_i}{d\eta_1}\frac{dn_i}{d\eta_1},n_i(\eta_2)n_i(\eta_2)\rangle_{\widehat{\Omega}}=\\
&\overline{-\langle e_{\ell 1}\frac{e_{m1}}{\det J}\frac{dn_i}{d\eta_1}\frac{dn_i}{d\eta_1}\rangle_{\omega}\cdot\langle n_i(\eta_2),n_i(\eta_2)\rangle_{\omega}}=d_{i,i}^{1\ell m}\ m_{i,i}\\
\mathcal{D}_{i,i+1}^{1\ell m}\ =\ &-\langle e_{\ell 1}\frac{e_{m1}}{\det J}\frac{\partial}{\partial\eta_1}N_i(\eta_1,\eta_2),\frac{\partial}{\partial\eta_1}N_{i+1}(\eta_1,\eta_2)\rangle_{\widehat{\Omega}}=\\
&-\langle e_{\ell 1}\frac{e_{m1}}{\det J}\frac{dn_i}{d\eta_1}n_i(\eta_2),\frac{dn_{i+1}}{d\eta_1}n_{i+1}(\eta_2)\rangle_{\widehat{\Omega}}=\\
&-\langle e_{\ell 1}\frac{e_{m1}}{\det J}\frac{dn_i}{d\eta_1}n_{i+1}(\eta_2),\frac{dn_{i+1}}{d\eta_1}n_{i+1}(\eta_2)\rangle_{\widehat{\Omega}}=\\
&-\langle e_{\ell 1}\frac{e_{m1}}{\det J}\frac{dn_i}{d\eta_1}\frac{dn_{i+1}}{d\eta_1},n_{i+1}(\eta_2)n_{i+1}(\eta_2)\rangle_{\widehat{\Omega}}=\\
&\overline{-\langle e_{\ell 1}\frac{e_{m1}}{\det J}\frac{dn_i}{d\eta_1},\frac{dn_{i+1}}{d\eta_1}\rangle_{\omega}\cdot\langle n_{i+1}(\eta_2),n_{i+1}(\eta_2)\rangle_{\omega}}=d_{i,i+1}^{1\ell m}\ m_{i+1,i+1}\qquad(9.133)\\
\mathcal{D}_{i,i+n-2}^{1\ell m}\ =\ &-\langle e_{\ell 1}\frac{e_{m1}}{\det J}\frac{\partial}{\partial\eta_1}N_i(\eta_1,\eta_2),\frac{\partial}{\partial\eta_1}N_{i+n-2}(\eta_1,\eta_2)\rangle_{\widehat{\Omega}}=\\
&-\langle e_{\ell 1}\frac{e_{m1}}{\det J}\frac{dn_i}{d\eta_1}n_i(\eta_2),\frac{dn_{i+n-2}}{d\eta_1}n_{i+n-2}(\eta_2)\rangle_{\widehat{\Omega}}=\\
&-\langle e_{\ell 1}\frac{e_{m1}}{\det J}\frac{dn_i}{d\eta_1}n_{i-1}(\eta_2),\frac{dn_{i-1}}{d\eta_1}n_{i+n-2}(\eta_2)\rangle_{\widehat{\Omega}}=\\
&-\langle e_{\ell 1}\frac{e_{m1}}{\det J}\frac{dn_i}{d\eta_1}\frac{dn_{i-1}}{d\eta_1},n_{i-1}(\eta_2)n_{i+n-2}(\eta_2)\rangle_{\widehat{\Omega}}=\\
&-\langle e_{\ell 1}\frac{e_{m1}}{\det J}\frac{dn_i}{d\eta_1}\frac{dn_{i-1}}{d\eta_1}\rangle_{\omega}\cdot\langle n_{i-1}(\eta_2),n_{i+n-2}(\eta_2)\rangle_{\omega}\simeq d_{i,i-1}^{1\ell m}\ m_{i-1,i+n-2}\\
\mathcal{D}_{i,i+n-1}^{1\ell m}\ =\ &-\langle e_{\ell 1}\frac{e_{m1}}{\det J}\frac{\partial}{\partial\eta_1}N_i(\eta_1,\eta_2),\frac{\partial}{\partial\eta_1}N_{i+n-1}(\eta_1,\eta_2)\rangle_{\widehat{\Omega}}=\\
&-\langle e_{\ell 1}\frac{e_{m1}}{\det J}\frac{dn_i}{d\eta_1}n_i(\eta_2),\frac{dn_{i+n-1}}{d\eta_1}n_{i+n-1}(\eta_2)\rangle_{\widehat{\Omega}}=
\end{aligned}
$$

$$
\begin{aligned}
& -\langle e_{\ell 1}\frac{e_{m1}}{\det J}\frac{dn_i}{d\eta_1}n_i(\eta_2),\frac{dn_i}{d\eta_1}n_{i+n-1}(\eta_2)\rangle_{\widehat{\Omega}} = \\
& -\langle e_{\ell 1}\frac{e_{m1}}{\det J}\frac{dn_i}{d\eta_1}\frac{dn_i}{d\eta_1},n_i(\eta_2)n_{i+n-1}(\eta_2)\rangle_{\widehat{\Omega}} = \\
& -\langle e_{\ell 1}\frac{e_{m1}}{\det J}\frac{dn_i}{d\eta_1},\frac{dn_i}{d\eta_1}\rangle_{\omega}\cdot\langle n_i(\eta_2),n_{i+n-1}(\eta_2)\rangle_{\omega}\simeq d_{i,i}^{1\ell m}\ m_{i,i+n-1} \\
\mathcal{D}_{i,i+n}^{1\ell m} \;=\; & -\langle e_{\ell 1}\frac{e_{m1}}{\det J}\frac{\partial}{\partial\eta_1}N_i(\eta_1,\eta_2),\frac{\partial}{\partial\eta_1}N_{i+n}(\eta_1,\eta_2)\rangle_{\widehat{\Omega}} = \\
& -\langle e_{\ell 1}\frac{e_{m1}}{\det J}\frac{dn_i}{d\eta_1}n_i(\eta_2),\frac{dn_{i+n}}{d\eta_1}n_{i+n}(\eta_2)\rangle_{\widehat{\Omega}} = \\
& -\langle e_{\ell 1}\frac{e_{m1}}{\det J}\frac{dn_i}{d\eta_1}n_{i+1}(\eta_2),\frac{dn_{i+1}}{d\eta_1}n_{i+n}(\eta_2)\rangle_{\widehat{\Omega}} = \\
& -\langle e_{\ell 1}\frac{e_{m1}}{\det J}\frac{dn_i}{d\eta_1}\frac{dn_{i+1}}{d\eta_1},n_{i+1}(\eta_2)n_{i+n}(\eta_2)\rangle_{\widehat{\Omega}} = \\
& -\langle e_{\ell 1}\frac{e_{m1}}{\det J}\frac{dn_i}{d\eta_1},\frac{dn_{i+1}}{d\eta_1}\rangle_{\omega}\cdot\langle n_{i+1}(\eta_2),n_{i+n}(\eta_2)\rangle_{\omega}\simeq d_{i,i+1}^{1\ell m}\ m_{i+1,i+n} \quad (9.134)
\end{aligned}
$$

9.9.2 η_2 Direction Operators

The determination of $d_{i,j}^{2\ell m}$ is attained via derivation of the exact decomposition of integrals $\mathcal{D}_{i,i-n+1}^{2\ell m}$, $\mathcal{D}_{i,i}^{2\ell m}$ and $\mathcal{D}_{i,i+n-1}^{2\ell m}$ along the principal η_2 sweep line $\{i-n+1,i,i+n-1\}$, (see Figure 9.1). The decomposition of integral $\mathcal{D}_{i,i-n+1}^{2\ell m}$ is

$$
\begin{aligned}
\mathcal{D}_{i,i-n+1}^{1\ell m} \;=\; & -\int_{\widehat{\Omega}} e_{\ell 2}\frac{e_{m2}}{\det J}\frac{\partial N_i(\eta_1,\eta_2)}{\partial\eta_2}\frac{\partial N_{i-n+1}}{\partial\eta_2}\,d\boldsymbol{\eta} = \\
& -\int_{\widehat{\Omega}} e_{\ell 2}\frac{e_{m2}}{\det J}\frac{dn_i}{d\eta_2}n_i(\eta_1)\frac{dn_{i-n+1}}{d\eta_2}n_{i-n+1}(\eta_1)\,d\boldsymbol{\eta} = \\
& -e_{\ell 2}(\boldsymbol{\eta}_1)\left(\frac{e_{m2}}{\det J}\right)_{\tilde{\boldsymbol{\eta}}_1}\int_{\widehat{\Omega}_1}\frac{dn_i}{d\eta_2}n_i(\eta_1)\frac{dn_{i-n+1}}{d\eta_2}n_i(\eta_1)\,d\boldsymbol{\eta} \\
& -e_{\ell 2}(\boldsymbol{\eta}_2)\left(\frac{e_{m2}}{\det J}\right)_{\tilde{\boldsymbol{\eta}}_2}\int_{\widehat{\Omega}_2}\frac{dn_i}{d\eta_2}n_i(\eta_1)\frac{dn_{i-n+1}}{d\eta_2}n_i(\eta_1)\,d\boldsymbol{\eta} = \\
& -\left(\int_{\omega_1}n_i(\eta_1)\,n_i(\eta_1)\,d\eta\right)\cdot\left(e_{\ell 2}(\boldsymbol{\eta}_1)\left(\frac{e_{m2}}{\det J}\right)_{\tilde{\boldsymbol{\eta}}_1}\int_{\omega_1}\frac{dn_i}{d\eta_2}\frac{dn_{i-n+1}}{d\eta_2}\,d\eta\right) \\
& -\left(\int_{\omega_2}n_i(\eta_1)\,n_i(\eta_1)\,d\eta\right)\cdot\left(e_{\ell 2}(\boldsymbol{\eta}_2)\left(\frac{e_{m2}}{\det J}\right)_{\tilde{\boldsymbol{\eta}}_2}\int_{\omega_1}\frac{dn_i}{d\eta_2}\frac{dn_{i-n+1}}{d\eta_2}\,d\eta\right)
\end{aligned}
$$

(9.135)

Equation (9.69) allows writing (9.135) as

$$\begin{aligned}
\mathcal{D}^{2\ell m}_{i,i-n+1} \;=\; & -\left(\int_{\omega_1} \mathrm{n}_i(\eta_1)\,\mathrm{n}_i(\eta_1)\;d\eta + \int_{\omega_2} \mathrm{n}_i(\eta_1)\,\mathrm{n}_i(\eta_1)\;d\eta\right)\times \\
& \left(\frac{1}{2}\left(e_{\ell 2}(\boldsymbol{\eta}_1)\left(\frac{e_{m2}}{\det J}\right)_{\tilde{\boldsymbol{\eta}}_1} + e_{\ell 2}(\boldsymbol{\eta}_2)\left(\frac{e_{m2}}{\det J}\right)_{\tilde{\boldsymbol{\eta}}_2}\right)\times\right. \\
& \left.\int_{\omega_1} \frac{d\mathrm{n}_i}{d\eta_2}\frac{d\mathrm{n}_{i-n+1}}{d\eta_2}\,d\eta\right) = \\
& -\left(\int_{\omega} \mathrm{n}_i(\eta_1)\,\mathrm{n}_i(\eta_1)\;d\eta\right)\times \\
& \left(\frac{1}{2}\left(e_{\ell 2}(\boldsymbol{\eta}_1)\left(\frac{e_{m2}}{\det J}\right)_{\tilde{\boldsymbol{\eta}}_1} + e_{\ell 2}(\boldsymbol{\eta}_2)\left(\frac{e_{m2}}{\det J}\right)_{\tilde{\boldsymbol{\eta}}_2}\right)\times\right. \\
& \left.\int_{\omega_1} \frac{d\mathrm{n}_i}{d\eta_2}\frac{d\mathrm{n}_{i-n+1}}{d\eta_2}\,d\eta\right)
\end{aligned} \tag{9.136}$$

In analogy with (9.115), the 1-D diffusion integral in this expression is multiplied by the average of two metric data expressions. Each expression is evaluated in the 2-D element that shares the 1-D element on which the relevant integral is computed. Consequently, this diffusion operator is obtained through the formula

$$\begin{aligned}
&\overline{\langle e_{\ell 2}\frac{e_{m2}}{\det J}\frac{d\mathrm{n}_i}{d\eta_2}, \frac{d\mathrm{n}_j}{d\eta_2}\rangle_\omega} \equiv \\
&\quad \sum_{k=1}^{2}\left(\frac{1}{2}\left(e_{\ell 2}\left(\boldsymbol{\eta}_{\widehat{\Omega}_{k1}}\right)\left(\frac{e_{m2}}{\det J}\right)_{\tilde{\boldsymbol{\eta}}_{\widehat{\Omega}_{k1}}} + e_{\ell 2}\left(\boldsymbol{\eta}_{\widehat{\Omega}_{k2}}\right)\left(\frac{e_{m2}}{\det J}\right)_{\tilde{\boldsymbol{\eta}}_{\widehat{\Omega}_{k2}}}\right)\int_{\omega_k}\frac{d\mathrm{n}_i}{d\eta_2}\frac{d\mathrm{n}_j}{d\eta_2}\,d\eta\right)
\end{aligned} \tag{9.137}$$

where the subscripts $\widehat{\Omega}_{k1}$ and $\widehat{\Omega}_{k2}$ respectively, denote the two 2-D elements that share the 1-D element ω_k. Insertion of this expression into (9.136) leads to the

formula

$$\mathcal{D}_{i,i-n+1}^{1\ell m} = -\langle \mathrm{n}_i, \mathrm{n}_i \rangle_\omega \cdot \overline{\langle e_{\ell 2} \frac{e_{m2}}{\det J} \frac{d\mathrm{n}_i}{d\eta_2}, \frac{d\mathrm{n}_{i-n+1}}{d\eta_2} \rangle_\omega} = -m_{i,i} \cdot \overline{\langle e_{\ell 2} \frac{e_{m2}}{\det J} \frac{d\mathrm{n}_i}{d\eta_2}, \frac{d\mathrm{n}_{i-n+1}}{d\eta_2} \rangle_\omega} \tag{9.138}$$

The decomposition of integral $\mathcal{D}_{i,i}^{2\ell m}$ is

$$\begin{aligned}
\mathcal{D}_{i,i}^{2\ell m} &= -\int_{\widehat{\Omega}} e_{\ell 2} \frac{e_{m2}}{\det J} \frac{\partial N_i}{\partial \eta_2} \frac{\partial N_i}{\partial \eta_2} \, d\boldsymbol{\eta} = \\
&-\int_{\widehat{\Omega}} e_{\ell 2} \frac{e_{m2}}{\det J} \frac{d\mathrm{n}_i}{d\eta_2} \mathrm{n}_i(\eta_1) \frac{d\mathrm{n}_i}{d\eta_2} \mathrm{n}_i(\eta_1) \, d\boldsymbol{\eta} = \\
&-e_{\ell 2}(\boldsymbol{\eta}_1) \left(\frac{e_{m2}}{\det J} \right)_{\tilde{\boldsymbol{\eta}}_1} \int_{\widehat{\Omega}_1} \frac{d\mathrm{n}_i}{d\eta_2} \mathrm{n}_i(\eta_1) \frac{d\mathrm{n}_i}{d\eta_2} \mathrm{n}_i(\eta_1) \, d\boldsymbol{\eta} \\
&-e_{\ell 2}(\boldsymbol{\eta}_2) \left(\frac{e_{m2}}{\det J} \right)_{\tilde{\boldsymbol{\eta}}_2} \int_{\widehat{\Omega}_2} \frac{d\mathrm{n}_i}{d\eta_2} \mathrm{n}_i(\eta_1) \frac{d\mathrm{n}_i}{d\eta_2} \mathrm{n}_i(\eta_1) \, d\boldsymbol{\eta} \\
&-e_{\ell 2}(\boldsymbol{\eta}_3) \left(\frac{e_{m2}}{\det J} \right)_{\tilde{\boldsymbol{\eta}}_3} \int_{\widehat{\Omega}_3} \frac{d\mathrm{n}_i}{d\eta_2} \mathrm{n}_i(\eta_1) \frac{d\mathrm{n}_i}{d\eta_2} \mathrm{n}_i(\eta_1) \, d\boldsymbol{\eta} \\
&-e_{\ell 2}(\boldsymbol{\eta}_4) \left(\frac{e_{m4}}{\det J} \right)_{\tilde{\boldsymbol{\eta}}_4} \int_{\widehat{\Omega}_4} \frac{d\mathrm{n}_i}{d\eta_2} \mathrm{n}_i(\eta_1) \frac{d\mathrm{n}_i}{d\eta_2} \mathrm{n}_i(\eta_1) \, d\boldsymbol{\eta} = \\
&-\left(\int_{\omega_1} \mathrm{n}_i(\eta_1) \mathrm{n}_i(\eta_1) \, d\eta \right) \cdot \left(e_{\ell 2}(\boldsymbol{\eta}_1) \left(\frac{e_{m2}}{\det J} \right)_{\tilde{\boldsymbol{\eta}}_1} \int_{\omega_1} \frac{d\mathrm{n}_i}{d\eta_2} \frac{d\mathrm{n}_i}{d\eta_2} \, d\eta \right) \\
&-\left(\int_{\omega_2} \mathrm{n}_i(\eta_1) \mathrm{n}_i(\eta_1) \, d\eta \right) \cdot \left(e_{\ell 2}(\boldsymbol{\eta}_2) \left(\frac{e_{m2}}{\det J} \right)_{\tilde{\boldsymbol{\eta}}_2} \int_{\omega_1} \frac{d\mathrm{n}_i}{d\eta_2} \frac{d\mathrm{n}_i}{d\eta_2} \, d\eta \right) \\
&-\left(\int_{\omega_1} \mathrm{n}_i(\eta_1) \mathrm{n}_i(\eta_1) \, d\eta \right) \cdot \left(e_{\ell 2}(\boldsymbol{\eta}_4) \left(\frac{e_{m2}}{\det J} \right)_{\tilde{\boldsymbol{\eta}}_4} \int_{\omega_2} \frac{d\mathrm{n}_i}{d\eta_2} \frac{d\mathrm{n}_i}{d\eta_2} \, d\eta \right) \\
&-\left(\int_{\omega_2} \mathrm{n}_i(\eta_1) \mathrm{n}_i(\eta_1) \, d\eta \right) \cdot \left(e_{\ell 2}(\boldsymbol{\eta}_3) \left(\frac{e_{m2}}{\det J} \right)_{\tilde{\boldsymbol{\eta}}_3} \int_{\omega_2} \frac{d\mathrm{n}_i}{d\eta_2} \frac{d\mathrm{n}_i}{d\eta_2} \, d\eta \right)
\end{aligned} \tag{9.139}$$

Use of the equality (9.88) allows writing (9.139) as

$$\begin{aligned}
\mathcal{D}_{i,i}^{2\ell m} &= -\left(\int_{\omega_1} \mathrm{n}_i(\eta_1) \mathrm{n}_i(\eta_1) \, d\eta + \int_{\omega_2} \mathrm{n}_i(\eta_1) \mathrm{n}_i(\eta_1) \, d\eta \right) \times \\
&\left(\frac{1}{2} \left(e_{\ell 2}(\boldsymbol{\eta}_1) \left(\frac{e_{m2}}{\det J} \right)_{\tilde{\boldsymbol{\eta}}_1} + e_{\ell 2}(\boldsymbol{\eta}_2) \left(\frac{e_{m2}}{\det J} \right)_{\tilde{\boldsymbol{\eta}}_2} \right) \int_{\omega_1} \frac{d\mathrm{n}_i}{d\eta_2} \frac{d\mathrm{n}_i}{d\eta_2} \, d\eta + \right. \\
&\left. \frac{1}{2} \left(e_{\ell 2}(\boldsymbol{\eta}_3) \left(\frac{e_{m2}}{\det J} \right)_{\tilde{\boldsymbol{\eta}}_3} + e_{\ell 2}(\boldsymbol{\eta}_4) \left(\frac{e_{m2}}{\det J} \right)_{\tilde{\boldsymbol{\eta}}_4} \right) \int_{\omega_2} \frac{d\mathrm{n}_i}{d\eta_2} \frac{d\mathrm{n}_i}{d\eta_2} \, d\eta \right) =
\end{aligned}$$

$$
\begin{aligned}
&-\left(\int_{\omega} n_i(\eta_1)\, n_i(\eta_1)\; d\eta\right) \times \\
&\left(\frac{1}{2}\left(e_{\ell 2}(\boldsymbol{\eta}_1)\left(\frac{e_{m2}}{\det J}\right)_{\tilde{\boldsymbol{\eta}}_1} + e_{\ell 2}(\boldsymbol{\eta}_2)\left(\frac{e_{m2}}{\det J}\right)_{\tilde{\boldsymbol{\eta}}_2}\right)\int_{\omega_1}\frac{dn_i}{d\eta_2}\frac{dn_i}{d\eta_2}\, d\eta\right. \\
&\left.+\frac{1}{2}\left(e_{\ell 2}(\boldsymbol{\eta}_3)\left(\frac{e_{m2}}{\det J}\right)_{\tilde{\boldsymbol{\eta}}_3} + e_{\ell 2}(\boldsymbol{\eta}_4)\left(\frac{e_{m2}}{\det J}\right)_{\tilde{\boldsymbol{\eta}}_4}\right)\int_{\omega_2}\frac{dn_i}{d\eta_2}\frac{dn_i}{d\eta_2}\, d\eta\right)
\end{aligned}
\tag{9.140}
$$

and the 1-D diffusion operator is again expressable via (9.137), hence $\mathcal{D}_{i,i}^{2\ell m}$ is cast as

$$
\mathcal{D}_{i,i}^{2\ell m} = -\langle n_i, n_i\rangle_{\omega}\cdot\overline{\langle e_{\ell 2}\frac{e_{m2}}{\det J}\frac{dn_i}{d\eta_2}, \frac{dn_i}{d\eta_2}\rangle_{\omega}} = -m_{i,i}\cdot\overline{\langle e_{\ell 2}\frac{e_{m2}}{\det J}\frac{dn_i}{d\eta_2}, \frac{dn_i}{d\eta_2}\rangle_{\omega}} \tag{9.141}
$$

Finally, the decomposition of integral $\mathcal{D}_{i,i+n-1}^{2\ell m}$ is

$$
\begin{aligned}
\mathcal{D}_{i,i+n-1}^{2\ell m} \;=\; & -\int_{\widehat{\Omega}} e_{\ell 2}\frac{e_{m2}}{\det J}\frac{\partial N_i}{\partial \eta_2}\frac{\partial N_{i+n-1}}{\partial \eta_2}\, d\boldsymbol{\eta} = \\
& -\int_{\widehat{\Omega}} e_{\ell 2}\frac{e_{m2}}{\det J}\frac{dn_i}{d\eta_2}n_i(\eta_1)\frac{dn_{i+n-1}}{d\eta_2}n_{i+n-1}(\eta_1)\; d\boldsymbol{\eta} = \\
& -e_{\ell 2}(\boldsymbol{\eta}_3)\left(\frac{e_{m2}}{\det J}\right)_{\tilde{\boldsymbol{\eta}}_3}\int_{\widehat{\Omega}_3}\frac{dn_i}{d\eta_2}n_i(\eta_1)\frac{dn_{i+n-1}}{d\eta_2}n_i(\eta_1)\; d\boldsymbol{\eta} \\
& -e_{\ell 2}(\boldsymbol{\eta}_4)\left(\frac{e_{m2}}{\det J}\right)_{\tilde{\boldsymbol{\eta}}_4}\int_{\widehat{\Omega}_4}\frac{dn_i}{d\eta_2}n_i(\eta_1)\frac{dn_{i+n-1}}{d\eta_2}n_i(\eta_1)\; d\boldsymbol{\eta} = \\
& -\left(\int_{\omega_1} n_i(\eta_1)\, n_i(\eta_1)\; d\eta\right)\cdot\left(e_{\ell 2}(\boldsymbol{\eta}_3)\left(\frac{e_{m2}}{\det J}\right)_{\tilde{\boldsymbol{\eta}}_3}\int_{\omega_2}\frac{dn_i}{d\eta_2}\frac{dn_{i+n-1}}{d\eta_2}\, d\eta\right) \\
& -\left(\int_{\omega_2} n_i(\eta_1)\, n_i(\eta_1)\; d\eta\right)\cdot\left(e_{\ell 2}(\boldsymbol{\eta}_4)\left(\frac{e_{m2}}{\det J}\right)_{\tilde{\boldsymbol{\eta}}_4}\int_{\omega_2}\frac{dn_i}{d\eta_2}\frac{dn_{i+n-1}}{d\eta_2}\, d\eta\right)
\end{aligned}
\tag{9.142}
$$

and continued use of (9.88) allows writing (9.142) as

$$
\begin{aligned}
\mathcal{D}_{i,i+n-1}^{2\ell m} \;=\; & -\left(\int_{\omega_1} n_i(\eta_1)\, n_i(\eta_1)\; d\eta + \int_{\omega_2} n_i(\eta_1)\, n_i(\eta_1)\; d\eta\right)\times \\
& \left(\frac{1}{2}\left(e_{\ell 2}(\boldsymbol{\eta}_3)\left(\frac{e_{m2}}{\det J}\right)_{\tilde{\boldsymbol{\eta}}_3} + e_{\ell 2}(\boldsymbol{\eta}_4)\left(\frac{e_{m2}}{\det J}\right)_{\tilde{\boldsymbol{\eta}}_4}\right)\int_{\omega_2}\frac{dn_i}{d\eta_2}\frac{dn_{i+n-1}}{d\eta_2}\, d\eta\right) =
\end{aligned}
$$

$$-\left(\int_{\omega} n_i(\eta_1)\, n_i(\eta_1)\; d\eta\right) \times$$
$$\left(\frac{1}{2}\left(e_{\ell 2}(\boldsymbol{\eta}_3)\left(\frac{e_{m2}}{\det J}\right)_{\tilde{\boldsymbol{\eta}}_3} + e_{\ell 2}(\boldsymbol{\eta}_4)\left(\frac{e_{m2}}{\det J}\right)_{\tilde{\boldsymbol{\eta}}_4}\right)\int_{\omega_2} \frac{dn_i}{d\eta_2}\frac{dn_{i+n-1}}{d\eta_2}\, d\eta\right) \tag{9.143}$$

which is recast via (9.137) as

$$\mathcal{D}^{2\ell m}_{i,i+n-1} = -\langle n_i, n_i\rangle_{\omega} \cdot \overline{\langle e_{\ell 2}\frac{e_{m2}}{\det J}\frac{dn_i}{d\eta_2}, \frac{dn_{i+n-1}}{d\eta_2}\rangle_{\omega}} = -m_{i,i} \cdot \overline{\langle e_{\ell 2}\frac{e_{m2}}{\det J}\frac{dn_i}{d\eta_2}, \frac{dn_{i+n-1}}{d\eta_2}\rangle_{\omega}} \tag{9.144}$$

Therefore, formulae (9.136), (9.140) and (9.143) can be made to coincide with the $\theta\Delta t d^2_{i,j}$ terms in (9.41)-(9.43) via the following definitions for $d^{2\ell m}_{i,j}$.

$$d^{2\ell m}_{i,i-n+1} = -\frac{1}{2}\left(e_{\ell 2}(\boldsymbol{\eta}_1)\left(\frac{e_{m2}}{\det J}\right)_{\tilde{\boldsymbol{\eta}}_1} + e_{\ell 2}(\boldsymbol{\eta}_2)\left(\frac{e_{m2}}{\det J}\right)_{\tilde{\boldsymbol{\eta}}_2}\right)\int_{\omega_1} \frac{dn_i}{d\eta_2}\frac{dn_{i-n+1}}{d\eta_2}\, d\eta \tag{9.145}$$

$$\begin{aligned} d^{2\ell m}_{i,i} = & -\frac{1}{2}\left(e_{\ell 2}(\boldsymbol{\eta}_1)\left(\frac{e_{m2}}{\det J}\right)_{\tilde{\boldsymbol{\eta}}_1} + e_{\ell 2}(\boldsymbol{\eta}_2)\left(\frac{e_{m2}}{\det J}\right)_{\tilde{\boldsymbol{\eta}}_2}\right)\int_{\omega_1} \frac{dn_i}{d\eta_2}\frac{dn_i}{d\eta_2}\, d\eta \\ & -\frac{1}{2}\left(e_{\ell 2}(\boldsymbol{\eta}_3)\left(\frac{e_{m2}}{\det J}\right)_{\tilde{\boldsymbol{\eta}}_3} + e_{\ell 2}(\boldsymbol{\eta}_4)\left(\frac{e_{m2}}{\det J}\right)_{\tilde{\boldsymbol{\eta}}_4}\right)\int_{\omega_2} \frac{dn_i}{d\eta_2}\frac{dn_i}{d\eta_2}\, d\eta \end{aligned} \tag{9.146}$$

$$d^{2\ell m}_{i,i+n-1} = -\frac{1}{2}\left(e_{\ell 2}(\boldsymbol{\eta}_3)\left(\frac{e_{m2}}{\det J}\right)_{\tilde{\boldsymbol{\eta}}_3} + e_{\ell 2}(\boldsymbol{\eta}_4)\left(\frac{e_{m2}}{\det J}\right)_{\tilde{\boldsymbol{\eta}}_4}\right)\int_{\omega_2} \frac{dn_i}{d\eta_2}\frac{dn_{i+n-1}}{d\eta_2}\, d\eta \tag{9.147}$$

In strict analogy with (9.124)-(9.126), these one dimensional operators contain 2-D metric data expressions. The structure of these operators induces a metric data approximation in the evaluation of the *off principal sweep line* TPF terms. Consider for example the evaluation of the representative term $\mathcal{D}^{2\ell m}_{i,i-1}$. According to the TPF formula (9.42) its value is represented via the principal sweep line operator

$d^{2\ell m}_{i-1,i-1}$. Consequently, following (9.145), (9.146) and (9.147) the associated TPF representation will embed the average of the four metric data expressions corresponding to the elements sharing node "i". However, the 2-D integral results from the contributions of elements $\widehat{\Omega}_1$ and $\widehat{\Omega}_4$ only, hence its exact expression contains two metric data expressions as evidenced by the following development.

$$
\begin{aligned}
\mathcal{D}^{2\ell m}_{i,i-1} \;=\; & -\int_{\widehat{\Omega}} e_{\ell 2}\frac{e_{m2}}{\det J}\frac{\partial N_i}{\partial \eta_2}\frac{\partial N_{i-1}}{\partial \eta_2}\, d\boldsymbol{\eta} = \\
& -\int_{\widehat{\Omega}} e_{\ell 2}\frac{e_{m2}}{\det J}\frac{dn_i}{d\eta_2}n_i(\eta_1)\frac{dn_{i-1}}{d\eta_2}n_{i-1}(\eta_1)\, d\boldsymbol{\eta} = \\
& -e_{\ell 2}(\boldsymbol{\eta}_1)\left(\frac{e_{m2}}{\det J}\right)_{\tilde{\boldsymbol{\eta}}_1}\int_{\widehat{\Omega}_1}\frac{dn_i}{d\eta_2}n_i(\eta_1)\frac{dn_{i-1}}{d\eta_2}n_{i-1}(\eta_1)\, d\boldsymbol{\eta} \\
& -e_{\ell 2}(\boldsymbol{\eta}_4)\left(\frac{e_{m2}}{\det J}\right)_{\tilde{\boldsymbol{\eta}}_4}\int_{\widehat{\Omega}_4}\frac{dn_i}{d\eta_2}n_i(\eta_1)\frac{dn_{i-1}}{d\eta_2}n_{i-1}(\eta_1)\, d\boldsymbol{\eta} = \\
& -\left(\int_{\omega_1} n_i(\eta_1)\,n_{i-1}(\eta_1)\, d\eta\right)\cdot\left(e_{\ell 2}(\boldsymbol{\eta}_1)\left(\frac{e_{m2}}{\det J}\right)_{\tilde{\boldsymbol{\eta}}_1}\int_{\omega_1}\frac{dn_{i-1}}{d\eta_2}\frac{dn_{i-1}}{d\eta_2}\, d\eta\right) \\
& -\left(\int_{\omega_1} n_i(\eta_1)\,n_{i-1}(\eta_1)\, d\eta\right)\cdot\left(e_{\ell 2}(\boldsymbol{\eta}_4)\left(\frac{e_{m2}}{\det J}\right)_{\tilde{\boldsymbol{\eta}}_4}\int_{\omega_2}\frac{dn_{i-1}}{d\eta_2}\frac{dn_{i-1}}{d\eta_2}\, d\eta\right) = \\
& -\left(\int_{\omega} n_i(\eta_1)\,n_{i-1}(\eta_1)\, d\eta\right)\times \\
& \left(e_{\ell 2}(\boldsymbol{\eta}_1)\left(\frac{e_{m2}}{\det J}\right)_{\tilde{\boldsymbol{\eta}}_1}\int_{\omega_1}\frac{dn_{i-1}}{d\eta_2}\frac{dn_{i-1}}{d\eta_2}\, d\eta\right. \\
& \left.+e_{\ell 2}(\boldsymbol{\eta}_4)\left(\frac{e_{m2}}{\det J}\right)_{\tilde{\boldsymbol{\eta}}_4}\int_{\omega_2}\frac{dn_{i-1}}{d\eta_2}\frac{dn_{i-1}}{d\eta_2}\, d\eta\right) \qquad (9.148)
\end{aligned}
$$

Here, the leading 1-D diffusion operator is obtained via formula (9.128). The TPF representation associated with (9.148) is

$$
\begin{aligned}
\mathcal{D}^{2\ell m}_{i,i-1} \;\simeq\; & -\left(\int_{\omega} n_i(\eta_1)\,n_{i-1}(\eta_1)\, d\eta\right)\times \\
& -\left(\frac{1}{2}\left(e_{\ell 2}(\boldsymbol{\eta}_1)\left(\frac{e_{m2}}{\det J}\right)_{\tilde{\boldsymbol{\eta}}_1}+e_{\ell 2}(\boldsymbol{\eta}_2)\left(\frac{e_{m2}}{\det J}\right)_{\tilde{\boldsymbol{\eta}}_2}\right)\int_{\omega_1}\frac{dn_{i-1}}{d\eta_2}\frac{dn_{i-1}}{d\eta_2}\, d\eta\right. \\
& \left.+\;\frac{1}{2}\left(e_{\ell 2}(\boldsymbol{\eta}_3)\left(\frac{e_{m2}}{\det J}\right)_{\tilde{\boldsymbol{\eta}}_3}+e_{\ell 2}(\boldsymbol{\eta}_4)\left(\frac{e_{m2}}{\det J}\right)_{\tilde{\boldsymbol{\eta}}_4}\right)\int_{\omega_2}\frac{dn_{i-1}}{d\eta_2}\frac{dn_{i-1}}{d\eta_2}\, d\eta\right)
\end{aligned}
$$

(9.149)

Therefore, comparing formulae (9.148) and (9.149) reveals that the TPF representation uses the following replacements

$$\begin{aligned} e^{i}_{\ell 2}(\boldsymbol{\eta}_1)\left(\frac{e_{m2}}{\det J}\right)^{i}_{\tilde{\boldsymbol{\eta}}_1} &\Rightarrow \frac{1}{2}\left(e^{i-1}_{\ell 2}(\boldsymbol{\eta}_1)\left(\frac{e_{m2}}{\det J}\right)^{i-1}_{\tilde{\boldsymbol{\eta}}_1} + e^{i-1}_{\ell 2}(\boldsymbol{\eta}_2)\left(\frac{e_{m2}}{\det J}\right)^{i-1}_{\tilde{\boldsymbol{\eta}}_2}\right) \\ e^{i}_{\ell 2}(\boldsymbol{\eta}_4)\left(\frac{e_{m2}}{\det J}\right)^{i}_{\boldsymbol{\eta}_4} &\Rightarrow \frac{1}{2}\left(e^{i-1}_{\ell 2}(\boldsymbol{\eta}_3)\left(\frac{e_{m2}}{\det J}\right)^{i-1}_{\tilde{\boldsymbol{\eta}}_3} + e^{i-1}_{\ell 2}(\boldsymbol{\eta}_4)\left(\frac{e_{m2}}{\det J}\right)^{i-1}_{\tilde{\boldsymbol{\eta}}_4}\right) \end{aligned} \tag{9.150}$$

where supesrcript $i-1$ indicates evaluation on the elements associated with node $i-1$.

A similar comparison with the expression for the remaining *off principal sweep line* terms shows that the TPF formulae (9.41)-(9.43) employ the replacements

$$\begin{aligned} e^{i}_{\ell 2}(\boldsymbol{\eta}_2)\left(\frac{e_{m2}}{\det J}\right)^{i}_{\tilde{\boldsymbol{\eta}}_2} &\Rightarrow \frac{1}{2}\left(e^{i+1}_{\ell 2}(\boldsymbol{\eta}_1)\left(\frac{e_{m2}}{\det J}\right)^{i+1}_{\tilde{\boldsymbol{\eta}}_1} + e^{i+1}_{\ell 2}(\boldsymbol{\eta}_2)\left(\frac{e_{m2}}{\det J}\right)^{i+1}_{\tilde{\boldsymbol{\eta}}_2}\right) \\ e^{i}_{\ell 2}(\boldsymbol{\eta}_3)\left(\frac{e_{m2}}{\det J}\right)^{i}_{\tilde{\boldsymbol{\eta}}_3} &\Rightarrow \frac{1}{2}\left(e^{i+1}_{\ell 2}(\boldsymbol{\eta}_3)\left(\frac{e_{m2}}{\det J}\right)^{i+1}_{\tilde{\boldsymbol{\eta}}_3} + e^{i+1}_{\ell 2}(\boldsymbol{\eta}_4)\left(\frac{e_{m2}}{\det J}\right)^{i+1}_{\tilde{\boldsymbol{\eta}}_4}\right) \end{aligned} \tag{9.151}$$

where supescript "$i+1$" indicates evaluation on the elements associated with node "$i+1$". Consequently, this approximation is inherently distinct from (9.130)-(9.131).

Finally, the following expressions show that the exact $\mathcal{D}^{2\ell m}_{i,j}$ are consistently represented by the TPF formulae (9.41)-(9.43)

$$\begin{aligned} \mathcal{D}^{2\ell m}_{i,i-n} &= -\langle e_{\ell 2}\frac{e_{m2}}{\det J}\frac{\partial}{\partial \eta_2}N_i(\eta_1,\eta_2), \frac{\partial}{\partial \eta_2}N_{i-n}(\eta_1,\eta_2)\rangle_{\widehat{\Omega}} = \\ &\quad -\langle e_{\ell 2}\frac{e_{m2}}{\det J}\frac{dn_i}{d\eta_2}n_i(\eta_1), \frac{dn_{i-n}}{d\eta_2}n_{i-n}(\eta_1)\rangle_{\widehat{\Omega}} = \end{aligned}$$

$$
\begin{aligned}
& -\langle e_{\ell 2}\frac{e_{m2}}{\det J}\frac{dn_{i-1}}{d\eta_2}n_i(\eta_1),\frac{dn_{i-n}}{d\eta_2}n_{i-1}(\eta_1)\rangle_{\widehat{\Omega}} = \\
& -\langle n_i(\eta_1)n_{i-1}(\eta_1),e_{\ell 2}\frac{e_{m2}}{\det J}\frac{dn_{i-1}}{d\eta_2}\frac{dn_{i-n}}{d\eta_2}\rangle_{\widehat{\Omega}} = \\
& -\langle n_i(\eta_1),n_{i-1}(\eta_1)\rangle_{\omega}\cdot\langle e_{\ell 2}\frac{e_{m2}}{\det J}\frac{dn_{i-1}}{d\eta_2},\frac{dn_{i-n}}{d\eta_2}\rangle_{\omega} \simeq m_{i,i-1}d^{2\ell m}_{i-1,i-n} \\
\mathcal{D}^{2\ell m}_{i,i-n+1} = & -\langle e_{\ell 2}\frac{e_{m2}}{\det J}\frac{\partial}{\partial\eta_2}N_i(\eta_1,\eta_2),\frac{\partial}{\partial\eta_2}N_{i-n+1}(\eta_1,\eta_2)\rangle_{\widehat{\Omega}} = \\
& -\langle e_{\ell 2}\frac{e_{m2}}{\det J}\frac{dn_i}{d\eta_2}n_i(\eta_1),\frac{dn_{i-n+1}}{d\eta_2}n_{i-n+1}(\eta_1)\rangle_{\widehat{\Omega}} = \\
& -\langle e_{\ell 2}\frac{e_{m2}}{\det J}\frac{dn_i}{d\eta_2}n_i(\eta_1),\frac{dn_{i-n+1}}{d\eta_2}n_i(\eta_1)\rangle_{\widehat{\Omega}} = \\
& -\langle n_i(\eta_1)n_i(\eta_1),e_{\ell 2}\frac{e_{m2}}{\det J}\frac{dn_i}{d\eta_2}\frac{dn_{i-n+1}}{d\eta_2}\rangle_{\widehat{\Omega}} = \\
& -\langle n_i(\eta_1),n_i(\eta_1)\rangle_{\omega}\cdot\langle e_{\ell 2}\frac{e_{m2}}{\det J}\frac{dn_i}{d\eta_2},\frac{dn_{i-n+1}}{d\eta_2}\rangle_{\omega} = m_{i,i}d^{2\ell m}_{i,i-n+1} \\
\mathcal{D}^{2\ell m}_{i,i-n+2} = & -\langle e_{\ell 2}\frac{e_{m2}}{\det J}\frac{\partial}{\partial\eta_2}N_i(\eta_1,\eta_2),\frac{\partial}{\partial\eta_2}N_{i-n+2}(\eta_1,\eta_2)\rangle_{\widehat{\Omega}} = \\
& -\langle e_{\ell 2}\frac{e_{m2}}{\det J}\frac{dn_i}{d\eta_2}n_i(\eta_1),\frac{dn_{i-n+2}}{d\eta_2}n_{i-n+2}(\eta_1)\rangle_{\widehat{\Omega}} = \\
& -\langle e_{\ell 2}\frac{e_{m2}}{\det J}\frac{dn_{i+1}}{d\eta_2}n_i(\eta_1),\frac{dn_{i-n+2}}{d\eta_2}n_{i+1}(\eta_1)\rangle_{\widehat{\Omega}} = \\
& -\langle n_i(\eta_1)n_{i+1}(\eta_1),e_{\ell 2}\frac{e_{m2}}{\det J}\frac{dn_{i+1}}{d\eta_2}\frac{dn_{i-n+2}}{d\eta_2}\rangle_{\widehat{\Omega}} = \\
& -\langle n_i(\eta_1),n_{i+1}(\eta_1)\rangle_{\omega}\cdot\langle e_{\ell 2}\frac{e_{m2}}{\det J}\frac{dn_{i+1}}{d\eta_2},\frac{dn_{i-n+2}}{d\eta_2}\rangle_{\omega} \simeq m_{i,i+1}d^{2\ell m}_{i+1,i-n+2}
\end{aligned}
\tag{9.152}
$$

$$
\begin{aligned}
\mathcal{D}^{2\ell m}_{i,i-1} = & -\langle e_{\ell 2}\frac{e_{m2}}{\det J}\frac{\partial}{\partial\eta_2}N_i(\eta_1,\eta_2),\frac{\partial}{\partial\eta_2}N_{i-1}(\eta_1,\eta_2)\rangle_{\widehat{\Omega}} = \\
& -\langle e_{\ell 2}\frac{e_{m2}}{\det J}\frac{dn_i}{d\eta_2}n_i(\eta_1),\frac{dn_{i-1}}{d\eta_2}n_{i-1}(\eta_1)\rangle_{\widehat{\Omega}} = \\
& -\langle e_{\ell 2}\frac{e_{m2}}{\det J}\frac{dn_{i-1}}{d\eta_2}n_i(\eta_1),\frac{dn_{i-1}}{d\eta_2}n_{i-1}(\eta_1)\rangle_{\widehat{\Omega}} = \\
& -\langle n_i(\eta_1)n_{i-1}(\eta_1),e_{\ell 2}\frac{e_{m2}}{\det J}\frac{dn_{i-1}}{d\eta_2}\frac{dn_{i-1}}{d\eta_2}\rangle_{\widehat{\Omega}} = \\
& -\langle n_i(\eta_1),n_{i-1}(\eta_1)\rangle_{\omega}\cdot\langle e_{\ell 2}\frac{e_{m2}}{\det J}\frac{dn_{i-1}}{d\eta_2},\frac{dn_{i-1}}{d\eta_2}\rangle_{\omega} \simeq m_{i,i-1}d^{2\ell m}_{i-1,i-1} \\
\mathcal{D}^{2\ell m}_{i,i} = & -\langle e_{\ell 2}\frac{e_{m2}}{\det J}\frac{\partial}{\partial\eta_2}N_i(\eta_1,\eta_2),\frac{\partial}{\partial\eta_2}N_i(\eta_1,\eta_2)\rangle_{\widehat{\Omega}} =
\end{aligned}
$$

$$-\langle e_{\ell 2}\frac{e_{m2}}{\det J}\frac{dn_i}{d\eta_2}n_i(\eta_1),\frac{dn_i}{d\eta_2}n_i(\eta_1)\rangle_{\widehat{\Omega}} =$$

$$-\langle e_{\ell 2}\frac{e_{m2}}{\det J}\frac{dn_i}{d\eta_2}n_i(\eta_1),\frac{dn_i}{d\eta_2}n_i(\eta_1)\rangle_{\widehat{\Omega}} =$$

$$-\langle n_i(\eta_1)n_i(\eta_1),e_{\ell 2}\frac{e_{m2}}{\det J}\frac{dn_i}{d\eta_2}\frac{dn_i}{d\eta_2}\rangle_{\widehat{\Omega}} =$$

$$-\langle n_i(\eta_1),n_i(\eta_1)\rangle_{\omega}\cdot\overline{\langle e_{\ell 2}\frac{e_{m2}}{\det J}\frac{dn_i}{d\eta_2},\frac{dn_i}{d\eta_2}\rangle_{\omega}} = m_{i,i}d_{i,i}^{2\ell m}$$

$$\mathcal{D}_{i,i+1}^{2\ell m} = -\langle e_{\ell 2}\frac{e_{m2}}{\det J}\frac{\partial}{\partial\eta_2}N_i(\eta_1,\eta_2),\frac{\partial}{\partial\eta_2}N_{i+1}(\eta_1,\eta_2)\rangle_{\widehat{\Omega}} =$$

$$-\langle e_{\ell 2}\frac{e_{m2}}{\det J}\frac{dn_i}{d\eta_2}n_i(\eta_1),\frac{dn_{i+1}}{d\eta_2}n_{i+1}(\eta_1)\rangle_{\widehat{\Omega}} =$$

$$-\langle e_{\ell 2}\frac{e_{m2}}{\det J}\frac{dn_{i+1}}{d\eta_2}n_i(\eta_1),\frac{dn_{i+1}}{d\eta_2}n_{i+1}(\eta_1)\rangle_{\widehat{\Omega}} =$$

$$-\langle n_i(\eta_1)n_{i+1}(\eta_1),e_{\ell 2}\frac{e_{m2}}{\det J}\frac{dn_{i+1}}{d\eta_2}\frac{dn_{i+1}}{d\eta_2}\rangle_{\widehat{\Omega}} =$$

$$-\langle n_i(\eta_1),n_{i+1}(\eta_1)\rangle_{\omega}\cdot\langle e_{\ell 2}\frac{e_{m2}}{\det J}\frac{dn_{i+1}}{d\eta_2},\frac{dn_{i+1}}{d\eta_2}\rangle_{\omega} \simeq m_{i,i+1}d_{i+1,i+1}^{2\ell m} \quad (9.153)$$

$$\mathcal{D}_{i,i+n-2}^{2\ell m} = -\langle e_{\ell 2}\frac{e_{m2}}{\det J}\frac{\partial}{\partial\eta_2}N_i(\eta_1,\eta_2),\frac{\partial}{\partial\eta_2}N_{i+n-2}(\eta_1,\eta_2)\rangle_{\widehat{\Omega}} =$$

$$-\langle e_{\ell 2}\frac{e_{m2}}{\det J}\frac{dn_i}{d\eta_2}n_i(\eta_1),\frac{dn_{i+n-2}}{d\eta_2}n_{i+n-2}(\eta_1)\rangle_{\widehat{\Omega}} =$$

$$-\langle e_{\ell 2}\frac{e_{m2}}{\det J}\frac{dn_{i-1}}{d\eta_2}n_i(\eta_1),\frac{dn_{i+n-2}}{d\eta_2}n_{i-1}(\eta_1)\rangle_{\widehat{\Omega}} =$$

$$-\langle n_i(\eta_1)n_{i-1}(\eta_1),e_{\ell 2}\frac{e_{m2}}{\det J}\frac{dn_{i-1}}{d\eta_2}\frac{dn_{i+n-2}}{d\eta_2}\rangle_{\widehat{\Omega}} =$$

$$-\langle n_i(\eta_1),n_{i-1}(\eta_1)\rangle_{\omega}\cdot\langle e_{\ell 2}\frac{e_{m2}}{\det J}\frac{dn_{i-1}}{d\eta_2},\frac{dn_{i+n-2}}{d\eta_2}\rangle_{\omega} \simeq m_{i,i-1}d_{i-1,i+n-2}^{2\ell m}$$

$$\mathcal{D}_{i,i+n-1}^{2\ell m} = -\langle e_{\ell 2}\frac{e_{m2}}{\det J}\frac{\partial}{\partial\eta_2}N_i(\eta_1,\eta_2),\frac{\partial}{\partial\eta_2}N_{i+n-1}(\eta_1,\eta_2)\rangle_{\widehat{\Omega}} =$$

$$-\langle e_{\ell 2}\frac{e_{m2}}{\det J}\frac{dn_i}{d\eta_2}n_i(\eta_1),\frac{dn_{i+n-1}}{d\eta_2}n_{i+n-1}(\eta_1)\rangle_{\widehat{\Omega}} =$$

$$-\langle e_{\ell 2}\frac{e_{m2}}{\det J}\frac{dn_i}{d\eta_2}n_i(\eta_1),\frac{dn_{i+n-1}}{d\eta_2}n_i(\eta_1)\rangle_{\widehat{\Omega}} =$$

$$-\langle n_i(\eta_1)n_i(\eta_1),e_{\ell 2}\frac{e_{m2}}{\det J}\frac{dn_i}{d\eta_2}\frac{dn_{i+n-1}}{d\eta_2}\rangle_{\widehat{\Omega}} =$$

$$-\langle n_i(\eta_1),n_i(\eta_1)\rangle_{\omega}\cdot\overline{\langle e_{\ell 2}\frac{e_{m2}}{\det J}\frac{dn_i}{d\eta_2},\frac{dn_{i+n-1}}{d\eta_2}\rangle_{\omega}} = m_{i,i}d_{i,i+n-1}^{2\ell m}$$

$$\mathcal{D}_{i,i+n}^{2\ell m} = -\langle e_{\ell 2}\frac{e_{m2}}{\det J}\frac{\partial}{\partial\eta_2}N_i(\eta_1,\eta_2),\frac{\partial}{\partial\eta_2}N_{i+n}(\eta_1,\eta_2)\rangle_{\widehat{\Omega}} =$$

$$-\langle e_{\ell 2}\frac{e_{m2}}{\det J}\frac{dn_i}{d\eta_2}n_i(\eta_1),\frac{dn_{i+n}}{d\eta_2}n_{i+n}(\eta_1)\rangle_{\widehat{\Omega}} =$$

$$-\langle e_{\ell 2}\frac{e_{m2}}{\det J}\frac{dn_{i+1}}{d\eta_2}n_i(\eta_1),\frac{dn_{i+n}}{d\eta_2}n_{i+1}(\eta_1)\rangle_{\widehat{\Omega}} =$$

$$-\langle n_i(\eta_1)n_{i+1}(\eta_1),e_{\ell 2}\frac{e_{m2}}{\det J}\frac{dn_{i+1}}{d\eta_2}\frac{dn_{i+n}}{d\eta_2}\rangle_{\widehat{\Omega}} =$$

$$-\langle n_i(\eta_1),n_{i+1}(\eta_1)\rangle_{\omega}\cdot\langle e_{\ell 2}\frac{e_{m2}}{\det J}\frac{dn_{i+1}}{d\eta_2},\frac{dn_{i+n}}{d\eta_2}\rangle_{\omega}\simeq m_{i,i+1}d^{1\ell m}_{i+1,i+n} \quad (9.154)$$

For the implicit primitive coordinate diffusion operators, both the parallel and cross derivative terms are expressed in terms of curvilinear coordinate operators. However, the present TPF dispenses with computational coordinate cross-derivative terms, whereas it accurately represents the leading two terms in the following primitive-coordinate 2^{nd} order differential operator formulae

$$\begin{aligned}\det J\left(\frac{\partial}{\partial x_1}\left((\cdot)\frac{\partial(\cdot)}{\partial x_1}\right)\right) &= e_{11}\left(\frac{\partial}{\partial\eta_1}\left(\frac{e_{11}}{\det J}(\cdot)\frac{\partial(\cdot)}{\partial\eta_1}\right)\right)+e_{12}\left(\frac{\partial}{\partial\eta_2}\left(\frac{e_{12}}{\det J}(\cdot)\frac{\partial(\cdot)}{\partial\eta_2}\right)\right)\\ &+ e_{11}\left(\frac{\partial}{\partial\eta_1}\left(\frac{e_{12}}{\det J}(\cdot)\frac{\partial(\cdot)}{\partial\eta_2}\right)\right)+e_{12}\left(\frac{\partial}{\partial\eta_2}\left(\frac{e_{11}}{\det J}(\cdot)\frac{\partial(\cdot)}{\partial\eta_1}\right)\right)\end{aligned} \quad (9.155)$$

$$\begin{aligned}\det J\left(\frac{\partial}{\partial x_1}\left((\cdot)\frac{\partial(\cdot)}{\partial x_2}\right)\right) &= e_{11}\left(\frac{\partial}{\partial\eta_1}\left(\frac{e_{21}}{\det J}(\cdot)\frac{\partial(\cdot)}{\partial\eta_1}\right)\right)+e_{12}\left(\frac{\partial}{\partial\eta_2}\left(\frac{e_{22}}{\det J}(\cdot)\frac{\partial(\cdot)}{\partial\eta_2}\right)\right)\\ &+ e_{11}\left(\frac{\partial}{\partial\eta_1}\left(\frac{e_{22}}{\det J}(\cdot)\frac{\partial(\cdot)}{\partial\eta_2}\right)\right)+e_{12}\left(\frac{\partial}{\partial\eta_2}\left(\frac{e_{21}}{\det J}(\cdot)\frac{\partial(\cdot)}{\partial\eta_1}\right)\right)\end{aligned} \quad (9.156)$$

$$\begin{aligned}\det J\left(\frac{\partial}{\partial x_2}\left((\cdot)\frac{\partial(\cdot)}{\partial x_1}\right)\right) &= e_{21}\left(\frac{\partial}{\partial\eta_1}\left(\frac{e_{11}}{\det J}(\cdot)\frac{\partial(\cdot)}{\partial\eta_1}\right)\right)+e_{22}\left(\frac{\partial}{\partial\eta_2}\left(\frac{e_{12}}{\det J}(\cdot)\frac{\partial(\cdot)}{\partial\eta_2}\right)\right)\\ &+ e_{21}\left(\frac{\partial}{\partial\eta_1}\left(\frac{e_{12}}{\det J}(\cdot)\frac{\partial(\cdot)}{\partial\eta_2}\right)\right)+e_{22}\left(\frac{\partial}{\partial\eta_2}\left(\frac{e_{11}}{\det J}(\cdot)\frac{\partial(\cdot)}{\partial\eta_1}\right)\right)\end{aligned} \quad (9.157)$$

$$\det J\left(\frac{\partial}{\partial x_2}\left((\cdot)\frac{\partial(\cdot)}{\partial x_2}\right)\right) = e_{21}\left(\frac{\partial}{\partial\eta_1}\left(\frac{e_{21}}{\det J}(\cdot)\frac{\partial(\cdot)}{\partial\eta_1}\right)\right)+e_{22}\left(\frac{\partial}{\partial\eta_2}\left(\frac{e_{22}}{\det J}(\cdot)\frac{\partial(\cdot)}{\partial\eta_2}\right)\right)$$

$$+ \quad e_{21}\left(\frac{\partial}{\partial \eta_1}\left(\frac{e_{22}}{\det J}(\cdot)\frac{\partial(\cdot)}{\partial \eta_2}\right)\right) + e_{22}\left(\frac{\partial}{\partial \eta_2}\left(\frac{e_{21}}{\det J}(\cdot)\frac{\partial(\cdot)}{\partial \eta_1}\right)\right) \tag{9.158}$$

where "$(\cdot)$" denotes a differentiable function.

9.10 TPF Error Structure

The precise structure of the TPF error is now derived, starting with the general form. Thereafter, the expressions specific to the convection and diffusion term errors are individually determined. The overall $O(\Delta t^2)$ error is then documented and subsequently the order of magnitude of all such errors is discussed.

9.10.1 Generic Error Expression

The TPF error is defined as

$$\varepsilon_{i,j} = a_{i,j} - \tilde{a}_{i,j} \tag{9.159}$$

The exact blocks $a_{i,j}$ are computed with (9.45)-(9.47), whereas the TPF blocks $\tilde{a}_{i,j}$ are computed using (9.41)-(9.43). Consequently, the error associated with the TPF expressions is

$$\begin{aligned}
\varepsilon_{i,i-n} &= \theta\Delta t\left(D^2_{i,i-n} - m_{i,i-1}d^2_{i-1,i-n}\right) + \theta\Delta t\left(D^1_{i,i-n} - d^1_{i,i-1}m_{i-1,i-n}\right) - \\
&\quad \theta^2\Delta t^2 d^1_{i,i-1}d^2_{i-1,i-n} \\
\varepsilon_{i,i-n+1} &= \theta\Delta t\left(D^1_{i,i-n+1} - d^1_{i,i}m_{i,i-n+1}\right) - \theta^2\Delta t^2 d^1_{i,i}d^2_{i,i-n+1}
\end{aligned}$$

$$\varepsilon_{i,i-n+2} = \theta\Delta t\left(D^2_{i,i-n+2} - m_{i,i+1}d^2_{i+1,i-n+2}\right) + \theta\Delta t\left(D^1_{i,i-n+2} - d^1_{i,i+1}m_{i+1,i-n+2}\right) - \theta^2\Delta t^2 d^1_{i,i+1}d^2_{i+1,i-n+2} \tag{9.160}$$

$$\begin{aligned}
\varepsilon_{i,i-1} &= \theta\Delta t\left(D^2_{i,i-1} - m_{i,i-1}d^2_{i-1,i-1}\right) - \theta^2\Delta t^2 d^1_{i,i-1}d^2_{i-1,i-1} \\
\varepsilon_{i,i} &= -\theta^2\Delta t^2 d^1_{i,i}d^2_{i,i} \\
\varepsilon_{i,i+1} &= \theta\Delta t\left(D^2_{i,i+1} - m_{i,i+1}d^2_{i+1,i+1}\right) - \theta^2\Delta t^2 d^1_{i,i+1}d^2_{i+1,i+1}
\end{aligned} \tag{9.161}$$

$$\varepsilon_{i,i+n-2} = \theta\Delta t\left(D^2_{i,i+n-2} - m_{i,i-1}d^2_{i-1,i+n-2}\right) + \theta\Delta t\left(D^1_{i,i+n-2} - d^1_{i,i-1}m_{i-1,i+n-2}\right) - \theta^2\Delta t^2 d^1_{i,i-1}d^2_{i-1,i+n-2}$$

$$\varepsilon_{i,i+n-1} = \theta\Delta t\left(D^1_{i,i+n-1} - d^1_{i,i}m_{i,i+n-1}\right) - \theta^2\Delta t^2 d^1_{i,i}d^2_{i,i+n-1}$$

$$\varepsilon_{i,i+n} = \theta\Delta t\left(D^2_{i,i+n} - m_{i,i+1}d^2_{i+1,i+n}\right) + \theta\Delta t\left(D^1_{i,i+n} - d^1_{i,i+1}m_{i+1,i+n}\right) - \theta^2\Delta t^2 d^1_{i,i+1}d^2_{i+1,i+n} \tag{9.162}$$

The subscript structure in these error formulae shows that the classic order Δt^2 error terms coexist with a metric-data approximation and a jacobian evaluation error. Therefore, the TPF spatial approximation, identified at the end of Section 5, appears in the form of both a replacement of some individual pieces of metric data with associated averages and an evaluation of some jacobians at locations adjacent to the exact ones. The latter occurs when the array f_α is a non-linear function of q. For this general case, the TPF formulae (9.41)-(9.43) exactly represent at all nodes the η_2 direction jacobian terms, whereas they render the η_1 direction jacobian terms precise at nodes $i-1$, i , $i+1$ and approximately correct at the six remaining

locations. Concerning the metric data representation, the TPF scheme replaces, at nodes $i-n$, $i-n+1$, $i-n+2$, $i+n-2$, $i+n-1$ and $i+n$, the local values of the metrics $e_{\ell 1}$ with metric data averages, see (9.82)-(9.83) and (9.130)-(9.131), whereas it yields the exact values at nodes $i-1$, i and $i+1$. Concurrently, the local value of the metrics $e_{\ell 2}$ at nodes $i-n$, $i-n+2$, $i-1$, $i+1$, $i+n-2$ and $i+n$ are analogously substituted with element averages, as indicated by (9.103)-(9.104) and (9.150)-(9.151), whereas an exact representation is obtained at nodes $i-n+1$, i and $i+n-1$. These metric-data errors directly depend upon the distribution of the computational-node primitive coordinates. Therefore, a smooth distribution of primitive coordinate data reduces this type of error in the TPF Jacobian.

The error (9.159) can be resolved into components

$$\varepsilon_{i,j} = \varepsilon^{c}_{i,j} + \varepsilon^{d}_{i,j} + \varepsilon^{\Delta t^2}_{i,j} \tag{9.163}$$

Here, $\varepsilon^{c}_{i,j}$ is the convection term error in the $\theta\Delta t$ jacobian components, and $\varepsilon^{d}_{i,j}$ is the diffusion term error in the same component. Simultaneously, $\varepsilon^{\Delta t^2}_{i,j}$ is the $O(\Delta t^2)$ error due to the product of the 1-D convection and diffusion terms. For the determination of the explicit form of these errors, the jacobian matrices must appear in the actual TPF 2-D jacobian expressions. These are obtained upon multiplication of the tensor product differential operators, (9.62) and (9.113), with appropriate Jacobian terms, as evaluated at the computational node indicated by the second subscript in the symbolic operators , see (9.60), (9.111). The following representative expressions

reiterate this jacobian decomposition, without implied repeated-index summation

$$\left(D^1_{i,i+1}\right)^c = d^{1\ell}_{i,i+1}\left[\frac{\partial f_\ell}{\partial q}\right]_{i+1} m_{i+1,i+1} = \mathcal{D}^{1\ell}_{i,i+1}\left[\frac{\partial f_\ell}{\partial q}\right]_{i+1} \tag{9.164}$$

$$\left(D^2_{i,i+n-1}\right)^c = m_{i,i} d^{2\ell}_{i,i+n-1}\left[\frac{\partial f_\ell}{\partial q}\right]_{i+n-1} = \mathcal{D}^{2\ell}_{i,i+n-1}\left[\frac{\partial f_\ell}{\partial q}\right]_{i+n-1} \tag{9.165}$$

the companion representative formulae for the diffusion operator are

$$\left(D^1_{i,i+1}\right)^d = d^{1\ell m}_{i,i+1}\left[\frac{\partial f_{\ell m}}{\partial q}\right]_{i+1} m_{i+1,i+1} = \mathcal{D}^{1\ell m}_{i,i+1}\left[\frac{\partial f_{\ell m}}{\partial q}\right]_{i+1} \tag{9.166}$$

$$\left(D^2_{i,i+n-1}\right)^d = m_{i,i} d^{2\ell m}_{i,i+n-1}\left[\frac{\partial f_{\ell m}}{\partial q}\right]_{i+n-1} = \mathcal{D}^{2\ell m}_{i,i+n-1}\left[\frac{\partial f_{\ell m}}{\partial q}\right]_{i+n-1} \tag{9.167}$$

The TPF formulae (9.41)-(9.43) are now expressed in terms of this jacobian decomposition and the error components are then derived.

9.10.2 Convection Term Errors

The actual TPF 2-D jacobian linear algebra statement for the convection terms is

$$\begin{aligned}
\tilde{a}_{i,i-n} &= M_{i,i-n} + \theta\Delta t m_{i,i-1} d^{2\ell}_{i-1,i-n}\left[\frac{\partial f_\ell}{\partial q}\right]_{i-n} + \theta\Delta t d^{1\ell}_{i,i-1} m_{i-1,i-n}\left[\frac{\partial f_\ell}{\partial q}\right]_{i-1} + \\
&\quad \theta^2\Delta t^2 d^{1\ell}_{i,i-1} d^{2\ell}_{i-1,i-n}\left[\frac{\partial f_\ell}{\partial q}\right]_{i-1}\left[\frac{\partial f_\ell}{\partial q}\right]_{i-n} \\
\tilde{a}_{i,i-n+1} &= M_{i,i-n+1} + \theta\Delta t m_{i,i} d^{2\ell}_{i,i-n+1}\left[\frac{\partial f_\ell}{\partial q}\right]_{i-n+1} + \theta\Delta t d^{1\ell}_{i,i} m_{i,i-n+1}\left[\frac{\partial f_\ell}{\partial q}\right]_{i} + \\
&\quad \theta^2\Delta t^2 d^{1\ell}_{i,i} d^{2\ell}_{i,i-n+1}\left[\frac{\partial f_\ell}{\partial q}\right]_{i}\left[\frac{\partial f_\ell}{\partial q}\right]_{i-n+1} \\
\tilde{a}_{i,i-n+2} &= M_{i,i-n+2} + \theta\Delta t m_{i,i+1} d^{2\ell}_{i+1,i-n+2}\left[\frac{\partial f_\ell}{\partial q}\right]_{i-n+2} + \theta\Delta t d^{1\ell}_{i,i+1} m_{i+1,i-n+2}\left[\frac{\partial f_\ell}{\partial q}\right]_{i+1} \\
&+ \theta^2\Delta t^2 d^{1\ell}_{i,i+1} d^{2\ell}_{i+1,i-n+2}\left[\frac{\partial f_\ell}{\partial q}\right]_{i+1}\left[\frac{\partial f_\ell}{\partial q}\right]_{i-n+2}
\end{aligned} \tag{9.168}$$

$$\begin{aligned}
\tilde{a}_{i,i-1} &= M_{i,i-1} + \theta\Delta t m_{i,i-1} d^{2\ell}_{i-1,i-1}\left[\frac{\partial f_\ell}{\partial q}\right]_{i-1} + \theta\Delta t d^{1\ell}_{i,i-1} m_{i-1,i-1}\left[\frac{\partial f_\ell}{\partial q}\right]_{i-1} + \\
&\quad \theta^2\Delta t^2 d^{1\ell}_{i,i-1} d^{2\ell}_{i-1,i-1}\left[\frac{\partial f_\ell}{\partial q}\right]_{i-1}\left[\frac{\partial f_\ell}{\partial q}\right]_{i-1}
\end{aligned}$$

$$
\begin{aligned}
\tilde{a}_{i,i} &= M_{i,i} + \theta\Delta t m_{i,i} d^{2\ell}_{i,i} \left[\frac{\partial f_\ell}{\partial q}\right]_i + \theta\Delta t d^{1\ell}_{i,i} m_{i,i} \left[\frac{\partial f_\ell}{\partial q}\right]_i + \\
&\quad \theta^2\Delta t^2 d^{1\ell}_{i,i} d^{2\ell}_{i,i} \left[\frac{\partial f_\ell}{\partial q}\right]_i \left[\frac{\partial f_\ell}{\partial q}\right]_i \\
\tilde{a}_{i,i+1} &= M_{i,i+1} + \theta\Delta t m_{i,i+1} d^{2\ell}_{i+1,i+1} \left[\frac{\partial f_\ell}{\partial q}\right]_{i+1} + \theta\Delta t d^{1\ell}_{i,i+1} m_{i+1,i+1} \left[\frac{\partial f_\ell}{\partial q}\right]_{i+1} + \\
&\quad \theta^2\Delta t^2 d^{1\ell}_{i,i+1} d^{2\ell}_{i+1,i+1} \left[\frac{\partial f_\ell}{\partial q}\right]_{i+1} \left[\frac{\partial f_\ell}{\partial q}\right]_{i+1}
\end{aligned} \tag{9.169}
$$

$$
\begin{aligned}
\tilde{a}_{i,i+n-2} &= M_{i,i+n-2} + \theta\Delta t m_{i,i-1} d^{2\ell}_{i-1,i+n-2} \left[\frac{\partial f_\ell}{\partial q}\right]_{i+n-2} + \theta\Delta t d^{1\ell}_{i,i-1} m_{i-1,i+n-2} \left[\frac{\partial f_\ell}{\partial q}\right]_{i-1} \\
&+ \theta^2\Delta t^2 d^{1\ell}_{i,i-1} d^{2\ell}_{i-1,i+n-2} \left[\frac{\partial f_\ell}{\partial q}\right]_{i-1} \left[\frac{\partial f_\ell}{\partial q}\right]_{i+n-2} \\
\tilde{a}_{i,i+n-1} &= M_{i,i+n-1} + \theta\Delta t m_{i,i} d^{2\ell}_{i,i+n-1} \left[\frac{\partial f_\ell}{\partial q}\right]_{i+n-1} + \theta\Delta t d^{1\ell}_{i,i} m_{i-1,i+n-1} \left[\frac{\partial f_\ell}{\partial q}\right]_i + \\
&\quad \theta^2\Delta t^2 d^{1\ell}_{i,i} d^{2\ell}_{i,i+n-1} \left[\frac{\partial f_\ell}{\partial q}\right]_i \left[\frac{\partial f_\ell}{\partial q}\right]_{i+n-1} \\
\tilde{a}_{i,i+n} &= M_{i,i+n} + \theta\Delta t m_{i,i+1} d^{2\ell}_{i+1,i+n} \left[\frac{\partial f_\ell}{\partial q}\right]_{i+n} + \theta\Delta t d^{1\ell}_{i,i+1} m_{i+1,i+n} \left[\frac{\partial f_\ell}{\partial q}\right]_{i+1} + \\
&\quad \theta^2\Delta t^2 d^{1\ell}_{i,i+1} d^{2\ell}_{i+1,i+n} \left[\frac{\partial f_\ell}{\partial q}\right]_{i+1} \left[\frac{\partial f_\ell}{\partial q}\right]_{i+n}
\end{aligned} \tag{9.170}
$$

The exact jacobian expressions are also cast via the developed jacobian decomposition. The resultant formulae are

$$
\begin{aligned}
a_{i,i-n} &= M_{i,i-n} + \theta\Delta t \mathcal{D}^{2\ell}_{i,i-n} \left[\frac{\partial f_\ell}{\partial q}\right]_{i-n} + \theta\Delta t \mathcal{D}^{1\ell}_{i,i-n} \left[\frac{\partial f_\ell}{\partial q}\right]_{i-n} \\
a_{i,i-n+1} &= M_{i,i-n+1} + \theta\Delta t \mathcal{D}^{2\ell}_{i,i-n+1} \left[\frac{\partial f_\ell}{\partial q}\right]_{i-n+1} + \theta\Delta t \mathcal{D}^{1\ell}_{i,i-n+1} \left[\frac{\partial f_\ell}{\partial q}\right]_{i-n+1} \\
a_{i,i-n+2} &= M_{i,i-n+2} + \theta\Delta t \mathcal{D}^{2\ell}_{i,i-n+2} \left[\frac{\partial f_\ell}{\partial q}\right]_{i-n+2} + \theta\Delta t \mathcal{D}^{1\ell}_{i,i-n+2} \left[\frac{\partial f_\ell}{\partial q}\right]_{i-n+2}
\end{aligned} \tag{9.171}
$$

$$
\begin{aligned}
a_{i,i-1} &= M_{i,i-1} + \theta\Delta t \mathcal{D}^{2\ell}_{i,i-1} \left[\frac{\partial f_\ell}{\partial q}\right]_{i-1} + \theta\Delta t \mathcal{D}^{1\ell}_{i,i-1} \left[\frac{\partial f_\ell}{\partial q}\right]_{i-1} \\
a_{i,i} &= M_{i,i} + \theta\Delta t \mathcal{D}^{2\ell}_{i,i} \left[\frac{\partial f_\ell}{\partial q}\right]_i + \theta\Delta t \mathcal{D}^{1\ell}_{i,i} \left[\frac{\partial f_\ell}{\partial q}\right]_i \\
a_{i,i+1} &= M_{i,i+1} + \theta\Delta t \mathcal{D}^{2\ell}_{i,i+1} \left[\frac{\partial f_\ell}{\partial q}\right]_{i+1} + \theta\Delta t \mathcal{D}^{1\ell}_{i,i+1} \left[\frac{\partial f_\ell}{\partial q}\right]_{i+1}
\end{aligned} \tag{9.172}
$$

$$
a_{i,i+n-2} = M_{i,i+n-2} + \theta\Delta t \mathcal{D}^{2\ell}_{i,i+n-2} \left[\frac{\partial f_\ell}{\partial q}\right]_{i+n-2} + \theta\Delta t \mathcal{D}^{1\ell}_{i,i+n-2} \left[\frac{\partial f_\ell}{\partial q}\right]_{i+n-2}
$$

$$
\begin{aligned}
a_{i,i+n-1} &= M_{i,i+n-1} + \theta\Delta t \mathcal{D}^{2\ell}_{i,i+n-1}\left[\frac{\partial f_\ell}{\partial q}\right]_{i+n-1} + \theta\Delta t \mathcal{D}^{1\ell}_{i,i+n-1}\left[\frac{\partial f_\ell}{\partial q}\right]_{i+n-1} \\
a_{i,i+n} &= M_{i,i+n} + \theta\Delta t \mathcal{D}^{2\ell}_{i,i+n}\left[\frac{\partial f_\ell}{\partial q}\right]_{i+n} + \theta\Delta t \mathcal{D}^{1\ell}_{i,i+n}\left[\frac{\partial f_\ell}{\partial q}\right]_{i+n}
\end{aligned} \tag{9.173}
$$

Consequently, the specific error

$$
\varepsilon^c_{i,j} \equiv (a_{i,j})^c_{\theta\Delta t} - (\tilde{a}_{i,j})^c_{\theta\Delta t} \tag{9.174}
$$

for the convection terms is

$$
\begin{aligned}
\varepsilon^c_{i,i-n} &= \theta\Delta t \left\langle N_i, \frac{\partial N_{i-n}}{\partial \eta_2}\right\rangle_{\widehat{\Omega}} \left[e^i_{\ell 2}(\eta_1) - \frac{1}{2}\left(e^{i-1}_{\ell 2}(\eta_1) + e^{i-1}_{\ell 2}(\eta_2)\right)\right]\left[\frac{\partial f_\ell}{\partial q}\right]_{i-n} + \\
&\quad \theta\Delta t \left\langle N_i, \frac{\partial N_{i-n}}{\partial \eta_1}\right\rangle_{\widehat{\Omega}} \left[e^i_{\ell 1}(\eta_1)\left[\frac{\partial f_\ell}{\partial q}\right]_{i-n} - \frac{1}{2}\left(e^i_{\ell 1}(\eta_1) + e^i_{\ell 1}(\eta_4)\right)\left[\frac{\partial f_\ell}{\partial q}\right]_{i-1}\right] \\
\varepsilon^c_{i,i-n+1} &= \theta\Delta t m_{i,i-n+1}\left\langle n_i, \frac{dn_i}{d\eta_1}\right\rangle_{\omega_1} \left[\left(e^i_{\ell 1}(\eta_1) - e^i_{\ell 1}(\eta_2)\right)\left[\frac{\partial f_\ell}{\partial q}\right]_{i-n+1} - \right. \\
&\quad \left. \frac{1}{2}\left(\left(e^i_{\ell 1}(\eta_1) + e^i_{\ell 1}(\eta_4)\right) - \left(e^i_{\ell 1}(\eta_2) + e^i_{\ell 1}(\eta_3)\right)\right)\left[\frac{\partial f_\ell}{\partial q}\right]_i\right] \\
\varepsilon^c_{i,i-n+2} &= \theta\Delta t \left\langle N_i, \frac{\partial N_{i-n+2}}{\partial \eta_2}\right\rangle_{\widehat{\Omega}} \left[e^i_{\ell 2}(\eta_2) - \frac{1}{2}\left(e^{i+1}_{\ell 2}(\eta_1) + e^{i+1}_{\ell 2}(\eta_2)\right)\right]\left[\frac{\partial f_\ell}{\partial q}\right]_{i-n+2} + \\
&\quad \theta\Delta t \left\langle N_i, \frac{\partial N_{i-n+2}}{\partial \eta_1}\right\rangle_{\widehat{\Omega}} \left[e^i_{\ell 1}(\eta_2)\left[\frac{\partial f_\ell}{\partial q}\right]_{i-n+2}\right. \\
&\quad \left. -\frac{1}{2}\left(e^i_{\ell 1}(\eta_2) + e^i_{\ell 1}(\eta_3)\right)\left[\frac{\partial f_\ell}{\partial q}\right]_{i+1}\right]
\end{aligned} \tag{9.175}
$$

$$
\begin{aligned}
\varepsilon^c_{i,i-1} &= \theta\Delta t m_{i,i-1}\left\langle n_{i-1}, \frac{dn_{i-1}}{d\eta_2}\right\rangle_{\omega_1} \left[\left(e^i_{\ell 2}(\eta_1) - e^i_{\ell 2}(\eta_4)\right) - \right. \\
&\quad \left. \frac{1}{2}\left(\left(e^{i-1}_{\ell 2}(\eta_1) + e^{i-1}_{\ell 2}(\eta_2)\right) - \left(e^{i-1}_{\ell 2}(\eta_3) + e^{i-1}_{\ell 2}(\eta_4)\right)\right)\right]\left[\frac{\partial f_\ell}{\partial q}\right]_{i-1} \\
\varepsilon^c_{i,i} &= 0 \\
\varepsilon^c_{i,i+1} &= \theta\Delta t m_{i,i+1}\left\langle n_{i+1}, \frac{dn_{i+1}}{d\eta_2}\right\rangle_{\omega_1} \left[\left(e^i_{\ell 2}(\eta_2) - e^i_{\ell 2}(\eta_3)\right) - \right. \\
&\quad \left. \frac{1}{2}\left(\left(e^{i+1}_{\ell 2}(\eta_1) + e^{i+1}_{\ell 2}(\eta_2)\right) - \left(e^{i+1}_{\ell 2}(\eta_3) + e^{i+1}_{\ell 2}(\eta_4)\right)\right)\right]\left[\frac{\partial f_\ell}{\partial q}\right]_{i+1}
\end{aligned} \tag{9.176}
$$

$$
\varepsilon^c_{i,i+n-2} = \theta\Delta t \left\langle N_i, \frac{\partial N_{i+n-2}}{\partial \eta_2}\right\rangle_{\widehat{\Omega}} \left[e^i_{\ell 2}(\eta_4) - \frac{1}{2}\left(e^{i-1}_{\ell 2}(\eta_4) + e^{i-1}_{\ell 2}(\eta_3)\right)\right]\left[\frac{\partial f_\ell}{\partial q}\right]_{i+n-2} +
$$

$$
\begin{aligned}
& \theta\Delta t \left\langle N_i, \frac{\partial N_{i+n-2}}{\partial \eta_1} \right\rangle_{\widehat{\Omega}} \left[e^i_{\ell 1}(\eta_4) \left[\frac{\partial f_\ell}{\partial q} \right]_{i+n-2} - \right. \\
& \left. \frac{1}{2} \left(e^i_{\ell 1}(\eta_1) + e^i_{\ell 1}(\eta_4) \right) \left[\frac{\partial f_\ell}{\partial q} \right]_{i-1} \right] \\
\varepsilon^c_{i,i+n-1} = \; & \theta\Delta t m_{i,i+n-1} \left\langle n_i, \frac{dn_i}{d\eta_1} \right\rangle_{\omega_1} \left[\left(e^i_{\ell 1}(\eta_4) - e^i_{\ell 1}(\eta_3) \right) \left[\frac{\partial f_\ell}{\partial q} \right]_{i+n-1} - \right. \\
& \left. \frac{1}{2} \left(\left(e^i_{\ell 1}(\eta_1) + e^i_{\ell 1}(\eta_4) \right) - \left(e^i_{\ell 1}(\eta_2) + e^i_{\ell 1}(\eta_3) \right) \right) \left[\frac{\partial f_\ell}{\partial q} \right]_i \right] \\
\varepsilon^c_{i,i+n} = \; & \theta\Delta t \left\langle N_i, \frac{\partial N_{i+n}}{\partial \eta_2} \right\rangle_{\widehat{\Omega}} \left[e^i_{\ell 2}(\eta_3) - \frac{1}{2} \left(e^{i+1}_{\ell 2}(\eta_4) + e^{i+1}_{\ell 2}(\eta_3) \right) \right] \left[\frac{\partial f_\ell}{\partial q} \right]_{i+n} + \\
& \theta\Delta t \left\langle N_i, \frac{\partial N_{i+n}}{\partial \eta_1} \right\rangle_{\widehat{\Omega}} \left[e^i_{\ell 1}(\eta_3) \left[\frac{\partial f_\ell}{\partial q} \right]_{i+n} \right. \\
& \left. - \frac{1}{2} \left(e^i_{\ell 1}(\eta_2) + e^i_{\ell 1}(\eta_3) \right) \left[\frac{\partial f_\ell}{\partial q} \right]_{i+1} \right]
\end{aligned}
\tag{9.177}
$$

9.10.3 Diffusion Term Errors

The actual TPF 2-D jacobian linear algebra statement for the diffusion terms is

$$
\begin{aligned}
\tilde{a}_{i,i-n} = \; & M_{i,i-n} + \theta\Delta t m_{i,i-1} d^{2\ell m}_{i-1,i-n} \left[\frac{\partial f_{\ell m}}{\partial q} \right]_{i-n} + \theta\Delta t d^{1\ell m}_{i,i-1} m_{i-1,i-n} \left[\frac{\partial f_{\ell m}}{\partial q} \right]_{i-1} + \\
& \theta^2\Delta t^2 d^{1\ell m}_{i,i-1} d^{2\ell m}_{i-1,i-n} \left[\frac{\partial f_{\ell m}}{\partial q} \right]_{i-1} \left[\frac{\partial f_{\ell m}}{\partial q} \right]_{i-n} \\
\tilde{a}_{i,i-n+1} = \; & M_{i,i-n+1} + \theta\Delta t m_{i,i} d^{2\ell m}_{i,i-n+1} \left[\frac{\partial f_{\ell m}}{\partial q} \right]_{i-n+1} + \theta\Delta t d^{1\ell m}_{i,i} m_{i,i-n+1} \left[\frac{\partial f_{\ell m}}{\partial q} \right]_{i} + \\
& \theta^2\Delta t^2 d^{1\ell m}_{i,i} d^{2\ell m}_{i,i-n+1} \left[\frac{\partial f_{\ell m}}{\partial q} \right]_{i} \left[\frac{\partial f_{\ell m}}{\partial q} \right]_{i-n+1} \\
\tilde{a}_{i,i-n+2} = \; & M_{i,i-n+2} + \theta\Delta t m_{i,i+1} d^{2\ell m}_{i+1,i-n+2} \left[\frac{\partial f_{\ell m}}{\partial q} \right]_{i-n+2} + \\
& \theta\Delta t d^{1\ell m}_{i,i+1} m_{i+1,i-n+2} \left[\frac{\partial f_{\ell m}}{\partial q} \right]_{i+1} + \\
& \theta^2\Delta t^2 d^{1\ell m}_{i,i+1} d^{2\ell m}_{i+1,i-n+2} \left[\frac{\partial f_{\ell m}}{\partial q} \right]_{i+1} \left[\frac{\partial f_{\ell m}}{\partial q} \right]_{i-n+2}
\end{aligned}
\tag{9.178}
$$

$$
\tilde{a}_{i,i-1} = M_{i,i-1} + \theta\Delta t m_{i,i-1} d^{2\ell m}_{i-1,i-1} \left[\frac{\partial f_{\ell m}}{\partial q} \right]_{i-1} + \theta\Delta t d^{1\ell m}_{i,i-1} m_{i-1,i-1} \left[\frac{\partial f_{\ell m}}{\partial q} \right]_{i-1} +
$$

$$
\begin{aligned}
& \theta^2\Delta t^2 d^{1\ell m}_{i,i-1} d^{2\ell m}_{i-1,i-1} \left[\frac{\partial f_{\ell m}}{\partial q}\right]_{i-1} \left[\frac{\partial f_{\ell m}}{\partial q}\right]_{i-1} \\
\tilde{a}_{i,i} &= M_{i,i} + \theta\Delta t m_{i,i} d^{2\ell m}_{i,i} \left[\frac{\partial f_{\ell m}}{\partial q}\right]_{i} + \theta\Delta t d^{1\ell m}_{i,i} m_{i,i} \left[\frac{\partial f_{\ell m}}{\partial q}\right]_{i} + \\
& \theta^2\Delta t^2 d^{1\ell m}_{i,i} d^{2\ell m}_{i,i} \left[\frac{\partial f_{\ell m}}{\partial q}\right]_{i} \left[\frac{\partial f_{\ell m}}{\partial q}\right]_{i} \\
\tilde{a}_{i,i+1} &= M_{i,i+1} + \theta\Delta t m_{i,i+1} d^{2\ell m}_{i+1,i+1} \left[\frac{\partial f_{\ell m}}{\partial q}\right]_{i+1} + \theta\Delta t d^{1\ell m}_{i,i+1} m_{i+1,i+1} \left[\frac{\partial f_{\ell m}}{\partial q}\right]_{i+1} \\
&+ \theta^2\Delta t^2 d^{1\ell m}_{i,i+1} d^{2\ell m}_{i+1,i+1} \left[\frac{\partial f_{\ell m}}{\partial q}\right]_{i+1} \left[\frac{\partial f_{\ell m}}{\partial q}\right]_{i+1}
\end{aligned} \tag{9.179}
$$

$$
\begin{aligned}
\tilde{a}_{i,i+n-2} &= M_{i,i+n-2} + \theta\Delta t m_{i,i-1} d^{2\ell m}_{i-1,i+n-2} \left[\frac{\partial f_{\ell m}}{\partial q}\right]_{i+n-2} + \\
& \theta\Delta t d^{1\ell m}_{i,i-1} m_{i-1,i+n-2} \left[\frac{\partial f_{\ell m}}{\partial q}\right]_{i-1} + \\
& \theta^2\Delta t^2 d^{1\ell m}_{i,i-1} d^{2\ell m}_{i-1,i+n-2} \left[\frac{\partial f_{\ell m}}{\partial q}\right]_{i-1} \left[\frac{\partial f_{\ell m}}{\partial q}\right]_{i+n-2} \\
\tilde{a}_{i,i+n-1} &= M_{i,i+n-1} + \theta\Delta t m_{i,i} d^{2\ell m}_{i,i+n-1} \left[\frac{\partial f_{\ell m}}{\partial q}\right]_{i+n-1} + \theta\Delta t d^{1\ell m}_{i,i} m_{i-1,i+n-1} \left[\frac{\partial f_{\ell m}}{\partial q}\right]_{i} \\
&+ \theta^2\Delta t^2 d^{1\ell m}_{i,i} d^{2\ell m}_{i,i+n-1} \left[\frac{\partial f_{\ell m}}{\partial q}\right]_{i} \left[\frac{\partial f_{\ell m}}{\partial q}\right]_{i+n-1} \\
\tilde{a}_{i,i+n} &= M_{i,i+n} + \theta\Delta t m_{i,i+1} d^{2\ell m}_{i+1,i+n} \left[\frac{\partial f_{\ell m}}{\partial q}\right]_{i+n} + \theta\Delta t d^{1\ell m}_{i,i+1} m_{i+1,i+n} \left[\frac{\partial f_{\ell m}}{\partial q}\right]_{i+1} \\
&+ \theta^2\Delta t^2 d^{1\ell m}_{i,i+1} d^{2\ell m}_{i+1,i+n} \left[\frac{\partial f_{\ell m}}{\partial q}\right]_{i+1} \left[\frac{\partial f_{\ell m}}{\partial q}\right]_{i+n}
\end{aligned} \tag{9.180}
$$

The exact jacobian expressions are also cast via the developed jacobian decomposition. The resultant formulae are

$$
\begin{aligned}
a_{i,i-n} &= M_{i,i-n} + \theta\Delta t \mathcal{D}^{2\ell m}_{i,i-n} \left[\frac{\partial f_{\ell m}}{\partial q}\right]_{i-n} + \theta\Delta t \mathcal{D}^{1\ell m}_{i,i-n} \left[\frac{\partial f_{\ell m}}{\partial q}\right]_{i-n} \\
a_{i,i-n+1} &= M_{i,i-n+1} + \theta\Delta t \mathcal{D}^{2\ell m}_{i,i-n+1} \left[\frac{\partial f_{\ell m}}{\partial q}\right]_{i-n+1} + \theta\Delta t \mathcal{D}^{1\ell m}_{i,i-n+1} \left[\frac{\partial f_{\ell m}}{\partial q}\right]_{i-n+1} \\
a_{i,i-n+2} &= M_{i,i-n+2} + \theta\Delta t \mathcal{D}^{2\ell m}_{i,i-n+2} \left[\frac{\partial f_{\ell m}}{\partial q}\right]_{i-n+2} + \theta\Delta t \mathcal{D}^{1\ell m}_{i,i-n+2} \left[\frac{\partial f_{\ell m}}{\partial q}\right]_{i-n+2}
\end{aligned} \tag{9.181}
$$

$$
\begin{aligned}
a_{i,i-1} &= M_{i,i-1} + \theta\Delta t \mathcal{D}^{2\ell m}_{i,i-1} \left[\frac{\partial f_{\ell m}}{\partial q}\right]_{i-1} + \theta\Delta t \mathcal{D}^{1\ell m}_{i,i-1} \left[\frac{\partial f_{\ell m}}{\partial q}\right]_{i-1} \\
a_{i,i} &= M_{i,i} + \theta\Delta t \mathcal{D}^{2\ell m}_{i,i} \left[\frac{\partial f_{\ell m}}{\partial q}\right]_{i} + \theta\Delta t \mathcal{D}^{1\ell m}_{i,i} \left[\frac{\partial f_{\ell m}}{\partial q}\right]_{i}
\end{aligned}
$$

$$a_{i,i+1} = M_{i,i+1} + \theta\Delta t\mathcal{D}^{2\ell m}_{i,i+1}\left[\frac{\partial f_{\ell m}}{\partial q}\right]_{i+1} + \theta\Delta t\mathcal{D}^{1\ell m}_{i,i+1}\left[\frac{\partial f_{\ell m}}{\partial q}\right]_{i+1} \tag{9.182}$$

$$\begin{aligned}
a_{i,i+n-2} &= M_{i,i+n-2} + \theta\Delta t\mathcal{D}^{2\ell m}_{i,i+n-2}\left[\frac{\partial f_{\ell m}}{\partial q}\right]_{i+n-2} + \theta\Delta t\mathcal{D}^{1\ell m}_{i,i+n-2}\left[\frac{\partial f_{\ell m}}{\partial q}\right]_{i+n-2} \\
a_{i,i+n-1} &= M_{i,i+n-1} + \theta\Delta t\mathcal{D}^{2\ell m}_{i,i+n-1}\left[\frac{\partial f_{\ell m}}{\partial q}\right]_{i+n-1} + \theta\Delta t\mathcal{D}^{1\ell m}_{i,i+n-1}\left[\frac{\partial f_{\ell m}}{\partial q}\right]_{i+n-1} \\
a_{i,i+n} &= M_{i,i+n} + \theta\Delta t\mathcal{D}^{2\ell m}_{i,i+n}\left[\frac{\partial f_{\ell m}}{\partial q}\right]_{i+n} + \theta\Delta t\mathcal{D}^{1\ell m}_{i,i+n}\left[\frac{\partial f_{\ell m}}{\partial q}\right]_{i+n}
\end{aligned} \tag{9.183}$$

Consequently, the specific error

$$\varepsilon^d_{i,j} \equiv (a_{i,j})^d_{\theta\Delta t} - (\tilde{a}_{i,j})^d_{\theta\Delta t} \tag{9.184}$$

for diffusion terms is

$$\begin{aligned}
\varepsilon^d_{i,i-n} &= \theta\Delta t\left\langle -\frac{\partial N_i}{\partial \eta_2}, \frac{\partial N_{i-n}}{\partial \eta_2}\right\rangle_{\widehat{\Omega}}\left[e^i_{\ell 2}(\eta_1)\left(\frac{e_{m2}}{\det J}\right)^i_{\tilde{\eta}_1} - \right. \\
&\quad \left.\frac{1}{2}\left(e^{i-1}_{\ell 2}(\eta_1)\left(\frac{e_{m2}}{\det J}\right)^{i-1}_{\tilde{\eta}_1} + e^{i-1}_{\ell 2}(\eta_2)\left(\frac{e_{m2}}{\det J}\right)^{i-1}_{\tilde{\eta}_2}\right)\right]\left[\frac{\partial f_{\ell m}}{\partial q}\right]_{i-n} + \\
&\quad \theta\Delta t\left\langle -\frac{\partial N_i}{\partial \eta_1}, \frac{\partial N_{i-n}}{\partial \eta_1}\right\rangle_{\widehat{\Omega}}\left[e^i_{\ell 1}(\eta_1)\left(\frac{e_{m1}}{\det J}\right)^i_{\tilde{\eta}_1}\left[\frac{\partial f_{\ell m}}{\partial q}\right]_{i-n} - \right. \\
&\quad \left.\frac{1}{2}\left(e^i_{\ell 1}(\eta_1)\left(\frac{e_{m1}}{\det J}\right)^i_{\tilde{\eta}_1} + e^i_{\ell 1}(\eta_4)\left(\frac{e_{m1}}{\det J}\right)^i_{\tilde{\eta}_4}\right)\left[\frac{\partial f_{\ell m}}{\partial q}\right]_{i-1}\right] + \\
&\quad \theta\Delta t\left(\mathcal{D}^{12\ell m}_{i,i-n} + \mathcal{D}^{21\ell m}_{i,i-n}\right)\left[\frac{\partial f_{\ell m}}{\partial q}\right]_{1-n} \\
\varepsilon^d_{i,i-n+1} &= \theta\Delta t\left\langle -\frac{\partial N_i}{\partial \eta_1}, \frac{\partial N_{i-n+1}}{\partial \eta_1}\right\rangle_{\widehat{\Omega}}\left[\frac{1}{2}\left(e^i_{\ell 1}(\eta_1)\left(\frac{e_{m1}}{\det J}\right)^i_{\tilde{\eta}_1}\right.\right. \\
&\quad \left.\left. + e^i_{\ell 1}(\eta_2)\left(\frac{e_{m1}}{\det J}\right)^i_{\tilde{\eta}_2}\right)\left[\frac{\partial f_{\ell m}}{\partial q}\right]_{i-n+1} - \right. \\
&\quad \frac{1}{2}\left(\frac{1}{2}\left(e^i_{\ell 1}(\eta_1)\left(\frac{e_{m1}}{\det J}\right)^i_{\tilde{\eta}_1} + e^i_{\ell 1}(\eta_4)\left(\frac{e_{m1}}{\det J}\right)^i_{\tilde{\eta}_4}\right)\right. \\
&\quad \left.\left.\left. + \frac{1}{2}\left(e^i_{\ell 1}(\eta_2)\left(\frac{e_{m1}}{\det J}\right)^i_{\tilde{\eta}_2} + e^i_{\ell 1}(\eta_3)\left(\frac{e_{m1}}{\det J}\right)^i_{\tilde{\eta}_3}\right)\right)\left[\frac{\partial f_{\ell m}}{\partial q}\right]_i\right] + \\
&\quad \theta\Delta t\left(\mathcal{D}^{12\ell m}_{i,i-n+1} + \mathcal{D}^{21\ell m}_{i,i-n+1}\right)\left[\frac{\partial f_{\ell m}}{\partial q}\right]_{1-n+1} \\
\varepsilon^d_{i,i-n+2} &= \theta\Delta t\left\langle -\frac{\partial N_i}{\partial \eta_2}, \frac{\partial N_{i-n+2}}{\partial \eta_2}\right\rangle_{\widehat{\Omega}}\left[e^i_{\ell 2}(\eta_2)\left(\frac{e_{m2}}{\det J}\right)^i_{\tilde{\eta}_2} - \right.
\end{aligned}$$

$$\frac{1}{2}\left(e_{\ell 2}^{i+1}(\eta_1)\left(\frac{e_{m2}}{\det J}\right)_{\tilde{\eta}_1}^{i+1}+e_{\ell 2}^{i+1}(\eta_2)\left(\frac{e_{m2}}{\det J}\right)_{\tilde{\eta}_2}^{i+1}\right)\left[\frac{\partial f_{\ell m}}{\partial q}\right]_{i-n+2}+$$
$$\theta\Delta t\left\langle-\frac{\partial N_i}{\partial \eta_1},\frac{\partial N_{i-n+2}}{\partial \eta_1}\right\rangle_{\hat{\Omega}}\left[e_{\ell 1}^{i}(\eta_2)\left(\frac{e_{m1}}{\det J}\right)_{\tilde{\eta}_2}^{i}\left[\frac{\partial f_{\ell m}}{\partial q}\right]_{i-n+2}-\right.$$
$$\left.\frac{1}{2}\left(e_{\ell 1}^{i}(\eta_2)\left(\frac{e_{m1}}{\det J}\right)_{\tilde{\eta}_2}^{i}+e_{\ell 1}^{i}(\eta_3)\left(\frac{e_{m1}}{\det J}\right)_{\tilde{\eta}_3}^{i}\right)\left[\frac{\partial f_{\ell m}}{\partial q}\right]_{i+1}\right]+$$
$$\theta\Delta t\left(\mathcal{D}_{i,i-n+2}^{12\ell m}+\mathcal{D}_{i,i-n+2}^{21\ell m}\right)\left[\frac{\partial f_{\ell m}}{\partial q}\right]_{1-n+2} \tag{9.185}$$

$$\begin{aligned}
\varepsilon_{i,i-1}^{d} &= \theta\Delta t\left\langle-\frac{\partial N_i}{\partial \eta_2},\frac{\partial N_{i-1}}{\partial \eta_2}\right\rangle_{\hat{\Omega}}\left[\frac{1}{2}\left(e_{\ell 2}^{i}(\eta_1)\left(\frac{e_{m2}}{\det J}\right)_{\tilde{\eta}_1}^{i}+e_{\ell 2}^{i}(\eta_4)\left(\frac{e_{m2}}{\det J}\right)_{\tilde{\eta}_4}^{i}\right)\right.\\
&\quad-\frac{1}{2}\left(\frac{1}{2}\left(e_{\ell 2}^{i-1}(\eta_1)\left(\frac{e_{m2}}{\det J}\right)_{\tilde{\eta}_1}^{i-1}+e_{\ell 2}^{i-1}(\eta_2)\left(\frac{e_{m2}}{\det J}\right)_{\tilde{\eta}_2}^{i-1}\right)\right.\\
&\quad\left.\left.+\frac{1}{2}\left(e_{\ell 2}^{i-1}(\eta_4)\left(\frac{e_{m2}}{\det J}\right)_{\tilde{\eta}_4}^{i-1}+e_{\ell 2}^{i-1}(\eta_3)\left(\frac{e_{m2}}{\det J}\right)_{\tilde{\eta}_3}^{i-1}\right)\right)\right]\left[\frac{\partial f_{\ell m}}{\partial q}\right]_{i-1}+\\
&\quad\theta\Delta t\left(\mathcal{D}_{i,i-1}^{12\ell m}+\mathcal{D}_{i,i-1}^{21\ell m}\right)\left[\frac{\partial f_{\ell m}}{\partial q}\right]_{i-1}\\
\varepsilon_{i,i}^{d} &= \theta\Delta t\left(\mathcal{D}_{i,i}^{12\ell m}+\mathcal{D}_{i,i}^{21\ell m}\right)\left[\frac{\partial f_{\ell m}}{\partial q}\right]_{i}\\
\varepsilon_{i,i+1}^{d} &= \theta\Delta t\left\langle-\frac{\partial N_i}{\partial \eta_2},\frac{\partial N_{i+1}}{\partial \eta_2}\right\rangle_{\hat{\Omega}}\left[\frac{1}{2}\left(e_{\ell 2}^{i}(\eta_2)\left(\frac{e_{m2}}{\det J}\right)_{\tilde{\eta}_2}^{i}+e_{\ell 2}^{i}(\eta_3)\left(\frac{e_{m2}}{\det J}\right)_{\tilde{\eta}_3}^{i}\right)\right.\\
&\quad-\frac{1}{2}\left(\frac{1}{2}\left(e_{\ell 2}^{i+1}(\eta_1)\left(\frac{e_{m2}}{\det J}\right)_{\tilde{\eta}_1}^{i+1}+e_{\ell 2}^{i+1}(\eta_2)\left(\frac{e_{m2}}{\det J}\right)_{\tilde{\eta}_2}^{i+1}\right)\right.\\
&\quad\left.\left.+\frac{1}{2}\left(e_{\ell 2}^{i+1}(\eta_4)\left(\frac{e_{m2}}{\det J}\right)_{\tilde{\eta}_4}^{i+1}+e_{\ell 2}^{i+1}(\eta_3)\left(\frac{e_{m2}}{\det J}\right)_{\tilde{\eta}_3}^{i+1}\right)\right)\right]\left[\frac{\partial f_{\ell m}}{\partial q}\right]_{i+1}+\\
&\quad\theta\Delta t\left(\mathcal{D}_{i,i+1}^{12\ell m}+\mathcal{D}_{i,i+1}^{21\ell m}\right)\left[\frac{\partial f_{\ell m}}{\partial q}\right]_{i+1}
\end{aligned} \tag{9.186}$$

$$\begin{aligned}
\varepsilon_{i,i+n-2}^{d} &= \theta\Delta t\left\langle-\frac{\partial N_i}{\partial \eta_2},\frac{\partial N_{i+n-2}}{\partial \eta_2}\right\rangle_{\hat{\Omega}}\left[e_{\ell 2}^{i}(\eta_4)\left(\frac{e_{m2}}{\det J}\right)_{\tilde{\eta}_4}^{i}-\right.\\
&\quad\left.\frac{1}{2}\left(e_{\ell 2}^{i-1}(\eta_4)\left(\frac{e_{m2}}{\det J}\right)_{\tilde{\eta}_4}^{i-1}+e_{\ell 2}^{i-1}(\eta_3)\left(\frac{e_{m2}}{\det J}\right)_{\tilde{\eta}_3}^{i-1}\right)\right]\left[\frac{\partial f_{\ell m}}{\partial q}\right]_{i+n-2}+\\
&\quad\theta\Delta t\left\langle-\frac{\partial N_i}{\partial \eta_1},\frac{\partial N_{i+n-2}}{\partial \eta_1}\right\rangle_{\hat{\Omega}}\left[e_{\ell 1}^{i}(\eta_4)\left(\frac{e_{m1}}{\det J}\right)_{\tilde{\eta}_4}^{i}\left[\frac{\partial f_{\ell m}}{\partial q}\right]_{i+n-2}-\right.\\
&\quad\left.\frac{1}{2}\left(e_{\ell 1}^{i}(\eta_1)\left(\frac{e_{m1}}{\det J}\right)_{\tilde{\eta}_1}^{i}+e_{\ell 1}^{i}(\eta_4)\left(\frac{e_{m1}}{\det J}\right)_{\tilde{\eta}_4}^{i}\right)\left[\frac{\partial f_{\ell m}}{\partial q}\right]_{i-1}\right]+\\
&\quad\theta\Delta t\left(\mathcal{D}_{i,i+n-2}^{12\ell m}+\mathcal{D}_{i,i+n-2}^{21\ell m}\right)\left[\frac{\partial f_{\ell m}}{\partial q}\right]_{i+n-2}
\end{aligned}$$

$$
\begin{aligned}
\varepsilon^d_{i,i+n-1} &= \theta\Delta t\left\langle -\frac{\partial N_i}{\partial \eta_1}, \frac{\partial N_{i+n-1}}{\partial \eta_1}\right\rangle_{\hat{\Omega}} \left[\frac{1}{2}\left(e^i_{\ell 1}(\eta_3)\left(\frac{e_{m1}}{\det J}\right)^i_{\tilde{\eta}_3}\right.\right. \\
&\quad \left.\left. + e^i_{\ell 1}(\eta_4)\left(\frac{e_{m1}}{\det J}\right)^i_{\tilde{\eta}_4}\right)\left[\frac{\partial f_{\ell m}}{\partial q}\right]_{i+n-1} - \right. \\
&\quad \frac{1}{2}\left(\frac{1}{2}\left(e^i_{\ell 1}(\eta_1)\left(\frac{e_{m1}}{\det J}\right)^i_{\tilde{\eta}_1} + e^i_{\ell 1}(\eta_4)\left(\frac{e_{m1}}{\det J}\right)^i_{\tilde{\eta}_4}\right)\right. \\
&\quad \left.\left. + \frac{1}{2}\left(e^i_{\ell 1}(\eta_2)\left(\frac{e_{m1}}{\det J}\right)^i_{\tilde{\eta}_2} + e^i_{\ell 1}(\eta_3)\left(\frac{e_{m1}}{\det J}\right)^i_{\tilde{\eta}_3}\right)\right)\left[\frac{\partial f_{\ell m}}{\partial q}\right]_i\right] + \\
&\quad \theta\Delta t\left(\mathcal{D}^{12\ell m}_{i,i+n-1} + \mathcal{D}^{21\ell m}_{i,i+n-1}\right)\left[\frac{\partial f_{\ell m}}{\partial q}\right]_{1+n-1} \\
\varepsilon^d_{i,i+n} &= \theta\Delta t\left\langle -\frac{\partial N_i}{\partial \eta_2}, \frac{\partial N_{i+n}}{\partial \eta_2}\right\rangle_{\hat{\Omega}} \left[e^i_{\ell 2}(\eta_3)\left(\frac{e_{m2}}{\det J}\right)^i_{\tilde{\eta}_3} - \right. \\
&\quad \left.\frac{1}{2}\left(e^{i+1}_{\ell 2}(\eta_4)\left(\frac{e_{m2}}{\det J}\right)^{i+1}_{\tilde{\eta}_4} + e^{i+1}_{\ell 2}(\eta_3)\left(\frac{e_{m2}}{\det J}\right)^{i+1}_{\tilde{\eta}_3}\right)\right]\left[\frac{\partial f_{\ell m}}{\partial q}\right]_{i+n} + \\
&\quad \theta\Delta t\left\langle -\frac{\partial N_i}{\partial \eta_1}, \frac{\partial N_{i+n}}{\partial \eta_1}\right\rangle_{\hat{\Omega}} \left[e^i_{\ell 1}(\eta_3)\left(\frac{e_{m1}}{\det J}\right)^i_{\tilde{\eta}_3}\left[\frac{\partial f_{\ell m}}{\partial q}\right]_{i+n} - \right. \\
&\quad \left.\frac{1}{2}\left(e^i_{\ell 1}(\eta_2)\left(\frac{e_{m1}}{\det J}\right)^i_{\tilde{\eta}_2} + e^i_{\ell 1}(\eta_3)\left(\frac{e_{m1}}{\det J}\right)^i_{\tilde{\eta}_3}\right)\left[\frac{\partial f_{\ell m}}{\partial q}\right]_{i+1}\right] + \\
&\quad \theta\Delta t\left(\mathcal{D}^{12\ell m}_{i,i+n} + \mathcal{D}^{21\ell m}_{i,i+n}\right)\left[\frac{\partial f_{\ell m}}{\partial q}\right]_{i+n}
\end{aligned}
\tag{9.187}
$$

Note in these expressions that the terms $\mathcal{D}^{12\ell m}_{i,j}$ and $\mathcal{D}^{21\ell m}_{i,j}$ account for the absence of the cross derivative diffusion relations in the TPF algorithm.

Comparing the convection and diffusion term errors shows that if $\frac{1}{Re} = O(\min_\alpha(\Delta x_\alpha))$, with $\frac{1}{Re}$ intrinsic to the diffusion jacobians $\frac{\partial f_{\ell m}}{\partial q}$, then these error expressions exhibit the same order of magnitude.

The magnitude of the diffusion term errors is directly proportional to Δt and inversely proportional to Re. Consequently, for large viscosity values, hence small Re, Δt must be reduced accordingly to prevent unbounded iteration growth, due to these diffusion jacobian errors, hence prevent instability. Therefore, this TPF algorithm is particularly efficient, i.e. the scheme remains stable for large time steps

Δt, for realistic aerodynamic flows where $Re \to \mathcal{O}\left(10^7\right)$

9.10.4 $O(\Delta t^2)$ Errors

Finally, the specific form of the order Δt^2 error is

$$\begin{aligned}
\varepsilon_{i,k}^{\Delta t^2} &= -\theta^2 \Delta t^2 d_{i,j}^1 d_{j,k}^2 = \\
&\quad -d_{i,j}^{1\ell} d_{j,k}^{2\ell} \left[\frac{\partial f_\ell}{\partial q}\right]_j \left[\frac{\partial f_\ell}{\partial q}\right]_k - d_{i,j}^{1\ell} d_{j,k}^{2\ell m} \left[\frac{\partial f_\ell}{\partial q}\right]_j \left[\frac{\partial f_{\ell m}}{\partial q}\right]_k \\
&\quad -d_{i,j}^{1\ell m} d_{j,k}^{2\ell} \left[\frac{\partial f_{\ell m}}{\partial q}\right]_j \left[\frac{\partial f_\ell}{\partial q}\right]_k - d_{i,j}^{1\ell m} d_{j,k}^{2\ell m} \left[\frac{\partial f_{\ell m}}{\partial q}\right]_j \left[\frac{\partial f_{\ell m}}{\partial q}\right]_k
\end{aligned} \tag{9.188}$$

9.10.5 Error Order of Magnitude

The values of the dependent variable q as computed with the TPF factorization can be second order accurate in time, since the variation $\Delta(q \cdot \det J)$ is of order (Δt). If no spatial approximation is present, then the order of the solution error in time becomes expressed as

$$O(\mathcal{E}_{TPF}^{\Delta t^2}) = O(\Delta t^2) \cdot O(\Delta(q \det J)) = O(\Delta t^3) \tag{9.189}$$

For non-vanishing spatial approximation error, the formal error in the Jacobian-term evaluation in matrices is of order $O(\max_\alpha(\Delta x_\alpha))$, since in the general non-linear case the following relations hold

$$\left[\frac{\partial f_\ell}{\partial q}\right]_{j+1} = \left[\frac{\partial f_\ell}{\partial q}\right]_j + \left\{\frac{\partial}{\partial q}\left[\frac{\partial f_\ell}{\partial q}\right]\right\}_j \Delta q + \cdots \tag{9.190}$$

$$\Delta q = q_{j+1} - q_j = \left[\frac{\partial q}{\partial \eta_\alpha}\right]_j \Delta \eta_\alpha + \cdots \tag{9.191}$$

$$\frac{\partial q}{\partial \eta_\alpha} = \frac{\partial q}{\partial x_j} \cdot \frac{\partial x_j}{\partial \eta_\alpha} \tag{9.192}$$

$$O\left(\frac{\partial x_j}{\partial \eta_\alpha}\right) = O(\Delta x_j) \text{ since } O(\Delta \eta_\alpha) = 1 \tag{9.193}$$

Hence, the error committed in the TPF computation of q is still of order $O(\Delta t^3)$, provided that $\max_\alpha(\Delta x_\alpha) \leq \Delta t$ and the metric data error is of order $O(\Delta x_\alpha)$. Finally, note that the spatial approximation error is still present for uniform rectangular grids if f_α is non-linear. Analogously, this error remains for linear fluxes if the grid is non-uniform.

9.11 An Alternative Iterative Solver

An optimal TPF for system (9.1) has been developed and the associated error ε_{ij} (9.175)-(9.177) and (9.185)-(9.187) is derived. If the error matrix E is defined as

$$E = [\varepsilon_{ij}] \tag{9.194}$$

then for $\delta k^{p+1} \equiv x$, (9.1) is expressed as

$$Ax = b \quad , \quad (A_{TPF} + E)x = b \quad , \quad A_{TPF} \equiv BC \tag{9.195}$$

System (9.195) can be used to define a novel iteration to solve (9.1). This is accomplished by writing

$$A_{TPF}x = b - Ex \tag{9.196}$$

hence

$$A_{TPF}x^{p+1} = b - Ex^p \tag{9.197}$$

where the superscript p is the inner iteration index.

Iteration (9.197) is clearly analogous to a standard linear algebra iterative procedure such as Jacobi or Gauss-Seidel. Note that such an iteration is stationary and can be embedded in any outer iteration, i.e. Newton. If only a reduced number of iterations is utilized, then the matrix product Ex^p is interpreted as a set of correction terms. System (9.196) is instrumental to investigate the convergence of this TPF iteration. Subtraction of (9.197) from (9.196) yields

$$A_{TPF}(x - x^{p+1}) = -E(x - x^p) \tag{9.198}$$

that is

$$\varepsilon^{p+1} = -A_{TPF}^{-1} E\varepsilon^p \tag{9.199}$$

$$\varepsilon^p \equiv x - x^p \tag{9.200}$$

Consequently

$$\|\varepsilon^{p+1}\| \leq \|(A_{TPF}^{-1}E)^p\| \cdot \|\varepsilon^0\| \tag{9.201}$$

Thus, convergence is achieved if the spectral radius of $A_{TPF}^{-1}E$ is less than one. In these conditions, the eigenvalues of the matrix

$$A_{TPF}^{-1}A = I + A_{TPF}^{-1}E \tag{9.202}$$

can be forced to cluster about unity for an appropriate Δt, since the norm of E is of order Δt. Expression (9.201) is further cast as

$$\|\varepsilon^{p+1}\| \leq \|A_{TPF}^{-1}\|^p \cdot \|E\|^p \cdot \|\varepsilon^0\| \tag{9.203}$$

Therefore, when the product $\|A_{TPF}^{-1}\| \cdot \|E\|$ is less than one, convergence is achieved. Note that the norm of matrix E is of order Δt, hence this iterative procedure can be always made to converge via appropriate choice of the time step.

9.12 Examples of Application

In this final section a demonstration is presented for formulae (9.54)-(9.56), defining the TPF mass matrix, and for (9.105)-(9.107) defining the TPF convection operator matrix.

With reference to Figure 9.8, the 1-D mass-matrix terms are

$$m_{i,i-1} = \frac{1}{3} \quad , \quad m_{i,i} = \frac{4}{3} \quad , \quad m_{i,i+1} = \frac{1}{3} \tag{9.204}$$

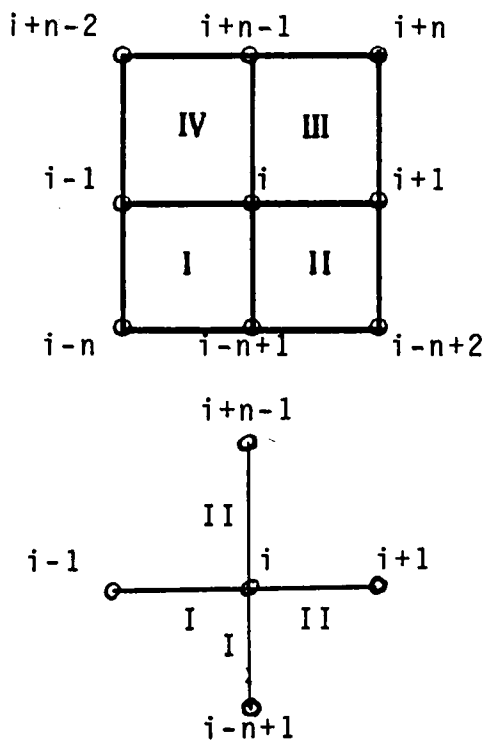


Figure 9.8: Representative TPF Computational Domain Correspondence

Utilization of (9.54)-(9.56) leads to the following values for the 2-D mass matrix terms

$$\begin{aligned} M_{i,i-n} &= m_{i,i-1} \cdot m_{i-1,i-n} = \frac{1}{3} \cdot \frac{1}{3} = \frac{1}{9} \\ M_{i,i-n+1} &= m_{i,i} \cdot m_{i,i-n+1} = \frac{4}{3} \cdot \frac{1}{3} = \frac{4}{9} \\ M_{i,i-n+2} &= m_{i,i+1} \cdot m_{i+1,i-n+2} = \frac{1}{3} \cdot \frac{1}{3} = \frac{1}{9} \end{aligned} \tag{9.205}$$

$$\begin{aligned} M_{i,i-1} &= m_{i,i-1} \cdot m_{i-1,i-1} = \frac{1}{3} \cdot \frac{4}{3} = \frac{4}{9} \\ M_{i,i} &= m_{i,i} \cdot m_{i,i} = \frac{4}{3} \cdot \frac{4}{3} = \frac{16}{9} \\ M_{i,i+1} &= m_{i,i+1} \cdot m_{i+1,i+1} = \frac{1}{3} \cdot \frac{4}{3} = \frac{4}{9} \end{aligned} \tag{9.206}$$

$$\begin{aligned} M_{i,i+n-2} &= m_{i,i-1} \cdot m_{i-1,i+n-2} = \frac{1}{3} \cdot \frac{1}{3} = \frac{1}{9} \\ M_{i,i+n-1} &= m_{i,i} \cdot m_{i,i+n-1} = \frac{4}{3} \cdot \frac{1}{3} = \frac{4}{9} \\ M_{i,i+n} &= m_{i,i+1} \cdot m_{i+1,i+n} = \frac{1}{3} \cdot \frac{1}{3} = \frac{1}{9} \end{aligned} \tag{9.207}$$

and these values indeed coincide with the actual 2-D mass-matrix terms [14], hence (9.54)-(9.56) are verified. The recursion formula associated with the convection integral

$$\mathcal{C}^1 = e_{\ell 1} \int_{\widehat{\Omega}} N_i \frac{\partial N_k}{\partial \eta_1} \, d\boldsymbol{\eta} \, \phi_k^\ell \tag{9.208}$$

is

$$\begin{aligned} \mathcal{C}^1 = & -\frac{1}{6} e_{\ell 1}(\boldsymbol{\eta}_1) \phi_{i-n}^\ell - \frac{4}{6} \left[\frac{1}{2} \left(e_{\ell 1}(\boldsymbol{\eta}_1) + e_{\ell 1}(\boldsymbol{\eta}_4) \right) \right] \phi_{i-1}^\ell - \frac{1}{6} e_{\ell 1}(\boldsymbol{\eta}_4) \phi_{i+n-2}^\ell \\ & -\frac{1}{6} \left[e_{\ell 1}(\boldsymbol{\eta}_2) - e_{\ell 1}(\boldsymbol{\eta}_1) \right] \phi_{i-n+1}^\ell \\ & -\frac{4}{6} \left[\frac{1}{2} \left(e_{\ell 1}(\boldsymbol{\eta}_2) + e_{\ell 1}(\boldsymbol{\eta}_3) \right) - \frac{1}{2} \left(e_{\ell 1}(\boldsymbol{\eta}_1) + e_{\ell 1}(\boldsymbol{\eta}_4) \right) \right] \phi_i^\ell \end{aligned}$$

$$-\frac{1}{6}\left[e_{\ell 1}(\boldsymbol{\eta}_3)-e_{\ell 1}(\boldsymbol{\eta}_4)\right]\phi^{\ell}_{i+n-1}$$
$$+\frac{1}{6}e_{\ell 1}(\boldsymbol{\eta}_2)\,\phi^{\ell}_{i-n+2}+\frac{4}{6}\left[\frac{1}{2}\left(e_{\ell 1}(\boldsymbol{\eta}_2)+e_{\ell 1}(\boldsymbol{\eta}_3)\right)\right]\phi^{\ell}_{i+1}+\frac{1}{6}e_{\ell 1}(\boldsymbol{\eta}_3)\,\phi^{\ell}_{i+n} \tag{9.209}$$

The jacobian terms associated to expression (9.209) are

$$\begin{aligned}
D^1_{i,i-n} &= -\frac{1}{6}e_{\ell 1}(\boldsymbol{\eta}_1)\left[\frac{\partial\phi^{\ell}}{\partial q}\right]_{i-n}\\
D^1_{i,i-n+1} &= -\frac{1}{6}\left[e_{\ell 1}(\boldsymbol{\eta}_2)-e_{\ell 1}(\boldsymbol{\eta}_1)\right]\left[\frac{\partial\phi^{\ell}}{\partial q}\right]_{i-n+1}\\
D^1_{i,i-n+2} &= +\frac{1}{6}e_{\ell 1}(\boldsymbol{\eta}_2)\left[\frac{\partial\phi^{\ell}}{\partial q}\right]_{i-n+2}
\end{aligned} \tag{9.210}$$

$$\begin{aligned}
D^1_{i,i-1} &= -\frac{4}{6}\left[\frac{1}{2}\left(e_{\ell 1}(\boldsymbol{\eta}_1)+e_{\ell 1}(\boldsymbol{\eta}_4)\right)\right]\left[\frac{\partial\phi^{\ell}}{\partial q}\right]_{i-1}\\
D^1_{i,i} &= -\frac{4}{6}\left[\frac{1}{2}\left(e_{\ell 1}(\boldsymbol{\eta}_2)+e_{\ell 1}(\boldsymbol{\eta}_3)\right)-\frac{1}{2}\left(e_{\ell 1}(\boldsymbol{\eta}_1)+e_{\ell 1}(\boldsymbol{\eta}_4)\right)\right]\left[\frac{\partial\phi^{\ell}}{\partial q}\right]_{i}\\
D^1_{i,i+1} &= +\frac{4}{6}\left[\frac{1}{2}\left(e_{\ell 1}(\boldsymbol{\eta}_2)+e_{\ell 1}(\boldsymbol{\eta}_3)\right)\right]\left[\frac{\partial\phi^{\ell}}{\partial q}\right]_{i+1}
\end{aligned} \tag{9.211}$$

$$\begin{aligned}
D^1_{i,i+n-2} &= -\frac{1}{6}e_{\ell 1}(\boldsymbol{\eta}_4)\left[\frac{\partial\phi^{\ell}}{\partial q}\right]_{i+n-2}\\
D^1_{i,i+n-1} &= -\frac{1}{6}\left[e_{\ell 1}(\boldsymbol{\eta}_3)-e_{\ell 1}(\boldsymbol{\eta}_4)\right]\left[\frac{\partial\phi^{\ell}}{\partial q}\right]_{i+n-1}\\
D^1_{i,i+n} &= +\frac{1}{6}e_{\ell 1}(\boldsymbol{\eta}_3)\left[\frac{\partial\phi^{\ell}}{\partial q}\right]_{i+n}
\end{aligned} \tag{9.212}$$

The relevant 1-D curvilinear coordinate sweep components $d^1_{i,j}$, as obtained from (9.76)-(9.78) are

$$d^1_{i,i-1} = -\frac{1}{2}\left[\frac{1}{2}\left(e_{\ell 1}(\boldsymbol{\eta}_1)+e_{\ell 1}(\boldsymbol{\eta}_4)\right)\right]\left[\frac{\partial\phi^{\ell}}{\partial q}\right]_{i-1} \tag{9.213}$$

$$d^1_{i,i} = -\frac{1}{2}\left[\frac{1}{2}\left(e_{\ell 1}(\boldsymbol{\eta}_2)+e_{\ell 1}(\boldsymbol{\eta}_3)\right)-\frac{1}{2}\left(e_{\ell 1}(\boldsymbol{\eta}_1)+e_{\ell 1}(\boldsymbol{\eta}_4)\right)\right]\left[\frac{\partial\phi^{\ell}}{\partial q}\right]_{i} \tag{9.214}$$

$$d^1_{i,i+1} = +\frac{1}{2}\left[\frac{1}{2}\left(e_{\ell 1}(\boldsymbol{\eta}_2)+e_{\ell 1}(\boldsymbol{\eta}_3)\right)\right]\left[\frac{\partial \phi^\ell}{\partial q}\right]_{i+1} \tag{9.215}$$

Utilization of (9.41)-(9.43), then leads to the following TPF representations for terms (9.210)-(9.212)

$$\begin{aligned}
D^1_{i,i-n} &\simeq d^1_{i,i-1}\cdot m_{i-1,i-n} = -\frac{1}{6}\left[\frac{1}{2}\left(e_{\ell 1}(\boldsymbol{\eta}_1)+e_{\ell 1}(\boldsymbol{\eta}_4)\right)\right]\left[\frac{\partial \phi^\ell}{\partial q}\right]_{i-1} \\
D^1_{i,i-n+1} &\simeq d^1_{i,i}\cdot m_{i,i-n+1} = -\frac{1}{6}\left[\frac{1}{2}\left(e_{\ell 1}(\boldsymbol{\eta}_2)+e_{\ell 1}(\boldsymbol{\eta}_3)\right)\right. \\
&\quad \left.-\frac{1}{2}\left(e_{\ell 1}(\boldsymbol{\eta}_1)+e_{\ell 1}(\boldsymbol{\eta}_4)\right)\right]\left[\frac{\partial \phi^\ell}{\partial q}\right]_{i} \\
D^1_{i,i-n+2} &\simeq d^1_{i,i+1}\cdot m_{i+1,i-n+2} = \frac{1}{6}\left[\frac{1}{2}\left(e_{\ell 1}(\boldsymbol{\eta}_2)+e_{\ell 1}(\boldsymbol{\eta}_3)\right)\right]\left[\frac{\partial \phi^\ell}{\partial q}\right]_{i+1}
\end{aligned} \tag{9.216}$$

$$\begin{aligned}
D^1_{i,i-1} &= d^1_{i,i-1}\cdot m_{i-1,i-1} = -\frac{4}{6}\left[\frac{1}{2}\left(e_{\ell 1}(\boldsymbol{\eta}_1)+e_{\ell 1}(\boldsymbol{\eta}_4)\right)\right]\left[\frac{\partial \phi^\ell}{\partial q}\right]_{i-1} \\
D^1_{i,i} &= d^1_{i,i}\cdot m_{i,i} = -\frac{4}{6}\left[\frac{1}{2}\left(e_{\ell 1}(\boldsymbol{\eta}_2)+e_{\ell 1}(\boldsymbol{\eta}_3)\right)\right. \\
&\quad \left.-\frac{1}{2}\left(e_{\ell 1}(\boldsymbol{\eta}_1)+e_{\ell 1}(\boldsymbol{\eta}_4)\right)\right]\left[\frac{\partial \phi^\ell}{\partial q}\right]_{i} \\
D^1_{i,i+1} &= d^1_{i,i+1}\cdot m_{i+1,i+1} = \frac{4}{6}\left[\frac{1}{2}\left(e_{\ell 1}(\boldsymbol{\eta}_2)+e_{\ell 1}(\boldsymbol{\eta}_3)\right)\right]\left[\frac{\partial \phi^\ell}{\partial q}\right]_{i+1}
\end{aligned} \tag{9.217}$$

$$\begin{aligned}
D^1_{i,i+n-2} &\simeq d^1_{i,i-1}\cdot m_{i-1,i+n-2} = -\frac{1}{6}\left[\frac{1}{2}\left(e_{\ell 1}(\boldsymbol{\eta}_2)+e_{\ell 1}(\boldsymbol{\eta}_3)\right)\right]\left[\frac{\partial \phi^\ell}{\partial q}\right]_{i-1} \\
D^1_{i,i+n-1} &\simeq d^1_{i,i}\cdot m_{i,i+n-1} = -\frac{1}{6}\left[\frac{1}{2}\left(e_{\ell 1}(\boldsymbol{\eta}_2)+e_{\ell 1}(\boldsymbol{\eta}_3)\right)\right. \\
&\quad \left.-\frac{1}{2}\left(e_{\ell 1}(\boldsymbol{\eta}_1)+e_{\ell 1}(\boldsymbol{\eta}_4)\right)\right]\left[\frac{\partial \phi^\ell}{\partial q}\right]_{i} \\
D^1_{i,i+n} &\simeq d^1_{i,i+1}\cdot m_{i+1,i+n} = \frac{1}{6}\left[\frac{1}{2}\left(e_{\ell 1}(\boldsymbol{\eta}_2)+e_{\ell 1}(\boldsymbol{\eta}_3)\right)\right]\left[\frac{\partial \phi^\ell}{\partial q}\right]_{i+1}
\end{aligned} \tag{9.218}$$

A direct comparison of (9.216)-(9.218) and (9.210)-(9.212) verifies the theoretical error formulae (9.175)-(9.177). Specifically, (9.217) exactly reproduces (9.211), while (9.216) and (9.218) consistently and accurately approximate (9.210) and (9.212).

Part IV

Validations

Chapter 10

Discussion and Results: Quasi-1D 2-D and Axisymmetric Solutions

The numerical procedures developed in Chapters 5, 6, 8, and 9 have been implemented in a versatile FORTRAN code. Numerical verifications have focused on benchmark quasi-1-D shocked inviscid flows, a linear 2-D model hyperbolic system with analytical solution, and several 2-D and axisymmetric transonic, supersonic, and hypersonic flows. The computational results confirm both the well posedness of the developed boundary conditions, with relevant implementation, and the effectiveness of the directionally biased minimally dissipative weak statement (MDS) algorithm to annihilate any unbounded spatial semi-discretization dispersive error. Further, these results document the relative accuracy and stability features of the backward Euler (EU) trapezoidal/Crank-Nicolson rule (CN) and implicit Runge-Kutta (IRK) algorithms.

10.1 Quasi-1-D Euler Benchmark

The quasi-one dimensional Euler equation set is obtained from (1.1) as

$$\frac{\partial \tilde{q}}{\partial t} + \nabla \cdot \tilde{f} - s = 0 \tag{10.1}$$

$$\tilde{q} \equiv \left\{ \begin{array}{c} \rho \\ m \\ E \end{array} \right\} , \tilde{f} \equiv \left\{ \begin{array}{c} m \\ m^2/\rho + p \\ (E+p)m/\rho \end{array} \right\} , s \equiv \left\{ \begin{array}{c} -m(\frac{d}{dx}(A(x)))/A(x) \\ -m^2/\rho(\frac{d}{dx}(A(x)))/A(x) \\ -(eEp)m/\rho(\frac{d}{dx}(A(x)))/A(x) \end{array} \right\} \tag{10.2}$$

where ρ is the density, $m = \rho u$ is the single momentum component, E is the volume specific total energy, p is static pressure and $A(x)$ is the nozzle cross-sectional area distribution.

The de Laval nozzle geometry and test problem specification of Liou and van Leer [48] have been utilized for this test. The computational experiment boundary conditions are $\rho(0,t) = \rho_{in}$, $E(0,t) = E_{in}$, $p(L,t) = p_{out}$. Solutions were generated using various constant integration time steps $0.005 \leq \Delta t \leq 0.3$, corresponding to the range $0.65 \leq CFL_{\max} \leq 35$. The initial condition was steady state isentropic subsonic flow throughout.

An appropriate specification to evaluate accuracy and stability is for an impulsive change from steady isentropic subsonic flow, as accomplished by a step decrease in exit pressure p_{out} at $t = 0$. The resultant rarefaction propagates upstream as an expansion wave which, upon reaching the nozzle throat, triggers the development of a normal shock wave. Liou and van Leer's steady-state problem definition pa-

rameters are

$$M_{in} = 0.2395 \quad , \quad p_{out}/p_{total\ in} = 0.84 \tag{10.3}$$

and the theoretical steady state predicts a normal shock at location $x/L = 0.65$ with shock Mach number $M_s = 1.40$.

Figure 10.1 sketches the nozzle geometry with cross-sectional area distribution

$$A(x) = \begin{cases} 1.75 - 0.75\cos[(x-0.5)\pi/0.5]; & 0.0 \leq x \leq 0.5 \\ \\ 1.25 - 0.25\cos[(x-0.5)\pi/0.5]; & 0.5 \leq x \leq 1.0 \end{cases} \tag{10.4}$$

A uniform $M = 100$ node spatial discretization was employed, in concert with a linear trial space finite element implementation of the Minimally Dissipative MDS semi-discrete formulation, as developed in Chapter 5.

The MDS steady state solution is graphically summarized in Figures 10.2-3 as momentum and Mach number distributions. Convergence to steady state using the IRK algorithm in a one-iteration mode was achieved within 60 steps, for the dynamically optimized MDS dissipation parameter $\beta_\tau = 0.164$. The fully discrete nodal solution is essentially non-oscillatory (ENO), and the shock is quite crisp being captured within 3 elements, Figure 10.2. Furthermore, its location and upstream Mach number are accurately predicted, Figure 10.3, and the associated discrete approximation to the Rankine-Hugoniot jump condition is clearly evident in Figure 10.2.

For comparison, Figure 10.3 also displays the solution Mach distributions obtained by Liou and van Leer using several first- and second order accurate flux

splitting algorithms. They report steady-state convergence was achieved within 159 time steps using the backwards Euler rule. The first-order van Leer splitting appears the only procedure that yields a solution devoid of the shock precursory overshoots present in all second-order solutions. Comparing data in Figure 10.3 thus verifies that the selected MDS semi-discrete algorithm can yield accurate results for the problem class to be addressed. Hence, a time-accurate evolution will be affected principally by Δt, the chosen time integration algorithm, and the number of Newton iterations, see Chapters 7, 8.

In the next data set, the unsteady solution evolutions obtained by several time algorithms are quantitatively compared at a specified time station and for various time step sizes, for the described de Laval nozzle problem. Figures 10.4a-f summarize the reference time-accurate solution in terms of the Mach number distribution as obtained at six pertinent time stations. This is computed using the IRK algorithm, in a one iteration mode, with $\Delta t = 0.005s$, which renders the time truncation error magnitude negligible. Specifically, Figures 10.4a-c illustrate the upstream propagation of the expansion wave travelling towards the throat as caused by the step decrease in exit pressure. The flow then chokes, and a normal shock wave forms and strengthens in moving downstream, Figures 10.4e-f. The nodal solution is essentially non-oscillatory (ENO) throughout with a crisp shock, which is captured across at most three elements at station $t = 1.8s$, and only two elements at station $t = 2.8s$. At these two time levels, the shock Mach numbers are $M_s = 1.220$ and

$M_s = 1.330$, respectively. Figures 10.5a-c graph the associated density, momentum and pressure solutions at $t = 1.8s$.

This solution sequence was then repeated to compare Mach number distributions at time levels $t = 1.0s$ and $t = 1.8s$ as computed with $0.2s \leq \Delta t \leq 0.3s$. Figures 10.6a-c are associated with Figure 10.4b and compare the EU, CN, and IRK algorithm solutions obtained at $t = 1.0s$ using $\Delta t = 0.2s$, with the EU and CN schemes implemented in a two iteration mode. The shock has not yet formed and the accurate peak Mach number is $M_p = 0.95$. The presence of the rarefaction wave is best defined in the IRK solution, and the computed Mach number is indeed $M_p = 0.95$. The trapezoidal CN rule also yields $M_p = 0.95$, but displays an unacceptable outlet oscillation. Conversely, the EU backwards Euler solution reaches $M_p = 0.99$ and is very diffused, in agreement with inequality (8.62), hence generally inaccurate.

Figures 10.7a-c are associated with Figure 10.4e and compare the nodal Mach number solutions at time level $t = 1.8s$ as obtained using $\Delta t = 0.2s$ for each of the three integration algorithms. The accurate upstream and downstream shock Mach numbers are $M_{s1} = 1.220$ and $M_{s2} = 0.824$. The EU backwards Euler solution is monotone; however, the shock is very diffused. The Mach number distribution smoothly curves to negotiate the discontinuity, and the shock Mach numbers are $M_{s1} = 1.16$ and $M_{s2} = 0.848$, respectively. In contrast, the trapezoidal rule CN shows a much sharper shock characterized by accurate shock Mach numbers. How-

ever, the post-shock solution is distorted and oscillatory, hence unacceptable. In distinction, the IRK solution remains ENO with a crisp shock with correct shock Mach numbers.

Finally, Figures 10.8a-c show the Mach number solution at time level $t = 1.8s$, as determined employing $\Delta t = 0.3s$ for each integration procedure. All three solutions suffer a decrease in accuracy due to increased temporal truncation error. The EU backwards Euler solution remains very diffused, the shock now is spread over four elements and the relevant shock Mach numbers are $M_{s1} = 1.10$ and $M_{s2} = 0.818$. The trapezoidal rule solution displays a crisper shock, in the vicinity of the upstream curve, and the shock Mach numbers are accurate. However, the downstream distribution is somewhat diffused and adversely affected by a non-linear instability, following the analysis in Section 8.3. In distinction, the IRK solution remains notably superior, with very little downstream distortion of a visibly crisp shock, which has been computed at the maximum Courant number CFL=35.

These results firmly indicate that the IRK algorithm in comparison to EU and CN is of superior accuracy and stability, and highly competitive for this problem statement. The quasi-one-dimensional Euler results thus indicate the IRK algorithm may be of significant value in time-accurate and/or rapid steady state prediction of unsteady Euler and Navier-Stokes solutions.

10.2 Linear Hyperbolic Conservation Law System Case

Following the analysis in Section 4.1, a model problem definition was developed as appropriate to evaluate and critically compare IRK algorithm performance. The selected hyperbolic conservation law statement is obtained from (1.1) through the specifications

$$\tilde{q} \equiv \left\{ \begin{array}{c} q_1 \\ q_2 \\ q_3 \end{array} \right\} \; , \; \{\tilde{f}_1\} = \{\tilde{f}_2\} \equiv \left\{ \begin{array}{c} q_1 \\ q_1 + q_2 \\ q_1 + q_2 + q_3 \end{array} \right\} \tag{10.5}$$

Equations (1.1) with (10.5) are coupled and emulate, to a certain extent, the Euler system for a subcritical compressible flow condition. For $r = 1, 2$, and 3, an analytical solution for (1.1) with (10.5) is

$$q_r(x_i, t) = \exp(-2rt + (x + y)) + (7.5r^2 - 27.5r + 30)(1 + \sin(x - y)) \tag{10.6}$$

Note that the steady state of (10.6) is not a constant, but rather a set of sinusoidal waves of uniform period.

Computational experiments generating approximate solutions to (1.1) with (10.5) can be conducted on any region $\Omega \subset \Re^2$. The domain shown in Figure 10.9 was selected, since it contains one curved boundary segment (A-B) and one straight segment (A-D) upon which temporally varying Dirichlet data are required specified according to the characteristics analysis. The initial condition is established from (10.6) for any time $t = t_0$; the specific selection was $q_i(x, y, 0)$ for $1 \leq i \leq 3$. The

spatial semi-discretization employs the Galerkin integral statement finite element formulation of Chapter 5, as implemented with $\beta_{\underline{r}} = 2$ using the bilinear tensor product basis under an isoparametric coordinate transformation.

The numerical tests were conducted for this specification using the EU, CN and IRK time integration procedures for a range of time steps Δt. Figure 10.10 graphs the analytical solution (10.6) for q_1 in a perspective surface rendering at $t = 2.0s$. Figures 10.11-10.12 provide the corresponding surface perspective view of numerical solutions for q_1 at $t = 2.0s$, as obtained using $\Delta t = 0.1s$ and $\Delta t = 0.2s$ for the EU , CN and IRK methods. The corresponding extremum Courant numbers are CFL=4.8 , 4.8 and 9.6, respectively, and the dominating error mechanism is clearly visible.

For a quantitative analysis, Figures 10.13-10.14 graph perspective plots of the associated discrete approximation error $\varepsilon^h(x, y, t_n)$ in each solution field, where

$$\varepsilon^h(x_i, t_n) \equiv q(x_i, t_n) - q^h(x_i, t_n) \tag{10.7}$$

It is quite apparent that the IRK solution exhibits a significantly reduced error magnitude distribution in the comparison. Another measure of performance is efficiency, recalling that the non-iterative IRK algorithm operation count is twice that of either single stage integration algorithm. The selected measure is the sup (max) norm of the algorithm residual at any time station. Computational experiments were conducted for $1 \leq \Delta t \leq 5$ for the one-stage algorithms, and $2 \leq \Delta t \leq 10$ for the IRK algorithm. The corresponding maximum Courant number range is

$48 \leq \text{CFL} \leq 480$, respectively. For equal computational work, it was found that all three algorithms yielded comparable residual magnitudes at $t_n = 96s$ for q_1. Conversely, for q_2 and q_3, the IRK algorithm solution is closer to the accurate steady-state by a factor of two ($\pm$).

The dominant error mechanism in this test problem is directly aggravated by the TPF jacobian factorization. Hence, it is quite apparent that a distinct optimal Δt may exist for each temporal algorithm, which is undoubtedly problem dependent, that would minimize the associated TPF amplification factor. Nevertheless, all issues considered, the implicit Runge-Kutta algorithm performance appears uniformly superior to both the CN and EU, in the selected quantitative measures, and for the same computational work, for this definitive model problem.

10.3 Transonic Aerodynamics Benchmarks

10.3.1 Inviscid Airfoil Flows

The two-dimensional Euler test investigates a transonic flow around a parabolic arc airfoil in a channel [34]. The airfoil thickness based on the chord length is 20%. The channel is three chords long and one chord wide. The non-uniform grid contains 65×35 bilinear finite elements, yielding 2376 nodes, and is body-fitted with vertical lines remaining parallel to the y axis, Figure 10.15, with modest mesh clustering near the airfoil surface. Dirichlet contraints on ρ, m_y and E are applied

at the inlet, while the exit boundary condition is static pressure p_{out} yielding a nomal shock of prescribed strength ($M_s \simeq 1.4$) in a strictly quasi-1-D solution. The unsteady solution leads to formation of a supersonic pocket, with associated shock wave, and allows critical evaluation of algorithm stability and accuracy.

The backwards Euler (EU), trapezoidal rule/Crank-Nicolson (CN) and non-linearly stable implicit Runge-Kutta (IRK) procedures were each implemented with the tensor product factorization (TPF) scheme to integrate the MDS generated ODE system (5.65)-(5.67)/(5.68)-(5.70), with dissipation parameter set $\beta_r = 0.2$, towards a steady state with extremum Mach number $M_s \simeq 1.5$. As detailed in Section 3.2, the initial condition was established numerically from an isentropic subcritical state for exit pressure ratio $p_{out}/p_\infty = 0.72$ and for $M_\infty = 0.675$ at inlet. The computed Mach number distribution at $t - t_0 = 2.0s$ is shown in perspective view in Figure 10.16a. The shock is not yet quite formed, and the ENO nature of the finite element solution is clearly visible, both at the airfoil leading and trailing edge singularities and at the outflow boundary. The further decreased pressure ratio $p_{out}/p_\infty = 0.62$ was then imposed upon this reference state to start the unsteady evolution tests.

Figures 10.16b-d show the resulting Mach number distributions at time $t - t_0 = 7.9s$ as obtained using $\Delta t = 0.1s$ with each of the three time algorithms. The EU and CN algorithms are implemented in a two iteration mode, while IRK utilizes a single iteration per stage. The CN solution has incurred a fatal non-linear instability,

recall Section 8.3, as evidenced in 10.16c by the unbounded error corrupting the solution at the airfoil trailing edge singularity. Conversely, the EU and IRK solutions are ENO and appear virtually identical with $M_s = 1.13$. Note that the Mach contour lines intersect the far field boundary orthogonally, indicating an accurate boundary condition enforcement accruing to the developments in Section 3.1

Since the CN solution subsequently diverges, the conclusion is that the upper limit on CN stable time step is smaller than that for the EU or IRK algorithms for this problem. Therefore, the comparison continued with only the latter two procedures. Now setting $\Delta t = 0.15s$, Figures 10.17a and 10.18a compare the static pressure distributions at time $t - t_0 = 14.65s$, while Figures 10.17b and 10.18b illustrate the relevant solution Mach number distributions. Both pressure surfaces clearly show peaks at the airfoil leading and trailing edge singularities, which are preceeded by a one-cell undershoot. (Presumably, this could be eliminated with an appropriate local grid refinement.) Away from these regions, the pressure surfaces are ENO along the forming shock, which extends over three elements, and everywhere along the farfield and outflow boundaries.

The associated contour plots of pressure indicate an emerging qualitative difference between these two MDS solutions. This can also be seen in the Mach number distributions, which display a crisper shock hence better accuracy for the IRK procedure. The EU Mach number curve along the airfoil appears somewhat rounded

two cells before the shock. Moreover, the peak Mach number ($M_s = 1.401$) is not attained on the airfoil surface, but instead lies on the adjacent streamwise grid line. Conversely, the IRK solution airfoil Mach number curve bends sharply to negotiate the shock; further, the Mach number monotonically decreases from $M_s = 1.46$ on the airfoil into the lateral field.

Continued use of the fixed $\Delta t = 0.15s$ caused the EU procedure to slowly diverge as the solution continued beyond this time level. This divergence was probably triggered by usage of only two Newton iterations. Conversely, the IRK procedure converged directly to a steady state, at the maximum Courant number $\mathrm{CFL}_{\mathrm{max}} = 100$. Hence, the IRK algorithm admits the largest stable time step, among the procedures investigated, for this benchmark problem.

The features of the final solution, documented in Figures 10.19-10.22, then only depend upon the properties of the spatially semi-discrete statement (5.65)-(5.70) at steady-state. Figure 10.20 shows the velocity field; note that the shock is located very close to the airfoil trailing edge singularity. Figure 10.19 presents the contour plots of entropy, Mach number and the x - component of momentum. The entropy contours illustrate the production of entropy along the shock front. They also indicate the MDS algorithm has generated a modest local increase in entropy starting from the leading edge; this singularity-induced error can presumably be eliminated with a local grid refinement. The contours of the x-component of momentum are ENO and contain virtually parallel segments orthogonally aligned along the shock.

This pattern represents the nominal momentum Rankine-Hugoniot jump condition approximation, also readily evident in Figure 10.2 for the de Laval nozzle test.

A further assessment of MDS solution quality is presented in Figure 10.21 containing the surface perspective representation and contour plots of each scalar component of momentum. In both surfaces, a one-cell wide transverse plateau in the mesh emanates from the airfoil and propagates upwards along the shock front. The local gradients in the surface of the principal momentum are quite substantial, especially at the leading and trailing edges, yet these singularities are negotiated without apparent under- or over- shoot. Note how the outflow principal momentum distribution remains planar from the upper wall to about mid-channel, at the upstream state, and then smoothly decreases towards the lower boundary as total pressure is lost. The regularity of this curve also reflects favorably on the outflow pressure boundary condition enforcement. Finally, Figure 10.22 shows the steady state Mach number and static pressure distributions. Again, the contour lines intersect the upper wall orthogonally. The pressure surface appears ENO everywhere, with the possible exception of the leading and trailing edges singularities. The Mach number distribution also exhibits this feature, and the shock is quite crisp and captured within three elements with $M_s = 1.528$.

10.3.2 Viscous Airfoil Flows at $Re = 2000$ and $Re = 4.6 \cdot 10^6$

The two-dimensional Navier-Stokes tests are two viscous flows at different Reynolds numbers, based on airfoil chord, in the channel geometry of the previous inviscid problem. The first test corresponds to $Re \approx 2000$ and the second to $Re = 4 \times 10^6$, as representative of a practical aerodynamics configuration. The relevant mesh for the first simulation, on a 20% thick parabolic arc, Figure 10.23a, contains $M = 65 \times 35$ elements, with a rather non-uniform distribution clustering nodes at the aerodynamic surface where $\Delta y_{\min} = 0.02$. This mesh has permitted numerical simulations characterized by satisfactory compressible boundary layer resolution for this Reynolds number, i.e. $Re \approx 2000$. The principal validation sought is adequacy of the derived viscous flow boundary condition specifications. Thereafter, the developed steady state can be used as flow field initialization for the larger Reynolds number case.

The onset flow corresponds to $M_\infty = 0.615$, and Dirichlet inlet side constraints on ρ, m_y and E are specified along with vanishing normal deviatoric traction. The various slip wall specifications enforce vanishing transverse momentum and tangential tractions. The airfoil surface constraints are vanishing momentum vector and heat flux, for an adiabatic wall specification. Finally, the exit boundary conditions are specified p_{out} with vanishing deviatoric traction and heat flux.

The $Re = 2000$ steady-state solution, as obtained with IRK in a one iteration mode, yields a maximum Mach number $M_{\max} = 0.95$ at about two-thirds chord and

is summarized in Figures 10.23-10.25. Figures 10.23b-c graph the Mach number perspective surface and velocity vector field as obtained for $\beta_r = 0.2$. The laminar boundary layer appears satisfactorily resolved, except perhaps the leading edge stagnation region gradients. The Mach number surface terminates with a negative transverse slope at the trailing edge, which signals separation and an emerging recirculation zone. This is confirmed in the velocity vector field close-up, Figure 10.24a. The Mach number isocline distribution, Figure 10.24b illustrates this flow characteristic, along with the smooth merging of the essentially inviscid outer flow with the boundary layer and viscous wake.

The latter is further illustrated in Figure 10.25 which graphs distributions of both components of the momentum vector as well as static pressure and temperature. The surface perspective presentations clearly illustrate flow detail . The single indication of non-smoothness is the leading edge stagnation point peak, wherein a modest one-cell wider undershoot occurs. Hence, $Re = 2000$ is indeed the maximum that this grid can support. Note that the outflow principal momentum distribution remains planar, from the upper wall to about mid-channel, and then smoothly declines towards the lower boundary value. This character is accompanied by a temperature increase, initiated at the leading edge and continuously progressing towards the outlet. The regularity of all solution distributions reflects favorably on both the viscous flow MDS algorithm accuracy capability, aand boundary condition definitions and enforcement procedure.

This solution was employed to initialize a subsequent simulation with substantially increased Reynolds number $Re = 4.6 \times 10^6$, to validate highly non-uniform meshings for a practical viscous transonic aerodynamics problem. The leading-edge pressure oscillation and steep gradients in the results of the previous viscous flow test indicate the need for a much more refined, i.e. solution adapted mesh. Hence, the sheared mesh for this test contains $M = 65 \times 45$ bilinear elements with exponential-progression node clustering at the trailing and leading edges as well as the aerodynamic surface. The airfoil is now a 4% thick parabolic arc, as shown with mesh in Figure 10.26a. In the aerodynamic surface region, the mesh has wall resolution with vertical measure of the surface element equal to $1/Re$, and the resultant mesh extremum aspect ratio is of order 10. The transverse physical diffusion components are thereby resolved to the same order as the longitudinal convection components. The MDS stability parameter set remained fixed at $\beta_r = 0.2$ and for the boundary conditions of the previous test, a nominal steady-state was achieved in about 800 time steps at the maximum Courant number $C_{\max} = 100$, with IRK in a one iteration mode. The corresponding inlet Mach number became $M_\infty = 0.7$. At this stage the sup norm, $\|R\|_\infty$, i.e. the absolute value of the normalized-residual maximum component, decreased to $O(10^{-5})$. It was noted that for single precision calculations, the values of this norm oscillated boundedly in the range $O(10^{-5}) \leq \|R\|_\infty \leq O(10^{-6})$. This behavior was localized on the second half of the airfoil, whereas $\|R\| \approx O(10^{-8})$ elsewhere on the computational domain.

Figures 10.26b-10.27a are contour plots of axial momentum distribution in physical cartesian space (x, y), and in the laterally-stretched cartesian-transverse nodal (x, η_2) space. Very little flow detail is visible in the former, whereas the latter presentation clearly shows that a local shock-induced massive separation occurs just past mid-chord and extends to well beyond the trailing edge. It is the flow within this region, according to the computations, that appeared marginally unsteady. Figure 10.27b graphs a perspective view of the axial momentum distribution, to correlate with Figures 10.21 and 10.25. The solution appears virtually ENO and the essential flow features appear sufficiently resolved. Note that the decrease of momentum (to zero), at the leading edge and along the airfoil surface, occurs smoothly, with the possible exception of a modest two-cell under- over-shoot preceding the stagnation point. The outlet variation of this variable is totally devoid of dispersive oscillations. This distribution remains virtually planar in the essentially inviscid flow region and then drastically decreases in the viscous layer in a monotone way. Therefore, the validity of the outlet boundary condition choice for this case, as discussed at the end of Section 3.1, is evidently supported by the regularity of these results.

The shock wave boundary layer interaction is very clearly illustrated in the region just past mid-chord. It consists of two recirculation zones, the second being wider than the first. This significant flow activity then subsides in a wavy pattern in the wake originating after the trailing edge. Figure 10.28 shows the associated persective distribution of static pressure, which appears ENO everywhere, including

the stagnation point. The main difference between these data, and those in Figure 10.25 lies in the recirculation zone pressure variation. The latter is detailed in the close-up graph in Figure 10.28b. A virtual pressure plateau exists in the primary recirculation zone, whereupon the local shock triggers the pressure rise. Possibly the attendant boundary layer thickening in this region significantly alters the cross sectional area distribution to the extent of producing a virtual converging channel for the outer inviscid originally-subsonic flow which, therefore, accelerates. This event seems compatible with a decrease in pressure following its rise across the shock. This low pressure area is then terminated by a second shock, and accompanying trailing edge region recompression. This second pressure increase then causes the second separation, as illustrated in the momentum distribution in Figure 10.27b.

This numerical simulation has been the first aerodynamics Reynolds number transonic viscous problem computed with the derived MDS algorithm. The results appear stable and ENO and seem to conform with expected shock-boundary layer interaction phenomena. However, no experimental data are known for a practical comparison, hence independent solution validation was not attainable.

10.4 Supersonic Cases

10.4.1 Gasdynamic Inviscid Flows

The first test in this group examines fast convergence to steady state, as well as accuracy and efficiency of prediction of shocked supersonic flows. The 2-D benchmark geometry is a 20^o wedge, with onset flow at $M_\infty = 3.0$. The initial condition is isentropic freestream throughout. The steady state exact solution contains an oblique shock emanating from the wedge tip at an inclination of 38^o. The flow downstream of the shock is at $M_{out} = 2.0$, hence the entire flow field remains supersonic. Accordingly, Dirichlet constraints were imposed on density, both momentum components and energy at the inlet, with no Dirichlet conditions specified elsewhere. The appropriate wall tangency boundary condition is imposed via deletion of the convection surface integrals in the weak statement finite element implementation as detailed in Section 3.1. The algorithm formulation uses no constraint on the upper boundary, thereby permitting the computed shock to cross this boundary without spurious reflection or oscillation.

Three solution-adapted discretizations were utilized, with each mesh containing 65 $\times$ 35 bilinear quadrilateral elements. The IRK temporal algorithm was employed in a one iteration mode. Figure 10.29a shows the initial, simple sheared cartesian uniform body-fitted mesh, and graphs the steady inviscid solution density distribution obtained after 20 time steps, reaching a maximum CFL number of 10, Figure 10.29. The solution is strictly monotone, and it resembles the analytical

steady-state but is grossly diffused (as expected for this mesh). The simulation was restarted on a two-block solution-adapted mesh, Figure 10.30a, which concentrates grid refinement to the shock region. After 40 additional time steps, with CFL number exceeding 100, the steady solution density field resolution is much sharper, Figure 10.30b, with predicted shock much closer to being acceptable. This isodensity graph is also absolutely devoid of isolated closed contours, a firm indication of the desired essentially non oscillatory (ENO) MDS solution character.

The accepted steady solution was achieved on the second solution-adapted mesh, Figure 10.31a, which strongly clusters grid along the shock with absolute disregard for mesh aspect ratio and/or grid orthogonality. Thus, the semi-discrete ODE system becomes extremely stiff, yet the IRK algorithm converged to steady state using adequate time steps. The sup norm ot the solution residual decreased four orders to 1.0E-08 with six more time steps, whereupon the solution is indeed at steady state. The maximum CFL number in this stage was 150 with no indication of oscillation or instability. The final solution density distribution, Figure 10.31b, displays a crisp ENO shock simulation.

Solution quality is additionally assessed in Mach number and static pressure contours and surface perspective plots, Figure 10.32a-b. The arrow shows onset flow direction, and the discontinuity is correctly a straight line inclined at the analytical solution angle to three significant digits. The shock front is absolutely free of under- or over-shoots, and the overall solution field is devoid of any spurious oscilla-

tions. This ENO character especially holds along the inlet and the wedge boundary, where flow angularity accurately follows the configuration geometry without any explicit nodal enforcement strategy. As Figure 10.32b verifies, pressure is accurately and fully determined in the process of solving numerically the semi-discrete ordinary differential equations approximating the fundamental Euler conservation law system.

The second benchmark test investigates reflection of a wedge-generated shock impinging on a flat plate. The onset is an $M_\infty = 2.2$ supersonic stream, and the initial condition is uniform isentropic, as before. The analytical steady state is constituted of a primary shock, at inclination angle 30^o (from a 3.15^o compression ramp) impinging and reflecting off the plate. The flow downstream of reflection remains supersonic, and $M_{out} = 2.05$ in the wedge-shaped flow region between the incident and reflected shocks. This reflected shock then intersects the upper inclined boundary and subsequently leaves the computational domain. This geometry is used to document relative performance of the EU and IRK algorithms for swift steady state solution attainment.

Three grid adaption levels are used, with each containing 65×35 bilinear finite elements. Figure 10.33a shows the initial sheared-cartesian uniform body-fitted grid. The EU and IRK solutions were each started from the isentropic initial condition and, on this grid, the maximum CFL number was limited to 14 via maximum $\Delta t = 0.9s$ prescribed. Significant convergence rates distinctions were recorded. The

EU algorithm required about 100 time steps in a 2-iteration mode for the residual sup norm to reach 1.0E-07. Conversely, this level was achieved in only twenty time steps with the IRK algorithm in a one-iteration mode, which corresponds to forty computational cycles since IRK is a two-stage method. However, even if EU is utilized in a single iteration (delta-form) mode, the IRK algorithm still required 60% less computational work to meet this residual tolerance.

Figure 10.33b graphs the density contour distribution for the twenty-step IRK solution, which sufficiently defines the steady-state solution weak shock character for a mesh adaptation. Improved resolution is achievable on the solution-adapted mesh, Figure 10.34a, with grid density enhanced in each shock region. The EU and IRK algorithm solutions were each continued to their final respective steady-state on this mesh, and significant convergence rate differences were observed. The IRK algorithm converged for CFL $\leq$ 360, corresponding to the maximum $\Delta t = 0.9s$. Conversely, the EU procedure incurred fatal divergence for a CFL number exceeding 240. The associated 2^{nd} order temporal truncation error, absent in the IRK rule, thus appears to affect adversely the stability of the tensor product factorization procedure at large Δt, recall the analysis in Section 9.10.

The corresponding IRK density solution is shown in Figure 10.34b. The solution is comparatively much sharper and remains totally devoid of dispersive oscillations. The accepted steady solution was achieved following twenty more time steps, at a maximum CFL $\leq$ 600, on the third adapted mesh increased to $M = 64 \times 74$

bilinear elements, Figure 10.35a, that truly clusters mesh without regard to aspect ratio or element skewness. Hence, the semi-discrete ordinary differential equation system again becomes extremely stiff. Figure 10.35b confirms a very crisp density distribution that accurately captures the shock reflection features. Solution quality and monotonicity are verified in Figures 10.36-10.38 in terms of Mach number, static pressure and entropy contour as well as surface perspective distributions. Both shock fronts are devoid of unphysical wiggles, yielding an accurate ENO middle-region plateau where $M = 2.05$. The arrow denotes free-stream flow direction in each plot, which is selected for perspective viewing clarity. It is emphasized that this steady state solution was achieved in sixty time steps using the MDS algorithm with IRK time integration on three sequential remeshings that are geometrically totally arbitrary via solution-adaptation.

An allied solution was obtained for this shock reflection problem by specifying a solid wedge surface to reflect the shock a second time. The initial grid and associated density contour distribution are shown in Figure 10.39a-b. Three mesh levels were again utilized, each containing $M = 64 \times 74$ bilinear elements, and the solution was advanced 20 time steps on each grid. Therefore, Figures 10.39a-b correlate with Figures 10.33a-b differing only in the second shock reflection. The final steady state was achieved in 60 time steps with IRK in a 1-iteration mode at a maximum CFL number exceeding 600. Figure 10.39c-d detail the final solution adapted mesh and associated density distribution. The perspective solution surface and contour

plots evidence an accurate shock reflection from the upper streamline boundary without spurious oscillation, although local mesh resolution at the second reflection is inadequate. Figure 10.40a-b verifies the monotone juxtaposition of the solution Mach plateaus and reflected shocks, with the fourth plateau intersecting the outflow boundary without warping.

10.4.2 Shock-Wave Flat-Plate Boundary Layer Interaction

The second viscous benchmark investigates and compares the separation of a supersonic laminar boundary layer induced by an impinging oblique shock wave. The specification for this problem was taken from [46,55] and Figure 10.41a illustrates the qualitative flow pattern. The steady state contains two primary shocks, one originating at the plate leading edge and the second emanating from the upper compression ramp, Figure 10.33a. This oblique shock is deflected in its interaction with the leading edge shock, and then triggers separation of the laminar boundary layer in its reflection. The onset flow Mach number is $M_\infty = 2.15$, and the Reynolds number is $Re = 0.96 \times 10^5$ based on the reference distance X_{sh} (80 mm) between the plate leading edge and the shock-impingement point. The Prandtl number is $Pr = 0.72$, and the freestream static pressure and temperature are $p_\infty = 1,000.660 N/m^2$ and $T_\infty = 148.873 K$.

Accordingly, the inlet boundary conditions are full Dirichlet. Vanishing y-momentum component and x-deviatoric traction were imposed upstream of and

downstream the plate boundary layer surface. Inviscid wall tangency is enforced along the upper boundary, and prescribed total surface tractions and vanishing heat flux are enforced at all outlet segments. These conditions are again enforced in the appropriate MDS surface integrals in the the weak statement (5.68)-(5.70). Finally, the no-slip conditiion is imposed on the flat plate which is also defined as an adiabatic wall.

Efficient progression to the steady state was promoted via intermediate computation of an allied inviscid flow, on the geometry, that promotes development of the described shock wave pattern. This auxiliary flow evolves from the previous benchmark Euler solution, Figure 10.35b, by inserting an isolated stagnation point at the lower plate boundary leading edge. This generates an "inviscid leading edge" shock wave that intersects the compression-corner wave. This steady state solution was achieved in 60 steps with the IRK procedure at a maximum CFL number exceeding 500.

The viscous simulation proceeds from this initial condition following linear extrapolation of both momentum components to zero in a suitable-size region above the plate surface. A nominal steady state was achieved with IRK in a 1-iteration mode, on a sheared cartesian $M = 64 \times 76$ mesh with wall minimum measure of order $\frac{1}{Re}$, after 400 time steps with CFL ≤ 200. Figures 10.41b-10.44b summarize the steady solution as contour and perspective surgace graphs for various thermodynamic variables, Mach number and axial momentum. As Figures 10.42b-10.44-b

indicate, the shock wave-boundary layer interaction pattern is apparent as well, as is the increase in temperature in the compressible flow boundary layer. Note that the solution is uniformly ENO including the outlet region which is totally undistorted. The impingment point is located at $X_{sh} = 0.77$mm from the plate leading edge, which is within 5% agreement with the value reported in [46]. Figure 10.44a-b presents the static pressure distributions for two upper wall boundary conditions, i.e. inviscid supersonic outflow and wall tangency. These pressure distributions differ significantly, locally, and in both cases the solution is ENO.

Robust convergence at large CFL and relevant solution ENO quality were attained provided that the variation of mesh metric data e_{kj} is smooth in the boundary layer separation region. Additional testing confirmed that abrupt non-parallelogram variations in element aspect ratios significantly reduced convergence rate, i.e. $\mathrm{CFL}_{\mathbf{max}}$, and could generate unphysical oscillations in the viscous separation regions of the solution field, where the local β_r was reduced to zero to verify uncompromized physical diffusion effects.

Figure 10.45 compares the plate surface pressure distribution of the present results with the experiment of [46]. The comparison with the experiment is very good upstream of and through the recirculation region, but thereafter the computed adverse pressure gradient is much larger than measured. This may be influenced by the outer wall tangency boundary condition and/or shock impingment location, which additional numerical experiments could verify. Further, the difference be-

tween computational and wind-tunnel boundary conditions, for the experiment in [46], can also contribute to the noted difference. Figure 10.46 compares wall skin friction distribution to the data of [46]. The axial extent of the recirculation region, shown in Figure 10.47, is correct, although the present results are shifted about 10 % downstream. The largest difference between computational and experimental peak pressure in the reattached flow is about 15%. The prolonged adverse pressure gradient thus delays firm reattachment of the boundary layer. Certainly, additional adapted mesh investigations of this benchmark case are warranted.

10.5 Hypersonic Cases

10.5.1 Blunt Body Inviscid Flow

The first inviscid test is formation of a detached bow shock for a parabolic blunt body in a mildly hypersonic freestream flow. The onset flow is at $M_\infty = 6.5$, and the steady state admits a strong shock that curves and progressively weakens as it wraps around the body, [53]. The outlet flow remains supersonic, hence full Dirichlet boundary conditions are used on inflow boundaries. The flow center line and body surface are streamlines, hence vanishing normal momentum flux is the inviscid constraint. A steady state was achieved in approximately 850 time steps, with IRK in a one iteration mode, on three different solution-adapted $M = 65 \times 35$ meshes, attaining the maximum $\mathrm{CFL}_{\mathrm{max}} \simeq 260$ on the final mesh. Figure 10.48a shows the

third level solution-adapted mesh with definition in the bow-shock and body nose tip regions. Figure 10.48b graphs the associated density contour quatifying solution accuracy and freedom from oscillations. The smooth contours in the region between the shock and the body further confirm the global ENO solution character.

10.5.2 Missile Inviscid and Viscous Flows

The second test is formation of the blunt body bow shock and shock layer about an axisymmetric sphere-biconic body in hypersonic flow with $M_\infty = 8$ for two sets of thermodynamic freestream conditions. The configuration consists of a $0.5''R_N$ nosetip, a 10.5^o forecone and a 7.0^o aft cone section with axial lengths 12.32in and 20.00in respectively. For this geometry, the shock layer abounds with significant expansion waves that interact with the bow shock inducing noticeable gradients in its curvature. The inlet Dirichlet constraints on density, momentum and specific total energy are appropriate. Vanishing radial momentum is enforced along the centerline, and both momentum components are set to zero at the stagnation point. Along the aerodynamic surface, vanishing momentum flux is imposed for the inviscid flow simulation, whereas the no-slip condition is enforced for the viscous flow prediction. The Rankine-Hugoniot conditions, along with Newtonian surface pressure distribution and available shock location estimates, are used for initial condition determination, as detailed in Section 3.22. Figure 10.49 shows the geometry of the computational domain, discretized with a body-fitted mesh that consists of

64×74 bilinear elements with non-dimensional $\Delta x_{\min} = O(10^{-5}) = O(1/Re)$ in the nosetip region.

For freestream thermodynamic conditions $p_\infty = 600.12 N/m^2$ and $T_\infty = 54.31^o K$, the ideal-gas viscous flow about this configuration is determined at the reference $Re_\infty = 500,000$, with the boundary layer initial condition obtained via linear interpolation to zero of the momentum components in a suitably narrow strip region about the aerodynamic surface. The machine zero steady state was achieved for $0.35 \leq \beta_r \leq 0.50$, and with IRK in a 1-iteration mode in approximately 800 time steps at the maximum CFL number exceeding 200. For an adiabatic wall, the boundary layer strongly interacts with the exterior essentially invisid flow. The terminal shock stand-off distance is $\delta \simeq 0.075$in, which agrees to within 1.5% with available correlations [22]. Figures 10.50-10.51 document this steady solution in terms of Mach number and temperature. The fundamental decrease to nought of Mach number in the boundary layer, paralleled by a drastic temperature increase are sharply defined and monotone, as well as totally free of numerical dispersion. The stagnation-point peak values for pressure and temperature are $p = 55383.87 N/\mathrm{m}^2$ and $T = 832.11^o$K. An important flow feature is the interaction of the hemisphere-cone juncture expansion wave with the bow shock, resulting in the deflection of the shock branch away from the nose, as illustrated by the pressure contours in Figure 10.52. In this plot, the contrasts with the invisid flow pressure distribution are evident, and clearly show the expected reduction in shock stand-off distance.

Note the apparent widening of the bow shock. This is only due to the distortion of the underlying grid, as caused by a non-linear magnification of the nose region. This magnification uses different scales for the x- and y- axes to achieve acceptable nose-region bow shock graphic resolution.

The associated invisid flow solution is obtained at a maximum CFL number exceeding 500, with maximum convergence rate occurring at CFL $\simeq$ 200. For the previous values of β_r, the solution is virtually monotone and devoid of spurious dispersive oscillations, and the computed stand-off distance $\delta \simeq 0.068$in agrees to within $\pm 4\%$ with available correlations [22].

Figures 10.53-10.54 summarize the steady solution in perspective view. The Mach number distribution is essentially monotone throughout the sharp-shock compresion and subsequent steep-gradient expansions. The associated shock expansion-wave interaction is evident in the intricate variations of density, from its rise across the shock and towards the stagnation point, to its sharp decrease along the body surface. Note the relevant gradients in the shock curvature and overall regularity of these distributions which verify the essentially non-oscillatory solution character.

Figure 10.55a graphs the distribution of pressure about the biconic body. The bow shock appears quite crisp and the compression towards the stagnation point is smooth, leading to the peak pressure $p = 55383.87 N/\mathrm{m}^2$. The subsequent flow expansion about the spherical nose is also smooth and clearly defined. No isolated close contours are present, thus the solution is devoid of unphysical wiggles. Note

that the shock contour concentration decreases away from the body tip, since the entropy rise diminishes as the bow shock wraps around the body. For the reference wind-tunnel free stream temperature of $T_\infty = 54.31°K$, the post shock and stagnation-point temperature values are $T = 773.2°K$ and $T = 832.11°K$. Hence, an ideal gas simulation in these conditions is adequate. However, for operating altitude, atmospheric freestream conditions, the temperature rise across the bow shock triggers non-negligible real gas effects. Hence, the invisid-flow is re-initiated with free stream conditions $T_\infty = 221.1°K$ and $p_\infty = 2.72 \times 10^{-2}$atm, corresponding to flight in standard atmosphere, with real gas effects simulated as described in Section 1.2.

For the previous values of β_r, the final steady state is directly achieved in approximately 400 time steps starting from the ideal-gas terminal solution, at maximum CFL number 200. Evidently, the continuous and accurate computation of the pressure derivatives for the implicit implementation promotes the observed monotone convergence. Figure 10.55b graphs the pressure contours for this more realistic case, as contrasted with the associated ideal-gas distribution. As indicated in this figure, real gas effects lead to a decrease of the shock stand-off distance to $\delta \simeq 0.056$in, almost 18% less than the associated ideal-gas value. This reduction is expected since in the real-gas case pressure does not appreciably vary, from the ideal-gas situation, whereas temperature substantialy decreases as shown in Figures 10.56-10.57. Therefore, the local density is higher, with respect to the ideal-gas value.

Consequently, the given freestream mass flow rate can be negotiated in a thinner shock layer.

The distribution of pressure along the stagnation streamline and aerodynamic surface is presented in Figure 10.56a. For the reference freestream conditions, the equilibrium air pressure distribution does not radically differ from that corresponding to the ideal gas case, with the exception of the shock location. Conversely, as indicated in Figure 10.56b and more in detail in Figure 10.57, the temperature fields are significantly different. For the same conditions, the post shock temperature for the ideal-gas simulation, corresponding to $T_\infty = 221.1^\circ K$, is $T = 3149.9^\circ K$, whereas the equilibrium gas value is $T = 2595.2^\circ K$, a decrease of almost 18% accounted for by the energy absorbed during exicitation of vibrational modes and eventual formation of nitric oxide and atomic oxygen. As indicated in Figures 10.58-10.59, these species are formed immediately after the shock, with peak production at the stagnation points. The mass fraction of nitric oxide is almost six times larger than the oxygen mass fraction, while only negligible traces of atomic nitrogen are present.

Thus, these results indicate that even for relatively low hypersonic Mach numbers, real gas effects for atmospheric flight free stream conditions significantly influence the air mixture chemical composition Consequently, the relevant temperature field appreciably varies in comparison with that associated with an ideal-gas prediction. In any case, the developed MDS implicit finite element algorithm has produced essentially monotone results even for this more challenging situation.

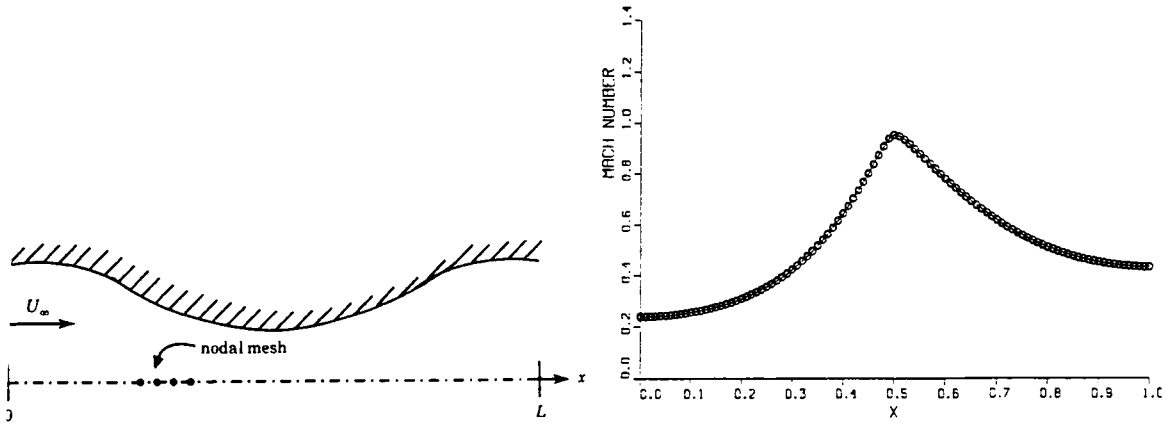


Figure 10.1: de Laval Nozzle and Initial Condition Mach Number Profile.

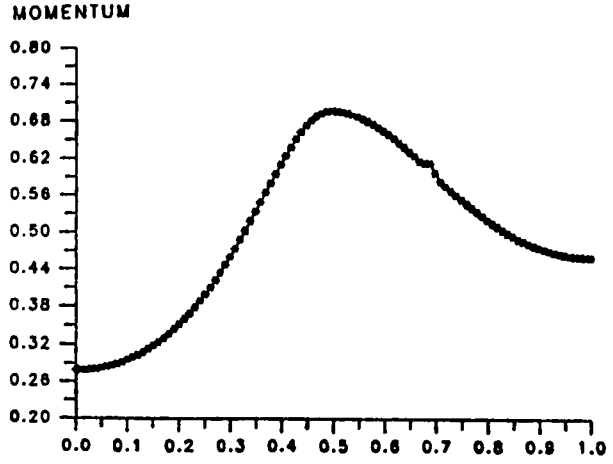


Figure 10.2: MDS Finite Element Quasi-1-D Euler Algorithm Steady-State Solution, $M_s \simeq 1.40$, Momentum Distribution

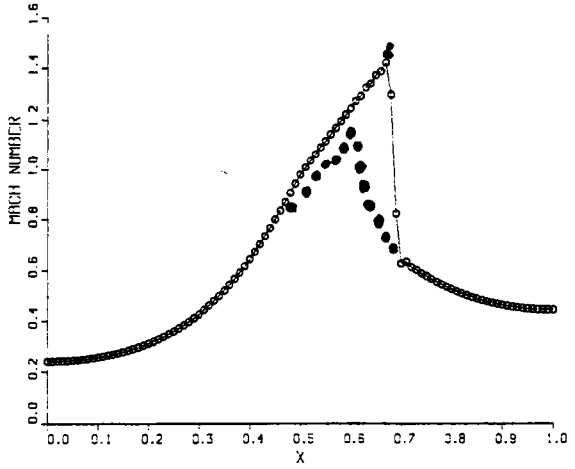


Figure 10.3: MDS Finite Element Quasi-1-D Euler Algorithm Steady-State Solution, $M_s \simeq 1.40$, Mach Number Distribution and Comparisons from [48].

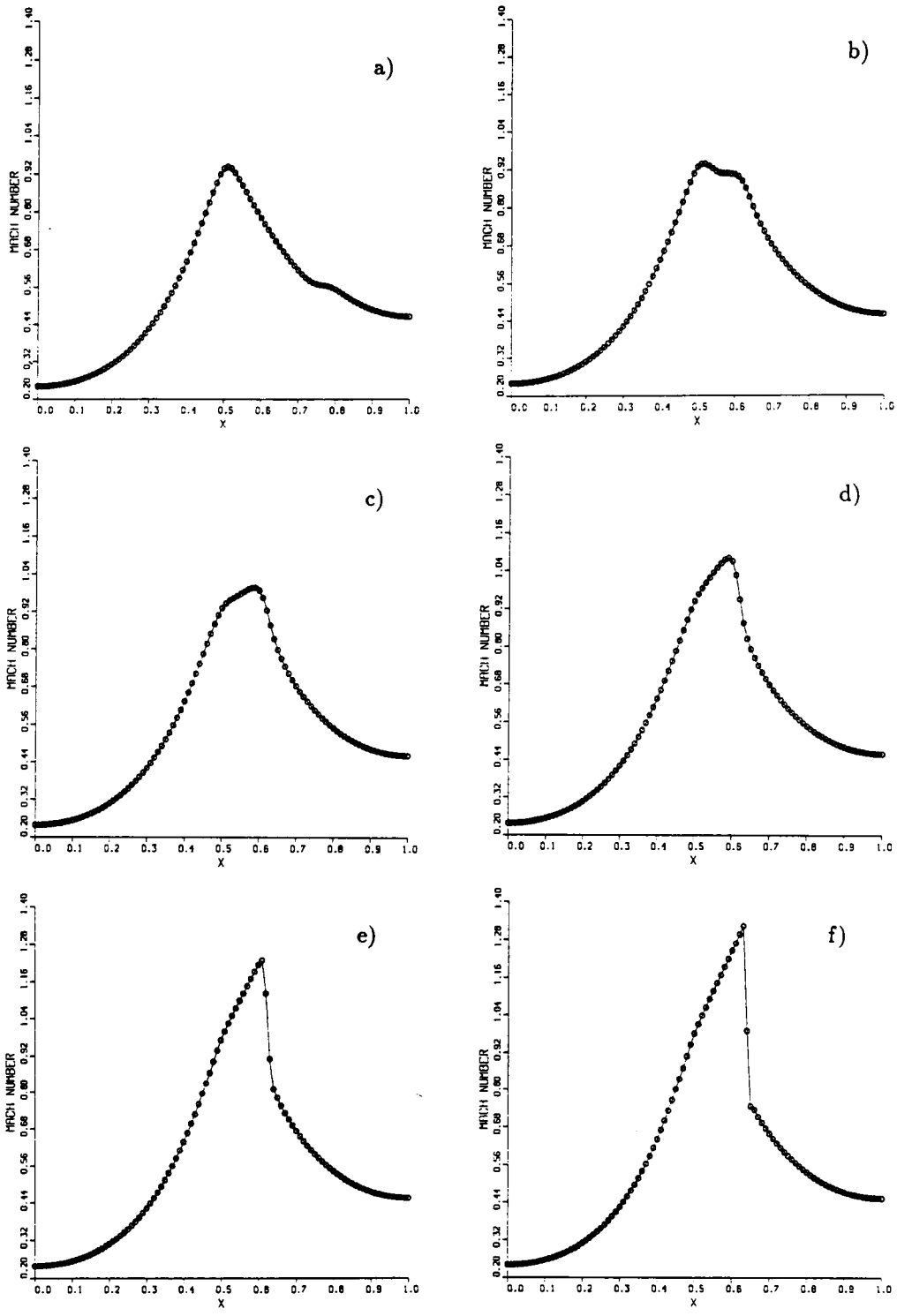


Figure 10.4: Unsteady Quasi-1-D Euler Solution. Implicit Runge-Kutta. Mach Number Profiles. $\Delta t = 0.005s$, a) $t = 0.4s$, b) $t = 1.0s$, c) $t = 1.2s$, e) $t = 1.8s$, f) $t = 2.8s$.

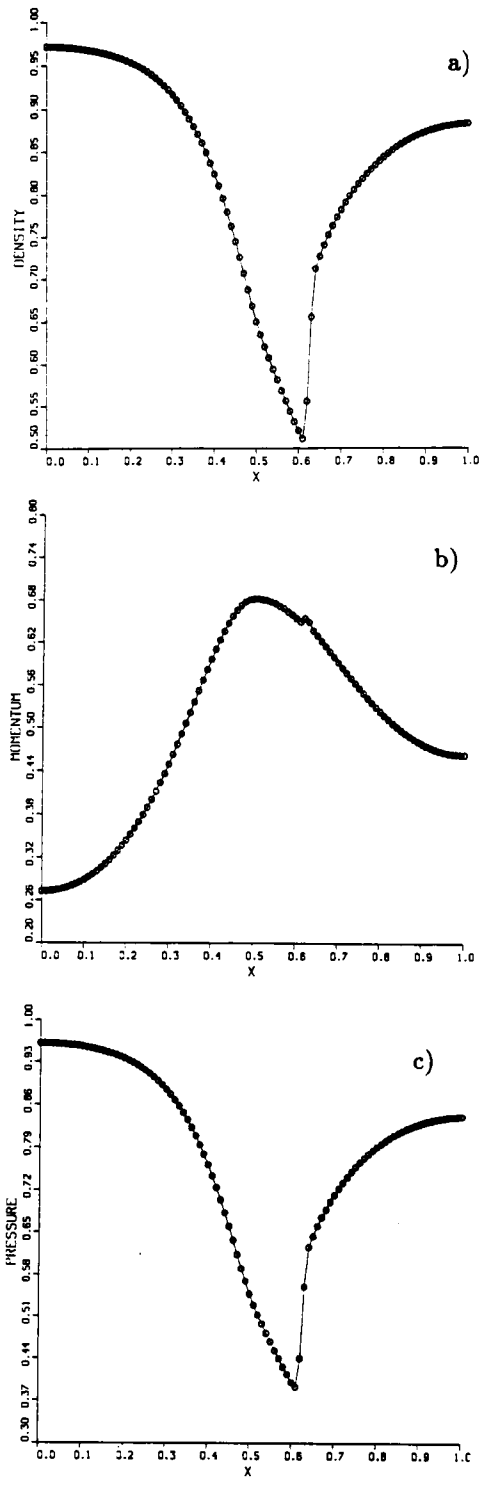


Figure 10.5: Unsteady Quasi-1-D Euler Solution. Implicit Runge-Kutta. $\Delta t = 0.005s$, $t = 1.8s$, a) Density, b) Momentum, c) Pressure.

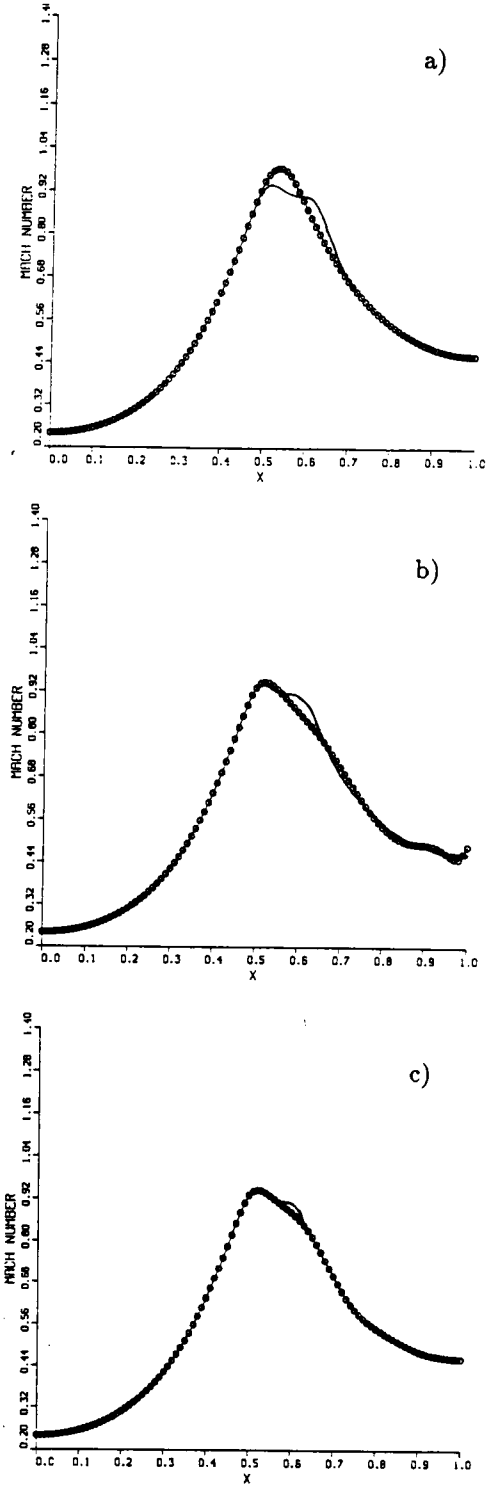
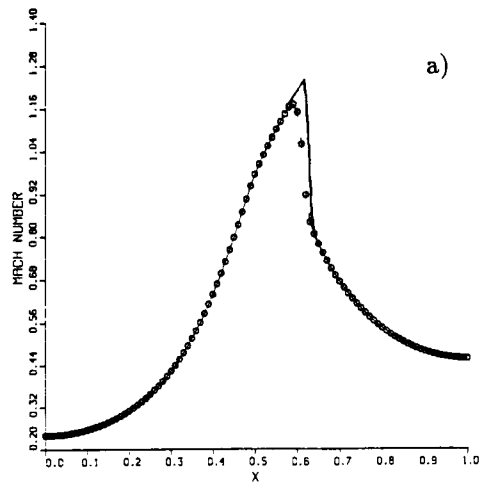
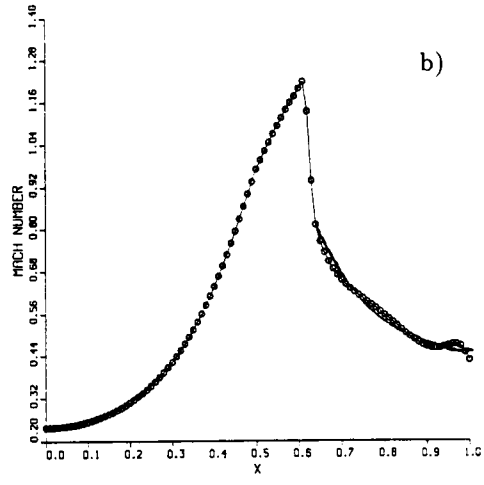


Figure 10.6: Unsteady Quasi-1-D Euler Solution Comparisons, $t = 1.0s$, $\Delta t = 0.2s$, —from Fig. 10.4b, a) EU, b) CN, c) IRK.





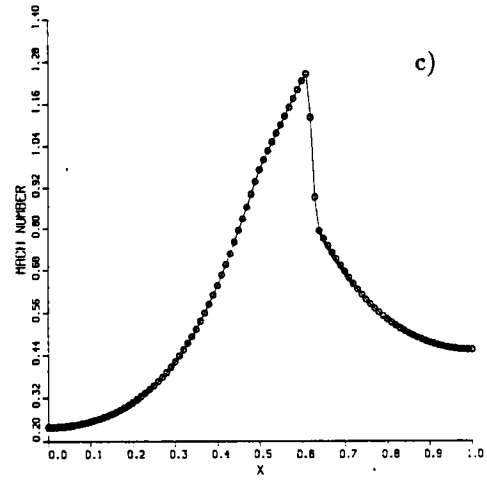
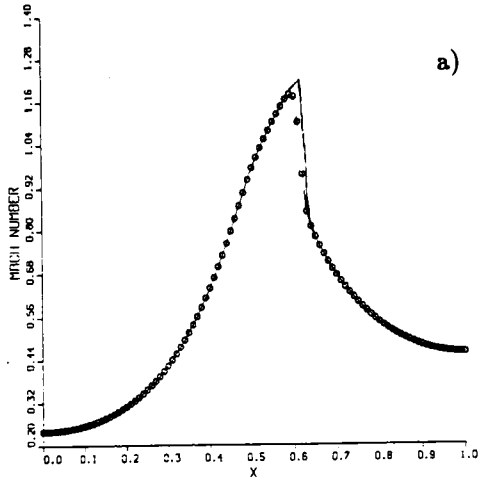
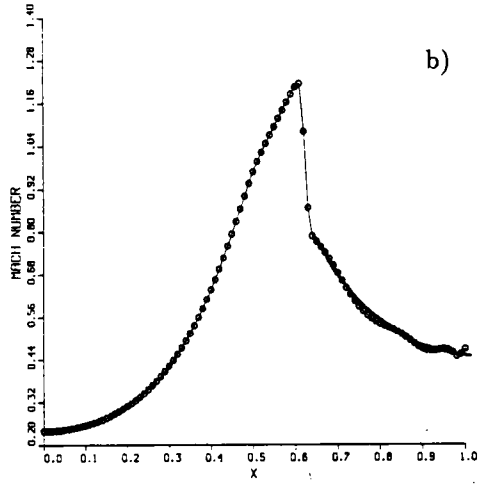


Figure 10.7: Unsteady Quasi-1-D Euler Solution, $t = 1.8s$, $\Delta t = 0.2s$, —from Fig. 10.4e, a) EU, b) CN, c) IRK.





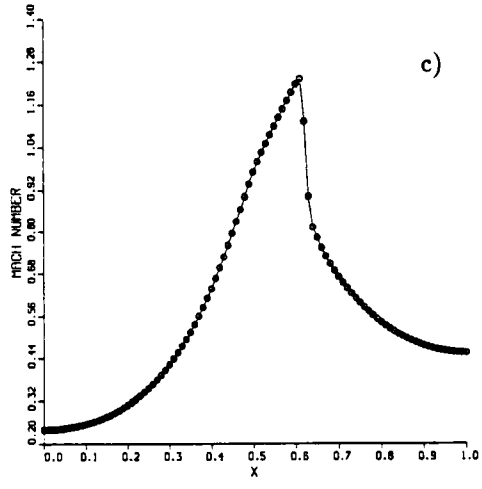


Figure 10.8: Unsteady Quasi-1-D Euler Solution, $t = 1.8s$, $\Delta t = 0.3s$, —from Fig. 10.4e, a) EU, b) CN, c) IRK.

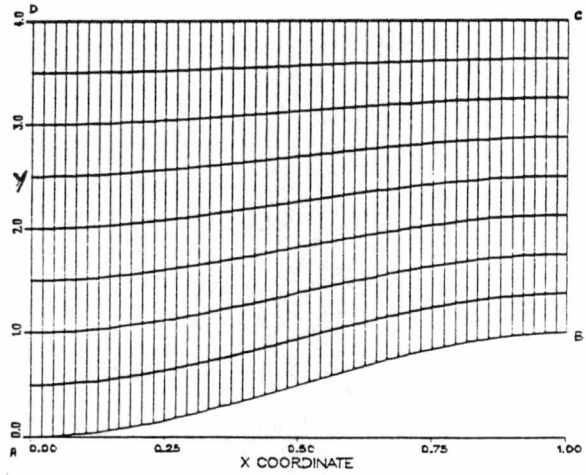


Figure 10.9: Two-Dimensional Linear Problem Domain and Discretization Ω^h.

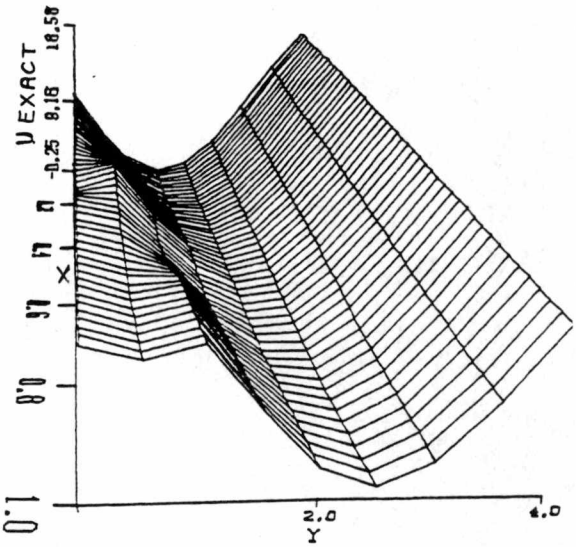


Figure 10.10: Analytical Solution Interpolation on Nodes of Ω^h for q_1, $t = 2.0s$.

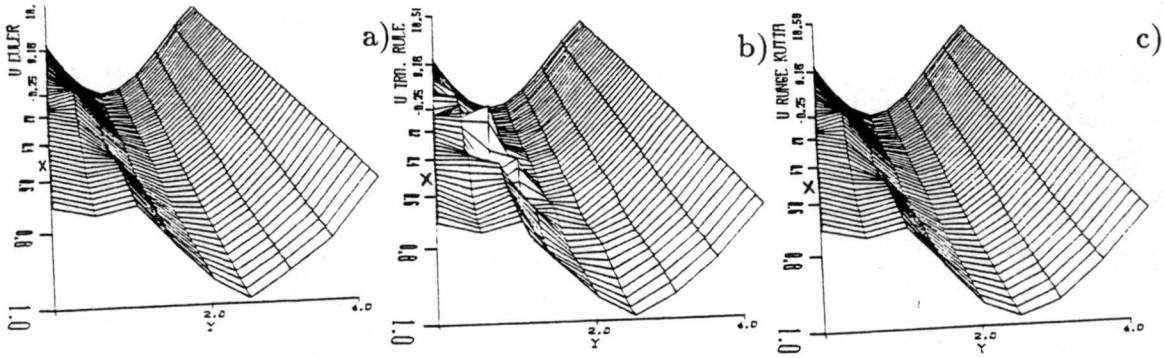


Figure 10.11: Computed Solution Surface Perspectives for q_1, $t = 2.0s$, $\Delta t = 0.1s$, a) Backwards Euler, b) Trapezoidal, c) Implicit Runge-Kutta.

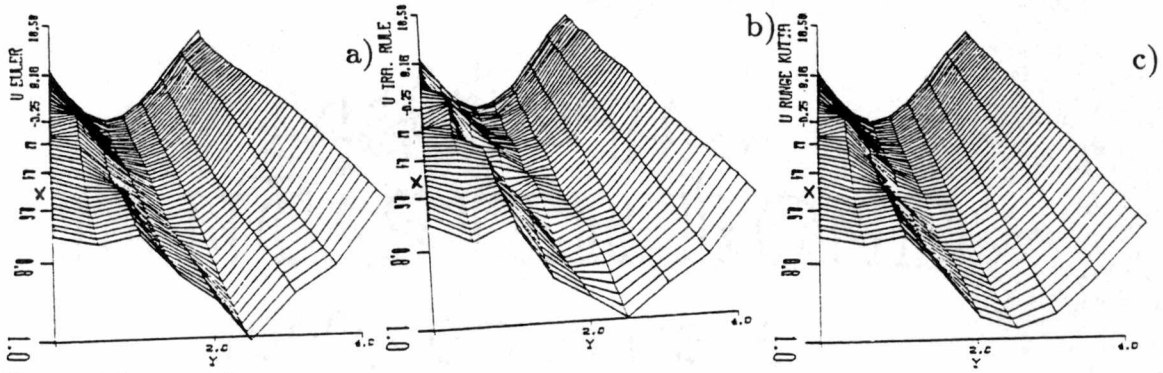


Figure 10.12: Computed Solution Surface Perspectives for q_1, $t = 2.0s$, $\Delta t = 0.2s$, a) Backwards Euler, b) Trapezoidal, c) Implicit Runge-Kutta.

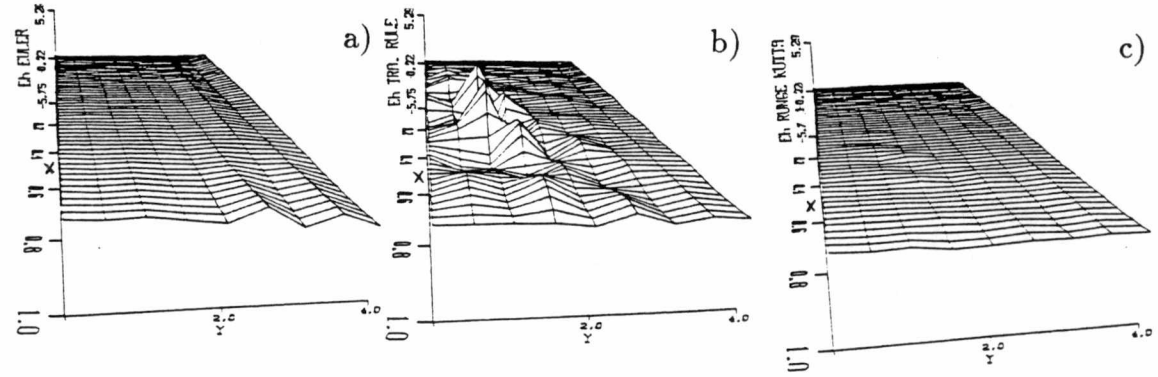


Figure 10.13: Error Distribution Perspective for q_1, $t = 2.0s$, $\Delta t = 0.1s$, a) Backwards Euler, b) Trapezoidal Rule, c) Implicit Runge-Kutta.

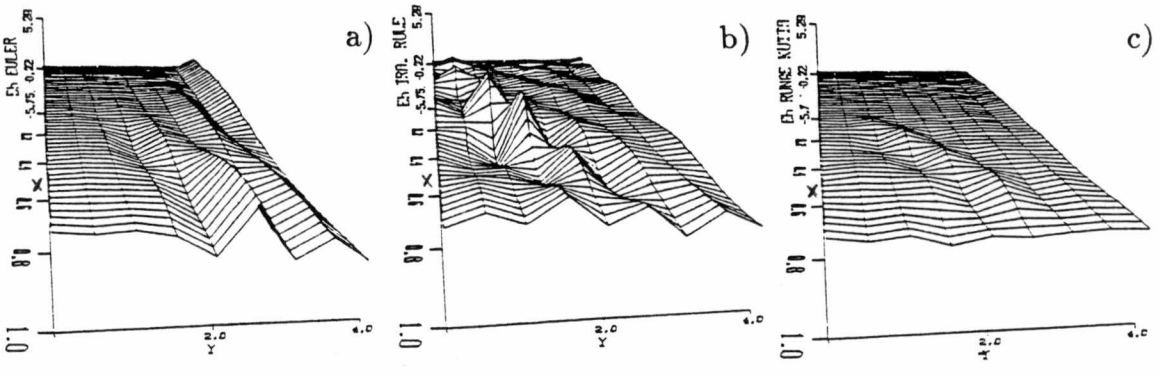


Figure 10.14: Error Distribution Perspective for q_1, $t = 2.0s$, $\Delta t = 0.2s$, a) Backwards Euler, b) Trapezoidal Rule, c) Implicit Runge-Kutta.

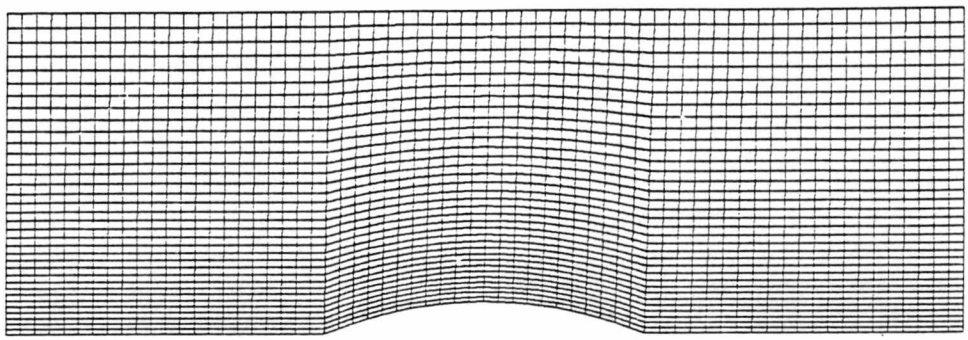


Figure 10.15: M=65 $\times$ 35 Nonuniform Mesh for Transonic Parabolic Arc Problem.

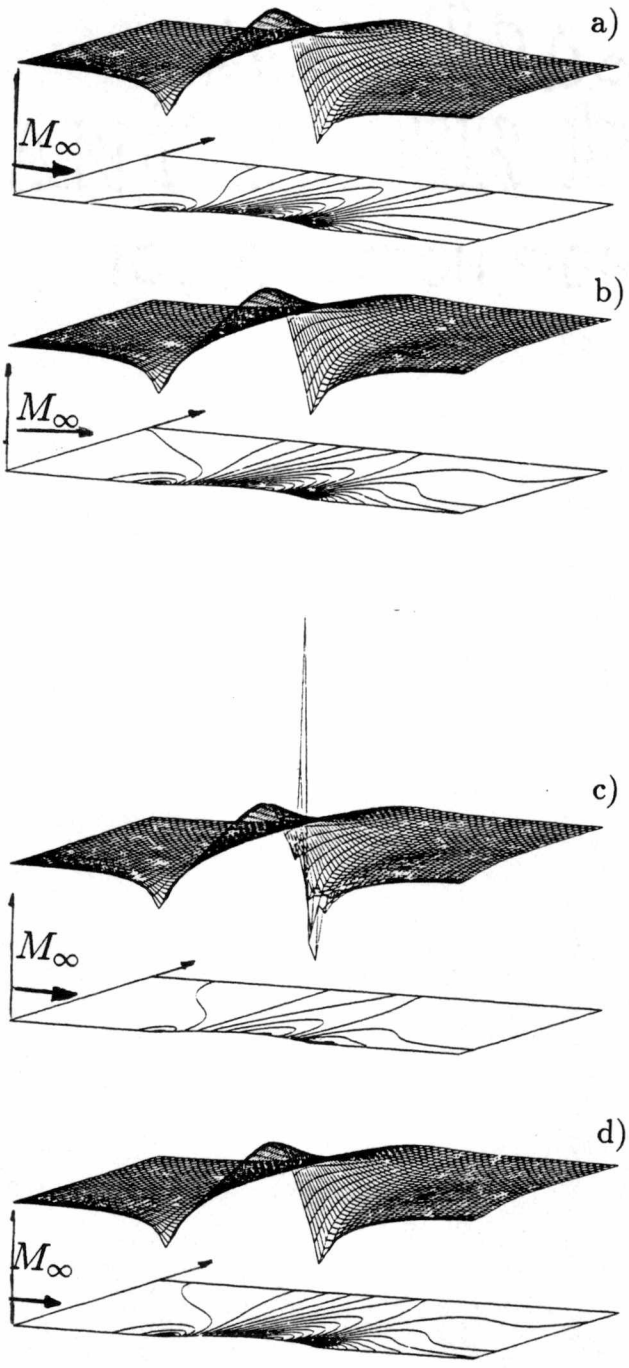


Figure 10.16: MDS Algorithm Unsteady Solution, Euler Equations, $t - t_0 = 2.0s$, Transonic Mach Number Surface Perspective and Contours, a) Initial State, b) Backwards Euler Rule, c) Trapezoidal Rule, d) Implicit Runge-Kutta.

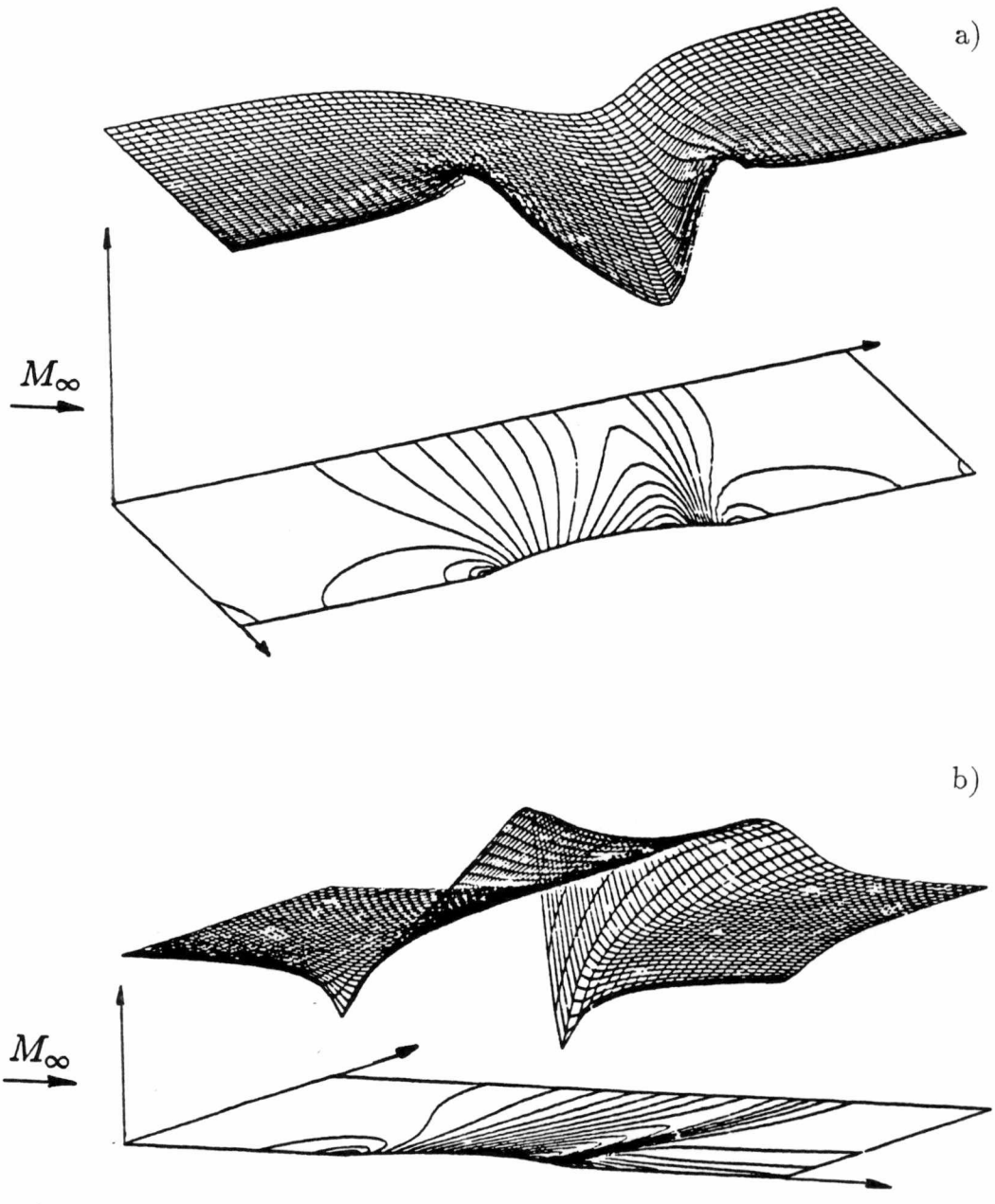


Figure 10.17: MDS Algorithm Unsteady Solution Perspective and Contours, Euler Equations, $t - t_0 = 14.65s$, $\Delta t = 0.15s$, Backwards Euler Rule, a) Pressure, b) Mach Number.

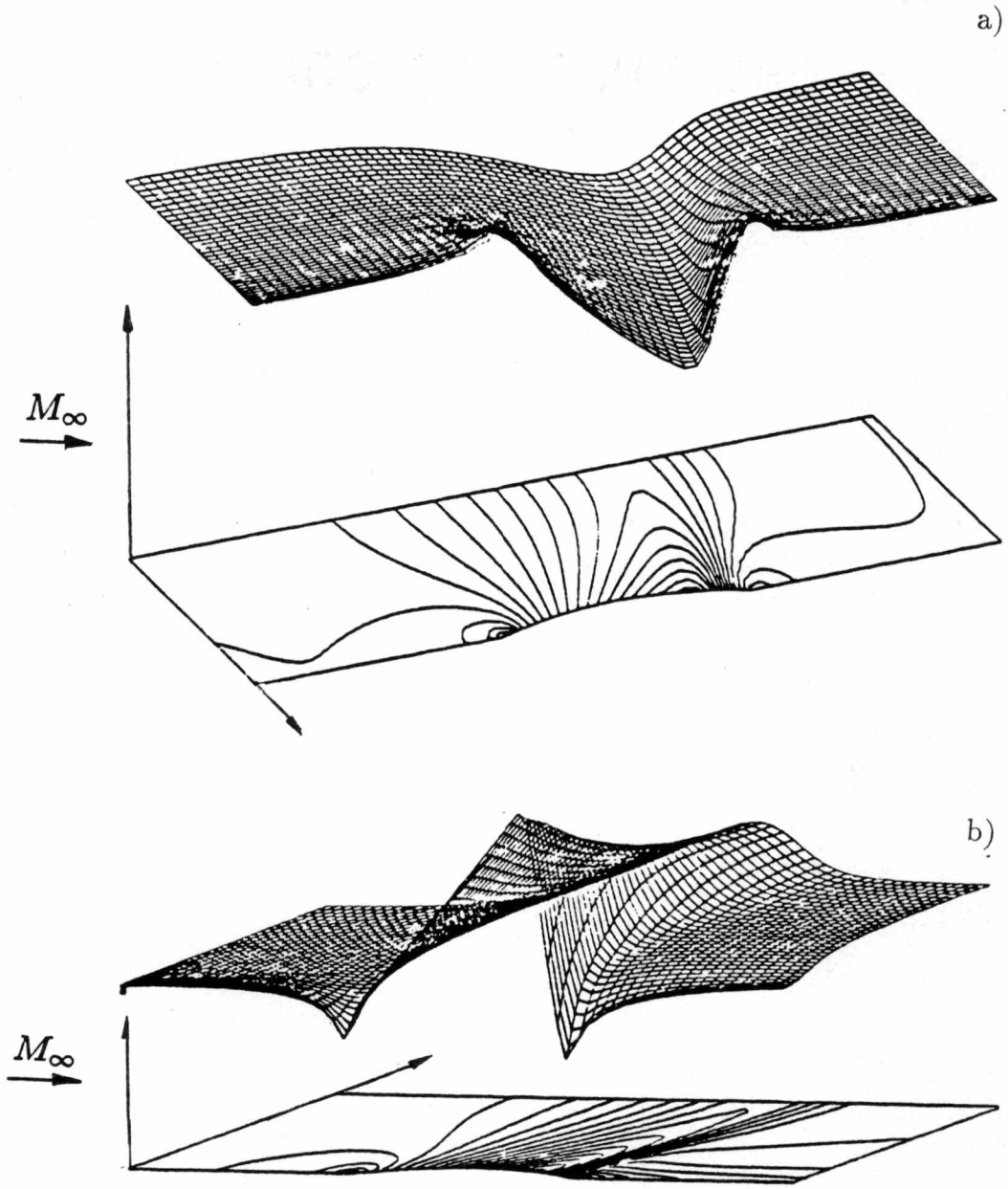


Figure 10.18: MDS Algorithm Unsteady Solution Perspective and Contours, Euler Equations, $t - t_0 = 14.65s$, $\Delta t = 0.15s$, Implicit Runge-Kutta, a) Pressure, b) Mach Number.

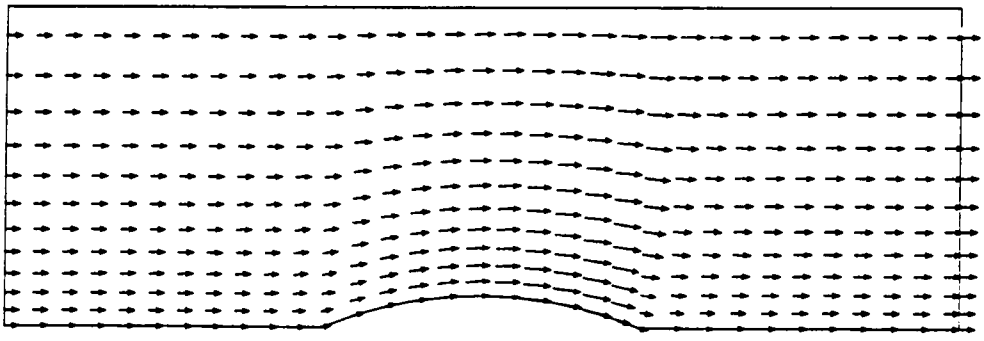
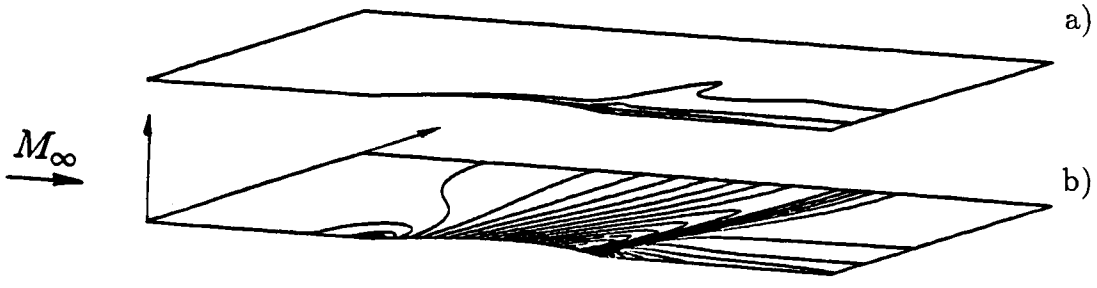


Figure 10.19: MDS Algorithm Steady-State Velocity Vector Field, Euler Equations, Parabolic Arc, $M_s \simeq 1.5$.



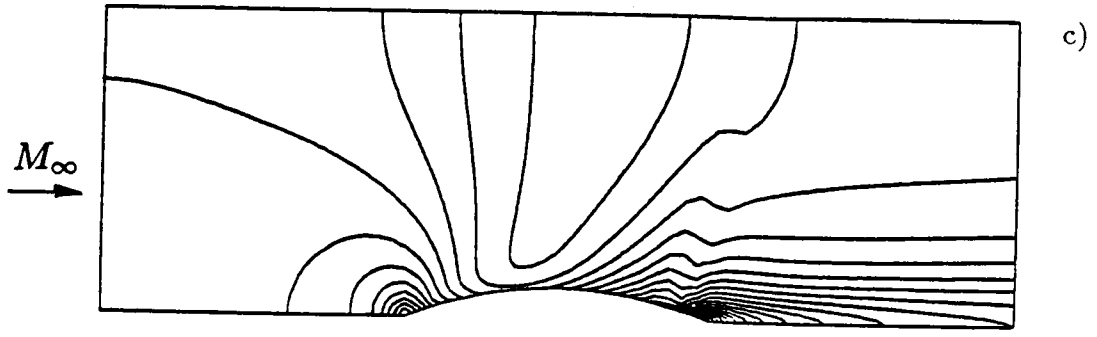


Figure 10.20: MDS Algorithm Steady-State Solution Contours, Euler Equations, Parabolic Arc, $M_s \simeq 1.5$, a) Entropy, b) Mach Number, c) Principal Momentum.

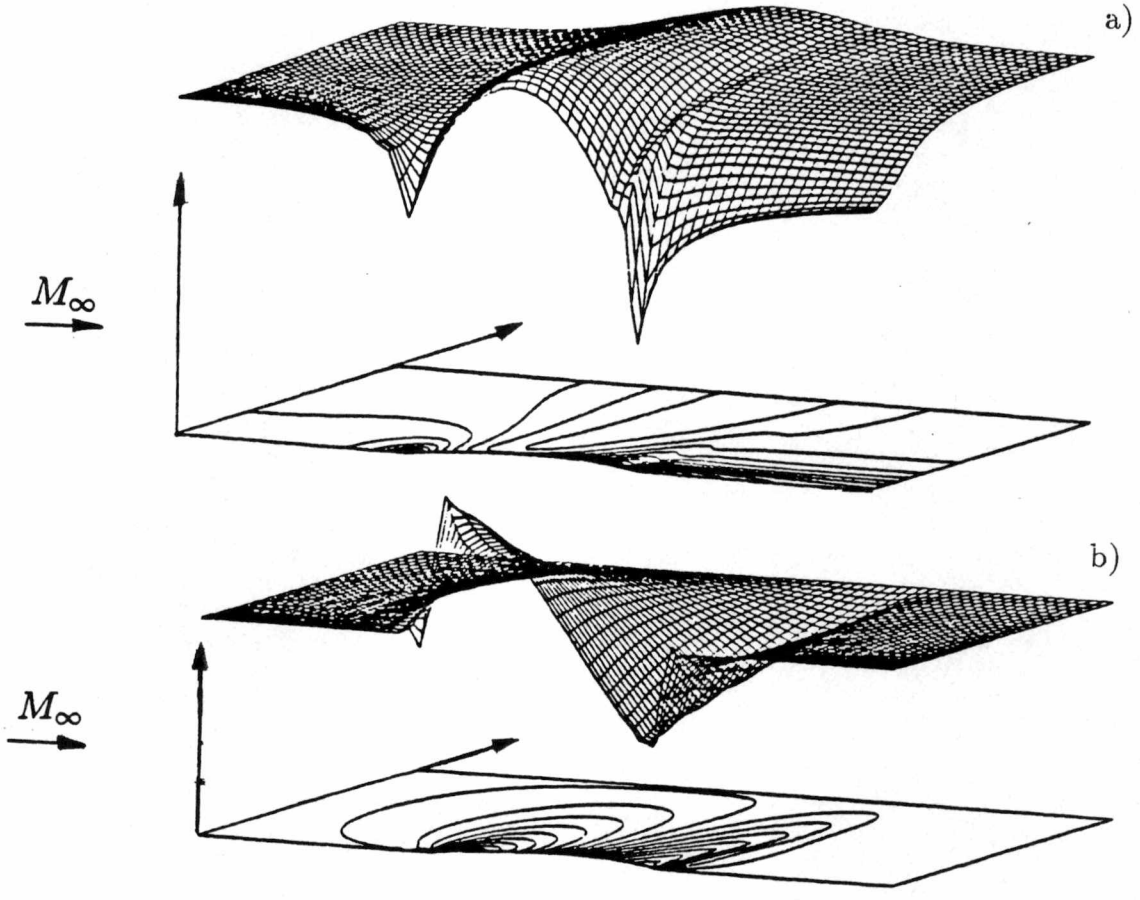


Figure 10.21: MDS Algorithm Steady-State Solution Perspectives and Contours, a) Principal Momentum, b) Transverse Momentum.

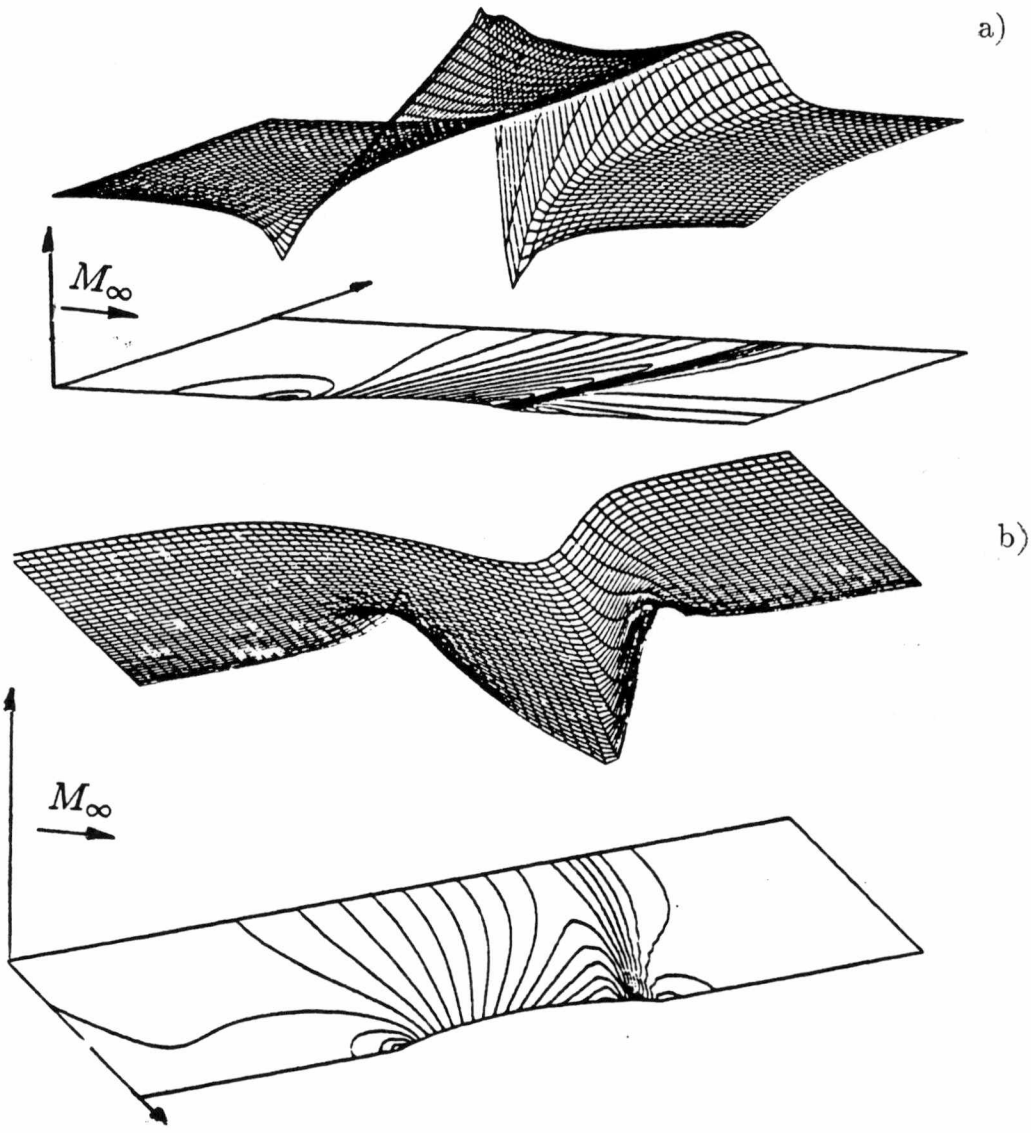


Figure 10.22: MDS Algorithm Steady-State Solution Perspectives and Contours, a) Mach Number, b) Pressure.

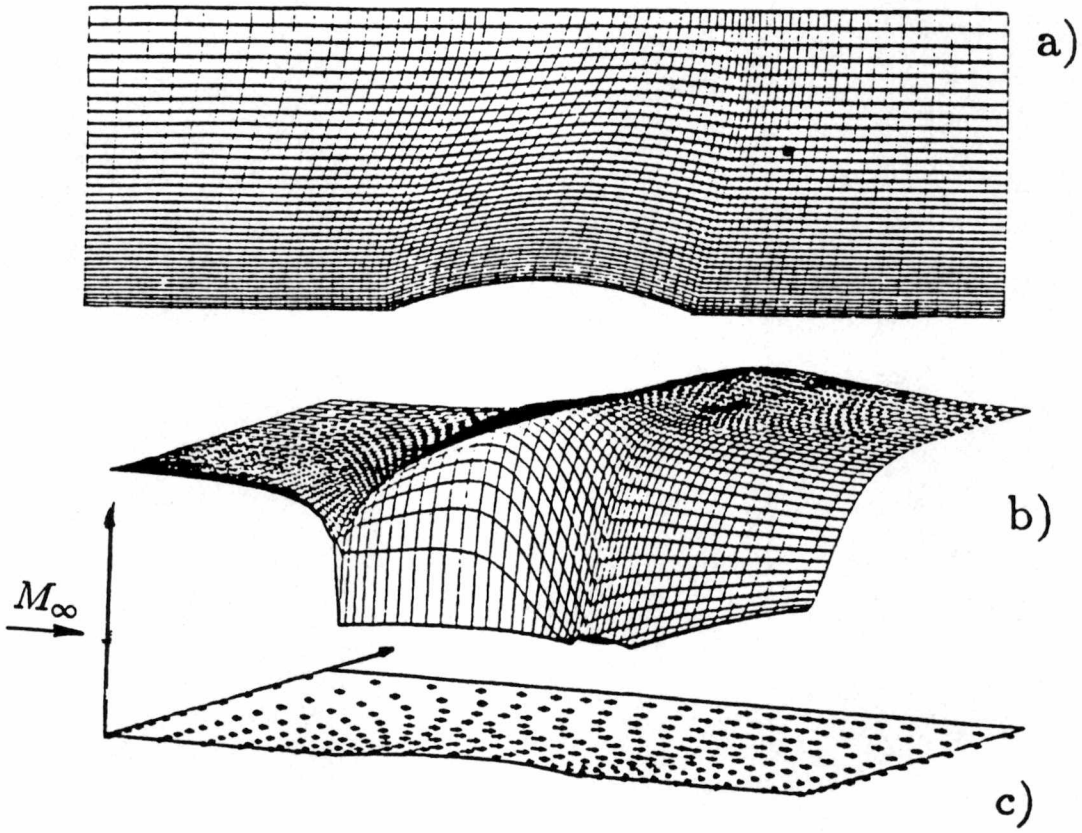


Figure 10.23: MDS Algorithm Steady-State Solution, Navier-Stokes Equations, Laminar $Re = 2000$, a) M=65 $\times$ 35 Element Discretization, b) Mach Number Distribution, c) Velocity Vector Field.

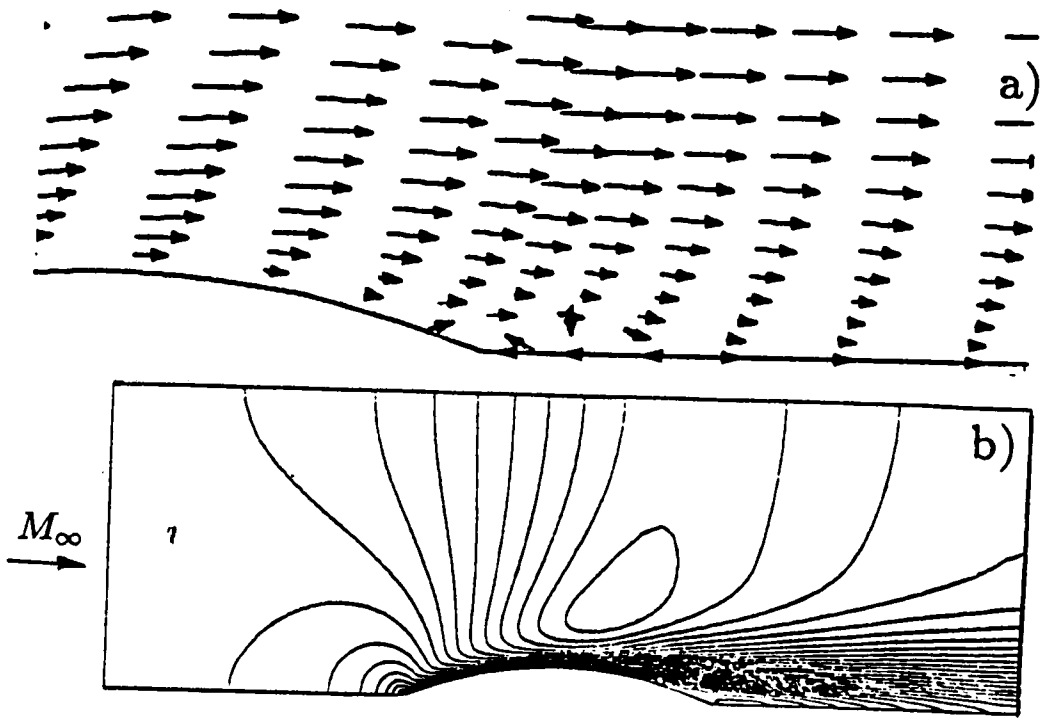


Figure 10.24: MDS Algorithm Steady-State Solution, Navier-Stokes Equations, Laminar $Re = 2000$, a) Trailing Edge Region Velocity Vector Field, b) Mach Number Isocline Distribution.

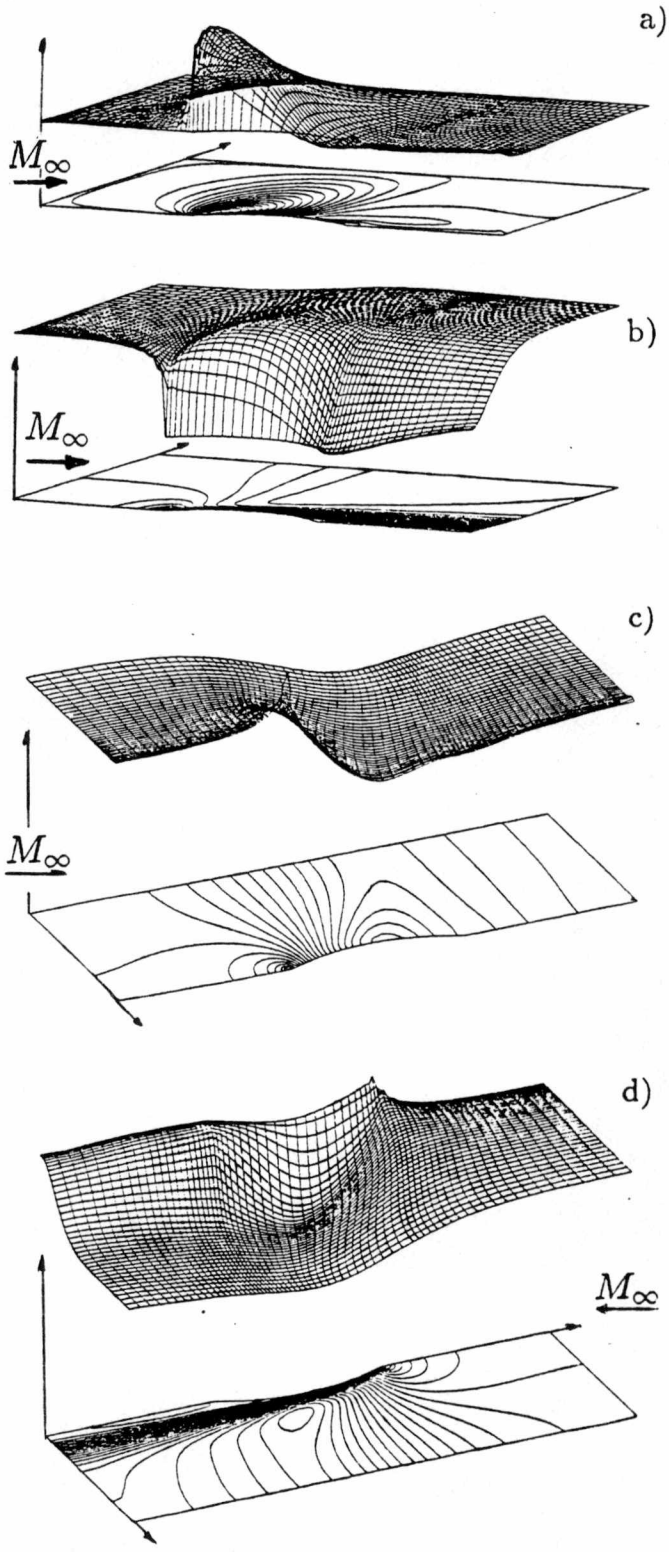


Figure 10.25: MDS Algorithm Steady-State Solution, Navier-Stokes Equations, Laminar $Re = 2000$, a) Transverse Momentum, b) Principal Momentum, c) Pressure, d) Temperature.

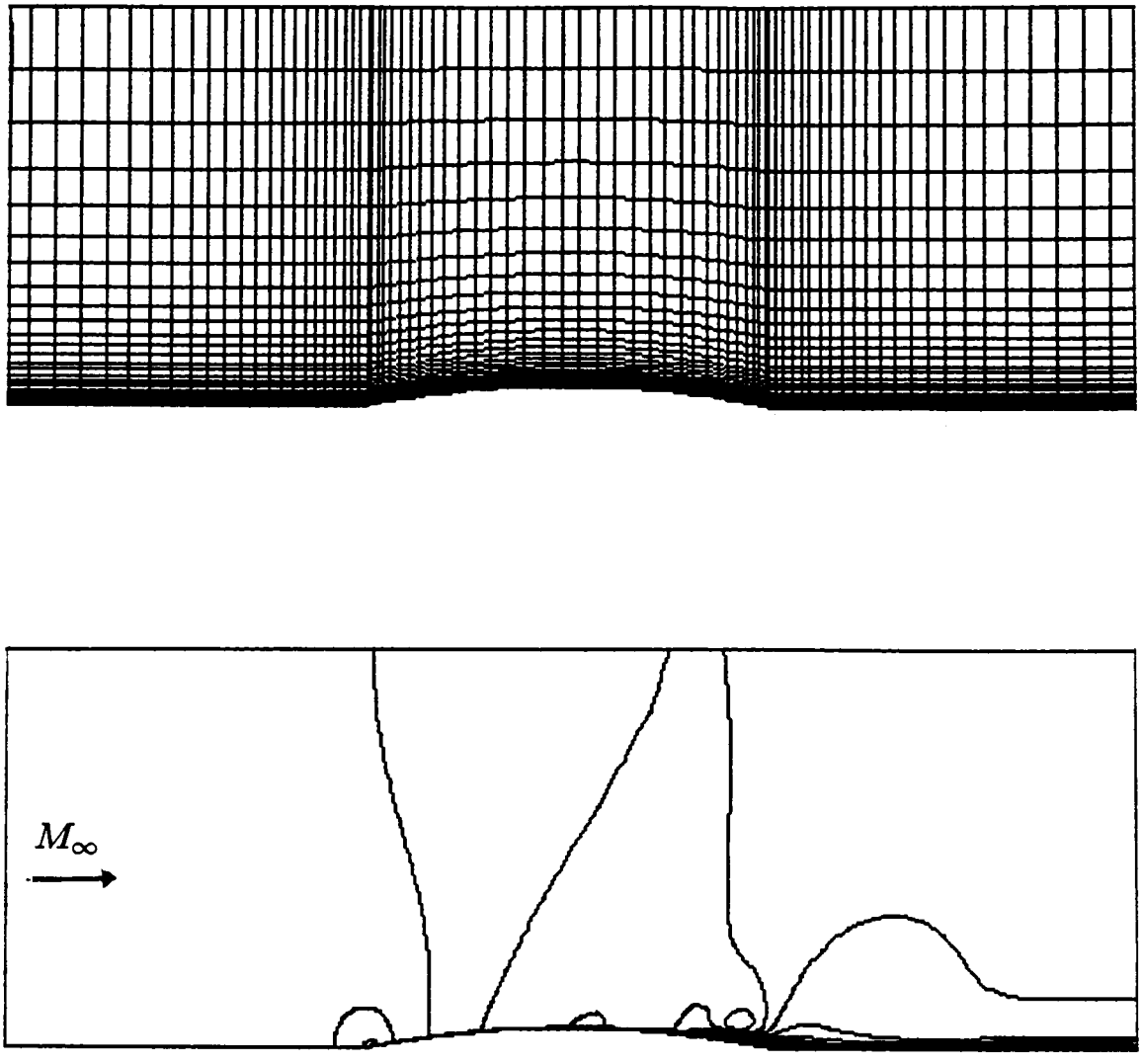


Figure 10.26: MDS Algorithm Steady-State Solution, Navier-Stokes Equations, Laminar $Re = 4 \times 10^6$, a) M=65 $\times$ 45 Element Discretization, b) Physical Space Principal Momentum Contour Distribution.

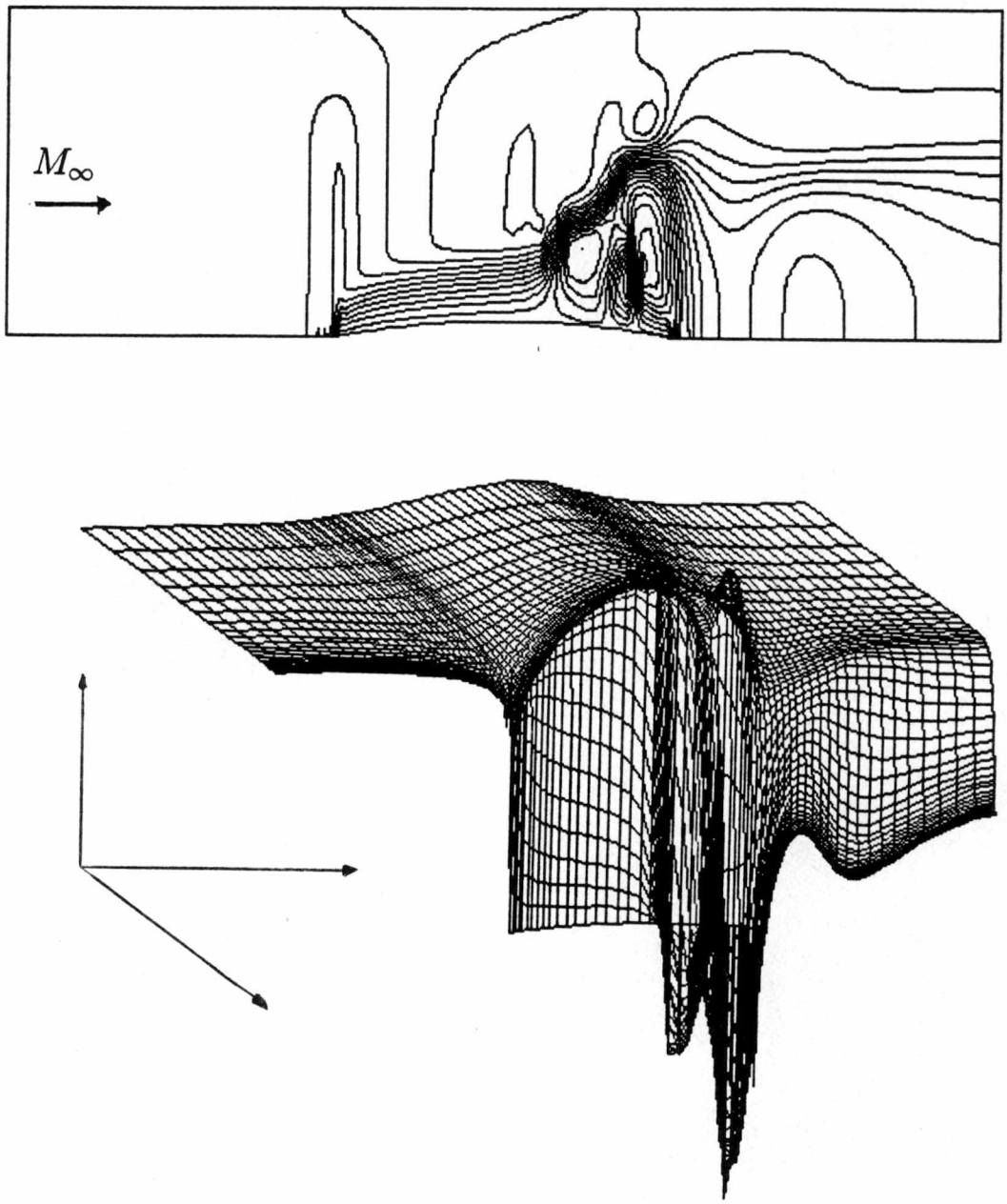


Figure 10.27: MDS Algorithm Steady-State Solution, Navier-Stokes Equations, Laminar $Re = 4 \times 10^6$, a) Transverse Nodal Space Contour Distribution, b) Perspective Surface Presentation.

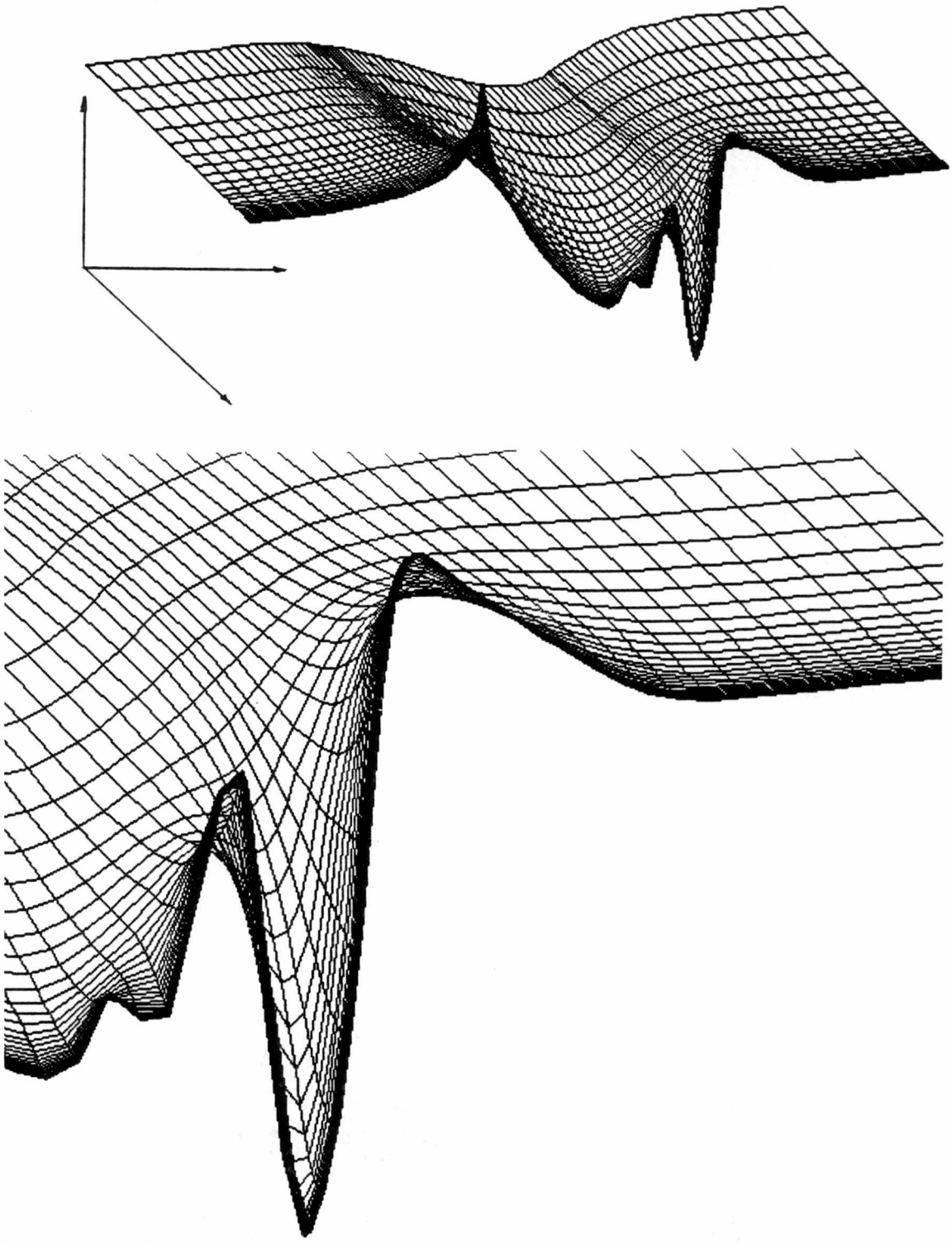


Figure 10.28: MDS Algorithm Steady-State Pressure Solution, Navier-Stokes Equations, Laminar $Re = 4 \times 10^6$, a) Global Distribution, b) Trailing Edge Region Detail.

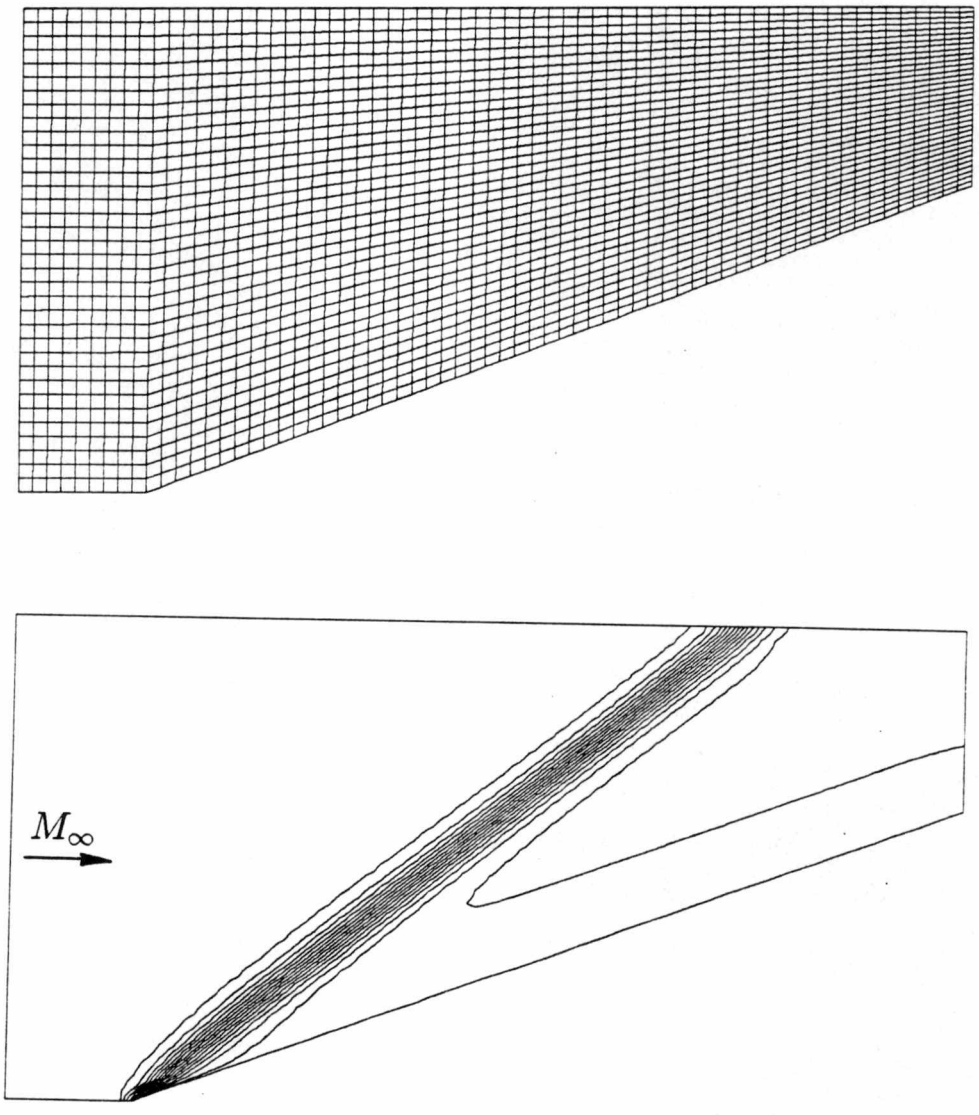


Figure 10.29: MDS Algorithm Steady-State Euler Solution, Supersonic Compression Ramp, $M_\infty = 3.0$, $\alpha = 20^o$, a) Sheared Cartesian Mesh, M=65 $\times$ 35 b) Density Distribution on Mesh 1.

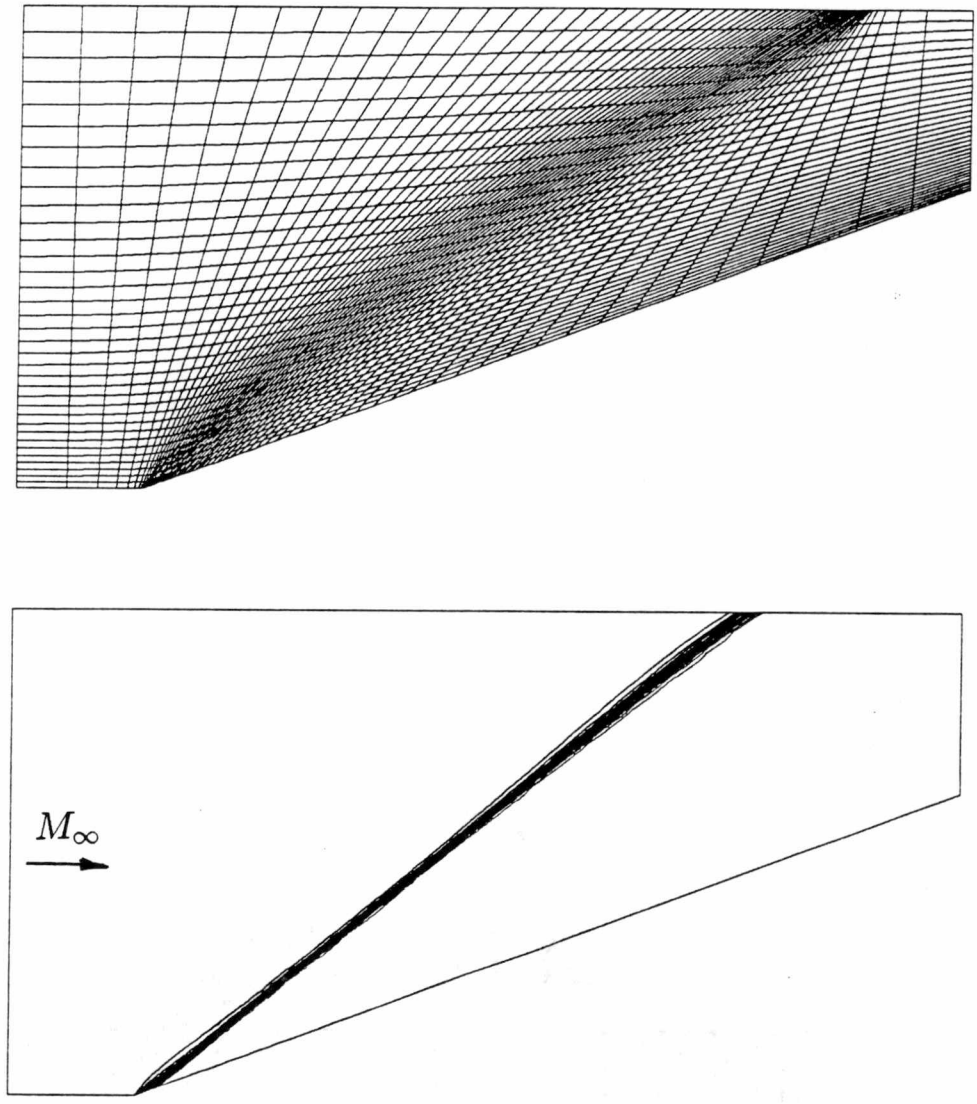


Figure 10.30: MDS Algorithm Steady-State Euler Solution, Supersonic Compression Ramp, $M_\infty = 3.0$, $\alpha = 20°$, a) First Solution-Adapted Mesh b) Density Distribution on Mesh 2.

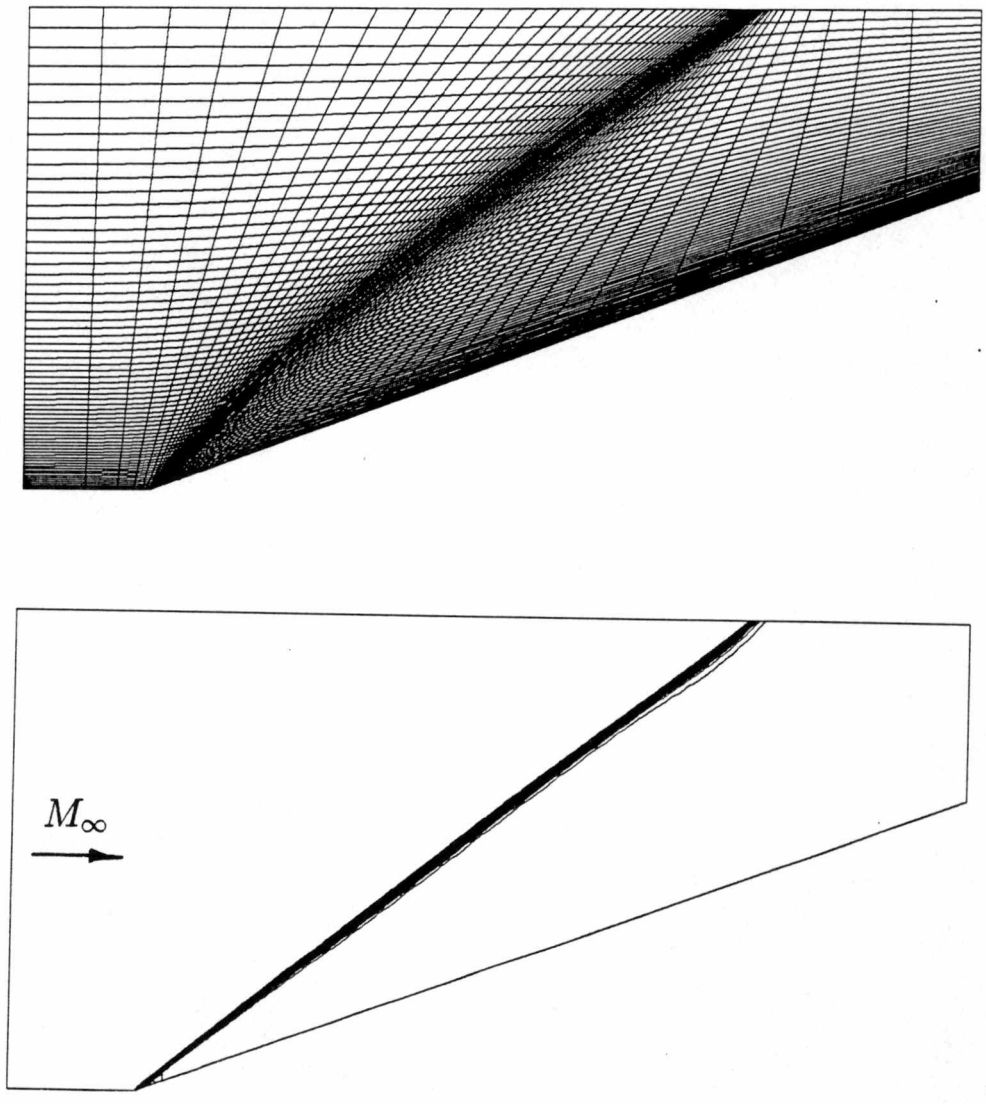


Figure 10.31: MDS Algorithm Steady-State Euler Solution, Supersonic Compression Ramp, $M_\infty = 3.0$, $\alpha = 20°$, a) Second Solution-Adapted Mesh b) Density Distribution on Mesh 3.

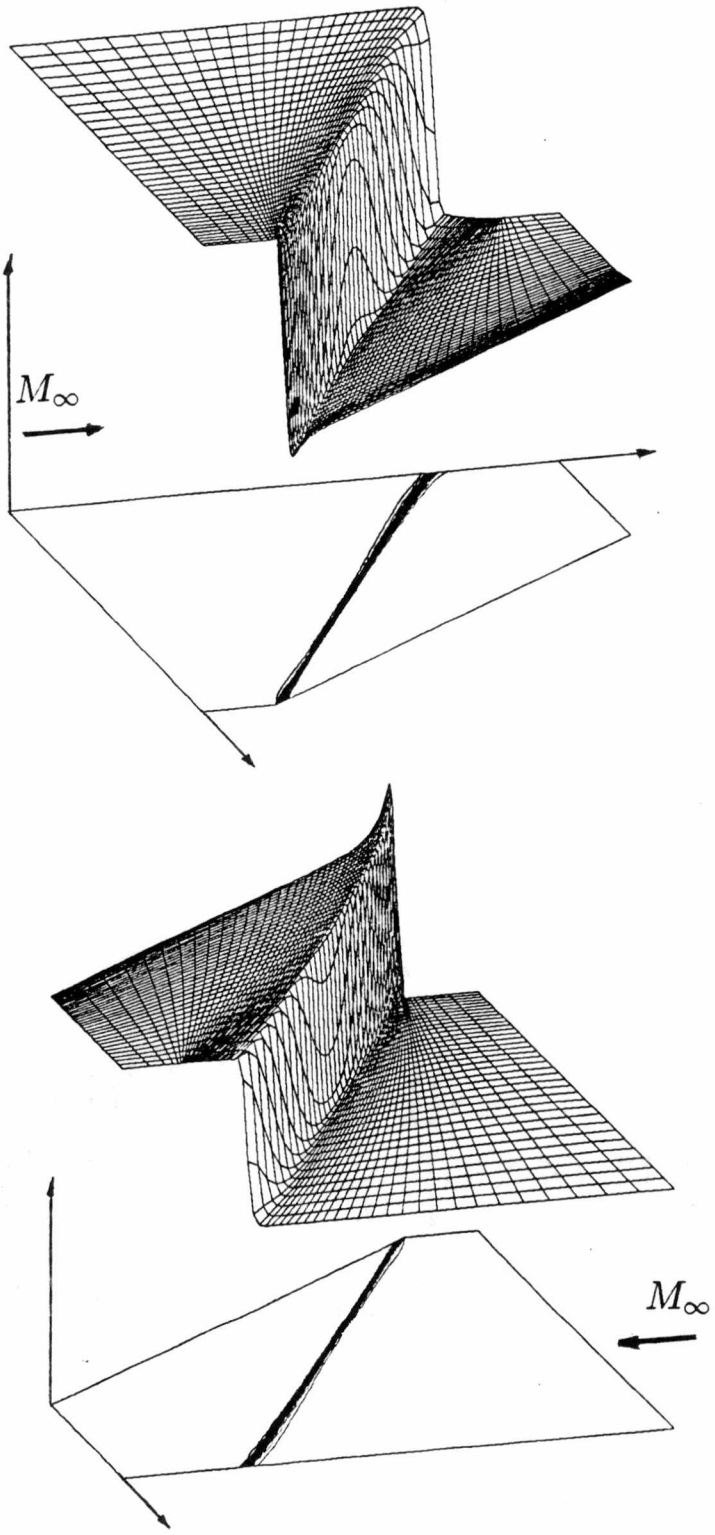


Figure 10.32: MDS Algorithm Steady-State Euler Solution, Supersonic Compression Ramp, $M_\infty = 3.0$, $\alpha = 20°$, Perspective Surface and Solution Contour Distributions, a) Mach Number, b) Pressure.

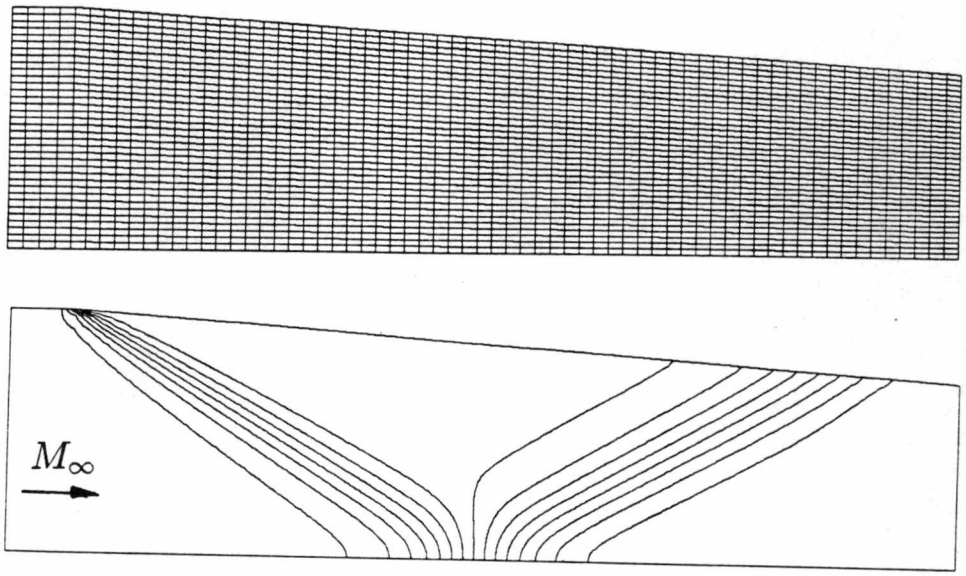


Figure 10.33: MDS Algorithm Steady-State Euler Solution, Supersonic Shock Reflection $M_\infty = 2.15$, $\alpha = -4^o$, a) Sheared Cartesian Mesh, M=65 $\times$ 35, b) Computed Density Distribution.

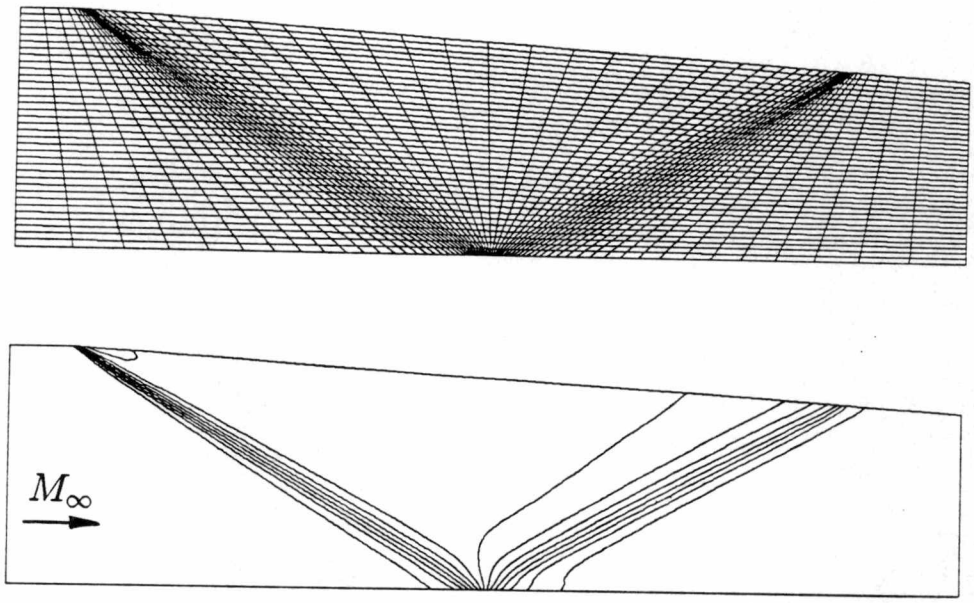


Figure 10.34: MDS Algorithm Steady-State Euler Solution, Supersonic Shock Reflection $M_\infty = 2.15$, $\alpha = -4^o$, a) First Solution-Adapted Mesh, b) Computed Density Distribution on Mesh 2.

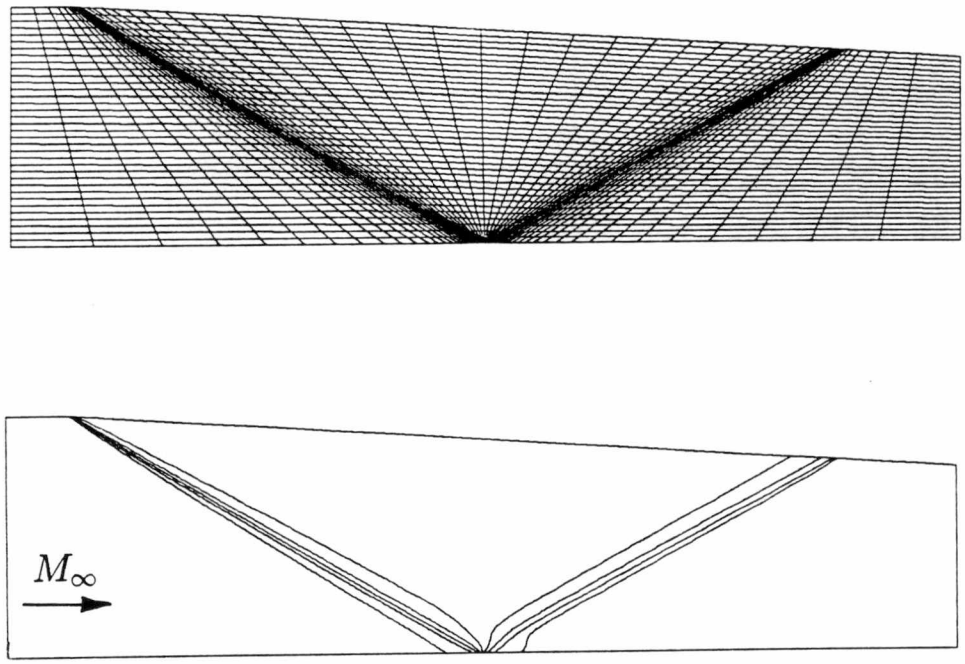


Figure 10.35: MDS Algorithm Steady-State Euler Solution, Supersonic Shock Reflection $M_\infty = 2.15$, $\alpha = -4^o$, a) Second Solution-Adapted Mesh, b) Computed Density Distribution on Mesh 3.

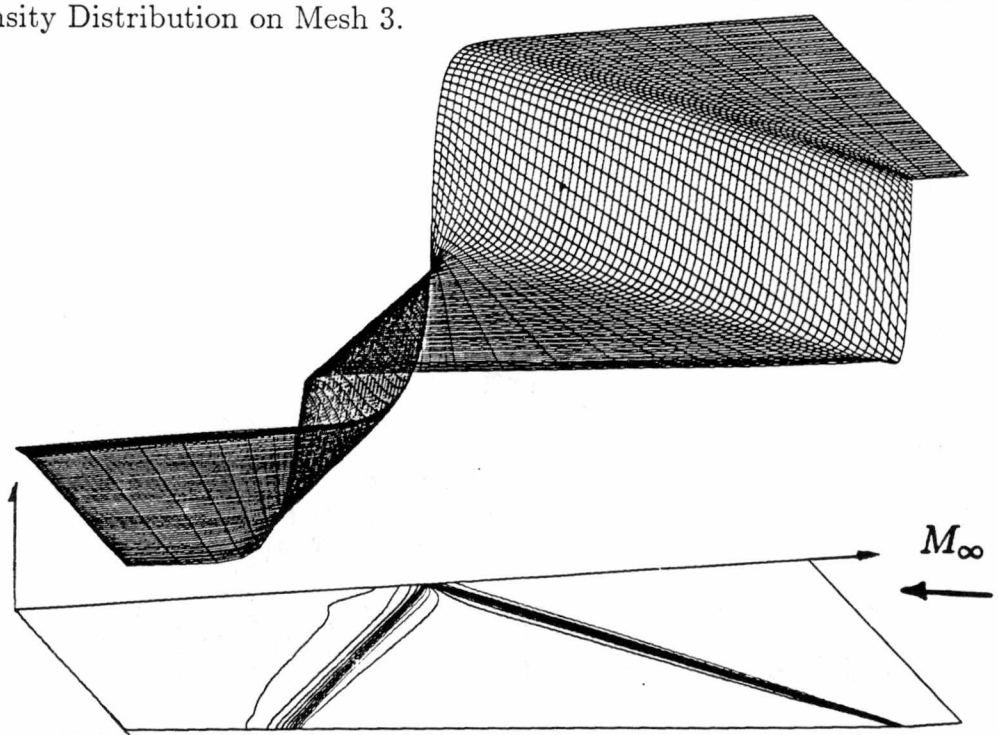


Figure 10.36: MDS Algorithm Steady-State Euler Solution, Supersonic Shock Reflection $M_\infty = 2.15$, $\alpha = -4^o$, Mach Number Solution Contour and Perspective Surface Distributions on Mesh 3.

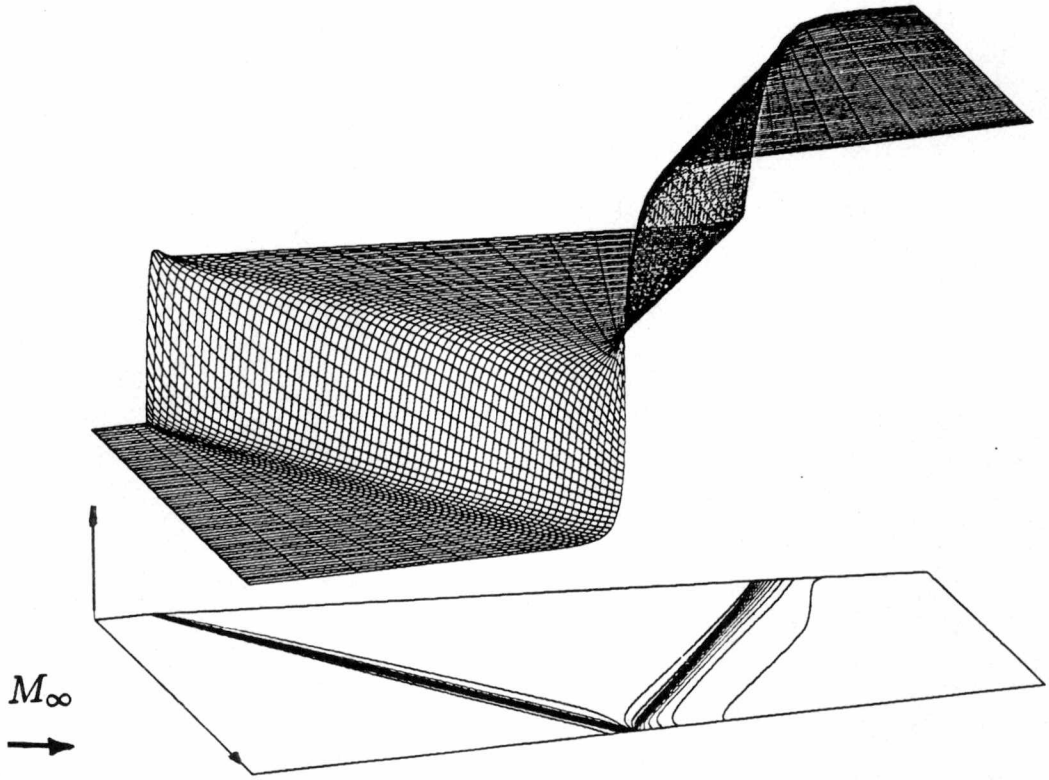


Figure 10.37: MDS Algorithm Steady-State Euler Solution, Supersonic Shock Reflection $M_\infty = 2.15$, $\alpha = -4^o$, Pressure Solution Contour and Perspective Surface Distributions on Mesh 3.

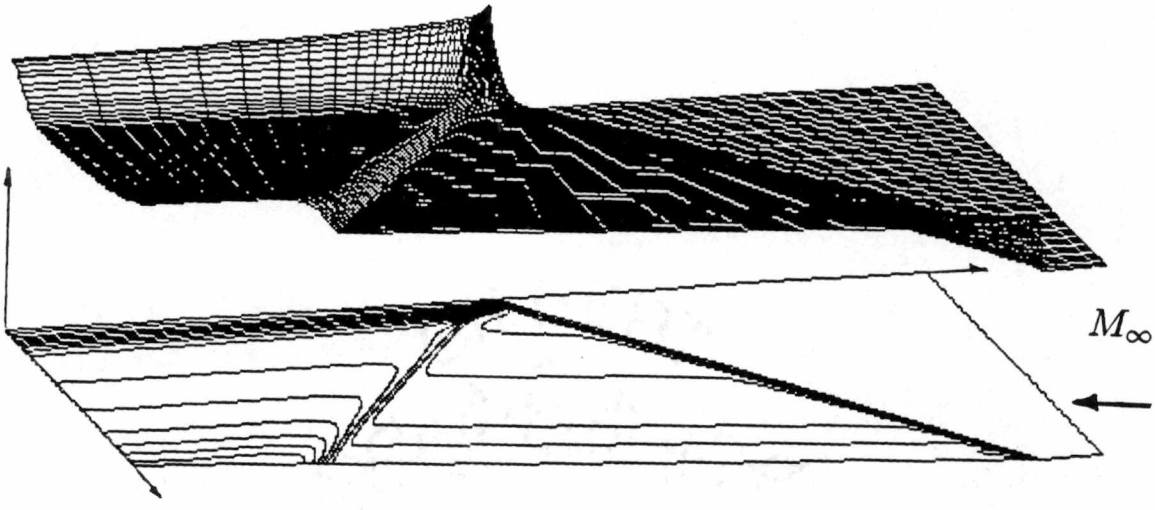


Figure 10.38: MDS Algorithm Steady-State Euler Solution, Supersonic Shock Reflection $M_\infty = 2.15$, $\alpha = -4^o$, Entropy Solution Contour and Perspective Surface Distributions on Mesh 3.

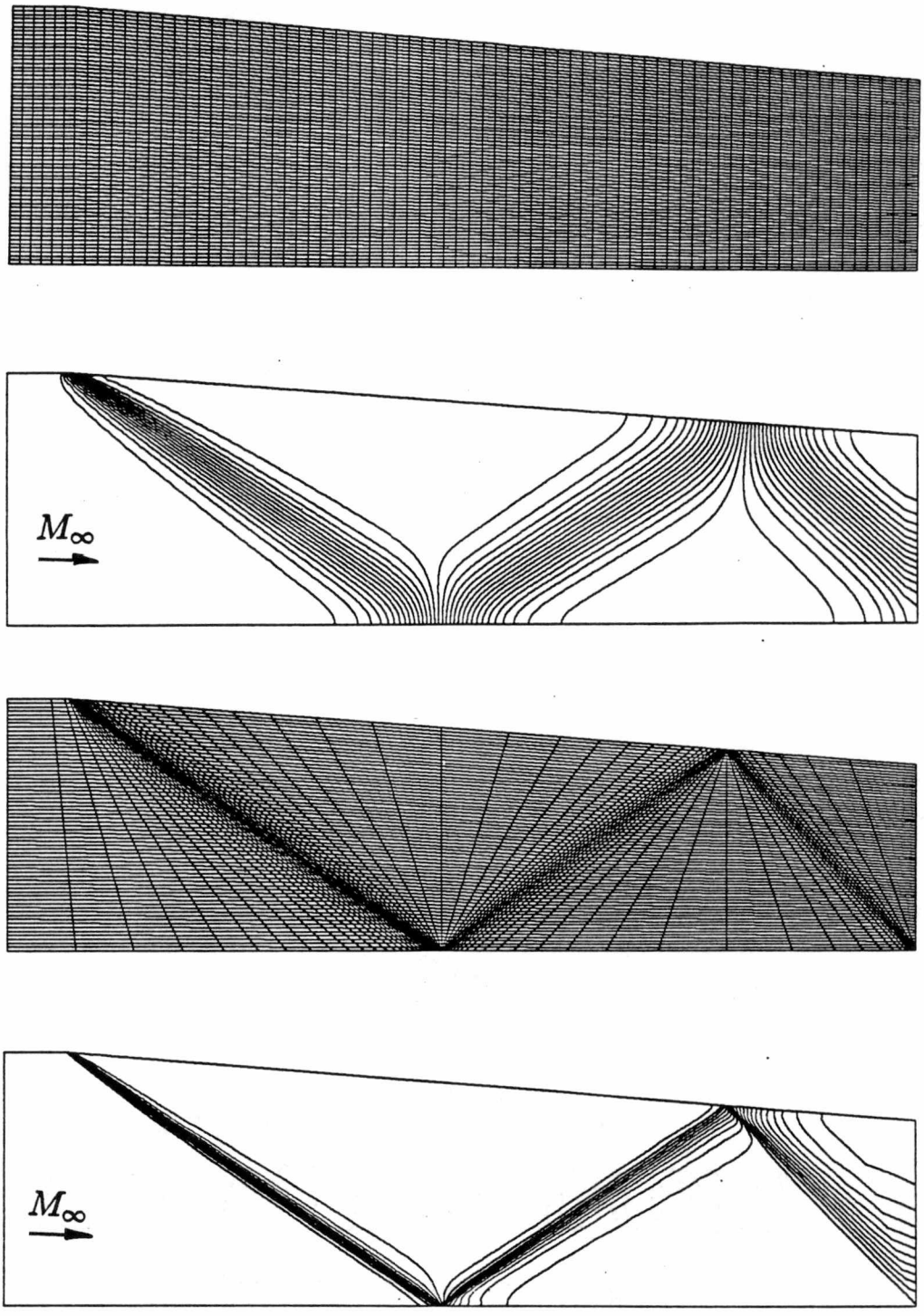


Figure 10.39: MDS Algorithm Steady-State Euler Solution, Double Supersonic Shock Reflection $M_\infty = 2.15$, $\alpha = -4°$, a) Sheared Cartesian Mesh, M=65 x 35, b) Computed Density Distribution, c) Final Solution-Adapted Mesh, d) Final Density Distribution.

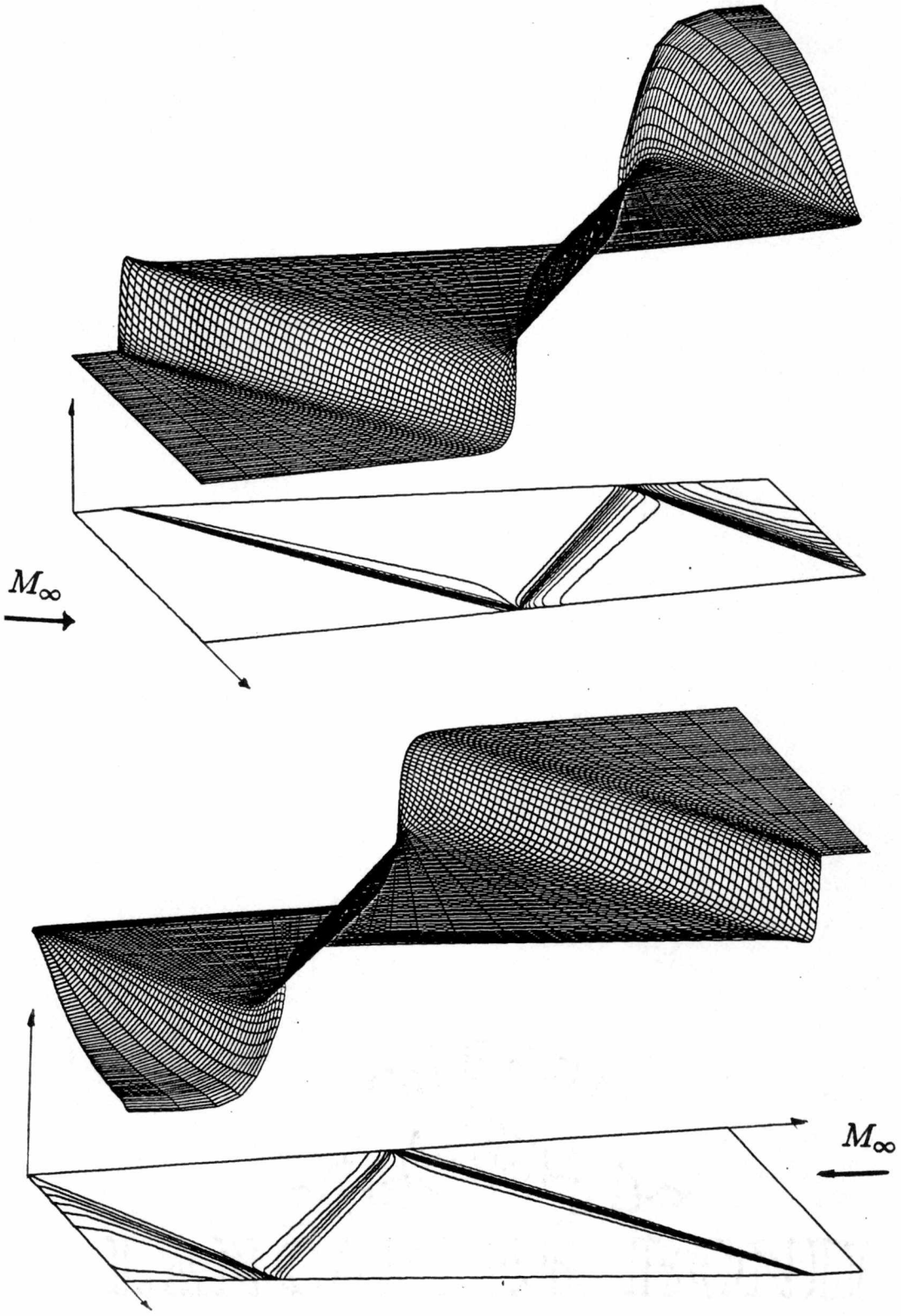
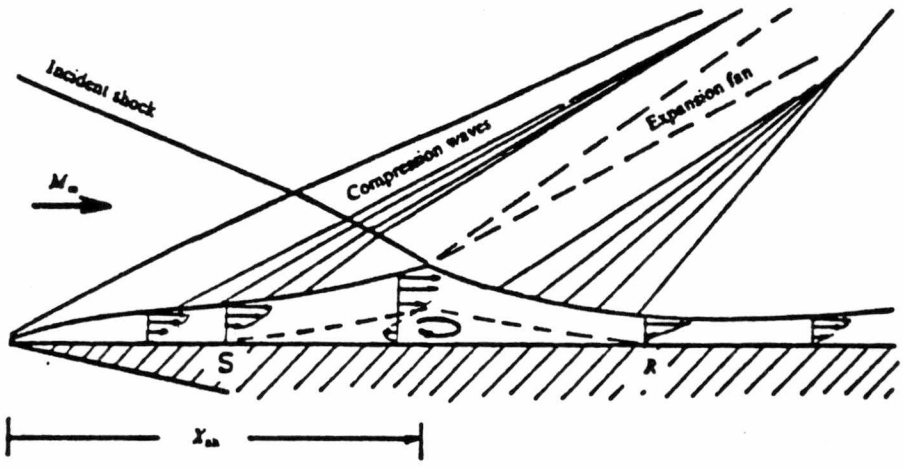


Figure 10.40: MDS Algorithm Steady-State Euler Solution, Double Supersonic Shock Reflection $M_\infty = 2.15$, $\alpha = -4^o$, Perspectives and Contour Distributions on Final Mesh, a) Static Pressure, b) Mach Number.



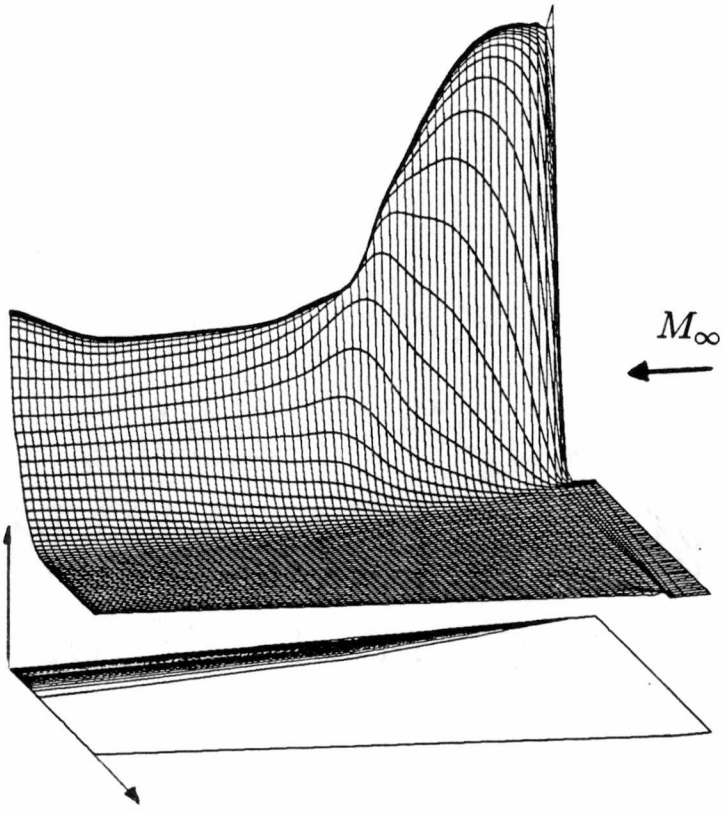


Figure 10.41: MDS Algorithm Steady-State Navier-Stokes Solution, Shock-Wave Laminar Boundary Layer Interaction, $M_\infty = 2.15$, $Re = 1 \times 10^5$, a) Problem Schematic, b) Entropy Perspective Solution Surface and Contour Distribution.

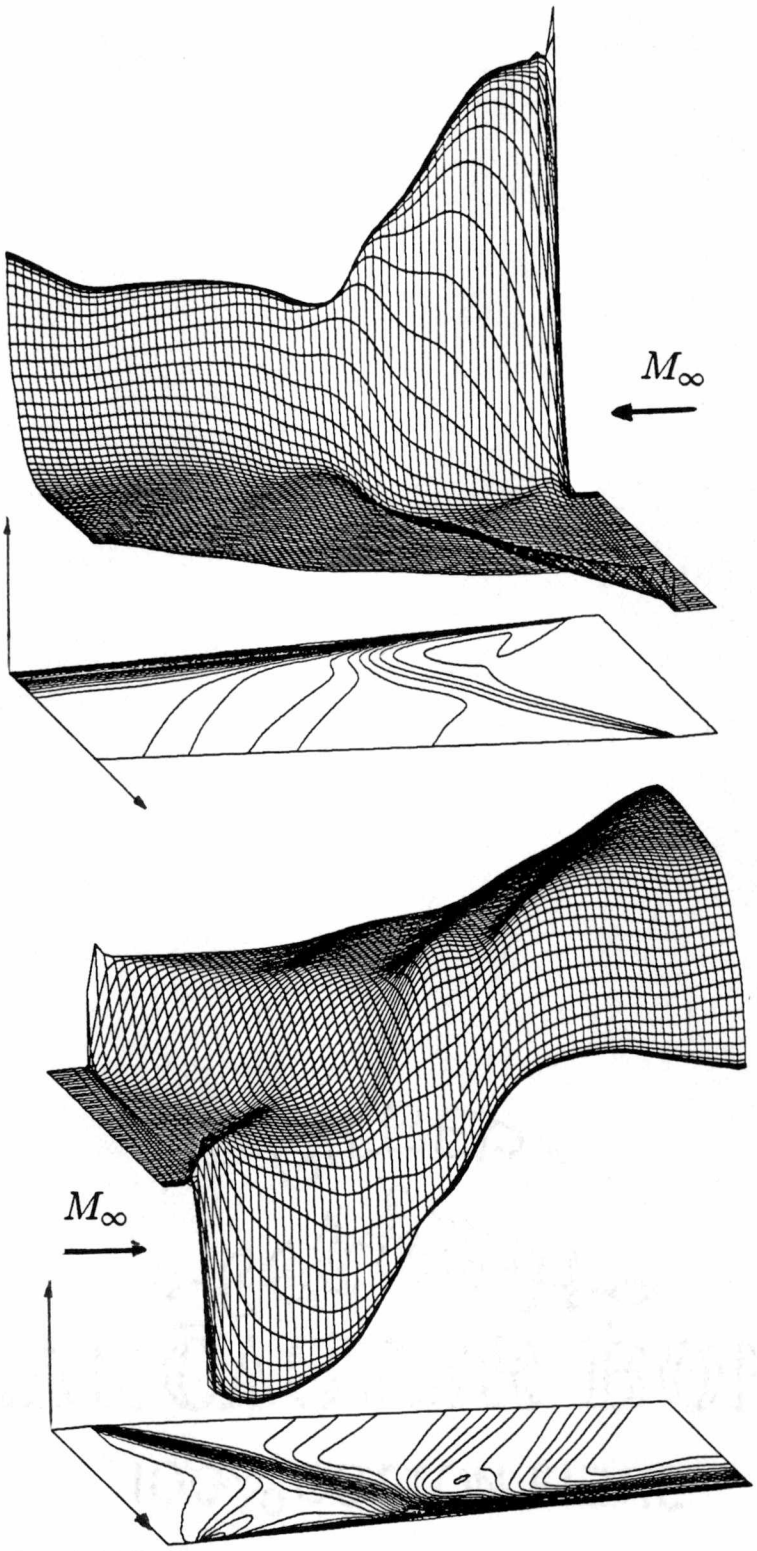


Figure 10.42: MDS Algorithm Steady-State Navier-Stokes Solution, Shock-Wave Laminar Boundary Layer Interaction, $M_\infty = 2.15$, $Re = 1 \times 10^5$, Perspective Solution Surface and Contour Distributions, a) Temperature, b) Density.

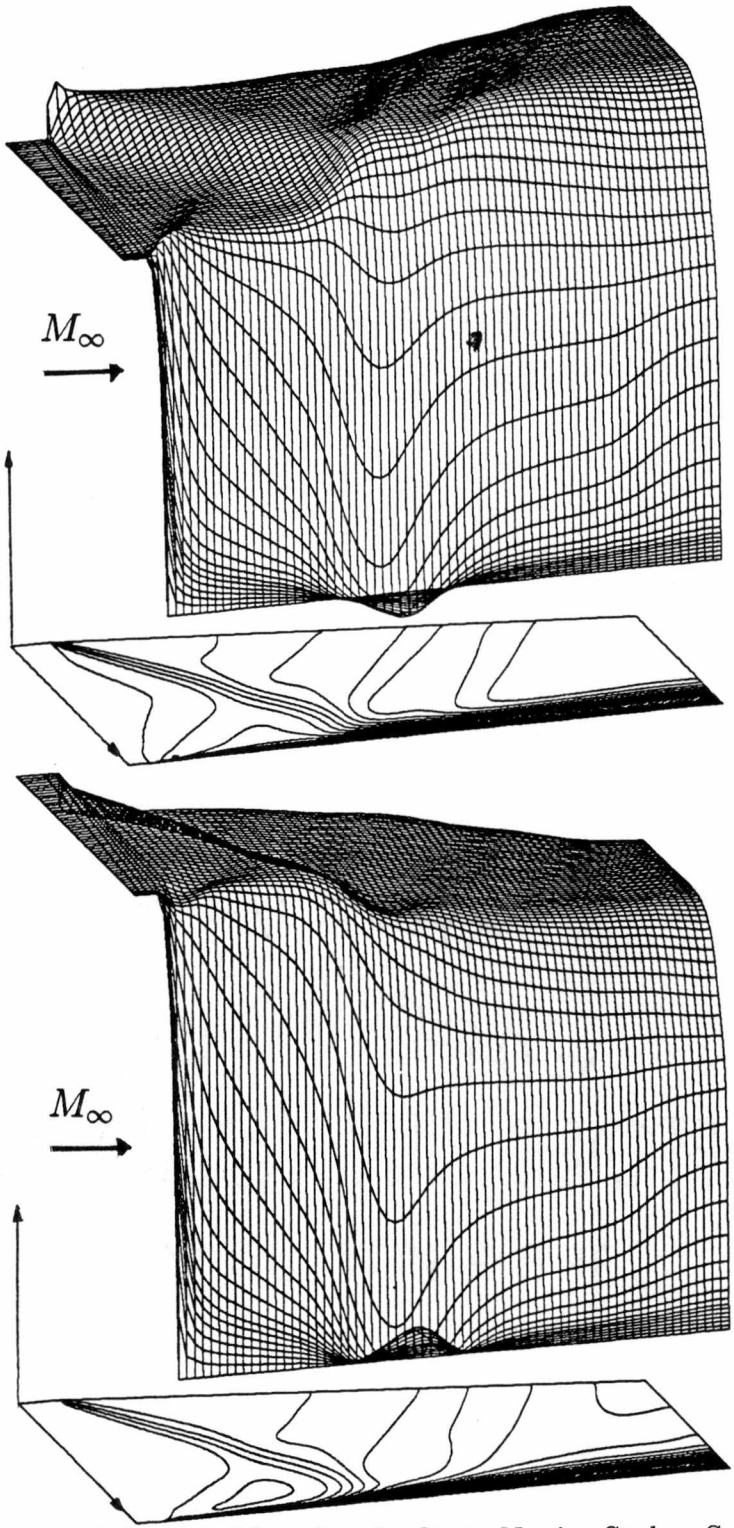


Figure 10.43: MDS Algorithm Steady-State Navier-Stokes Solution, Shock-Wave Laminar Boundary Layer Interaction, $M_\infty = 2.15$, $Re = 1 \times 10^5$, Perspective Solution Surface and Contour Distributions, a) Axial Momentum b) Mach Number.

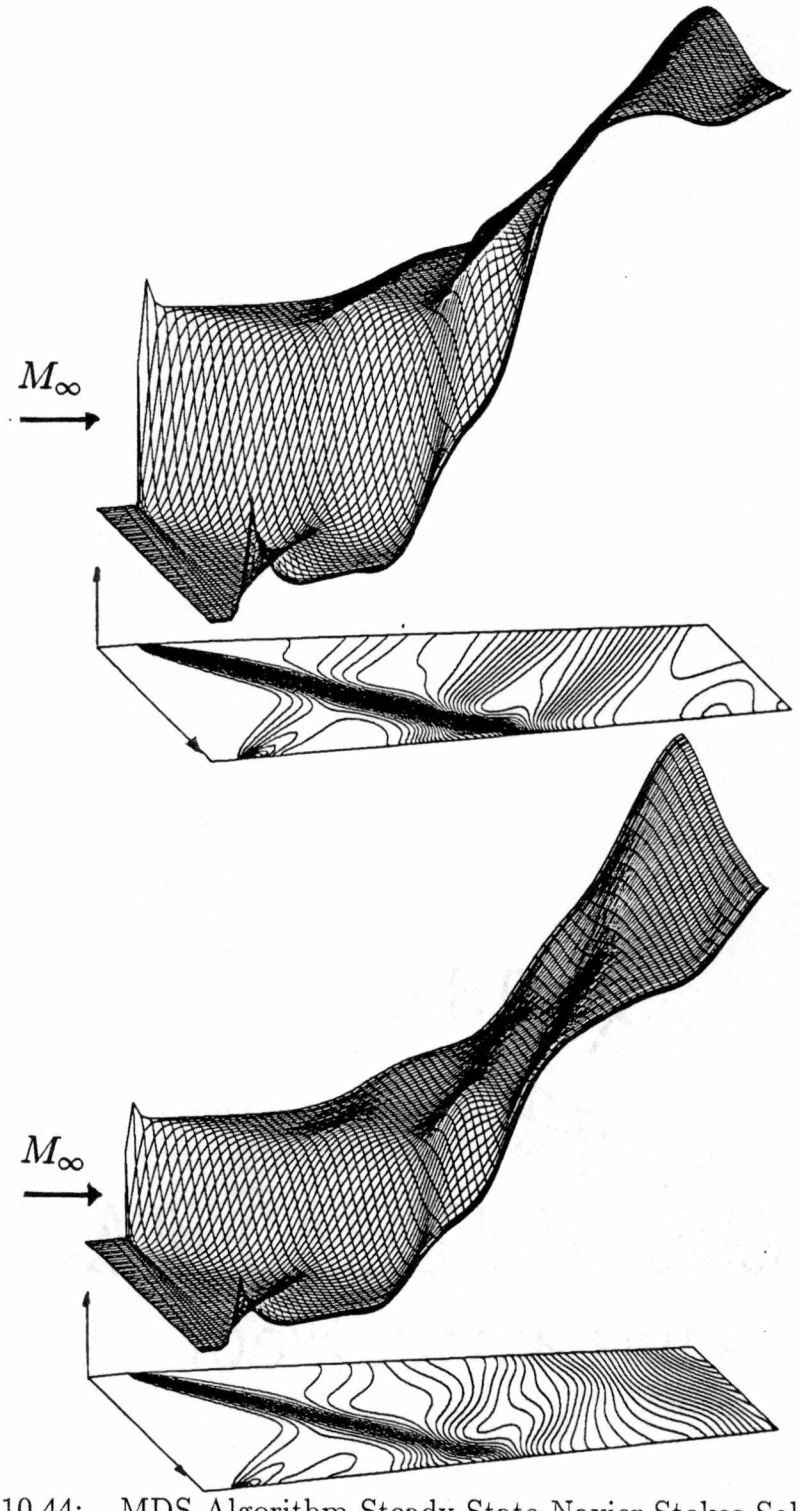


Figure 10.44: MDS Algorithm Steady-State Navier-Stokes Solution, Shock-Wave Laminar Boundary Layer Interaction, $M_\infty = 2.15$, $Re = 1 \times 10^5$, Pressure Perspective Solution Surface and Contour Distributions, a) Single Reflection, b) Double Reflection.

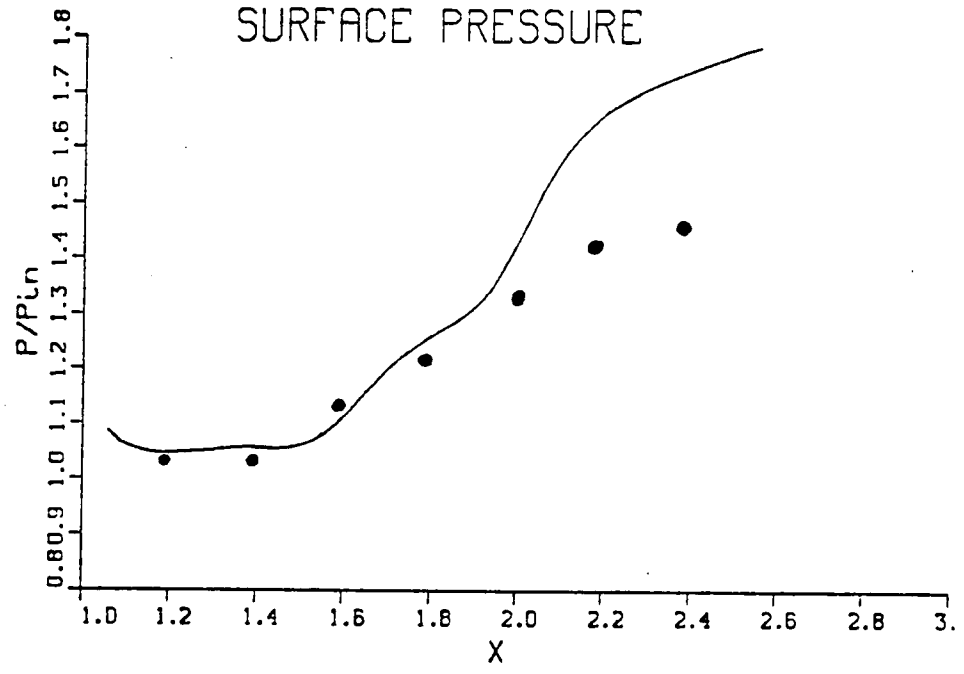


Figure 10.45: Surface Pressure Distributions and Comparisons from [46], Shock Boundary Layer Interaction, $M_\infty = 2.15$

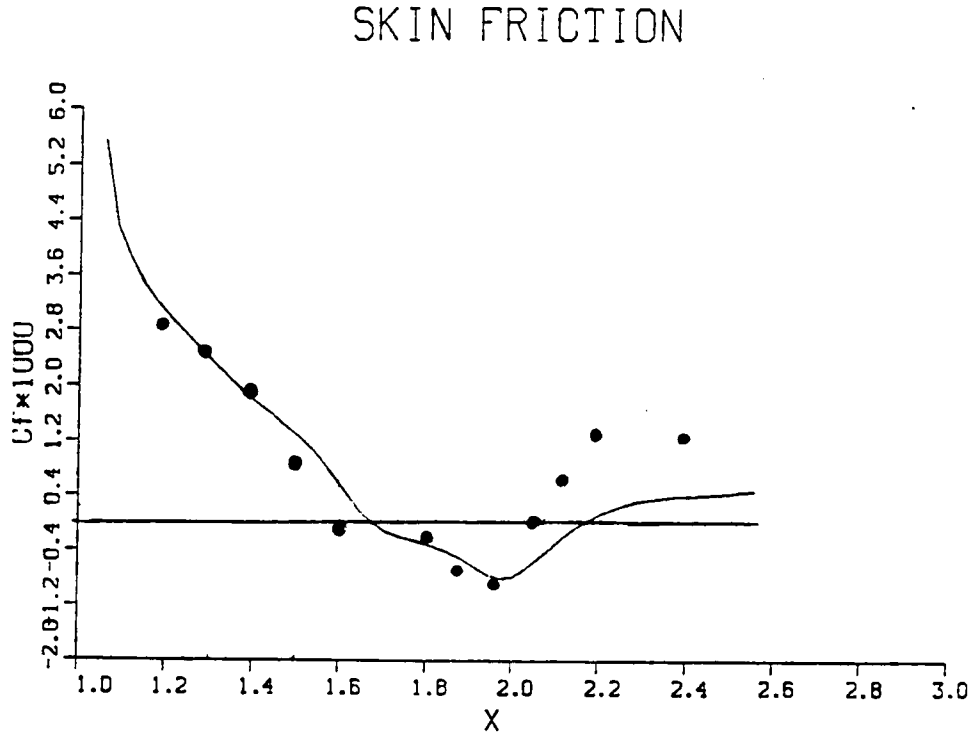


Figure 10.46: Surface Skin Friction Distributions and Comparisons from [46], Shock Boundary Layer Interaction, $M_\infty = 2.15$

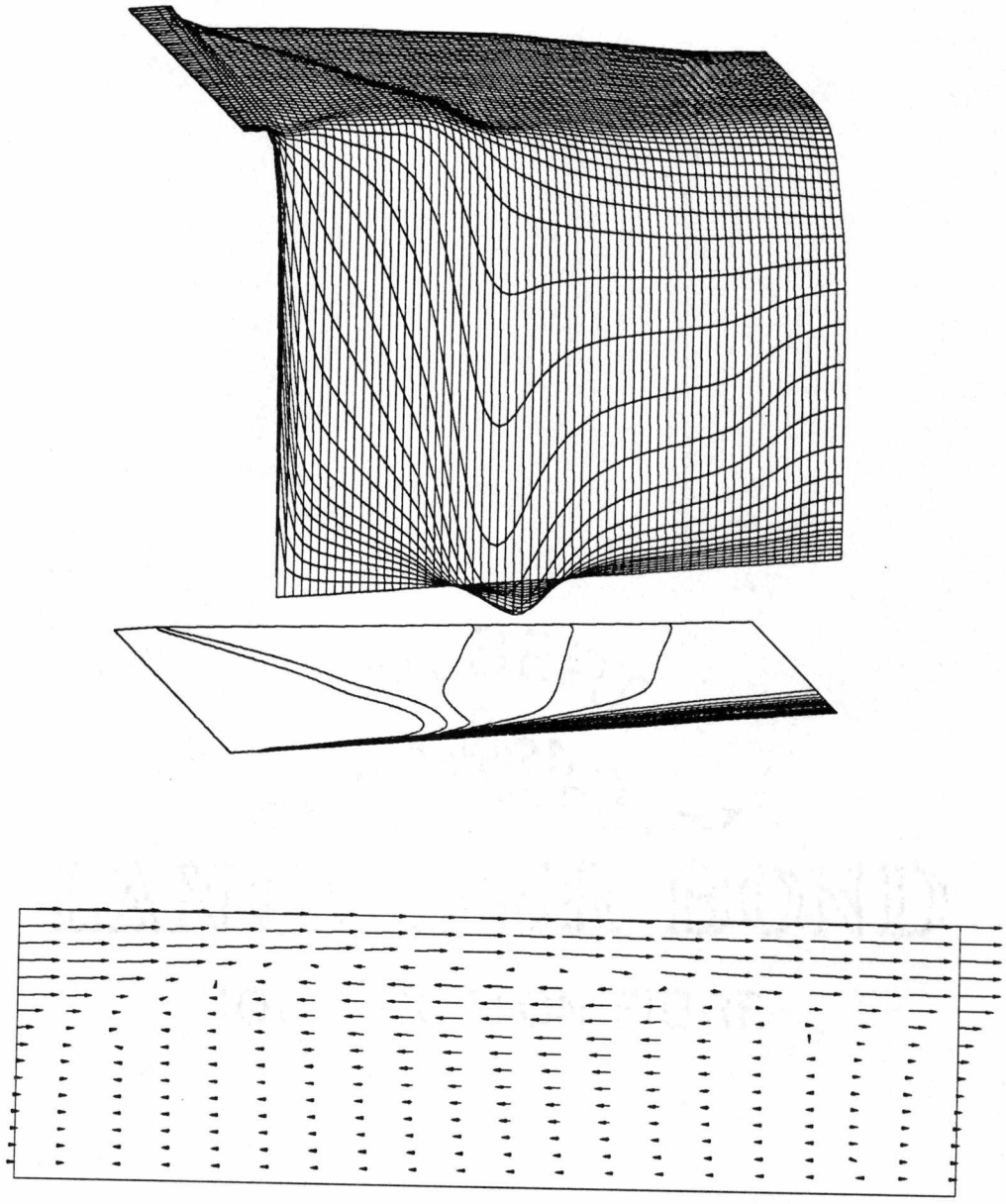


Figure 10.47: Steady-State Navier-Stokes Solution, Shock-Boundary Layer Interaction, $M_\infty = 2.15$, $Re = 1 \times 10^5$, a) Axial Velocity Surface Perspective and Contour Distribution, b) Recirculation Region Velocity Field Close-Up.

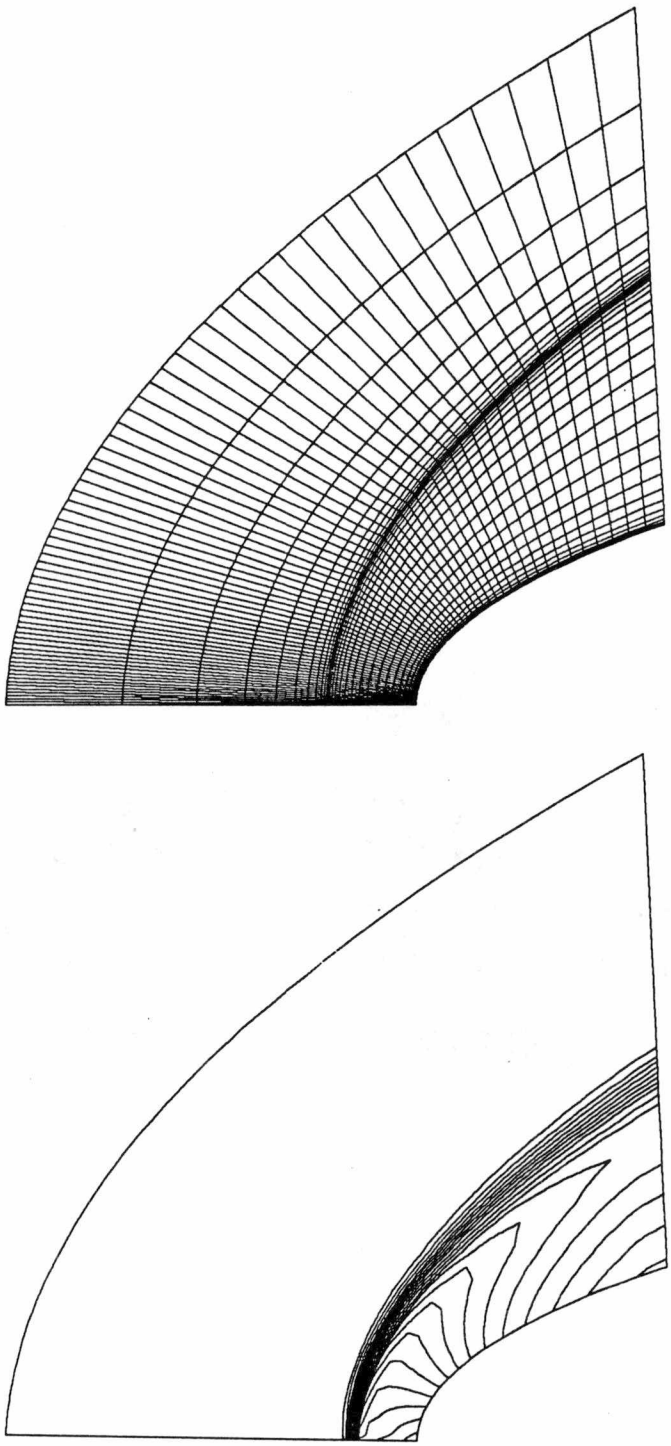


Figure 10.48: MDS Algorithm Steady-State Euler Solution, Hypersonic Blunt Body, $M_\infty = 6.5$, a) Third Solution-Adapted Mesh, M=65 $\times$ 35, b) Density Contour Distribution

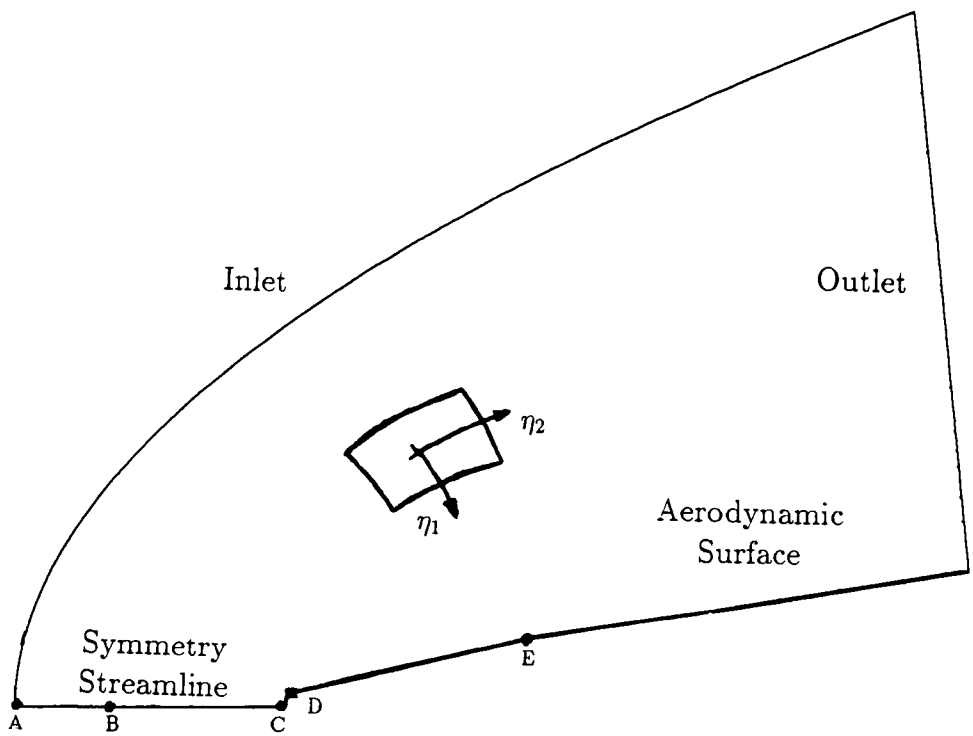


Figure 10.49: Sphere-Biconic Axisymmetric Body, Computational Domain, A) Symmetry Streamline Inlet Point, B) Symmetry Streamline Shock Point, C) Stagnation Point, D) Sphere-Cone Juncture, E) Bicone Juncture.

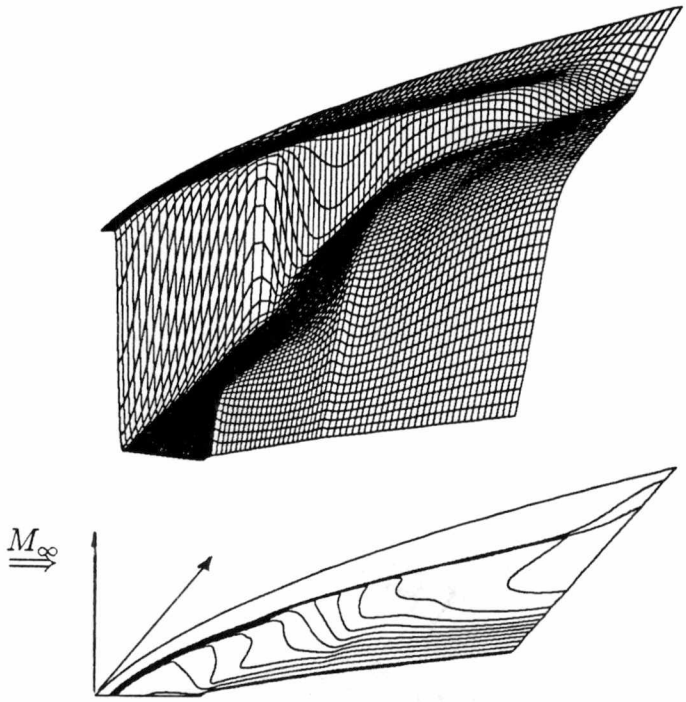


Figure 10.50: $M_\infty = 8$ Hypersonic Viscous Flow Past Sphere-Biconic Axisymmetric Body, $Re_\infty = 500,000$, Steady State Perspective Surface and Contour Distributions, Mach Number.

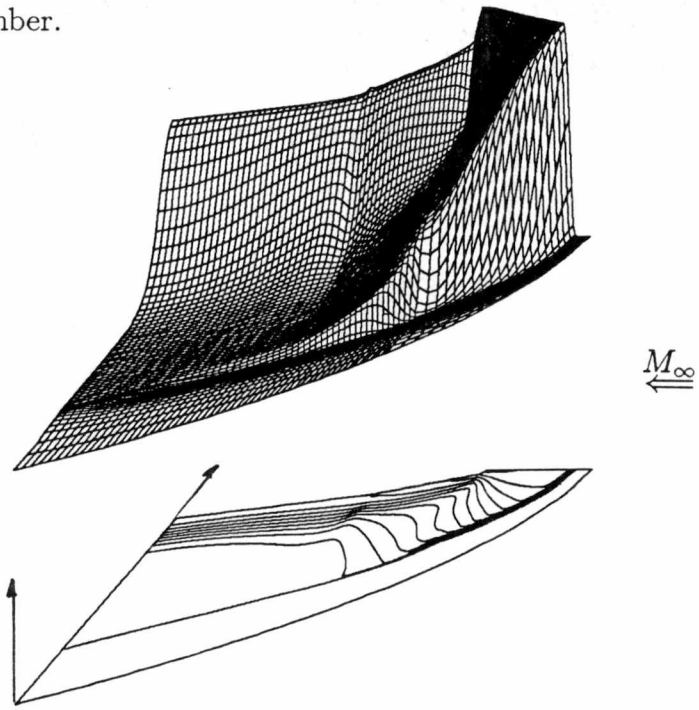


Figure 10.51: $M_\infty = 8$ Hypersonic Viscous Flow Past Sphere-Biconic Axisymmetric Body, $Re_\infty = 500,000$, Steady State Perspective Surface and Contour Distributions, Temperature.

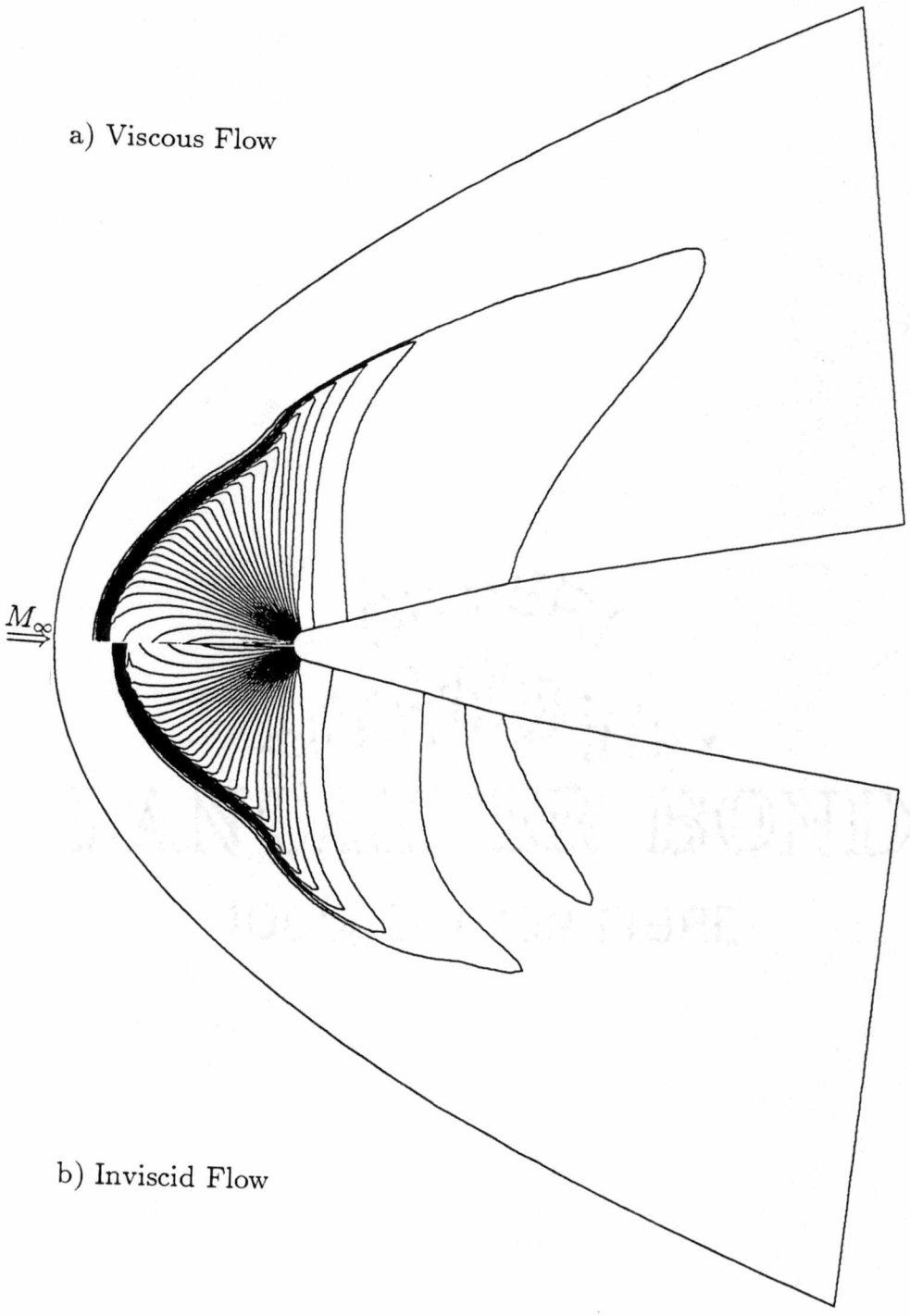


Figure 10.52: $M_\infty = 8$ Hypersonic Flow Past Sphere-Biconic Axisymmetric Body, Steady State Contour Distributions, Pressure, a) $Re_\infty = 500,000$ Viscous Flow, b) Inviscid Flow. Magnification-Induced Bow Shock Distortion.

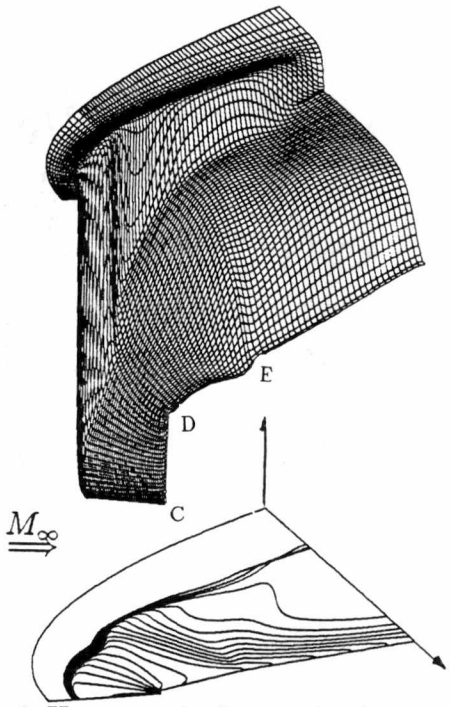


Figure 10.53: $M_\infty = 8$ Hypersonic Inviscid Flow Past Sphere-Biconic Axisymmetric Body, Steady State Perspective Surface and Contour Distributions, Mach Number, C) Stagnation Point, D) Sphere-Cone Juncture, E) Bicone Juncture.

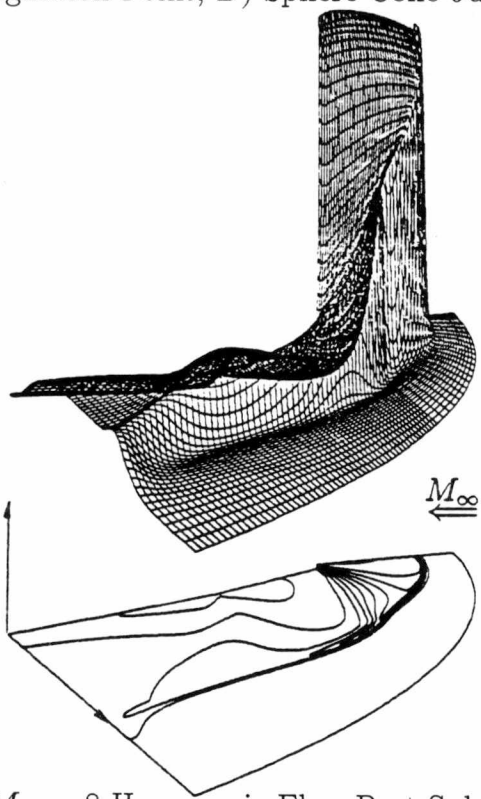


Figure 10.54: $M_\infty = 8$ Hypersonic Flow Past Sphere-Biconic Axisymmetric Body, Steady State Perspective Surface and Contour Distributions, Density.

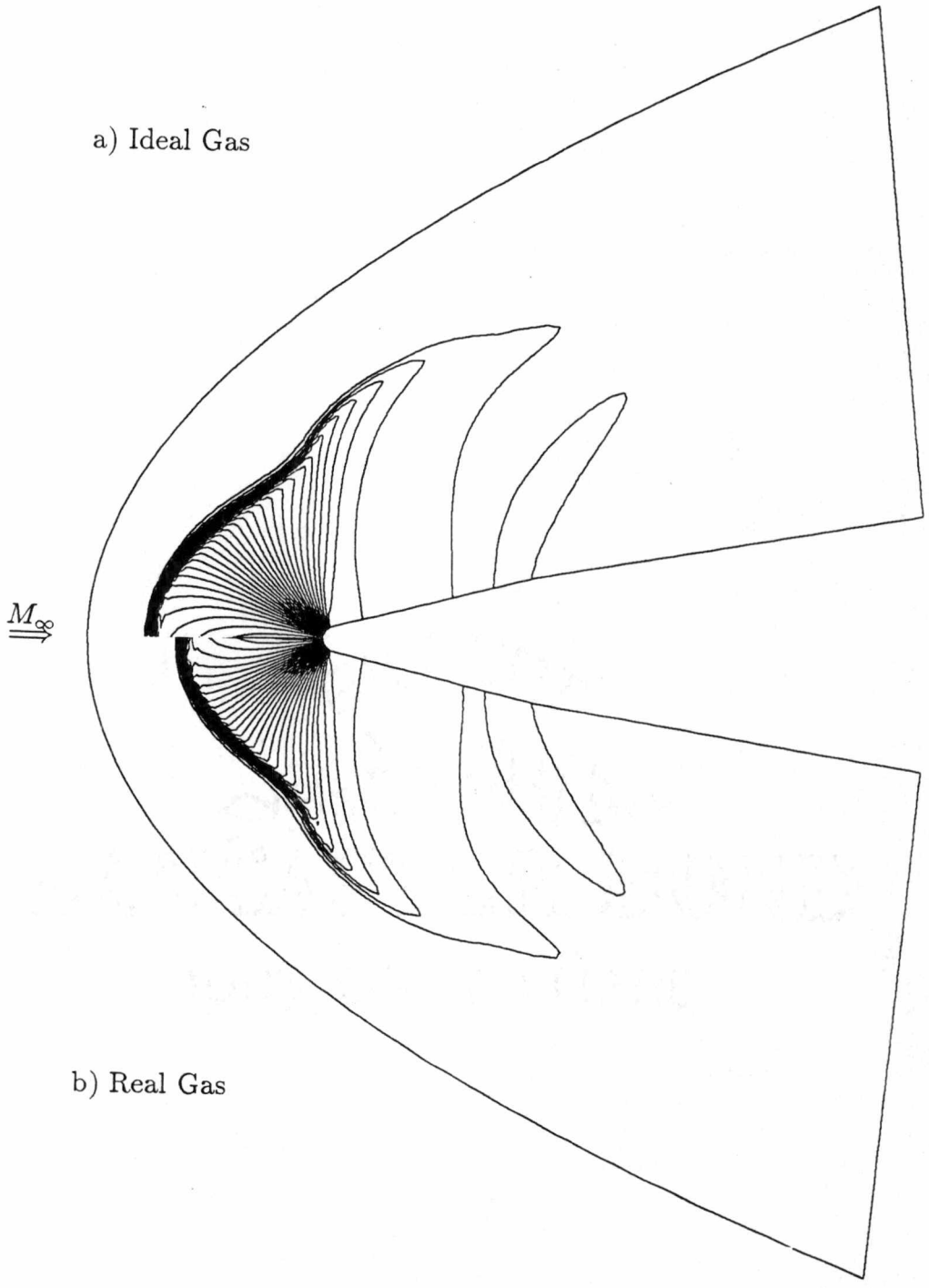


Figure 10.55: $M_\infty = 8$ Hypersonic Inviscid Flow Past Sphere-Biconic Axisymmetric Body, Steady State Contour Distributions, Pressure, a) Ideal Gas, b) Real Gas. Magnification-Induced Bow Shock Distortion.

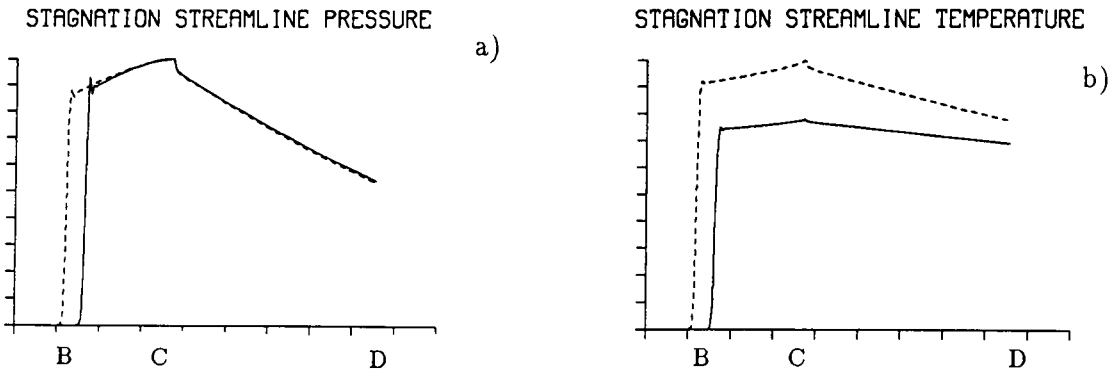


Figure 10.56: $M_\infty = 8$ Hypersonic Inviscid Flow Past Sphere-Biconic Axisymmetric Body, Steady State Stagnation Streamline Distributions, B-Shock Point, C-Stagnation Point, D-Sphere Cone Juncture, – – – – Ideal Gas, —— Real Gas, a) Pressure, b) Temperature.

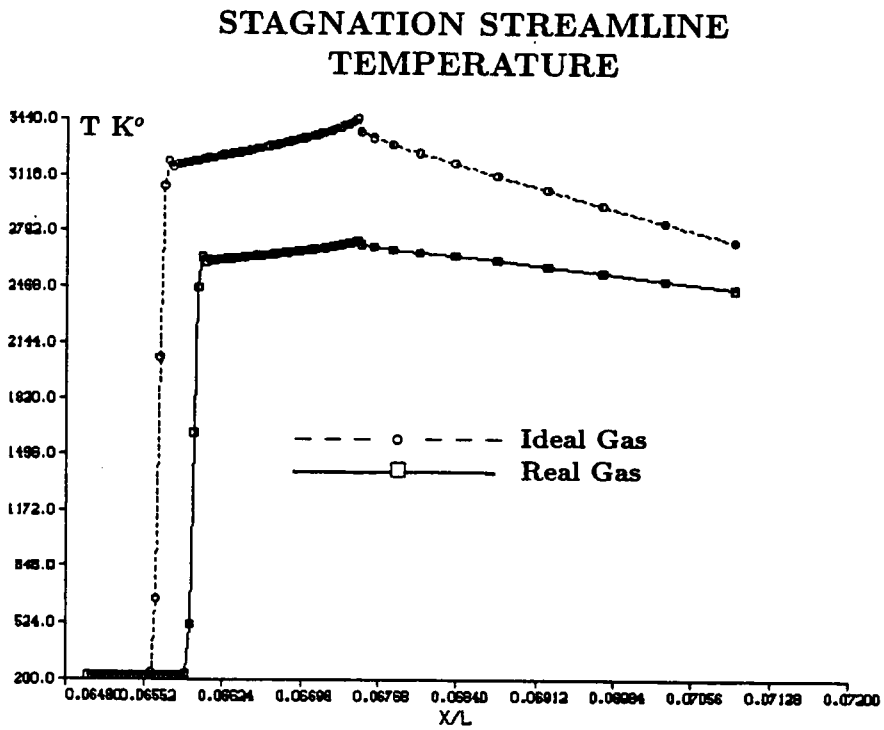


Figure 10.57: $M_\infty = 8$ Hypersonic Inviscid Flow Past Sphere-Biconic Axisymmetric Body, Detailed Steady-State Stagnation-Streamline Temperature Distributions.

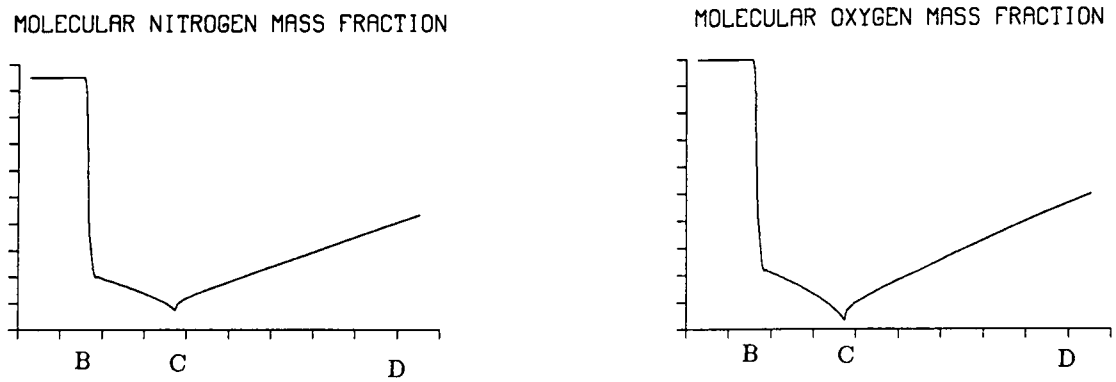


Figure 10.58: $M_\infty = 8$ Hypersonic Inviscid Flow Past Sphere-Biconic Axisymmetric Body, Steady State Stagnation-Streamline Distributions, B-Shock Point, C-Stagnation Point, D-Sphere Cone Juncture, Mass Fractions, a) Molecular Nitrogen, b) Molecular Oxygen.

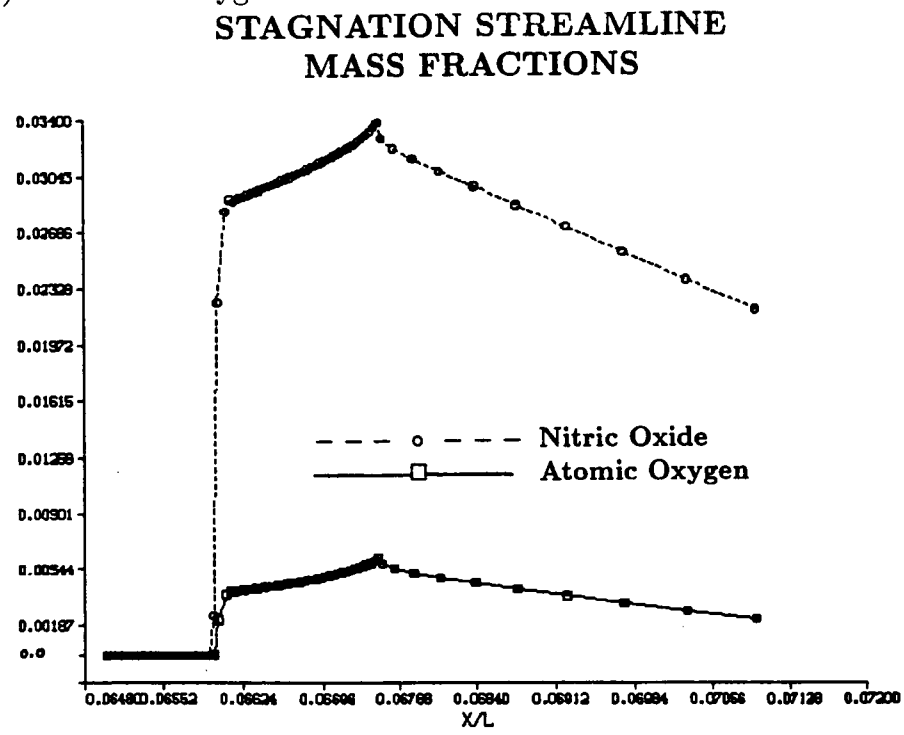


Figure 10.59: $M_\infty = 8$ Hypersonic Inviscid Flow Past Sphere-Biconic Axisymmetric Body, Detailed Steady-State Stagnation-Streamline Distributions for Nitric Oxide and Atomic Oxygen Mass Fractions.

Chapter 11

Summary and Conclusions

A non-linearly stable and accurate finite element CFD algorithm for the laminar compressible Navier-Stokes and Euler conservation law systems is developed and validated. The procedure is constituted by the union of a minimally dissipative integral statement (MDS), an optimal metric-data Galerkin finite element semi-discretization, a non-linearly stable implicit Runge-Kutta integration algorithm, and a matrix tensor product approximate factorization linear algebra procedure. Further, the study contains the full theoretical development of well posed boundary conditions for all Reynolds and Mach numbers. These conditions constrain the surface total tractions and momentum and heat flux and are directly enforceable through the surface integrals exposed in weak statement constructions.

The MDS procedure plays a central role in the achievement of stable solutions by yielding a suitably dissipative semi-discrete ODE system, with dissipation level controlled with the parameter $\beta_{\underline{r}}$. The terminal algorithm is proven robust and

stable over a wide range of challenging inviscid and viscous flow benchmark problems for a uniformly constant value of β_r independent of mesh distribution and element aspect ratio, as especially revealed by the 2-D adapted mesh inviscid-flow results.

The theoretical analysis comparing the developed non-linearly stable IRK scheme and the "θ" implicit algorithms indicates that IRK remains accurate and stable without introducing substantial additional numerical dissipation. The quasi-1-D tests then confirm that the IRK procedure yields uniformly more accurate and stable results than those generated by the equivalently second order accurate trapezoidal rule. Further, the 2-D inviscid-flow tests indicate that IRK affords the largest useable Courant number.

The numerical results for the selected benchmarks validate the algorithm and verify its robustness for curvilinear-coordinate computations on totally arbitrary grids of bilinear elements. The evolution towards a steady state is achieved without indication of numerical instabilities and the terminal solutions are essentially non-oscillatory. For inviscid and viscous flows, including real gas effect simulation, the results are accurate and conform to the fundamental physics of the problems investigated. In particular, the captured shocks are resolved monotonically, even for the challenging real gas simulations in the missile flow field prediction. For this more realistic case, the shock stand-off distance and peak temperature are reduced by 18 %, in comparison with the corresponding ideal-gas values.

This implicit finite-element algorithm has consistently yielded accurate results

for several transonic, supersonic and hypersonic flows under diverse boundary conditions and geometry combinations. Hence, it can be considered a robust "Navier-Stokes" solver and therefore appears to constitute a reliable and advantageous alternative on arbitrary meshes to implicit fully upwind finite difference and finite volume procedures now in general use in CFD aerodynamics codes.

Part V

Bibliography

Bibliography

[1] A. H. Shapiro, *The Dynamics and Thermodynamics of Compressible Fluid Flow*, Vol. I & II, Ronald Press Co., New York, NY (1954).

[2] N. Coburn, *Vector and Tensor Analysis*, The MacMillian Company, New York, NY (1955).

[3] H. W. Liepman, and A. Roshko, *Elements of Gasdynamics*, John Wiley, New York, NY (1957).

[4] V. I. Zubov, *Methods of A. M. Lyapunov and their Application*, US Atomic Energy Commission AEC-52-4439, Office of Technical Services, Department of Commerce, Washington, D.C. (1961).

[5] W. Hahn, *Theory and Application of Lyapunov's Direct Method*, Prentice-Hall, Inc., Englewood Cliffs, NJ (1963).

[6] W. G. Vincenti, and C. H. Kruger, *Introduction to Physical Gasdynamics*, John Wiley, New York, NY (1965).

[7] T. Yoshizawa, *Stability Theory by Lyapunov's Second Method*, The Mathematical Society of Japan (1966).

[8] W. Hahn, *Stability of Motion*, Springer-Verlag, New York, NY (1967).

[9] R. D. Richtmyer and K. W. Morton, *Difference Methods for Initial Value Problems*, Interscience Publishers, New York, NY (1967).

[10] J. D. Lambert, *Computational Methods in Ordinary Differential Equations*, John Wiley, New York, NY (1973).

[11] F. M. White, *Viscous Flow*, McGraw-Hill, New York, NY (1978).

[12] V. Hutson and J. S. Pym, *Applications of Functional Analysis and Operator Theory*, Academic Press, New York, NY (1980).

[13] J. D. Anderson Jr., *Modern Compressible Flow with Historical Perspective*, Mc Graw-Hill, New York, NY (1982).

[14] A. J. Baker, *Finite Element Computational Fluid Mechanics*, Hemisphere Publishers, Washington, DC (1983).

[15] K. Dekker and J.G. Verwer, *Stability of Runge-Kutta Methods for Stiff Nonlinear Differential Equations*, Elsevier Publishers, New York, NY (1984).

[16] C. A. Fletcher, *Computational Galerkin Methods*, Springer-Verlag, New York, NY (1984).

[17] P. R. Garabedian, *Partial Differential Equations*, Chelsea, New York, NY (1986).

[18] J. C. Butcher, *The Numerical Analysis of Ordinary Differential Equations: Runge-Kutta and General Linear Methods*, John Wiley, New York, NY (1987).

[19] J. P. Keener, *Principles of Applied Mathematics*, Addison-Wesley, New York, NY (1988).

[20] E. Zauderer, *Partial Differential Equations of Applied Mathematics*, John Wiley, New York, NY (1989).

[21] R. Courant and D. Hilbert, *Methods of Mathematical Physics*, John Wiley, New York, NY (1989).

[22] J. D. Anderson Jr., *Hypersonic and High Temperature Gas Dynamics*, Mc Graw-Hill, New York, NY (1989).

[23] M. E. O' Neil, and F. Chorlton, *Viscous and Compressible Fluid Dynamics*, Ellis Horwood Limited, Chichester, England (1989).

[24] B. van Leer "Towards the Ultimate Conservative Difference Scheme, II Monotonicity and Conservation Combined in a Second Order Scheme", Journal of Computational Physics, 14, 361-370 (1974).

[25] R. M. Beam and R. F. Warming "An Implicit Finite-Difference Algorithm for Hyperbolic Systems in Conservation-Law Form", Journal of Computational Physics, 22, 87-110 (1976).

[26] J. C. Strickwerda, "Initial Boundary Value Problems for Incompletely Parabolic Systems", Comm. Pure Appl. Math., 30, 797-822 (1977).

[27] K. Burrage and J. C. Butcher, "Stability Criteria for Implicit Runge-Kutta Methods", SIAM J. Numer. Anal. 16, 46-57 (1979).

[28] L. J. Hayes, "Implementation of Finite Element Alternating Direction Methods on Non-Rectangular Regions", Int. J. Num. Mtd. Engr., 16, 35-49 (1980).

[29] L. J. Hayes, "Galerkin Alternating-Direction Methods for Non-rectangular Regions Using Patch Approximations", SIAM J. Num. Anal., 18, 627-643 (1981).

[30] W. H. Hundsdorfer and M. N. Spijker, "A Note on B-Stability of Runge-Kutta Methods", Numer. Math., 36, 319-331 (1981).

[31] P. Kaps and G. Wanner, "A Study of Rosenbrock-Type Methods of High Order", Numer. Math., 38, 297-298 (1981).

[32] P. L. Roe, "Approximate Riemann Solvers, Parameter Vectors, and Difference Schemes", Journal of Computational Physics, 43, 357-372 (1981).

[33] J. L. Steger and R. F. Warming, "Flux Vector Splitting of the Inviscid Gasdynamics Equations with Applications to Finite Difference Methods", Journal of Computational Physics, 40, 263-293 (1981).

[34] G. M. Johnson, "Relaxation Solution of the Full Euler Equations", Springer-Verlag, Lecture Notes in Physics, 170, 273-279 (1982).

[35] B. van Leer, "Flux-Vector Splitting for the Euler Equations", Lecture Notes in Physics, 170, 507-512 (1982).

[36] C. K. Lombard, J. Oliger, and J.Y. Yang, "A Natural Conservative Flux Difference Splitting for the Hyperbolic Systems of Gasdynamics", Tech. Paper AIAA 82-0976, 3rd Joint Thermophysics, Fluids, Plasma and Heat Transfer Conference, St. Louis, Missouri (1982).

[37] T. E. Tezduyar and T. J. R. Hughes, "Finite Element Formulations for Convection Dominated Flows with Particular Emphasis on the Compressible Euler Equations", Tech. Paper AIAA 83-0125, 21st Aerospace Sciences Meeting, Reno NV (1983).

[38] A. Lerat, "Implicit Methods of Second-Order Accuracy for the Euler Equations", Tech. Paper AIAA 83-1925, 6th Computational Fluid Dynamics Conference, (1983).

[39] J. Donea "A Taylor-Galerkin Method for Convective Transport Problems", Int. Journal Num. Mtd. in Eng., 20, 101-119 (1984).

[40] M. A. Celia and G. F. Pinder, "An Analysis of Alternating Direction Methods for Parabolic Equations", Num. Mtd. Partial Dif. Eqn., 1, 57-70 (1985).

[41] W. K. Anderson, J. L. Thomas and B. van Leer, "A Comparison of Finite Volume Flux Vector Splittings for the Euler Equations", Tech. Paper AIAA 85-0122, 23rd Aerospace Sciences Meeting, Reno NV (1985).

[42] C. Park, "On Convergence of Computation of Chemically Reacting Flows", Tech. Paper, AIAA 85-0247, 23rd Aerospace Sciences Meeting, Reno, NV (1985).

[43] J. L. Thomas, B. van Leer and R. W. Walters, "Implicit Flux-Split Schemes for the Euler Equations", Tech. Paper AIAA 85-1680, 18th Fluid Dynamics, Plasmadynamics and Lasers Conference, Cincinnati, OH (1985).

[44] T. H. Pulliam, "Efficient Solution Methods for the Navier-Stokes Equations", Lecture Notes, Von Karman Institute Lecture Series, Numerical Techniques for Viscous Flow Computation in Turbomachinery Bladings, Brussels, Belgium (1986).

[45] J. T. Oden, T. Strouboulis, and P. Devloo, "Adaptive Finite Element Methods for the Analysis of Inviscid Compressible Flow: Part I. Fast Refinement/Unrefinement and Moving Mesh Methods for Unstructured Meshes", Computer Methods In Applied Mechanics And Engineering, 59, 327-362 (1986).

[46] G. Degrez, C. H. Boccadoro, and J. F. Wendt, "The interaction of an Oblique Shock Wave with a Laminar Boundary Layer Reviseted. An Experimental and Numerical Study", Journal of Fluid Mechanics, 177, 243-263 (1987).

[47] A. J. Baker, and J. W. Kim, "A Taylor Weak Statement Algorithm for Hyperbolic Conservation Laws", Int. J. Num. Mtd. Fluids, 7, 489-520 (1987).

[48] M. S. Liou and B. van Leer, "Choice of Implicit and Explicit Operators for the Upwind Differencing Method", Tech. Paper AIAA 88-0624, 26th Aerospace Sciences Meeting, Reno NV (1988).

[49] P. Dutt, "Stable Boundary Conditions and Difference Schemes for Navier-Stokes Equations", SIAM J. Num. Anal., 25, 245-267 (1988).

[50] M. S. Liou and B. van Leer, "Splitting of Inviscid Fluxes for Real Gases", NASA Tech. Memorandum 100856 ICOMP-88-7 (1988).

[51] G. C. Paynter, "CFD Technology for Hypersonic Vehicle Design", Computers and Structures, 30, 1/2, 39-46 (1988).

[52] T. R. A. Bussing, and S. Eberhardt, "Chemistry Associated with Hypersonic Vehicles", AIAA Journal of Thermophysics, 3, 3, 245-253 (1989).

[53] R. K. Prabhu, J. R. Stewart, and R. R. Thareja, " A Navier-Stokes Solver for High Speed Equilibrium Flows and Application to Blunt Bodies", AIAA 89-0668, 27th Aerospace Sciences Meeting, Reno, NV (1989).

[54] Y. Liu, and M. Vinokur, "Equilibrium Gas Flow Computations. I. Accurate and Efficient Calculation of Equilibrium Gas Properties", Tech. Paper, AIAA 89-1736, 24th Thermophysics Conference, Buffalo, New York (1989).

[55] M. S. Liou, "A Newton/Upwind Method and Numerical Study of Shock Wave Boundary Layer Interactions", International Journal for Numerical Methods in Fluids, 9, 747-761 (1989).

[56] K. G. Powell, and B. van Leer "A Genuinely Multi-Dimensional Upwind Cell-Vertex Scheme for the Euler Equations", NASA Tech. Memorandum 102029 ICOMP-89-13 (1989).

[57] C. Park, and S. Yoon, "A Fully-Coupled Implicit Method for Thermo-Chemical Non-Equilibrium Air at Sub-Orbital Flight Speeds", Tech. Paper, AIAA 89-1974, 9th Computational Fluid Dynamics Conference, Buffalo, New York (1989).

[58] D. W. Levy, K. G. Powell and B. van Leer, "An Implementation of A Grid Independent Upwind Scheme for The Euler Equations", Tech. paper 89-1931, 9th Computational Fluid Dynamics Conference, Buffalo, NY (1989).

[59] D. P. Rizzetta, and K. D. Mach, " Comparative Numerical Study of Hypersonic Compression Ramp Flows " Tech. Paper AIAA-89-1877, (1989).

[60] Y. Kronzon, *et al.*, "Gas Flows in Rocket Motors", Tech. Report AL-TR-89-011, AFSC, AL/LSCF, Edwards AFB, CA (1989)

[61] B. Simpson, "Unsteady Three-Dimensional Thin Layer Navier- Stokes Solutions on Dynamic Blocked Grids", Tech. Report AFATL-TR-89-19, ABAB, AF Armament LAB, Eglin AFB, FL (1989).

[62] P. Colella, "Multidimensional Upwind Methods for Hyperbolic Conservation Laws", Journal of Computational Physics, 87, 171-200 (1990).

[63] H. C. Yee, G. H. Klopfer, and J. L. Montagne, "High Resolution Shock-Capturing Schemes for Inviscid and Viscous Hypersonic Flows", Journal of Computational Physics, 88, 31-61 (1990).

[64] J.-A. Desideri, N. Glinsky, and E. Hettena, "Hypersonic Reacting Flow Computations", Computers and Fluids, Vol. 18, No. 2, 151-182 (1990).

[65] B. Grossman, and P. Cinnella, "Flux-Split Algorithms for Flows with Non-equilibrium Chemistry and Vibrational Relaxation", Journal of Computational Physics, 88, 131-168 (1990)

[66] M. S. Liou, B. van Leer, and J. S. Shuen, "Splitting of Inviscid Fluxes for Real Gases", Journal of Computational Physics, 87, 1-24 (1990).

[67] M. Vinokur, and J. L. Montagne', " Generalized Flux-Vector Splitting and Roe Average for an Equilibrium Real Gas", Journal of Computational Physics, 89, 276-300 (1990).

[68] J. S. Shuen, M. S. Liou, and B. van Leer, "Inviscid Flux-Splitting Algorithms for Real Gases with Non-equilibrium Chemistry", Journal of Computational Physics, 90, 371-395 (1990).

[69] C. L. Rumsey, B. van Leer, and P. L. Roe, "A Grid-Independent Approximate Riemann Solver With Applications to the Euler and Navier-Stokes Equations", AIAA 91-0239, 29th Aerospace Sciences Meeting, Reno NV (1991).

[70] N. Kroll, D. Gaitonde, and M. Aftosmis, "A Systematic Comparative Study of Several High Resolution Schemes for Complex Problems in High Speed Flows", AIAA 91-0636, 29th Aerospace Sciences Meeting, Reno NV (1991).

VITA

Giuseppe S. Iannelli was born in Susa, province of Turin in Italy, on July 22, 1961. He lived in northern Italy for a little while before moving to the southern Italian town of Palermo. Towards the end of July 1979 he graduated from the local "V Liceo Scientifico" (scientific high school), and then he enrolled in the aeronautical engineering program of the University of Palermo.

In September 1984 he went to the Von Karman Institute for Fluid Dynamics in Rhode St. Genese, near Brussels, Belgium, where he graduated with the Von Karman Diploma in Fluid Dynamics. By the end of 1985 he returned to Italy, and in November 1986 he graduated with a "Laurea" in aeronautical engineering, the equivalent of a B.S. and M.S. in the same field.

In December 1986 he accepted a teaching and research assistanship at the University of Tennessee, Knoxville, and began to study towards a PH.D., in Engineering Science. This degree was awarded in May 1991. Dr. Iannelli will be employed by the University of Tennessee as a professor in the department of Engineering Science & Mechanics.